Vol. 66 May, 1962 No. 5

THE JOURNAL OF PHYSICAL CHEMISTRY

(Registered in U. S. Patent Office)

CONTENTS

Contents continued on inside front cover

THE JOURNAL OF PHYSICAL CHEMISTRY

(Registered in U. S. Patent Office)

Published monthly by the American Chemical Society at 20th and Northampton Sts., Easton, Pa. Second-class postage paid at Easton, Pa.

The *Journal of Physical Chemistry* is devoted to the publication of selected symposia in the broad field of physical chemistry and to other contributed papers.

Manuscripts originating in the British Isles, Europe, and Africa should be sent to F. C. Tompkins, The Faraday Society, 6 Gray's Inn Square, London W. C. 1, England.

Manuscripts originating elsewhere should be sent to W. Albert Noyes, Jr., Department of Chemistry, University of Rochester, Rochester 20, N. Y.

Correspondence regarding accepted copy, proofs, and reprints should be directed to Assistant Editor, Allen D. Bliss, Department of Chemistry, Simmons College, 300 The Fenway, Boston 15, Mass.

Advertising Office: Reinhold Publishing Corporation, 430 Park Avenue, New York 22, N. Y.

Articles must be submitted in duplicate, typed, and double spaced. They should have at the beginning a brief Abstract, in no case exceeding 300 words. Original drawings should accompany the manuscript. Lettering at the sides of graphs (black on white or blue) may be pencilled in and will be typeset. Figures and tables should be held to a minimum consistent with adequate presentation of information. Photographs will not be printed on glossy paper except by special arrangement. All footnotes and references to the literature should be numbered consecutively and placed in the manuscript at the proper places. Initials of authors referred to in citations should be given. Nomenclature should conform to that used in *Chemical Abstracts*, mathematical characters be marked for italic, Greek letters carefully made or annotated, and subscripts and superscripts clearly shown. Articles should be written as briefly as possible consistent with clarity and should avoid historical background unnecessary for specialists.

Remittances and orders for subscriptions and for single copies, notices of changes of address and new professional connections, and claims for missing numbers should be sent to the Subscription Service Department, American Chemical Society, 1155 Sixteenth St., N. W., Washington 6, D. C. Changes of address for the *Journal of Physical Chemistry* must be received on or before the 30th of the preceding month. Please include an old address label with the notification.

Claims for missing numbers will not be allowed (1) if received more than sixty days from date of issue (because of delivery hazards, no claims can be honored from subscribers in Central Europe, Asia, or Pacific Islands other than Hawaii), (2) if loss was due to failure of notice of change of address to be received before the date specified in the preceding paragraph, or (3) if the reason for the claim is "missing from files."

Subscription rates (1962): members of American Chemical Society, $12.00 for 1 year; to non-members, $24.00 for 1 year. Postage to countries in the Pan-American Union $0.80; Canada, $0.40; all other countries, $1.20. Single copies, current volume, $2.50; foreign postage, $0.15; Canadian postage $0.10; Pan-American Union, $0.10. Back volumes (Vol. 56–65) $30.00 per volume; foreign postage, per volume $1.20, Canadian, $0.40; Pan-American Union, $0.80. Single copies: back issues, $3.00; for current year, $2.50; postage, single copies: foreign, $0.15; Canadian, $0.10; Pan-American Union, $0.10.

The American Chemical Society and the Editors of the *Journal of Physical Chemistry* assume no responsibility for the statements and opinions advanced by contributors to This Journal.

The American Chemical Society also publishes *Journal of the American Chemical Society*, *Chemical Abstracts*, *Industrial and Engineering Chemistry*, International Edition of *Industrial and Engineering Chemistry*, *Chemical and Engineering News*, *Analytical Chemistry*, *Journal of Agricultural and Food Chemistry*, *Journal of Organic Chemistry*, *Journal of Chemical and Engineering Data*, *Chemical Reviews*, *Chemical Titles*, *Journal of Chemical Documentation*, *Journal of Medicinal and Pharmaceutical Chemistry*, *Inorganic Chemistry*, *Biochemistry*, and *CA — Biochemical Sections*. Rates on request.

THE JOURNAL OF PHYSICAL CHEMISTRY

(Registered in U. S. Patent Office) (© Copyright, 1962, by the American Chemical Society)

VOLUME 66 MAY 16, 1962 NUMBER 5

THE STRUCTURE OF N-MONO AND N,N'-DISUBSTITUTED AMIDINES[1]

BY DUSAN C. PREVORSEK[2]

Laboratoires des Recherches Physiques, Sorbonne, Paris and Textile Research Institute, Princeton, New Jersey

Received April 19, 1961

The infrared spectra of several N-mono- and N,N'-disubstituted amidines have been studied in order to obtain information about their rotational isomerism and factors influencing the position of the tautomeric equilibria. It is shown that rotational isomerism in N,N'-disubstituted amidines is not sufficient to explain all experimental findings. The possibility of tautomerism is re-examined and the suggestion is made that both tautomerism and rotational isomerism may occur simultaneously. The electronic structure of the amidoxime grouping is discussed.

Introduction

Amidines are monoacid bases characterized by the structural grouping

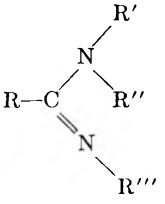

and may be classified into five general types depending on the number and distribution of the substituents on the nitrogen atoms.

A. Unsubstituted 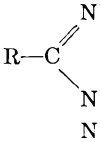

B. Monosubstituted 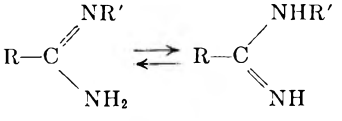

C. N,N'-disubstituted 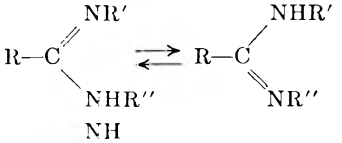

D. N-disubstituted 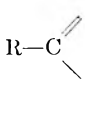

E. Trisubstituted 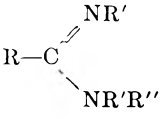

One expects that mono- and N,N'-disubstituted amidines having different groups on the nitrogen atoms would exhibit tautomerism. Although there is a considerable amount of experimental data favoring this supposition, no proof for the existence of the two tautomeric forms has been presented as yet.[3] Numerous attempts have been made to isolate the two tautomeric forms, but they apparently all failed.[4]

Experimental findings favoring the possibility of tautomerism are: (1) a single amidine results from a reaction designed to prepare two tautomeric forms; (2) the alkylation of an amidine yields two products; (3) the hydrolysis of N,N'-disubstituted amidines produces a mixture of amides and amines.[5]

Although these findings sometimes led to correct conclusions, their value is questionable, because the mechanism of reactions involved could not be studied adequately before the structure of these compounds had been determined.

Because of the lack of systematic work regarding tautomeric equilibria the infrared spectra of a series of mono- and N,N'-disubstituted amidines have been studied. Thus we obtained information about the position of the characteristic bands associated

(1) Paper presented at the 138th National Meeting of the American Chemical Society, Division of Physical Chemistry, September, 1960, New York.

(2) Textile Research Institute, Princeton, New Jersey.

(3) M. Kuna and M. J. Kopac, *Ann. N. Y. Acad. Sci.*, **58**, 263 (1954); *Chem. Abstr.*, **49**, 6176[b] (1955).

(4) R. Delaby, J. V. Harispe, and S. H. Renard, *Bull. soc. chim. France*, **11**, 227 (1944).

(5) R. L. Shriner and F. W. Neuman, *Chem. Revs.*, **35**, 351 (1944).

TABLE I: CHARACTERISTIC FREQUENCY ASSIGNMENT IN THE 2–7 μ REGION N-MONOSUBSTITUTED AND N,N-DISUBSTITUTED AMIDINES

General formula $R'N{=}CR{-}NR'R''$ or $R^2N{-}CR{=}NR''$ R	R′	R″	Solution ν(OH)	Solution ν_{as}(NH₂)	Solution ν_{s}(NH₂)	Solution ν(=NHR)	Solution ν(=NH)	Amidine I [ν_{as}(N=C—N)]? Solid or condensed phase	Amidine I [ν_{as}(N=C—N)]? Solution	Amidine I [ν_{as}(N=C—N)]? Deut. species Solid	Amidine I [νC=N)]? Solid or condensed phase	Amidine I [νC=N)]? Solution	Amidine I [νC=N)]? Deut. species solid	δ(NH₂) Solid	δ(NH₂) Solution	Amidine II Solid	Amidine II Solution	Amidine II Deut. species solid
	H–	HO–	3568[a]	3505[a]	3400[a]	....	....	1641s	n.i.	1604s	...	...	...	1578m	n.i.	....	....	....
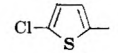	H–	HO–	3575[a]	3510[a]	3415[a]	....	....	1641s	n.i.	1611s	...	...	...	1581m	n.i.	....	....	....
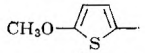	H–	HO–	3570[a]	3510[a]	3412[a]	....	....	1656s	n.i.	n.i.	...	...	...	1581m	n.i.	....	....	....
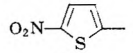	H–	HO–	3575[a]	3515[a]	3412[a]	....	....	1643s	n.i.	1617s	...	...	...	1586m	n.i.	....	....	....
	H–	HO–	3584[a]	3515[a]	3395[a]	....	....	1643s	n.i.	1618s	...	...	...	1544m	n.i.	....	....	....
	H–	HO–	3560[a]	3509[a]	3400[a]	....	....	1643s	n.i.	n.i.	...	...	...	1609m	n.i.	....	....	....
	H–	HO–	3560[a]	3510[a]	3396[a]	....	....	1627s	n.i.	1609s	...	...	...	1591m	n.i.	....	....	....
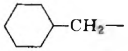	H–		...	3497m	3401m	....	....	1633s	1640s	1620s	...	...	...	1601m	1587m	....	....	....
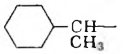	H–		...	3497m	3401m	....	....	1630s	1640s	n.i.	...	...	...	1610m	1597m	....	....	....
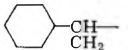	H–		...	3497m	3401m	....	....	1635s	1640s	n.i.	...	...	...	1610m	....	....	....	....
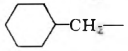	H–	CH_3CH_2–	...	3510vw	....	3448m	3310w		1648sh	n.i.	1588s	1615s	1580s	....	....	1571m	1510m	1410m
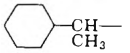	H–	CH_3CH_2–	...	3500vw	....	3446m	3310w	1642m,sh	1647m,sh	n.i.	1605s	1601s	n.i.	....	....	1540m	1506m	n.i.
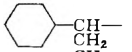	H–	CH_3CH_2–	...	3510vw	....	3448m	3332w	1640m,sh	1642m,sh	n.i.	1610s	1610s	n.i.	....	....	1540m	1505m	n.i.
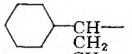	H–	CH_3CH_2–	...	3510vw	....	3442m	3310w	1648m,sh	1650m,sh	n.i.	1608s	1610s	n.i.	....	....	1544m	1505m	n.i.
	H–	CH_3–	...	3510vw	....	3450m	3310w	1640m	1652m,sh	n.i.	1602s	1612s	n.i.	....	....	1540m	1525m	....
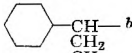 [b]	CH_3CH_2–	CH_3CH_2–	...	.....	....	....	3305w	.....	.....	...	1588s	n.i.	n.i.	....	....	....	....	....
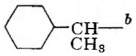 [b]	CH_3CH_2–	CH_3CH_2–	...	.....	....	....	3305w	.....	.....	...	1588s	n.i.	n.i.	....	....	....	....	....

[a] Solution too dilute to estimate the relative intensities. [b] N,N-Disubstituted amidines $HN{=}CR{-}NR'R''$

Band characteristics and relative intensities: w = weak; m = medium; s = strong; v = very; sh = shoulder; b = broad; n.i. = not investigated.
Scale of relative intensities in percentage transmission: vw, >85; m, 30–70; w, 70–85; s, <30.

TABLE II

CHARACTERISTIC FREQUENCY ASSIGNMENT IN THE 2–7 μ REGION N,N'-DISUBSTITUTED AMIDINES

General formula

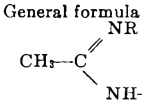

R	R'	ν(NH) Solid	ν(NH) Soln.	ν(NH) Deut. species solid	Amidine I Solid	Amidine I Soln.	Amidine I Deut. species solid	Amidine II (Amidine II') Solid	Amidine II (Amidine II') Soln.	Amidine II (Amidine II') Deut. species solid
		3245m 3205m 3105m	3448m 3390m	2314m,b	1628s	1655s 1633m,sh	1618s	1531s	1515s	1406m
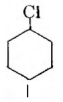		3236m 3184m 3012m	3448m 3370w	2300m,b	1628s	1652s	1618s 1610s	1540s	1508s	1408m
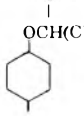		3278m 3205m 3105m	3448m 3390m	2304m,b	1636s 1628s	1647s	1615s 1605s	1531s	1517s	1398m
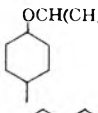	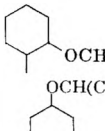	3290m 3246m 3236m 3115m	3446m	2358m,b	1636s 1631s	1647s	1615s 1600s	1550s 1533s	1519s	1396m
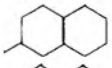	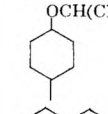	3400m	3448m 3378m	2518m	1644s 1628s	n.i.	1639s 1623s	1531s	1517s	1404m
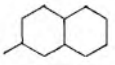	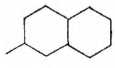	3412m	3448m 3378m	2518m	1647s 1620s	1655s 1630m,sh	1639s 1615s	1540s	1526s	1400m
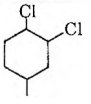	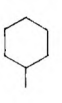	n.i.	3448m 3358w	n.i.	n.i.	1650s	n.i.	n.i.	1506m	n.i.
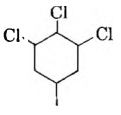	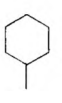	n.i.	3448m 3350w	n.i.	n.i.	1648s	n.i.	n.i.	1505m	n.i.

Band characteristics and relative intensities: w = weak; m = medium; s = strong; v = very; sh = shoulder; b = broad; n.i. = not investigated. Scale of relative intensities in percentage transmission: vw, >85; m, 30–70; w, 70–85; s, <30.

with the vibrations of the two tautomeric forms, the structure of amidines in general, and the principal factors influencing the equilibrium.

Experimental

Apparatus and Technique.—Infrared absorption spectra were recorded using a Perkin-Elmer (Model 21) double-beam spectrophotometer equipped with NaCl and CaF_2 optics. The crystalline specimens were melted as a thin film between rock-salt plates and allowed to crystallize or examined as Nujol and hexachlorobutadiene mulls. With $CHCl_3$ solutions matched cells of path-length 0.1–10 mm. were used.

The spectra of the deuterated species also were recorded. The deuterium exchange procedure resulted in at least 75% exchange of deuterium for acidic hydrogens.

Assignment of Characteristic Frequencies in the 2–7 μ Region.—Because the complete description of the spectra is not within the scope of this work we shall limit the discussion to frequencies associated with vibrations of the amidine grouping in the 2–7 μ region. Bands associated with vibrations of the amidine grouping can be distinguished from bands associated with vibrations of the rest of the molecule on the basis of frequency shifts in solution and behavior on deuteration. The results pertinent for the discussion of configuration are given in Tables I and II.

In Table I are not included the data for amidoximes in the 3 μ region in the solid state. In the solid state both OH and NH bonds are strongly hydrogen bonded. Thus the associated vibrational bands are strong and broad. Such factors as the non-linearity of the X–H. . . .Y grouping and variation of the environment affect the hydrogen bond frequencies. Further, it also has been suggested that a number of molecules might be involved in bridge mechanisms leading to a delocalization of protons.[6] Therefore we were unable to give an unequivocal frequency assignment which would permit us to obtain unambiguous information regarding the configuration.

a. **Monosubstituted Amidines.**—With amidoximes and N-phenylamidines we found two bands appearing near 3500 and 3400 cm.$^{-1}$. In the spectra of amidoximes there is another band appearing near 3590 cm.$^{-1}$ which clearly arises from the OH stretching mode. The monomeric ν(OH) band in acetoxime[7] which contains the structural unit =N—OH occurs at 3604 cm.$^{-1}$.

The frequencies of NH stretching vibrations in molecules having a similar structure have been summarized by Orville-Thomas and Parsons.[8] The observed frequencies are in close agreement with those found for the $\nu_{as}(NH_2)$ and $\nu_s(NH_2)$ modes in formamide (3533, 3411 cm.$^{-1}$) and acetamide (3533, 3415 cm.$^{-1}$), which indicates that amidoxime and N-phenylamidines contain very probably a terminal amino group.

The symmetrical and asymmetrical NH stretching frequencies in primary amines have been studied extensively by Bellamy and Williams.[9] It has been shown that in dilute solutions these two frequencies are related by the expression

$$\nu_s = 345.5 + 0.876\nu_{as}$$

We found that this correlation applies also for hydrazides of carboxylic acids.[10] The agreement is very satisfactory

(6) D. Hall and F. T. Llewellyn, *Acta Cryst.*, **9**, 408 (1956).

(7) S. Califano and W. Lüttke, *Z. physik. Chem.*, **5**, 240 (1955).

(8) W. J. Orville-Thomas and A. E. Parsons, *Trans. Faraday Soc.*, **54**, 460 (1958).

(9) L. J. Bellamy and R. L. Williams, *Spectrochim. Acta*, **9**, 341 (1957).

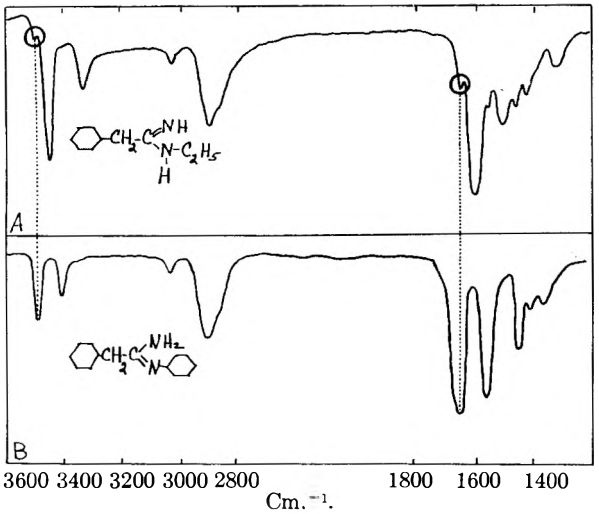

Fig. 1.—Infrared spectra of (A) N-ethylphenylacetamidine and (B) N-phenylphenylacetamidine, solution in $CHCl_3$; ○, absorption bands associated with the less stable tautomeric form.

also for amidoximes and N-phenylamidines, hence we considered this as another supporting argument for a terminal amino group. Somewhat larger deviations for amidoximes very probably are due to the inequality in the NH links introduced by the intramolecular hydrogen bond.

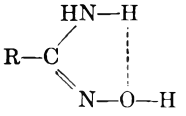

It also is clear that these compounds are not a tautomeric mixture of the two forms, because in such a case one would expect four NH and two OH stretching modes to appear in this region.

Additional evidence for the presence of a terminal amino group in these compounds is the appearance of a band near 1600 cm.$^{-1}$. This band moves to lower frequencies in solution and is reduced greatly in intensity or disappears in deuterated species, which indicates that this mode involves the deformation of hydrogen atoms. A band in this region of the spectrum has been assigned to the bending mode of $-NH_2$ group in a large number of compounds. Bands arising from the deformation of =NH and –NH–R groups generally are found at lower frequencies.[8,11] A strong band near 1640 cm.$^{-1}$ which alters but little on deuteration and shifts in solution to higher frequencies probably is described best as ν_{as} 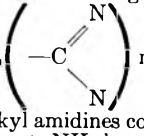 mode.

The spectra of N-alkyl amidines contain three bands in the region where we expect NH bond-stretching vibrations. The band at 3510 cm.$^{-1}$ is very weak, while the bands near 3450 and 3310 cm.$^{-1}$ are much stronger. The band near 3450 cm.$^{-1}$ has been assigned to the NH stretching vibrations of the —N—R group. The observed values for this band are in agreement with those found with secondary amides[11] and N,N'-disubstituted amidines.[12] The band at 3310 cm.$^{-1}$ is assigned to the vibration of the =N—H group. This assignment has been verified by the spectra of N-diethylamidines having the configuration

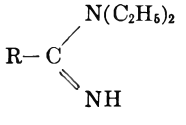

The ν(=NH) absorption in these compounds occurs near 3305 cm.$^{-1}$ (see Table I).

The infrared spectra of N-alkyl amidines indicate therefore that these compounds exist predominantly in the form having a terminal imino group. With the 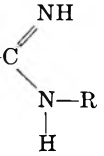 group, which is very similar to the configuration of secondary amides, one can expect a strong interaction of the ν(C–N) and δ(NH) modes. In N-substituted amides the ν(C–N) and δ(NH) vibrations are strongly coupled since their unperturbed frequencies lie close to one another.[13,14]

As a consequence of this interaction the vibrations split about the common value, the higher frequency occurs near 1560 cm.$^{-1}$ (amide II band); the lower near 1290 cm.$^{-1}$ (amide III band). Miyazawa, *et al.*,[15] who carried out the normal coördinate treatment for methylacetamide and calculated the displacement vectors, give this assignment for the absorption bands under discussion

Amide II 60% NH in plane bending and 40% C–N stretching

Amide III 40% C–N stretching, 30% NH in plane bending, 20% CH_3–C stretching

As expected, on deuteration the coupling is broken and bands appearing near 1400 and around 950 cm.$^{-1}$ can be described approximately as ν(C–N) and δ(ND).

The spectra of all investigated N-alkyl amidines contain in the 6μ region a strong band near 1550 cm.$^{-1}$. This band is sensitive to deuteration and changes of state. In solution the band is shifted to lower frequencies (near 1510 cm.$^{-1}$), while in deuterated species its intensity is greatly reduced and a new intense band appears near 1400 cm.$^{-1}$. The observed frequency shifts are very similar to the observations made with the amide II band with N-monosubstituted amides.

Evidently both 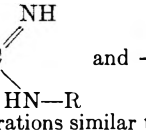 and 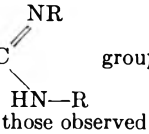 groupings give rise to normal vibrations similar to those observed with secondary amides. Because of their complexity some of the absorption bands cannot be described adequately (even approximately) by the displacements of two atoms only. Especially the attribution of any of the observed bands to ν(C–N) and δ(N–H) would be misleading. Therefore the use of terms amidine I, II, III, etc., band (as generally accepted for amides) is recommended.

Amidine I band arising principally from a ν(C=N) mode occurs near 1600 cm.$^{-1}$. This band is very strong and shows only small shifts with alteration of phase.

There remain to be assigned bands appearing at 3500 and 1640 cm.$^{-1}$. Both bands are very weak and they cannot be allocated to fundamental frequencies of the form having a terminal imino group. The frequency at 3500 cm.$^{-1}$ cannot be explained satisfactorily as a combination or an overtone. The band at 3500 cm.$^{-1}$ does not appear in the solid N-ethylphenylacetamidine (the only compound of this series that can be prepared in crystalline form) in deuterated species and in N,N-diethylamidines. The frequency of this band is in close agreement with the value for the $\nu_{as}(NH_2)$ stretching vibration in amidoximes and N-phenylamidines. Hence we considered the presence of a band in this region as a very strong indication that N-ethylamidines exist in solution as a tautomeric mixture. This view is confirmed by the appearance of a weak band near 1640 cm.$^{-1}$. This frequency does not occur in N-diethylamidines but it appears in the spectra of all the amidoximes and N-phenylamidines we investigated, and it has been assigned

(10) D. Prevorsek, *Bull. soc. chim. France*, **6**, 795 (1958).

(11) L. J. Bellamy, "The Infrared Spectra of Complex Molecules," Methuen, London, Second Edition, 1958, p. 219.

(12) D. Prevorsek, *Bull. soc. chim. France*, 788 (1958).

(13) D. B. Frazer and W. C. Price, *Nature*, **170**, 490 (1952).

(14) I. Sandeman, *Proc. Roy. Soc.* (London), **A232**, 105 (1955).

(15) T. Miyazawa, T. Shimanouchi, and S. Mizushima, *J. Chem. Phys.*, **29**, 611 (1958).

to ν_{as} 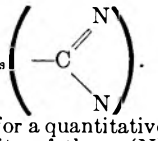 . The intensity of these two bands is too low for a quantitative determination. Assuming that the intensity of the $\nu_{as}(NH_2)$ band in N-ethylamidines is of the same magnitude as observed with N-phenylamidines, one can estimate that the amount of less stable configuration at room temperature in $CHCl_3$ solution is below 5%.

These experimental data suggest further that it is possible to obtain additional confirmatory evidence as to the type of configuration of N-monosubstituted amidines by comparing the position of the amidine I band associated with a ν(C=N) or ν_{as} 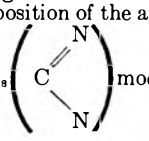 mode. A strong band near 1640 cm.$^{-1}$ which was tentatively assigned to the ν_{as} 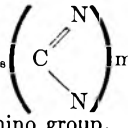 mode indicates a structure having a terminal amino group. The amidine I band in N-alkyl and N-diethylamidines which probably is described best as a ν(C=N) mode occurs at lower frequencies near 1600 cm.$^{-1}$. The assignment of these two bands to ν_{as} 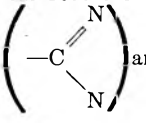 and ν(C=N) is somewhat arbitrary. We assigned the band occurring with the 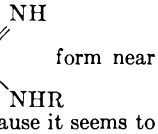 form near 1600 cm.$^{-1}$ to a C=N stretching mode, because it seems to be justified to extend the findings obtained with amides to amidines.[16] Both the similarity of the electronic configuration and the infrared spectra of these compounds favor such an assumption.

There is much less information available about the nature of the band appearing near 1640 cm.$^{-1}$ with the 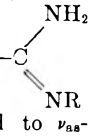 form. This band has been tentatively assigned to ν_{as}  because it is possible that the observed frequency shift is caused by a stronger interaction between ν(C=N) and ν(C-N) modes. As a consequence of such an interaction the separation of the two frequencies is expected to become larger, which is in agreement with the shift of the ν(C=N) band to higher frequencies. Because of the complexity of spectra we were unable to identify the ν(C-N) or ν_s 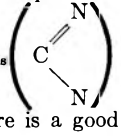 band so that it remains uncertain whether there is a good reason for such an assignment or not.

b. N,N'-Disubstituted Amidines.—The spectra of all investigated N,N'-disubstituted amidines (with the exception of N-(*p*-isopropoxy)-phenyl-N'-(*o*-isopropoxy)-phenylacetamidine) contain in the NH stretching region two bands near 3450 and 3380 cm.$^{-1}$. Because the relative intensities of these two bands remain unaffected by dilution provided $c \times l$ = constant (c = concentration, l = path length) it is evident that they both are associated with the vibrations of the monomeric form of the molecule. The high frequency band always is stronger and its position changes little in the series of investigated compounds. The low frequency band varies in intensity and frequency depending on the substituents on the nitrogen atoms. It is strongest with amidines having identical substituents on the nitrogen atoms and diminishes in intensity if one of the substituents is replaced by either a more or less electronegative one. In the solid state we found either a broad absorption band with several peaks between 3300 and 3100 cm.$^{-1}$ or a narrow band near 3400 cm.$^{-1}$. With deuterated species the intensity of these bands is greatly reduced, and new peaks appear near 2300 or 2520 cm.$^{-1}$. Because the narrow absorption band at 3400 cm.$^{-1}$ (near 2520 cm.$^{-1}$ in deuterated species) occurs with N-β-naphthyl derivatives one can infer that the bulky naphthyl group causes a steric hindrance preventing the formation of a strong hydrogen bond in this compound. It is interesting to note that the compounds that show only one absorption band associated with ν(NH) vibration in the solid state also contain two bands in the spectra of solutions.

A strong band near 1630 cm.$^{-1}$ that shifts toward higher frequencies in solution has been attributed to a ν(C=N) mode. The frequency shifts accompanying changes of state probably are due to a certain extent to the breaking or formation of hydrogen bonds on the C=N groups. The fact that similar frequency shifts have been observed also with the ν(C=N) band in N,N'-β-dinaphthylacetamidine suggests that the changes of state from solid to solution are accompanied by a polarization of the amidine group in favor of the homopolar structure.

In deuterated species the ν(C=N) band shifts slightly to lower frequencies, which indicates that the normal vibrations associated with this frequency also contain displacements of the NH group.

A very characteristic feature of the ν(C=N) band is its asymmetry in solution. In some cases the band shows on its low frequency side a well defined shoulder. The occurrence of two ν(C=N) bands in N,N'-disubstituted amidines in solution has been reported previously.[17] Shigorin and Syrkin[17a] suggested that the appearance of two ν(C=N) bands is due to rotational isomerism around the C–N bond. This view is supported also by the appearance of two ν(NH) bands.

The spectra of N,N'-disubstituted amidines in the solid state contain a very strong band near 1540 cm.$^{-1}$. This band shifts in solution toward lower frequencies and occurs near 1515 cm.$^{-1}$. In most cases this band appears less intense in solution than in the solid state. In the case of N-deuterated species the intensity of this band is reduced and a new peak appears near 1400 cm.$^{-1}$. The behavior of this band therefore is very similar to the behavior of the amide II band, which nature has been discussed with the spectra of N-alkyl amidines. The presence of an amide II band with N-monosubstituted amides indicates that the compounds possess a *trans*-CONH group. With a *cis*-CONH group the interaction between δ(NH) and ν(CN) modes is negligible and vibrations associated predominantly with N–H bonding and a C–N stretching mode occur near 1450 and 1350 cm.$^{-1}$.[18]

The fact that the intensity of the amidine II band is reduced in solution in proportion to the intensity of the ν(NH) band associated with the *cis* form indicates that this observation applies also for amidines.

We considered therefore the occurrence of the amidine II band in the spectra of N-alkyl amidines and N,N'-disubstituted amidines as evidence that these compounds possess in the solid state the configuration

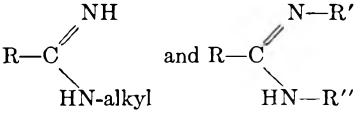

Discussion

Neglecting weak energy differences of the two tautomeric forms of the unsubstituted amidines that could arise if the radical R were to destroy the existing identity of the tautomers we can assume that both forms are equally stable and that

(16) The nature of amide I band is discussed in ref. 15.

(17) (a) D. N. Shigorin and Y. K. Syrkin, *Zhur. Fiz. Khim.*, **23**, 241 (1949); (b) T. Fabian, M. Legrand, and P. Poirier, *Bull. soc. chim. France*, 1499 (1956).

(18) T. Miyazawa, *J. Mol. Spectroscopy*, **4**, 155 (1960).

at least in solution these substances exist as a mixture of approximately equal quantities.

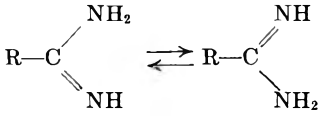

The substitution of a hydrogen atom of the amidine grouping by an electron donating substituent (for example ethyl) increases the negative charge of that particular nitrogen atom, which in turn exhibits a more pronounced tendency to attract the proton and the equilibrium should displace as

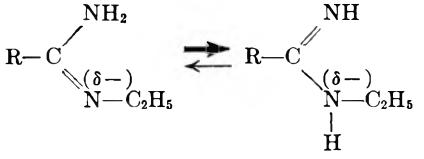

as in fact it does.

In the case of an aromatic substitution (for example, phenyl) the formation of the charge on the nitrogen atom under consideration is a result of two factors. First, the introduction of an aromatic residue is accompanied by a displacement of charges toward the nucleus because of its electronegativity, second we have to consider also the resonance effects of the lone pair electrons of nitrogen with the π-electron system of the aromatic ring as

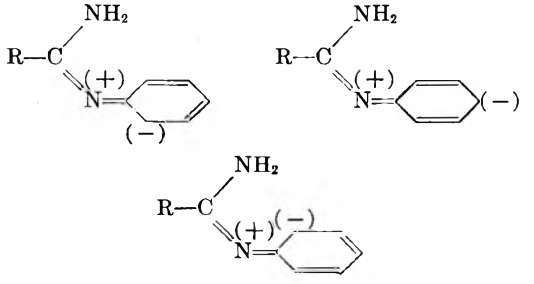

The resulting accumulation of positive charge on the nitrogen atom attached to the aromatic residue should decrease the basic character of this atom and we expect the equilibrium to be displaced in favor of the form I, which has been confirmed by our experimental work.

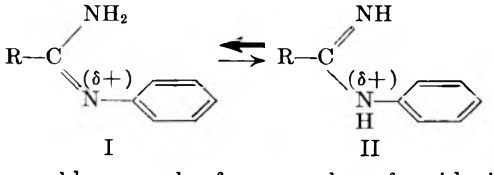

I II

We could prove also for a number of amidoximes whose structure has (with a few exceptions) not been known previously[19] that they all exist in the form III, which again is in agreement with the considerations presented above.

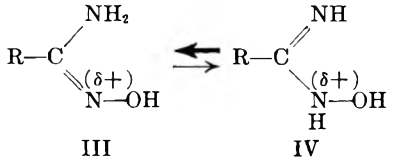

III IV

(19) J. Barrans, R. Mathis-Noel, and F. Mathis, *Compt. rend.*, **245**, 19 (1957).

With amidoximes and N-phenyl monosubstituted amidines, the infrared spectra were interpreted to mean that the equilibrium is shifted to such an extent that the less stable form cannot be detected in the spectrum. With N-alkyl derivatives we were able to observe both forms, although the configuration V

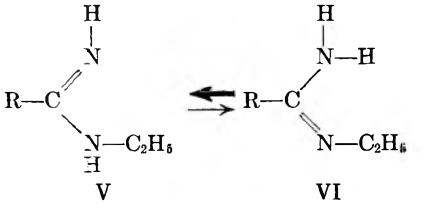

V VI

was much more abundant in the mixture at which the observations were made (condensed phase or solution in $CHCl_3$ at room temperature). This gave us valuable information about the frequencies of the characteristic bands of both tautomeric forms.

The tautomeric equilibrium in N-monosubstituted amidines is displaced therefore in proportion to the electronegativity of the substituents on the nitrogen atoms. The radical to which the amidine group is attached has a negligible effect on the position of the equilibrium.

N,N'-Disubstituted amidines can be prepared in two ways[20,21] and the reaction generally results

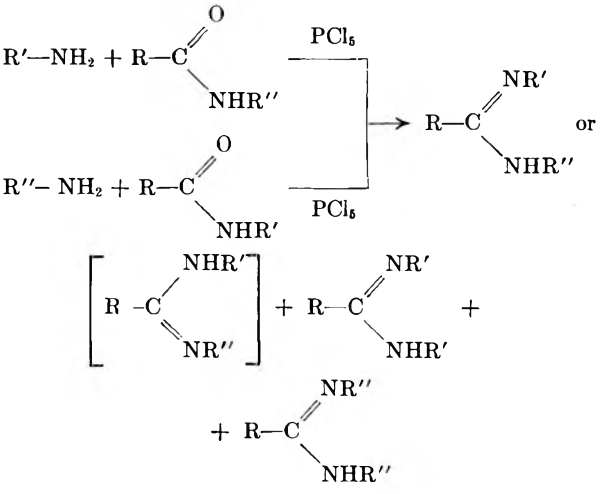

in a mixture of three derivatives, but the asymmetrical disubstituted amidine (the most abundant in the mixture) is always the same regardless which way is used for the preparation.

The spectra of N,N'-disubstituted amidines show in dilute solutions in the 3 μ region two bands near 3450 and 3380 cm.$^{-1}$ associated with NH stretching vibrations. The strong absorption band in the 6 μ region due to the ν(C=N) mode is apparently a doublet too, since it shows a well defined shoulder on the low frequency side. The relative intensities of these bands do not depend on the concentration, so that we eliminate the possibility that the lower frequency band is due to an associated form.

(20) G. Tsatsas, R. Delaby, A. Quevauvillier, R. Damiens, and O. Blanpin, *Ann. pharm. franç.*, **14**, 607 (1956).

(21) G. Tsatsas and R. Delaby, *ibid.*, **14**, 621 (1956).

It therefore is evident that we have either two forms of monomer or a single form giving rise to two bands in this region.[12] Consequently we have to discuss the following possibilities:

1. Geometrical isomerism with respect to the double bond

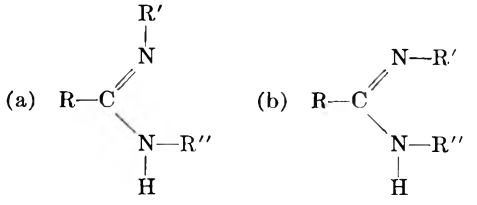

The occurrence of the form (b) is in our case quite unlikely because of the steric factors involved with the substituted aromatic rings or naphthyl groups used in this study.

2. Rotational isomerism with respect to the single C–N bond, which has considerable double bond character

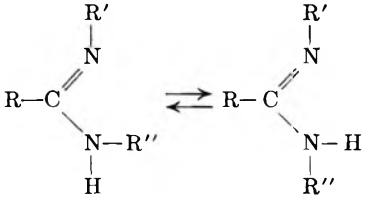

3. The possibility of tautomerism

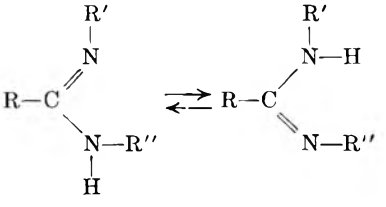

which was rejected previously because the two bands have been observed with amidines having the same substituents on both nitrogen atoms. Before the nature of the amide II band had been fully understood it had been assumed that the configuration of N,N'-disubstituted amidines is probably such as represented below.[5]

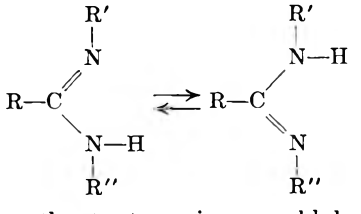

In this case the tautomerism would lead to two identical configurations provided R' = R''.

Since it has been established that in amides only the *trans* configuration gives rise to the amide II band and we have strong evidence that this interpretation can be extended also to amidines, we believe that the possibility of tautomerism has to be reconsidered.

The spectrum of a mixture of tautomeric forms as represented above (3) should be very similar to the spectrum of a mixture of rotational isomers (2). However the migration of the proton in (3) not only leads to a change of the *trans*-CNNH group into a *cis*-CNNH group as in rotational isomers

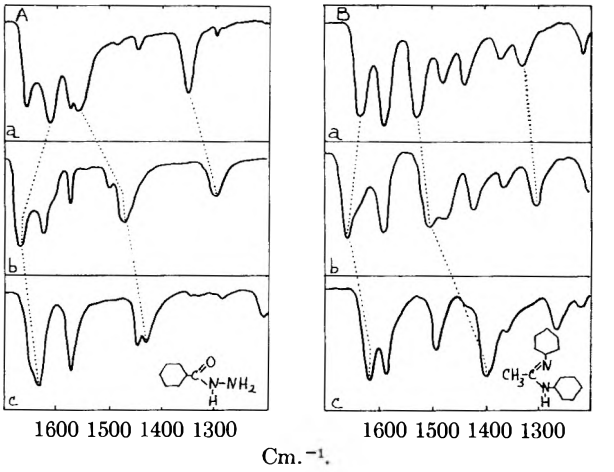

Fig. 2.—Infrared spectra of (A) benzhydrazide and (B) N,N'-diphenylacetamidine with the frequency shifts of amide I, II, III and amidine I, II, III bands: (a) solid; (b) solution in $CHCl_3$; (c) deuterium compound solid.

but changes also the *trans*- 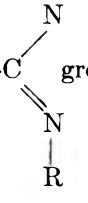 group into a *cis*-

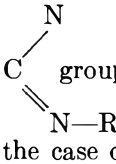 group. Consequently one can expect that in the case of tautomers the differences in ν(C=N) frequency might be larger than in the case of rotational isomers.

4. It also is possible that one of the bands in the 3 μ region is due to an overtone of the fundamental C=N stretching vibration near 6 μ. This is very improbable since it would imply a substantial anharmonicity for the vibration and of the opposite sign than usually is found. The frequency of the stretching C=N vibration is near 1650 cm.$^{-1}$. The frequencies of the bands in the 3 μ region are at 3450 and 3380 cm.$^{-1}$. In either case the anharmonicity factor would have to be negative.

If Fermi resonance were occurring between the first overtone of the C=N stretching and N–H stretching vibrations this anharmonicity might have to be even more negative. Most probably we have to chose between rotational isomerism or tautomerism.

The presence of two ν(N–H) and two ν(C=N) bands in solution has been attributed to rotational isomerism.[12,17a,22] Such rotational isomerism has been observed also with secondary amides by Russell and Thompson.[23] However, they report smaller differences in frequencies for two ν(N–H) bands ($\sim$ 30 cm.$^{-1}$) than we measured with amidines ($\sim$70 cm.$^{-1}$). Since no noticeable asymmetry of the ν(C=O) band has been reported as yet, one could infer that rotation around the C–N

(22) D. N. Shigorin and Y. K. Syrkin, *Izvest. Akad. Nauk, S.S.S.R. Ser. Fiz.*, **9**, 225 (1945).

(23) R. A. Russell and H. W. Thompson, *Spectrochim. Acta*, **8**, 138 (1956).

bond in amides is accompanied by smaller shifts of the carbonyl frequency then we found for the two ν(C=N) bands with N,N′-disubstituted amidines (30–40 cm.$^{-1}$), which is somewhat unexpected.

Besides larger frequency differences for the two ν(N–H) and ν(C=N) absorption bands as compared with the data obtained with amides, we noticed also that the proportion of the *cis* form as estimated by the relative intensities of the two ν-(N–H) bands is greatest with symmetrical derivatives and decreases if one of the substituents is replaced either by a more or a less electronegative one.

In particular this last observation suggests that the interpretation of the appearance of the two ν-(N–H) bands by rotational isomerism is not necessarily correct. There is no satisfactory explanation as to why any change in the polar character of the substituents should result in a shift of the equilibrium in the favor of the *trans* form (confirmed also by intensity changes in the amidine II band). No such effect has been observed for amides, where the shifts in equilibrium have been successfully attributed to steric effects.[24] On the other hand the displacement of the equilibrium can be explained easily assuming tautomerism and that the low frequency ν(N–H) band (~3370 cm.$^{-1}$) is associated with the less stable tautomeric form.

To clarify this question, a series of N,N′-disubstituted amidines has been prepared (following the method of Tsatsas, *et al.*,[11,12]) such that the differences in the relative electronegativities of the substituents increased gradually. According to the reaction scheme both asymmetrically disubstituted forms would be expected, however, these workers isolated only one form in the solid phase.

According to what we found with N-monosubstituted amidines, where the position of the equilibrium has been determined easily by infrared spectra, an increased positive charge induced on the nitrogen atom (attached to the chlorinated

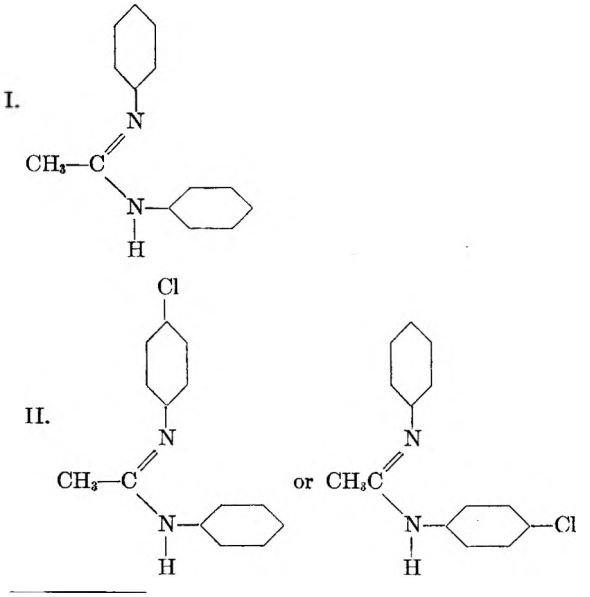

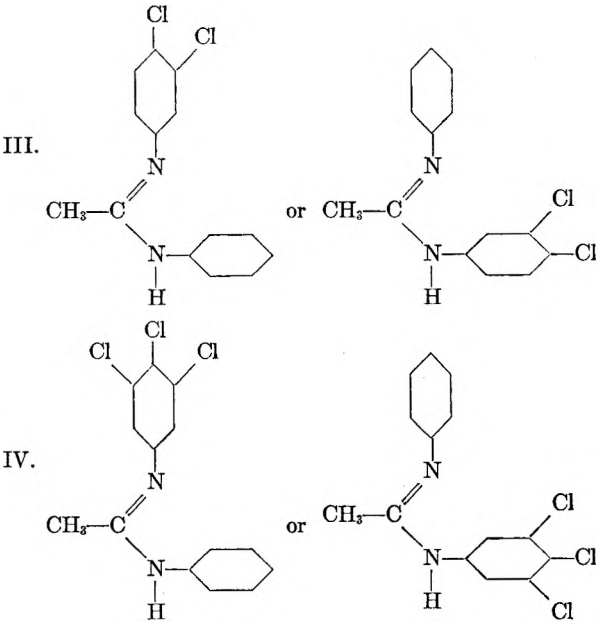

phenyl radical) by increased chlorination should result at least in solution in a gradual shift of the equilibrium in favor of form A.

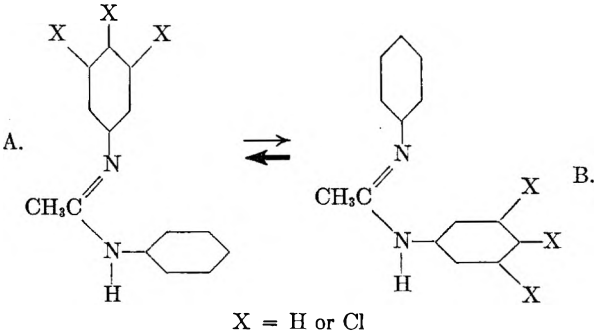

X = H or Cl

This supposition not only finds support in the observed displacement of the equilibrium in solution, but also in frequency shifts observed for the two ν(N–H) bands. The band at 3448 cm.$^{-1}$ associated with the *trans* configuration is practically unaffected by the introduction of the chlorine atoms, while the band at 3370 cm.$^{-1}$ exhibits displacements toward lower frequencies as the number of exchanged hydrogen atoms increases.

Therefore we concluded that N,N′-disubstituted amidines very probably exhibit in solution a tautomerism leading at the same time to a geometrical isomerism, with respect to both single and double CN bonds, which explains also the appearance of the two ν(N–H) and ν(C=N) bands for derivatives with identical substituents. The inability to isolate the two tautomeric forms therefore can be considered as a consequence of the shift of the equilibrium in favor of the more stable form accompanying the transition from solution into the crystalline phase.

The presence of two ν(N–H) and two ν(C=N) bands in the spectra of N,N′-disubstituted amidines (having identical substituents on the nitrogen atoms) has been used by previous workers to conclude that tautomers in this series of compounds do

(24) I. Suzuki, M. Tsuboi, T. Shimanouchi, and S. Mizushima, *Spectrochem. Acta*, **16**, 471 (1960).

not exist. This error was due to the fact that their argument failed to take into account the possibility of the existence of the *trans* configuration. This work has shown that the *trans* configuration is always more stable (at least in the series of investigated compounds) and the only one giving rise to the amidine II band.

By analogy with the spectra of monosubstituted amides having a *cis* CONH group, one can expect the C–N stretching and N–H bending frequencies associated with the vibrations of the *cis* CNNH group to occur near 1450 and 1350 cm.$^{-1}$.[18]

We were, however, unable to locate these bands. This probably is due to the fact that the amount of *cis* form was in our case always smaller than the amount of *trans* form. In addition to that these frequencies fall in the region of CH_3 and CH_2 deformation vibrations and it is quite possible that δ(NH) and ν(CN) modes associated with the *cis* form are overlapped by other stronger bands in this region.

Electronic Structure of Amidines

Infrared spectra of mono- and di-substituted amidines indicate an electronic configuration similar to that of amides, for which the importance of the ionic form has been stressed. In the valence bond representation this can be formulated as

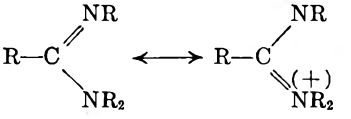

The partially ionic character manifests in a shortening of the carbon–nitrogen single bond length and higher C–N frequencies.

Another important consequence of the partially ionic character of the valence bond structure is the quadrivalent nature of the amine nitrogen atom leading to an approximate over-all planarity of the amidine grouping.

A particularly sensitive criterion of the hybridization of the nitrogen atom is afforded by a comparison of the stretching and bending frequencies of the $-NH_2$ grouping[8] in amidoximes and N-phenyl monosubstituted amidines with the corresponding frequencies in methylamine, aniline, and formamide; the nitrogen atom in methylamine and aniline being approximately sp^3 hybridized, while in formamide it is close to being sp^2 hybridized as established by microwave spectra.

TABLE III

FREQUENCIES AND HYBRIDIZATION OF $-NH_2$ GROUPING

	$\nu_{as}(NH_2)$	$\nu_s(NH_2)$	$\delta(NH_2)$	Hybridization
$H_2N—CH_3$	3427	3361	1625	sp^3 (25)
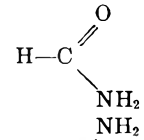	3545	3450	1572	sp^2 (26)
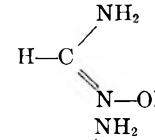	3525	3410	1572	sp^2 (27)
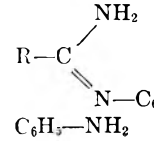	3500	3410	1585	sp^2
$C_6H_5—NH_2$	3440	3360	1618	sp^3 (28)

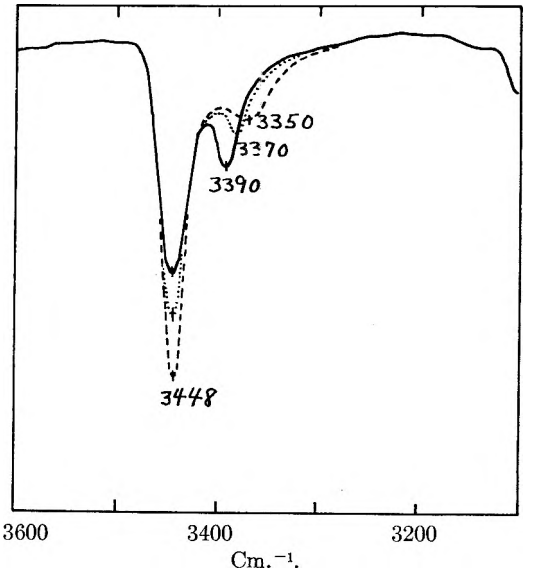

Fig. 3.—Infrared spectra of N,N'-diphenylacetamidine ———, N-phenyl-N'-*p*-chlorophenylacetamidine . . . . . , and N-phenyl-N',3,4,5,-trichlorophenylacetamidine– – –, in $CHCl_3$ solution.

When the nitrogen atom is in the sp^2 hybridized state it combines with adjacent atoms in an all planar configuration and the lowest energy bonding orbitals consist of: (a) three σ type molecular orbitals visualized as being formed from sp^2 hybrid atomic orbitals of nitrogen and suitable orbitals of adjacent atoms; (b) a π bonding molecular orbital arising from the pure p atomic orbitals on the nitrogen and neighboring atoms; (c) a π^* non-bonding molecular orbital formed from p atomic orbitals on nitrogen and neighboring atoms.[29]

The lone pair electrons originally with the configuration $N(2s)^2$ are in this case in a pure p orbital and form π and π^* type bonding and non-bonding molecular orbitals mentioned above.

The quadrivalent valence state of the nitrogen atom can be visualized as

$$N[(1s)^2(2sp^2)^2(2p_z)^2]$$

The low frequency 3315 cm.$^{-1}$ for the ν(=N–H) stretching vibration of the imino grouping as found with N-ethyl monosubstituted amidines suggests a larger atomic radius of the imino than amino nitrogen.

Coulson[30] has shown that the length of a carbon *n* hydrogen bond depends on the state of hybridization of the carbon atom The more s character is possessed by the carbon atomic orbitals, the shorter will be its radius and the greater will be the value of the C–H stretching force constant. This view has been extended to the nitrogen atom by

(25) A. P. Gray and R. C. Lord, *J. Chem. Phys.*, **26**, 690 (1957).
(26) J. Ewans, *ibid.*, **22**, 1228 (1954).
(27) W. J. Orville-Thomas and A. E. Parsons, *Trans. Faraday Soc.*, **54**, 460 (1958).
(28) J. C. Ewans, *Spectrochim. Acta*, **16**, 428 (1960).
(29) W. J. Orville-Thomas, *Chem. Revs.*, **57**, 1179 (1957).
(30) C. A. Coulson, "Victor Henry Memorial Volume," Desoer, Liége (1948).

TABLE IV

FREQUENCIES AND OTHER PARAMETERS OF H—N=X GROUPING

	H—N=C=O[25]	H—N—C=S[25]	H—N=N=N[25]	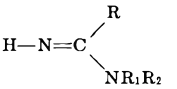
ν(N–H), cm.$^{-1}$	3531	3536	3335	3315
f(N–H), dyn./cm.	6.9×10^5	7.0×10^5	6.2×10^5	6.0×10^5
α H—N=X	128° 5′	130° 32′	112° 39′	112° (est.)
r (N–H), Å.	0.987	1.013	1.021	1.02 (est.)

Orville-Thomas[29] and strengthened by experimental data. An increase in the force constant of a pure N–H therefore can be taken as an indication of a change in the hybridization at the nitrogen atom leading to orbitals containing more s character.

By comparing the ν(N–H) frequencies of the imino grouping in N-ethyl monosubstituted amidines with those found with isocyanic, isothiocyanic, and hydrazoic acids,[31] for which the H—N=X angles are known and vary between 112–130°, one might expect the corresponding angle on the imino nitrogen in N-ethylamidines is of the same range or smaller than that found in hydrazoic acid (112°) and the N–H distance greater than 1.02 Å.

This nitrogen is therefore three-valent and its valence state consists of two σ type molecular orbitals N(2p + δ2s) forming σ bonds with the carbon and hydrogen atoms, the lone pair electrons are in the hybrid N(2s + δ2p) orbital forming an atomic dipole, and there is a $2p_z$ orbital remaining to form a π type delocalized bonding.

$$N[(1s)^2(2s + \delta 2p)^2(2p + \delta_1 2s)(2p + \delta_2 2s)(2p_z)]$$

The carbon atom is hybridized in its sp^2 state with three planar bonding orbitals—with interbond angle close to 120°, the fourth orbital is a p orbital at right angle to the sp^2 hybrid forming the π type molecular orbital

$$C[(1s)^2(2sp^2)^3(2p_z)]$$

Although the relationship between C–N frequencies and C–N bond character has been studied extensively, it is difficult to obtain even an approximative picture of the C–N bond length in amidines from their infrared spectra. There is no normal vibration which could be assigned to the C–N stretching mode alone. In N-ethyl monosubstituted and N,N′-disubstituted amidines we found a similar type of normal vibrations as discussed with monosubstituted amides.[13,15] We have much less information about the nature of normal vibrations in amidoximes and N-phenyl monosubstituted amidines, where the ν(C=N) and ν(C–N) bands can be considered as well as the symmetrical and asymmetrical stretching frequencies of the 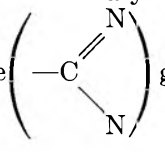 grouping. The best values for a hypothetical C–N stretching frequency we can probably obtain from the frequency of the amidine II′ band in deuterated compounds, for which at least the contribution of the ND bending mode is eliminated almost completely.[15]

In Table V the frequencies of the amidine II′ band in some amidines are listed.

TABLE V

FREQUENCIES OF THE AMIDINE II′ BAND

General formula 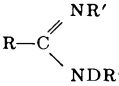 R	R′	R″	Amidine II′ frequency ν(C–N) cm.$^{-1}$
$-CH_3$	$-C_6H_5$	$-C_6H_5$	1406
$-CH_3$	$-C_6H_4$-*p*-Cl	$-C_6H_5$	1408
$-CH_3$	$-C_6H_5$	$-C_6H_4$-*p*-$OCH(CH_3)_2$	1398
$-CH_3$	$-C_6H_4$-*o*-$OCH(CH_3)_2$	$-C_6H_4$-*p*-$OCH(CH_3)_2$	1396
$-CH_3$	$-\beta$-$C_{10}H_7$	$-C_6H_4$-*p*-$OCH(CH_3)_2$	1404
$-CH_3$	$-\beta$-$C_{10}H_7$	$-\beta$-$C_{10}H_7$	1400
$-C_6H_5$	-D	$-CH_3$	1400

Taking into account that the C=N group in oximes absorbs near 1680 cm.$^{-1}$,[1,32] and that the C–N stretching frequency in methylamine[25] has been found at 1044 cm.$^{-1}$, we can assume that the C–N bond in the investigated amidines possesses considerable double bond character.

Using Lüttke's correlation[33] for the C–N bond length and C–N stretching frequencies, the observed frequency at 1400 cm.$^{-1}$ would correspond approximately to a C–N bond length of 1.36 Å. This value is in reasonable agreement with the value reported by Hall and Llewellyn[6] (1.33 Å.).

Acknowledgments.—The author wishes to express his sincere thanks to Dr. J. Lecomte for his interest and helpful discussions, and to Professors G. Tsatsas and P. Reynaud, who furnished many of the substances studied. The indebtedness of the author to the late Professors R. Delaby and R. Damiens, who suggested this work, is gratefully acknowledged.

(31) W. J. Orville-Thomas, *Trans. Faraday Soc.*, **49**, 855 (1953).

(32) L. J. Bellamy, "Infrared Spectra of Complex Molecules," Methuen, London, 2nd Ed., 1958, p. 268.

(33) W. Lüttke, "Habilitationsschrift," Freiburg, 1956; and *Chem. Revs.*, **57**, 1183 (1957).

RADIATION CHEMISTRY OF IONIC SOLIDS. II. FREE RADICALS DETECTED IN IRRADIATED POTASSIUM NITRATE BY ELECTRON PARAMAGNETIC RESONANCE[1]

BY JOSEPH CUNNINGHAM*

Argonne National Laboratory, Argonne, Illinois

Received May 22, 1961

Crystals of $K^{14}NO_3$ and $K^{15}NO_3$ have been irradiated and studied at 4 and 77°K. Six distinct species were indicated by the electron paramagnetic resonance (e.p.r.) spectra. Tentative identification of individual e.p.r. patterns with radical species in fixed orientations is attempted. The magnetic parameters of patterns assigned to $(NO_2^-)^-$, NO_2, $(NO_3^-)^-$, NO_3, NO, and O_2^- radicals are shown to be not inconsistent with previous results and with orbital representation. Results are described on optical removal of the e.p.r. signals. The relationship of radical formation and orientation to the radiation chemistry of nitrates is considered.

I. Introduction

The decomposition of crystalline nitrates under ionizing radiation can be represented by $NO_3^- \rightsquigarrow NO_2^- + {}^1/_2O_2$. In crystals with absorbed dose greater than $\sim 10^{21}$ e.v. g.$^{-1}$ nitrite ions have been detected by their infrared[2] and ultraviolet[3] absorption. Molecular oxygen in quantity equivalent to the nitrite has been shown to exist occluded in the crystals after irradiation at *ca.* 320°K.[4] The primary radiation-induced process, which results in the build-up of nitrite and oxygen, has been represented in the first paper of this series as the dissociation of excited nitrate ions.[5] $G_{NO_2^-}$ for concentrated aqueous solutions of nitrate,[6] or for the molten salts,[5] were independent of the fraction of energy initially absorbed by the cations. The latter result suggests that ionization electrons from the cations contribute to dissociation of nitrate ions. Electron paramagnetic resonance (e.p.r.) studies on nitrate crystals were undertaken to provide information on such electronic processes. Previous[7,8] studies of the e.p.r. spectra of nitrate crystals were made principally at room temperature. Observed signals were attributed to NO_2 radicals. Possible effects of radiation on nitrates may be represented schematically by

Ionization and excitation, $NO_3^- \rightsquigarrow NO_3$, NO_3^{-*}, K^{++}

Primary dissociation events:

$$NO_3 \longrightarrow NO_2 + O \quad (1a)$$
$$NO_3 \longrightarrow NO + O_2 \quad (1b)$$
$$NO_3^{-*} \longrightarrow NO_2^- + O \quad (2a)$$
$$NO_3^{-*} \longrightarrow NO_2 + O^- \quad (2b)$$
$$NO_3^{-*} \longrightarrow NO + O_2^- \quad (2c)$$

Electron capture $\longrightarrow (NO_3^-)^-$, K^0, $(NO_2^-)^-$

Magnetic parameters have been reported for NO_2 in the gas phase[9] and frozen in an argon matrix,[10] and for NO, $(NO_2^-)^-$, and $(NO_3^-)^-$ observed in KCl/KNO_3 crystals.[11,11a] The present work attempts to correlate signals observed in irradiated nitrate crystals with previously identified radicals. Because the number of probable radical species is smaller in radiation-resistant nitrite crystals, the e.p.r. spectra of irradiated $NaNO_2$ were studied for comparison with nitrate results.

II. Experimental

Reagents.—Materials used were reagent grade KNO_3, and $K^{15}NO_3$ enriched to 99.6% in ^{15}N. Nitrates were twice recrystallized and crystals grown by slow evaporation from aqueous solution. Crystallographic axes were located by X-ray diffraction or from crystal habit[12] or growth characteristics.[13] Crystals were γ-irradiated at dose rates of 10^{18} e.v. g.$^{-1}$ min.$^{-1}$, under either vacuum or low pressure of helium. Samples irradiated at 77°K. were transferred under liquid N_2 to unirradiated holders. Since such transfer was not feasible at 4°K., crystals were wedged into the desired position in high purity silica holders and thus irradiated and studied on an X-band spectrometer which displayed the second derivative of the absorption. Crystals could be rotated around a vertical axis, termed here the rotation axis, R. R was perpendicular to the applied magnetic field, H. Crystals were rigidly mounted either with the crystallographic c-axis parallel to R, (C$\parallel$R), or perpendicular to R, (C$\perp$R).

III. Results

E.p.r. spectra of a $K^{14}NO_3$ crystal after γ-irradiation of *ca.* 1.8×10^{19} e.v. g.$^{-1}$ at 77°K. are shown in Fig. 1. Spectra were taken at 5° intervals with the crystal c-axis parallel to the rotation axis, R, and perpendicular to the static magnetic field, H. The symmetry of KNO_3 is orthorhombic, its space group being V_h^{16}-Pbnm. Therefore, if radicals produced by irradiation were oriented according to the lattice symmetry, the sequence of e.p.r. spectra should show two mirror planes, m_1 and m_2. Figure 1 illustrates the symmetry around m_1. It was less clearly observed around m_2.

The spectral features of Fig. 1 are: (a) the central complex pattern with incompletely resolved structure showing the symmetry of the lattice; (b) two similar lines of spacing 64 ± 2 gauss observed to be

* Armour Research Foundation, Chicago 16, Illinois.

(1) Based on work performed under the auspices of the U. S. Atomic Energy Commission.

(2) J. Cunningham and H. G. Heal, *Trans. Faraday Soc.*, **56**, 1355 (1958).

(3) P. Pringsheim, *J. Chem. Phys.*, **23**, 369 (1955).

(4) G. Hennig, R. Lees, and M. Matheson, *ibid.*, **21**, 664 (1953).

(5) J. Cunningham, *J. Phys. Chem.*, **65**, 628 (1961).

(6) H. A. Mahlman and G. K. Schweitzer, *J. Inorg. & Nuclear Chem.*, **5**, 213 (1958).

(7) W. B. Ard, *J. Chem. Phys.*, **23**, 1967 (1955).

(8) B. Bleaney, W. Hayes, and P. M. Llewellyn, *Nature*, **179**, 140 (1957).

(9) J. G. Castle and R. Beringer, *Phys. Rev.*, **80**, 114 (1950).

(10) C. K. Jen, S. N. Foner, E. L. Cochran, and V. A. Bowers, *ibid.*, **112**, 1169 (1958).

(11) C. Jaccard, *Phys. Rev.*, **124**, 60 (1961).

(11a) NOTE ADDED IN PROOF.—The symbol $(NO_2^-)^-$ or $(NO_3^-)^-$ was used to preserve the possibility that an additional electron might be associated with NO_2^- or NO_3^- through trapping at defect sites involving these ions. It becomes clear in the discussion that in fact the additional electron moves in orbitals of the species $NO_2^=$ or $NO_3^=$.

(12) R. W. G. Wyckoff "Crystal Structures," Interscience Publishers, New York, N. Y., 1957.

(13) J. D. Dana, "System of Mineralogy," 7th Ed., Vol. II, John Wiley and Sons, New York, N. Y., 1944.

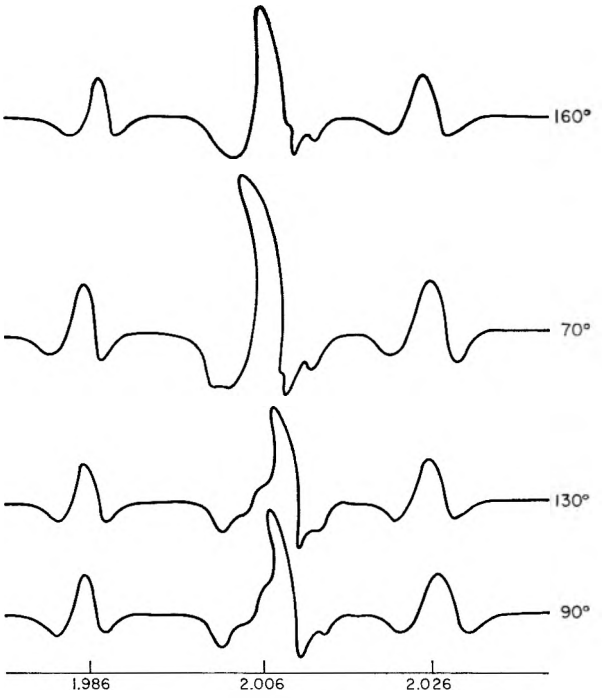

Fig. 1.—E.p.r. spectra of $K^{14}NO_3$ crystal γ-irradiated at 77°K. to 2×10^{18} e.v. g.$^{-1}$. Crystal c-axis $\parallel$ rotation axis and $\perp H$. Mirror plane m_I occurred at 112 ± 3°. Pairs of spectra (160 and 70°) or (90 and 130°) are identical because taken at *ca.* equal angles from m_I.

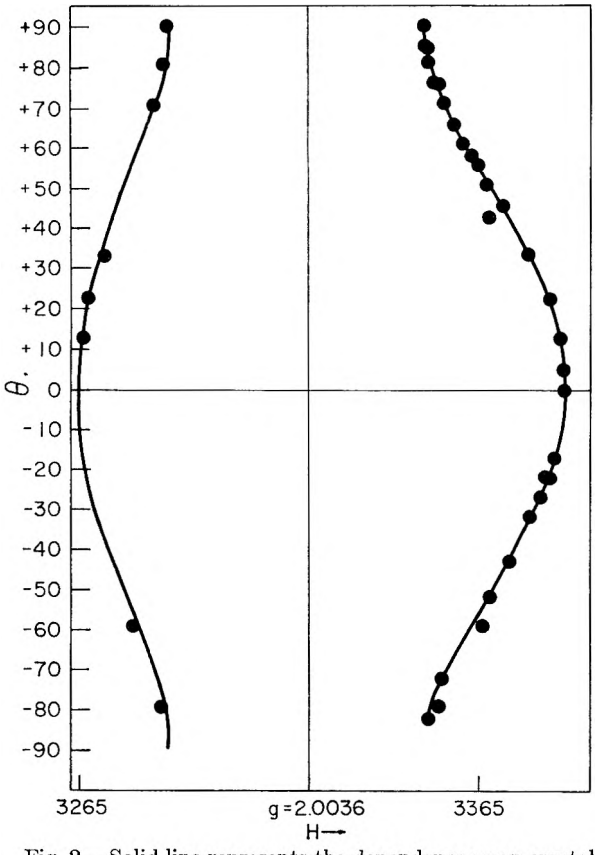

Fig. 2.—Solid line represents the dependence upon crystal orientation calculated for the energy levels of the symmetric radical of Table I using eq. 1. Points represent the observed positions of the high and low field members of the triplet identified with $(NO_2^-)^-$.

isotropic with $g = 2.006 \pm 0.001$. For $K^{15}NO_3$, similarly mounted and irradiated, lines of comparable intensity and spacing 45 ± 2 gauss were observed. These results are consistently accounted for by a triplet or doublet arising, respectively, from hyperfine interaction with $^{14}N(I = 1)$ or ^{15}N $(I = 1/2)$ nuclei. The ratio of the splittings is equal to the ratio of the magnetic moments of the isotopic nitrogen nuclei.

With the crystal c-axis perpendicular to the rotation axis and in the plane of the magnetic field, (C⊥R), maximum and minimum total hyperfine splitting (HFS) of 122 and 64 gauss were observed for $K^{14}NO_3$ with associated g values of 2.002 and 2.006. These data, showing the absence of anisotropy in the C||R sequence and the existence of maximum and minimum values of both HFS and g in the C⊥R sequence, may be fitted to an axially symmetric spin Hamiltonian. The values of HFS and g-factor parallel to this axis of cylindrical symmetry are denoted by A and $g_{||}$. Those perpendicular to the axis are B and $g_\perp$. The dependence of the eigen values of the appropriate axially symmetric Hamiltonian, upon θ, the angle between the axis of cylindrical symmetry and the magnetic field H, may be described by

$$E_\pm = \pm 1/2\, H\,(g_{||}^2 \cos^2\theta + g_\perp^2 \sin^2\theta) \pm 1/2\, M_I\,[A^2\cos^2\theta + B^2\sin^2\theta]^{1/2} \quad \text{(I)}$$

With the experimental values for A, B, $g_{||}$, and $g_\perp$ shown in Table I, the dependence on θ calculated using eq. I is represented by solid lines in Fig. 2 on a gauss scale. (Since $g_{||} \approx g_\perp \approx 2$, separations in gauss equal $E/2\beta$.) The experimentally observed dependence of the HF lines on the angle between H and the crystallographic c-axis is in good agreement with this calculation. The axis of cylindrical symmetry of the spin Hamiltonian, and so of the orbital of the unpaired electron in the radical species, therefore is parallel to the crystallographic c-axis. Markedly similar values obtained by Jaccard also are listed in Table I. Jaccard observed in his crystals of KCl, to which nitrate had been added before irradiation, that the species in Table I was greatly reduced by hole capture. He therefore tentatively identified the species responsible as $(NO_3^-)^-$ to represent its electron-excess nature. An optical absorption band at 355 mμ has been observed after irradiation in KCl/NO_3^- crystals[14] similar to Jaccard's and in $NaNO_3$[3] and KNO_3[15] single crystals. The optical absorption has been assigned[14] to a nitrite ion with which another electron is associated, *i.e.*, $(NO_2^-)^-$.

This optical absorption band was observed[14] in KNO_3 crystals exposed to irradiation dosage at 77°K. equal to that which produced the e.p.r. signal of Table I. Exposure to light of wave length 320–520 mμ bleached both the optical band[15] and the e.p.r. signal (see Fig. 3d). Both Jaccard's observations and this bleaching effect are consistently accounted for by identifying the e.p.r. signal of Table I with $(NO_2^-)^-$ radicals.

Spectra at Increasing Dose.—The increase in intensity of the central and $(NO_2^-)^-$ signals was

(14) E. Hutchinson and P. Pringsheim, *J. Chem. Phys.*, **23**, 1113 (1955).

(15) J. Cunningham, unpublished work.

TABLE I

PRINCIPAL VALUES FOR A RADICAL SPECIES DETECTED IN KNO_3 AFTER SHORT γ-IRRADIATION

Salt	Temp., °K.	$g_\parallel$ (values ±0.001)	$g_\perp$	a	B (values ±2 gauss)	A	
$K^{14}NO_3$	77	2.002	2.006	±41.7 ± 1.0	±32	±61	
$K^{15}NO_3$	77	..	2.006	...	±22.5	..	This
$K^{14}NO_3$	4	2.002	2.006	±43.7 ± 1.7	±34	±63	work
$K^{15}NO_3$	4	2.002	2.006	±32 ± 1.3	±25	±46	
$KCl/^{14}NO_3^-$	77	2.0017	2.0068	±40.8	±30.5	±61.5	Jaccard

followed by comparing the signal strength to standard DPPH samples. Instrument power was maintained at a low level to minimize saturation effects. The signals reached maximum free radical concentration, S, at absorbed dose *ca.* 3×10^{20} e.v. g.$^{-1}$. S for the central signal was 4×10^{17} g.$^{-1}$. For each outer member of the $(NO_2^-)^-$ triplet, S reached 2×10^{17} g.$^{-1}$ and showed evidence of a slow decrease at doses $>3 \times 10^{20}$ e.v. g.$^{-1}$. As these signals approached saturation, others appeared (see Fig. 3). With C||R the new signals appeared as two lines which overlapped the $(NO_2^-)^-$ signals at some settings (Fig. 3c). Because of this overlap the measured minimum HFS of 75 ± 5 contained greater uncertainty than the observed maximum separation of 110 ± 2 gauss. Sequences of spectra, taken with the crystallographic *c*-axis perpendicular to R, showed that the greatest HFS, then observed for this new signal, occurred when the *c*-axis made an angle of 55° with the magnetic field. Two magnetic axes of this e.p.r. signal therefore must be non-coincident with the *c* and *a*, (or *b*), crystallographic axes. The exact relation between the magnetic axes of this signal and the crystallographic axes was not determined because (a) overlap between the members of this signal and those of $(NO_2^-)^-$ occurred over two considerable ranges of angular settings (*ca.* 20°) and greatly enhanced the difficulty of obtaining a reliable and detailed description of its orientation dependence, and (b) the results of studies on powdered KNO_3 distinguished clearly between this signal and $(NO_2^-)^-$ and provided evidence on the possible identity of the radical species.

In powdered $K^{14}NO_3$ after short irradiation *ca.* 10^{18} e.v. g.$^{-1}$, two broad signals of total separation 66 ± 3 gauss were observed. The theoretical[16] value predicted for the species with parameters in Table I was 64 gauss. In good agreement with the single crystal results, only the $(NO_2^-)^-$ triplet was observed after short irradiation. Irradiations $>3 \times 10^{20}$ e.v. g.$^{-1}$ produced another set of lines at greater spacing than the $(NO_2^-)^-$ powder pattern. The observed total splitting in $K^{14}NO_3$ and $K^{15}NO_3$ powders (Table II) are in the ratio expected for species with HFS resulting from interaction with the ^{14}N or ^{15}N nuclear magnetic moments.

This value derived from powdered KNO_3 compares favorably with a value of total splitting 115.6 gauss measured for NO_2 frozen in an argon matrix.[10] Zeldes and Livingston have made a detailed analysis[17] of a triplet observed in single crystals of

(16) S. M. Blinder, *J. Chem. Phys.*, **33**, 748 (1960).
(17) H. Zeldes and R. Livingston, *ibid.*, in press.

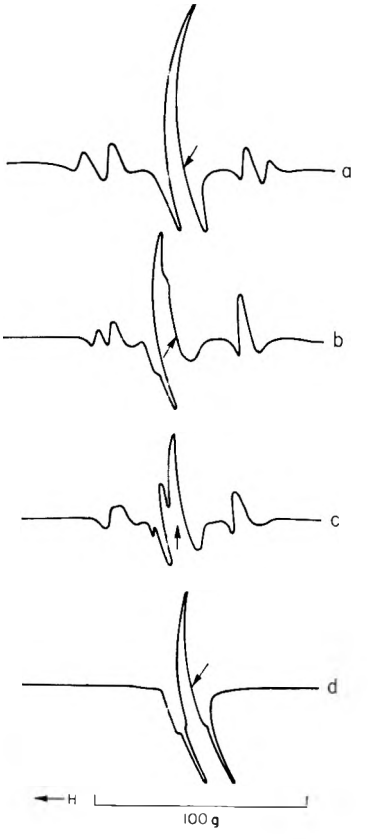

Fig. 3.—E.p.r. spectra of $K^{14}NO_3$ γ-irradiated at 77°K. to *ca.* 3×10^{20} e.v. g.$^{-1}$. Crystal *c*-axis ∥ R and ⊥H. Outer lines of (3a) are dependent on orientation and in (b) and (c) they move in on top of the isotropic $(NO_2^-)^-$ lines. (d) represents spectrum after bleaching by light of λ = 320–530 mμ. The arrow at the level of the base line indicates the position, on an arc, of g = 2.006.

TABLE II

EXPERIMENTAL VALUES MEASURED IN TWO CRYSTAL PLANES OF IRRADIATED KNO_3 FOR A SPECIES FORMED WITH ITS MAGNETIC AXES INCLINED TO THE CRYSTAL AXES

Salt	Crystal *c*-axis orientation		g_α	$g_{\alpha+90°}$	$A_{\alpha+90°}$
$K^{14}NO_3$	∥R	2.001	2.005	110 ± 2	75 ± 5
$K^{14}NO_3$	⊥R	2.005	2.008	118 ± 2	63 ± 2
			$g_{av.}$		$A_{av.}$
$K^{14}NO_3$	Powder		1.999		113
$K^{15}NO_3$	Powder		1.999		80
$^{14}NO_2$	In argon matrix		2.0037		115.6

NOTE: The setting α in the C⊥R sequence corresponded to 55° rotation from the position of C||H.

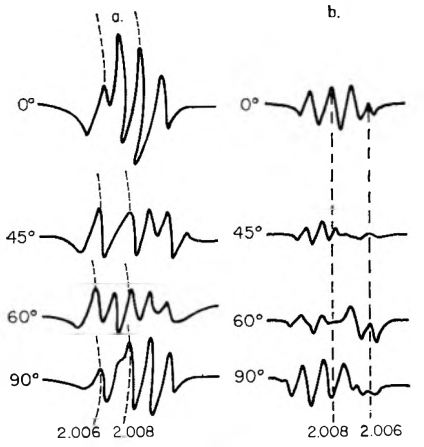

Fig. 4.—Orientation dependence of detail resolved on broad pattern centered at $g = 2.006$: (a) $K^{14}NO_3$ crystal after γ-irradiation at 77°K. C||R; (b) Same crystal after bleach with 320–530 mμ light.

$NaNO_2$ which they have identified as NO_2. The total separation for random orientation in powdered $NaNO_2$ calculated[18] from their values is 110 gauss. The averaged g-value should be 1.9994. These values again are in reasonable agreement with the value observed here in powdered KNO_3. These experimental observations favor the tentative identification of the signals, detailed in Table II, with NO_2 radicals. It is expected that NO_2 centers would be electron accepting to give stable nitrite ions. Figure 3 illustrates that removal of the $(NO_2^-)^-$ e.p.r. signal by electron release with 320–520 mμ light resulted also in the disappearance of the NO_2 triplet.

Pattern at *ca.* $g = 2.006$ in Crystals Irradiated at 77°K.—The partially resolved structure on the central line at *ca.* $g = 2.006$ had the symmetry of the lattice (Fig. 1) thus indicating radicals occupying fixed lattice positions. For $K^{14}NO_3$ with C||R, using high resolution, the structure shown in Fig. 4a was seen. This pattern was difficult to analyze because of contributions from the central members of $(^{14}NO_2^-)^-$ and $^{14}NO_2$ triplets. These triplets were bleached by 320–520 mμ light and the pattern shown in Fig. 4b resulted.

The principal feature of Fig. 4b is a triplet of invariant separation = 3.5 gauss between members. During rotation around the c-axis the center of this pattern moved reproducibly between a maximum of $g_a = 2.010$ and a minimum $g_b = 2.008$.

For crystals of $K^{15}NO_3$ the NO_2 or $(NO_2^-)^-$ radicals result in doubtlets with no central member to distort the central pattern. Without optical bleach a doublet of invariant total spacing 4 ± 0.5 gauss was distinguished. Its g-values were similar to those of the triplet in Fig. 4b, and the total splitting was reduced in the ratio of the nuclear magnetic moments of ^{15}N and ^{14}N.

The spectra of the central region (see Fig. 4a) contain a small underlying singlet signal at $g = 2.006 \pm 0.001$ which did not change position during rotation with C||R. Studies of the orientation dependence of the triplet signal for rotation with C⊥R were hampered by the overlap with the singlet signal and the central members of the

(18) H. Zeldes, private communication.

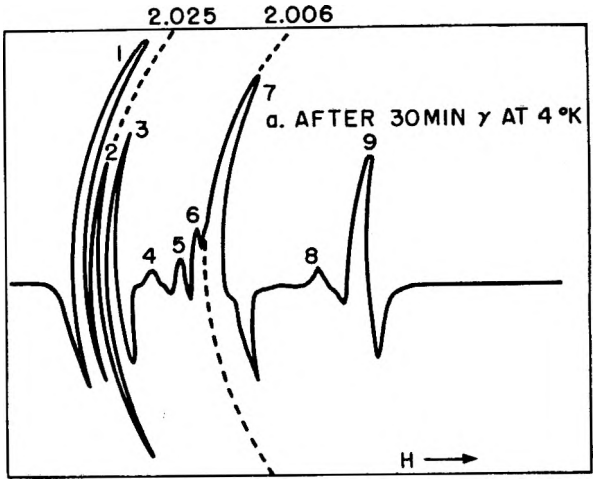

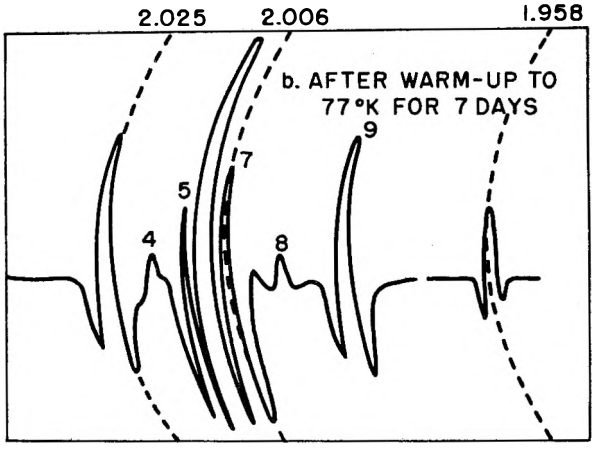

Fig. 5.—E.p.r. spectra recorded at 4°K. for $K^{14}NO_3$ irradiated at 4°K. Crystal c-axis ⊥H. The numbered peaks are tentatively assigned to radicals as follows. Peaks 1, 2, and 3 arise from $(NO_3^-)^-$ radicals with $g = 2.025$. They are distorted by overlap with the third member of the $(NO_2^-)^-$ triplet whose other members are peaks 7 and 9 in 5a. Peaks 4 and 8 in 5a arise from NO radicals with the molecular axis in the NO_3^- plane. (Compare Fig. 7a). Peaks 5 and 6 in Fig. 5a arise from one set of NO radicals with the molecular axis || c-axis and the third member is not resolved from peak 7. In Fig. 5b peaks 1, 2, and 3 have annealed out, peak 4 and 8 appear almost unchanged. Peaks 5 and 6 appear increased. The new peak at $g = 1.958$ is recorded at gain × 25 relative to the other parts and arises from O_2^-.

$^{14}NO_2$ and $(^{14}NO_2^-)^-$ triplets. The triplet showed a maximum total HFS of 63 ± 2 gauss centered at $g = 2.005$ with C||H. Within the experimental error of the measured values of g and HFS, the data may be fitted to an axially symmetric Hamiltonian, with $A = 32$, $B = 3.5$, $g_{\|} = 2.005$, and $g_{\perp} = 2.009$. It must be noted, however, that the difference between the g_a and g_b values was real and reproducible so that the g-factor of this species was not truly axially symmetric around the c-axis. Jaccard has evaluated principal values of g and A for a radical species which he observed in irradiated KCl/NO_3^- crystals at 260°K. His values are very similar (see Table IV) to those reported here. He has deduced good evidence for assigning these values to NO radicals fixed in interstitial positions and has identified the magnetic z-axis with the molecular axis of NO. Because of the strong

similarity to the values of Jaccard, and the evidence from isotopic substitution of ^{15}N that the radical contains bound nitrogen, the signals recorded at 77°K. (see Table IV) in KNO_3 are identified with NO radicals oriented with the molecular axis parallel to the crystallographic c-axis.

E.p.r. Spectra at 4° of Crystals Irradiated at 4°K.—Spectra of KNO_3 γ-irradiated to a dose of 3×10^{18} e.v. g.$^{-1}$ at 4°K. are shown in Fig. 5 for the c-axis parallel to the axis of rotation. A triplet with high intensity is evident at $g = 2.025$. It had not been observed in crystals irradiated at 77°K. The high field member of the $(^{14}NO_2^-)^-$ triplet is evident but the low field member overlaps and distorts the triplet at 2.025. Within the uncertainty introduced by this distortion the new triplet remained isotropic at $g = 2.025$ with C||R. With C⊥R the spectrum is represented in Fig. 6. The position of maximum splitting of the $(^{14}NO_2^-)^-$ triplet at C||H corresponded to minimum g (= 2.008) for the new triplet. Observed parameters for the triplet and a comparable doublet in $K^{15}NO_3$ are shown in Table III. The invariant total splittings of 9 ± 0.5 and 6 ± 0.5 observed in $K^{14}NO_3$ and $K^{15}NO_3$ could arise from a Hamiltonian with no anisotropic contribution to the HFS and isotropic splitting arising from contact fermi interaction with ^{14}N or ^{15}N nuclei. The marked anisotropy of the g-values excluded the possibility that the radicals were $^4S_{3/2}$ nitrogen atoms. Observations made on crystals of $NaNO_2$ irradiated and measured at 4°K. make it appear improbable that the triplet of Table III could arise from radicals of the general form $(NO_2)^{-n}$, where $n = 0, 2, 4$. These crystals of $NaNO_2$ did not show any triplet with parameters resembling those of Table II, after equal or longer irradiation. It therefore seems more probable that the triplet arises from an $(NO_3)^{-n}$ species where $n = 0$ or 2. It previously has been argued[5] that NO_3 radicals would not display HFS. For this reason, and others detailed below, the triplet of Table III is attributed to $(NO_3^-)^-$ radicals.

TABLE III

PRINCIPAL VALUES OF A RADICAL SPECIES DETECTED ONLY IN SAMPLES IRRADIATED AND MEASURED AT 4°K.

Salt	Orientation of crystal c-axis	$g_a = g_b$	g_c	$A_a = A_b = A_c$
$K^{14}NO_3$	‖R	2.025	...	±9 ± 0.5
$K^{14}NO_3$	⊥R	2.025	2.008	±9 ± 0.5
$K^{15}NO_3$	⊥R	2.025	2.008	±6 ± 0.5

Other signals than NO_2 and $(NO_3^-)^-$ are evident in Fig. 5a and 6 and are shown in greater detail in Fig. 7. The formation of NO radicals by decompositions such as (1b) and (2c) could occur with equal probability that any one of the equivalent N–O bonds in an $(NO_3)^{-n}$ species would remain unbroken. Therefore 3 sets of NO radicals mutually at 120° to each other would be predicted, if the NO were not free to move. Using the parameters measured for the one set of NO radicals observed at 77°K. (Table IV), the positions of the e.p.r. lines were predicted for 3 sets of NO radicals with the intermolecular axis of each set parallel to one of the original N–O bonds of NO_3^-.

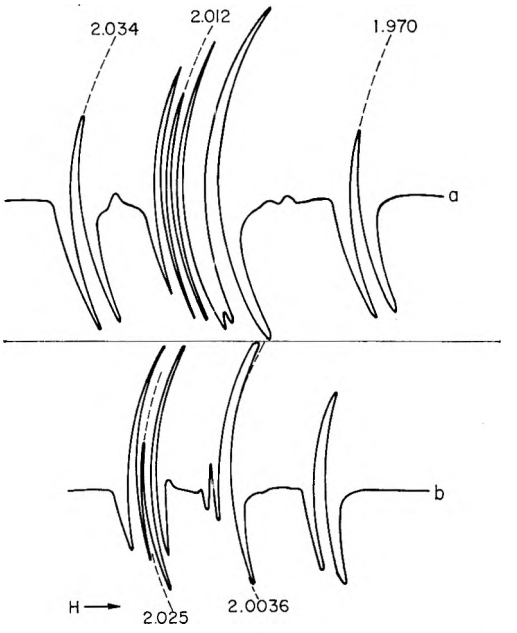

Fig. 6.—Spectra at 4°K. of $K^{14}NO_3$ irradiated at 4°K. Taken with C⊥R. (a). Spectra at intermediate setting (θ approx. 30°) showing the $(NO_3^-)^-$ triplet at $g = 2.012$ well separated from the $(NO_2^-)^-$ peaks. (b). Spectrum with C⊥H and $(NO_3^-)^-$ at $g = 2.025$ overlapping one $(NO_2^-)^-$ member.

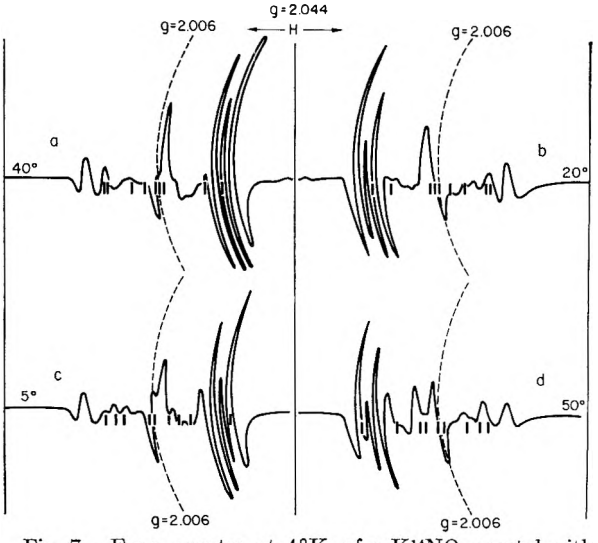

Fig. 7.—E.p.r. spectra at 4°K. of a $K^{14}NO_3$ crystal with C||R after irradiation at 4°K. Field shown increasing from central $g = 2.044$ line in all spectra. Angles correspond to those made with H by the molecular axis of one set of NO radicals. Small vertical lines indicate calculated positions of nine lines resulting from 3 sets of NO radicals.

The positions of the lines so calculated are compared in Fig. 7 with e.p.r. spectra taken with C||R. The fixed 0° position (not shown) corresponded to measurement with the axes of one N–O set parallel to H. It is seen that the majority of the small lines and their orientation dependence thus are well accounted for.

The principal unexplained feature of the 4°K. spectra with C||R is the signal of intensity intermediate between the $(NO_2^-)^-$ and $(NO_3^-)^-$ signals in Fig. 7, with g not varying significantly from 2.006. With C⊥R, the signal was observed to move be-

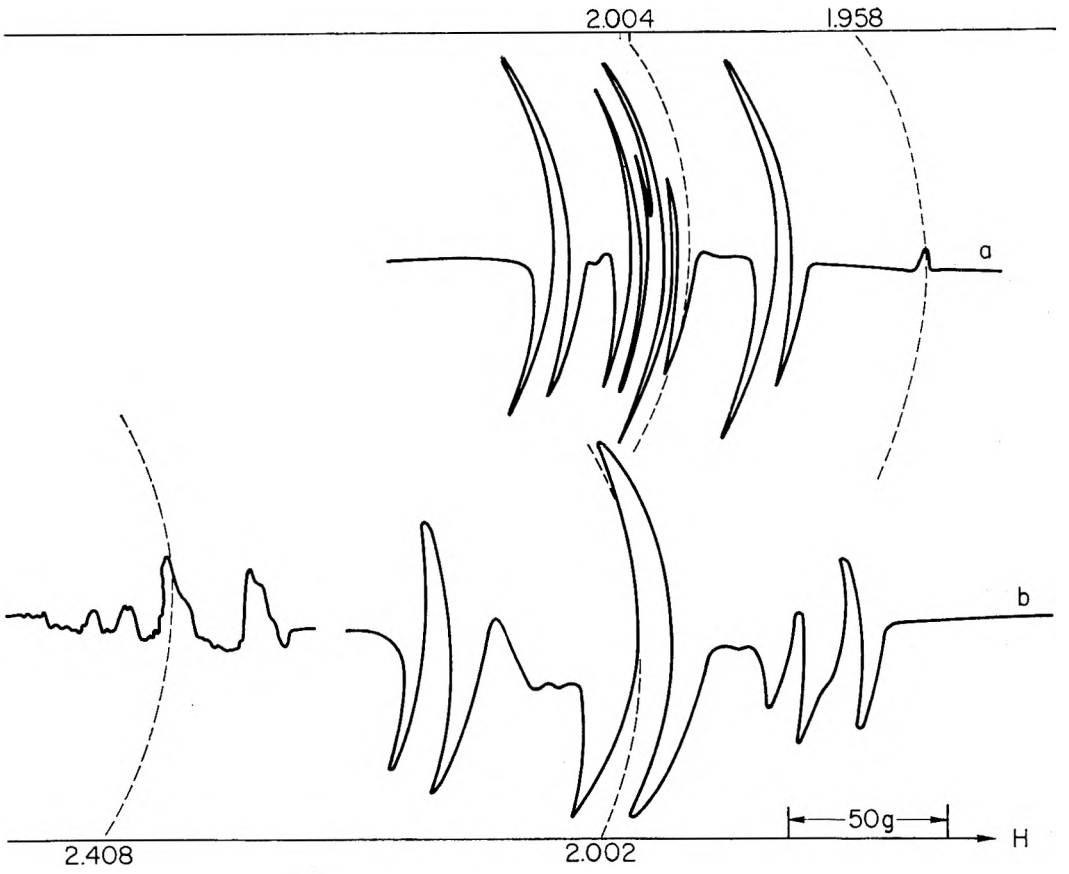

Fig. 8.—E.p.r. spectra recorded at 4° for $K^{14}NO_3$ crystals γ-irradiated at 77°K. to *ca.* 10^{21} e.v. g.$^{-1}$. (a) Crystal *c*-axis $\perp H$ showing single line at $g = 1.958$ recorded at equal gain to central pattern. (b) Crystal *c*-axis $\parallel H$ pattern at $g = 2.408$ was recorded at increased gain relative to central pattern.

tween $g = 2.006$ and $g = 2.001$ at 90° intervals. A radical with no measurable HFS and with cylindrical symmetry of its *g*-factor about the *c*-axis thus is indicated. Because an electron deficient species is required to provide electrons for $(NO_3^-)^-$ and $(NO_2^-)^-$, and because NO_3 is expected to show no HFS, it is speculated that this e.p.r. signal arises from NO_3.

Changes Produced in E.p.r. Spectra Taken at 4° by Warm-up to 77°K.—Figure 5 illustrates the disappearance of the $(NO_3^-)^-$ triplet after warming to 77°K. for 7 days a KNO_3 crystal irradiated at 4°K. Spectra recorded after only 2-hr. warm-up to 77°K. showed that the $(NO_3^-)^-$ triplet had decreased by a factor of 2. Both these crystals were oriented with C||R and, simultaneous with the decay of their $(NO_3^-)^-$ triplets, a single isotropic line appeared with $g = 1.958$ (Fig. 5). All attempts to locate a line at this position immediately after irradiation at 4°K. were unsuccessful. The radical species responsible for the single line at $g = 1.958$ apparently required temperatures of *ca.* 77°K. for its appearance. This conclusion was supported by the detection of the single line in KNO_3 crystals irradiated at 77° and measured at 4°K. For C||R the single line was observed clearly (Fig. 8a) at $g = 1.958$ at all settings. The e.p.r. signal for O_2^- ions in KCl crystals has been reported with a *g*-value along the intermolecular axis of 2.436 and values of 1.951 and 1.955 in the other orthogonal directions.[19] The observed *g*-values with C||R in KNO_3 were consistent with O_2^- ions aligned with their molecular axis parallel to the *c*-axis. The *g*-value then would be expected, by analogy with results in KCl, to vary from *ca.* 2.4 to 1.96 with the *c*-axis in the plane of rotation. Figure 8b shows that a pattern was observed at $g = 2.408$ when the *c*-axis was parallel to *H*. The splitting of the single line, which could result from hyperfine coupling to non-bonded potassium ($I = 3/2$) or nitrogen ($I = 1$) nuclei, was not investigated further. With small rotation away from the C||H position, the center of the pattern moved in agreement with the movement calculated for *g*-values of 2.408 and 1.958. The agreement with previous values for O_2^- is good evidence for identifying as O_2^- this radical species, which appeared only when the crystal temperature reached 77°K. during or after irradiation.

It is apparent in Fig. 5 that the pattern close to $g \approx 2.006$ was greatly altered by the warm-up treatment which removed the $(NO_3^-)^-$ peaks 1, 2, and 3. The changes can be accounted for by enhancement of the small triplet only partially resolved on the large central peak in Fig. 5a (peaks 5 and 6). One outer member of the triplet, peak 5, appears with greatly increased intensity in Fig. 5b. The other members overlap with the NO_3 singlet to give the greatly increased central peak 6 in Fig. 5b. Values estimated for the triplet are total HFS = 8 ± 2 gauss and $g \approx 2.008$. These are

(19) W. Kanzig and M. H. Cohen, *Phys. Rev. Letters*, **3**, 509 (1959).

TABLE IV

PRINCIPAL VALUES AND ORIENTATION OF NO RADICALS OBSERVED IN IRRADIATED $K^{14}NO_3$

Crystal c-axis	Temp., °K.	g_a	g_b	g_c	$A_a = A_b$	A_c	Orientation of molecular axis
‖R	77	2.008	2.010	..	3.5	..	‖C
⊥R	77		2.010	2.005	4.0	31	‖C
‖R	4						
3 sets			2.009	2.004	3.5	30	⊥C
⊥R	4						
3 sets		2.009		..	4.0	..	⊥C
1 set		..	2.010	2.003	4.0	32	‖C
		g_x	g_y	g_z	$A_x = A_y$	A_z	
KCl/NO_3	260	2.007	2.0097	2.0038	4.9	32.5	Jaccard

similar to the values in Table III for NO radicals with their molecular axis perpendicular to *H*. It especially is to be noted that the small peaks indicated by 4 and 8 in Fig. 5 were not increased significantly by the warm-up. Since these correspond to NO radicals with their molecular axis in the plane of the NO_3^- ions, the conclusion to be drawn is that warm-up preferentially increased the number of NO radicals oriented with their molecular axes parallel to the crystal *c*-axis. The results at 77°K. indicated that this latter set was of much greater intensity than those NO radicals with their molecular axes in the *c*-plane.

IV. Discussion

It is not presently possible *a priori* to calculate magnetic parameters for radical species in the crystalline field of KNO_3. The use of the e.p.r. values to support the tentative assignments made in the preceding section therefore is necessarily limited to considerations showing that the parameters and symmetry properties observed for the e.p.r. signals are not inconsistent with the properties of the assigned radicals.

Orbital Representation.—Walsh has presented a general treatment[20] of the orbital representation of non-linear triatomic molecules. According to this picture the unpaired electron of NO_2 in its ground state occupies an a_1s_A orbital. The nature of this orbital is such that for a linear B–A–B molecule with 17 electrons it would be a $p\pi$ orbital localized on the central atom. For the extreme case of a bent BAB molecule, with 90° between the AB bonds, it would be a pure s orbital localized on the central atom. The apex angle in NO_2 has been reported as 135°.[21] It represents an intermediate case in which the a_1s_A orbital retains part of the s character of the bent 90° case. The orbital remains largely localized on the nitrogen atom according to this analysis. The large contact term splitting reported by Zeldes and Livingston,[17] and indicated by the powder KNO_3 spectra, is consistent with this representation and with the recently calculated[20] charge density of 0.17 for the contribution of the nitrogen 2s orbital to the M.O. containing the unpaired electron.

It follows from this treatment that variation in the contact term HFS of NO_2 may occur in different solids. Greater s character, and so greater HFS, would be predicted if the apex angle of NO_2 were decreased by space restrictions of the host lattice. This may be a factor contributing to the substantial differences observed between contact terms HFS of 48 and 54.3 gauss reported for NO_2 in the gaseous state[9] or in the $NaNO_2$ lattice,[17] respectively.

Walsh's general treatment predicts for 19-electron AB_2 molecules an apex angle of *ca.* 115°, and places the unpaired electron in a b_1 orbital. For both the 90 and 180° cases this is built from a p orbital on A overlapping out of phase with a p orbital on each B atom. It is B ↔ B bonding but A ↔ B antibonding in the bent molecule case and more localized on the A atoms. Four values of the contact term, $a = \pm 41\ 2/3$ and $a = \pm 1$, satisfy the requirements of eq. 1. Since the sign of A or B is not discernible from the data presented here some consideration of both numerical values is required. *Case A*, $a = \pm 1$, would correspond closely with the absence of contact-term splitting, which the above simple M.O. considerations predict for $(NO_2^-)^-$. The expanded form of the term describing the angular dependence of the HFS in eq. 1 may be written[16] as

$$[a^2 - 2aB_\perp (3\cos^2\theta - 1) + B_\perp^2 (3\cos^2\theta + 1)]^{1/2}$$

since $A^2 = (a + B_\parallel)^2$ and $B^2 = (a + B_\perp)^2$, and $B_\parallel = -2B_\perp$. $B_\parallel$ and $B_\perp$ are, respectively, the parallel and perpendicular components of the dipolar contribution. In case A, since $|a|$ is negligibly small relative to $B_\parallel$ and $B_\perp$, the expression reduces to $\pm B\ (3\cos^2\theta + 1)^{1/2}$. Figure 2 therefore would represent the comparison between the experimental values and an angular dependence varying as $(3\cos^2\theta + 1)^{1/2}$. This is the angular dependence predicted by Zeldes, *et al.*,[22] for an electron in a pure p orbital, and the agreement in Fig. 2 would constitute evidence that the unpaired electron is largely in a p-orbital with axis of cylindrical symmetry pointing along the *c*-axis of the crystal. The M.O. representation of $(NO_2^-)^-$ radicals with the radical plane in the plane of the parent NO_3^- ions would consistently account for this symmetry. *Case B*, $a = \pm 41\ 2/3$, would require admixture by configuration interaction of a state having high s-electron character on the nitrogen. The observed total HFS splitting of 66 ± 3 gauss for this signal in powdered KNO_3, and its relatively small line width, are more consistent with the solution $a = \pm 41\ 2/3$. This follows because the line widths in powdered salts have been predicted[16] to increase generally with increasing

(20) A. D. Walsh, *J. Chem. Soc.*, 2266 (1953).

(21) M. Green and J. W. Linnett, *Trans. Faraday Soc.*, **57**, 1 (1961).

(22) H. Zeldes, G. T. Trammell, R. Livingston, and R. W. Holmberg, *J. Chem. Phys.*, **32**, 618 (1960).

$|B_\perp|$, and the small observed width of *ca.* 8 gauss thus is more consistent with case B, giving $|B_\perp| = 9\ 2/3$, than case A, giving $|B_\perp| = 32$. Jaccard has chosen a solution equivalent to case B for his data set out in Table I. He observed that his anisotropic signal of Table I disappeared in a reversible way at 128°K. It was replaced above this temperature by an isotropic triplet. The HFS splitting of the isotropic triplet was exactly equal to the contact term of the anisotropic triplet, but only if calculated for A and B with the same sign. He postulated that in fact the anisotropic and isotropic triplets arose from the same species, $NO_3^=$ radicals, which, he said, underwent rapid tumbling motions above 128°K. This interpretation does not explain how $(NO_3^-)^-$ ions could undergo rapid tumbling above 128°K. when the smaller NO_3^- ion cannot undergo even hindered rotation below 400°K.[23] Neither does it account for the observed difference between the average of the anisotropic g-values (av. = 2.0031) and the g observed for the isotropic triplet ($g = 2.0052$). Thus, neither from analogy with Jaccard's results, nor from the present data, can an unambiguous choice be made between the $|a| = 41\ 2/3$ and $|a| = 1$.

Some disagreement exists in the literature on the correct M.O. description of the electronic configuration of NO_3^-. Following Walsh, both 23 (*e.g.*, NO_3) and 24 (*e.g.*, NO_3^-) electron-containing AB_3 molecules should be planar. The top orbital (containing the unpaired electron of NO_3 or a pair of electrons in NO_3^-) should be a_2', meaning that it is built from a lone-pair p orbital on each oxygen atom. This orbital is slightly B ↔ B antibonding and A ↔ B non-bonding, (*i.e.*, n type). The lowest unfilled orbital would be $\bar{a}_2''$, which is A ↔ antibonding and B ↔ B bonding and is constructed from a p orbital on A overlapping out of phase with a p orbital on each B atom (*i.e.*, π^* type). Because of the strong B ↔ B bonding character, Walsh concludes that occupancy of this $\bar{a}_2''$ orbital would favor the closest approach of the B atoms. Thus either the 25-electron radical $(NO_3^-)^-$, or the first excited state of NO_3^-, should tend toward a pyramidal shape. From their observed spectra of $NaNO_3$ crystals Friend and Lyons[24] have claimed that the intensity of the absorption at ~300 mμ is consistent with a forbidden $\pi^* \leftarrow$ n transition. They claimed that the appearance of out-of-plane vibration intervals on the electronic transition showed the tendency toward pyramidal form in the excited state. This M.O. representation would consistently account for the magnetic parameters assigned to NO_3 and $(NO_3^-)^-$ because: (a) The unpaired electron in NO_3 has no HFS because the a'_2 orbital is built from p orbitals on oxygen. It has an axis of threefold rotation symmetry perpendicular to the plane of the NO_3 group. The observed cylindrical symmetry of g for NO_3 would arise from this threefold axis, for NO_3 radicals in the position of the parent NO_3^- ions. (b) The cylindrical symmetry of g for the triplet identified as $(NO_3^-)^-$ would arise in like manner for an electron in the $\bar{a}_2''$ orbital. The nature of the orbital is such that, while it would have pure p character on the central atom for planar $(NO_3^-)^-$ molecules, it would acquire an amount of s character on the central atom which would increase as the distortion from the planar (and toward the pyramidal) geometryi ncreased. The small observed HFS of 4.5 gauss indicates slight distortion of $(NO_3^-)^-$ from a planar form on this M.O. representation.

From a detailed analysis of the optical absorption of nitrate crystals Sayre[25] has concluded that the highest filled orbital of (NO_3^-) is $(1e'')^4$ and the lowest unfilled orbital $2a_2''$. Both of these orbitals in a planar AB_3 molecule are constructed from a p orbital on A overlapping with a p orbital on each oxygen. This representation of the low energy transition as $\pi^* \leftarrow \pi$ in type, and so allowed, is difficult to reconcile with the very low intensity ($\epsilon \cong 25$) for the ~300 mμ band. It would predict for planar NO_3 and $(NO_3^-)^-$ an absence of HFS. Sayre also claimed that the first excited state of NO_3^- was planar, and this interpretation would infer that $(NO_3^-)^-$ also probably would be planar. The HFS here attributed to $(NO_3^-)^-$ then could be accounted for only by configurational interaction. Other recent work casts doubt on the validity of Sayre's conclusions that the transition is $\pi^* \leftarrow \pi$ and that the excited state is planar. McEwen[26] has calculated the relative energy levels of the NO_3^- ion and considers that type $\pi^* \leftarrow$ n or $\sigma^* \leftarrow$ n transitions would be consistent with the energy, intensity, and symmetry of the 300 mμ transition in NO_3^-. The suggestion that the upper state might be σ^* probably would require much greater HFS than the observed 4.5 gauss for $(NO_3^-)^-$. The HFS could arise naturally from the alternative $^*\pi$-type, non-planar upper state suggested by Walsh, Friend, and McEwen (see above). Sayre observed that predissociation accompanied promotion of an electron into the upper orbital. The observed instability of the species here identified as $(NO_3^-)^-$ is in accord with this observation, if similar M.O. descriptions are accepted for the first excited state of NO_3^- and the ground state of $(NO_3^-)^-$.

Satisfactory agreement between an orbital description of O_2^- and an e.p.r. signal with parameters similar to those here assigned to O_2^- has been achieved by previous workers.[19] The agreement between parameters previously identified with NO and those here assigned to this species also is satisfactory. Because the $^2\pi_{1/2}$ non-paramagnetic state of NO is lower in energy than its paramagnetic $^2\pi_{3/2}$ state, the former should be occupied almost exclusively at 4°K. The experimentally observed e.p.r. signals showing HFS at 4°K. indicate an orbital description of NO involving configurational interaction between the ground state and states having s character on the nitrogen nucleus.

Radical Orientation.—Layers of planar NO_3^- ions alternate with cation layers in KNO_3. The layer planes are perpendicular to the crystal c-axis. The cylindrical symmetry around the c-axis of the g-factors of NO_3 and $(NO_3^-)^-$ has been shown

(23) A. R. Ubbelohde, *Brit. J. Appl. Phys.*, **7**, 313 (1956).
(24) J. A. Friend and L. E. Lyons, *J. Chem. Soc.*, 1572 (1959).
(25) E. V. Sayre, *J. Chem. Phys.*, **31**, 73 (1959).
(26) K. L. McEwen, *ibid.*, **34**, 547 (1961).

above to result naturally from these radical species fixed in the nitrate layer. It also has been seen that N–O radicals produced at 4.2°K. had 3 fixed orientations in the nitrate layer. It therefore seems improbable that the larger $(NO_2^-)^-$, or NO_2, fragments formed at 4°K. would rotate away from their positions of formation. Six sets of $(NO_2^-)^-$ fragments approximately related to each other by 60° rotation around the *c*-axis then would result. The experimental observations for $(NO_2^-)^-$ signals were cylindrical symmetry about the *c*-axis and line width of *ca.* 4 gauss at 4°K. which was not significantly reduced by going to lower microwave power. The cylindrical symmetry observed with lines of this width does not preclude the possibility that the *g* and/or HFS components in the nitrate plane differ by *ca.* ±0.002 or ±2 gauss, respectively. Overlap between signals from 6 sets then could result in the irreducible line width and apparent cylindrical symmetry. The exact orientation of the NO_2 radicals is not known, but it is possible that the increase in the O–N–O bond angle from 120° in NO_3^- to 135° in NO_2 may require that the oxygens be displaced toward the more open cation layers with resultant tilt of the magnetic axes.

Conclusion

The tentative identification of e.p.r. signals observed in irradiated KNO_3 with the radicals $(NO_2^-)^-$, NO_2, $(NO_3^-)^-$, NO_3, NO, and O_2^- is seen to be not inconsistent with the orbital and orientation requirements. The identification of these radicals, if valid, has these important applications to the mechanism of radiolysis of these salts: (1) The formation of $(NO_3^-)^-$ and the observation that it decays at a measurable rate at 77°K. provide the first indication of dissociative mechanisms of the types

$$(NO_3^-)^- \longrightarrow (NO)^{-n} + O_2^{n-2} \qquad (3a)$$

$$(NO_3^-)^- \longrightarrow (NO_2)^{-n} + O^{n-2} \qquad (3b)$$

where $n = 0$, 1, or 2. Since these mechanisms depend on electron capture by NO_3^- ions they could account for the observed efficiency[5,6] of γ-ray energy, initially absorbed by the cations with release of electrons, for dissociation of the nitrate ion. (2) The detection of the species $(NO_2^-)^-$ after even the shortest irradiations at 4.2 or 77°K. ($\sim 10^{18}$ e.v. g.$^{-1}$) and with an initial $G \cong 2$ for their production also indicates the existence of the mechanism $(NO_3^-)^- \rightarrow (NO_2^-)^- + O$. This seems a much more probable process for the production of $(NO_2^-)^-$ with the observed efficiency than the alternative requiring first a dissociation leading to NO_2^- and then capture of electrons by the then very small concentration ($<10^{-6}$ *M*) of NO_2^- ions. (3) The existence of NO radicals after irradiation at 4.2 or 77°K. suggests that mechanisms of type 3a, in particular for $n = 0$, contribute to the initial decomposition of NO_3^-. That NO results from NO_3^{-n} fragments and not *via* NO_2^{-n} intermediates is further suggested by the observations of Zeldes and Livingston and this author that no NO radicals were detected in irradiated $NaNO_2$.

The importance of these NO radicals in the chemical changes and annealing processes in irradiated nitrate crystals is being studied by a chemical method. Saturation concentrations of *ca.* 10^{-4} *M* at dose of *ca.* 3×10^{22} e.v. mole^{-1} have been detected, in good agreement with the observations on saturation of the central e.p.r. signal to which NO contributes. Studies are being completed on the radiation-induced absorption in nitrate crystals. It is hoped that such independent means of investigation may provide the means of removing the uncertainties remaining in the identifications derived by e.p.r.

Acknowledgments.—It is a pleasure to acknowledge the generous assistance of Dr. B. Smaller and Dr. J. A. McMillan without whose help this work could not have been completed. The assistance of E. Yasaitis with the measurements at 4°K. also is gratefully acknowledged. Copies of their manuscripts, prior to publication, received from Dr. C. Jaccard and Drs. H. Zeldes and R. Livingston were of considerable assistance in formulating the discussion.

THE HEAT CAPACITY OF DIAMMONIUM DICADMIUM SULFATE FROM 15 TO 300°K.

BY C. C. STEPHENSON AND O. R. LUNDELL

Department of Chemistry, Massachusetts Institute of Technology, Cambridge 39, Massachusetts

Received July 17, 1961

The heat capacity of diammonium dicadmium sulfate has been measured from 15 to 300°K. There is a gradual transition, the maximum in the heat capacity occurring at about 92°K. The entropy of diammonium dicadmium sulfate was calculated to be 116.09 ± 0.24 cal. deg.$^{-1}$ mole^{-1} at 298.16°K. The estimated excess enthalpy and entropy attributed to the transition are 216 ± 2 cal. mole^{-1} and 2.36 cal. deg.$^{-1}$ mole^{-1}.

Order–disorder transitions which involve reorientation of the ammonium ions have been found in a number of ammonium salts.[1] Several ammonium salts, for example ammonium sulfate and ammonium fluoroberyllate, are ferroelectric or antiferroelectric. A more recently discovered ferroelectric substance is diammonium dicadmium sulfate,[2] $(NH_4)_2Cd_2(SO_4)_3$. The dielectric constant of this salt had been measured by Pepinsky, *et al.*,

(1) C. C. Stephenson, R. W. Blue, and J. W. Stout, *J. Chem. Phys.*, **20**, 1046 (1952).

(2) F. Jona and R. Pepinsky, *Phys. Rev.*, **103**, 1126 (1956).

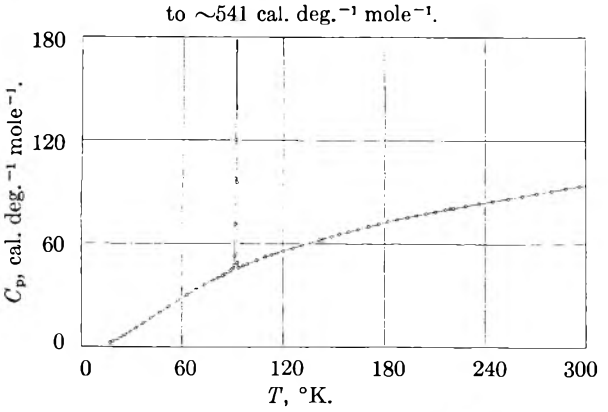

Fig. 1.—The heat capacity of $(NH_4)_2Cd_2(SO_4)_3$.

from about 80°K. to room temperature and reaches a maximum at approximately 89°K. Thermal analysis done by Pepinsky[3] and in this Laboratory revealed a transition near 90°K.

In this study, heat capacity measurements have been made from 15 to 300°K. An anomaly in the heat capacity has been found, the heat capacity maximum occurring near 92°K. This maximum is extremely sharp, and the transition extends over a relatively small temperature interval.

Material.—The diammonium dicadmium sulfate used for the heat capacity measurements was prepared by a method outlined in an unpublished thesis.[3] A solution containing 0.333 mole of $3CdSO_4 \cdot 8H_2O$, 0.500 mole of ammonium sulfate, 400 cc. of boiling distilled water, and 4 cc. of concentrated sulfuric acid was allowed to evaporate slowly in an oven at 85 ± 5°. Before evaporation was complete, the solution was decanted rapidly, and the crystals were washed on a suction filter with hot distilled water and then with hot absolute alcohol. The crystals were pressed on filter paper, placed in an oven at 100° for five hours, and stored in a desiccator over magnesium perchlorate.

In an analysis for cadmium sulfate, the samples were heated gently until most of the ammonium sulfate was driven off. They then were subjected to prolonged heating at 550°. Three samples gave a mean of 75.84 weight % cadmium sulfate. The average deviation from the mean was 0.03%. The theoretical percentage of cadmium sulfate in diammonium dicadmium sulfate is 75.93%. The heat capacity measurements gave no indication of eutectic melting below 273°K. due to solution inclusion nor any evidence of the transition at 220°K. due to free ammonium sulfate. These are very sensitive tests and rule out the presence of significant quantities of included solution or ammonium sulfate.

All measurements were made on a single loading of 210.531 g., *in vacuo*, or 0.38340 mole with a molecular weight of 549.11.

Apparatus and Method.—The cryostat and calorimeter have been described in the literature.[4] The calorie was taken as equivalent to 4.1833 international joules, and the absolute temperature of the ice point was taken as 273.16°K.

Heat Capacity Measurements.—The experimental heat capacities are given in Table I and Table II and shown in Fig. 1. The values given in Table II were obtained through the transition region and do not represent differential heat capacities near the maximum. Values of the heat capacity taken from a smooth curve through the experimental points are listed in Table III.

The accuracy of the measurements is believed to be within 5% below 20°K., 1% between 20 and 30°K., and 0.2% above 30°K., except in the transition region where the temperature intervals are very small.

Heat Capacity Measurements.—The experimental heat capacities are given in Tables I and II and shown in Fig. 1. The values given in Table II were obtained through the transition region in a continuous series of measurements. They do not represent differential heat capacities near the maximum; no curvature correction has been applied. Values of the heat capacity taken from a smooth curve through the experimental points are listed in Table III, and the molal entropy, enthalpy, and free energy are given in Table IIIa.

TABLE I

THE HEAT CAPACITY OF $(NH_4)_2Cd_2(SO_4)_3$ IN CAL. DEG.$^{-1}$ MOLE^{-1}

T, °K.	C_p	T, °K.	C_p	T, °K.	C_p
17.23	2.63	88.88	44.80	170.37	70.22
18.95	3.38			176.70	71.73
		Transition region			
22.18	5.04			182.31	73.21
24.18	6.19	94.50	46.70	187.61	74.44
26.40	7.46	95.60	47.10	193.26	75.58
29.06	9.08	98.92	48.23	199.00	76.75
32.72	11.40	104.13	50.42	204.83	77.97
36.84	14.04	109.39	52.25	210.48	78.92
41.45	16.96	114.39	54.08	216.63	80.12
46.46	20.16	116.25	54.67	221.13	81.03
51.85	23.62	120.42	56.09	228.57	82.40
57.68	27.18	125.81	57.80	236.41	83.75
62.85	30.33	131.24	59.46	244.73	85.22
68.00	33.33	136.49	60.94	253.26	86.62
73.16	36.20	141.58	62.44	261.88	88.07
78.36	38.96	144.05	63.02	270.61	89.61
83.61	41.75	148.71	64.39	279.10	90.95
85.15	42.55	153.66	65.78	287.68	92.31
87.92	44.13	158.89	67.28	296.37	93.56
88.20	44.27	164.37	68.69		

TABLE II

THE HEAT CAPACITY OF $(NH_4)_2Cd_2(SO_4)_3$ THROUGH THE TRANSITION REGION IN CAL. DEG.$^{-1}$ MOLE^{-1}

T, °K.	C_p	T, °K.	C_p	T, °K.	C_p
89.91	45.72	91.73	120.5	92.18	385.0
90.21	45.88	91.86	172.3	92.24	340.2
90.52	46.04	91.95	278.2	92.30	300.9
90.82	47.87	92.01	423.7	92.38	205.8
91.11	53.02	92.05	538.1	92.51	96.75
91.36	71.70	92.09	541.1	92.75	49.17
91.56	98.01	92.13	432.5		

The temperature at which the measured heat capacity has its maximum value lies between 92.05 and 92.10°K. Two warming curves made on the sample in the calorimeter gave a temperature of 92.08 ± 0.03°K. However, the minimum in the cooling rate curve occurred at 91.72 ± 0.03°K.

Three measurements of the total enthalpy change from 80 to 95°K. were made, and the results are given in Table IV. The mean value is assumed to be correct to 0.1%. A total enthalpy change of 866.9 cal. mole^{-1} was obtained from the measurements made at small temperature intervals.

The Entropy of Diammonium Dicadmium Sulfate at 298.16°K.—A summary of the entropy calculation from the calorimetric data appears in Table V. A Debye function, 21°D(181), which fitted the data to 22°K., was used for the calculation from 0 to 15°K.

The Transition in Diammonium Dicadmium Sulfate.—Because the transition occurs over such a small temperature range, a fairly reliable estimate of the excess enthalpy and entropy of transition can be made. A smooth curve was drawn through the heat capacity points above and below the transition region. The difference between the total enthalpy change from 80 to 95°K. and that estimated from the smooth curve is 216 ± 2 cal. mole^{+1}. The estimated excess entropy of transition is 2.36 cal. deg.$^{-1}$ mole^{-1}.

If it is assumed that the entropy of transition in diammonium dicadmium sulfate is related to the reorientation of the ammonium ions, the entropy which can be attributed to

(3) R. P. Eastman. Thesis, The Pennsylvania State University. 1957, "Thermal, Dielectric and Optical Studies of Some New Ferroelectrics."

(4) R. W. Blue and J. F. G. Hicks, *J. Am. Chem. Soc.*, **59**, 1962 (1937).

TABLE III

THE HEAT CAPACITY OF $(NH_4)_2Cd_2(SO_4)_3$ FROM A SMOOTH CURVE THROUGH THE EXPERIMENTAL POINTS IN CAL. DEG.$^{-1}$ MOLE^{-1}

T, °K.	C_p	T, °K.	C_p	T, °K.	C_p
16	2.08	62	29.83	155	66.17
17	2.53	64	31.01	160	67.52
18	2.96	66	32.18	165	68.84
19	3.41	68	33.63	170	70.13
20	3.90	70	34.45	175	71.38
21	4.41	72	35.56	180	72.60
22	4.95	74	36.65	185	73.79
23	5.51	76	37.72	190	74.92
24	6.08	78	38.77	195	75.98
25	6.65	80	39.82	200	76.98
26	7.23	82	40.88	205	77.96
27	7.82	84	41.93	210	78.92
28	8.42	86	43.01	215	79.86
29	9.04	88	44.26	220	80.79
30	9.67	Transition		225	81.72
32	10.95	region		230	82.64
34	12.21	94	46.50	235	83.50
36	13.49	96	47.30	240	84.37
38	14.76	98	48.08	245	85.24
40	16.04	100	48.84	250	86.10
42	17.32	105	50.70	255	86.95
44	18.59	110	52.52	260	87.80
46	19.87	115	54.28	265	88.64
48	21.15	120	55.94	270	89.47
50	22.42	125	57.54	275	90.29
52	23.69	130	59.08	280	91.10
54	24.95	135	60.55	285	91.89
56	26.18	140	61.98	290	92.66
58	27.40	145	63.40	295	93.40
60	28.62	150	64.79	300	94.09

TABLE IIIa

MOLAL ENTROPY, ENTHALPY, AND FREE ENERGY OF $(NH_4)_2Cd_2(SO_4)_3$

T, °K.	S^0, cal. deg.$^{-1}$	$H^0 - H_0^0$, cal.	$-(F^0 - H_0^0)$, cal.
15	0.62	6.96	2.3
20	1.39	20.89	6.9
25	2.55	47.10	16.7
30	4.03	87.75	33.1
35	5.75	143.7	57.5
40	7.68	215.9	91.3
45	9.75	304.0	144.5
50	11.94	408.2	188.8
60	16.58	663.5	331.3
70	21.44	949.2	551.6
80	26.40	1321	791
90	30.79	1743	1028
100	38.65	2428	1437
110	43.48	2935	1847
120	48.20	3478	2306
130	52.80	4051	2813
140	57.29	4658	3363
150	61.66	5292	3957
170	70.10	6642	5275
180	74.18	7356	5996
190	78.17	8094	6758
200	82.06	8853	7559
210	85.87	9633	8400
220	89.58	10430	9276
230	93.21	11250	10190
240	96.76	12080	11140
250	100.25	12940	12130
260	103.66	13800	13150
270	107.00	14700	14190
280	110.28	15600	15280
290	113.51	16250	16400
300	116.68	17460	17550
298.16	116.09	17280	17330

TABLE IV

THE ENTHALPY CHANGE FROM 80 TO 95°K.

	ΔH, cal. mole^{-1}
Run I	867.55
Run II	867.57
Run III	867.91
Mean	867.68 ± 0.9

TABLE V

THE ENTROPY OF DIAMMONIUM DICADMIUM SULFATE

	^1S, cal. deg.$^{-1}$ mole^{-1}
0–15 °K.	0.62
15–89.75 °K.	30.67
89.75–92.89 °K. $\Sigma(C_p/T)\Delta T$	3.86
92.89–298.16 °K. (graphical integration)	80.94
	116.09 ± 0.24

each mole of ammonium ions is 1.18 cal. deg.$^{-1}$. If each ammonium ion could be oriented in two different ways above the transition temperature, the entropy due to the disordering of the ions should be $R \ln 2$ or 1.38 cal. deg.$^{-1}$ mole^{-1}. However, all of the ammonium ions probably do not occupy equivalent positions. A study[5] of the crystal structure of an isomorph, $K_2Mg_2(SO_4)_3$, reveals that the lattice positions occupied by the potassium ions are of two different types.

(5) Anna Zemann and J. Zemann, *Acta Cryst.*, **10**, 409 (1957).

COÖRDINATION COMPOUNDS. III. CHELATE COMPOUNDS OF THE URANYL ION WITH HYDROXY, MERCAPTO, AND AMINO ACIDS[1]

BY MICHAEL CEFOLA, ROBERT C. TAYLOR, PHILIP S. GENTILE, AND A. V. CELIANO

Department of Chemistry, Fordham University, New York, N. Y.

Received July 17, 1961

This investigation involved a potentiometric study of the chelates formed by the uranyl ion with the amino, hydroxy, and mercapto analogs of acetic, propionic, and succinic acids. The order of decreasing stability was aspartic, β-alanine, glycine, malic, thiomalic, β-hydroxypropionic, glycolic, and thioglycolic acids. The stability of chelates with analogs of acetic, propionic and succinic acids decreases for any given acid as the donor group changes from NH_2 to OH to SH. This decrease parallels the order of decreasing basicity in any given series. Considering acids which contain the same donor group (NH_2 or OH or SH) decreasing stability is observed in the analogs of succinic, propionic, and acetic acids, in that order.

Titration studies of the uranyl ion with acids and complexing agents has been virtually neglected except for a few ligands.[2-8]

This investigation was undertaken to establish the stabilities of the uranyl chelates of several hydroxy, mercapto, and amino acids, and to determine trends in their stabilities. The ligands were chosen so as to be able to determine the effect of ring size, ligand basicity, and nature of the donor atom on the stabilities. A polarographic study of these compounds, as well as of the uranyl chelates of β-diketones and several types of organic sulfur compounds, also was undertaken and will be reported at a later date. Little work has been done with compounds containing sulfur coördinating groups because of their tendency to oxidize to disulfides, especially in the presence of metal ions.

Experimental

Materials.—All chemicals used were either reagent grade or purified. Organic acids were prepared at a concentration of 0.1 *M* and were diluted for each titration so that the final solution contained about 1×10^{-3} mole of acid. β-Hydroxypropionic acid was prepared by dissolving β-propiolactone in hot water, to convert the lactone to the acid.[9] The acids, with the exception of glycine and β-alanine, were standardized by potentiometric titration with potassium hydroxide. Glycine and β-alanine were standardized with potassium hydroxide in the presence of formaldehyde.[10] The uranyl nitrate solution was prepared at a concentration of 0.033 *M* and diluted so that the final solution contained between 1×10^{-3} and 1×10^{-5} mole of metal ion. It was standardized by the addition of hydrogen peroxide and the titration of the nitric acid formed by the resulting reaction.[11] Potassium hydroxide was prepared carbonate-free at a concentration of 0.1 *M* by the method of Schwarzenbach and Biedermann[12] and standardized with potassium acid phthalate.

Apparatus and Procedure.—The experimental method consisted of the potentiometric titration of the organic acids in the absence and in the presence of uranyl ion. The acids employed were glycolic acid, thioglycolic acid, glycine, malic acid, thiomalic acid, aspartic acid, β-hydroxypropionic acid, and β-alanine.

The ionic strength was maintained at 0.1 by using 0.1 *M* potassium chloride as a supporting electrolyte. All measurements were carried out in an atmosphere of prepurified nitrogen at a constant temperature of 30.0 ±0.1°. Titrations were carried out using 1:1, 2:1, and 10:1 ratios for the acid to metal ion concentration. The *p*H values were determined with a Beckman Model G *p*H meter with extension glass and calomel electrodes.

Interpretation of the data is simplified if hydrolysis, which is *p*H dependent, may be neglected. It is possible by varying metal and ligand concentration to find a region of negligible hydrolysis. The agreement of the values of stability constants obtained at the different metal ion concentrations indicates that the amount of hydrolysis was negligible in the region between *p*H values of 2 and 4. It has been established[13,14] that UO_2^{++} is the species of hexavalent uranium existing in solution of *p*H approximately equal to 3. Due to early precipitation of the metal hydroxide in the 10:1 runs for glycine and β-alanine, calculations could not be made. Formation function curves did not permit calculation of K_2 for uranyl aspartate. The values reported are the averages of several runs. Acid dissociation constants were determined potentiometrically and agree well with previously reported values.[15-19]

The logarithms of the stability constants of the uranyl chelates are listed in Table I and were calculated by Bjerrum's graphical method.[20] The error limits[21] are: ±5% for K_1, ±10% for K_2. This corresponds to the errors: ±0.02 for log K_1, ±0.05 for log K_2.

Discussion

The over-all order of decreasing stability for the ligands was aspartic, β-alanine, glycine, malic,

TABLE I

STABILITY CONSTANTS OF MONOBASIC AND DIBASIC ACIDS WITH URANYL NITRATE

Acid	log K_1	log K_2
Aspartic	8.00	..
β-Alanine	7.78	7.53
Glycine	7.53	7.15
Malic	5.50	3.63
Thiomalic	3.56	3.42
β-Hydroxypropionic	3.25	2.88
Glycolic	2.97	2.40
Thioglycolic	2.88	2.40

(1) This study was supported by a grant from the U. S. Atomic Energy Commission, AT-(30-1)906.

(2) M. Cabell, *Analyst*, **77**, 859 (1952).

(3) R. Irving and H. Rossotti, *J. Chem. Soc.*, 2910 (1954).

(4) S. Ahrland, *Acta Chem. Scand.*, **5**, 199 (1951).

(5) S. Ahrland, *ibid.*, **3**, 783 (1949).

(6) S. Ahrland, *ibid.*, **7**, 485 (1953).

(7) J. Rodgers and W. Newman, Atomic Energy Commission Report AECO-2218, August 11, 1948.

(8) R. M. Izatt, W. C. Fernelius, and B. P. Block, *J Phys. Chem.*, **59**, 80 (1955).

(9) T. L. Gresham, J. E. Jansen, and W. Shaver, *J. Am. Chem. Soc.*, **70**, 998 (1948).

(10) I. Kolthoff and N. Furman, "Volumetric Analysis," John Wiley and Sons, Inc., New York, N. Y., 1929, p. 164.

(11) W. Bunce, G. Morrison, W. Chorney, and R. Nundy, Atomic Energy Commission Report No. 2-1044, July 7, 1944.

(12) G. Schwarzenbach and W. Biedermann, *Helv. Chim. Acta*, **31**, 339 (1948).

(13) S. Ahrland, *Acta Chem. Scand.*, **3**, 374 (1949).

(14) M. Crandall, *J. Chem. Phys.*, **17**, 602 (1949).

(15) R. Canaan and A. Kibrick, *J. Am. Chem. Soc.*, **60**, 2314 (1938).

(16) N. C. Li and R. A. Manning, *ibid.*, **77**, 5225 (1955).

(17) H. Kroll, *ibid.*, **74**, 2034 (1952).

(18) R. Taylor and M. Cefola, Doctoral Dissertation, Fordham University, June, 1957.

(19) N. C. Li and E. Doody, *J. Am. Chem. Soc.*, **72**, 1891 (1950).

(20) J. Bjerrum, "Metal Ammine Formation in Aqueous Solution," P. Haase and Son, Copenhagen, 1941.

(21) G. R. Choppin, private communication.

thiomalic, β-hydroxypropionic, glycolic, and thioglycolic acids, as shown in Table I.

The stability of chelates with analogs of acetic, propionic, and succinic acids decreases for any given acid as the donor group changes from NH_2 to OH to SH. This decrease parallels the order of decreasing basicity in any given series. Considering acids which contain the same donor group (NH_2 or OH or SH) decreasing stability is observed in the analogs of succinic, propionic, and acetic acids, in that order. This order is found to be unusual in that the six-member ring chelates of the propionic acid analogs are more stable than the five-member ring chelates of the acetic acid analogs. Succinic acid analogs, although the weakest bases, form the strongest chelates in any group. These would be expected to be the least stable inasmuch as a decrease in ligand basicity results in a corresponding lower affinity for metal ions.

The behavior of succinic acid analogs may be attributed to the formation of either a bidentate or tridentate complex. The bidentate complexes possibly may possess either a five- or six-membered ring, thus taking on the structure of acetic acid analogs with a substituted carboxylmethyl group, or of propionic acid analogs with a substituted carboxyl group. In either case, the bidentate chelates would be expected to be only slightly stronger than those of the acetic acid or propionic acid analogs, whereas tridentate formation would be expected to give a large increase in the stability constant (~2 log units).[22] Such an increase is observed only for malic acid. Lumb and Martell[23] have observed that aspartic acid forms bidentates with alkaline earth ions and for these chelates the stability constant was 0.2 log unit higher than the glycine, the small increase being attributed to the inductive effect of the negative carboxylate group in aspartic acid, which can lend stability to the structure by increasing the basicity of the donor group toward the metal ion. The difference between the stabilities of the aspartate and β-alinate chelates of uranyl ion is approximately 0.2 log unit, thus indicating formation of a bidentate chelate with aspartic acid. In all probability aspartic acid forms a six-membered ring since the β-alinate is more stable than the glycinate.

Table II lists the relative position of UO_2^{+2} in a series of metal ions for the formation of glycinates and aspartates.

TABLE II

STABILITY CONSTANTS OF VARIOUS METALS WITH GLYCINE AND ASPARTIC ACID

Glycine		Aspartic acid	
Metal ion	log K_1	Metal ion	log K_1
Cu(II)	8.62 (24)	Cu(II)	8.57 (25)
UO_2	7.53	UO_2	8.00
Ni(II)	6.18 (24)	Ni(II)	7.12 (25)
Zn(II)	5.52 (24)	Co(II)	5.90 (25)
Co(II)	5.23 (24)	Zn(II)	5.64 (25)
Pb(II)	5.47 (24)	Cd(II)	4.37 (25)
Mn(II)	3.44 (24)	Hg(II)	2.43 (23)
Ag(II)	3.51 (24)	Ca(II)	1.60 (23)

(22) M. Cefola, A. Tompa, A. V. Celiano, and P. S. Gentile, *Inorg. Chem.*, **1**, 290 (1962).

(23) R. F. Lumb and A. E. Martell, *J. Phys. Chem.*, **57**, 690 (1953).

(24) G. Monk, *Trans. Faraday Soc.*, **47**, 297 (1951).

(25) S. Chaberek and A. E. Martell, *J. Am. Chem. Soc.*, **74**, 6021 (1952).

THE HEATS OF COMBUSTION OF ReS_2 AND Re_2S_7 AND THE THERMODYNAMIC FUNCTIONS FOR TRANSITION METAL SULFIDES[1,2]

BY J. E. MCDONALD[3] AND J. W. COBBLE

Department of Chemistry, Purdue University, Lafayette, Indiana

Received July 24, 1961

The heats of combustion of ReS_2 and Re_2S_7 have been measured by bomb calorimetry. The heat and free energy of formation at 25° of ReS_2 are -42.7 ± 1.2 kcal. mole^{-1} and -41.5 ± 1.2 kcal. mole^{-1}, respectively. The similar quantities for Re_2S_7 are -107.9 ± 1.8 kcal. mole^{-1} and -101.0 ± 1.8 kcal. mole^{-1}, respectively. With data on these key sulfides, along with recalculated heats of formation from previous vapor pressure measurements, it has been possible to estimate the thermodynamic functions for a number of sulfides not previously available.

I. Introduction

Very few thermodynamic data have been available on transition element sulfides in spite of their potential interest in solid state and high temperature chemistry. Certain vapor pressure measurements of Biltz, Juza, and their co-workers fix the heats of formation of PtS_2, PtS,[4] Ir_2S_3, IrS_2,[5] ReS_2,[6] RuS_2,[7] and OsS_2[8] if the assumption is made that the only vaporizing species is gaseous sulfur. Since ReS_2 can be directly sublimed at ~1000°, this assumption needs independent verification.

The purpose of this communication is to report the calorimetric determination of the thermody-

(1) This research was supported by the United States Air Force through the Air Force Office of Scientific Research of the Air Research and Development Command under contract AF 18(600)-1525. Reproduction in whole or part is permitted for any purpose of the United States Government.

(2) This constitutes communication number VIII in our previous series on rhenium and technetium chemistry. For the previous paper in this series see *J. Am. Chem. Soc.*, **82**, 2111 (1960).

(3) From the Ph.D. thesis of J. E. McDonald, Purdue University, 1961; Dow Chemical Co. Fellow, 1959–1960; Procter and Gamble Fellow, 1960–1961.

(4) W. Biltz and R. Juza, *Z. anorg. Chem.*, **190**, 161 (1930).

(5) W. Biltz, J. Laar, P. Ehrlich, and K. Meisel, *ibid.*, **233**, 257 (1937).

(6) R. Juza and W. Biltz, *Z. Elektrochem.*, **37**, 498 (1931).

(7) R. Juza and W. Meyer, *Z. anorg. Chem.*, **213**, 273 (1933).

(8) R. Juza, *ibid.*, **219**, 129 (1934).

namic functions for ReS_2 and Re_2S_7. With these data it now is possible to check the nature of the vaporization process in these and similar sulfides. Further, because of the central and key position of rhenium sulfides among the other transition elements, thermodynamic functions for many other sulfides can be estimated which have not been available previously.

II. Experimental

Chemicals.—Rhenium heptasulfide was prepared by precipitation from a strongly acid perrhenate solution with hydrogen sulfide gas. The black precipitate was washed repeatedly with water, carbon bisulfide, and finally ether, and dried under vacuum over P_2O_5. The carbon bisulfide–ether extractions were repeated until the dried solid had attained a constant composition. The material was analyzed for both rhenium and sulfur content, the former by reduction to the metal with hydrogen at 700°. The sulfur was determined by oxidation with aqueous hydrogen peroxide and precipitation of the sulfate so formed as barium sulfate. The composition of the product was: Re, 62.24%; S, 37.05%, corresponding to $ReS_{3.49}$.

Rhenium disulfide was prepared by the thermal decomposition of Re_2S_7 under a stream of dry nitrogen at 450°. The product was analyzed by reduction to the metal with hydrogen as before. The composition, Re, 74.39%, corresponded to a material $ReS_{2.02}$.

Equipment.—The calorimeter consisted of a Parr microbomb of 50-ml. capacity immersed in a 2-l. calorimeter vessel. The vessel was a brass container with a double wall which could be evacuated, and had a lucite cover lid. The calorimeter assembly was submerged in a 15-gal. temperature-controlled (±0.005°) thermostat. Access tubes for the stirrer, heater, and connections were provided in the lucite cover. The bomb was held in a bearing-mounted collar which could be rocked or rotated by a pulley arrangement through the access tubes. This feature was not utilized in the present experiments because of subsequent chemical side reactions. The bomb calorimeter system (hereafter designated CMC-1) was calibrated using a benzoic acid sample from the National Bureau of Standards (obsd.: 6319 ± 19.0 cal. g.$^{-1}$; NBS: 6318.3 cal. g.$^{-1}$).

The thermistor temperature measuring and recording system was essentially identical to that previously described.[9] However, the thermal range was expanded somewhat to accommodate larger heats (up to 90 cal. per mv.). The firing system was of a conventional type and firing energy corrections for the fuse wire (2 in. of #32 gage platinum) and the fuse (1 in. of #50 cotton thread) under the combustion conditions were determined to be 4.45 ± 0.16 cal.

Procedure.—The bomb containing the sample in a small platinum boat was assembled and flushed a few times with oxygen. The combustions all were made at a standard pressure of 30 atm. The calorimeter system first was electrically calibrated, then a combustion run was made, followed by a second electrical calibration. The average electrical equivalent from the two calibrations was used in the calculations.

After the final calibration, the bomb was removed and the combustion gases slowly vented into a series of washing bottles containing known amounts of a standardized basic hypochlorite solution. The contents of the wash bottles then were analyzed to determine the change in hydroxide and hypochlorite concentrations. On the assumption that the gases were either SO_2 or SO_3, these analyses along with the original weight of sulfide provided the information necessary to fix the combustion reaction. Examination of the contents of the bomb after each run demonstrated that no solid residue remained in the case of the ReS_2 combustions, although quantities of solids varying from 1–2.5 mg., which were shown to be Re_2S_7, sometimes were recovered from the heptasulfide combustions. A final test of the stoichiometry was made by spectrophotometric analysis of the perrhenate ion obtained by washing out the contents of the bomb.

(9) J. E. McDonald, J. P. King, and J. W. Cobble, *J. Phys. Chem.*, **64**, 1345 (1960).

III. Experimental Results

The combustion of Re_2S_7 produces both SO_2 and SO_3

$$Re_2S_7(c) + \frac{21}{2}O_2(g) \longrightarrow Re_2O_7(c) + 7SO_2(g) \quad (1)$$

$$Re_2S_7(c) + 14O_2(g) \longrightarrow Re_2O_7(c) + 7SO_3(g) \quad (2)$$

Experimentally, the fraction of sulfur which appears as SO_2 in the combustion products was found to be 0.883 ± 0.019, independent of the amount of sulfide burned. The thermal data for the sum of reactions 1 and 2 are summarized in Table I. The average ΔE for the processes in eq. 1 and 2 is −1.1743 ± 0.0019 cal. mg.$^{-1}$ of Re_2S_7. Corrected to 100% SO_3, and changing ΔE to ΔH,[10] the heat of combustion for reaction 2 becomes $\Delta H_2^0 = -849.9 \pm 1.7$ kcal. mole^{-1} Re_2S_7. Using necessary auxiliary thermodynamic data[11] and a heat of formation of $Re_2O_7(c)$ of −296.7 ± 0.8 kcal. mole^{-1},[12] the heat of formation of Re_2S_7 becomes −107.9 ± 1.8 kcal. mole^{-1} at 25°.

Table I

The Energy of Combustion of Re_2S_7 at 25°

Sample wt. (mg.)	Heat[a] (cal.)	ΔE (cal. mg.$^{-1}$)
35.43	41.814	1.1802
31.46	36.814	1.1702
50.32	59.201	1.1765
44.45	52.171	1.1737
34.45	40.331	1.1707
	Av.	1.1743 ± 0.0019[b] cal. mg.$^{-1}$

[a] Corrected for firing energy. [b] Standard deviation.

The combustion of rhenium disulfide takes place according to reactions 3 and 4

$$2ReS_2(c) + \frac{15}{2}O_2(g) \longrightarrow Re_2O_7(c) + 4SO_2(g) \quad (3)$$

$$2ReS_2(c) + \frac{19}{2}O_2(g) \longrightarrow Re_2O_7(c) + 4SO_3(g) \quad (4)$$

In this case the fraction of sulfur which forms SO_2 is 0.817 ± 0.019. The thermal data for ReS_2 are summarized in Table II. From this data, the average value for the energy of combustion is −254.71 ± 0.73 kcal. mole^{-1} of ReS_2. Changing this quantity to the heat of combustion,[10] and correcting to 100% SO_3, $\Delta H_4^0 = -294.58 \pm 1.13$ kcal. mole^{-1} ReS_2. Using auxiliary thermodynamic data,[11,12] the heat of formation of ReS_2 becomes −42.7 ± 1.2 kcal. mole^{-1} at 25°.

IV. Discussion

Volatilization Processes for $ReS_2(c)$.—By making certain estimations[13,14] of the ΔC_p of vaporization and the entropy of the solid sulfides, it is possible to predict the vapor pressures of ReS_2 and Re_2S_7 at high temperatures. Assuming $\overline{\Delta C_p}$ for the process

$$ReS_2(c) = Re(c) + S_2(g) \quad (5)$$

(10) The Washburn corrections are estimated to be small compared to the experimental error.

(11) U. S. Bureau of Standards, Circular 500, "Selected Values of Chemical Thermodynamic Properties," 1952.

(12) G. E. Boyd, J. W. Cobble, and W. T. Smith, Jr., *J. Am. Chem. Soc.*, **75**, 5783 (1953).

(13) Based upon data given in K. K. Kelley, U. S. Bur. of Mines Bull. 584 (1960).

(14) K. K. Kelley, U. S. Bur. of Mines Bull. 406 (1937).

TABLE II

THE ENERGY OF COMBUSTION OF ReS_2 AT 25°

Sample wt. (mg.)	Heat[a] (cal.)	$-\Delta E$ (cal. g.$^{-1}$)
64.89	65.984	1.0169
55.73	57.089	1.0244
61.82	62.463	1.0104
60.35	61.336	1.0162

Av. 1.0170 ± 0.0029[b] cal. g.$^{-1}$

[a] Corrected for firing energy. [b] Standard deviation.

is −1.5 between 0 and 298°K., ΔH_0^0 for the vaporization process is calculated to be 73.2 kcal. mole^{-1}. If $\overline{\Delta C_p}$ for the same process over the temperature range 0 and 1400–1500°K. is −3.0 and ΔS_6 at 298°K. is 42.5 gbs. mole^{-1}, then it follows

$$-\log P_{(atm)} = \frac{15.6 \times 10^3}{T} + 2.16 \log T - 15.5 \quad (6)$$

This equation should be valid up to 1500°K. However, vapor pressures calculated from equation 6 are not in agreement with the data of Juza and Biltz,[6] by about a factor of ~10 (see Table III). One concludes that either the vaporization process for ReS_2 is not wholly described by eq. 5, or that the direct vapor pressure measurements are in error. In this respect, it was reported[6] that the quartz container used in the vapor pressure measurements showed evidence of chemical attack. If volatile components (such as SO_2) were produced, then the observed vapor pressures would be too high.

It also is possible to estimate the effect of molecular vaporization of $ReS_2(g)$

$$ReS_2(c) = ReS_2(g) \quad (7)$$

It was noted[6] that ReS_2 only slowly sublimed at 1000°. This probably indicated that the partial pressure of $ReS_2(g)$ at this temperature was about 10^{-5} atm. $\Delta S_7 = 45$ is probably a reasonable estimate for the vaporization process and although there is very little data upon which to make reasonable heat capacity estimates, $\Delta C_{p7} = 0$ will not cause a serious error. Therefore, the chemistry of the situation enables one to predict that $\Delta H_0^0 = 86.5$ kcal. mole for the molecular vaporization given in eq. 7, and

$$-\log P_{(atm)} = \frac{18.9 \times 10^3}{T} - 9.83 \quad (8)$$

This equation also predicts vapor pressures too low to account for the data of Juza and Biltz.[6] The situation can be summarized in Table III.

TABLE III

HIGH TEMPERATURE VAPOR PRESSURES FOR ReS_2

T, °K.	$P_{obsd.}$,[a] mm.	$P_{calcd.}$,[b] mm. $S_2(g)$	$P_{calcd.}$,[c] mm. $ReS_2(g)$
1383	13	1.1	0.1
1462	55	4.2	0.6
1498	96	7.3	1.2

[a] Experimental vapor pressures of Juza and Biltz, ref. 6. [b] Calculated from thermal data, eq. 6. [c] Calculated from eq. 8.

The conclusion from the vapor pressures given in Table III is that the original vapor pressure data in reference 6 are not correct. However, it also is evident that in this region of the periodic table, the direct molecular volatilization may contribute significantly to the total pressure. Consequently, the heats of formation commonly calculated for these sulfides, particularly for OsS_2 and RuS_2, from total pressure measurements alone may be subject to some errors.

Vaporization Process for $Re_2S_7(c)$.—The thermal data obtained on $Re_2S_7(c)$ are consistent with the observations on the rapid decomposition of $Re_2S_7(c)$ into $ReS_2(c)$ in the 700–800°K. temperature range. Assuming that the decomposition can be represented as

$$Re_2S_7(c) \longrightarrow 2ReS_2(c) + 3/2S_2(g) \quad (9)$$

ΔH^0 at 298°K. is 67.4 kcal. mole^{-1} from the thermal experiments. Estimating the entropy of Re_2S_7 to be 48 gbs., and reasonable ΔC_p values[13,14] for eq. 9 it follows

$$-\log P_{(atm)} = \frac{14.8 \times 10^3}{T} + 2.01 \log T - 23.0 \quad (10)$$

This equation predicts $\Delta H_0^0 = 67.9$ kcal. mole^{-1} and vapor pressures of 0.01 and 3.2 mm. at 700° and 800°K., respectively, and therefore is in agreement with the chemical behavior of Re_2S_7.

TABLE IV

THERMOCHEMICAL DATA FOR SELECTED TRANSITION ELEMENT SOLID SULFIDES AT 25°[a]

Compound	$-\Delta Hf^0$ (kcal. mole^{-1})	$-\Delta Ff^0$ (kcal. mole^{-1})	S^{0b} (gbs. mole^{-1})
TcS_2	53.5	51.6	17
TcS_3	66.0	62.8	20
$TcS_{3.5}$	73.5	69.4	21
RuS	39.2	38.5	12
RuS_2[c]	47.0	44.1	12.4 (18)
RhS	37.2	36.2	12
$RhS_{1.5}$	40.8	39.9	16
RhS_2	42.5	41.1	18
PdS[c]	35.8	34.4	12
PdS_2	39.0	37.1	18
ReS_2	42.7	41.5	20
ReS_3	49.8	47.2	23
$ReS_{3.5}$	53.95	50.5	24
OsS	26.4	25.4	12
OsS_2[c]	37.4	37.2	22.3 (20)
OsS_3	42.6	40.3	23
OsS_4	48.0	44.3	26
IrS	23.0	21.7	12
$IrS_{1.5}$[c]	28.1	27.9	15.1
IrS_2[c]	31.0	31.5	25.6 (20)
PtS[c]	20.2	18.6	12.0
PtS_2[c]	26.6	24.3	17.3 (20)

[a] Underlined values are from experimental measurements. [b] In general, entropy values have been estimated from additivity rules and comparison with corresponding oxides. When experimental values have been available, the estimated value is given parenthetically, and serves to indicate the magnitude of errors involved in both the experimental determinations and estimation of the entropy. [c] From the compilation of K. K. Kelley, ref. 14; see, however, text for possible sources of error due to molecular volatilization.

Summary of Thermochemical Data.—Table IV contains a summary of the thermodynamic functions for rhenium sulfides determined in the

present research. These data also make it possible to estimate similar functions for neighboring sulfides which have not been available previously. Some other values available in the literature also have been included for convenience and reference.

Acknowledgment.—The authors are indebted to Professor Alan W. Searcy for his helpful comments on the manuscript.

NON-EQUILIBRIUM SOOT FORMATION IN PREMIXED FLAMES

BY ROGER C. MILLIKAN

General Electric Research Laboratory, Schenectady, N. Y.

Received August 17, 1961

Soot deposition has been studied in a series of large, flat, premixed ethylene–air flames burning on porous metal burners. The mixture ratios bracketed those at which soot first appears. Using combined optical and probe sampling techniques, spatially resolved measurements were made of C_2H_2, CH_4, OH, and soot concentrations as functions of burned gas temperature. It was found that acetylene and methane (in smaller amounts) are produced in the reaction zone and survive to form about 1% of the burned gas. The pyrolysis of these hydrocarbons competes with an oxidation reaction involving OH. The balance between these reactions determines whether or not soot is set free. The dark space between the reaction and soot zones is a region of high oxidizing power due to the OH concentration in excess of equilibrium. The critical mixture ratio at which soot appears is temperature dependent. This temperature dependence leads to a value of -34 ± 10 kcal./mole for the difference in activation energy between the soot oxidation and formation reactions.

Introduction

Soot formation occurs in many premixed flames when it should not—if chemical equilibrium were attained. The onset of soot deposition in certain ethylene–air flames can be observed for mixtures with a carbon to oxygen atom ratio as low as 0.58. If equilibrium prevailed, soot would not be set free until this ratio exceeded unity. That is, even though there is more than enough oxygen present to oxidize all the carbon to CO, this does not happen. Instead soot is liberated. Such non-equilibrium behavior was established by Street and Thomas[1] for premixed flames of a variety of fuels burning in air. This aspect of soot formation is but one of the puzzles[2] which adds scientific interest to a problem of obvious industrial importance.

The purpose of this work was to find an explanation for the occurrence of non-equilibrium soot deposition, and to elucidate the mechanisms involved. Theories of soot formation are many. They have been well summarized,[1,2] and will not be recounted here. The difficulty lies in the lack of sufficient experimental data on a well characterized system to limit the possibilities to one mechanism.

We have chosen for study a set of large, flat ethylene–air flames whose mixture ratios bracket those at which soot first appears. By using a combination of optical and probe sampling techniques, an experimental description of these flames has been obtained which is complete enough to severely limit speculation on the mechanisms of soot formation. A key point in the present work has been a determination of the temperature dependence of soot formation. This turned out to be an important factor which has not been recognized in earlier work.

Experimental

The flames studied were burned on porous metal burners of the type developed by Kaskan.[3] Burners used ranged from a 2.5 × 5 cm. rectangular one to circular ones 7 cm. in diameter. All were of the compound design so that the flame could be shielded from its surroundings by a sheath of N_2 gas. The use of such porous metal burners aided this work in two ways. They gave large flat flames which could be probed optically with good spatial resolution. More important is that on such burners the burned gas temperature becomes a variable independent of mixture ratio. Consequently we have been able to observe the temperature dependence of soot formation at constant over-all composition. Since the gas flow is normal to the burner at a calculable velocity, the scale of distance from the burner can be converted to a time scale. For all the flames considered here this conversion is of the order of 1 msec. per mm. Measurements have been made of burned gas temperature, C_2H_2, CH_4, OH, and soot concentrations. In addition, the critical mixture ratio at which soot luminosity appears has been determined. Most of the techniques of measurement have been described previously. The following is only a brief account of the procedures used.

A. **Apparatus.**—The ethylene was of C.P. grade. Air was supplied from a 2000 p.s.i. reservoir and compressor. Both were metered with calibrated critical flow orifice meters to within 0.5%. Details of the narrow beam optical setup have been given.[4,5]

B. **Flames.**—The ethylene–air flames used all fell within the region defined by the following ranges of these variables: mixture ratio $0.5 <$ atomic $C/O < 0.7$, linear gas velocity $7 < v_{25} < 20$ cm./sec. NTP, temperature $1600 < T < 2000°$ K. The characteristics of some of the individual flames used are given in Table I. Noted there for each flame is the atomic C/O ratio ϕ, the linear gas velocity entering the flame, v_{25}, and the maximum burned gas temperature.

C. **Temperature Measurements.**—Gas temperatures were measured in one case by a fine wire thermocouple. Such couples soon became brittle and broke when exposed to these reducing flames. Subsequent measurements were made by the sodium D-line reversal method.[4] They are believed accurate to ±50°K. Soot luminosity and scattering from even the richest of our flames were so feeble that no errors in the temperature measurements arose from that source.

D. **Concentration Measurements.**—The OH radical concentration was determined by the ultraviolet line absorption method of Kaskan.[6] Since the level of OH was low, it was necessary to pass the light beam twice through a 7 cm.

(1) J. C. Street and A. Thomas, *Fuel*, **34**, 4 (1955).

(2) A. G. Gaydon and H. G. Wolfhard, "Flames, Their Structure Radiation and Temperature," Second ed., Chapman and Hall, Ltd., London, 1960, pp. 175–209.

(3) W. E. Kaskan, "Sixth Symposium (International) on Combustion," Reinhold Publ. Corp., New York, N. Y., 1957, p. 134.

(4) R. C. Millikan, *J. Opt. Soc. Am.*, **51**, 535 (1961).

(5) R. C. Millikan, *Combustion and Flame*, **5**, 349 (1961).

(6) W. E. Kaskan, *ibid.*, **2**, 229 (1958); *J. Chem. Phys.*, **29**, 1420 (1958).

TABLE I

FLAME CONDITIONS

Atomic C/O	v_{25}, cm./sec.	T_{max}, °K.
0.583	7.0	1720
.53	19.5	1950
.663	14.0	1900
.577	11.5	1820
.607	11.6	1820
.640	11.7	1820
.673	11.7	1815
.710	11.8	1810

diam. flame to secure enough absorption for adequate measurement.

Acetylene and methane were measured at high levels in the flames by extracting samples with fine quartz probes and analyzing them with a mass spectrometer. Similar analyses for CO_2 were shown to agree with values derived from equilibrium calculations,[6] so that the probe analyses are thought to be reliable. Concurrently, measurements were made of the emission and absorption of infrared light by acetylene at 13.7 μ. The results of the probe analyses were used to calibrate the infrared method of measuring C_2H_2. The infrared method then was used to determine the spatial distribution of C_2H_2 in different flames.[5]

The soot produced has been characterized by measurements of light absorption and emission by the particles in the flames over the 4000–10,000 A. wave length range.[4] Soot deposits from the flames were studied similarly by light absorption. Particle sizes were determined by electron microscope examination of those caught on a cool target *in vacuo* after being extracted from the flame by a quartz critical flow orifice.[7,8]

The equilibrium composition for the burned gases of all our flames have been obtained from the published tables of Fremont, *et al.*,[9] using the measured values of flame temperatures.

Results

The temperature and emission profiles for flame 1 are given in Fig. 1. These are for a highly quenched flame that is just rich enough to show soot luminosity. There is a distinct dark space at 4 mm. from the burner which is bounded on one side by the reaction zone emission, and on the other side by the increasing emission of soot. Such a dark zone has been observed previously by others using flat flames.[10,11] Since it represents a delay in the deposition of soot, the dark space is an important feature of the flame which must be accounted for by any proposed theory of soot formation. It should be noted that the ordinates in Fig. 1 are different for the different species. The sensitivities for CH and soot are very great, while that for C_2H_2 is low.

The behavior of the OH radical concentration is shown in Fig. 2 for a non-luminous flame above and for a sooty flame below. The dashed lines give the calculated equilibrium OH concentrations. The equilibrium values fall off slowly due to the gradual decrease in burned gas temperature (*cf.* Fig. 1).

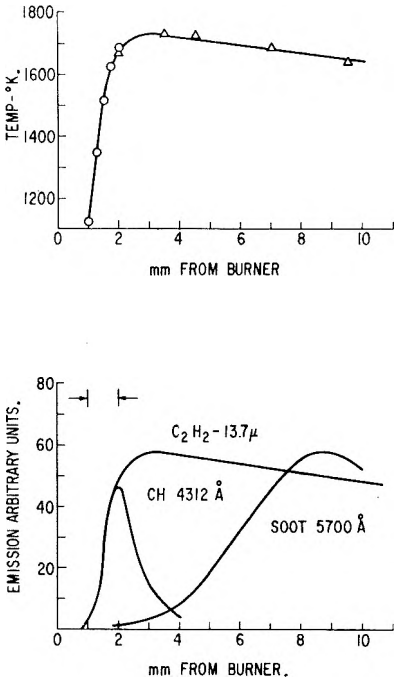

Fig. 1.—Above, temperature profile for soot forming flame 1: O, determined with a thermocouple. Δ determined by Na D-line reversal. Below, emission profiles for the same flame. The location of the lower abscissa scale is uncertain with respect to the upper one by 0.5 mm. Ordinate scale is different for each species.

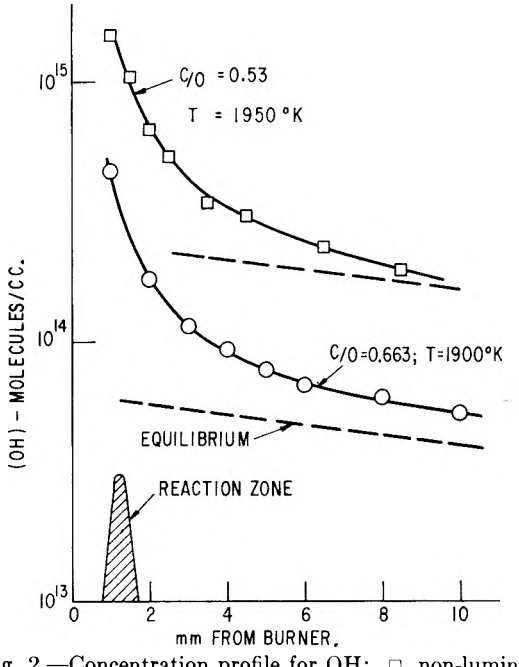

Fig. 2.—Concentration profile for OH: □, non-luminous flame 2; O, soot forming flame 3. Location of reaction zone indicated by CH emission.

The agreement between the calculated equilibrium values and the measured ones at large distances from the burner is within the experimental accuracy.

The onset of soot luminosity occurs abruptly at a reproducible mixture ratio when one begins with a non-luminous flame and gradually makes it richer in fuel. We found that this critical mixture ratio,

(7) R. C. Millikan, *J. Opt. Soc. Am.*, **51**, 698 (1961).

(8) R. C. Millikan, "Fourth Symposium on Temperature, Its Measurement and Control in Science and Industry," Vol. 3, in press, 1961.

(9) H. A. Fremont, H. N. Powell, A. Shaffer, and S. N. Suciu, "Properties of Combustion Gases, System C_nH_{2n}-Air," General Electric Company, 1955.

(10) C. P. Fenimore, G. W. Jones, and G. E. Moore, "Sixth Symposium (International) on Combustion," Reinhold Publ. Corp., New York, N. Y., 1957, p. 242.

(11) J. M. Singer and J. Grumer, "Seventh Symposium (International) on Combustion," Butterworths Scientific Publ., London, 1959, p. 559.

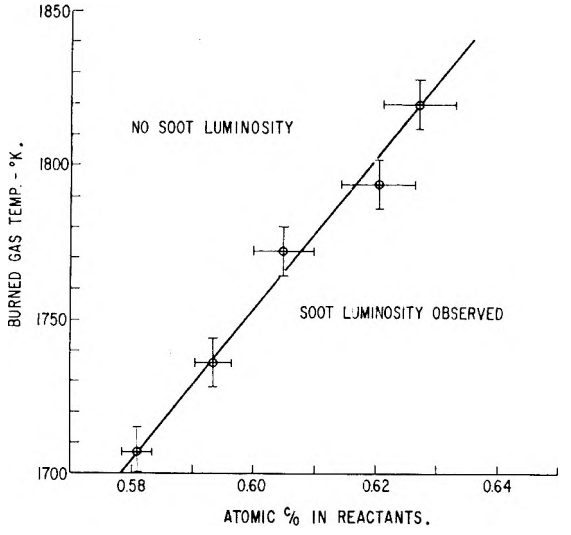

Fig. 3.—Critical mixture ratio at which soot luminosity first is observed *vs.* burned gas temperature. Ethylene–air flames on a 2.5 × 5 cm. porous plug burner.

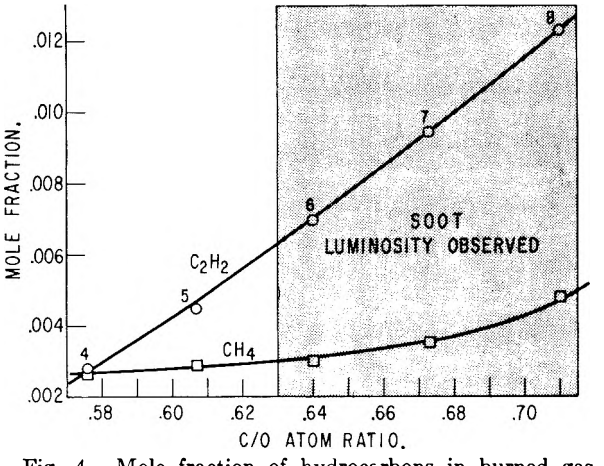

Fig. 4.—Mole fraction of hydrocarbons in burned gas against mixture ratio. Probe samples taken 12 mm. above burner. All flame temperatures between 1800 and 1820°K. O, C_2H_2; □, CH_4. Point numbers refer to the rows of Table I.

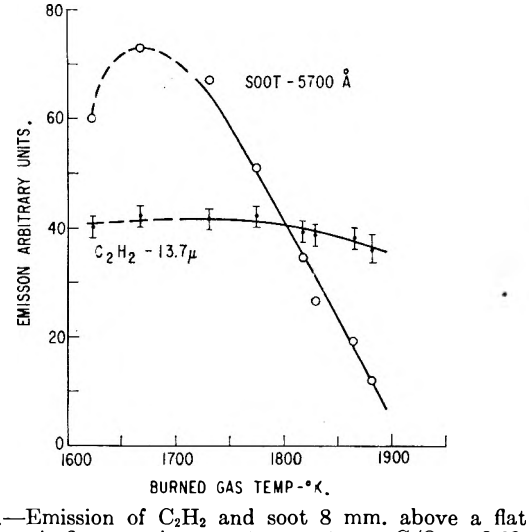

Fig. 5.—Emission of C_2H_2 and soot 8 mm. above a flat ethylene–air flame against gas temperature; C/O = 0.68.

ϕ_{CR}, at which soot deposition begins varies with the gas flow rate through the porous burner. The important variable which is being changed when the flow velocity is varied is the burned gas temperature. This temperature was determined for five of the critical ratio flames, and the results are shown in Fig. 3. The mixture ratio at which soot appears is seen to be temperature dependent. This observation should be quantitatively explained by an adequate theory of soot deposition.

The amount of acetylene and methane produced in the reaction zone and surviving into the burned gas next was measured for flames of different mixture ratios, but all with temperatures between 1800 and 1820°K. The data obtained by probe analyses 12 mm. above the burner are shown in Fig. 4. It is clear that as the mixture ratio is increased through that at which soot appears, the acetylene concentration continues to rise smoothly. The same is true of the methane, but the rise is more gradual. Other hydrocarbons were not detected by the mass spectrometer.

It is possible on the porous burner to burn a flame which shows considerable soot luminosity at low flow velocities, but which becomes non-luminous at high flow velocities, the mixture ratio being kept constant. The visible emission of soot and the infrared emission of C_2H_2 were measured 8 mm. above the burner for a set of such flames of constant composition. The data are given in Fig. 5 plotted against the measured temperature of the flames. The low temperature portions of the curves are dotted since those flames were weak and unsteady. Edge effects were more important for them, and no doubt account for the fall in soot emission for the 1625° point. The data are plotted as obtained, and have not been adjusted to account for the temperature dependence of the black body function. Were this done, the C_2H_2 curve in terms of concentration would be little affected because of the long wave length, but the soot curve would become much steeper. Evidently the acetylene concentration is little affected by the flame temperature, but the soot concentration is very sensitive to it.

The data of Fig. 2 showed that the concentration of OH was considerably above equilibrium for a short distance downstream of the reaction zone. This suggested that the dark zone might be a region in which oxidation processes still are dominant. To see if this were so, the following experiment was performed. A sooty flame similar to flame 1, which showed a distinct dark space, was lit. A one mil platinum wire was slowly lowered into the soot zone while the tip of the wire was observed through the telescope of a micro optical pyrometer. During the course of a few minutes the tip became covered with a deposit of soot. This could be distinguished because of the different emissivities of platinum and soot. The wire next was lowered until its tip extended into the dark space of the flame, but not into the reaction zone. The soot deposit on the end of the wire was seen to slowly disappear until the wire was bare. This deposition of soot in the luminous zone and its removal in the dark space could be repeated over and over. It is no wonder that soot cannot be deposited in the dark space,

whose oxidizing characteristics are made so evident in this experiment.

Discussion

We now set forth a description of the soot deposition process which qualitatively accounts for all of the observations just given. In addition, it quantitatively accounts for the data of Fig. 3 in terms of reasonable kinetic parameters for the reactions involved. Certain simplifying features of these flames should be noted first. Beyond the dark space, that is, beyond 5 mm. from the burner, thermal equilibrium prevails. This was shown in a previous paper[4] in two ways. The measured rate of temperature drop in the burned gas was shown to be that calculated for pure thermal radiation by the flame gases. Secondly, the soot particle temperature was shown to equal the gas temperature even during the deposition process. Thus the measured temperatures have a well defined meaning. There also exists in this same downstream region of the burned gases a state of partial chemical equilibrium. As can be seen from Fig. 2, the OH radical concentration has essentially reached its equilibrium level at distances beyond 5 mm. from the burner. This is likely true for the other flame radicals as well since, according to Sugden, *et al.*,[12] the flame radicals are equilibrated among themselves by rapid bimolecular reactions even in the absence of equilibration with the final products. Essentially equilibrium amounts also were found[5] for CO_2 by probe sampling of the burned gases. The species which are not at chemical equilibrium in the burned gases are the hydrocarbons acetylene and methane produced in the reaction zone, plus the soot. These species make up about one volume per cent. of the gas, and do not greatly change the concentrations of the other products.

The data of Fig. 4 show that the burned gases of these flames contain hydrocarbons, mainly acetylene and methane. The infrared emission profile given in Fig. 1 reveals that the C_2H_2 is produced in the reaction zone (well before the soot luminosity appears), and that its concentration remains relatively constant in the region of burned gas studied here. Both acetylene and methane are thermodynamically unstable with respect to carbon and hydrogen at these temperatures. Thus their thermal decomposition would account for the soot formed if two conditions are met. These are: (a) that the rate of decomposition and particle nucleation be sufficiently rapid, and (b) that there be no competing reactions such as oxidation that are fast enough to remove the soot as quickly as it forms. Condition (a) is especially relevant in view of the dark space, which represents some sort of delay in soot precipitation. Fortunately, there are recent shock tube results which are applicable to this question. Hooker[13] has measured the induction time required for carbon luminosity to appear when mixtures of 2% acetylene in argon were shocked to temperatures and pressures comparable to those reached in our flames. He finds this induction time to be less than 100 μsec. for our conditions. The residence time represented by the spatial extent of the dark space is over ten times longer than that. We therefore conclude that the dark space cannot be accounted for by induction time effects or delays in nucleation. The reproducibility of these flame profiles also argues against the supposition that nucleation effects are important.

The idea of competing oxidation reactions is the natural alternative for explaining the occurrence of the dark space. It was shown that the dark space is a region of sufficient oxidizing power to remove previously deposited soot from a wire. We attribute this oxidizing power to the concentration of OH radicals in excess of equilibrium. The data of Fig. 2 show that just downstream of the reaction zone the OH concentration is about 8 times its equilibrium value. During the space of a millimeter or two, which coincides with the dark space, the excess radicals are disappearing. Even though the CH_4 and C_2H_2 are being thermally decomposed in this region, the oxidation by the excess OH is sufficiently rapid to prevent formation of free soot. Apparently it is only after the OH concentration drops to a low value corresponding to equilibrium that the decomposition reactions dominate, and soot appears. The oxidation reaction also may involve other species such as O atoms or H_2O and CO_2 molecules. None of these, however, are likely to be as important as OH. For these rich flames the O atom concentration at equilibrium is only 10^{-4} that of OH; the O atoms constitute only 10^{-9} mole fraction of the burned gas. Oxidation of soot predominantly by H_2O and CO_2 will not account either for the dark space or the temperature dependence of soot formation. Oxidation by OH accounts for both.

To see if the mechanism just proposed gives the correct variation of the critical mixture ratio at which soot appears, ϕ_{CR}, with temperature we proceed as follows. Assume the main reactions are

$$\text{Formation: } C_2H_2 \xrightarrow{k_f} \text{Soot precursor} \longrightarrow \text{Soot} \qquad (1)$$

$$\text{Oxidation: Soot precursor} + OH \xrightarrow{k_{ox}} \text{Products} \qquad (2)$$

Then the rate of soot precursor formation is

$$\frac{dSp}{dt} = k_f(C_2H_2) - k_{ox}(OH) \qquad (3)$$

Now at the critical mixture ratio at which soot just appears, the rate of soot precursor formation may be taken as zero.

$$\left(\frac{dSp}{dt}\right)_{\phi=CR} = 0 = k_f(C_2H_2) - k_{ox}(OH) \qquad (4)$$

where ϕ represents the carbon to oxygen atom ratio fed. Thus at the critical ratio

$$(OH)_{\phi=CR} = \frac{k_f}{k_{ox}}(C_2H_2) \qquad (5)$$

or, when the rate constants are written in Arrhenius' form

$$(OH)_{\phi=CR} = \frac{A_f}{A_{ox}}(C_2H_2)\exp\left[\frac{E_{ox} - E_f}{RT}\right] \qquad (6)$$

We note that the OH concentration here is the equilibrium value, since we are concerned with whether or not soot appears well out in the burned

(12) E. M. Bulewicz, C. G. James, and T. M. Sugden, *Proc. Roy. Soc.* (London), **A235**, 89 (1956).

(13) W. J. Hooker, "Seventh Symposium (International) on Combustion," Butterworths Scientific Publ., London, 1959, p. 949.

gas at the given mixture ratio. The equilibrium OH concentration is a function of ϕ, the mixture ratio, and the temperature. By plotting the extensive data in ref. 9 we have derived an analytical function which gives the equilibrium OH concentrations for mixture ratios $0.5 < \phi_{\text{eff}} < 0.83$ and temperatures $1650 < T°\text{K.} < 2000$. This function is

$$\log (\text{OH}) = -1.54 \left(\frac{10^4}{T}\right) + 5.15 - 3\phi_{\text{eff}} \quad (7)$$

The accuracy of this representation may be judged by observing in Table II the comparison of OH values given by eq. 7 with those computed by Fremont, *et al.*[9] It is seen to fit within 20% over the range of interest. A correction to make this equation apply to our flames is required to account for the unburned hydrocarbons in the burned gas. They are not included in the tables of Fremont, *et al.* The way of making this correction has been given in ref. 5. There we defined an effective mixture ratio, ϕ_{eff}, which is arrived at by assuming that each C_2H_2 molecule and every two CH_4 molecules found in the burned gas detract from the nominal fuel–air ratio as if they were ethylene molecules. On this basis, using the gas analyses given in Fig. 4

$$\phi_{\text{eff}} = 0.5\phi + 0.26 \quad (8)$$

When this is put into eq. 7, we obtain

$$\log (\text{OH}) = -1.54 \left(\frac{10^4}{T}\right) + 5.41 - 1.5\phi \quad (9)$$

At the critical ratio, $\phi = \phi_{\text{CR}}$ and $(\text{OH}) = (\text{OH})_{\text{CR}}$. By taking the logarithm of eq. 6 and substituting for log (OH) from (9), we obtain

$$1.5\phi_{\text{CR}} = -\frac{1}{T}\left[\frac{E_{\text{ox}} - E_{\text{f}}}{2.3R} + 1.54(10^4)\right] + 5.41 - \log\left[\frac{A_{\text{f}}}{A_{\text{ox}}}(C_2H_2)\right] \quad (10)$$

Now on the basis of the data given in Fig. 5 we say (C_2H_2) is not a function of temperature. That is, all the temperature dependence is ascribed to the variation of the equilibrium OH concentration with temperature. However, (C_2H_2) is a function of ϕ as shown in Fig. 4. A little curve fitting shows that this may be represented by

$$\log (C_2H_2) = 4.63\phi - 5.17 \quad (11)$$

for our flames. When this is substituted into (10), we finally obtain an equation relating the critical mixture ratio to the temperature

$$6.13\phi_{\text{CR}} = -\frac{1}{T}\left[\frac{E_{\text{ox}} - E_{\text{f}}}{2.3R} + 1.54(10^4)\right] - \log\left(\frac{A_{\text{f}}}{A_{\text{ox}}}\right) + 0.24 \quad (12)$$

If $6.13\phi_{\text{CR}}$ is plotted against $1/T$, a straight line should be obtained whose slope leads directly to the difference in activation energies for the soot oxidation and formation reactions.

In Fig. 6 the data on the temperature dependence of the critical mixture ratio have been so plotted. A straight line is obtained whose slope gives $E_{\text{ox}} - E_{\text{f}} = -34$ kcal. Uncertainties in this figure arise from three sources. The slope determination in Fig. 6 is ±2 kcal. Possible errors in the equilibrium OH temperature dependence as given in eq. 7 account for ±4 kcal./mole. More difficult to evaluate is the accuracy of the statement that the amount of acetylene and methane produced in the reaction zone do not change with flame temperature. That this is approximately true is shown in Fig. 5. Taking ±4 kcal./mole as a reasonable uncertainty from this cause we conclude that $E_{\text{ox}} - E_{\text{f}} = -34 \pm 10$ kcal./mole.

TABLE II

MOLE FRACTION (OH) COMPUTED FROM EQUATION 7 COMPARED TO THE VALUES OF FREMONT, *et al.*[9]

ϕ_{eff} C/O atom ratio	T, °K.	(OH) Eq. 7	(OH) Ref. 9
0.583	1722	2.88×10^{-6}	2.56×10^{-6}
.583	1890	1.78×10^{-5}	1.35×10^{-5}
.667	1722	1.62×10^{-6}	1.72×10^{-6}
.667	1890	1.0×10^{-5}	9.05×10^{-6}

In order to compare this value with data from other sources we want to separate the contributions of the formation and oxidation reactions. The experimental data indicated that the oxidation reaction is probably a free radical attack of OH upon some intermediate between acetylene and soot, or upon the soot itself. If this is so then the activation energy of the oxidation reaction will be very low, and we may consider the 34 ± 10 kcal./mole as representing the activation energy of the formation reaction that produces soot from acetylene.

The pyrolysis of acetylene between 1400 and 2500°K. has been reinvestigated recently by Aten and Greene[14] using a shock tube. For the homogeneous pyrolysis of C_2H_2 in argon they find an activation energy of 39 kcal./mole. This they consider compatible with the values of earlier workers, namely 47,[15] 50,[16] and 39 kcal./mole.[13] Thus our rather indirectly deduced value is in agreement with these determinations.

We take this agreement as evidence that the mechanism advanced to account for the observed temperature dependence of the onset of soot formation succeeds quantitatively when reasonable values are used for the activation energies involved.

Relation to Previous Work.—Measurement of hydrocarbons existing in the burned gases of rich flames has been made by a number of authors.[10,11,17] To that body of data we add the direct evidence of Fig. 1 to show that the acetylene is produced in the reaction zone of the flame, well before soot formation begins. This is not a surprising result, but it is almost a necessary one if the acetylene theory of soot formation is to remain tenable.

Porter has revitalized the acetylene theory of soot formation by arguing that hydrocarbons in premixed flames would decompose to acetylene. The polymerization and simultaneous dehydration of this acetylene would then, in his view, lead to soot.[18]

Fenimore, Jones, and Moore[10] advanced the idea

(14) C. F. Aten and E. F. Greene, *Combustion and Flame*, **5**, 55 (1961).

(15) G. J. Minkoff, D. M. Newitt, and P. Rutledge, *J. Appl. Chem.*, **7**, 406 (1957).

(16) C. G. Silcocks, *Proc. Roy. Soc.* (London), **A242**, 411 (1957).

(17) P. H. Kydd, *Combustion and Flame*, **3**, 133 (1959).

(18) G. Porter, "Fourth Symposium (International) on Combustion," Williams and Wilkins Co., Baltimore, Md., 1953, p. 248.

that soot deposition is controlled by the balance between the rate of decomposition of simple hydrocarbons, and the rate of oxidation by hydroxyl. This mechanism accounted for their experimental data on the pressure dependence of the critical mixture ratio for soot formation. We have arrived at the same mechanism in studying the temperature dependence of soot formation. Their speculation that the dark space is due to the large excess of OH emerging from the reaction zone is given strong support by the experiments reported here.

Street and Thomas,[1] as part of their extensive study of carbon formation in premixed flames, determined the effect of temperature on the critical mixture ratio. They did this by preheating the mixture going to the burner. Their result was that "increasing temperature allows somewhat richer mixtures to be burned without producing carbon, but the effect is not marked." Since the markedness of the temperature dependence is important to this paper, let us consider it further. For 400° of preheat Street and Thomas found the critical air–fuel ratio (by weight) to decrease from 10.0 to 8.6 for propane–air flames. In terms of the units used here this is a change in the C/O atom ratio from 0.47 to 0.55. It should be remembered, however, that the heat capacity of the burned gas is about 1.5 times that of the original mixture. Consequently, 400° of preheat causes a change in burned gas temperature of about 270°. On this basis we deduce that Street and Thomas observed a change in the critical C/O atom ratio of 0.03 unit per 100° change in burned gas temperature. This rate of change is in agreement with our data shown in Fig. 3.

In previous studies, when the carbon forming tendencies of flames of various fuels have been compared, the final temperatures reached usually have not been controlled or determined. The work given here suggests this temperature may be one of the more important variables. For instance, Street and Thomas found that carbon could be obtained from ethane–air flames much leaner relative to the stoichiometric carbon point than was possible for acetylene–air flames. This was taken as evidence against the acetylene theory of soot formation. Yet their flames were nearly adiabatic, so that the acetylene–air flame was hotter. This means mainly that the OH oxidation reactions were faster in that flame, and that no information about relative isothermal soot formation tendencies can be had from such a comparison.

Conclusions

1. The hydrocarbons found in the burned gas of rich flames in amounts in excess of equilibrium are produced in the reaction zone, well before the region of soot deposition.

2. The dark space lying between the reaction zone and the soot zone is an oxidizing region due to the concentration of OH in excess of equilibrium.

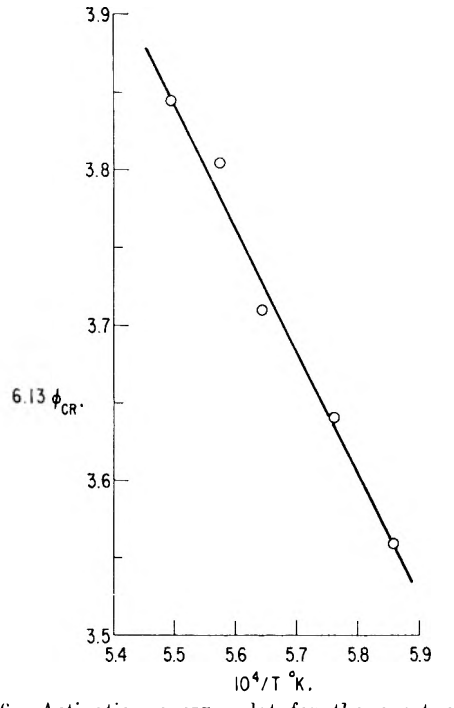

Fig. 6.—Activation energy plot for the onset of soot formation. ϕ_{CR} is the critical C/O atom ratio at which soot first appears.

3. Non-equilibrium soot formation results from thermal decomposition of the acetylene and, to a much lesser extent, the methane produced in the reaction zone. This pyrolysis is opposed at some stage by an oxidation reaction involving mainly OH as the oxidizer. It is the balance between these two reactions which determines whether or not soot is set free.

4. The critical mixture ratio at which soot first is observed is temperature dependent. With certain assumptions, this temperature dependence leads to a value of 34 ± 10 kcal./mole for the activation energy of the soot deposition reaction. This is in agreement with shock tube results on the pyrolysis of acetylene–argon mixtures.

5. Care must be used in drawing valid conclusions about the mechanism of soot formation by comparing the sooting tendencies of flames of different fuels. Different flame temperatures are encountered in such comparisons, but this usually has been ignored. The temperature, in fact, is one of the more important variables determining the balance between the pyrolysis and oxidation reactions.

Acknowledgment.—Much of the experimental work was performed by W. I. Foss. G. W. Jones helped with the mass spectrometer analyses. The author is grateful for discussions with G. E. Moore, W. E. Kaskan, C. P. Fenimore, and P. H. Kydd concerning this work.

HYDROXYL CONTENT IN SILICA GEL "AEROSIL"

BY J. J. FRIPIAT AND J. UYTTERHOEVEN

Laboratoire des colloides (I.N.E.A.C.) et de Chimie Minérale, Agronomic Institute of the University, Heverlee, Louvain, Belgium

Received August 24, 1961

Changes in the hydroxylic surface of silica gel as a function of temperature are studied by different techniques. From the comparison between infrared data and thermogravimetric determination, a distinction can be clearly made between constitution and adsorbed water. New chemical methods for the determination of surface hydroxyls also are described, using the reaction either with CH_3MgI or CH_3Li and volumetric measurement of the CH_4 evolved. The discussion and interpretation of the results collected from physical and chemical methods permit the distinction between adsorbed water, inner hydroxyls, and surface hydroxyls.

I. Introduction

The relative distribution of the two classes of hydroxyls in silica gels, one corresponding to physically adsorbed water and the other to constitution hydroxyls, never has been completely resolved. Thermogravimetric or differential thermal analysis does not permit the distinction since, upon heating silica gels, a continuous loss of water occurs over a large temperature range.

Infrared spectroscopy gives considerably more information: the H_2O deformation band around 6 μ and the –OH stretching vibration in the 3 μ region do not overlap but water hydroxyls contribute to the intensity of the last one and the separation between inner and surface hydroxyls is not easy.

The diborane technique allows, according to Shapiro and Weiss,[1] and Naccache and Imelik,[2] the distinction between hydroxyls and adsorbed water by studying the hydrogen/diborane ratio as a function of the outgassing temperature. Their assumption is based on the fact that, following the increase in the distance between hydroxyls, this ratio will change from two to one. However, whether hydroxyls in close proximity will behave as water molecules or not is still open to question. These authors found that a portion of the hydroxyls are located inside the gel particles.

The objective of this paper was to combine infrared and chemical determinations in order to distinguish adsorbed water from constitution hydroxyls and, by a new method, to separate inner and surface hydroxyls.

The basis of the chemical technique was to use OH^- specific organometallic reagents. Zugaeff and Zerewitinoff[3] were the first to make use of methylmagnesium iodide (CH_3MgI), while Gilman, Benkeser, and Dunn[4] proposed methyllithium (CH_3Li), in which the stronger ionic character of the carbon–metal bond increases the reactivity. In both cases, reaction with water or hydroxyls occurs as

$$H_2O + MCH_3 \longrightarrow CH_4 + MOH$$

or

$$\equiv Si{-}OH + MCH_3 \longrightarrow \equiv SiOM + CH_4$$

M represents either MgI or Li.

Deuel[5] was the first to propose the application of methylmagnesium iodide to the quantitative determination of surface hydroxyls in clays by volumetric measurement of methane.

Fripiat, Gastuche, and Uytterhoeven[6] published a comparison of data obtained for kaolinite from isotopic exchange and by an organometallic reaction.

II. Experimental

(1) **Sample.**—Aerosil "Degussa" was used for this research. It is a high purity silica gel, prepared by flame-hydrolysis of $SiCl_4$. The B.E.T. surface area amounts to 180 $m.^2\ g.^{-1}$. Granulometric distribution, as given by the maker, shows a sharp maximum for a diameter of 20 μ. The surface distribution as a function of the average pore radius is given in Fig. 1, according to the Pierce[7] method. Even the narrower pores allow an easy accessibility of the whole surface to both kinds of organometallic molecules.

Films suitable for infrared study were made by spreading 20 to 40 mg. of the gel between two polished steel blocks. Pressing under about 2000 p.s.i. for 5 min. produces a film, weighing 10 to 20 $mg./cm.^2$, coherent enough to permit careful handling.

(2) **Chemical Device.**—The control of the sample hydration level is absolutely necessary: for this reason a device was built in order to allow preparation of sample and reagent under vacuum. It is represented in Fig. 2.

Samples were dehydrated in furnace 1 under vacuum at a given temperature. This operation requires about 15 hr., down to a residual pressure of 10^{-5} mm. The stopcock between I and II is closed and reagent is introduced into vessel II and outgassed for half an hour. The sample is introduced in vessel II by withdrawing the magnetic rod supporting the sample holders in furnace I. A good mixing is obtained with a magnetic stirrer. The methane is purified by distillation at low temperature in 3a and 3b, trapped in 3c, according to a technique proposed by Coppens,[8] and introduced in volumetric vessel 5 by means of a Töpler pump 4.

Mass spectrometric analysis has confirmed the purity of methane collected. Averaged results for several analyses were the following: 99.30% of CH_4; 0.44% N_2; 0.15% O_2; 0.11% C_2 hydrocarbons.

(3) **Reagents.**—CH_3MgI was easily produced by mixing CH_3I and Mg in anisol; its concentration is about 0.2 mole $l.^{-1}$.

CH_3Li is obtained in diisoamylic ether by mixing Li and CH_3I, added progressively with good stirring and under nitrogen atmosphere. A concentration of about 0.2 mole $l.^{-1}$ was obtained.

(4) **Infrared Spectroscopy.**—The thin film is carefully inserted in a copper block having a rectangular hole 2 × 1 cm. The film was held in place by a thin platinum screen. The block, containing a heating wire and a thermocouple, can be introduced in a vacuum cell, the design of which

(1) J. Shapiro and H. G. Weiss, *J. Phys. Chem.*, **57**, 219 (1953); H. G. Weiss, J. A. Knight, and I. Shapiro, *J. Am. Chem. Soc.*, **81**, 1823 (1959).

(2) Cl. Naccache, J. François-Rosetti, and B. Imelik, *Bull. soc. chim. France*, 404 (1959); Cl. Naccache and B. Imelik, *ibid.*, 553 (1961).

(3) V. Grignard, G. Dupont, and R. Locquin, "Traité de Chimie Organ.," Tome V, Masson et Cie., Paris, 1937.

(4) H. Gilman, R. A. Benkeser, and G. E. Dunn, *J. Am. Chem. Soc.*, **72**, 1689 (1950).

(5) H. Deuel and G. Huber, *Helv Chim. Acta*, **34**, 1697 (1951).

(6) J. J. Fripiat, M. C. Gastuche, and J. Uytterhoeven, *Pédologie*, **7**, 39 (1957).

(7) C. Pierce, *J. Phys. Chem.*, **57**, 149 (1953).

(8) L. Coppens, *Bull. soc. chim. Belg.*, **43**, 335 (1934).

has been given elsewhere.[19] The spectra can be recorded either under vacuum or at atmospheric pressure. Infrared spectra were obtained using a Beckman IR4 double beam, fitted with CaF_2 optics.

Two spectral regions were covered: the first around 2.8 μ for the OH stretching band and the second one around 6.1 μ for the H_2O deformation band. In this region, a harmonic of a SiO vibration could be expected, according to Little and Mathieu.[9] Tatlock and Rochow[10] have shown that absorption at 6.1–6.2 μ appears in molecules where a silicon atom carries two hydroxyls but the same band—even more intense—is observed for the corresponding disodium salts. Moreover, from theoretical considerations of the expected frequency of the $Si\langle^{OH}_{OH}$ deformation, it may be concluded that geminal hydroxyl pairs carried by silicon cannot produce an absorption band in the frequency range where the water deformation band is found.

III. Theoretical Basis

1. Infrared Determinations.—Let I be the integrated intensity of either considered band

$$I = \int_{\nu_1}^{\nu_2} A_\nu \, d\nu \qquad (1)$$

where A_ν is the absorbance at the frequency ν.

We will prove that the Beer–Lambert law is obeyed, but radiation loss by scattering must be taken in account. If X represents the individual OH belonging to the gel and Y the water molecules physically absorbed, the total hydroxyl content N is given by

$$N = X + 2Y \qquad (2)$$

Therefore

$$I_3 = k_3 l N - A_3 \qquad (3a)$$

and

$$I_6 = k_6 l Y - A_6 \qquad (3b)$$

Where k_3 and k_6 are the absorption coefficients, l the optical path through the sample, A_3 the scattering loss in the 3 μ region, and A_6 the scattering loss in the 6 μ region plus the absorbance due to an eventual SiO harmonic. I_3 and I_6 are obtained by graphical integration of the curve of absorbance *vs.* wave number. They are measured at different temperatures, in other words, at different OH and H_2O contents, and can be compared with gravimetric determinations.

From (2) and (3), we may write

$$N \frac{I_6}{I_3^*} = \frac{k_6}{k_3} Y - \frac{A_6}{k_3 l} \qquad (4)$$

Where $I_3^* = I_3 + A_3$. A_3 is calculated from extrapolation to $N \rightarrow 0$ of the linear plot I_3 *vs.* N, N being known from gravimetric determinations (Fig. 3). Let us write formally the differential of (2) and (3) with respect to N. The optical path l is equal to $(1/k_3)(dI_3^*/dN)$ and

$$2 \frac{k_3}{k_6} \left(\frac{dI_6}{dN}\right) \Big/ \left(\frac{dI_3^*}{dN}\right) = 1 - \frac{dX}{dN} \qquad (5)$$

If we consider a *theoretical rehydration process*, X will reach slowly a constant value when N increases, since the surface becomes saturated in hydroxyls. Therefore, by measuring the derivatives dI_6/dN and dI_3^*/dN at the beginning of the dehydration process of a saturated gel, the ratio of absorption coefficients k_3/k_6 is given by (5), assuming $dX/dN = 0$.

It follows that, in relationship 6 written as

$$N \frac{k_3}{k_6} \left(\frac{I_6}{I_3^*}\right) = Y - \frac{A_6}{k_6 l} \qquad (6)$$

the first member contains known values only. If plotted against temperature, it will decrease until reaching the $A_6/k_6 l$ constant level. This ratio is graphically determined. Introduced in (6), Y is calculated in the range of temperature where physically adsorbed water exists upon the surface. When it disappears, N is equal to X according to relationship 2.

In this way, hydration water and hydroxyls can be distinguished and estimated. The main implicit approximation involves assuming k_3 constant whatever the kind of hydroxyls included in the band.

(2) Chemical Determinations.—Reactions between organometallic molecules and hydroxyls proceed fundamentally in two steps. The first one is characterized by a very rapid methane evolution which becomes much slower during the second step. In this case, the amount of gas collected increases linearly with time. We believe that the

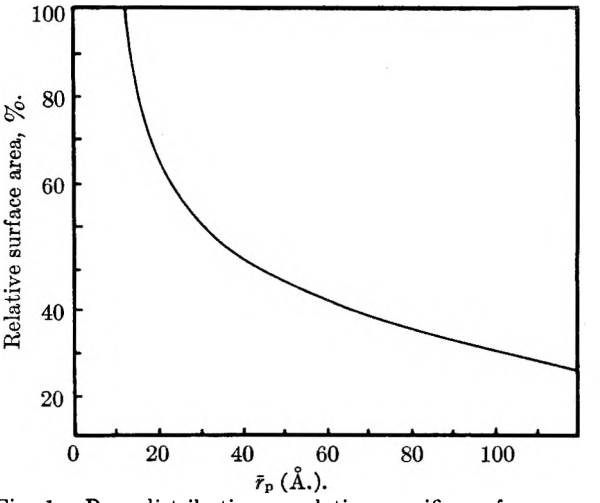

Fig. 1.—Pore distribution: relative specific surface area developed by pores with radii wider than $\bar{r}_p$ (in Å.).

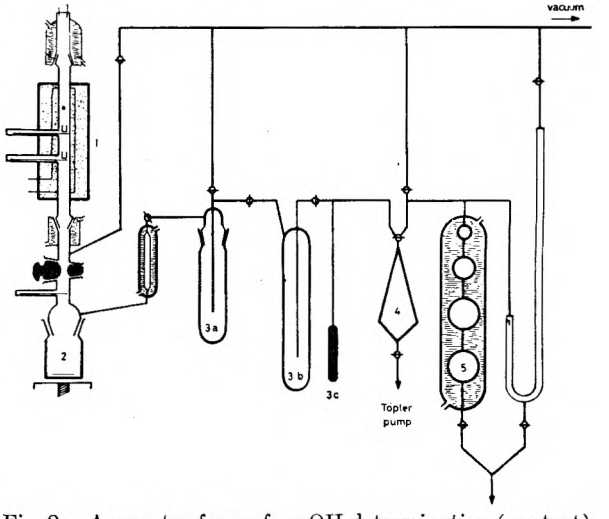

Fig. 2.—Apparatus for surface OH determination (see text).

(9) L. H. Little and M. V. Mathieu, *Actes, II Intern. Congr. Catalysis, Paris*, **1**, 771 (1961).

(10) W. S. Tatlock and E. G. Rochow, *J. Org. Chem.*, **17**, 1555 (1952).

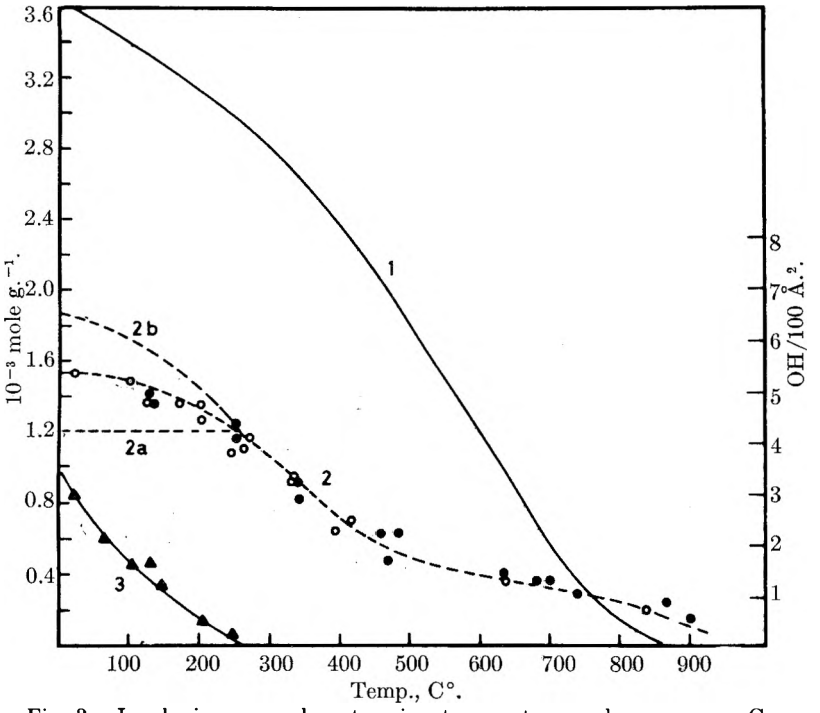

Fig. 3.—In abscissa: sample outgassing temperature under vacuum. Curve 1, OH (gravimetric) content (including H_2O); curve 2, evolved CH_4 for the reaction with CH_3Li (○) and CH_3MgI (●); curve 2a, correction for physically adsorbed water (see text); curve 2b, true OH surface content; curve 3, H_2O content (in OH) as determined by infrared.

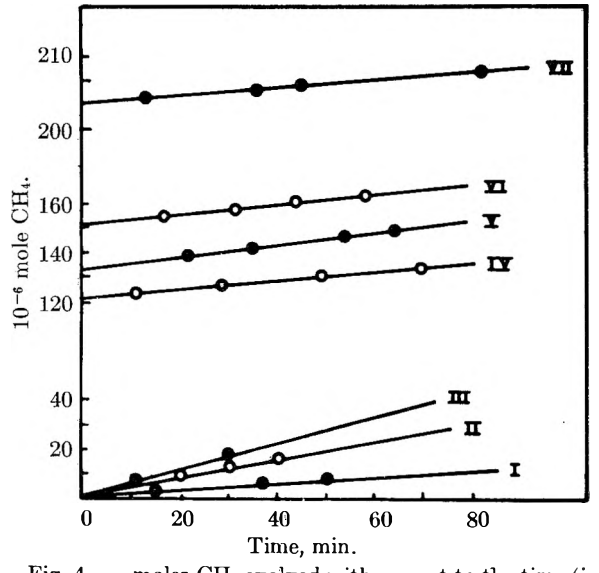

Fig. 4.—μ-moles CH_4 evolved with respect to the time (in min.): I, autolysis of CH_3MgI; II and III, autolysis of CH_3Li; IV, V, VI, and VII, reaction with increasing amounts of β-naphthol (see Table I).

first step characterizes the reaction with hydroxyls belonging either to water or surface hydroxyls and the second an autolysis of the reagent.

In order to prove this hypothesis the amount of methane produced during the reaction with β-naphthol was measured. Results are reproduced in Fig. 4.

Extrapolation of the linear plot to the ordinate axis gives figures in close relation with expected ones, as shown in Table I.

This graphical procedure thus was used for the silica gel study.

The apparatus does not allow the kinetic study of the first step: it is impossible to measure volumetrically the CH_4 produced within the first 10 min., and beyond this limit the first step is over.

As far as reagent autolysis is concerned, opinions differ widely according to experimenters[11-13] but they agree in concluding that decomposition compounds contain mainly C_2 hydrocarbons. This seems in contradiction with our mass spectrometer measurements. L. A. Wood[14] observed some methane evolution from methyl derivatives of Li and Mg. He considers a possible uptake of hydrogen from ether molecules, used as solvent. With triphenylmethane and anisol, methyllithium reacts either with hydrogen located in the *ortho* position of the aromatic ring or directly with the methane hydrogen.

In our experiments, the spontaneous CH_4 evolution during the second step amounted to 0.3 mole

TABLE I

REACTION OF ORGANOMETALLICS WITH β-NAPHTHOL

Run	Introduced amt. (μmoles)	CH_4 evolved (μmoles)	Reagent
IV	118	121	CH_3Li
V	124	133	CH_3Li
VI	154	153	CH_3Li
VII	192	201	CH_3MgI

min.$^{-1}$ at 20° in the usual concentration range, about 0.2 mole l.$^{-1}$. As compared with the first step, errors due to autolysis accounted for a few per cent. only.

IV. Experimental Results

(1) **Chemical Determinations.**—Experimental results are gathered in Fig. 3. It may be observed that both organometallic derivatives give the same results. This suggests the absence of steric hindrance since the radii of CH_3MgI and CH_3Li molecules are very different. In close packing, the MgI radical covers about 17 Å. The solvation also must be considered, CH_3MgI forming a very stable "dietherate" complex. However, results obtained with this reagent using anisol or isoamyl ether as solvent do not differ.

The pore size distribution in aerosil allows probably a complete accessibility of the whole surface.

(2) **Infrared Determinations.**—When silica gel films are heated, it is well known that the OH stretching band in the 3 μ region changes ap-

(11) W. H. Carothers and D. D. Coffman, *J. Am. Chem. Soc.*, **51**, 588 (1929); **52**, 1254 (1930).
(12) E. Wiberg and R. Bauer, *Chem. Ber.*, **85**, 593 (1952).
(13) A. H. Haubein, *Iowa State Coll. J. Sci.*, **18**, 48 (1943).
(14) L. A. Wood, *ibid.*, **19**, 67 (1944).

preciably. The low frequency OH, corresponding to strongly hydrogen bonded hydroxyls disappears before the high frequency OH, from the weaker hydrogen bridges.

Young,[15] Sidorov[16], Zhdanov,[17] and Kiselev and Lygin[18] already have observed this fact. In favorable conditions three components at least may be distinguished: isolated OH are responsible for the 3750 cm.$^{-1}$ band, hydrogen bonded hydroxyls for the 3660 cm.$^{-1}$ component, and adsorbed water for the low frequency one, at 3456 cm.$^{-1}$.

In the OH range, the distinction is not very clear but it appears clearly in the OD region according to Fripiat, Gastuche, and Brichard.[19]

From the study of the OD stretching, they were able to calculate the relative OD contents corresponding with the three main absorption peaks observed in this spectral range. In Table III, these figures are compared with the ones obtained by the method under discussion. The two independent sets of measurements can be considered in accord despite the poor distinction of the three main stretching characteristics.

The intensity of the H_2O deformation band at 6 μ decreases regularly with increasing temperature.

Figure 5 gives, for different film weights, the variation in the ratio $I_3^*(T^0)/I_3^*(20°)$ against the $N(T^0)/N$ (20°) ratio. The linearity of the experimental results verifies relationship 3a. The k_3/k_6 ratio was calculated for six experiments, run with six different films. The mean value amounts to 14.8 ± 0.9.

Table II contains the OH (X) and H_2O (Y) contents, calculated according to the theory given above (relationship 6), taking into account the experimental gravimetric content of Fig. 3. At temperatures higher than 300°, adsorbed water has completely disappeared.

As soon as the H_2O (Y) content is known, experimental curves of Fig. 3 may be corrected since, when reacting with organometallics, a water molecule accounts for one hydroxyl only (see Fig. 3).

TABLE II

WATER (Y) AND HYDROXYL CONTENT (X) FROM INFRARED DETERMINATIONS (IN 10^{-3} MOLE G.$^{-1}$)

Under vacuum			At atm. pressure		
Temp. (°C.)	Y	X	Temp. (°C.)	Y	X
20	0.42	2.76	25	1.56	2.78
60	.30	2.90	60	0.942	2.92
100	.23	2.75	100	.44	3.10
140	.17	2.96	140	.24	2.97
200	.06	3.03	200	.10	2.95
240	.03	2.94			
Av. hydroxyls content: 2.89 (below 300°)			Av. hydroxyls content: 2.94 (below 300°)		

(15) G. I. Young, *J. Colloid Sci.*, **13**, 67 (1958).

(16) A. N. Sidorov, *Optics and Spectroscopy*, **8**, 424 (1960).

(17) S. P. Zhdanov, *Zhur. Fiz. Khim.*, **32**, 669 (1958).

(18) A. V. Kiselev and V. I. Lygin, *Colloid J.*, **21**, 561 (1959); *Proc. Sec. Intern. Congr. Surface Activity, London*, II, 1957; A. V. Kiselev, 10th Colston Symposium, Butterworths, London, 1958, p. 210.

(19) J. J. Fripiat, M. C. Gastuche, and R. Brichard, *J. Phys. Chem.*, **66**, 805 (1962).

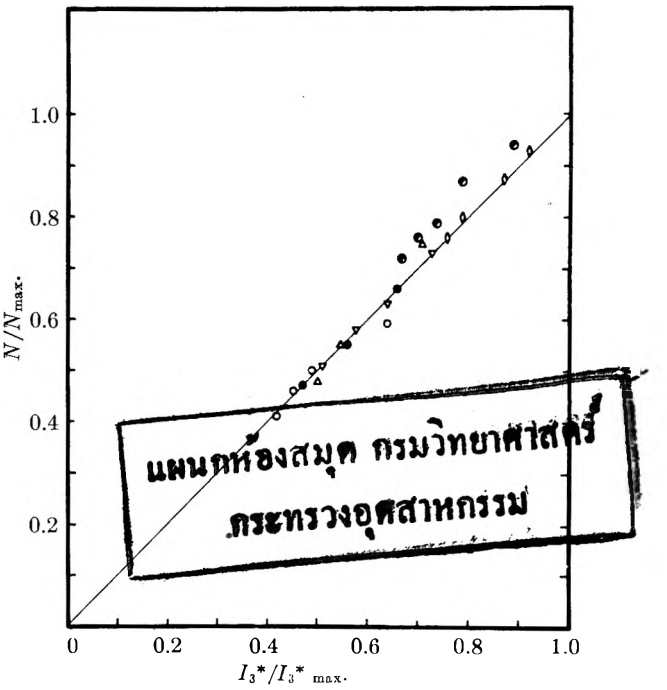

Fig. 5.—$I_3^*(T°)/I_3^*(20°)$ plotted against $N(T°)/N(20°)$ for different film weights: ○, 22.2 mg.; ●, 21.2 mg.; ▽, 27.5 mg.; △, 24.5 mg.; ◇, 28.6 mg.; ●, 27.8 mg. per cm.^{2}.

TABLE III

COMPARISON BETWEEN Y AND X OBTAINED FROM RELATIONSHIP 6 AND THE CORRESPONDING VALUES CALCULATED ON THE BASIS OF THE OD ABSORPTION BAND[19] (Y OR X IN 10^{-3} MOLE G.$^{-1}$ AT ATMOSPHERIC PRESSURE)

Temp., °C.	Y	D_2O	X	Isolated OD + deuterium bonded deuteroxyls
25	1.56	1.27	2.78	3.37
60	0.94	0.83	2.92	3.13
90	.44	.54	3.10	2.97
140	.24	.34	2.97	2.76
200	.10	.18	2.95	2.67

The averaged hydroxyl contents measured under vacuum or at atmospheric pressure agree very well and may be considered as constant below 300°. Beyond this limit, X becomes confounded with N (gravimetric), since $Y = 0$.

Since corrected results for organometallics and gravimetric curves do not coincide, it may be concluded that only a portion of the hydroxyls is located on the surface.

The ratio of surface hydroxyl to total hydroxy content can be estimated from the ratio $[(CH_4) - Y]/X$, where (CH_4) represents evolved methane. Calculated values are expressed with respect to temperature in Fig. 5.

The ratio is constant and approximately equal to 42% below 240°. Above this limit, it decreases and reaches a minimum at about 500°, afterwards it increases sharply up to 100%. O'Reilly,[20] from n.m.r. determinations, has shown that above 500° residual protons in silica gel belong to isolated and randomly distributed silanols.

(20) E. D. O'Reilly, Am. Chem. Soc. National Meeting, Boston, April, 1959, Abstracts, p. 157.

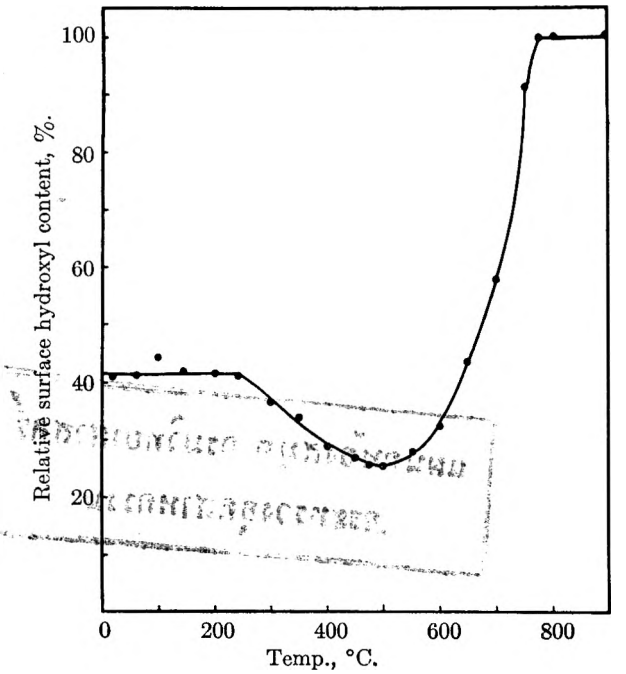

Fig. 6.—Relative surface hydroxyl content as a function of outgassing temperature.

V. Discussion

de Boer, *et al.*, have shown from adsorption isotherms that physical adsorption of water vapor on silicas ceases at temperature above 120°.

The results of Table II demonstrate that individual water molecules still exist beyond this limit.

The main argument which supports this viewpoint is that either *under vacuum* or at *atmospheric pressure*, numbers of water molecules represented by the *Y* values of Table II reach zero simultaneously at approximately 300°. On the other hand it seems that the intimate structure of silica gels affects the temperature of removal of adsorbed water. The same argument holds for the distribution of constitution hydroxyls.

Young,[14] by infrared, and Shapiro and Weiss[1] and Naccache and Imelik,[2] from the diborane technique, arrived at the conclusion that a part of the hydroxyl content must be located inside the primary particles. From their results, it follows that the nature of the gel has a deep influence. In Table IV, we compare our results with those found by others and indicate also the critical temperature range beyond which the removal of *individual* water molecules is completed.

The data obtained from infrared spectra agree satisfactorily with the observations of Naccache and Imelik.[2]

TABLE IV

RELATIVE SURFACE HYDROXYL CONTENT AS A FUNCTION OF TEMPERATURE

Gel	Ref.	Temperature 155°	400°	750°	Critical temp. range, °C.
Xerogel	1	73%	..	100%	...
Xerogel	2	68%	95%	...	300–400
Aerogel	2	48%	93%	...	300
Aerosil	This work	42%	30%	90%	300

In order to compare our results concerning hydroxyl distribution with those of others, the physically adsorbed water must be taken into consideration. In our calculations, it has been discarded as indicated. This was not done for the data of the other authors cited in Table IV. Since only temperatures higher than 155° are used, errors should not be very considerable. It follows that Aerogel and Aerosil have a low relative surface hydroxyl content as compared with Xerogel.

At the right side of Fig. 3, a OH surface density scale has been drawn, taking into account the B.E.T. surface area. It may be observed that the hydroxyl packing below 300° amounts to 4.2 units per 100 Å.^{2}. de Boer and Vleeskens,[21] when dehydrating and rehydrating silica gels several times, have shown the maximum OH density never exceeds 4.6 units per 100 Å.^{2}. Aerosil, by the preparation used here, presents a close analogy with the gels studied by de Boer and Vleeskens. Stöber,[22] from structural considerations, proposes 4.4 OH per 100 Å.^{2} as a theoretical value for the surface hydroxyl density; experimentally he found 3.75 for aerosil. Our result agrees very well with predicted surface density and confirms indirectly the hypothesis previously exposed.

Iler[23] estimated, from a structural analogy between silica gel and cristobalite, the OH surface density to be equal to 7.85 OH groups per 100 Å.^{2}, while Dzisko *et al.*,[24] proposed 6.70 OH per 100 Å.^{2}. It is probable that surface density for xerogels tends toward this value while aerogels, or aerosil, are characterized by a lower surface density, closer to the value proposed by Stöber, *i.e.*, 4.4 OH/100 Å.^{2}. In the first case, a high percentage of surface silicon is bonded to two hydroxyls, in the second one the average ratio (OH/Si) would be closer to one.

Naccache and Imelik,[2] Bastick,[25] and Young[15] observe that the sintering temperature of an aerogel is lower than for a xerogel (500° against 700°). It generally is accepted that sintering results from condensation of OH groups belonging to different primary particles followed by siloxane-bridge formation. The change of the relative hydroxyl content of the surface with respect to temperature (Fig. 6) suggests, however, another interpretation. Between 300 and 500° dehydroxylation takes place by condensation of surface hydroxyls, as indicated by the decrease of the relative OH surface density. At higher temperature, diffusion of inner hydroxyls toward the surface becomes very important. At the same time, sintering occurs and it may be that it is the diffusion of inner constitution water rather than the condensation of OH belonging to different particles which is at the origin of the phenomenon. The diffusion of internal water may greatly modify the gel structure. This hypothesis needs further investigation.

(21) J. H. de Boer and J. H. Vleeskens, *Koninkl. Ned. Akad. Wetenschap. Proc.*, **B61**, 3 (1958).

(22) W. Stöber, *Kolloid-Z.*, **145**, 17 (1956).

(23) R. K. Iler, "The Colloid Chemistry of Silica and Silicates," Cornell Univ. Press, Ithaca, N. Y., 1955.

(24) V. A. Dzisko, A. Vishneskaja, and V. S. Chesalova, *Zhur. Fiz. Khim.*, **24**, 1416 (1950).

(25) J. Bastick, *Bull. soc. chim. France*, **20**, 437 (1953); *Chim. & Ind.* (Paris), **78**, 9 (1957).

The experimental results presented here also may contribute to the knowledge of water absorption sites on silica gel surfaces. Sidorov[16] and Zhdanov[17] published experimental evidence that hydroxyl pairs (as opposed to isolated OH) may be the main adsorption sites, but they define "sites of second kind" as oxygen from siloxane bridges. Young[15] does not distinguish between hydroxyls and considers the silanol radical as the water adsorption site. Kiselev and Lygin[18] emphasize the importance of hydroxyl pairs resulting in the formation of the "ring" structure.

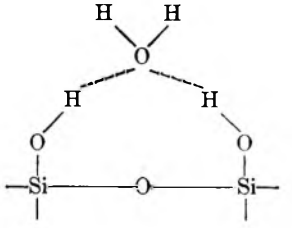

Between 20° and 250–300°, the amount of surface hydroxyls (Fig. 3, curve 2a) remains constant and equal to 1.2×10^{-3} mole g.$^{-1}$. If each water molecule is held by two hydroxyls, the surface provides a maximum of 0.6×10^{-3} mole g.$^{-1}$ adsorption sites. On the other hand, a primary adsorbed molecule can act as a center for further condensation.

Table II gives the amounts of adsorbed water either under vacuum or at atmospheric pressure. By assuming that under vacuum, "primary" molecules only subsist, it may be concluded that the amount of physically adsorbed water does not exceed the possibilities offered by hydroxyl pairs but remains far below the theoretical value given for isolated hydroxyls. This is not presented as a direct argument for Kiselev and Lygin's model but as an indication favorable to it.

Fripiat, Gastuche, and Brichard,[19] by isotopic exchange, have given more direct evidence which agrees with this viewpoint. Young[15] has shown that after silica gel has been activated at a temperature higher than 650°, rehydration produces a OH stretching absorption band where the shoulder at 3456 cm.$^{-1}$, attributed to water hydroxyls, decreases in intensity and finally disappears under vacuum. The thermal activation beyond 650° causes the surface available for water to decrease simultaneously.

Results given in Table III show that the intensity of adsorption at 3460 cm.$^{-1}$ follows approximately the evolution of the water content (Y) and disappears completely only above 300°.

Young's results may be explained on the basis that the activation procedure eliminates the more powerful adsorption sites.

SURFACE HETEROGENEITY IN SILICA GEL FROM KINETICS OF ISOTOPIC EXCHANGE OH–OD

By J. J. Fripiat, M. C. Gastuche, and R. Brichard

Laboratoire des colloïdes (I.N.E.A.C.), Institut Agronomique, Université de Louvain, Héverlé-Louvain, Belgium

Received November 2, 1961

The heterogeneity of the hydroxylic surface of a silica gel is demonstrated by following the isotopic exchange OH–OD by infrared spectroscopy using the three main components of the stretching vibration band. The first-order law is obeyed but the rate constants—which can be measured separately—differ according to the OH species. These are introduced in the Marcus relationships assuming limitative models in order to decrease to three the number of transport coefficients. The nature of the hydroxylic surface and the values of the first-order constants permit the use of the most likely diffusion model as

vapor phase → bridged hydroxyls → isolated hydroxyls
bridged hydroxyls → adsorbed water

The privileged location in this sequence of the bridged hydroxyls probably comes from the fact that they constitute the main adsorption sites.

I. Introduction

Several studies dealing with surface heterogeneity have been published during recent years.

Isotopic exchange has been widely used in order to investigate the number of different adsorption sites present at the solid–gas interface.[1] Generally, the change of isotope atomic fraction x in the gas phase is followed in function of the time t. For homogeneous surfaces, a first-order law in the distance from equilibrium is observed. For heterogeneous ones, this must be replaced by a sum of exponentials such as

$$1 - \frac{x}{x^\infty} = \sum_{i=1}^{i=n-1} A_i e^{-a_i t} \qquad (1)$$

where x^∞ represents the equilibrium value in the gas phase; i, the index number of the different site classes; $(n - 1)$ site classes being present in the solid phase, and finally A_i and a_i are kinetic constants.

When observing the gas phase only, the development of the experimental function $(1 - x/x^\infty)$ into $(n - 1)$ exponentials is only theoretical, because, in the most favorable case, the resolution does not allow the calculation of $[n + (n/2)(n - 1)]$ unknown coefficients since $2(n - 1)$ parameters only are given.[2] Hence, it becomes necessary to make a limitative choice among the possible exchange processes in order to decrease the number of unknowns.

Sheppard and Householder[3] have studied the

(1) G. Z. Roginsky, *J. chim. phys. U.R.S.S.*, **4**, 737 (1958).

(2) W. K. Hall, private communication.

(3) C. W. Sheppard and A. S. Householder, *J. Appl. Phys.*, **22**, 510 (1951).

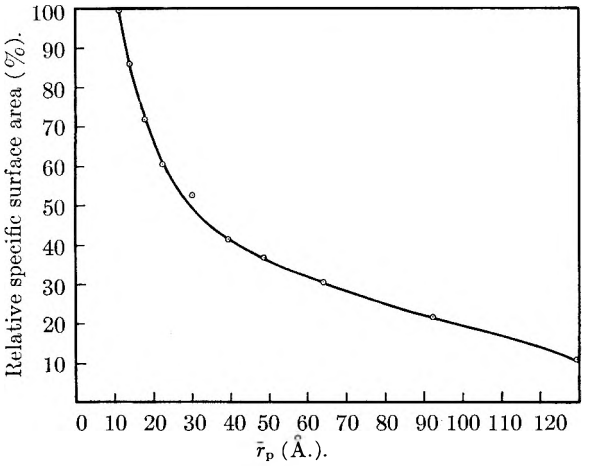

Fig. 1.—Pore distribution: relative specific surface area developed by pores with radii wider than $\bar{r}_p$ (in Å).

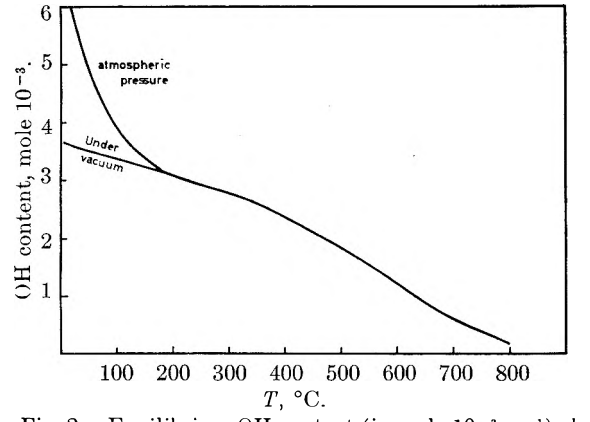

Fig. 2.—Equilibrium OH content (in mole 10^{-3} g.$^{-1}$) obtained on long heating at the temperature given by the abscissa.

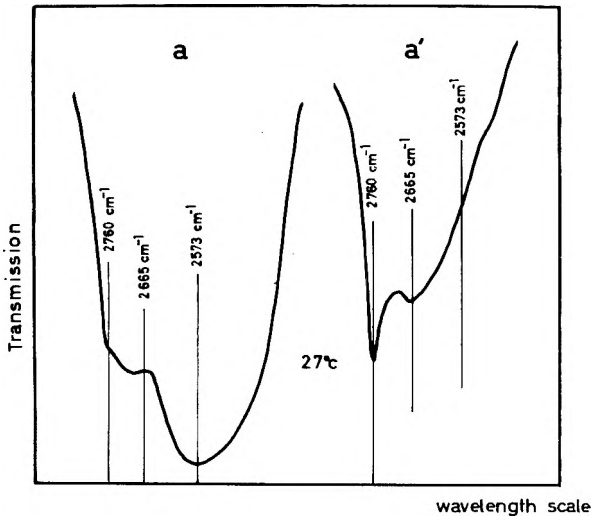

Fig. 3.—Infrared spectra of the OD stretching vibration band. Transmission against wave length at 27°: a', under vacuum; a, P_{D_2O} = 4.5 mm.

theoretical problem while Abell, Bonner, and Goishi[4] considered the system including a gas and a "two-compartment" solid phase.

If the measurement of every separate exponential term but one were possible, the resolution of eq. 1 would be easy within the limits indicated.

From this viewpoint, as far as OH–OD exchange is concerned, silica gel offers an interesting possibility from the fact that the evolution of different kinds of OH groups may be followed by infrared spectroscopy.

The stretching frequency of OH groups in silica gel ranges between 3750 and 3480 cm.$^{-1}$, according to the degree of hydrogen bonding.[5-8]

The difference in hydrogen bond strength possibly may produce different exchange classes.[9] This hypothesis can be tested by following the isotopic exchange for each component of the vibration band, since silica gel films are easily made which allow good transmission in the infrared region.

II. Experimental

(1) **Sample.**—Silica gel Aerosil "Degussa" was used for this research. The B.E.T. surface area (N_2 at −196°) amounts to 176 m.^{2} g.$^{-1}$; the pore size distribution was calculated following the method of Pierce,[10] Fig. 1. The surface area does not change noticeably under the various conditions of heating adopted here. The water content, including constitution OH's and hydration water, were gravimetrically determined under vacuum and at atmospheric pressure; the data are shown in Fig. 2.

The OH content under a water vapor pressure of 4.5 mm. is identical to the one observed under atmospheric pressure.

The OD vibration band shows clearly three components, the wave lengths of which are located, respectively, at 3.628, 3.750, and 3.890 μ (Fig. 3). In the corresponding OH spectral range, the separation between those components is not so clear.

In Table I wave lengths and frequencies are given for OH and OD bands. $\Delta\nu$ represents the difference between the "free" OH frequency (*i.e.*, 3750 cm.$^{-1}$) and the observed ones. From Lippincott and Schroeder's relationship[11] the OH–O lengths are estimated and given as R_{O-O}.

TABLE I
WAVE LENGTHS AND FREQUENCIES OF OH AND OD STRETCHING VIBRATIONS

ODν (cm.$^{-1}$)	2760	2665	2573
λ (μ)	3.628	3.750	3.890
OHν (cm.$^{-1}$)	3740	3607	3480
λ (μ)	2.675	2.772	2.875
$\Delta\nu$ (cm.$^{-1}$)	10	143	270
R_{O-O} (Å.)	3.20	3.00	2.87

The three differently hydrogen bonded hydroxyls will be considered as forming three exclusive different "boxes," characteristics for the solid phase.

Suitable silica gel films were produced as follows: 20 to 40 mg. of air-dried gel was spread as equally as possible on a "parchment" paper laying on a flat steel bloc, covered with another parchment sheet and steel bloc and pressed under 2000 p.s.i. for 5 min.

The film is coherent enough to be removed from the paper and introduced into the cell. The density ranges between 10 and 20 mg. cm.$^{-2}$.

(2) **Exchange Device.**—The apparatus is schematically drawn in Fig. 4. The circulation pump necessarily must produce a vapor flow high enough in order to allow the ex-

(4) D. F. Abell, N. A. Bonner, and W. Goishi, *J. Chem. Phys.*, **27**, 658 (1957).

(5) A. N. Siderov, *Optics and Spectroscopy*, **8**, 424 (1960).

(6) A. V. Kiselev and V. I. Lygin, *Proc. Sec. Intern. Congr. Surface Activity, London*, **II**, 204 (1957); A. V. Kiselev and V. I. Lygin, *Colloid J.*, **21**, 561 (1959).

(7) A. V. Kiselev, 10th Colston Symposium, Butterworths, London, 1958, p. 210.

(8) R. S. MacDonald, *J. Am. Chem. Soc.*, **79**, 850 (1957); *J. Phys. Chem.*, **62**, 1168 (1958).

(9) J. B. Peri, *ibid.*, **64**, 1526 (1960).

(10) C. Pierce, *ibid.*, **57**, 149 (1953).

(11) E. Lippincott and R. Schroeder, *J. Chem. Phys.*, **23**, 1099 (1955).

change rate process not to be limited by the heavy water diffusion in the reaction cell.

If V and v represent the apparatus and the cell volumes, the first one being filled with D_2O, the second with H_2O at the initial time, an elementary theory shows the hydrogen atomic fraction x in the cell will change with respect to time as

$$x = x^\infty + (1 - x^\infty)\, e^{-q(V+v/vV)t} \qquad (2)$$

where q is the flow rate and x^∞ the ratio $v/(v + V)$. In our apparatus $q = 17 \times 10^{-6}$ moles sec.$^{-1}$, $V = 12 \times 10^3$ cm.^{3}, and $v = 250$ cm.^{3}. When introducing these data in relationship 2 it is easy to calculate that x becomes smaller than 0.3 after 5 sec. under a pressure of 4.5 mm. at 30°.

The pump would become the limiting factor for a first-order rate constant (k_i from relationship 3) amounting to 0.26 sec.$^{-1}$. In fact, the highest observed value has been 0.044 sec.$^{-1}$ at 100°, $P_{D_2O} \simeq 8$ mm. for the "3.75 μ" box, the other ones being generally smaller than 0.03 sec.$^{-1}$.

(3) **"Quenching" Procedure.**—Net transfer of matter during isotopic exchange must be reduced to the lowest possible level in order to simplify the mathematical treatment.

The silica gel film thus is carefully equilibrated against a given water vapor pressure just before the run. The pressure is kept constant in the cell until the heavy water vapor is allowed to circulate. The water vapor in the reaction cell C_2 is not removed but the amount is so small that it does not matter. The pressure during the exchange process is exactly the same as during the equilibration. This can be obtained when C_1 and C_3 (Fig. 4) are brought to the same temperature, the small difference between H_2O and D_2O vapor pressures not being taken into consideration.

The "zero" time corresponds to the beginning of the pen drift, corresponding with the absorbance change recorded by the infrared spectrograph.

(4) **Optics.**—A Beckman double beam IR4, fitted with CaF_2 optics, was used. The wave lengths were selected as indicated in Table I for the OD vibration bands.

The Beer–Lambert law is observed almost within the complete range of OH and OD contents. This can be proved as follows. The OH and OD absorbance bands are graphically integrated for various OH and OD contents. Let $I_{OH} = \int_{3300}^{3900} A\, d\nu$ and $I_{OD} = \int_{2500}^{2900} A\, d\nu$ be, respectively, the integrated intensities for the OH and OD regions. If they are plotted against the OH and OD content, known from gravimetric determinations given in Fig. 2, linear relationships appear.

These have negative intercepts which are due to the radiation loss from scattering.

A calibration curve is carefully established for each film after exchange runs. Regeneration is brought about by admitting H_2O into the cell several times.

The absorbance of H_2O or D_2O vapor is quite negligible (less than 3% in transmission units), due to both short cell length and low pressure.

(5) **General Procedure.**—Before each run, the film is equilibrated and the OH band recorded. The wave length is selected and the pen recorder set into operation. The D_2O vapor is allowed to circulate into the cell. When an equilibrium has been reached, the OD band is recorded. From calibration curves, OH and OD contents at the beginning and at the end of the exchange are known from graphical integration of both bands. Let ρ^{-1} be the ratio of the initial OH to the final OD contents.

From the plot of the OD absorbance at the chosen wave length *vs.* the time, the ratio $A_{OD}(t)/A_{OD}^\infty(t = \infty)$ is calculated. Let α be this ratio. The hydrogen atomic fraction x for a "box" corresponding to a selected frequency is given by $(1 - \alpha\rho)$. Figure 5 gives some examples which demonstrate that the data are represented quite satisfactorily by the relationship $\log x = -kt$. Similar results are obtained for all three boxes or selected frequencies of Table I but each box, i, has its own characteristics, k_i. The reason each box can be evaluated separately and follows

$$\frac{dx}{dt} = -k_i (x - x^\infty) \qquad (3)$$

is that (a) observation is made within each box separately and (b) an important excess of D_2O exists so that the results obtained for one box are not appreciably affected by exchange in another. However the following theory will demonstrate the necessity to know the contents of each box (V_i). This requirement can be approximately achieved as follows. The sum $(A_a^\infty + A_b^\infty + A_c^\infty)$ is proportional to the OD equilibrium content known, as already indicated. A_a^∞, A_b^∞, and A_c^∞ correspond with the equilibrium absorbance for the three boxes. V_a, V_b, and V_c will be calculated easily assuming V_i proportional to A_i^∞.

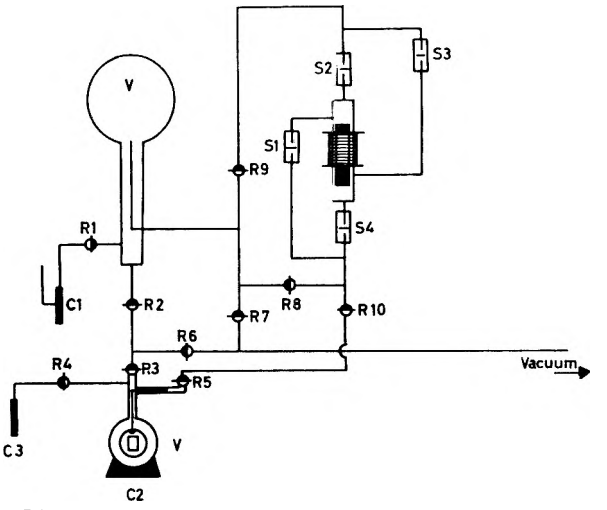

Fig. 4.—Apparatus: R_1, R_2, R_3, R_4, R_5, R_6, R_7, R_8, R_9, and R_{10} are stopcocks; S_1, S_2, S_3, and S_4 are valves of the circulation pump; C_2, reaction cell set in the infrared beam (volume v); V, D_2O vapor storage vessel (volume V); C_1 and C_3, storage vessels of D_2O and H_2O.

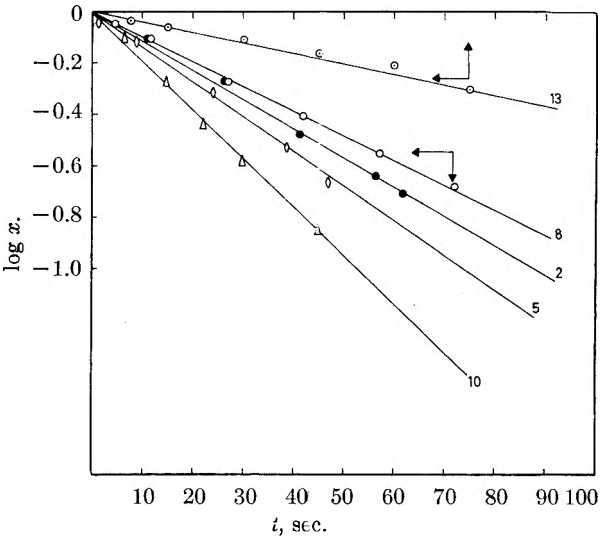

Fig. 5.—Linear relationship between the log of the hydrogen atomic fraction (x) with respect to the time: film weight, 250 mg.; selected frequency, 2665 cm.$^{-1}$; P_{D_2O} = 4.5 mm.; ○ at 27°; ◇ at 95°; ● at 237°. At 100°: ΔP_{D_2O} = 8.85 mm.; ⊙ P_{D_2O} = 1.36 mm.

III. Theory

In order to represent the system silica gel–water vapor, a four-compartment model will be considered including three "boxes" a, b, c, in the solid phase, the last one being the gas phase, g.

Let V_a, V_b, V_c, and V_g be the (H + D) contents of the four compartments and x, y, z, and u the corresponding hydrogen atomic fractions. The V_i contents are constant throughout the complete run, thanks to the adopted quenching procedure.

$$V_T = V_a + V_b + V_c + V_g \qquad (4)$$

At the equilibrium, $u^\infty = x^\infty = y^\infty = z^\infty$ and from the conservation of hydrogen atoms

$$uV_g = xV_a + yV_b + zV_c = V_T u^\infty \qquad (5)$$

We shall postulate that the isotopic effect is negligible. The Marcus relationships for the system become

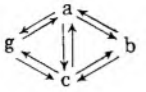

$$\left.\begin{aligned} V_g \frac{du}{dt} &= R_{ga}(u-x) + R_{gb}(u-y) + R_{gc}(u-z) \\ V_a \frac{dx}{dt} &= R_{ag}(x-u) + R_{ab}(x-y) + R_{ac}(x-z) \\ V_b \frac{dy}{dt} &= R_{bg}(y-u) + R_{ba}(y-x) + R_{bc}(y-z) \\ V_c \frac{dz}{dt} &= R_{cg}(z-u) + R_{ca}(z-x) + R_{cb}(z-y) \end{aligned}\right\} \qquad (6)$$

The sum of the first members being equal to zero in order to keep constant the number of hydrogen atoms, it follows that $R_{ij} = R_{ji}$.

From (3), (4), (5), and (6) it can be written

$$\left.\begin{aligned} F_a + (a_1 + k_a)x + a_2 y + a_3 z &= 0 \\ F_b + b_1 x + (b_2 + k_b)y + b_3 z &= 0 \\ F_c + c_1 x + c_2 y + (c_3 + k_c)z &= 0 \end{aligned}\right\} \qquad (8)$$

where

$$F_a = -\left(\frac{V_T R_{ag}}{V_g V_a} + k_a\right) u^\infty;\quad F_b = -\left(\frac{V_T R_{bg}}{V_g V_b} + k_b\right) u^\infty$$

$$F_c = -\left(\frac{V_T R_{cg}}{V_g V_c} + k_c\right) u^\infty$$

and

$$a_1 = \frac{1}{V_a}\left(R_{ag}\left(1 + \frac{V_a}{V_g}\right) + R_{ab} + R_{ac}\right)$$

$$b_1 = -\frac{1}{V_b}\left(R_{ag} - R_{bg}\frac{V_a}{V_g}\right);\quad c_1 = -\frac{1}{V_c}\left(R_{ac} - R_{cg}\frac{V_a}{V_g}\right)$$

$$a_2 = -\frac{1}{V_a}\left(R_{ab} - R_{ag}\frac{V_b}{V_g}\right)$$

$$b_2 = \frac{1}{V_b}\left(R_{bg}\left(1 + \frac{V_b}{V_g}\right) + R_{ab} + R_{bc}\right)$$

$$c_2 = -\frac{1}{V_c}\left(R_{bc} - R_{cg}\frac{V_b}{V_g}\right)$$

$$a_3 = -\frac{1}{V_a}\left(R_{ac} - R_{ag}\frac{V_c}{V_g}\right);\quad b_3 = -\frac{1}{V_b}\left(R_{bc} - R_{bg}\frac{V_c}{V_g}\right)$$

$$c_3 = \frac{1}{V_c}\left(R_g\left(1 + \frac{V_c}{V_g}\right) + R_{ac} + R_{cb}\right)$$

In relationships 8 the k_i first-order constants are calculated from experimental results, x, y, and z are known at all times, and V_T, V_g, and V_i are measured as previously indicated. Therefore the six R_{ij} coefficients are the unknowns.

Three kinds of special cases will be selected.

(a) Mamillary Model.—

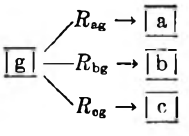

The gas phase exchanges separately with every box. It follows

$R_{ab} = R_{bc} = R_{ac} = 0$ and

$$\left.\begin{aligned} R_{ag} &= -\frac{V_a V_g k_a (x - u^\infty)}{(V_g + V_a)x + V_b y + V_c z - V_T u^\infty} \\ R_{bg} &= -\frac{V_b V_g k_b (y - u^\infty)}{V_a x + (V_g + V_b)y + V_c z - V_T u^\infty} \\ R_{cg} &= -\frac{V_c V_g k_c (z - u^\infty)}{V_a x + V_b y + (V_c + V_g)z - V_T u^\infty} \end{aligned}\right\} \qquad (9)$$

V_T is quite large as compared with V_a, V_b, and V_c, thus $V_T \simeq V_g$. It follows $R_{ag} = -V_a k_a$, $R_{bg} = -V_b k_b$, and $R_{cg} = -V_c k_c$.

(b) Catenary Models.—We shall admit two possibilities.

(1) g − R_{ag} → a − R_{ab} → b − R_{bc} → c

For this first case

$R_{ac} = R_{gb} = R_{gc} = 0$ and

$$\left.\begin{aligned} R_{ag} &= -(k_a V_a + V_c k_c e^{(k_a - k_c)t} + V_b k_b e^{(k_a - k_b)t} \\ R_{ab} &= -\frac{V_c k_c e^{-k_c t} + V_b k_b e^{-k_b t}}{e^{-k_b t} - e^{-k_a t}} \\ R_{bc} &= -\frac{V_c k_b e^{-k_c t}}{e^{-k_c t} - e^{-k_b t}} \end{aligned}\right\} \qquad (10)$$

because of the assumption $V_T \simeq V_g$.

In order to allow the diffusion to take place following the sequence a → b → c, the following inequality $u \geq x \geq y \geq z$ must be observed at all times, in other words, $k_a \geq k_b \geq k_c$. This last condition, which contains experimental values only, will indicate the diffusion mechanism among the three boxes.

(2) g − R_{ag} → a, with R_{ab} → b and R_{bc} → c

We call this case the branched catenary case: one favored compartment is connected with both others.

Here, we have $R_{bc} = R_{bg} = R_{cg} = 0$ and

$$\left.\begin{aligned} R_{ac} &= -\frac{V_c k_c e^{-k_c t}}{e^{-k_c t} - e^{-k_a t}} \\ R_{ab} &= -\frac{V_b k_b e^{-k_b t}}{e^{-k_b t} - e^{-k_a t}} \\ R_{ag} &= -(k_a V_a + k_b V_b e^{(k_a - k_b)t} + k_c V_c e^{(k_a - k_c)t}) \end{aligned}\right\} \qquad (11)$$

Diffusion will proceed only if $k_a \geq k_b$ and $k_a \geq k_c$.

(c) Alternative Model.—

g, with R_{ag} → a and R_{bg} → b − R_{cg} → c

We assume a mamillary model for two compartments and a catenary for the last two ones. In this case $R_{ab} = R_{ac} = R_{gc} = 0$, and

$$\left.\begin{aligned} R_{ag} &= -k_a V_a \\ R_{bg} &= -(k_b V_b + V_c k_c e^{(k_b - k_c)t} \\ R_{bc} &= -\frac{V_c k_c e^{-k_c t}}{e^{-k_c t} - e^{-k_b t}} \end{aligned}\right\} \qquad (12)$$

k_b necessarily must be higher than k_c.

In order to select the right model, every possible factor must be taken into consideration: the nature of the surface and the influence of temperature and pressure upon the exchange process.

IV. Experimental Results

(1) Experiments have been undertaken under

a constant vapor pressure of 4.5 mm. at increasing temperature or at 100° under increasing pressure.

In every case, films of different weights (or thicknesses) have been used. Figures 6 and 7 give, respectively, the variations of V_i and V_ik_i as a function of the temperature under a vapor pressure of 4.5 mm. Figures 8 and 9 reproduce the same variations as a function of the vapor pressure at 100°.

TABLE II[a]

MEAN RESULTS OBTAINED UNDER A CONSTANT PRESSURE OF 4.5 MM. AT INCREASING TEMPERATURE

Temp., °C.			30	100	180	260
Wave length						
3.628 μ	V_ak_a	10^7	5.60	8.60	10.50	11.70
	V_a	10^3	1.49	1.82	1.86	1.86
	k_a	10^4	3.76	4.72	5.64	6.29
3.750 μ	V_bk_b	10^7	12.30	7.50	4.60	3.40
	V_b	10^3	1.88	1.11	0.83	0.77
	k_b	10^4	6.54	6.82	5.54	4.41
3.890 μ	V_ck_c	10^7	10.30	5.60	3.00	1.80
	V_c	10^3	2.40	1.00	0.57	0.40
	k_c	10^4	4.29	5.60	5.26	4.51

[a] V_ik_i are expressed in mole sec.$^{-1}$, V_i in g.$^{-1}$ mole^1. k_i's are given in sec.$^{-1}$ for a "theoretical" 1-g. film.

It must be well understood that by "temperature" we mean the film and not the gas temperature, the last one always being approximately equal to 30°.

TABLE III[a]

MEAN RESULTS OBTAINED AT 100° UNDER INCREASING PRESSURE

Pressure, mm.			2	4.5	8	16
Wave length						
3.628 μ	V_ak_a	10^7	3.50	8.60	9.60	10.00
	V_a	10^3	1.71	1.71	1.71	1.71
	k_a	10^4	2.05	5.03	5.33	5.85
3.750 μ	V_bk_b	10^7	2.60	7.40	8.80	10.60
	V_b	10^3	0.87	1.07	1.07	1.07
	k_b	10^4	2.99	6.93	8.20	9.92
3.890 μ	V_bk_b	10^7	2.30	5.00	5.10	5.30
	V_b	10^3	0.63	0.90	0.91	0.91
	k_b	10^4	3.65	5.56	5.61	5.83

[a] V_ik_i are expressed in mole sec.$^{-1}$, V_i in g.$^{-1}$ mole^1. k_i's are given in sec.$^{-1}$ for a "theoretical" 1-g. film.

From Fig. 6 and 7 are extracted the mean results of Table II, and from Fig. 8 and 9 the mean results of Table III. They will be useful for the discussion.

(2) **Nature of the Surface Hydroxyl Groups.**— Experimental results of Fig. 6 show the variation of the content of each "box" as a function of temperature. It may be particularly pointed out: (1) the OD content of the "3.63 μ box" increases with temperature; (2) the OD contents of "3.75 and 3.89 μ boxes" decrease; (3) the OD content of the "3.89 μ box" falls even more rapidly.

Let us represent, respectively, by the a, b, and c symbols the three boxes containing respectively, at the beginning of the run

a, the weaker hydrogen bonded species or "isolated OH"
b, the stronger hydrogen bonded species or "bridged OH"
c, the strongest hydrogen bonded species belonging mainly to physically adsorbed water

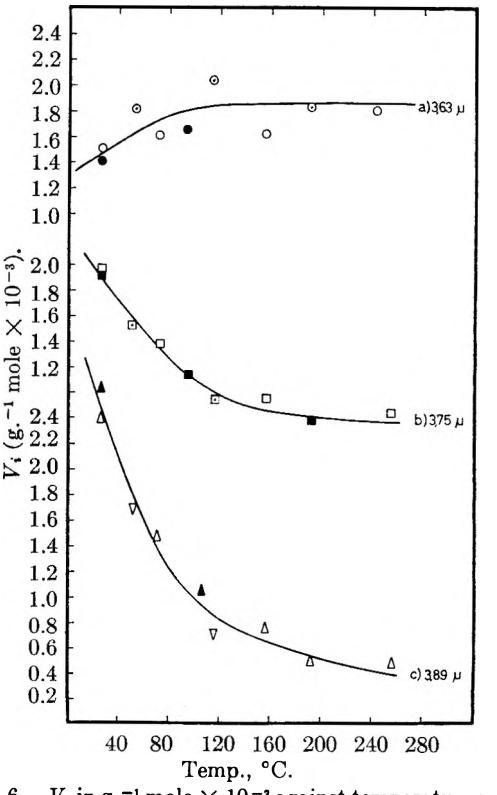

Fig. 6.—V_i in g.$^{-1}$ mole × 10^{-3} against temperature under a constant pressure of 4.5 mm. for different film weights: 40.0 mg.: ○, □, △; 25.0 mg.: ●, ■, ▲; 32.3 mg.: ⊙, ⊡, ◬, according to the compartment.

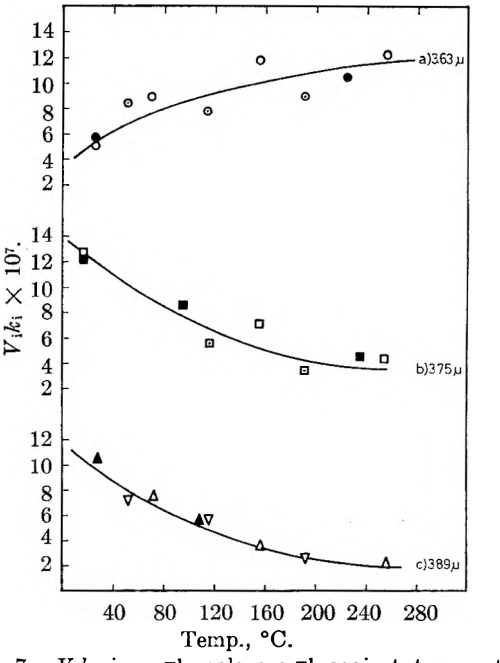

Fig. 7.—V_ik_i in g.$^{-1}$ mole sec.$^{-1}$ against temperature under a constant pressure of 4.5 mm. for different film weights: 40.0 mg.: ○, □, △; 25.0 mg.: ●, ■, ▲; 32.3 mg.: ⊙, ⊡, ▽, according to the compartment.

With rising temperature, "bridged OH" tend to disappear and the number of isolated OH increases accordingly.

Siderov[5] and Kiselev and Lygin[6] consider bridged hydroxyls as probable adsorption sites ac-

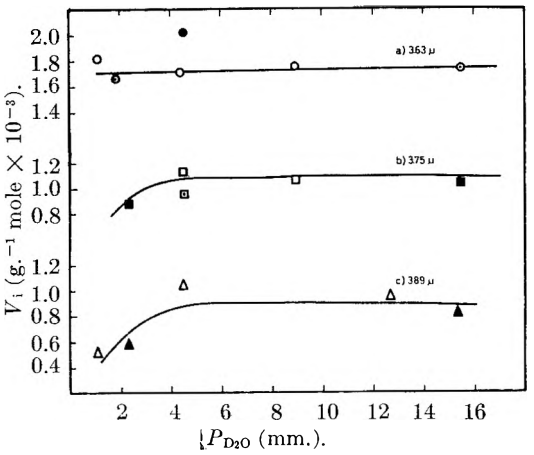

Fig. 8.—V_i in g.$^{-1}$ mole × 10^{-3} against pressure at a constant temperature of 100° for different film weights: 25.0 mg.: ○, ◇, △; 29.2 mg.: ⊙, ■, ▲; 32.2 mg.: ●, ⊡, according to the compartment.

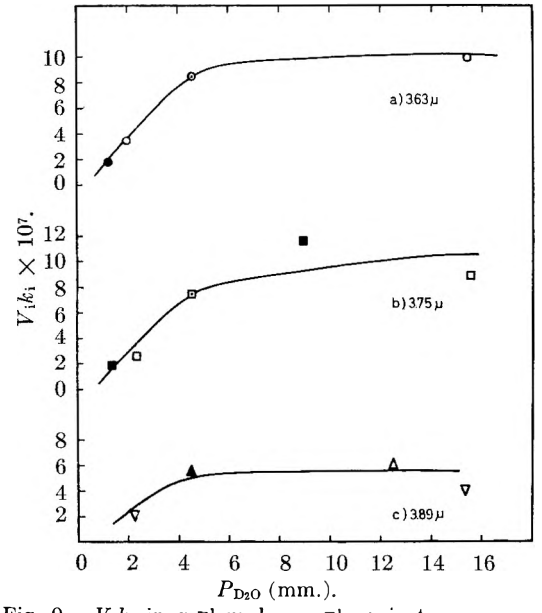

Fig. 9.—$V_i k_i$ in g.$^{-1}$ mole sec.$^{-1}$ against pressure at a constant temperature of 100° for different film weights: 25.0 mg.: ●, ■, △; 29.2 mg.: ○, □, ▽ Mean results at 100° under 4.5 mm.: ⊙, ⊡, ▲, according to the compartment.

cording to

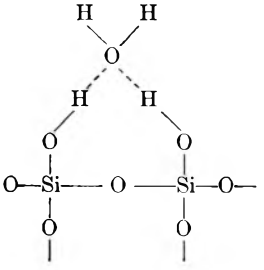

From this viewpoint a strong connection exists between the b and c boxes: this can explain the similar evolution of their contents as a function of temperature or pressure (Fig. 6 and 8). This situation, however, possibly may change and at higher temperatures the isolated OH would contribute to the adsorption of minute amounts of water.

In our Laboratory, Uytterhoeven has measured the surface OH with lithium methyl and Grignard reagents.[12] These still unpublished data are reproduced in the fifth column of Table IV.

TABLE IV

OH CONTENTS IN MOLE × 10^3 G.$^{-1}$ UNDER A H_2O VAPOR PRESSURE OF 4.5 MM.

Temp., °C.	Isolated OH (a)	Bridged OH (b)	Sum a + b	Surface hydroxyls (Uytterhoeven's results[12])
30	1.49	1.88	3.37	1.50
60	1.66	1.47	3.13	1.49
90	1.79	1.18	2.97	1.44
120	1.83	1.11	2.80	1.42
160	1.86	0.91	2.72	1.37
200	1.86	0.80	2.67	1.32
260	1.86	0.77	2.63	1.12

From the comparison between the amounts of bridged and surface hydroxyls, it follows effectively that, at 30°, isolated OH are almost entirely located inside the particles. At higher temperatures, a part of "a" box content accounts for surface hydroxyls.

V. Discussion

R_{ij} parameters measure the flow of hydrogen from the i to the j compartment. Since the rate process of the whole exchange is limited by the exchange process of the more crowded compartment, the flow decreases when the content of a given box becomes smaller.

An increase in temperature contributes to the change of R_{ij} parameters by two antagonistic effects: the usual increase ruled by the temperature coefficient on the one hand and the depressing influence of emptying the boxes on the other hand.

The temperature coefficient for such isotopic exchanges is never very high: it follows that R_{ij} may either increase or decrease with increasing temperature. This conclusion must be kept in mind for the following discussion.

We first shall consider the experiments at increasing temperature under constant pressure. From the nature of the silica gel hydroxylic surface, a mamillary model must be discarded because a connection certainly must exist between the solid phase compartment; *i.e.*, this model would imply that there is no relationship between bridged hydroxyls and adsorbed water or between isolated OH and bridged hydroxyls, which was experimentally proved not to be true.

In order to discuss the catenary models, let us consider the experimental data of Table II. A change in the constants is observed according to the temperature: below 180°, $k_b >> k_c > k_a$; above 180°, $k_a > k_c \simeq k_b$.

The theoretical considerations show the following diffusion processes are allowed

Below 180: g → b → c → a or g → b → c, b → a

Above 180°: g → a → b, a → c

The first model seems inadequate: there is no reason to accept a connection between adsorbed

(12) J. Uytterhoeven, "Contribution à l'étude de la surface hydroxylique des silicates," Ph.D. Thesis, Agronomic Institute, Louvain University, Belgium, 1961.

TABLE V

R_{ij} PARAMETERS FOR THE BRANCHED CATENARY MODEL (P_{D_2O} = 4.5 MM.) (RELATIONSHIPS (11))

	g → b (a, c) 30°			g → b (a, c) 100°			g → a (b, c) 260°		
$-R_{bg}10^6$	$-R_{ba}10^6$	$-R_{bc}10^6$	$-R_{bg}10^6$	$-R_{ba}10^6$	$-R_{bc}10^6$	$-R_{ag}10^6$	$-R_{ab}10^6$	$-R_{ac}10^6$	Time, sec.
2.80	∞	∞	2.2	∞	∞	1.7	∞	∞	0
2.90	7.8	21.5	2.2	17.4	20.4	1.7	6.1	4.0	250
3.00	4.2	9.3	2.3	8.7	12.1	1.7	3.8	2.4	500
3.10	2.9	6.2	2.3	7.0	9.7	1.8	3.1	1.7	750
3.30	2.2	4.7	2.4	5.5	7.9	1.8	2.6	1.6	1000
3.40	1.8	4.1	2.5	4.3	7.0	1.8	2.2	1.3	1250
3.50	1.6	3.1	2.6	3.5	5.9	1.9	1.7	1.0	1500
3.70	1.4	3.1	2.7	2.7	4.3	1.9	1.4	0.9	1750

TABLE VI

R_{ij} PARAMETERS AT 100° UNDER INCREASING PRESSURE

Pressure = 2 mm. Model: g → c → b → a (Relationships (10))

t (sec.)	$-R_{ab}10^6$	$-R_{bc}10^6$	$-R_{cg}10^6$
0	∞	∞	0.84
250	21.3	28.1	.86
500	9.2	17.5	.88
750	5.3	14.7	.89
1000	3.9	10.1	.91
1200	3.6	8.7	.93

P = 4.5 mm. Model: g → b (c, a) P = 8 mm. Model: g → b (c, a) P = 16 mm. Model: g → b (c, a)

(Relationships (11))

(sec.)	$-R_{ba}10^6$	$-R_{bc}10^6$	$-R_{bg}10^6$	$-R_{ba}10^6$	$-R_{bc}10^6$	$-R_{bg}10^6$	$-R_{ba}10^6$	$-R_{bc}10^6$	$-R_{bg}10^6$
0	∞	∞	2.1	∞	∞	2.3	∞	∞	2.5
250	15.78	10.80	2.2	18.00	11.90	2.4	11.30	5.90	2.8
500	8.30	9.18	2.2	8.40	5.20	2.6	5.70	2.90	2.9
750	5.90	6.25	2.3	5.50	3.40	2.7	3.80	1.90	3.1
1000	4.60	3.20	2.3	4.00	2.40	2.8	2.90	1.40	3.3
1200	4.00	1.80	2.4	3.40	1.90	2.9	2.50	1.00	3.5

water and isolated hydroxyls, and not between these two and bridged hydroxyls. Above 180°, "b" box empties and the order of the diffusion process is changed. The isolated hydroxyls act as adsorption sites for small amounts of residual adsorbed water. The branched catenary model explains very well the observed results, although alternative models cannot be discarded if the following combinations are taken into consideration

Below 180°: g → b → c (a) Above 180° g → a → c (b)

or g → a → b (c)

All are compatible with k_i calculated values. It is difficult, however, to understand why bridged and isolated hydroxyls would be connected only through the gas phase. Above 180°, the last combination would implicate no direct exchange between isolated OH and adsorbed water. Therefore it may be concluded that the alternative models do not represent the right processes.

Table V contains the calculated R_{ij} parameters for the branched catenary models.

At 30 and 100°, the flow rate R_{bc} always is higher than R_{ba}: a stronger connection exists between bridged OH (b) and adsorbed water (c) than between isolated OH (a) and bridged OH (b). At 260°, R_{ab} is higher than R_{ac}; the diffusion inside the gel particles is activated.

The antagonistic influences of compartment content and temperature upon the R_{ij} values show their effects when considering, for example, the R_{ba} change with respect to temperature.

We now shall study the experiments run at 100°, under increasing pressure. Results obtained below a 2 mm. pressure differ from theon es obtained at higher pressure, as shown in Table III.

Below 2 mm., $k_c > k_b > k_a$; above this limit, $k_b >> k_c \geqslant k_a$ So, the exchange process differs at low and high pressure. *At high pressure,* the already proposed mechanism maintains, *i.e.*, g → b (c, a). *At low pressure,* the exchange process initiates by box c (adsorbed water), but the small difference between k_a and k_b does not allow one to decide between other diffusion orders.

Table VI gives the R_{ij} parameters, assuming the g → c → b → a sequence under low pressure. For the "branched" catenary model, the R_{bg} coefficient remains almost constant but R_{bc} and R_{ba} decrease when the pressure rises from 8 to 16 mm. From relationships (11) and the k_i values of Table V, this change results from a relatively strong variation of

k_b, as compared with k_a and k_c. Higher pressure induces a faster exchange between the vapor phase and the bridged hydroxyls.

From both sets of experiments, either under constant pressure and increasing temperature or at constant temperature and increasing pressure, it appears clearly that exchange processes can be summarized as follows.

Below 180° and under D_2O vapor pressures ranging between 4 and 16 mm., the more probable model is

vapor phase → bridged hydroxyls (b box) → isolated hydroxyls (a box); adsorbed water (c box)

Above 180°, under a D_2O vapor pressure of 4.5 mm., the a and b boxes are interverted. At 100° and under a D_2O vapor pressure of 2 mm., the exchange initiates from the c compartment.

It would have been expected that at low temperature and high pressure, the physically adsorbed water (c) would be connected with the gas phase and the other two compartments would interact with it.

The privileged situation of the bridged hydroxyls derives probably from the fact that they constitute the main absorption sites, according to the views expressed by Siderov,[4] Kiselev,[6,7] and others.

Acknowledgments.—We wish to thank Dr. W. K. Hall of the Mellon Institute, Pittsburgh, Pa., and Dr. B. Delmon, of the Chemistry Department of the University of Louvain, Belgium, for interesting discussions.

HIGH TEMPERATURE ADSORPTION STUDIES ON VARIOUS ION-EXCHANGED FORMS OF ZEOLITES A AND X

BY P. E. EBERLY, JR.

Esso Research Laboratories, Humble Oil & Refining Company, Baton Rouge Refinery, Baton Rouge, Louisiana

Received August 31, 1961

Pulse flow techniques were used to measure the heats of adsorption of benzene and *n*-hexane on various ion-exchanged forms of zeolite X at 260–482°. The monovalent materials (Li^+, Na^+, and K^+) gave values of about 16.0 and 12.0 kcal./mole for benzene and *n*-hexane, respectively. Considerable variation was observed in benzene heats of adsorption on the divalent ion-exchanged forms. The Mg^{++}, Ca^{++}, Zn^{++}, Sr^{++}, Cd^{++}, and Ba^{++} forms of zeolite X exhibited 11.6, 21.8, 11.2, 23.3, 24.0, and 10.0 kcal./mole for benzene, respectively. Similar data were obtained with hexene-1 and *n*-hexane on several divalent ion-exchanged forms of zeolite A. Cadmium zeolite A gave the highest heat of adsorption of hexene-1, which amounted to 21.5 kcal./mole. This compares to 16.4 kcal./mole observed on calcium zeolite A.

Introduction

Synthetic zeolites A and X are crystalline, sodium aluminosilicates which have large surface areas on the order of 700–800 $m.^2/g.$[1-3] Also, they possess the unique characteristic of having uniform pore diameters. In view of these properties, these so-called molecular sieves have constituted a new class of adsorbents for separation processes. Since they belong to the zeolite family, the sodium ions in the aluminosilicate framework can be easily exchanged with cations of Groups I and II of the periodic table. Therefore, it is of interest to determine the effect of ion-exchange on the adsorption properties of these synthetic zeolites.

In the present report, heats of adsorption were determined in the temperature range of 260–482° for (1) benzene and *n*-hexane on ion-exchanged forms of zeolite X and (2) hexene-1 and *n*-hexane on ion-exchanged forms of zeolite A. To avoid decomposition, flow techniques similar to those reported previously were used to determine the heats of adsorption.[1,4,5]

At the present time, very little is known concerning the effect of ion-exchange on adsorptive properties. Barrer and Stuart[3] observed differences in the heats of adsorption on several ionic forms of zeolite X (synthetic faujasite) with nitrogen and argon at low temperatures. In regard to high temperature adsorption, the only data available are those obtained with benzene and *n*-hexane on sodium zeolite X.[1] The heats of adsorption were 15.5 and 10.8 kcal./mole, respectively, in the range of 260–454°.

Experimental

In the preparation of the ion-exchanged materials, 200 g. of the original sodium zeolite A or X powder was contacted with an aqueous solution of the chloride salt of the metal for a period of 2 hr. at 66°. Solution compositions are listed in Tables I and II. In most cases, the treatment was repeated three times, a fresh solution being used for each treatment. After the final exchange, the material was washed repeatedly with distilled water until no chloride was detectable in the filtrate. This usually required 10 to 15 washings. The solid was preliminarily dried at 110° for a period of four hours, pelletized, and finally ground to 48–60 mesh (250–300 μ) particle size.

In general, the exchanging solutions listed in Tables I and II contained a two- to sixfold excess of cation equivalents per equivalent of sodium in the original zeolite. These large concentrations were used to induce a maximum amount of exchange. With certain large ions such as Sr^{++} and Ba^{++} either lower concentrations or single exchange treatments were used in an attempt to avoid destruction of the crystalline lattice.

The apparatus and experimental methods for determining the heats of adsorption by pulse flow techniques have been reported previously.[1,6] In brief, the unit consisted of a pulse injection system connected in series to a packed column of the exchanged zeolite and a thermal conductivity cell.

(1) P. E. Eberly, Jr., *J. Phys. Chem.*, **65**, 68 (1961).

(2) D. W. Breck, W. G. Eversole, R. M. Milton, T. B. Reed, and T. L. Thomas, *J. Am. Chem. Soc.*, **78**, 5963 (1956).

(3) R. M. Barrer and W. I. Stuart, *Proc. Roy. Soc.* (London), **A249**, 464 (1959).

(4) S. A. Greene and H. Pust, *J. Phys. Chem.*, **62**, 55 (1958).

(5) P. E. Eberly, Jr., and E. H. Spencer, *Trans. Faraday Soc.*, **57**, 289 (1961).

(6) P. E. Eberly, Jr., and C. N. Kimberlin, Jr., *ibid.*, **57**, 1169 (1961).

Helium, a non-adsorbable gas, was selected as the carrier gas and permitted to flow at a rate of 50 cc. (STP)/min. A six-port Perkin–Elmer injection valve was employed to inject 0.5 cc. of a mixture of 8 mole % hydrocarbon in argon into the helium stream. The column consisted of 1.5 cc. of the molecular sieve (250–300 μ particle size) packed into a 0.18 in. i.d. stainless steel tube resulting in a bed length of 9.1 cm. Prior to the pulse flow experiments, the zeolite was flushed with dry helium at 538° for a period of 16 hr. to remove adsorbed water. The adsorbent column was maintained at the desired temperatures by use of a fluidized-solids sand bath. Because of reversible adsorption, the hydrocarbon in the pulse mixture was separated from the non-adsorbable argon. The difference in emergence times of the hydrocarbon and argon, as detected by the conductivity cell, was equal to the hydrocarbon retention time (t_m) through the packed section of the column.[7]

By determining the retention times as a function of temperature, heats of adsorption were calculated by means of the equation[1,4,6]

$$\log t_m(\text{corr.}) = C - \frac{\Delta H}{2.303R}\left(\frac{1}{T}\right) \qquad (1)$$

where

$$t_m\,(\text{corr.}) = t_m(\text{obsd.})\,\frac{T}{298}\,3/2\,\frac{(P_i/P_0)^2 - 1}{(P_i/P_0)^3 - 1} \qquad (2)$$

P_i and P_0 are the pressures at the column inlet and outlet, respectively. The constant C is a function of the entropy of adsorption, the dimensions of the column, and the carrier gas flow rate. If these factors are kept constant, then a plot of the logarithm of the corrected retention time against the reciprocal of the absolute temperature $1/T$ should yield a straight line the slope of which is proportional to the heat of adsorption.

Sodium zeolites A and X were obtained in powder form from Linde Air Products Co. The benzene, *n*-hexane, and hexene-1 were research grade hydrocarbons having mole % purities of 99.93, 99.96, and 99.99, respectively, and were obtained from the Phillips Petroleum Company. The gases were commercially available. The purities of the helium and argon were 99.99 and 99.995%, respectively.

Results

Ion Exchange.—Data on the properties of the ion-exchanged forms of zeolite X are listed in Table I. The Li^+, K^+, and Ca^{++} exchanges resulted in nearly 90–97% replacement of the original sodium ions. This is somewhat less than that reported by Barrer and Stuart,[3] who obtained 100% exchange with Li^+ and K^+ and 98% exchange for Ca^{++}. With the magnesium exchanges, only about two-thirds of the sodium was replaceable. Two separate preparations yielded the same degree of exchange. It is difficult to understand the poor performance of magnesium in comparison with other larger ions of groups I and II metals. A similar phenomenon, however, was reported previously by Breck, *et al.*,[2] in the exchange of sodium zeolite A. Only two-thirds of the sodium was exchangeable with magnesium ions. Two separate batches of strontium zeolite X were prepared. Three exchanging treatments were used to prepare batch A, resulting in 90% exchange, whereas only one treatment was used with batch B, resulting in 50% exchange. Although only relatively mild conditions were selected for the barium exchange, destruction of the crystalline lattice apparently occurred.

The residual chloride contents of the ionic forms of zeolite X all were quite low. With the exception of the Ca^{++} form, the materials contained less than 0.1 wt. % chloride. This is of the same order of magnitude as the 0.05% present on the original sodium zeolite X powder. A qualitative measure of crystallinity was obtained from the relative intensities of X-ray diffraction peaks. Good crystallinity was observed with most of the materials. The Zn^{++} and Sr^{++} forms, however, exhibited only fair crystallinity. The Ba^{++} form gave a rather poor X-ray diffraction pattern, indicating a severe loss in crystalline structure. Presumably, some of the pores in the zeolite structure through which barium has to travel in order to exchange with sodium are sufficiently small in comparison to the radius of the barium ion so that disintegration of the crystalline lattice occurs.

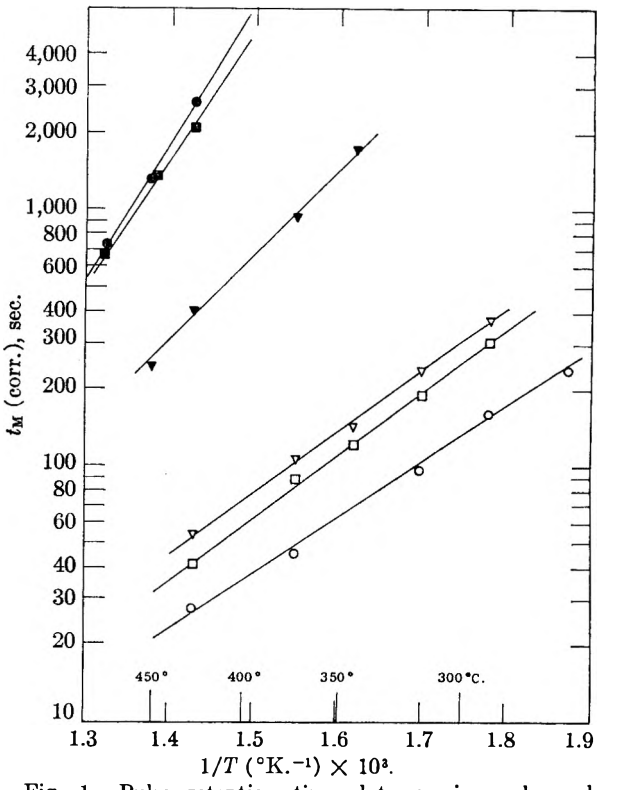

Fig. 1.—Pulse retention time data on ion-exchanged forms of zeolite X. The solid and open points represent data with benzene and *n*-hexane, respectively. The Cd^{++}, Ca^{++}, and Na^+ forms are indicated by the circle, square, and triangle, respectively.

Properties of the ion-exchanged forms of zeolite A are given in Table II. Only Group II metals were used for these exchanges since apparently only divalent ions produce a structure having pore diameters sufficiently wide to permit adsorption of straight chain hydrocarbons.[2] The degree of exchange is similar to that observed with the X zeolites. No barium exchange was attempted since it apparently destroys the crystalline structure.[2,8] Some of the residual chloride contents were higher in comparison with those observed with the X zeolites. The Ca^{++} and Cd^{++} forms had 0.35 and 0.31 wt.% chloride. The finer pore structure of zeolite A evidently causes more difficulty in washing off occluded chlorides. The Mg^{++} and Sr^{++} forms had much lower residual chloride. The crystallinity was good for most of the materials.

(7) The time required for argon to flow through the packed section was negligible in comparison to that of the hydrocarbon.

(8) R. M. Barrer and W. M. Meier, *Trans. Faraday Soc.*, **54**, 1074 (1958).

TABLE I

PREPARATION AND PROPERTIES OF ION-EXCHANGED FORMS OF ZEOLITE X

Exchanging ion	Ionic radius[a] of cation, Å.	Exchanging solution: Molality	Exchanging solution: Equiv. cation in soln./ equiv. Na in sieve	Exchanged zeolite X: Wt. % Cl	Exchanged zeolite X: % Na^+ exchanged	Exchanged zeolite X: Crystallinity
Li^+	0.78	0.0101 *M* LiCl	6.4	0.1	97	Good
Na^+	0.98	.....	..	.05	0	Good
K^+	1.33	.00517 *M* KCl	3.3	.08	89	Good
Mg^{++} (Batch A)	0.78	.00260 *M* $MgCl_2 \cdot 6H_2O$	3.3	.07	67	Good
Mg^{++} (Batch B)	0.78	.00260 *M* $MgCl_2 \cdot 6H_2O$	3.3	.08	70	Good
Ca^{++}	1.06	.00354 *M* $CaCl_2$	4.5	.14	92	Good
Zn^{++}	0.83	.00156 *M* $ZnCl_2$	2.1	.10	86	Fair
Sr^{++} (Batch A)	1.27	.000857 *M* $SrCl_2 \cdot 6H_2O$	1.1	.03	89	Fair
Sr^{++} (Batch B)[b]	1.27	.000857 *M* $SrCl_2 \cdot 6H_2O$[b]	1.1	.05	50	Fair
Cd^{++}	1.03	.00257 *M* $CdCl_2 \cdot 2.5H_2O$	3.3	.05	92	Good
Ba^{++}[b]	1.43	.000351 *M* $BaCl_2 \cdot 2H_2O$[b]	0.52	.04	51	Poor

[a] T. Moeller, "Inorganic Chemistry," John Wiley and Sons, Inc., New York, N. Y., 1953. [b] In these preparations the original sodium zeolite X was treated only once with the indicated solution at 66° for 2 hr.

TABLE II

PREPARATION AND PROPERTIES OF ION-EXCHANGED FORMS OF ZEOLITE A

Exchanging ion	Ionic radius[a] of cation, Å.	Exchanging solution: Molality	Exchanging solution: Equiv. of cation in soln./ equiv. of Na in sieve	Exchanged zeolite A: Wt. % Cl	Exchanged zeolite A: % Na^+ exchanged	Exchanged zeolite A: Crystallinity
Na^+	0.98	.....	..	0.00	0	Good
Mg^{++}	0.78	0.00260 *M* $MgCl_2 \cdot 6H_2O$	2.6	.07	67	Good
Ca^{++}	1.06	.00354 *M* $CaCl_2$	3.6	.35	91	Good
Sr^{++} (Batch A)	1.27	.000857 *M* $SrCl_2 \cdot 6H_2O$	0.87	.05	80	Poor
Sr^{++} (Batch B)[b]	1.27	.000857 *M* $SrCl_2 \cdot 6H_2O$[b]	0.87	.00	56	Fair
Cd^{++}	1.03	.00257 *M* $CdCl_2 \cdot 2.5H_2O$	2.6	.31	90	Good

[a] T. Moeller, "Inorganic Chemistry," John Wiley and Sons, Inc., New York, N. Y., 1953. [b] The original sodium zeolite A was treated only once with the indicated solution at 66° for 2 hr.

The exhaustively exchanged Sr^{++} zeolite (batch A) lost most of its crystalline structure whereas the more mildly exchanged material (batch B) showed less degradation.

Benzene and *n*-Hexane Adsorption on Ion-Exchanged Forms of Zeolite X.—Heats of adsorption of benzene and *n*-hexane, as determined by pulse flow techniques, are listed in Table III for the temperature range of 260–482°. Corrected pulse retention time data are plotted in Fig. 1 for the sodium, calcium, and cadmium forms. For all materials and temperatures, the retention time of benzene was larger than that of *n*-hexane. As predicted from theory, the retention times (corrected to room temperature and pressure) increased logarithmically with reciprocal temperature.

With the monovalent ion-exchanged materials, little variation was observed in the heats of adsorption. Benzene varied from 15.5 kcal./mole for sodium zeolite X to 16.6 kcal./mole for the lithium form. These values agree well with the 16.8 kcal./mole reported by Barrer, Bultitude, and Sutherland[9] for the sodium form. Heats of adsorption of *n*-hexane varied only from 10.8 to 13.0 kcal./mole. The retention time ratio of benzene to *n*-hexane also showed little change. Potassium zeolite X gave a value of 5.2, which is slightly lower than the 7.1–7.4 for the lithium and sodium forms.

The behavior observed with the divalent ion-exchanged materials was decidedly different from

TABLE III

ADSORPTION MEASUREMENTS AT 260–482° ON ION-EXCHANGED FORMS OF ZEOLITE X

Ion-exchanged zeolite X: Type	% Na^+ exchanged	ΔH of adsorption, kcal./mole: Benzene	ΔH of adsorption, kcal./mole: *n*-Hexane	t_M (Benzene)/t_M (*n*-Hexane at 427°
Li^+	97	16.6	12.1	7.1
Na^+	0	15.5	10.8	7.4
K^+	89	15.8	13.0	5.2
Mg^{++} (A), run 1	67	11.7	..	..
Mg^{++} (A), run 2	67	12.1	8.71	2.7
Mg^{++} (B)	70	11.0	8.94	2.5
	Av.	11.6	8.82	2.6
Ca^{++}	92	21.8	10.5	53
Zn^{++}	86	11.2	10.2	4.2
Sr^{++} (A)	89	23.3	11.7	48
Sr^{++} (B)	50	21.1	10.5	24
Cd^{++}	93	24.0	7.3	96
Ba^{++}	51	10.0	[a]	..

[a] *n*-Hexane was not adsorbed in this temperature range.

that of the monovalent ion-exchanged forms. Also, the adsorptive properties were strongly dependent on the type of divalent ion used in the exchange and the degree of replacement of the sodium ions. With the exception of the Mg^{++}, Zn^{++}, and Ba^{++} forms, the divalent ion-exchanged materials exhibited much higher values for the heats of adsorption of benzene relative to *n*-hexane. Thus, the Ca^{++}, Sr^{++}, and Cd^{++} zeolites had values for benzene ranging from 21.1 to 24.0 kcal./mole.

(9) R. M. Barrer, F. W. Bultitude, and J. W. Sutherland, *Trans. Faraday Soc.*, 1111 (1957).

Also, the pulse retention time ratios were three to fourteen times higher than those found on the monovalent ion-exchanged forms. The Cd^{++} form is particularly unusual in that it exhibits the highest heat of adsorption for benzene and at the same time gives the lowest heat for *n*-hexane. This is accompanied by an extremely high pulse retention time ratio of 96 at 427°. Dependence of the adsorptive properties on the degree of exchange is illustrated by the data on the two strontium sieves.

The Mg^{++} zeolite X was investigated more thoroughly since its behavior did not fit the general picture. In contrast to the Ca^{++}, Sr^{++}, and Cd^{++} forms, it gave lower heats of adsorption and lower pulse retention time ratios than even the monovalent ion-exchanged materials. Two separate batches were prepared. Pulse retention time data are shown in Fig. 2 and were quite reproducible. X-Ray diffraction patterns of the material both before and after the adsorption measurements were identical, indicating no loss in crystalline structure during high temperature exposure.

The low heats of adsorption observed with the Zn^{++} form presumably can be attributed to some loss in crystalline structure. This is more obviously true with the Ba^{++} form since its X-ray diffraction pattern indicated that the material was largely amorphous. Its adsorptive properties were rather poor. No adsorption of *n*-hexane could be detected even at the lowest temperature of 260°.

n-Hexane and Hexene-1 Adsorption on Ion-Exchanged Forms of Zeolite A.—Heats of adsorption of *n*-hexane and hexene-1 at 260–482° on ion-exchanged A zeolites are listed in Table IV. Pulse retention time data on the Mg^{++}, Ca^{++}, and Cd^{++} forms are plotted in Fig. 3.

TABLE IV

ADSORPTION MEASUREMENTS AT 260–482° ON ION-EXCHANGED FORMS OF ZEOLITE A

Ion-exchanged zeolite A		ΔH of adsorption, kcal./mole		t_M (Hexene-1) / t_M (*n*-Hexane)
Type	% Na^+ exchanged	Hexene-1	*n*-Hexane	at 427°
Mg^{++}	67	15.6	11.7	1.7
Ca^{++}	91	16.4	13.0	1.7
Sr^{++} (Batch A)	80	[a]	[a]	[a]
Sr^{++} (Batch B)	56	13.1	9.2	1.8
Cd^{++}	90	21.5	12.2	9.0

[a] No adsorption observed.

In contrast to the behavior of the corresponding X zeolites, the Mg^{++} and Ca^{++} forms exhibited very similar adsorptive properties. The heats of adsorption for hexene-1 and *n*-hexane were about 16 and 12 kcal./mole, respectively. Also, the ratios of the pulse retention times were identical.

Cadmium exchange markedly affected the adsorptive properties of zeolite A in a manner analogous to that previously observed with benzene and *n*-hexane on zeolite X. The heat of adsorption of hexene-1 was increased relative to that of *n*-hexane. This was associated with over a fourfold increase in the pulse retention time ratio.

The 80% exchanged strontium form showed no adsorption of either hydrocarbon even at the lowest temperature of 260°. An X-ray diffraction pattern indicated that most of the crystalline structure was lost in this exchange. The more mildly exchanged Sr^{++} form (batch B) exhibited some adsorptive properties.

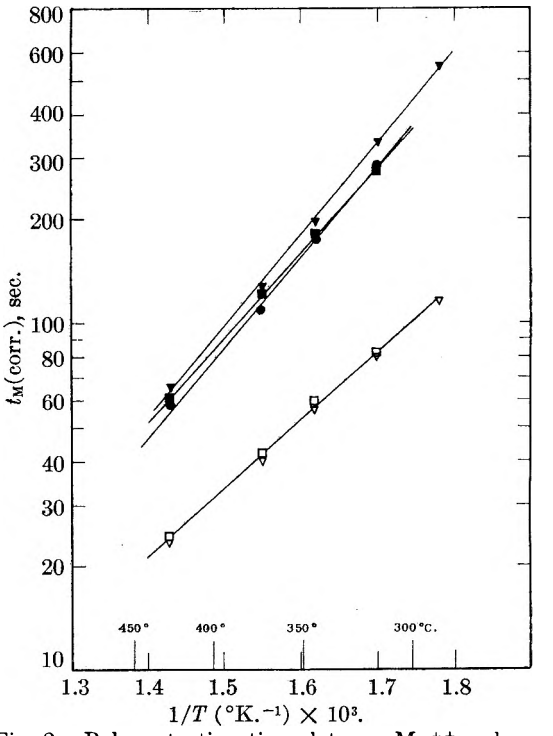

Fig. 2.—Pulse retention time data on Mg^{++}-exchanged forms of zeolite X. The symbols have the following significance: ●, benzene on Mg-X (A), run 1; (▼), benzene on Mg-X (A), run 2; ▽, *n*-hexane on Mg-X (A), run 2; ■, benzene on Mg-X (B); □, *n*-hexane on Mg-X (B).

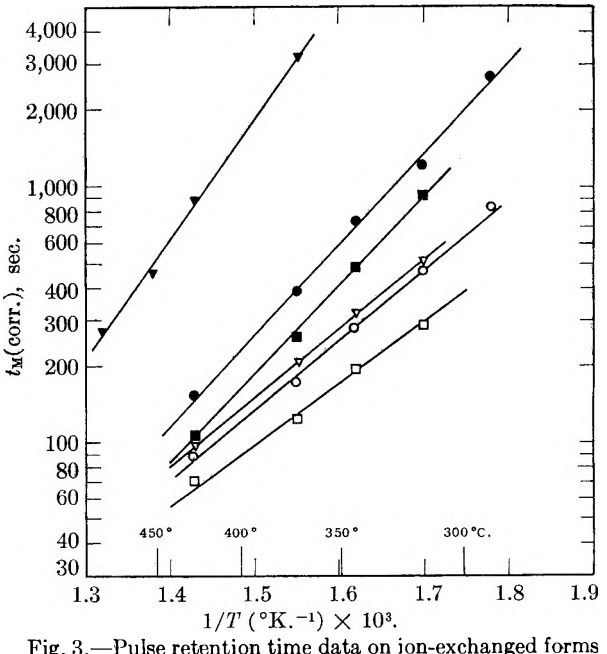

Fig. 3.—Pulse retention time data on ion-exchanged forms of zeolite A. The symbols have the following significance: ●, hexene-1 on Ca-A; ○, *n*-hexane on Ca-A; ■, hexene-1 on Mg-A; □, *n*-hexane on Mg-A; ▼, hexene-1 on Cd-A; ▽, *n*-hexane on Cd-A.

Discussion

The results of this work show that marked changes in adsorptive properties of synthetic zeolites A and X can be brought about by replacing the original sodium ions with other metallic ions of groups I and II of the periodic table. As such, a variety of surfaces having different adsorptive properties can be easily produced by ion-exchange. Theoretically, it is difficult to predict the effect of ion-exchange on adsorptive properties of these synthetic zeolites. Other variables in addition to ionic radius or ionization potential must be taken into consideration. These include among others (1) degree of exchange, (2) position of exchanged ions in crystal lattice, and (3) degree of retention of crystalline structure.

In the temperature range of 260–482°, the heats of adsorption are essentially constant with temperature since the plots of log t_M(corr.) *vs.* $1/T$ are nearly linear in all cases. Apparently, this near constancy extends to even broader temperature ranges. Barrer and his co-workers,[9] for instance, observed a heat of adsorption of benzene on sodium zeolite X of 16.8 kcal./mole at 25–70°. This agrees quite well with our value of 15.5 kcal./mole determined at high temperatures.

The heats of adsorption and retention time ratios are important quantities which characterize (1) the resolving power of solid adsorbents for gas chromatography and (2) the dependence of the resolving power on temperature. The retention time (t_M) of the pulse maximum is related to column variables by the following relationship[5]

$$t_M = \frac{\beta' L}{U_e} \qquad (3)$$

where L is the length of the column and U_e the superficial linear velocity of the carrier gas stream. β' is an adsorption equilibrium constant equal to the moles adsorbed/cm.^{3} of column divided by the moles in the gas/cm.^{3} gas. In general, most adsorptions are not linear with pressure and the value of t_M or β' would change with pressure. In gas–solid chromatography, the pressures in the pulse are normally on the order of 1 mm. or less; consequently, the t_M or β' values in this report should correspond to the limiting slopes of the isotherms at very low pressures.

With the same column at a given temperature and carrier gas flow rate, the retention times of the pulse maxima for two different hydrocarbons are related by the equation

$$\frac{t_{M1}}{t_{M2}} = \frac{t_{M1}(\text{corr.})}{t_{M2}(\text{corr.})} = \frac{\beta'_1}{\beta'_2} \qquad (4)$$

Thus, the retention time ratios listed in Tables III and IV are equal to the ratios of the limiting slopes of the respective isotherms at low pressure. Consequently, they serve to characterize the resolving power of the solid adsorbents. High values of the ratio mean high resolving power. The ratios as listed, however, would not necessarily have the same value at higher pressures.

Also, by use of eq. 1, the following relationship may be derived

$$t_{M1}/t_{M2} = K \exp\left[-(\Delta H_1 - \Delta H_2)/RT\right] \qquad (5)$$

which gives the temperature dependency of the retention time ratio. Heats of adsorption have negative values and consequently the exponent in eq. 5 is positive if ΔH_1 is assumed to have the higher numerical value. Thus, the retention time ratio increases exponentially as the temperature is lowered, and the rate of increase is governed by the differences in the heat of adsorption of the two hydrocarbons.

According to this theoretical development, the cadmium exchanged zeolites have unusual properties. Cadmium zeolites X and A give much higher retention time ratios for benzene to *n*-hexane and hexene-1 to *n*-hexane, respectively, than the other ion-exchanged forms. Also, the differences in the heats of adsorption for the respective hydrocarbons are greatest for the cadmium zeolites. Hence, they should show considerable promise in analytical, high temperature gas–solid chromatography.

Acknowledgment—The author wishes to express his sincere appreciation to Mr. J. E. Landry, Jr., for his excellent work in the assembly and calculation of data.

THE OXIDATION OF COPPER FILMS TO $CuO_{0.67}$

BY HAROLD WIEDER AND A. W. CZANDERNA

Parma Research Laboratory, Union Carbide Corporation, Parma 30, Ohio

Received September 7, 1961

Low temperature oxidation studies of copper films have been carried out employing microgravimetric, optical, and diffraction techniques. A composition of $CuO_{0.67}$ can be formed in 100 Torr of oxygen from about 110 to 200° for thicknesses up to 1085 Å., depending on the time and temperature, and is stable *in vacuo* up to at least 350°. Results of diffraction, optical, and density measurements were used to conclude that this composition is a gross defect structure of Cu_2O.

Introduction

Numerous investigations of the low temperature oxidation of copper have been carried out in an effort to understand the mechanism of oxidation.[1,2] These studies have included the determinations of the surface oxide phases formed, using diffraction techniques, and of the rates of oxidation, by optical, gravimetric, coulometric and diffraction techniques. It is apparent from the recent review of the oxidation of copper[2] that the com-

(1) R. F. Tylecote, *J. Inst. Metals*, **78**, 259 (1950–51).
(2) A. Rönnquist and H. Fischmeister, *ibid.*, **89**, 65 (1960–61).

position of the oxides formed on the surface in these studies has been inferred from reasonable assumptions but has not been determined directly. This is not surprising because the stoichiometry of a thin oxide layer formed on bulk copper is very difficult to characterize. For example, if oxidation temperatures exceed ~200°, more than one oxide layer is formed. At temperatures below ~ 200°, the thin oxide formed is difficult to separate from the bulk copper for direct analysis. Complete oxidation of a copper slab below 200° would require an impractical amount of time.

In this sudy, the stoichiometry of completely oxidized copper films has been measured directly and correlated with other physical properties. As a result of this additional parameter, unexpected information was obtained about the oxidation of copper films.

Experimental

In the principal experiment, a thin film of copper was evaporated onto a transparent substrate suspended from a microbalance. During the subsequent oxidation of the film, the mass of oxygen incorporated into the film and the optical transmission of the film were continuously and simultaneously measured. The mass measurements were used to determine the oxygen uptake; the optical measurements provided both fundamental physical information about the film and a "fingerprint" of the extent of oxidation, as will be discussed later.

Mass Measurements and Vacuum Technique.—Mass changes were determined with the vacuum microbalance shown in Fig. 1. A detailed description of the construction, operation, calibration, and limitation of the balance has been reported.[3] In the present set of experiments, the balance reproducibility was ±0.1 μg. The sensibility of the balance was 0.1 μg. in high vacuum or ±1 μg. at the oxygen and hydrogen pressures utilized. The change in sensibility arises because of buoyancy and thermomolecular flow effects.[4]

"Pyrex" glass plates, 0.25 mm. thick and 40 mm. in diameter, weighing about 0.7 g., were suspended from the balance as shown in Fig. 1. One plate served as a substrate for the copper film, the other was provided to maintain symmetry.[4] A 6 mm. diameter hole was drilled in the field lens to allow adequate clearance of the suspension fiber.

The temperature of the hinged tube furnace mounted about each "Pyrex" plate was controlled to ±0.5°. The furnace temperature was determined from the e.m.f. of "Chromel Alumel" thermopiles which were cemented to the furnaces as near as possible to the sample and dummy plates. Prior to the oxidation studies, the actual sample temperature was calibrated as a function of the thermopile temperature with a thermocouple tip placed against the plate. Thereafter, the thermopile e.m.f. was measured and the sample temperature was obtained from the calibration curve.

The vacuum system consisted of two mercury diffusion pumps in series backed with a forepump, a gas handling section, a mercury manometer, and an ionization gage. Liquid nitrogen was used to trap mercury vapor.

Oxygen was prepared by the thermal decomposition of chemically pure $KMnO_4$, dried with $MgClO_4$, and stored in bulbs. Reagent grade hydrogen was obtained in 1-l. break seal flasks.

Optical Measurements.—The optical transmission of the films was measured using the arrangement shown in Fig. 1.

Monochromatic light was obtained from a ribbon filament tungsten light source which was incident on a Bausch and Lomb grating monochromator. The exit slit of the monochromator was focused on an intermediate field lens and then refocused on an opal glass disk located immediately in front of an RCA 6217 photomultiplier tube. A slit

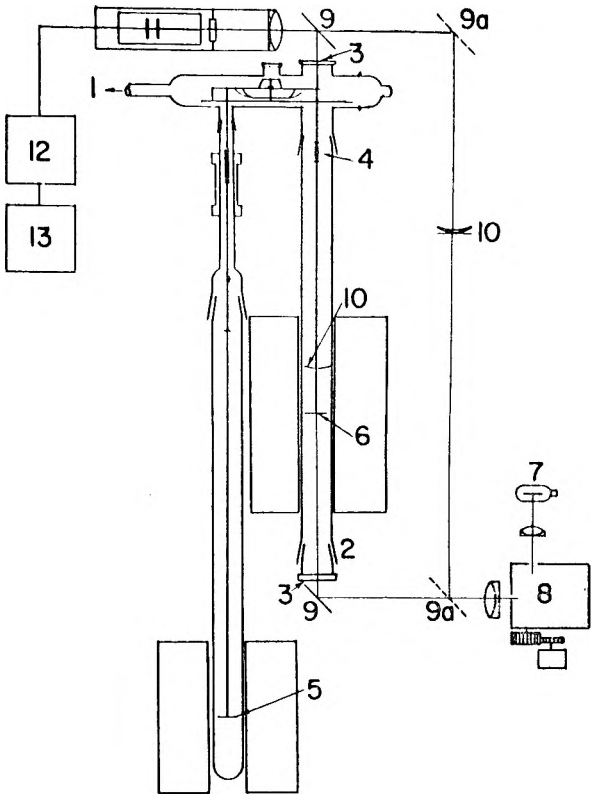

Fig. 1.—Schematic diagram of the apparatus: (1) to vacuum system; (2) ground glass joint; (3) optical window; (4) glass counterweights; (5) dummy plate; (6) sample plate; (7) tungsten light source; (8) monochromator; (9) mirrors; (10) field lens; (11) photomultiplier tube; (12) amplifier; (13) recorder.

width corresponding to a 10 Å. band width was found convenient for optical scanning. The center portion of the slit was masked to prevent scattering from the hole in the field lens.

A motor drive on the wave length drum enabled the 0.4 to 0.8 μ region to be scanned and recorded in 1 min. For each run this was done twice, once with the mirrors in position 9 and again with the mirrors in position 9a. The relative transmission at any wave length is the ratio of the transmission through the sample to that through the equivalent blank path. Residual scattering from the microbalance components was determined in a run made prior to film evaporation, and was used to correct all subsequent transmission measurements.

During each transmission run the composition of the film remained unchanged.

Film Preparation.—For preparation of the copper film, the lower optical window, shown in Fig. 1, was replaced with an evaporator assembly which also had a getter tube and ionization gage tube attached to side arms. The copper charge, which was formed from 99.99$_7$% copper sheet, was evaporated from a molybdenum boat. A magnetic shield was employed to cover or expose the copper charge as desired. A masking tube was provided to collect all the copper that did not condense on the substrate or in the evaporator assembly. The 25 cm. distance from the boat to the substrate should yield a film uniformity of about 1%.

Prior to the actual deposition of copper, the vacuum system, evaporator assembly, hangdown tubes, and copper charge were heated and outgassed until a vacuum of 1 μ-Torr (1 μTorr = 10^{-6} mm.) was achieved with the furnaces, ion gage, getter bulb, and copper charge hot. Upon cooling to room temperature, a pressure of 0.1 μT. or better was achieved. The copper charge then was heated. Onset of deposition was observed as an apparent mass loss resulting from the momentum transfer of the impinging copper. Deposition was allowed to continue until a pressure of 2 μT. was observed. When a pressure of 0.1 μT. or less again was obtained by gettering and pumping, evaporation

(3) A. W. Czanderna and J. M. Honig, *Anal. Chem.*, **29**, 1206 (1957).

(4) A. W. Czanderna, "Vacuum Microbalance Techniques," Plenum Press, 1961, p. 129.

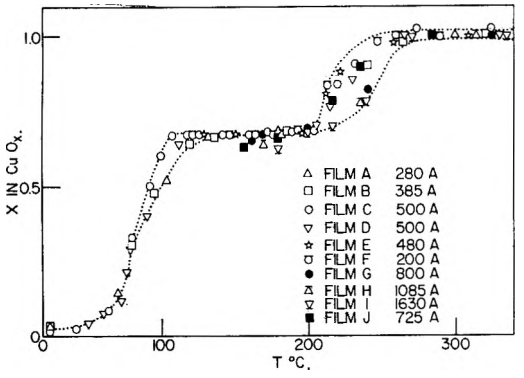

Fig. 2.—Extent of copper oxidation *vs.* temperature in 100 Torr of oxygen for various film thicknesses.

was resumed. In the preparation of Film C, which was a typical preparation, 550 μg. of copper was evaporated in ten separate steps. Each evaporation interval varied from 15 to 30 sec.; the total deposition time was 6 min. and the integral of Pdt was about 2 μT.-min. The amount of deposition was measured with the microbalance during the pumpdown interval. Thus, any desired film thickness could be attained. After the evaporation was completed, the evaporator assembly was removed under a positive pressure of helium and the optical window was inserted. The flow of helium was terminated simultaneously with resealing the wax joint. The system then was evacuated to 0.1 μT.

Hydrogen was employed to remove any oxide formed on the film. In general, the mass loss during the low temperature (160°) hydrogen treatment corresponded to about three atomic layers of oxide. Reduction at higher temperatures did not remove additional mass but resulted in agglomeration of the film.

Oxidation of the film was achieved by heating the film in 100 Torr of oxygen. Except where otherwise noted, film thicknesses reported in this paper were calculated from the measured mass and area of the film by assuming the bulk density of copper. It has been shown that the density of copper films condensed on "Pyrex" substrates approaches the bulk density of copper at 200 Å.[5]

Additional Film Studies.—In addition to the principal experiment, films were studied by X-ray and electron diffraction, electron microscopy, and interferometry techniques. The films were prepared in a vacuum chamber equivalent in every way to the one already described except that the substrates were not suspended from a microbalance. Oxidation of these films was carried out at 100 Torr of oxygen in the same temperature range as was used for the films prepared on the microbalance.

Results

Thirty films were studied during the course of this investigation, of which eighteen were studied with the microbalance-transmission apparatus. The eighteen films ranged in thickness from 200 to 1630 Å., prior to oxidation. The measurements were carried out at least twice for each film thickness, except for films thicker than 800 Å. As a result of this study, it was found that the optimum sensitivity and reproducibility for both the optical transmission and gravimetric measurements could be achieved with a 500 Å. film. Accordingly, six films of this thickness were studied with the apparatus.

In the discussions which follow, the amount of oxygen incorporated into the film is presented as a value of x in CuO_x. This does not imply that the oxygen is homogeneously distributed throughout the film except for single phase regions. The actual distribution of oxygen will be treated in the discussion of the results.

Formation of $CuO_{0.67}$ by Oxidation of Copper Films at Progressively Higher Temperatures.—Oxidation data for films of different thicknesses were obtained by heating the films to progressively higher temperatures in 100 Torr of oxygen. In general, a film was allowed to oxidize until no further mass change could be detected for a 24 to 48 hr. period. The total oxidation time at a given temperature varied up to a maximum of 160 hr. The temperature then was lowered to 25° to determine the amount of uptake as accurately as possible. Further oxidation was obtained by heating to higher temperatures. When the film was finally oxidized to stoichiometric CuO, it was reduced to copper by heating in hydrogen at 250°. The mass of copper measured during evaporation and the amount calculated from the mass loss during hydrogen reduction of CuO agreed to 2% for the thinnest films and 1% or less for the thicker films.

Careful progressive oxidation of Films A–D produced the over-all shape of the curve shown in Fig. 2. Films E–J then were oxidized in one step, (*i.e.*, direct oxidation) at a temperature between 122 and 180° and thereafter progressively. The data shown in Fig. 2 were reproduced once for all films except H and I. These additional data are not plotted to avoid further crowding of the points.

There are five regions to the curve which are approximately bounded by the following temperatures: (1) Below 70°, (2) 70–110°, (3) 110–200°, (4) 200–270°, and (5) 270–330°. The results obtained in regions (1), (2), (4), and (5) are not unexpected. In region (1), oxidation occurs by growth of an amorphous oxide. This region of oxide growth has been treated both theoretically[6] and experimentally.[7]

In regions (2) and (4) the oxidation is rate limited. The presence of a slope in each of these regions and the decrease in slope with increasing film thickness both are characteristic of a rate limited process. The flat region (5) corresponds to cupric oxide. The unusual feature of region (3) is that a constant composition is exhibited not at $CuO_{0.5}$, as might be expected from previous studies, but at $CuO_{0.67}$. The value of 0.67 for x is reproducible from film to film over a wide range of temperatures, film thicknesses, and oxidizing conditions.

The composition $CuO_{0.67}$ can be reached asymptotically in time by direct oxidation (Fig. 3) and first is obtained at a temperature which depends on the film thickness. In the case of a very thick film, such as Film I (1630 Å.), the flat region in the progressive oxidation curve becomes sloped with an inflection point at $CuO_{0.67}$.

From the study of Films A–J, it may be concluded that: (1) The composition $CuO_{0.67}$ can be formed for films of different thicknesses (200–1085 Å.), and hence is not a consequence of substrate interactions or anomalies in the evaporated surface; (2) The composition may be obtained either by

(5) N. Wainfran, N. J. Scott, and L. G. Parratt, *J. Appl. Phys.*, **30**, 1604 (1959).

(6) N. Cabrera and N. F. Mott, *Repts. Prog. in Phys.*, **12**, 163 (1949).

(7) T. N. Rhodin "Advances in Catalysis," Vol. 5, Academic Press, Inc., New York, N. Y., 1953.

progressive oxidation (Films A–D) or by direct oxidation at some temperature along the flat (Films E–J), and hence is not a consequence of the heating cycle employed.

In addition to being stable in oxygen up to about 200°, $CuO_{0.67}$ is stable *in vacuo* up to at least 350°. The vacuum stability was determined microgravimetrically by heating in a bakable, greaseless vacuum system, with a limiting pressure of 2×10^{-8} Torr.

Optical Transmission of a 500 Å. Film.—During the oxidation of films A–J, hundreds of optical transmission spectra were obtained at various stages of the oxidation. It was found that, for a given film thickness and the oxidizing conditions employed in this study, there is a unique relationship between the optical transmission spectrum and the x in CuO_x, regardless of whether the oxidation is progressive or direct. As many as 40 curves were obtained during oxidation of a single film to $CuO_{0.67}$. A typical set of such curves, taken during progressive oxidation of a 500 Å. film (Film C), are presented in Fig. 4. The arrows along the oxidation curve in the inset of Fig. 4 indicate at what stages of the oxidation the correspondingly numbered transmission curves were measured. A comparison of these data shows that, except for the temperature region 186–206°, the optical transmission changes only when the x in CuO_x changes. Other features of the optical curves are discussed in the next section.

X-Ray Diffraction, Electron Diffraction, and Electron Microscopy Studies of Films K, L, and M.—The repeated appearance of a flat at $CuO_{0.67}$ in the oxidation curve suggested that the oxidation be studied by diffraction methods. An additional 500 Å. film (Film K) was prepared and oxidized at progressively higher temperatures in a second vacuum system. After oxidizing at each temperature, the film was cooled to room temperature and removed from the chamber. The transmission was measured, a small area of film was scraped from the substrate for X-ray analysis, and the film was replaced in the chamber for further oxidation. This process required about 15 min.

Since no transmission changes have been observed in partially oxidized films exposed to air for as long as 24 hr., it is probable that there are no macroscopic changes in the film during such exposures. Hence, it is reasonable to assume that there was no significant change in film composition during the 17-hr. exposures required for powder pattern analyses.

The x in CuO_x for film K was inferred from its transmission spectrum by comparison with the transmission curves of Film C (Fig. 4). Hence this experiment enabled a correlation to be made between the x and the phases present in the film.

The experiment was repeated with two 300 Å. Films, one prepared in the microbalance apparatus (Film L) and one prepared in the auxiliary vacuum system (Film M). In this case, small areas of film M were stripped and examined by electron microscopy and selected area electron diffraction. The additional diffraction lines obtained by this

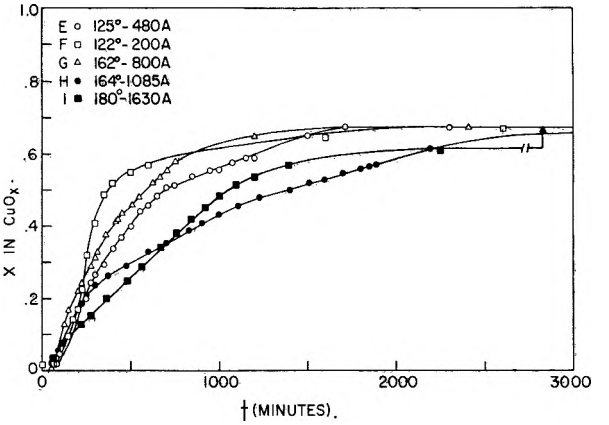

Fig. 3.—Rate of copper film oxidation in 100 Torr of oxygen at various temperatures and thicknesses for Films E-I. The temperature was increased to 200° at the break in the curve for Film I. $CuO_{0.67}$ was obtained after 100 hr. at 200°.

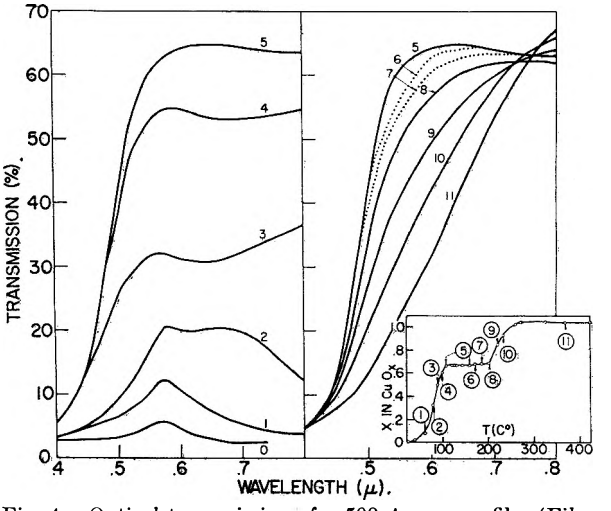

Fig. 4.—Optical transmission of a 500 A. copper film (Film C) during oxidation to CuO.

method served to substantiate the conclusions obtained by X-ray diffraction of Film K.

Although the small particle size in the film resulted in broadening of the X-ray lines, it was possible to distinguish readily the Cu, Cu_2O, and CuO lines and to identify mixtures of the lines. As many as five (and not less than three) lines were used to identify each phase by X-ray diffraction. Electron diffraction yielded as many as eight lines of a single phase.

In the early stages of the oxidation, only Cu lines were found. This confirms that the initial oxide formation is amorphous. A typical transmission spectrum is shown by curve 1 of Fig. 4.

The appearance of Cu_2O lines, in addition to the Cu lines, was accompanied by the appearance of an absorption edge (curves 2 and 3). The intensity of the Cu lines gradually diminished (curve 4) and finally disappeared, leaving only Cu_2O lines (curve 5). The shape of the transmission curve differs from that of bulk Cu_2O[8] only in that the fundamental absorption edge is shifted to shorter wave lengths.

(8) J. Bloem, *Philips Research Repts.*, **13**, 167 (1958).

Eventually CuO lines began to appear in addition to Cu_2O lines (curve 8).[9] The Cu_2O lines grew weaker (curves 9, 10) and finally vanished, leaving only CuO lines (curve 11). Transmission curves of bulk CuO have not been published, to our knowledge, probably because of its extreme opacity. Hence, a comparison of the film results with that of bulk CuO is not possible.

The most significant aspect of these measurements is that $CuO_{0.67}$ yields the same diffraction lines as those of Cu_2O and only those lines.[10] Subtle differences in the intensities and positions of the lines, if present, are obscured by line broadening.

Density of $CuO_{0.67}$.—In electron microscope studies, magnifications as high as 36,000× revealed no gaps in the evaporated films or at any stage of the progressive oxidation up to CuO. Hence, it was felt that density measurements of $CuO_{0.67}$ would be meaningful.

The density of $CuO_{0.67}$ was inferred from a measurement of the film thickness, since the two quantities are directly proportional for homogeneous films. The thickness measurements were made by the Tolansky technique,[11] using a device for measuring across film areas ~1 mm. in diameter.[12] This technique, which measures the distance across an air gap, is to be preferred to thickness measurements which require the prior knowledge of the refractive index of the material.

To carry out the measurement it first was necessary to prepare a set of films of equal thickness. This was accomplished by simultaneous deposition onto three substrates located 25 cm. away from the molten copper. The thickness of one film was measured immediately after evaporation, another was measured after oxidation to $CuO_{0.67}$, and a third was measured after oxidation to CuO.

Since the actual mass of copper deposited during evaporation was not measured, an absolute determination of the density could not be made by this technique. Instead the density of the oxidized films was calculated relative to an assumed bulk density for that of the evaporated copper films. As mentioned earlier, Cu films exceeding 200 Å. in thickness do have the density of bulk copper. Since measurements were made on a set of films 230 Å. thick and another set 480 Å. thick, the bulk density assumption probably is valid.

TABLE I

A COMPARISON OF MEASURED DENSITIES OF COPPER OXIDE FILMS WITH BULK DENSITIES OF COPPER OXIDE

Materia	Bulk density relative to copper	Measured density relative to copper 1st set	2nd set
Cu_2O	0.68		
CuO	0.72	0.80	0.64
$CuO_{0.67}$		0.51	0.53

(9) No X-ray information is available corresponding to curves 6 and 7, which were measured at 186 and 202°, respectively. Because of a slight temperature dependence in the absorption edge position, these curves are shown dotted. All other curves were measured at 25°.

(10) For $CuO_{0.67}$ X-ray diffraction of Film K showed the 110, 111, 200, 220, and 311 lines of Cu_2O. Electron diffraction of Film M yielded the same lines, as well as the 211, 400, and 331 lines of Cu_2O.

(11) S. Tolansky, "Multiple Beam Interferometry," Oxford University Press, 1948.

(12) G. D. Scott, *J. Opt. Soc. Am.*, **48**, 858 (1958).

The measured relative densities of $CuO_{0.67}$ and CuO are presented together with the relative bulk densities of Cu_2O and CuO in Table I.

It is apparent that the density of the CuO film approaches that of bulk CuO within the accuracy of the experiment (~10%). It then is very striking that the density of $CuO_{0.67}$ is 20 to 25% less than that of bulk Cu_2O.

Discussion

It is of interest to consider a possible structure for $CuO_{0.67}$. From the optical and diffraction measurements, it is concluded that no CuO is present. If CuO were, in fact, present, in *any* form (whether as a mixed phase, as a thin layer on the surface of voids, or in minute nuclei distributed throughout the volume), it would have to be: (1) of such a special size that it remains undetected by diffraction or optical absorption techniques; (2) of such a structure as not to increase in amount between 110 and 200°; (3) of such a special quantity as to yield invariably an over-all composition of $CuO_{0.67}$ along the flat for film thicknesses of 200–1085 Å.

It seems highly improbable that CuO could be present in such an unusual form.

Since it generally is accepted that the oxidation of copper to Cu_2O proceeds by the diffusion of copper ion vacancies, it seems logical to postulate that $CuO_{0.67}$ is a gross defect structure of Cu_2O. The composition of $CuO_{0.67}$ corresponds to one vacancy per unit cell, on the average. Therefore, the flat region of the oxidation curve could imply that this is the maximum number of vacancies which can be supported by the Cu_2O structure. A random orientation of vacancies would explain the diffraction, density, and mass measurements. However, a deviation from stoichiometric Cu_2O of this magnitude has not been reported previously.

Some consideration has been given to the possibility that the defects are ordered and that $CuO_{0.67}$ is, in fact, a unique metastable phase, Cu_3O_2. Experiments are now in progress in an effort to resolve this question.

Differences in crystallite size between films and bulk material lead to differences in their optical properties.[13] This may account for the shift of the absorption edge of $CuO_{0.67}$ to shorter wave lengths than that reported for bulk Cu_2O. It also is possible that the shift is characteristic of the gross defect structure, as distinguished from stoichiometric Cu_2O. The optical characteristics of this material will be the subject of a later communication.

It is interesting to note that Cu lines are present in the diffraction pattern almost to the point where the composition reaches $CuO_{0.67}$. Thus the formation of a defect structure does not appear to depend on the prior formation of stoichiometric Cu_2O. Analysis of the transmission curves reveals that it is possible that the defect structure is formed immediately upon recrystallization of the amorphous oxide.

At the temperatures and pressures studied, CuO is apparently the only thermodynamically

(13) See, for example, O. S. Heavens, "Optical Properties of Thin Solid Films," Butterworth, 1955.

stable phase. The formation of defect cuprous oxide then presumably occurs not only because this oxide is more stable than copper in an oxygen ambient but also because it has a smaller activation energy than that for oxidation to CuO. Thus, the rate of formation of the more stable cupric oxide is too low below 200° to convert a measurable amount of the metastable $CuO_{0.67}$ to CuO.

It has been shown by the progressive oxidation of Films A–J that CuO begins to form on $CuO_{0.67}$ at about the same temperature for $CuO_{0.67}$ thicknesses of 440 to 2400 Å. Thus, the onset of CuO formation in thin copper films depends only on the relative activation energies for oxidation to $CuO_{0.67}$ and CuO, and not on the underlying thickness of $CuO_{0.67}$ present.

Conclusions

It has been shown that $CuO_{0.67}$ is formed during the oxidation of copper films. This new information isolates a temperature, pressure, and thickness region for copper oxidation where only one oxide composition is formed. Further study of the formation of $CuO_{0.67}$ could lead to better understanding of copper oxidation in the 100 to 10,000 Å. region.

The simultaneous measurement of microgravimetric and optical transmission changes is the first reported and has realized considerable value in the study of copper oxidation. Studies of this type could produce similar information about other materials.

Acknowledgments.—It is a pleasure to acknowledge the many ways in which the authors benefited from stimulating discussions with A. W. Smith. Discussions with Prof. C. S. Smith also proved very helpful. We are grateful to P. M. Stier for continued encouragement. We thank M. L. Alley for making the X-ray diffraction measurements and L. I. Forrest for carrying out the gravimetric measurements.

THE REACTIONS OF PHENYL RADICALS IN THE GAS PHASE AND THE CARBON–HYDROGEN DISSOCIATION ENERGY IN BENZENE

BY W. FIELDING AND H. O. PRITCHARD

Chemistry Department, University of Manchester, Manchester 13, England

Received September 7, 1961

An exploratory study has been made of the abstraction of hydrogen atoms by phenyl radicals from hydrogen, methane, and fluoroform. The results taken in conjunction with other kinetic and thermochemical data lead to two estimates for the C–H dissociation energy in benzene of 104.2 and 103.1 kcal./mole.

The C–H dissociation energy in benzene was determined by Szwarc and Williams[1] *via* the pyrolysis of bromobenzene. They measured the activation energy for dissociation into a phenyl radical and a bromine atom, and assuming zero activation energy for the reverse process calculated a value of about 102 kcal./mole for D(Ph-H). Unfortunately, this determination suffers from two disadvantages, first that it requires a knowledge of the heat of formation of bromobenzene which is most uncertain[2,3] and second that the temperature range of the experiment is approaching the limit of usefulness of the toluene carrier technique. Nevertheless, this value receives further support from the analogous pyrolysis of iodobenzene, for which Szwarc[4] got an activation energy of >57 kcal., corresponding[3] to a value of >101 kcal. for D(Ph-H).

Shortly afterwards, the position was complicated by the publication of two discordant electron-impact values. In the former of these, Kandel[5] measured the appearance potential of CH_3^+ from toluene, and assuming the ionization process to be

$$PhCH_3 + e \longrightarrow Ph + CH_3^+ + 2e$$

he obtained a heat of formation for the phenyl radical corresponding to D(Ph-H) = 107 kcal./mole. However, the abundance of the mass 15 peak in the spectrum of toluene is no greater than the mass 15 peak from toluene-αd_3[6] showing that the neutral fragment(s) accompanying the formation of CH_3^+ cannot be a phenyl radical. In the other experiment, Field and Franklin[7] measured the appearance potential of $C_2H_3^+$ from ethylbenzene, and assuming the ionization process to be

$$PhC_2H_5 + e \longrightarrow Ph + C_2H_3^+ + H_2 + 2e$$

one gets D(Ph-H) = 99 kcal.; this determination probably is open to the same criticism as Kandel's work, and therefore neither can be considered as a definitive determination of D(Ph-H).

We therefore embarked on an exploratory study of the reactions of phenyl radicals, aiming to measure D(Ph-H) by the classical kinetic method. The activation energies of the two reactions

$$CH_3 + PhH \longrightarrow CH_4 + Ph \qquad (3)$$

$$CF_3 + PhH \longrightarrow CF_3H + Ph \qquad (3')$$

are known,[8,9] and therefore a knowledge of the

(1) M. Szwarc and D. Williams, *J. Chem. Phys.*, **20**, 1171 (1952).

(2) K. Hartley, H. O. Pritchard, and H. A. Skinner, *Trans. Faraday Soc.*, **47**, 254 (1951).

(3) C. L. Chernick, H. A. Skinner, and I. Wadsö, *ibid.*, **52**, 1088 (1956).

(4) M. Szwarc, *Chem. Revs.*, **47**, 75 (1950).

(5) R. J. Kandel, *J. Chem. Phys.*, **22**, 1496 (1954).

(6) H. O. Pritchard, unpublished work.

(7) F. H. Field and J. L. Franklin, *J. Chem. Phys.*, **22**, 1895 (1954).

(8) A. F. Trotman-Dickenson and E. W. R. Steacie, *ibid.*, **19**, 329 (1951).

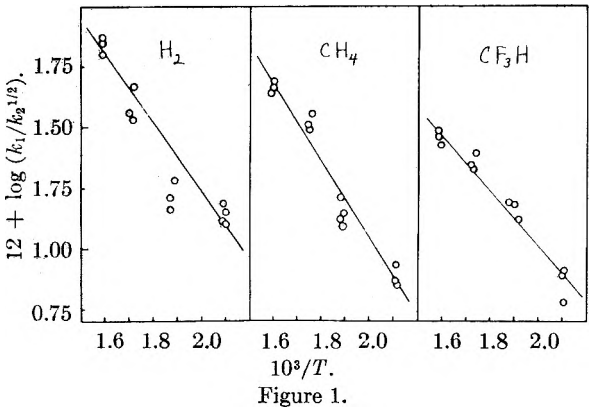

Figure 1.

activation energies for the pair of reactions

$$Ph + CH_4 \longrightarrow PhH + CH_3 \quad (1)$$

$$Ph + CF_3H \longrightarrow PhH + CF_3 \quad (1')$$

leads (in principle—see Discussion) to two independent values for D(Ph-H). We have measured these two activation energies relative to (half) that for the reaction

$$Ph + Ph \longrightarrow \text{diphenyl} \quad (2)$$

and these experiments are described below, together with some preliminary studies on D_2 and H_2. Our results confirm the essential correctness of Szwarc's conclusions.

Experimental

Source of Phenyl Radicals.—Benzophenone, azobenzene, and mercury diphenyl were considered as possible sources of phenyl radicals. Each was photolyzed in turn in the presence of a large excess of hydrogen at 250° using a low pressure mercury lamp. Benzophenone decomposed but gave no benzene or diphenyl; azobenzene did not decompose; mercury diphenyl gave both benzene and diphenyl, indicating the production of phenyl radicals. There are, however, two complicating factors to the use of mercury diphenyl—its low vapor pressure (10^{-6} mm. at room temperature[10]) and its high extinction coefficient (log ϵ = 3.1 at 2537 Å.); these will be referred to later.

Experiments with Deuterium.—98% D_2, 2% HD was prepared by the reaction of D_2O vapor with sodium. About 10 mg. of mercury diphenyl was placed in a 300-ml. spherical quartz flask and sublimed while pumping to remove any traces of occluded methanol (used as a solvent in recrystallization). This quantity of mercury diphenyl is sufficient to give a vapor pressure of the order of 1 mm. in the reaction flask, and, provided experiments are carried out above about 180°, it is all present in the vapor phase. After the sublimation, D_2 (2–3 cm.) was introduced into the flask which then was sealed off from the vacuum system and transferred to a furnace at 250–300°. After photolysis, the flask was reattached to the vacuum system and the benzene fraction removed for mass-spectral analysis. The product consisted solely of benzene and benzene-d_1: there were no substances of higher mass number, *i.e.*, hexenes or hexanes, indicating that under the conditions of our experiment, atoms did not add to the benzene produced in the reaction. However, the benzene analysis was unexpected in that benzene, and not benzene-d_1, was the major component. After varying the conditions and the photolysis times, we concluded from the isotopic constitution of the products that, while some of this benzene came from attack of phenyl radicals on mercury diphenyl, the greater part of it was being produced by the reaction of phenyl radicals with the benzene-d_1 accumulated from the primary reaction, *i.e.*

$$C_6H_5 + C_6H_5D \longrightarrow C_6H_6 + C_6H_4D$$

This eliminated our hopes for a rapid comparison of the reactivity of phenyl radicals with a number of hydrocarbons by an isotopic comparison technique[11] and we were forced to use only the comparison of the rates of formation of benzene and diphenyl where this exchange reaction is irrelevant, *i.e.*

$$\frac{R_{\text{benzene}}}{R^{1/2}_{\text{diphenyl}}} = \frac{k_1[RH]}{k_2^{1/2}}$$

Analysis of Benzene–Diphenyl Mixtures.—After the reacting gas RH (*i.e.*, H_2, CH_4 or CF_3H) had been pumped away, the benzene was distilled into a calibrated volume and the pressure of benzene vapor was measured with a mercury manometer and cathetometer. The benzene then was returned to the reaction flask and the whole contents were concentrated in a small depressed area directly opposite the neck by refrigeration. Some 0.3 ml. of (benzene-free) toluene then was distilled on top of the products, and on allowing to warm up, the benzene and diphenyl formed in the reaction were dissolved in this toluene. The solution was transferred by pipet to a small sample tube for analysis using a Pye argon chromatograph with a silicone oil-celite column. Using a hypodermic syringe, about 20 μl. of this solution was placed on top of the column (at 20°). After the benzene and the toluene (which grossly overloaded the detector) had come through, the column temperature was raised rapidly to 100° in order to elute the diphenyl. The apparent ratio of benzene:diphenyl was found by comparison of the peak areas, but as the detector sensitivity varies with temperature, calibration with known benzene–diphenyl mixtures was needed to give the true ratio. The rates of formation of benzene and diphenyl then can be calculated assuming that benzene vapor obeys the perfect gas laws at room temperature.

Possible Side Reactions.—The principal reaction of phenyl radicals with aromatic systems in solution is addition and we therefore must rule out the possibility that some of our diphenyl comes from direct addition of a phenyl radical to benzene, followed by removal of a hydrogen atom. It previously has been pointed out by Jaquiss and Szwarc[12] that this type of reaction does not occur in the gas phase at 600°, and we already have ruled out the simple addition of H or D atoms to benzene under our experimental conditions. Furthermore, we found no evidence for the formation of toluene or xylenes in our experiments with methane, nor benzotrifluoride or bis-trifluoromethylbenzenes in our experiments with fluoroform (by choosing instead of toluene a solvent less volatile than any of these compounds). Finally, we photolyzed mercury diphenyl in the presence of chlorobenzene vapor, but failed to find any chlorinated diphenyl, suggesting that the addition of phenyl to benzene is unimportant in the gas phase.

It also is possible that some diphenyl is formed by the mercury-photosensitized decomposition of benzene,[13] but irradiation of benzene with 10 mg. of added mercury did not yield any diphenyl under our experimental conditions. We conclude therefore that the production of diphenyl is accounted for by reaction 2.

Effect of a High Extinction Coefficient.—When the radical source has a high extinction coefficient (ϵ), there is a concentration-gradient of the radicals in the system. If this gradient can be kept fairly small, we can rule out of the kinetic equations the diffusion of radicals along the concentration-gradient. Thus, if the source concentration is kept down, or if the radicals react very quickly, this will be the case. In our experiments using a spherical vessel of about 10 cm. diameter, about 10% of the light is transmitted across the vessel: this will mean that the concentration of radicals falls much less than a factor of 10 across the vessel because of the second-order reaction 2, which probably takes place on every collision; we therefore neglect diffusion effects in what follows. It is of course necessary to integrate the rate equations over the path length of the photolyzing radiation, and this leads to a most complicated equation. However, in the limiting cases of very high light intensity (about 10^{16} quanta/cm.²/sec.) or very low light

(9) S. W. Charles and E. Whittle, *Trans. Faraday Soc.*, **56**, 794 (1960).

(10) A. S. Carson, D. R. Stranks, and B. R. Wilmshurst, *Proc. Roy. Soc.* (London), **A244**, 75 (1958).

(11) G. O. Pritchard, H. O. Pritchard, H. I. Schiff, and A. F. Trotman-Dickenson, *Trans. Faraday Soc.*, **52**, 849 (1956).

(12) M. T. Jaquiss and M. Szwarc, *Nature*, **170**, 312 (1952).

(13) E. J. Y. Scott and E. W. R. Steacie, *Can. J. Chem.*, **29**, 233 (1951).

intensity (about 10^{12} quanta/cm.^{2}/sec.) simple expressions of the type

$$\frac{R_{\text{benzene}}}{R^{1/2}_{\text{diphenyl}}} = \frac{k_1[\text{RH}]}{k_2^{1/2}} \times f(\epsilon,c,L)$$

are obtained,[6] where c is the source concentration and L is the path length; approximating our 10 cm. spherical vessel to a cylinder of $L = 7$ cm., these functions $f(\epsilon,c,L)$ come out to 2.6 and 2.3, respectively, for the limiting cases. The important point is that this modifying function is independent of temperature (provided ϵ and the quantum yield of the primary photolytic step, which we assume is always 2, are both temperature independent), and therefore the activation energy differences which we measure will be correct.

Results

Kinetic experiments were carried out over the range 180–350°; it is inconvenient to go much outside this range because of the low volatility of mercury diphenyl below 180°, and because of the onset of thermal decomposition of mercury diphenyl above 350°. Photolyses were carried out for the shortest time which would give sufficient products for analysis (about 15 min. with $I_0 \approx 10^{14} - 10^{15}$ quanta/cm.^{2}/sec. at 2357 Å.). The results are shown in Fig. 1 and the derived activation energies and *apparent* A-factors are given in Table I; it is not possible to quote absolute values for $A_1/A_2^{1/2}$ because the analysis given in the preceding section is complicated by the build-up during the photolysis of diphenyl which absorbs strongly at 2537 Å. No correction was made for the attack of phenyl radicals on the mercury diphenyl source because separate experiments showed that this would be negligible under our experimental conditions.

Discussion

No abstraction reactions of phenyl radicals have been measured previously, and our observations show that their activation energies are lower than the corresponding reactions of other free radicals, assuming that $E_2 \approx$ zero. The A-factor ratios, although uncorrected, are clearly of the correct order of magnitude.

Using our data on methane and fluoroform, we are now in a position to make two estimates for

TABLE I[a,b]

ARRHENIUS FACTORS FOR THE REACTION Ph + RH → PhH + R

RH	$k_1/k_2^{1/2}$ (apparent) at 182° (molecule$^{-1/2}$ cm.$^{3/2}$ sec.$^{-1/2}$)	$E_1 - {}^1/_2E_2$ (kcal./mole)	$A_1/A_2^{1/2}$ (apparent) (molecule$^{-1/2}$ cm.$^{3/2}$ sec.$^{-1/2}$)
H_2	9.4×10^{-12}	6.5 ± 1	1.2×10^{-8}
CH_4	5.2×10^{-12}	7.5 ± 0.5	2.0×10^{-8}
CF_3H	6.2×10^{-12}	5.2 ± 0.5	1.9×10^{-9}

[a] For convenience of comparison with other radical data, approximate rate-constant ratios are quoted at 182° although this temperature is just at the limit of our range. [b] The last two columns in this table represent the equations of the lines drawn in Fig. 1. These lines were drawn by eye and the error limits quoted represent the largest reasonable amount by which we feel they may be skewed. In the particular case of H_2, the three points at $10^3/T \approx 1.9$ have been given less weight than the others because the photolysis time for these particular points was too long, and they are certainly somewhat low on this account.

D(Ph-H) by comparing reactions 1 and 3, and 1′ and 3′. Assuming that all the recombination reactions have zero activation energy (*i.e.*, methyl, trifluoromethyl, and phenyl) we have

$$D(\text{Ph–H}) = D(\text{CH}_3\text{–H}) + E_3 - E_1$$
$$= 102.5 \pm 1 + 9.2 \pm 0.2 - 7.5 \pm 0.5 = 104.2 \pm 1.7 \text{ kcal./mole}$$

and

$$D(\text{Ph–H}) = D(\text{CF}_3\text{–H}) + E_3' - E_1'$$
$$= 102.0 \pm 2 + 6.3 \pm 0.2 - 5.2 \pm 0.5 = 103.1 \pm 2.7 \text{ kcal./mole.}$$

These two determinations would be independent except for the fact that $D(\text{CF}_3\text{-H})$ is at present directly related to $D(\text{CH}_3\text{-H})$.[11,14]

Finally, consideration of our results for hydrogen gives additional confirmation of the essential correctness of these values: the activation energy for the attack of H atoms on benzene[15] is $E < 7$ kcal., which, taken in conjunction with our results gives D(Ph-H) < 104.5 kcal./mole.

(14) We have used $D(\text{CH}_3\text{–H}) = 102.5 \pm 1$ to be consistent with earlier work[11] but recent measurements by G. C. Fettis and A. F. Trotman-Dickenson [*J. Chem. Soc.*, 3037 (1961)] suggest that this might need raising a little.

(15) H. I. Schiff and E. W. R. Steacie, *Can. J. Chem.*, **29**, 1 (1951).

ON THE ADSORPTION OF POLYELECTROLYTES AT PLANAR DIELECTRIC SUBSTRATES

BY H. L. FRISCH AND F. H. STILLINGER

Bell Telephone Laboratories, Inc., Murray Hill, New Jersey

Received September 11, 1961

We have examined the effect of charges on polyelectrolytes on the adsorption free energy at a dielectric interface. We restrict ourselves initially to summing over all charges the electrical image forces, and then estimate separately the nonelectrostatic contributions to the free energy. We discuss the effect of pH changes and added electrolyte on the adsorption isotherm.

1. Introduction

A number of experimental investigations of the adsorption of natural[1] and synthetic[2-4] polyelectrolytes have been carried out recently or are under way. It therefore appears desirable to extend the theory of polymer adsorption,[5] particularly at the

(1) A. D. McLaren, *J. Phys. Chem.*, **58**, 129 (1954); A. D. McLaren, G. H. Peterson, and I. Barshad, *Soil. Sci. Soc. Amer. Proc.*, 22 (1958).

(2) T. L. Pugh and W. Heller, *J. Polymer Sci.*, **47**, 219 (1960).

(3) I. R. Miller, *Trans. Faraday Soc.*, **57**, 301 (1961); I. R. Miller and D. C. Grahame, *J. Colloid Sci.*, **16**, 23 (1961).

(4) R. J. Lauria, W. Schmidt, and F. R. Eirich, to be published.

solid–liquid interface, to the case of electrically charged macromolecules and/or solid adsorbents carrying electrical charges. A number of formidable problems arise in attempting to do this which become especially severe as the polymer concentration in the bulk solution, in contact with the solid adsorbent, increases. In view of this we shall in our theory be almost exclusively concerned with the most dilute concentration region in which the expected electrical potentials surrounding the macroion in bulk and at the interface are adequately described by appropriate solutions of the linearized Poisson–Boltzmann equation. A second consequence of considering only very dilute macroion solutions is that the adsorption isotherm relating the surface concentration c_s to the bulk macroion concentration c will be linear[5]

$$c_s = Kc + O(c^2) \qquad (1.1)$$
$$\left(\frac{\partial c_s}{\partial c}\right)_{c\to 0} = K$$

where K is a constant sometimes called the affinity.[4] This relationship is in many ways analogous to an interfacial Henry's law. We wish to compute K.

A further difficulty encountered with polyelectrolytes is their ability in some instances to modify their shape and dimension drastically with changes in their electrical environment. Thus an essentially randomly coiled polyion can for instance straighten out into an effectively rod-like or cigar-like shape on being brought from the bulk solution to the immediate vicinity of the adsorbent surface. This change in shape furthermore can affect the electrical environment as well as modify the adsorption behavior of the macroion. In this paper we restrict ourselves for simplicity to a model polyion which is a long rigid rod structure along which point charges Ze are distributed at random. There are $N\alpha$ such charges where N is the total number of ionizable groups and α represents the fraction ionized in solution. We assume that α is the same on the surface although clearly at high degrees of surface coverage by macro-or microions this cannot strictly be the case. Our α thus is essentially to be obtained from the bulk titration curve. Reasoning only by analogy to the adsorption behavior of uncharged polymers,[5] we expect that this simple model may at least qualitatively reproduce the adsorption behavior of real polyelectrolytes (even when their shapes depart from a rod-like structure) if the effective parameters of the rod-like model are suitably interpreted. The next section will be devoted to the affinity calculation for a rigid rod-like polycation or polyanion and the modification of these results for the case of a polyampholyte.

As the concentration of the bulk polyelectrolyte solution increases one expects to observe saturation of the adsorbent, merely because of the depletion of free surface sites and the small tendency even uncharged polymers show for extensive multilayer formation. The description of the shape and the capacity[4] of the complete adsorption isotherm is beyond the limits of the theory we shall develop. Nevertheless we shall make certain qualitative observations concerning these characteristics in a subsequent section. In the last section we shall make some comparisons of the theory with available experimental information. In part, the value of even such a simplified model theory as the one we shall develop is to indicate clearly the necessity for studying experimentally the affinity and capacity as well as the zeta potential of the pure adsorbent in the given solvent as a function of pH, temperature, etc., at constant ionic strength.

2. **The Affinity.**—We assume that our rigid rod polycation or polyanion solution is essentially so dilute as to be ideal, except for effects due to the ion atmospheres around the ionized groups on the polymer. To compute the free energy change on adsorption of our macroion we shall: (1) initially discharge the designated macroion in the bulk of solution; (2) bring the uncharged rod to the immediate vicinity of the adsorbent surface (which we take to be planar), arranged so as to assume the most probable final orientation which turns out to be parallel to the surface; and (3) finally recharge the rod so as to attain a random distribution of $N\alpha$ ionized groups along its length.

We refer chemical potentials to the ideal, bulk solution of uncharged rods, for which we can write

$$\mu = \mu^{(0)}(T) + kT \ln c \qquad (2.1)$$

Similarly on the surface, the chemical potential of these uncharged rods can be written

$$\mu = \mu_s^{(0)}(T) + kT \ln c_s \qquad (2.2)$$

If the rods remain uncharged, the condition for equilibrium which is the equality of μ as given by (2.1) and (2.2) yields immediately the linear relation

$$c_s = \exp\left[\frac{\mu^{(0)}(T) - \mu_s^{(0)}(T)}{kT}\right] c \qquad (2.3)$$

Comparing (2.3) with (1.1) we see that for the unionized rods the affinity is, as expected, independent of ionic strength, pH, as well as the surface charge σ on the adsorbent, if any. If the rod now is allowed to ionize, the affinity K will involve an additional electrical adsorption free energy W and (2.3) becomes

$$\frac{c_s}{c} = K = \exp\left[\frac{\mu^{(0)}(T) - \mu_s^{(0)}(T) - W}{kT}\right] \qquad (2.4)$$

where W may be interpreted as the reversible electric work that must be done in bringing the charged rod up to the surface. This work can be written as a product of the charge on the rod times one-half the change in mean electrostatic potential (caused by bringing the rod up to the surface) measured at the position of a typical ionized group on the linear macromolecule.

Fortunately, Stillinger[6] previously has considered in sufficient detail the appropriate solutions for this mean potential of the linearized Poisson–Boltzmann equation for boundary conditions corresponding to fixed point charge ions near the planar boundary between an electrolyte solution and a dielectric substrate. In what follows we shall pursue closely the basic theory developed in reference 6 which incidentally sketches the implications for simple (micro) ionic adsorption processes. Our

(5) H. L. Frisch and R. Simha, *J. Chem. Phys.*, **24**, 652 (1956).

(6) F. H. Stillinger, Jr., *Ibid.*, **35**, 1584 (1961).

model rod within the framework of this theory corresponds to a rigid linear distribution of monomer units which may ionize to yield point charges along the rod's axis. Using essentially eq. 20 of reference 6 adapted for our model, one finds that the mean potential is highly peaked in favor of a parallel orientation of the rod to the planar substrate. Adapting immediately this orientation, with only negligible error, one finds that W can be written as a sum of 4 contributions. Only the last of these involves the surface charge density σ of the substrate.

The first contribution to W is the unshielded image work per ionized group which amounts for $N\alpha$ groups to

$$N\alpha W \tag{2.5}$$

where w is the shift in adsorption free energy, A, for a monomer unit in pure solvent, caused by ionization, *i.e.*,

$$w = A_{\text{ionized}} - A_{\text{un-ionized}} \tag{2.6}$$

We are particularly interested in the dielectric constant dependence of w. Denoting by D and D_s the dielectric constants of the solution and adsorbent, respectively, we expect w to be positive if $D_s < D$ and negative if $D_s > D$. This contribution amounts to the work which has to be done in bringing an unshielded ionized group against the potential due to the single image charge within the surface, to an effective distance l. This distance, l, which is a characteristic of the adsorption system, is essentially determined by the molecular attractive surface forces responsible for the adsorption as well as the finite size of the adsorbing monomer units. With this characteristic cutoff distance l we can formally write for w

$$w = \frac{D - D_s}{D + D_s} \times \frac{(Ze)^2}{4\pi D l} \tag{2.7}$$

as would be expected from simple electrostatic theory (Poisson's equation).

The second contribution to W is the atmosphere displacement work, equal to (*cf.* eq. 24 of ref. 6)

$$\frac{N\alpha(Ze)^2\kappa}{D} F(\gamma) \tag{2.8}$$

where κ is the Debye shielding parameter,[7] which depends on the ionic strength, γ is $D/(D + D_s)$ and

$$F(\gamma) = {}^1/_2 - \gamma^2 \int_0^\infty \mathrm{d}l \, \frac{[(1 + l^2)^{1/2} - l]}{\gamma[(1 + l^2)^{1/2} - l] + l} \tag{2.9}$$

The function $F(\gamma)$ is plotted *vs.* γ in Fig. 2 of ref. 6, while for very small γ, $F(\gamma) \cong \gamma^2 \ln \gamma + {}^1/_2$. This contribution represents the reversible work required to displace the ion atmospheres surrounding the ionized groups into one hemisphere as each of these charges is brought up to the interface from the bulk solution.

The third contribution to W which must be considered arises because of the change in the shielded interaction, between surface and bulk, for pairs of ionized groups along the rod. If the rod is sufficiently long[8] so that end effects can be neglected

(7) This Debye κ refers only to small ions.

(8) Strictly speaking in the limit as the length of the rod and N approach infinity in such a way that average charge density on the rod remains constant.

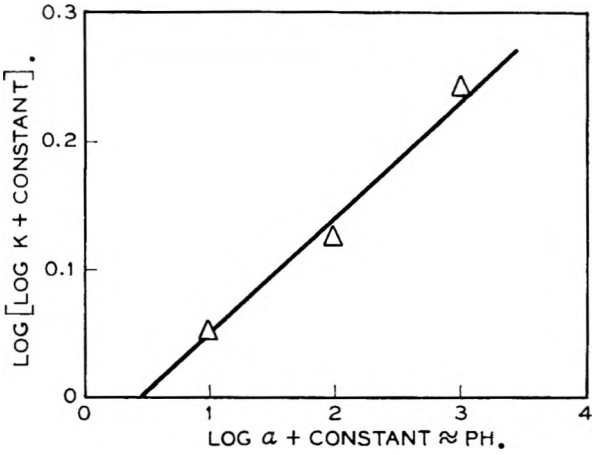

Fig. 1.—Plot of log [log (10^6K)] *vs.* log α + constant $\approx$ *p*H for aqueous polyacrylic acid ($M = 6 \times 10^5$) adsorbed on anatase (TiO_2) at a constant ionic strength of 0.1 at 25°. (K is dimensionless, being expressed as grams of polymer adsorbed per gram of adsorbent divided by grams of polymer per gram of polymer solution.)

and the average distance between neighboring randomly distributed ionized groups is a we can set this contribution equal to

$$\frac{N\alpha^2(Ze)^2\kappa}{D} \sum_{j=1}^{\infty} \int_0^\infty \mathrm{d}l \, J_0[(\kappa j a) l] \left\{ \frac{2\gamma}{\gamma[(1 + l^2)^{1/2} - l] + l} - \frac{1}{(1 + l^2)^{1/2}} \right\} \tag{2.10}$$

with $J_0(x)$ the zeroth order Bessel function of the first kind of x, by virtue essentially of eq. 25, etc., of ref. 6, applied once for the mean surface potential and once for the mean bulk potential. When $\gamma \neq 1$, the dominant small κ behavior is rigorously obtained from (2.10) by replacing, in the integrand, $2\gamma/\{\gamma[(1 + l^2)^{1/2} + l] - l\}$ by $2\gamma/(1 + l^2)^{1/2}$. Equation 2.10 then simplifies to

$$\frac{N\alpha^2(Ze)^2\kappa}{D} \left(\frac{D - D_s}{D + D_s}\right) \sum_{j=1}^{\infty} \frac{e^{-\kappa j a}}{\kappa j a} = -\frac{N\alpha^2(Ze)^2\kappa}{D} \left(\frac{D - D_s}{D + D_s}\right) \frac{1}{\kappa a} \ln(1 - e^{-\kappa a}) \tag{2.11}$$

As can be seen from (2.11) the change of interaction between pairs of ionized groups along the rod can in this limiting case be calculated as if the ion atmosphere of one group acted independently of the other. Even for larger κ, the integrand simplification of (2.10) still gives qualitatively the correct behavior. For very large κ this effect is completely negligible as can be seen directly from (2.10).

The final contribution to W is the work of bringing the charged rod up to the adsorbent surface, which itself bears a uniform surface charge density σ.[9] The zeta potential ζ for such a surface, computed from the appropriate solution of the linearized Poisson–Boltzmann equation is just

$$\zeta = \frac{4\pi\sigma}{\kappa D} \tag{2.12}$$

The corresponding reversible work for bringing up the charged rod is

$$N\alpha Ze\zeta = \frac{4\pi N\alpha Ze\sigma}{\kappa D} \tag{2.13}$$

(9) In the $c \to 0$ limit, σ is due only to small ions.

Combining (2.5), (2.7), (2.8), (2.11), and (2.13) we find that

$$W = \frac{N\alpha(Ze)^2}{D}\left\{\frac{1}{4l}\left(\frac{D-D_s}{D+D_s}\right) + F(\gamma)\kappa - \alpha\left(\frac{D-D_s}{D+D_s}\right)\frac{1}{a}\ln(1-e^{-\kappa a}) + \frac{4\pi\sigma}{\kappa Ze}\right\} \quad 2.14$$

and using (2.4)

$$\ln K = \ln K_{\text{un-ionized}} - \frac{W}{kT} \quad (2.15)$$

with

$$K_{\text{un-ionized}} = \exp\left\{\frac{\mu^{(0)}(T) - \mu^{(0)}(T)}{kT}\right\} \quad (2.16)$$

of (2.3).

The pH dependence of eq. 2.15, at constant ionic strength, resides completely in the pH dependence of α and σ, which we presume to be given functions of the pH. For vanishingly small κ, the second and third terms on the right-hand side of (2.14) can be neglected in comparison with the first and fourth terms. In this case, if σ furthermore is constant with changes in pH, at constant κ, we see that the pH dependence of ln K is directly proportional to the pH dependence of α. The importance of the dielectric constant immediately is apparent from (2.15). Given two polyelectrolytes, their adsorption behavior from solution onto a given substrate, if their electrical properties and environments are the same, is essentially determined by $K_{\text{un-ionized}}$. Then the affinity is the larger the smaller the solubility of the polymer in the given solvent.

To extend the previously developed theory of the affinity of polycations or polyanions to polyampholytes, we recognize that the generalization required is notational rather than conceptual. Thus, in place of a single charged state Ze previously available per monomer unit, it is necessary generally to admit states $Z_1e, Z_2e, \ldots, Z_ne$, representing, respectively, $N\alpha_1, N\alpha_2, \ldots, N\alpha_n$ point charges along the axis of the rod-like macromolecule.[10] For evaluation of the modified electrostatic contribution W to the affinity K, (2.9), we exhibit each of the four contributions previously discussed is the simpler case. Analogous to the previous presumption, the quantities $\alpha_1, \ldots, \alpha_n$ will be treated as experimentally available from bulk solution properties such as the titration curve.

The unshielded image work obviously becomes

$$\sum_{i=1}^{n} N\alpha_i w_i,\ w_i = \frac{D-D_s}{D+D_s} \times \frac{(Z_ie)^2}{4Dl_i} \quad (2.17)$$

One should of course be prepared to admit the necessity of distinct length parameters l_i for each monomer unit charge state; nevertheless it probably is true that these quantities do not differ drastically from one another, being equal to one or two Ångstrom units, unless the ionizing monomer units undergo radical steric changes with change in charge state.

The atmosphere displacement work, like the unshielded image work (2.17), is additive for all monomer units; its generalization is

$$\sum_{i=1}^{n} \frac{N\alpha_i(Z_ie)^2\kappa}{D} F(\gamma) \quad (2.18)$$

That contribution to W arising from the change in shielded interaction between ionized monomer units, in passing from bulk to interface, can depend upon the mean distribution of units along the rod (*e.g.*, atactic or isotactic distribution of acidic and basic monomers). For simplicity, we suppose that the various charge states of the monomers are randomly placed along the rod. The corresponding analog of expression (2.11) is

$$-\frac{N\kappa}{D}\left[\sum_{i=1}^{n}\alpha_i(Z_ie)\right]^2\left(\frac{D-D_s}{D+D_s}\right)\frac{1}{\kappa a}\ln(1-e^{-\kappa a}) \quad (2.19)$$

Finally, electrostatic work of polyampholyte adsorption against the (adsorbed microion) surface charge σ mean potential, the ζ potential has the form

$$\frac{4\pi N\sigma}{\kappa D}\sum_{i=1}^{n}\alpha_i(Z_ie) \quad (2.20)$$

The sum of the four expressions (2.17)–(2.20) is the appropriate polyampholyte W, which, when inserted into (2.9), yields the affinity K.

3. Qualitative Considerations Concerning the Isotherm and the Capacity.—Although mathematical difficulties preclude a quantitative theory of the complete adsorption isotherm we can make certain speculations concerning the shape of the isotherm on the basis of our knowledge of the adsorption behavior of non-ionic polymers. In more concentrated solutions the affinity calculated in the previous section no longer acts as the adsorption equilibrium constant. This is due to a number of effects, *e.g.*: (1) The effect due to the non-ideality of the solution which introduces activity corrections, which arise because in more concentrated solutions the concentrations in (2.1) and (2.2) have to be replaced by the corresponding activities. (2) The reversible electrical work W has to be replaced by $W(\theta)$, the modified reversible work of bringing up an ionized macroion to a surface of which a fraction θ of the sites already are occupied by previously deposited polymer segments. (3) The effects due to, in general, non-athermal lateral interactions between deposited polymer molecules. For small θ we can, by virtue of the known limiting behavior, write for the equilibrium adsorption coefficient $K_{\text{is}}(\theta)$

$$K_{\text{is}}(\theta) = K(1 + 0(\theta)) \quad (3.1)$$

with K the previously calculated affinity.[11]

The shape of the isotherm also will strongly depend on the extent of deposition of the segments of the adsorbed polyelectrolyte. In the presence of sufficiently strong attractive electrical forces between the substrate and the adsorbed macromolecule the fraction p of segments anchored at the adsorbent surface can be an appreciable fraction of the total number of segments.[5] A theory of this factor has been given[12] and a more refined version was

(10) For most polyampholytes, of course, $n = 2$ and Z_1 and Z_2 are just $+1$ and -1. The more general scheme here includes the possibility of monomer units being themselves, for example, polybasic acids.

(11) By $0(\theta)$ as $\theta \to 0$ we mean a function of θ which approaches zero faster than θ.

developed by Higuchi.[13] This indeed is experimentally found to be the case for both ionized and un-ionized aqueous polyvinylpyridine, polymethacrylic acid, and polyacrylic acid at a mercury surface.[3] Thus the number of anchor segments ν will be of the order of the total number of segments. An immediate consequence of this will be found in the great difficulty of completely reversibly removing deposited polymer with the same solvent, etc. At constant ionic strength and surface charge σ a change in a parameter such as the extent of ionization of the polyion will increase strongly the attractive forces if $D_s > D$ and thus cause a tendency for ν to increase. Since more segments now are deposited per polymer molecule, saturation is reached with fewer deposited polymer molecules, *i.e.*, at a lower capacity.

In studying polyelectrolyte adsorption, particularly at higher concentrations and varying ionic strengths, it must be remembered that polyelectrolyte not only competes for surface sites with the solvent but also with all the other ionic species in solution including any introduced by the substrate itself. Thus the surface charge density σ itself may vary drastically in the course of the adsorption and at arbitrary θ σ now must be taken as due to both adsorbed micro- and macro-ions. We already have mentioned effects due to relatively sudden changes in shape of the polymer molecule with the extent of ionization. This certainly can drastically affect ν, particularly for the more rigid polymers.

Since a large number of segments has to be deposited per polymer molecule an adsorption isotherm like that suggested for non-polar macromolecules[5] is indicated. In any case the Langmuir isotherm is a special case of this class of isotherms.

4. Relation to Experiment.—It has been the major purpose of this paper to point out the nature of the various types of electrostatic interactions which affect the polyelectrolyte adsorption affinity K, as well as to estimate their relative contribution to this quantity for the rod-like macromolecule model. In view of our results, the ideal experiments with which quantitatively to compare our theory would determine K as a function of pH, *at constant ionic strength or* κ. Separate determinations, also at constant κ, are of course required for the pH dependence of the α's and of σ.

We readily acknowledge that the most serious limitation of the present model computation lies in the rigid rod assumption concerning coil conformation. Many polyelectrolytes (those with a helical structure, well known among proteins) come rather close geometrically to this ideal. Others, however, have a random coil structure whose appearance is quite different. In any event, the major effect of coil geometry lies in the value of the affinity for the *uncharged* polymer, as exhibited in eq. 2.3, because this quantity contains the entropy lost in properly orienting the coil (whatever its form) at the surface for adsorption to take place. Each of the additional electrostatic contributions to the actual affinity, on the other hand, show only modest sensitivity to coil geometry; in fact, of the four contributions (2.7), (2.8), (2.11), and (2.13) to the work of bringing $N\alpha$ charged groups up to the interface, only the third has explicitly utilized the rod assumption. A less regular coil would still possess an analogous quantity to (2.11) where the summation

$$\sum_{j=1}^{\infty} \frac{e^{-\kappa j a}}{\kappa j a}$$

has been replaced by a more general expression taking into account the less regular distribution of charge–charge distances adsorbed on the surface. The qualitative effects of κ and dielectric constant variation of the more general version of (2.11), however, remain unchanged upon relaxing the rod assumption. The two reasons for presenting these computations for the rigid rod model therefore are: (1) The impossibility of exhibiting for all contributions explicit results for κ and dielectric constant effects on the affinity except for this simple case. (2) The insensitivity of these electrostatic contributions to the actual coil geometry.

Suitable detailed experimental data appear to be rather scarce. That the electrostatic effects discussed in this paper often seem to be important, though, is evident from measurement of the stabilization of negatively charged gold sols by polycations, even at low added polyelectrolyte concentrations,[2] for the observations are indicative of the strong electrostatic tendency to adsorb on a surface not only charged oppositely to that of the ionized monomer units, but on a surface whose dielectric constant (infinity for gold, an electrical conductor) is greater than that of the solution. Accordingly, both expressions (2.5) and (2.13) are negative.

Miller and Grahame[3] furthermore apparently have observed the rapid onset of saturation of the adsorption isotherm of polyvinylpyridines on mercury surfaces, indicative of the power of attractive electrical image forces to constrain a polyelectrolyte to lie flat on the substrate, and therefore consume a large area available for adsorption.

Recently the affinity of aqueous polyacrylic acid onto anatase (TiO_2) at the constant ionic strength of 0.1 has been measured as a function of pH between one and three pH units.[4,14] Fortunately, within this pH range estimates of σ from sedimentation rate studies indicate a less than twofold variation in σ, and σ is not tremendously large ($\zeta \sim 20$ mv.).[14] Within the same pH range, α (the extent of ionization) varies by a factor of 100.[14] The dielectric constant difference between the solution ($D \sim 78$) and the substrate ($D_s \sim 114$) is quite favorable ($D_s > D$). Letting $a = 3 \times 10^{-8}$ cm. and $l \sim 0.5 \times 10^{-8}$ cm. we find that the four contributions to $WD/N\alpha(Ze)^2$ are

$$\frac{1}{4l}\left(\frac{D - D_s}{D + D_s}\right) \sim 10^7 \text{ cm.}^{-1}$$

$$F(\gamma)\kappa \sim 0.275 \times 10^7 \text{ cm.}^{-1}$$

$$-1.9 \times 10^4 \text{ cm.}^{-1} \leq -\alpha\left(\frac{D - D_s}{D + D_s}\right)\frac{1}{a}\ln(1 - e^{-\kappa a})$$

(12) H. L. Frisch, *J. Phys. Chem.*, **59**, 633 (1955).

(13) W. I. Higuchi, *ibid.*, **65**, 487 (1961).

(14) We are indebted to Professor F. R. Eirich and Dr. R. J. Lauria for supplying us with these data.

$$\leq -1.9 \times 10^{2} \text{ cm.}^{-1} \text{ and}$$

$$\frac{4\pi\sigma}{\kappa Ze} \lesssim 10^{7} \text{ cm.}^{-1}$$

Thus, the most important terms are due to the unshielded image work per ionized group and the work of bringing the charged rod up to the adsorbent surface. We expect, therefore, W to be a linear function of α with positive slope. Equations 2.14 and 2.15 suggest that in this case the affinity should increase rapidly with pH. Figure 1 shows a plot of log [log K + constant] *vs.* log α + constant $\approx$ pH which is linear as expected in this case on taking the logarithm of (2.15). In the same pH range, at the constant ionic strength of 0.1, the capacity[4,14] decreases monotonically (*cf.* section 3).

CHAIN TRANSFER CONSTANT OF VINYLPYRROLIDONE WITH DEXTRAN

BY KWEI-PING S. KWEI[1] AND F. R. EIRICH

Institute of Polymer Research, Polytechnic Institute of Brooklyn, Brooklyn, N. Y.

Received September 11, 1961

The chain transfer constant of vinylpyrrolidone with a polymeric chain transfer agent, *e.g.*, dextran, was determined by modifying the conventional method to avoid the viscosity effect of the polymeric medium on the rate of polymerization. The chain transfer constant of vinylpyrrolidone with dextran was determined to be 5.87×10^{-4}.

In the course of our study of graft copolymerization of vinylpyrrolidone (VP) on dextran, initiated by azo-bis-isobutyronitrile in aqueous medium, the kinetics of the chain transfer reaction of the growing polyvinylpyrrolidone (PVP) chain radicals with dextran was examined. The latter, as a branched polyglucopyranose, contains tertiary hydrogen atoms and secondary hydroxy groups.

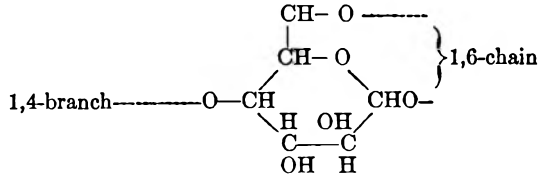

The chain transfer activity of low molecular weight secondary alcohols in the polymerization of styrene has been measured[2] and the secondary hydrogen on the carbon atom was found to be involved. Other chain transfer studies of alcohols[3-5] also confirm that displacement takes place on a hydrogen attached to the carbon bearing the –OH group. In addition, the C–H bonds in methylal have been found[6] to be activated by the two ether groups. Hence, the growing PVP chain radical likely will abstract a certain number of secondary or tertiary hydrogen atoms, leaving free radicals on dextran capable of initiating polymerization. We shall describe here a study of the rate of polymerization of VP and the chain transfer activity of VP chain radicals toward dextran.

Experimental

The detailed procedure for the preparation of the PVP–dextran graft copolymer and the isolation and characterization of the respective homo- and copolymers has been described previously.[6] A typical polymerization mixture consists of *n*-vinylpyrrolidone, dextran, azo-bis-isobutyronitrile, and water. All polymerization mixtures were rigorously degassed under high vacuum before use. The polymerization temperature was 50° and the total volume of each polymerization mixture was 50 ml. The polymerization time in each experiment was varied so that less than 5% conversion occurred. The molecular weight of PVP was determined from intrinsic viscosity measurements[7]

$$[\eta] = 5.65 \times 10^{-3} M_w^{0.55} \quad (1)$$

$$M_w = 197\,[\eta]^{1.8} \quad (2)$$

at 25° in water.

Results and Discussion

Even after repeated degassing of the polymerization mixture at 10^{-6} mm. (4 times) a prolonged induction period was observed. Further degassing did not seem to reduce the length of the induction period. The presence of dextran in the polymerization mixture lengthens the induction period but does not appear to affect the rate of polymerization. Chain transfer of PVP chain radical with dextran, however, is evidenced by the decrease of the $\overline{DP}$ of the free PVP homopolymer. Consequently, the conventional kinetic scheme was used.

$$1/\overline{DP} = 1/\overline{DP}_0 + C_s \frac{(S)}{(M)} + C_I \frac{(I)}{(M)} \quad (3)$$

Where

$C_s = k_{tr.s.}/k_p$, $C_I = k_{tr.I}/k_p$

M = monomer, S = solvent, I = catalyst

$\overline{DP}_0 = \overline{DP}$ when no transfer agent is present

For azo-bis-isobutyronitrile, which does not chain transfer with PVP radicals, the third term of eq. 3 can be eliminated. Two "solvents" are present, namely, water and dextran, and chain transfer reactions to both may occur. The transfer to water probably can be neglected. The transfer constant, C_s, thus has been assigned to be that of dextran.

It is well known that the rate of polymerization changes if the viscosity of the medium is raised.[8-10]

(1) Chemistry Department, Newark College of Engineering, Newark 2, New Jersey.

(2) M. Morton, J. A. Cala, and I. Piirma, *J. Am. Chem. Soc.*, **78**, 5394 (1956).

(3) C. T. Walling, "Free Radicals in Solution," John Wiley and Sons, Inc., New York, N. Y., 1957, p. 156, p. 285.

(4) R. A. Gregg and F. R. Mayo, *J. Am. Chem. Soc.*, **75**, 3530 (1953).

(5) W. R. Urry, F. W. Stacey, E. S. Huyser, and O. O. Juveland, *ibid.*, **76**, 450 (1954).

(6) K. P. S. Kwei and F. R. Eirich, *J. Polymer Sci.*, **53**, 81 (1961).

(7) G. B. Levy and H. P. Frank, *ibid.*, **17**, 247 (1955).

(8) P. J. Flory, "Principles of Polymer Chemistry," Cornell University Press, Ithaca, N. Y., 1953, p. 124.

The average degree of polymerization of the polymer at constant given conversion is also a function of viscosity. When increasing amounts of dextran were added to the polymerizing system, the solutions sharply increased in viscosity until at a dextran concentration of 12 g./100 ml. the relative flow time was eight times that of the solution without dextran. Therefore, the transfer constant could not be determined by the usual method of adjusting the catalyst concentration so as to keep the ratio $(I)^{1/2}/(M)$ constant while varying the concentration of the chain transfer agent.

The method for the evaluation of the chain transfer constant was modified accordingly in the following way. The viscosity of the medium was kept practically constant by using a constant concentration of dextran within the 50 ml. and varying the ratio of water to vinylpyrrolidone. The catalyst concentration was adjusted with the varying concentration of the monomer so as to keep $(I)^{1/2}/(M)$ constant. In this way, the plots of $1/\overline{DP}$ *vs.* (D)/(M) yielded straight lines from which the transfer constant was obtained by the slopes. Two different viscosity levels of the dextran solutions, *e.g.*, 1.5 g./50 ml. and 6 g./50 ml., were used and the two series of experiments gave parallel straight lines as shown in Fig. 1. It should be emphasized that utmost care must be taken in the isolation and purification of the PVP homopolymer from the reaction mixture in order to obtain accurate $\overline{DP}$ values.[7]

In Fig. 1, the ratio $(I)^{1/2}/(M)$ was kept constant at 1.8340×10^{-2}. The concentration of dextran was expressed in moles of base units, *e.g.*, $(C_6H_{10}O_5)$, per liter. The weight average molecular weight of dextran was 76,400. The percentage of conversion was below 4%.

The data of the series of experiments using a constant concentration of vinylpyrrolidone while varying the amounts of dextran showed that the molecular weights of the polymers obtained increased with the amounts of dextran because of the change in viscosity. The transfer constants derived from Fig. 1 at the two constant levels of viscosity were 5.92×10^{-4} and 5.82×10^{-4} in excellent agreement with each other.

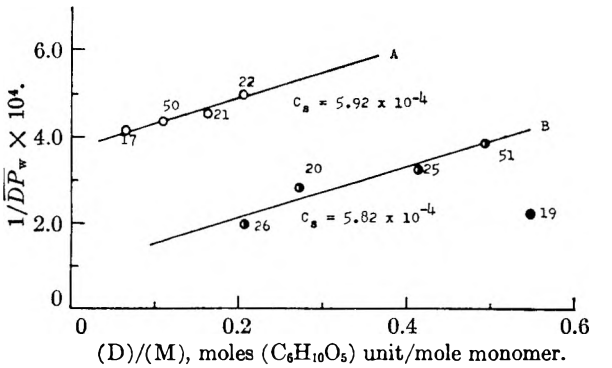

Fig. 1.—Chain transfer constant of dextran in the polymerization of vinylpyrrolidone: A, 1.5 g. dextran in 50 ml. H_2O; B, 6.0 g. dextran in 50 ml. H_2O; 19, 12.0 g. dextran in 50 ml. H_2O; $(I)^{1/2}/(M) = 1.834 \times 10^{-2}$; polymerization temperature = 50°; initiator = azo-bis-isobutyronitrile.

Comparing the mean value of these numbers, 5.87×10^{-4} at 50° (per mole of $(C_6H_{10}O_5)$ unit) with the available transfer constant of cyclohexanol with hexene-1 radicals,[5] it is seen to be one seventieth of the transfer constant of cyclohexanol (3.9×10^{-2} at 135°). The differences are quite reasonable if one considers the differences in the temperatures at which these transfer constants were measured and in the physical natures of cyclohexanol and of dextran, which is a macromolecular transfer agent.

Recently, the chain transfer constant of methyl-β-D-glucoside (or α-) with polyacrylonitrile radicals in dimethylformamide was measured to be 2×10^{-3} at 60°.[11] This certainly agrees very well with our data.

(9) S. W. Benson and A. M. North, *J. Am. Chem. Soc.*, **81**, 1339 (1959).

(10) A. M. North and G. A. Reed, *Trans. Faraday Soc.*, **57**, 859 (1961).

(11) G. Machell and G. N. Richards, *J. Chem. Soc.*, 3308 (1961).

INTERMITTENT CURRENT EFFECTS IN FREE ELECTROPHORESIS[1]

BY JAMES C. NICHOL

Department of Chemistry, University of Minnesota, Duluth, Duluth 12, Minnesota

Received September 15, 1961

The phenomena accompanying the interruption of current in the course of moving boundary experiments are discussed. During the period of current interruption diffuse boundaries of varying degrees of skewness are produced from the original steady state moving boundaries. On restoration of the current each of these sharpens and moves ahead, but at the same time a new stationary boundary appears at its trailing edge. The new boundary tends to disappear at a rate which depends on the current strength, with the original steady state eventually being restored. The same effect can be demonstrated on passage of current across mechanically formed boundaries if the concentrations are chosen correctly. Therefore, the observed phenomena arise as a result of conditions inherent at any diffuse electrolyte boundary. An explanation is presented in terms of fundamental moving boundary theory, and the experimental behavior is predicted qualitatively. The effect of current interruption on the electrophoresis of proteins is considered.

Introduction

Although the effect of current interruption on moving boundary behavior in free electrophoresis has not been discussed extensively in the literature, a few results have been reported. MacInnes and his co-workers[2,3] investigated the factors responsible for the maintenance of sharp boundaries in moving boundary transference experiments with strong electrolytes. They found that interruption or even reversal of the current for a few minutes in the course of an experiment did not affect the values of the transference numbers calculated from the steady state boundary velocities. The boundaries, which diffused rapidly during current interruption, were quickly restored to their original sharpness on resumption of current flow in the original direction. At the time that these experiments were performed, optical devices for determining the variation of refractive index with height in the cell channel were not available. Consequently, no observations were reported concerning the details of the diffusion of the boundary and restoration of the steady state. Stern and Reiner[4] investigated boundary anomalies and artifacts, and noted that an a.c. ripple in the d.c. current supply caused serious convection disturbances. Longsworth,[5] in a study of the moving boundary separation of salt mixtures, commented on the complexity of certain two-salt boundaries as manifested by their diffusion behavior on interruption of the current. Cann[6] carried out a detailed study on intermittent current electrophoresis of bovine serum albumin in acidic media, and concluded that the rate of growth of new boundaries which developed following current interruption should be interpreted in terms of the rate of diffusion of the buffer ions rather than the rate of an isomerization reaction, which originally had been thought to occur.

In the present paper, a detailed study of intermittent current effects (observed using schlieren and Rayleigh optics) in systems consisting for the most part of simple low molecular weight electrolytes is decribed, and the results are predicted qualitatively in terms of moving boundary theory.

Experimental

All experiments were performed at 1.00°, using a Spinco Model H electrophoresis apparatus. Rayleigh integral fringe photographs and schlieren photographs (Wolter phase plate) were taken simultaneously. Reagent grade chemicals were used without further purification. Compensation, where necessary, was carried out at a rate of 1 ml. per hr. with an electrolytic compensator. Rayleigh fringe displacements were measured, using a Gaertner Model M2001P comparator, as described previously.[7]

Moving boundaries were formed in the usual manner for 18 different systems involving compounds of known structure. The effects of interrupting the current for a range of time intervals were studied in detail. The experimental arrangements varied from simple strong electrolyte three-ion systems, of the type used in transference number determinations (Fig. 1a–1c), to weak electrolyte systems analogous to the electrophoresis of two proteins in a buffer (Fig. 1d). A number of special experiments were also carried out and are described below.

Results and Discussion

The experimental observations may be summarized as follows.

(a) In all cases, the characteristic feature was the appearance of a new, approximately stationary boundary at the trailing edge of each originally sharp moving boundary, following current interruption and restoration (Fig. 1). The phenomenon was observed regardless of the skewness developed by the moving boundary schlieren pattern upon current interruption. Some such diffusing patterns were almost Gaussian, some were definitely skew, as in Fig. 1a, and one ($NaCl$–$NaC_2H_3O_2$) even showed a tendency to split into two peaks. The phenomenon also was observed regardless of the current strength (0.25 to 4 mamp. for the iodide–phosphate system)[8] and of the duration of current interruption (from 5 min. to 2 hr.).

(b) The higher the current strength and the shorter the period of interruption, the more rapidly did the new boundary disappear and the more rapidly did the moving boundary regain its original steady state. For example, in the case of the iodide–phosphate system of Fig. 1, it was

(1) Presented in part at the 138th National Meeting of the American Chemical Society, New York, N. Y., September, 1960. This investigation was supported by a research grant (A-2240) from the National Institutes of Health, United States Public Health Service.

(2) D. A. MacInnes and I. A. Cowperthwaite, *Proc. Natl. Acad. Sci. U. S.*, **15**, 18 (1929).

(3) D. A. MacInnes and L. G. Longsworth, *Chem. Revs.*, **11**, 171 (1932).

(4) K. G. Stern and M. Reiner, *J. Electrochem. Soc.*, **97**, 213 (1950).

(5) L. G. Longsworth, Natl. Bur. Standards Circ. 524, 1953, p. 59.

(6) J. R. Cann, *J. Phys. Chem.*, **63**, 210 (1959).

(7) J. C. Nichol, E. B. Dismukes, and R. A. Alberty, *J. Am. Chem. Soc.*, **80**, 2610 (1958).

(8) Instead of field strengths, which vary markedly from phase to phase in the cell channel in a single experiment, current strengths are indicated in this paper. By way of illustration, however, it may be noted that the field strength is about 0.6 volt cm.$^{-1}$ in a solution of 0.075 *M* NaI at 1° when the current is 2 mamp. and the standard Tiselius cell of 0.75 cm.^{2} cross section is used.

observed that for a one-quarter hr. interruption with current restoration at 2 mamp., the boundary almost completely disappeared after 1 hr., while with a 1 mamp. current it was still of appreciable magnitude after 2 hr. With an interruption of 2 hr., application of a 2 mamp. current for 2 hr. was required to restore the original conditions. Pronounced convective effects frequently were noted at higher current strengths, and undoubtedly hastened the disappearance of the new boundaries. Convection often was preceded by the appearance of a marked inverted refractive index gradient immediately ahead of the new boundary. A corresponding inverted density gradient would reasonably account for the convection.

To make sure that changes were occurring only in the region of the sharpening moving boundary, and that there was no net transport of material out of the cell channel, fringe displacements were determined for all boundaries in the cell channel for which the fringes were sufficiently resolved to be counted. For experiments involving very sharp boundaries, diffusion was allowed to take place at the end of the run, and the total number of fringes was checked with that at the beginning of the run. The only significant changes occurred in the neighborhood of the diffuse boundaries as they sharpened. Table I illustrates the constancy of total fringe displacements in the cell channel for the iodide–phosphate experiment at 1 mamp. It also illustrates the persistence of the new boundary (column 4).

TABLE I

FRINGE DISPLACEMENTS FOR IODIDE–PHOSPHATE EXPERIMENT AT 1 MAMP.

(1) Min. after current applied	(2) Initial boundary	(3) Moving boundary	(4) New boundary	(5) Total (2) + (3) + (4)
0[a]	30.47	87.90	0	118.37
23	30.46	87.94[b]		118.40
49	30.48	85.51	2.38	118.40
57	30.44	85.96	1.97	118.37
73	30.44	86.25	1.68	118.37
136	30.44	86.88	1.02	118.34

[a] Following a current interruption of 17 min. [b] Resolution between boundaries (3) and (4) insufficient for analysis.

(c) Once the steady state was restored, the velocity of the moving boundary was found to be the same as the original boundary velocity (*cf.* MacInnes, *et al.*[2,3]). For example, for the iodide–phosphate system of Fig. 1, the boundary velocity was observed to be constant and identical to the velocity prior to current interruption to within 0.1% as calculated from observations beginning 26 min. after current restoration (4 mamp.), following an interruption of 22 min. (In the initial period following current restoration, before the steady state was attained, the boundary was changing shape and it was felt that its location could not be clearly defined for the purpose of determining boundary velocity.)

(d) The magnitude of the refractive index change across the new boundary, determined as soon as the latter was sufficiently resolved from the moving boundary to be measured, varied for the different

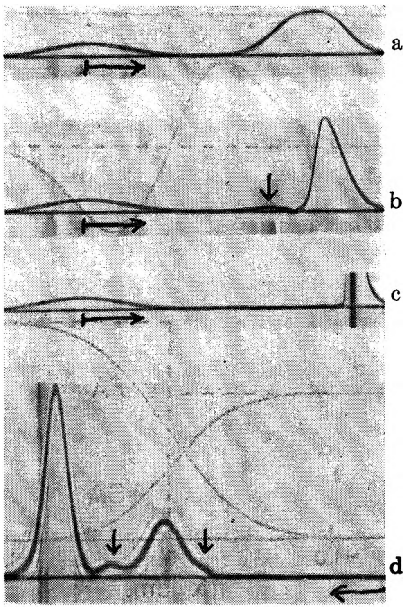

Fig. 1.—Tracings of schlieren patterns illustrating the intermittent current effect. Patterns a–c, descending system 0.075 *M* NaI (α) ← 0.0445 *M* NaH_2PO_4 (β)::0.025 *M* NaH_2PO_4 (γ) (see ref. 7 for notation): (a) diffuse boundary 120 min. after current interruption; (b) 19 min. after restoration of 2 mamp. current which was turned on just after picture (a) was taken; (c) 41 min. after (b) (only the bottom portion of the very sharp boundary is shown). Pattern (d), ascending system 0.10 *M* NaOH, 0.15 *M* HOAc (δ) ← NaOH, HOAc, HAsp (γ) ← NaOH, HOAc, HAsp, HGlut (β)::0.10 *M* NaOH, 0.15 *M* HOAc, 0.03 *M* HAsp, 0.03 *M* HGlut (α), 19 min. after restoration of 16 mamp. current, following a 35 min. current interruption (OAc = acetate, Asp = aspartate, Glut = glutamate). The initial boundary lies beyond the right edge of (d). Vertical arrows indicate new boundaries; horizontal arrows indicate direction of boundary movement.

systems from 2 to 14% of that across the moving boundary.

The new boundary effect also was observed upon application of a current to mechanically formed diffusing boundaries, such as the initial boundary in an electrophoresis experiment, provided that the concentration of the original indicator solution were made exactly equal to that of the adjusted phase produced behind the boundary on passage of current. For example, flow of current across a mechanically formed boundary between 0.075 *M* sodium iodide and 0.0445 *M* monosodium dihydrogen phosphate, in the direction required to make the sodium iodide the leading electrolyte, gave rise to a new temporary boundary. This boundary was practically identical in size and in rate of disappearance with that observed on passage of the same current across the corresponding electrophoretically formed boundary which had been allowed to diffuse for the same length of time. The 0.0445 *M* concentration value for the phosphate solution was determined by conductometric analysis of the adjusted phase formed in a moving boundary experiment. Similar results were obtained with other properly adjusted systems. In the usual electrophoresis experiment the above adjustment of concentrations is not made, a permanent boundary remains near the site of the initial boundary, and a temporary gradient is not detected. It may be concluded, then, that the new

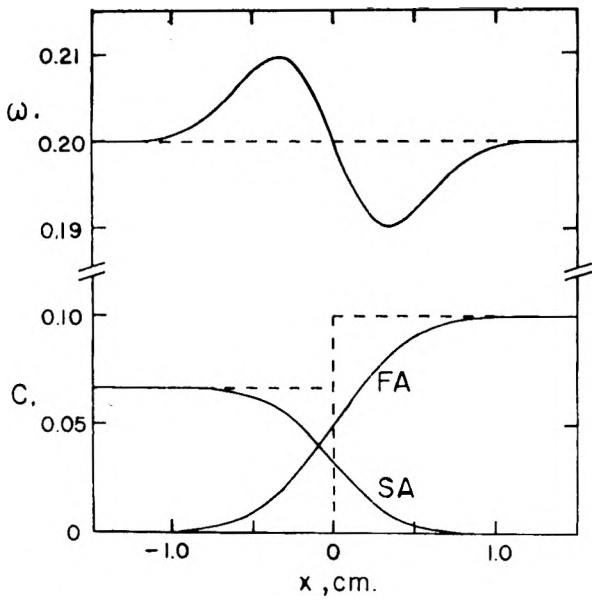

Fig. 2.—Kohlrausch regulating function, ω, and equivalent concentration, C, as a function of distance along the cell channel for a diffusion boundary between electrolytes FA and SA (see text): ----, values at the instant of boundary formation; ———, values after diffusion for 3600 sec.

boundary effect will be observed regardless of the method—mechanical or electrophoretic—of formation of a boundary between two electrolyte solutions provided that the concentrations are chosen correctly in the mechanical case.

The above phenomena can be explained by considering the fundamental laws of moving boundary behavior.[9] The discussion will be restricted to strong electrolytes, although undoubtedly the explanation for weak electrolyte systems is essentially the same, since the same experimental behavior is observed. The concentrations of the electrolytes present in the two phases on either side of a moving boundary are governed by the requirement of constancy, across the boundary, of the Kohlrausch regulating function $\omega = \Sigma C_i/r_i$, where C_i is the equivalent ion concentration and r_i is the relative mobility of ion i.[10] Immediately upon cessation of current (or immediately after the two solutions come in contact in the case of a mechanically formed boundary) diffusion commences, whereupon ω no longer maintains its steady state value, but varies with distance along the cell in the diffusion zone. The form of this variation is illustrated in the top half of Fig. 2 for strong electrolytes FA and SA. The ions of these electrolytes are considered to have approximately the relative mobilities of the ions in KCl and LiCl ($r_F = -r_A = 2r_S = 1$), so that $\sqrt{D_{FA}/D_{SA}} = 1.225$, where the D's are diffusion constants. D_{FA} is taken to be 2×10^{-5} cm.^{2} sec.$^{-1}$, which is the approximate experimental value for KCl at 25°. Flow coupling during diffusion is neglected. The concentrations of the original solutions are taken as $C_{FA} = 0.1\ M$ and $C_{SA} = 0.0667\ M$, the latter value being that calculated, with the aid of the regulating function, for the adjusted phase behind a 0.1 M FA solution in a moving boundary experiment. The concentration profiles are shown for comparison with ω in the bottom half of Fig. 2.

The passage of an electric current across this boundary brings about the restoration of the constancy of ω in the diffusion zone. The mechanism of the restoration can be envisaged as follows: Let us suppose that the diffuse boundary does not change continuously with distance, x, but rather consists of a large number of phases of constant composition meeting at infinitely sharp boundaries. Further, let us suppose that the composition of each phase is that which would exist at the midpoint of the phase if the concentrations were to vary with distance in the continuous and Gaussian manner of Fig. 2. Now upon passage of current across the series of stepwise boundaries, the junction of each pair of phases constitutes an initial boundary in a three-ion moving boundary system. Since for an n-ion system, $n - 1$ boundaries (including a stationary boundary) are expected on passage of current,[10] we predict two boundaries at each junction, one moving, and the other remaining at the site of the junction. The situation at each junction will be, in fact, like that described by Longsworth[11] for the system $K,Cl,IO_3(\alpha) \leftarrow K,Cl,IO_3(\beta) :: K,Cl,IO_3(\gamma)$, except that each of the large number of moving boundaries sooner or later will overtake other stationary and moving boundaries ahead of it. When a stationary boundary is overtaken, the phase behind it is replaced by the phase behind the overtaking boundary, and at the same time a new boundary moves out ahead. When a moving boundary is overtaken, the only effect is the reduction of the number of boundaries by one, with the disappearance of the intermediate phase, since ω is the same throughout the three phases involved. The readjustment of phases continues until a steady state is achieved.

Although a rigorous mathematical treatment for the time-dependent behavior in the limiting real case of an infinitely large number of steps has not yet been developed, calculations carried out assuming a small number of steps predict the formation of the new temporary boundary and lend support to the validity of the model. This is illustrated in Fig. 3 for electrolytes FA and SA, which are assigned the same end concentrations as in Fig. 2. The graph of refractive index *vs.* arbitrary distance units along the cell channel for a hypothetical step-wise boundary made up of five phases (including the end phases) is shown in Fig. 3a. The equivalent refractions are taken as 10.00 and 8.73 in arbitrary units for FA and SA.[12] The concentrations of FA and SA, selected so that there are equal jumps in C_{FA}, are indicated in Fig. 3a. It is a simple, if rather tedious, matter to calculate the refractive index profile at any time, from the known relative mobilities, equivalent refractions, and initial concentrations. This is done in Fig. 3b

(9) The author is indebted to one of the referees for his comments which greatly aided in strengthening the original explanation, particularly as regards the effect of diffusion on the Kohlrausch regulating function, and for his suggestion of the regulating function plot shown in Fig. 2.

(10) V. P. Dole, *J. Am. Chem. Soc.*, **67**, 1119 (1945).

(11) L. G. Longsworth, *ibid.*, **67**, 1109 (1945).

(12) L. G. Longsworth, *ibid.*, **66**, 449 (1944).

and 3c. The time t from the start of the experiment is given in arbitrary units. It is assumed that diffusion is negligible and that all boundaries remain infinitely sharp. At $t = 0.65$, two moving boundaries still are present while at $t = 1.00$, the second has just overtaken the first, and no region containing both FA and SA remains. It is evident that the model does indeed predict qualitatively the experimental behavior, both as regards the development of the new boundary (a rise in n at the left of the diagrams) and the inversion of refractive index immediately ahead of it. Furthermore, a similar profile is obtained for the density (Fig. 3d), assuming that the electrolytes are KCl and LiCl and that each contributes independently to the density of the solution. The predicted density minimum would lead to gravitational instability and the convective effects observed for real systems. No assumption has been made as to whether the boundary is ascending or descending, and the model, therefore, predicts the same results for both cases, which is in accordance with experiment. The predicted absence of leading electrolyte from the region of the new boundary once the latter is well separated from the moving boundary was confirmed experimentally for the iodide–phosphate system of Fig. 1. No trace of iodide could be detected in a sample removed from behind the moving boundary 25 min. after resumption of current.

Calculations similar to those above were carried out with similar results on a system analogous to the electrophoresis of a single protein in a buffer. The idealized calculations thus do predict qualitatively the significant observed effects in both transference number and protein–buffer type systems.

Consideration was given to the possibility that the development of inverted conductivity gradients during diffusion might account, at least in part, for the intermittent current phenomena. In moving boundaries, Longsworth[12] has demonstrated that the maxima of different electrolyte gradients do not in general coincide. This explains the frequent occurrence of skewed schlieren patterns, the skewness of which often becomes more apparent as diffusion proceeds following current interruption. However, calculations of concentration and conductivity gradients across some of the diffuse boundaries studied, using values for the diffusion coefficients obtained from the limiting ion conductances, and correcting for interacting flows,[13,14] although predicting the skewness of the schlieren patterns, showed at the most only slight fluctuations in a steady increase of conductivity from the low to high conductivity phases on either side of the boundary. Conductance measurements obtained by drawing the contents of the cell channel slowly through a micro conductance cell, with readings at short intervals, confirmed this. Finally, the fact that essentially identical results are obtained in experiments with electrophoretically and mechanically formed boundaries suggests that the non-coincidence of the electrolyte gradient maxima in the former plays an insignificant role in the phenomena observed.

The phenomena discussed in this paper appear to be perfectly general, and to be inherent in the

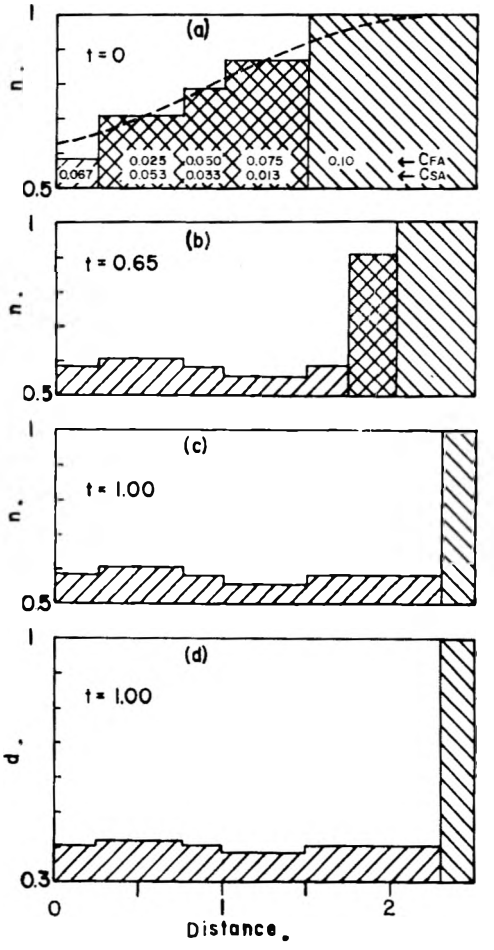

Fig. 3.—Plots illustrating the effect of passage of an electric current on a highly idealized diffuse boundary. The refractive index contributions, n, and the density contributions, d, in excess of the solvent values are plotted in arbitrary units against distance in the cell, also in arbitrary units (shown only in (d)), for various times of current passage, t. The distance scale is the same in all four plots //////, SA present; \\\\\\, FA present.

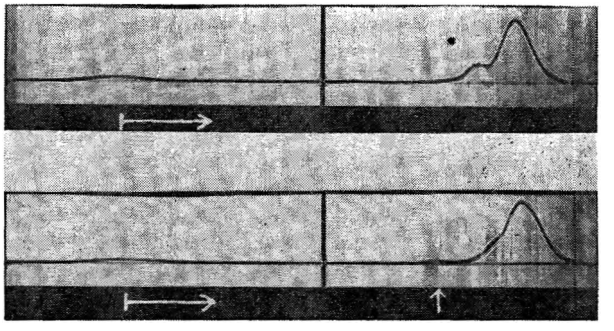

Fig. 4.—Effect of current interruption on electrophoresis of crude egg albumin preparation. Top, 16 mamp. for 234 min.; bottom, 16 mamp. for total of 234 min. with current interruption of 252 min. after 162 min. of electrophoresis. Vertical arrow indicates new boundary; the vertical line in the center is a reference line.

(13) L. J. Gosting, "The Structure of Electrolytic Solutions," ed. by Walter J. Hamer, John Wiley and Sons, Inc., New York, N. Y., 1959, pp. 175 ff.

(14) L. J. Gosting, "Advances in Protein Chemistry," M. L. Anson, K. Bailey, and J. T. Edsall, eds., Vol. XI, Academic Press, Inc., New York, N. Y., 1956, p. 540.

conditions produced in any diffusing boundary by the act of diffusion itself, regardless of whether the boundaries are produced mechanically or in the course of electrophoresis. In any free electrophoresis experiment, including those with proteins or other macromolecules in buffers in which a current interruption occurs, the formation of new boundaries of varying degrees of persistence is to be expected. Since one of the most important applications of electrophoresis is in the study of proteins, an intermittent current experiment was carried out on a crude preparation of egg albumin, using a sodium diethylbarbiturate buffer of 0.1 ionic strength. The sample was very thoroughly dialyzed. The results of a 2-hr. interruption are shown in Fig. 4. The patterns with and without current interruption are distinctly different, and, as expected, a new stationary peak indeed is observed at the trailing edge of the rear peak on restoration of current (vertical arrow in Fig. 4b).

From the results reported in this paper, it would appear that current interruptions should be avoided whenever possible once a run is started since they give rise to new peaks which, as far as can be seen at present, have no significance themselves in revealing new data about the system and easily can give rise to incorrect quantitative analyses with an undetermined error, since they disappear at very variable rates, depending on the conditions. This is especially true when more than one component is present and resolution is poor, as Fig. 4 clearly demonstrates.

Acknowledgment.—The author wishes to thank Dr. L. J. Gosting for helpful discussions in connection with the diffusion coefficient calculations.

SPECTROSCOPIC STUDIES ON THE COLOR REACTION OF ACID CLAY WITH AMINES. II. THE REACTION WITH AROMATIC TERTIARY AMINES

BY HAJIME HASEGAWA

Department of Applied Chemistry, Faculty of Science and Engineering, Waseda University, Tokyo, Japan

Received September 16, 1961

The color reaction of acid clay in benzene with the aromatic tertiary amines tri-*p*-tolylamine, di-*p*-tolylphenylamine, triphenylamine, tetra-*p*-tolylbenzidine, and tetraphenylbenzidine, was studied spectroscopically between 300 and 900 mμ, using the opal glass transmission method for translucent materials. In parallel with these observations, the products on oxidation of these amines without acid clay were analyzed by both spectroscopic and potentiometric titrations. The analysis of the products revealed that the radicals of the three tertiary monoamines and the semiquinone and quinoid compounds of the two benzidine derivatives are responsible for the color reaction with acid clay.

Introduction

In a previous study on the color reaction of acid clay with benzidine and tetramethylbenzidine,[1] it was found that the quinoid and meriquinoid forms of these reagents were responsible for the color reactions. This result suggested that the transfer of an electron from the nitrogen atoms of the reagents to acid clay plays an important role in the formation of the colored compounds, so that a radical of amine is formed on acid clay. In the present study, the absorption spectra of the colored acid clay with three tertiary monoamines (tri-*p*-tolylamine, di-*p*-tolylphenylamine, and triphenylamine) and two benzidine derivatives (tetra-*p*-tolylbenzidine and tetraphenylbenzidine) were measured by the opal glass transmission method, which recently was developed for obtaining sharp absorption bands of translucent materials,[2] in order to prove the formation of the radicals in these reactions. The spectra thus obtained were compared with the data obtained for the products on oxidation of these reagents without acid clay. The results clarified not only the formation of radicals for the tertiary monoamines in the primary act of acid clay, but also the further reaction, the formation of semiquinones and quinoid compounds for the benzidine derivatives.

(1) H. Hasegawa, *J. Phys. Chem.*, **65**, 292 (1961).

(2) K. Shibata, "Spectrophotometry of Translucent Biological Materials—Opal Glass Transmission Method," in "Methods of Biochemical Analysis," D. Glick, ed., Vol. VII, Interscience Publishers, Inc., New York, N. Y., 1959.

Experimental

Preparation of Samples.—The Itoigawa Clay of Montmorillonite group was used for this research. It was washed with water and dried *in vacuo* before its use. The tri-*p*-tolylamine, di-*p*-tolylphenylamine, and triphenylamine used in this study were purified by recrystallizing them from their ethanol solutions; the melting points of the purified samples were 116.5, 108.5, and 127°, respectively. Tetra-*p*-tolylbenzidine and tetraphenylbenzidine were prepared from di-*p*-tolylphenylamine and triphenylamine, respectively, using CrO_3 as the oxidizing agent, and the products were purified chromatographically on alumina with benzene as solvent. The melting points of tetra-*p*-tolylbenzidine and tetraphenylbenzidine were 224.5 and 210°, respectively. The colored acid clay suspensions were obtained by adding 0.1–6.0 ml. of 0.1% solution of amine in benzene to 40 ml. of 1.0% clay suspension. Tri-*p*-tolylamine perchlorate used to compare its spectrum with the spectrum of colored acid clay was prepared by the method of Weitz and Werner.[3]

Spectroscopic Observations.—The absorption spectra of colored acid clay suspensions were measured by the opal glass transmission method with a Shimadzu Model RS-27 recording spectrophotometer, using cells 1 mm. thick.

Results and Discussion

(I) The Coloration with Aromatic Tertiary Monoamines.—When tri-*p*-tolylamine was added to the clay suspension in benzene, a bright blue color appeared. The colored acid clay thus obtained showed a spectrum with a sharp band at 680 mμ and a low band at 590 mμ (Table I). This spectrum is similar to the spectrum of the radical, $(CH_3C_6H_4)_3N\bullet^+$, of tri-*p*-tolylamine, obtained by Granick and Michaelis[4] on its chemical oxida-

(3) E. Weitz and H. Werner, *Ber.*, **59**, 2307 (1926).

tion and by Lewis and Lipkin[5] on its photooxidation, although the two bands of the colored acid clay are located at slightly longer wave lengths as compared with those of the radical. A similarity also was found between the spectrum of the colored acid clay and the spectrum of the chloroform solution of tri-*p*-tolylamine perchlorate with bands at 670 and 580 mμ. One may, therefore, presume that the coloration on the acid clay is due to the formation of a radical of tri-*p*-tolylamine, if the red shift may be attributed to a change of the electronic state due to adsorption. This possibility was examined by observing the spectrum of the mixture of acid clay with tri-*p*-tolylamine perchlorate in chloroform. The blue perchlorate in solution was completely adsorbed by mixing it with the clay; the supernatant then becomes colorless. The spectrum of the mixture was in good agreement both in shape and in maximum position with the spectrum of the colored acid clay.

TABLE I

THE ABSORPTION MAXIMA AND RELATIVE INTENSITIES OF THE COLORED CLAY WITH AROMATIC TERTIARY MONOAMINES

Reagent	Vol. of the reagent soln., ml.	Absorption, max., mμ	Relative intensity
Tri-*p*-tolylamine	0.1	590	0.250
		680	.615
Di-*p*-tolylphenylamine	.1	575	.290
		683	.700
Triphenylamine	.1	580	.355
		678	.540
	.2	480	.580
		580	.420
		678	.735

The acid clay was treated with di-*p*-tolylphenylamine in benzene. The spectrum of the colored suspension was similar in shape to the spectrum of the colored clay with tri-*p*-tolylamine. However, the positions of the major and minor peaks were shifted slightly to 683 and 575 mμ as shown in Table I. The similarity of the bands suggests the formation of a radical, $(CH_3C_6H_4)_2(C_6H_5)N\bullet^+$, of di-*p*-tolylphenylamine on the acid clay.

Complication arises when one deals with triphenylamine. Upon addition of 0.1 ml. of its benzene solution to 40 ml. of a clay suspension, the mixture gave a result qualitatively similar to the spectrum of the colored clay with tri-*p*-tolylamine. The absorption spectrum of the mixture has two bands at 678 and 580 mμ in the Soret region (Table I). However, another different peak appeared at 480 mμ when we treated the clay with 0.2 ml. of the same benzene solution of triphenylamine. One may, therefore, infer that the bands at 678 and 580 mμ are due to the radical, $(C_6H_5)_3N\bullet^+$, of triphenylamine, and the additional band at 480 mμ arises from a compound different from the radical, which is discussed later in more detail.

(4) S. Granick and L. Michaelis, *J. Am. Chem. Soc.*, **62**, 2241 (1940).

(5) N. Lewis and D. Lipkin, *ibid.*, **64**, 2801 (1942).

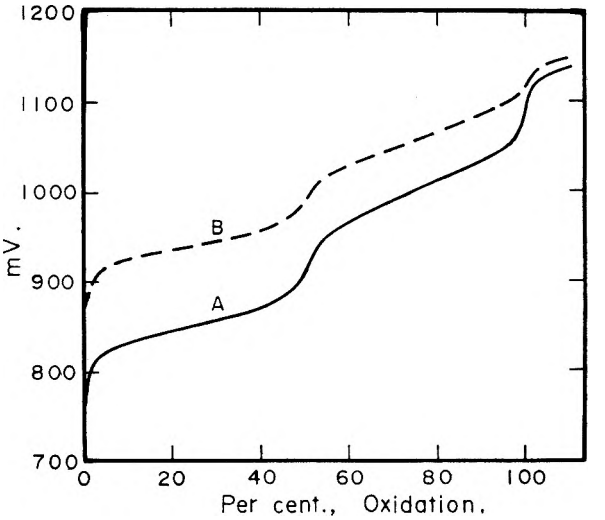

Fig. 1.—Potentiometric titration curves of tetra-*p*-tolylbenzidine (concentration, 2.8×10^{-4} *M*) and tetraphenylbenzidine (concentration, 2.6×10^{-4} *M*) with potassium bichromate (concentration, 16.5×10^{-4} *M*): curve A, tetra-*p*-tolylbenzidine; curve B, tetraphenylbenzidine.

(II) The Coloration with Tetra-*p*-tolylbenzidine and Tetraphenylbenzidine.—The absorption spectra of the clay suspension colored with tetra-*p*-tolylbenzidine in benzene have two bands as shown in Table II. When 0.4 ml. of 0.1% solution of tetra-*p*-tolylbenzidine was added to 40 ml. of the clay suspension, a high band appeared at 740 mμ and a low band at 490 mμ. The increase of the volume of the amine solution to 6.0 ml. caused the intensification of the 490 mμ band and the lowering of the 740 mμ band. This fact suggests that two different compounds each having a different absorption band are formed in this color reaction.

TABLE II

THE ABSORPTION MAXIMA AND RELATIVE INTENSITIES OF THE COLORED CLAY WITH BENZIDINE DERIVATIVES

Reagent	Vol. of the reagent soln., ml.	Absorption, max., mμ	Relative intensity
Tetra-*p*-tolylbenzidine	0.4	490	0.760
		740	1.180
	6.0	490	1.150
		740	0.640
Tetraphenylbenzidine	0.4	480	0.650
		700	1.060
	6.0	480	0.975
		700	0.470

The spectra of the mixtures of clay with tetraphenylbenzidine showed two peaks at 700 and 480 mμ. Similarly as above, the relative height of the 480 mμ band to that of the 700 mμ band was increased when the volume of the tetraphenylbenzidine solution was raised from 0.4 to 6.0 ml. It is clear from these results that the color reaction affords two different products which are characterized by their absorption bands at 480–490 and 700–740 mμ, respectively.

(III) Potentiometric Titration of Tetra-*p*-tolylbenzidine and Tetraphenylbenzidine.—The above spectroscopic observations of the colored clay suspensions *in situ* clarified that the products formed by coloration with tri-*p*-tolylamine and

di-*p*-tolylphenylamine and the major product formed with triphenylamine are their radicals. We have, however, unknown products which are the minor product formed from triphenylamine having a band at 480 mμ, and two different groups of compounds formed with the benzidine derivatives described above. In order to determine the structure of these compounds, spectroscopic and potentiometric titrations were conducted for the oxidation products of tetra-*p*-tolylbenzidine and tetraphenylbenzidine without acid clay.

Forty ml. of 2.8×10^{-4} *M* tetra-*p*-tolylbenzidine solution and 2.6×10^{-4} *M* tetraphenylbenzidine solution were titrated with 16.5×10^{-4} *M* potassium bichromate under nitrogen gas. Glacial acetic acid, containing sulfuric acid in 0.25% by volume, was used as the solvent, and was found to stabilize the products formed with tetraphenylbenzidine. The values of the oxidation–reduction potential are plotted against the degree of oxidation in Fig. 1. As seen from this figure, two different compounds are formed on oxidation; one is observed at 50% oxidation, and the other at 100% oxidation. The absorption spectra were observed at these stages of oxidation, and the results are shown in Table III, which shows a great difference in the absorption maxima between the products formed at these oxidation stages. The peak positions of the products from tetra-*p*-tolylbenzidine and tetraphenylbenzidine were 490 and 480 mμ at 50% oxidation and 740 and 700 mμ at 100% oxidation, respectively. It is, therefore, certain that the product obtained by coloration of acid clay with these benzidine derivatives is different depending upon the degree of oxidation. The product of 50% oxidation would be their semiquinone, and the 100% oxidation product would be their quinoid compound. The fact that the minor product of coloration of acid clay with triphenylamine has an absorption band at 480 mμ indicates that it may be the same compound as described above, which is the semiquinone of tetraphenylbenzidine. The mechanism of its formation is, therefore, the dehydrogenation of two molecules of triphenylamine, which affords tetraphenylbenzidine.

TABLE III

THE ABSORPTION MAXIMA AND RELATIVE INTENSITIES OF THE OXIDIZED PRODUCTS OF BENZIDINE DERIVATIVES

Sample	Degree of oxidation, %	Absorption, max., mμ	Relative intensity
Tetra-*p*-tolylbenzidine	50	490	0.560
		740	.040
	100	490	.040
		740	.875
Tetraphenylbenzidine	50	480	.550
		700	.040
	100	480	.060
		700	.720

Summarizing the results obtained in the present study, the color reactions of acid clay with aromatic tertiary monoamines and benzidine derivatives are the oxidation of these reagents. With tri-*p*-tolylamine and di-*p*-tolylphenylamine as the reagent, a single compound of its radical is formed. With triphenylamine, two products are formed; they are its radical and the semiquinone of tetraphenylbenzidine. The semiquinone may be formed from the radical of the primary product. We obtain also two different products with benzidine derivatives: one their semiquinones and the other quinoid compounds obtained by further oxidation of semiquinones. The initial products of these semiquinones may be regarded as the radicals of benzidines. It therefore may be concluded that the coloration of acid clay with aromatic tertiary monoamines and benzidine derivatives is due to the transfer of an electron of the reagent molecule to acid clay.

Acknowledgment.—The author wishes to express his hearty thanks to Prof. K. Shibata for his kind guidance and valuable suggestions throughout this research, and to Asahi Glass Co. for the financial support in carrying out this investigation.

THE KINETICS OF THE DECARBOXYLATION OF CINNAMALMALONIC ACID IN AROMATIC AMINES

BY LOUIS WATTS CLARK

Department of Chemistry, Western Carolina College, Cullowhee, N. C.

Received September 23, 1961

Kinetic data are reported for the decarboxylation of cinnamalmalonic acid in six aromatic amines—aniline, *o*-toluidine, *o*-chloroaniline, N,N-dimethylaniline, quinoline, and 8-methylquinoline. The parameters of the Eyring equation are evaluated and compared with those for malonic acid obtained previously. The enthalpy–entropy plots of both sets of data are linear. Both the enthalpy and entropy of activation for the cinnamalmalonic acid reaction in a given solvent generally are lower than are those of malonic acid, reflecting the stronger acidity and greater bulk of the derivative.

Kinetic studies on the decarboxylation of malonic acid in polar solvents have yielded a wealth of information on the energetics and mechanism of the reaction.[1] Since the rate-determining step of the reaction is an electrophilic attack by the malonic acid on the nucleophilic center of a solvent molecule,[2] differences in the nucleophilicity of organic molecules are revealed by differences in the enthalpies of activation of the reaction among the various solvents.[1]

While, potentially, an unlimited number of mono- and disubstituted malonic acids may be prepared,

(1) L. W. Clark, *J. Phys. Chem.*, **64**, 692 (1960), and previous papers in this series.

(2) G. Frankel, R. L. Belford, and P. E. Yankwich, *J. Am. Chem. Soc.*, **76**, 15 (1954).

all of which may undergo decarboxylation, very few such derivatives have been investigated kinetically.[3] The substitution of various groups in place of one or both of the hydrogens on the central methylene group of malonic acid would be expected to exert characteristic inductive and steric effects on the decarboxylation reaction. It was with the view of determining some of these characteristic effects in a given case that cinnamalmalonic acid was prepared in this Laboratory and the kinetics of its decarboxylation in various aromatic amines was studied. The results of this investigation are reported herein.

Experimental

Preparation of Cinnamalmalonic Acid.—The cinnamalmalonic acid used in this research was prepared by the condensation of cinnamaldehyde with malonic acid in acetic acid at 95°, according to the procedure described in the literature,[4] and was purified by crystallization. The yellow crystals melted at 205° and yielded the quantitative amount of CO_2 on decarboxylation.

Solvents.—The amines used in this research were reagent grade chemicals and were redistilled at atmospheric pressure directly into the dried reaction flask immediately before the beginning of each decarboxylation experiment.

Apparatus and Technique.—The apparatus and technique used in this research have been described previously.[5] The temperature of the thermostat (controlled to within ± 0.05°) was determined by means of a thermometer calibrated by the U. S. Bureau of Standards. The buret used to collect the evolved CO_2 likewise was calibrated by the Bureau of Standards. In each experiment a 0.3917-g. sample of cinnamalmalonic acid (the amount needed to furnish 40.0 ml. of CO_2 at STP on complete reaction) was weighed quantitatively into a fragile glass capsule and was introduced in the usual manner into the solvent previously saturated with dry CO_2 gas.

Results

The decarboxylation of cinnamalmalonic acid in the six solvents studied was first order. Reactions in each solvent were carried out two or three times at three or four different temperatures over a 20° temperature range. The average values of the apparent first-order rate constants for the decarboxylation reaction in the various solvents at the different temperatures studied were obtained in the usual manner from the slopes of the experimental logarithmic plots. The experimental data are reproduced in Table I. Shown in Table II are the parameters of the Eyring equation, based upon the data in Table I, along with supplementary data for malonic acid obtained previously which is included for comparison.

Discussion of Results

Figure 1 is a plot of ΔH^* *vs.* ΔS^* for both the malonic acid and the cinnamalmalonic acid reactions in the six solvents under discussion, based upon the data shown in Table II. It will be seen in Fig. 1 that a good linear relationship exists for the cinnamalmalonic acid reaction in aniline and its derivatives, while a separate parallel line might be drawn for the data for the reaction in quinoline and in 8-methylquinoline. The plot also is approximately linear for the malonic acid reaction in the various liquids. Such linearity is good evidence that the mechanisms of both reactions in the various amines are the same.[9]

The ΔH^* values for the malonic acid reaction in aniline and quinoline are nearly equal, as are those for the cinnamalmalonic acid reaction in these two liquids (see lines 1 and 2 of Table II). This is in line with the fact that these two amines are approximately equally basic (pK for aniline is 9.42, for quinoline 9.20).[10] The difference in ΔH^* between the malonic acid and the cinnamalmalonic acid reactions in these two solvents probably results from the withdrawal of electrons from the carbonyl carbon atom in the latter due to resonance. In both these solvents the ΔS^* values for the cinnamalmalonic acid reaction are much lower than

TABLE I

APPARENT FIRST-ORDER RATE CONSTANTS FOR THE DECARBOXYLATION OF CINNAMALMALONIC ACID IN SEVERAL AROMATIC AMINES

Solvent	Temp. (°C. cor.)	$k \times 10^4$ (sec.$^{-1}$)	Av. dev.[a]
N,N-Dimethylaniline	125.16	4.39	0.02
	131.07	7.98	.03
	144.43	28.47	.05
o-Chloroaniline	111.15	2.75	.01
	121.01	5.38	.01
	131.07	10.27	.01
Aniline	115.84	4.61	.01
	120.49	6.72	.02
	127.38	11.57	.02
	135.53	21.35	.03
o-Toluidine	107.10	3.13	.01
	115.15	5.82	.01
	126.48	13.38	.03
Quinoline	119.39	1.92	.02
	130.07	4.44	.02
	138.24	8.14	.02
8-Methylquinoline	128.88	2.68	.02
	138.64	5.18	.02
	149.00	10.20	.03

[a] Values shown are average deviations between duplicate runs. For example, in the two experiments at 144.43° in N,N-dimethylaniline $k \times 10^4$(sec.$^{-1}$) values were 28.42 and 28.52; in the two experiments at 135.53° in aniline corresponding values were 21.32 and 21.38.

TABLE II

KINETIC DATA FOR THE DECARBOXYLATION OF MALONIC ACID AND CINNAMALMALONIC ACID IN SEVERAL AROMATIC AMINES[a]

Solvent	Malonic acid ΔH^* (kcal./mole)	Malonic acid ΔS^* (e.u./mole)	Cinnamalmalonic acid ΔH^* (kcal./mole)	Cinnamalmalonic acid ΔS^* (e.u./mole)
Aniline[6]	26.9	−4.5	23.8	−13.2
Quinoline[7]	26.7	−2.4	23.5	−16.2
o-Chloroaniline[6]	26.6	−6.9	19.6	−24.0
o-Toluidine[6]	25.7	−7.1	21.9	−17.5
N,N-Dimethylaniline[8]	25.4	−8.0	31.2	+ 3.8
8-Methylquinoline[7]	24.4	−10.5	21.6	−21.8

[a] The superscript after the name of the solvent refers to the source of the malonic acid data.

(3) J. Muus, *J. Phys. Chem.*, **39**, 343 (1935); **40**, 121 (1936).
(4) L. F. Fieser and M. Fieser, "Introduction to Organic Chemistry," D. C. Heath and Co., Boston, Mass., 1957, p. 443.
(5) L. W. Clark, *J. Phys. Chem.*, **60**, 1150 (1956).
(6) L. W. Clark, *ibid.*, **62**, 79 (1958).
(7) L. W. Clark, *ibid.*, **62**, 500 (1958).
(8) L. W. Clark, *ibid.*, **61**, 1975 (1957).
(9) J. E. Leffler, *J. Org. Chem.*, **20**, 1202 (1955).
(10) N. A. Lange, Ed., "Handbook of Chemistry," 9th Ed., Handbook Publishers, Inc., Sandusky, Ohio, 1956, p. 1202.

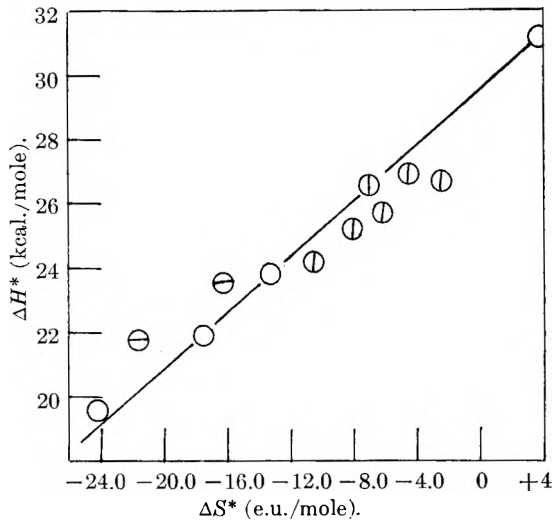

Fig. 1.—The enthalpy–entropy relationship for the decarboxylation of malonic acid and cinnamalmalonic acid in various amines. Symbols: ○, cinnamalmalonic acid in aniline and its derivatives; ⊖, cinnamalmalonic acid in quinoline and 8-methylquinoline; ⓓ, malonic acid in various amines.

are those for malonic acid, a reflection of the greater bulk of the malonic acid derivative.

The ΔH^* values for both the malonic acid and the cinnamalmalonic acid reaction are about 2 kcal./mole lower in 8-methylquinoline than in quinoline, a fact which is consistent with the increased nucleophilicity of the quinoline derivative (see lines 2 and 6 of Table II). The strong steric effect of the methyl group in the 8 position of quinoline is shown by the large decrease in ΔS^* of both reactions on going from quinoline to 8-methylquinoline.

Comparing lines 1 and 4 of Table II it will be seen that the ΔH^* values of both reactions decrease on going from aniline to *o*-toluidine. This is consistent with the increase in nucleophilicity of the amine as a result of the +I effect of the methyl group. At the same time a rather large decrease takes place in the entropy of activation of both reactions, indicative of the strong steric effect of the *ortho* substituent.

In all these solvents the ΔS^* values for the cinnamalmalonic acid reaction are considerably smaller than are those for malonic acid, corresponding with the greater size of the derivative. In every case, also, the cinnamalmalonic acid reaction has a lower enthalpy of activation, in line with its greater acidity.

The abnormally high value of ΔH^* of the cinnamalmalonic acid reaction in N,N-dimethylaniline (line 5 of Table II) suggests the possibility that it is the mono-anion, and not the un-ionized di-acid, which is involved here in the rate-determining step. Since the anion would exhibit less association than the di-acid, the reactive species would be smaller, and hence the ΔS^* of the reaction should have a higher positive value, as is indeed the case.

Acknowledgments.—(1) The support of this research by the National Science Foundation, Washington, D. C., is gratefully acknowledged. (2) The synthesis of the cinnamalmalonic acid was carried out by Donald McCoy.

THE LUMINESCENCE OF FLUORESCEIN DYES[1]

BY LESLIE S. FORSTER AND DANIEL DUDLEY

Department of Chemistry, University of Arizona, Tucson, Arizona

Received September 23, 1961

The fluorescence and phosphorescence yields and triplet state lifetimes have been determined for a number of halogenated fluorescein dyes in EPA solutions. The lifetimes decrease progressively as the number of halogen atoms is increased in both the bromine and iodine series of derivatives and the lifetime always is less in the iodine than in the corresponding bromine derivative. The results indicate that the diminution of the fluorescence yield that accompanies bromine and iodine substitution is not due primarily to an increase in intersystem crossing but rather to increased internal conversion from the excited singlet state to the ground state.

Introduction

Considerable evidence has been accumulated, since the pioneering study of Lewis and Kasha,[2] to support the view that a general energy level scheme is applicable to organic molecules.[3] Excitation to a high vibrational level of the lowest excited singlet state, S′, is followed by the rapid radiationless removal of this vibrational energy by the surroundings. The short-lived (10^{-8}–10^{-9} sec.) state, S′, then decays radiatively, S′ → S (k_2), or non-radiatively S′ → S(k_3) to the singlet ground state, S, or alternatively to the lowest triplet state, S′ → T(k_4). The relatively long-lived triplet state ($\geq 10^{-4}$ sec.) then is converted radiatively, T → S (k_5), or non-radiatively T → S (k_6) to the ground state. Non-radiative transitions between electronic states generally are termed internal conversions, although if a change in multiplicity is involved, the term intersystem crossing may be used. Considerable interest has been manifested in the effect of environment on these internal conversion processes, but little quantitative information has been accumulated.[4] It has been shown that halogen substitution increases the efficiency of S′ → T in the order I > Br > Cl > H.[5] This presumably is due to the increased spin-orbit coup-

(1) Supported by a grant from the Atomic Energy Commission.

(2) G. N. Lewis and M. Kasha, *J. Am. Chem. Soc.*, **66**, 2100 (1944).

(3) M. Kasha and S. McGlynn, *Ann. Rev. Phys. Chem.*, **7**, 403 (1956).

(4) H. Sponer, *Radiation Research*, **Suppl. 1**, 558 (1959); E. J. Bowen, *Discussions Faraday Soc.*, **27**, 40 (1959); G. Jackson, R. Livingston, and A. Pugh, *Trans. Faraday Soc.*, **56**, 1635 (1960).

(5) M. Kasha, *Radiation Research*, **Suppl. 2**, 243 (1960).

ling that accompanies the substitution of atoms with large Z. However, kinetic evidence has been obtained which indicates that the reduction in fluorescence efficiency ($S' \rightarrow S$) that accompanies the halogenation of fluorescein dyes is not primarily the result of increased $S' \rightarrow T$ but rather of increased non-radiative $S' \rightarrow S$.[6] It is the purpose of the present work to present further evidence bearing on this problem.

Experimental

The dyes were purified by paper chromatography.[7] Geometric isomers were not separated. The bromine derivatives were identified spectrophotometrically.[8] The absorption maximum shifts to longer wave lengths as the number of bromine atoms is increased. The iodine derivatives were identified by assuming the same shift with increasing iodination. This shift is correlated with decreasing migration velocity on the paper chromatogram. The spots were cut out and the dyes eluted with 5% ammonia. The samples were prepared by evaporation of the water followed by addition of EPA to the dry salt. The samples were protected from light as much as possible during this procedure to minimize photodecomposition.

The samples were contained in a 1-cm. cuvette which was placed in a cryostat that was a modification of a previously described design.[9] The 4358 Å. excitation was obtained from a filtered AH-4 lamp and the emission at 45° was passed through a Farrand grating monochromator to a cooled Dumont 6911 photomultipler tube. The output of this tube was fed into a recorder coupled to the wave length drive of the monochromator.

The monochromator–photomultiplier system was calibrated against a standard tungsten lamp. In the 510–580 $m\mu$ region the calibration curve so obtained agreed ($\pm 10\%$) with the calibration curve determined by utilizing quinine sulfate in conjunction with the known emission distribution for this substance.[10]

The dye concentrations were kept in the 10^{-5}–10^{-6} M range to minimize reabsorption, self-quenching, and dimerization. The absorbance at 4358 Å. was measured at 25° in a 10-cm. cell and the absorbance in 1-cm. path length computed from this measurement.

By using the above procedure and assuming a value of $\Phi_F = 0.92$ for the fluorescence yield of aqueous fluorescein dianion, $\Phi_F = 0.18$ was obtained for the aqueous eosin dianion. This can be compared with the directly measured value of 0.19.[11]

The phosphorescence lifetimes, τ, were measured in EPA glasses at −183° by the flash technique. A Dumont 6911 photomultiplier also was used in this apparatus to increase sensitivity in the red and near infrared regions.

Results

A meaningful interpretation of dye luminescence data can be made only if the emitting species can be identified. In aqueous solution fluorescein can exist as the cation, mono- and dianions, and neutral molecule. Only at a sufficiently high pH is the dianion the predominant species.[12] The absorption and emission spectra for each dye are, except for a small solvent shift, very nearly the same in EPA as in the corresponding ammoniacal solution. This fact coupled with the observation that dimerization of fluorescein and eosin dianions becomes appreciable only when the concentration exceeds 10^{-3} M,[13] leads to the conclusion that in each case the predominant species is the dianion.

(6) A. Adelman and G. Oster, *J. Am. Chem. Soc.*, **78**, 3977 (1956).
(7) E. Lederer and M. Lederer, "Chromatography," Elsevier, Amsterdam, 1951, p. 236.
(8) C. Graichen and J. C. Molitor, *J. Assoc. Offic. Agr. Chemists*, **42**, 149 (1959).
(9) T. O. Jones and J. Willard, *Rev. Sci. Instr.*, **27**, 1037 (1956).
(10) W. Melhuish, *J. Phys. Chem.*, **64**, 762 (1960).
(11) G. Weber and F. Teale, *Trans. Faraday Soc.*, **53**, 646 (1957).
(12) L. Lindqvist, *Arkiv. Kemi*, **16**, 79 (1960).

The results are given in Table I. The emission spectra can be grouped into three classes. $FlCl_2$ and Fl exhibit negligible phosphorescence; $FlBr_4$ and $FlBr_4Cl_4$ have poorly resolved phosphorescence bands; while the remaining compounds show well resolved phosphorescence bands at −183°. The phosphorescence yields, Φ_P, of $FlBr_4$ and $FlBr_4Cl_4$ consequently are less reliable than those of the other dyes. The light absorption was not measured at −183° and only $\chi = \Phi_P/\Phi_F$ and τ can be considered as primary data at −183°. The fluorescence yields, Φ_F, are the primary data at 25°. The Φ_P then can be computed by assuming Φ_F is independent of temperature. This assumption has been verified for Fl, $FlBr_4$, and FlI_4 dianions and presumably is valid for the other halogenated fluoresceins.[14] It has been shown that oxygen has no effect on the fluorescence of fluorescein,[12] but it cannot be assumed that the phosphorescence also is unaffected by oxygen, even at low temperature and in a rigid medium.[5] We compared the phosphorescence of a carefully degassed eosin solution with that of an air-saturated solution and found no quenching by oxygen. However, the room temperature photodecomposition of alcoholic solutions of eosin is reduced considerably in the presence of oxygen[15] and we found that more reliable results could be obtained by the use of air-saturated solutions.

TABLE I

LUMINESCENCE OF DIANIONS OF FLUORESCEIN DYES IN EPA

Dye	λ_{max} fluorescence ($m\mu$, 25°)	λ_{max} phosphorescence ($m\mu$ −183°)	Φ_F[a] (25°)	$\chi = \Phi_P/\Phi_F$ (−183°)	τ (msec. −183°)	χ/τ (rel.)
Fl	527	..	0.83	0	..	..
FlBr	535	634	.60	.13	50	22
$FlBr_2$	540	650	.29	.21	44	48
$FlBr_4$	549	(690)[b]	40	.082	9.4	86
FlI	531	642	15	.67	15.8	420
FlI_3	544	667	054	1.05	10.4	1000
FlI_3	549	671	061	0.71	5.1	1400
FlI_4	560	686	066	.40	1.3	3100
$FlBr_4Cl_4$	572	(660)[b]	56	.15	5.6	270
$FlCl_2$	538	..	79	0	..	..

[a] Referred to aqueous fluorescein dianion $\Phi_F = 0.92$. [b] Phosphorescence band insufficiently resolved to determine maximum accurately.

Examination of Table I reveals the following trends: (i) τ diminishes progressively with halogenation in both the bromine and iodine series. This is to be contrasted with the results for naphthalene derivatives, where no simple correlation was found[16,17]; (ii) the lifetime of a given bromine derivative is 4–7 times as long as the lifetime of the corresponding iodine derivative; (iii) χ/τ increases regularly with halogenation in both the bromine and

(13) T. Förster and E. König, *Z. Elektrochem.*, **61**, 344 (1957).
(14) V. Zanker and H. Rammensee, *Z. physik. Chem.* (Frankfurt), **16**, 168 (1960).
(15) M. Imamura and M. Koizumi, *Bull. Chem. Soc. Japan*, **29**, 899 (1956).
(16) D. S. McClure, *J. Chem. Phys.*, **17**, 905 (1949).
(17) V. Ermolaev and A. Terenin, *J. chim. phys.*, **55**, 698 (1958).

iodine series and is 20–40 times larger for a given iodine derivative than for the bromine analog.

Discussion

The number of independent data determined in this study are insufficient to determine unambiguously the effect of halogenation on the individual rate constants k_2–k_6. However, from the several trends indicated above some meaningful conclusions may be drawn. From the relation $\tau = 1/k_5 + k_6$ it can be seen that $k_5 + k_6$ increases with halogenation and is larger for the iodine derivatives than for the bromine derivatives. The increased spin-orbit coupling due to iodine would increase k_5. The effect of such substitution on k_6 cannot be determined from the lifetime data alone, but there is evidence that chlorine substitution on naphthalene increases both k_5 and k_6 by a factor of five.[18]

The integrated absorption, a measure of the natural lifetime of S', $\tau_0 = 1/k_2$, varies by less than 30% within the group of halogen derivatives in aqueous solution.[6,8] The values of τ_0 computed from $\Phi_F = \tau/\tau_0$ vary by a factor of two between fluorescein and eosin.[19] In the following discussion we will assume that k_2 is nearly the same for all of the dyes in EPA solution.

The intersystem crossing ratio, χ, sometimes is nearly equal to k_4/k_2.[5] This is not necessarily true in the case of the fluorescein dyes where we cannot be certain that $k_6 << k_5$, *i.e.*, that non-radiative T → S is negligible. From a steady-state treatment it is found that $\chi/\tau = k_4k_5/k_2$.[20] If k_2 is constant the trends for χ/τ are the trends for k_4k_5. It is difficult to decide whether the increase of k_4k_5 with increasing extent of halogenation is due mainly to an increase in k_4 or k_5 or both. It is not surprising that changing the substituent from bromine to iodine increases k_4k_5 by a factor of 20 or more, for such a change probably would increase both k_4 and k_5. This last statement is not in conflict with the kinetic results of Adelman and Oster,[6] where substitution of iodine for bromine in $FlBr_2$ and $FlBr_4$ resulted in a decreased quantum yield for S' → T. Such a decreased quantum yield would be observed in spite of an increased k_4 if k_3 increases more rapidly than k_4. This is precisely the conclusion reached in the kinetic study, which was made with aqueous solutions.

With the exception of the unsubstituted fluorescein dianion, Φ_F always is larger in EPA than in water. Nevertheless the same qualitative trend is observed in both solvents, *i.e.*, Φ_F decreases in the sequence H > Br > I. The kinetic results have shown that in aqueous solutions the decrease in Φ_F is due to the increase of k_3. The parallel trends suggest that a similar situation prevails in EPA solutions. This conclusion is supported further by examination of the trends within the group of iodine derivatives. $\Phi_F = k_2/(k_2 + k_3 + k_4)$ and since Φ_F is about 0.1, $1/\Phi_F \cong (k_3 + k_4)/k_2$. k_4k_5 increases progressively with the number of iodine atoms, while Φ_F does not decrease in a similar progression. It would seem that if $k_4 >> k_3$ such a trend would exist.

One final point must be emphasized. The decrease in Φ_F is not accompanied by an increase in Φ_P. The sum $\Phi_P + \Phi_F$ decreases with substitution in the order H = Cl > Br > I, therefore at least one of the non-radiative processes, S' → S or T → S, becomes more important in this sequence.

(18) M. de Groot and J. Van der Waals, *Mol. Phys.*, **4**, 189 (1961).
(19) P. Pringsheim, "Fluorescence and Phosphorescence," Interscience Publ., New York, N. Y., 1949, p. 316; T. Förster, "Fluorescenz Organischer Verbindungen," Vandenhoeck and Ruprecht, Göttingen, 1951, p. 149.
(20) L. Forster, S. Greenberg, R. Lyons, and M. Smith, *Spectrochim. Acta*, **16**, 128 (1960).

THE KINETICS OF CYCLIZATION OF SOME 2,2'-DIPHENIC ACIDS IN SULFURIC ACID

BY D. M. MARCH[1] AND T. HENSHALL

Department of Chemistry, Sir John Cass College, London, England

Received September 25, 1961

The kinetics of cyclization of some 2,2'-diphenic acids in concentrated sulfuric acid have been studied using a spectrophotometric method of analysis. Simple first-order kinetics were found in each case, and also a linear dependence of log k on the Hammett acidity function. The energy and entropy parameters were found to vary in a characteristic manner. A mechanism is proposed and is discussed.

The kinetics of cyclization of 2,2'-diphenic acid to fluorenone-4-carboxylic acid[2] have been studied in aqueous sulfuric acid, and in sulfuric–acetic acid mixtures over the ranges 77–100% and 60–100% w./w., respectively.

The measurements also have been extended to certain 5,5'-disubstituted-2,2'-diphenic acids containing substituents of well defined electronic character; these were studied in the aqueous medium only.

In every case, a linear dependence was found of log k on the Hammett acidity function H_0 but the slopes differed from unity.

The activation energies and entropies have been found to depend markedly on the solvent composition; a probable interpretation is offered (Discussion).

(1) Material taken from a thesis in partial fulfillment of the requirements for the Ph.D., London University, 1961.
(2) C. Graebe and C. Aubin, *Ann.*, **247**, 261 (1888).

Experimental

Materials.—These various diphenic acids were prepared for study; 2,2′-diphenic acid; 5,5′-dimethyl-; 5,5′-diethyl-; 5,5′-di-*t*-butyl-; 5,5′-dichloro-; 5,5′-dibromo-; and 5,5′-dinitro-2,2′-diphenic acids.

Of these, the 5,5′-diethyl-, and 5,5′-di-*t*-butyl acids have not been reported previously; the physical constants and analytical figures are, respectively: M.p. 247°. *Anal.* Calcd. for $C_{18}H_{18}O_4$: C, 72.5; H, 6.09. Found: C, 72.5; H, 6.20. M.p. 306°. *Anal.* Calcd. for $C_{22}H_{26}O_4$: C, 74.6; H, 7.40. Found: C, 74.7; H, 7.52.

Preparation of Reaction Solvents. (i) 100% Sulfuric Acid.—A commercial acid containing a slight excess of sulfur trioxide was partially frozen by immersion in iced-water. Distilled water then was added dropwise from a microburet, with stirring, until the melting point rose to a maximum of 10.4° and remained constant as the whole was frozen.

The stock acid then was kept in a tightly stoppered bottle, whose neck was protected by a Polythene sleeve. The melting point was checked periodically. (ii) **Mixtures of sulfuric acid with water, and with acetic acid** were prepared by the dilution of the stock acid. A known weight of the acid was diluted by the gradual addition of distilled water or glacial acetic acid, cooled in a desiccator and reweighed.

The Analytical Method.—The fluorenone-4-carboxylic acids possess characteristic absorption spectra in the ultraviolet region; maxima occur around 2850 and 3150 Å., the former being the more intense.

The diphenic acids themselves show an appreciable absorption in the ultraviolet but the intensities of alkaline solutions decrease with increasing wave length, becoming negligible above 3000 Å.

Consequently the cyclization reaction is most conveniently followed by absorption spectrophotometry; and absorption above 3000 Å. shown by samples of reaction mixture after dilution by $N/10$ sodium hydroxide is due almost entirely to the reaction product.

Obedience to Beer's law was tested for each acid studied. Optical density measurements were made in quartz cells on a Unicam photoelectric spectrophotometer, model SP 500[3]; and a typical plot is shown in Fig. 1 which relates to fluorenone-4-carboxylic acid itself.

Reaction Vessels and Temperature Control.—The kinetic runs on 2,2′-diphenic acid itself were carried out in 40-ml. tubes fitted with ground glass stoppers.

However, due to the decreased solubilities of the disubstituted acids in sulfuric acid of concentration less than 95% w./w., it was necessary in these cases to use the apparatus shown in Fig. 2 in order to obtain reaction solutions sufficiently concentrated for rate studies.

In operation, the solvent is held in A by the entrapped air. The reactant is added, and when sufficient has dissolved, the reaction solution is transferred to B by removing the ground-glass stopper and applying slight suction; undissolved material is retained by the sintered-glass plate.

This procedure was found to be highly satisfactory; and by using 3–4 cm. quartz cells for the measurement of optical density, rate studies could be made in solutions of lower acidity than otherwise would have been possible.

For kinetic runs in the range 10–70°, a conventional thermostat was used which could be controlled to ±0.05°; while steady temperatures in the range 70–150° were achieved by a vapor-bath as described and used previously.[4]

The Kinetic Procedure.—The reaction tube containing approximately 10 ml. of the standard acid was allowed to equilibrate in the thermostat. A preheated sample of the diphenic acid then was added, the mixture was quickly and vigorously stirred to effect solution, and the first sample quickly withdrawn by an automatic pipet and discharged into a graduated flask containing $N/10$ NaOH solution.

Further samples were withdrawn at fixed time intervals. Between sampling operations the reaction tube was kept firmly stoppered, and the pipet was held in a separate tube in the thermostat. The sampling of the reaction mixture could be completed in less than 10 sec. At the completion of the run, the solutions were made to the mark with $N/10$ NaOH and measurements made of optical density

$$k = \frac{2.303}{t} \log \frac{\alpha_\infty - \alpha_0}{\alpha_\infty - \alpha_s} \qquad (1)$$

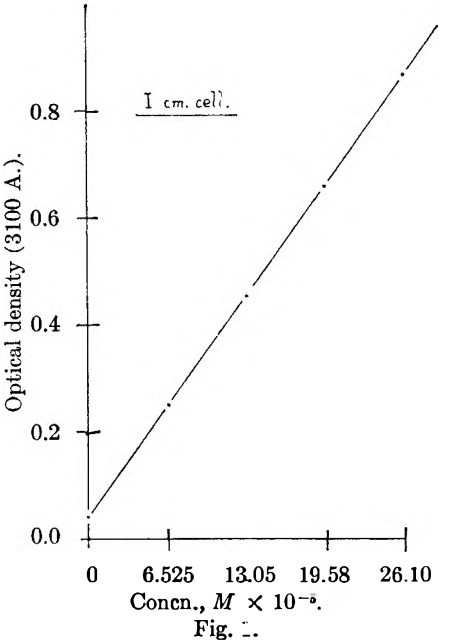

Fig. 1.

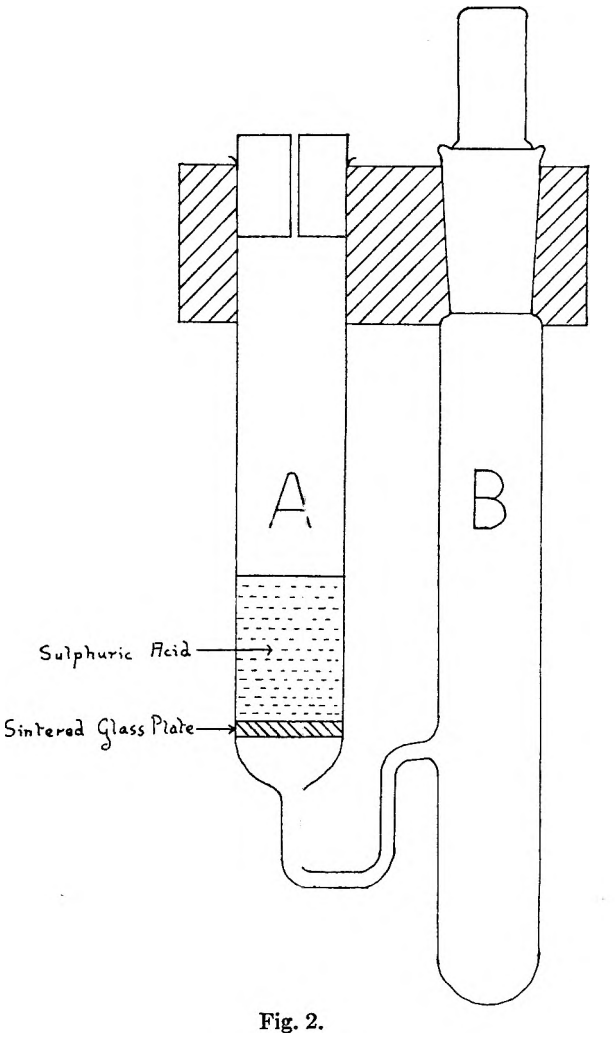

Fig. 2.

(3) Unicam Instruments, Cambridge, England.

(4) T. Henshall, W. E. Silbermann, and J. G. Webster, *J. Am. Chem. Soc.*, **77**, 6656 (1955); W. E. Silbermann and T. Henshall, *ibid.*, **79**, 4107 (1957).

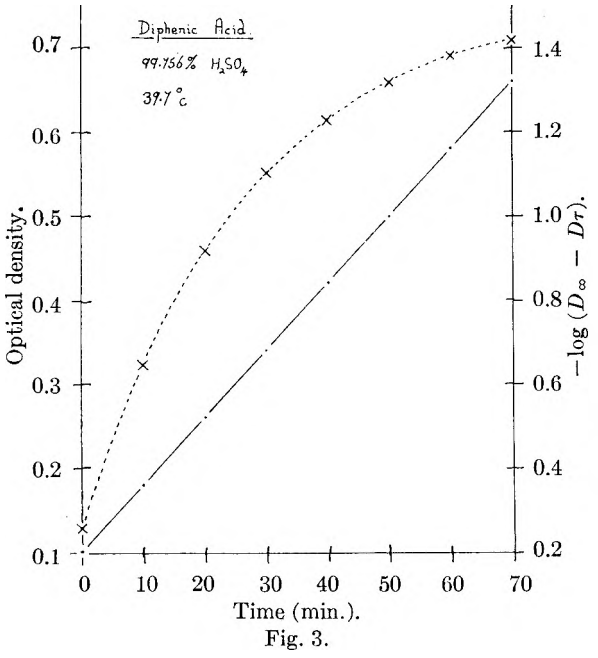

Fig. 3.

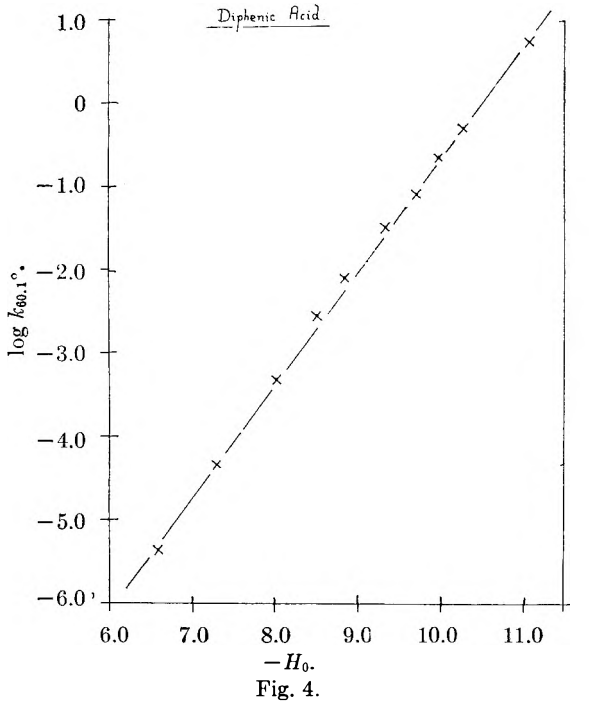

Fig. 4.

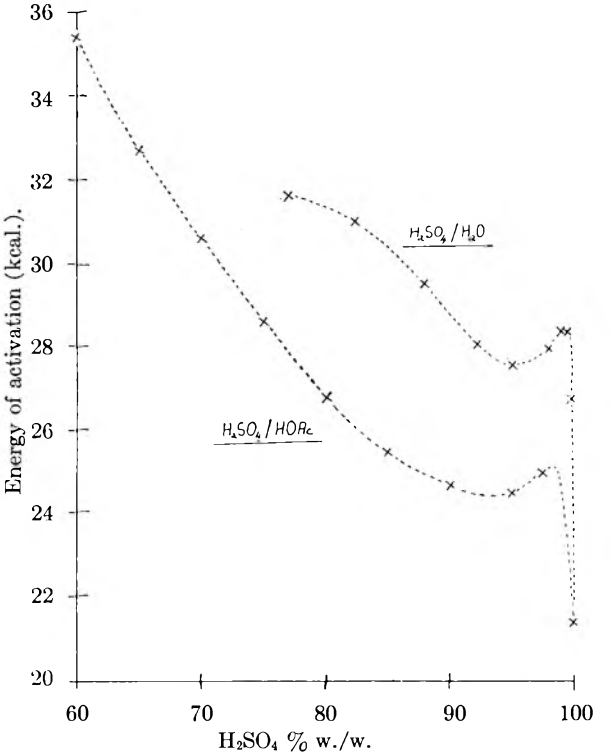

Fig. 5.

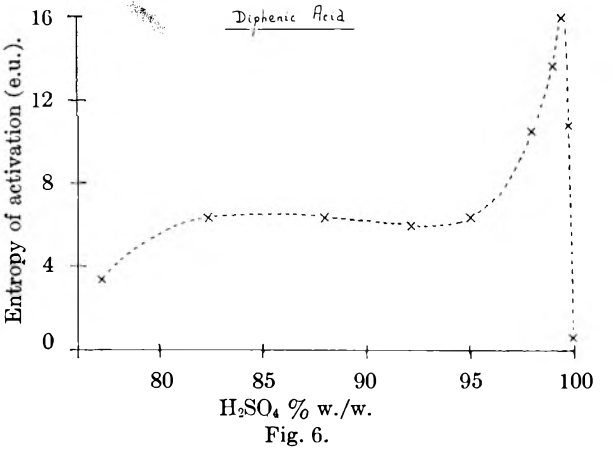

Fig. 6.

For the calculation of rate constants, "infinity" values are required (eq. 1). These initially were obtained by heating the tube and contents in a boiling water-bath to effect completion of the reaction. However, such a procedure was found to lead to inconsistencies due to further attack of the reaction product by sulfuric acid. Accordingly an alternative procedure was adopted for the calculation of the infinity value (in which the optical density was extrapolated to infinite time). This is justified, since first-order kinetics first were established by using Guggenheim's procedure.[5] Kinetic runs always were taken to at least 90% completion to ensure maximum accuracy in this calculation. A typical kinetic run is shown in Fig. 3.

The Effect of Solvent Composition.—The composition of the solvent was found to have a marked effect on the reaction rate, and on the activation energies and entropies. Rate studies were made in as wide a range of solvent composition as possible; the upper limit was set by the maximum rate which could conveniently be measured, the lower limit by the solubility of the diphenic acids. The ranges for the various acids are given in Table I.

TABLE I

2,2′-Diphenic acid	77–100% H_2SO_4
5,5′-Dimethyl-2,2′-diphenic acid	85–99
5,5′-Diethyl-2,2′-diphenic acid	85–99
5,5′-Di-*t*-butyl-2,2′-diphenic acid	90–99
5,5′-Dichloro-2,2′-diphenic acid	90–100
5,5′-Dibromo-2,2′-diphenic acid	90–100

For all the acids studied, a linear dependence was found of log k on H_0; but the slopes of these plots varied considerably, being close to unity for 5,5′-diethyl-2,2′-diphenic acid; 1.34 for 2,2′-diphenic acid (Fig. 4); and 1.5 for 5,5′-dichloro-2,2′-diphenic acid.

The rate constants used in the construction of these plots were arbitrarily chosen to correspond to a temperature of 60.1°, and were made from the plots of log k against $1/T$ used in the evaluation of activation energy.

The form of the dependence of activation energy on

(5) E. A. Guggenheim, *Phil. Mag.*, **1**, 538 (1926).

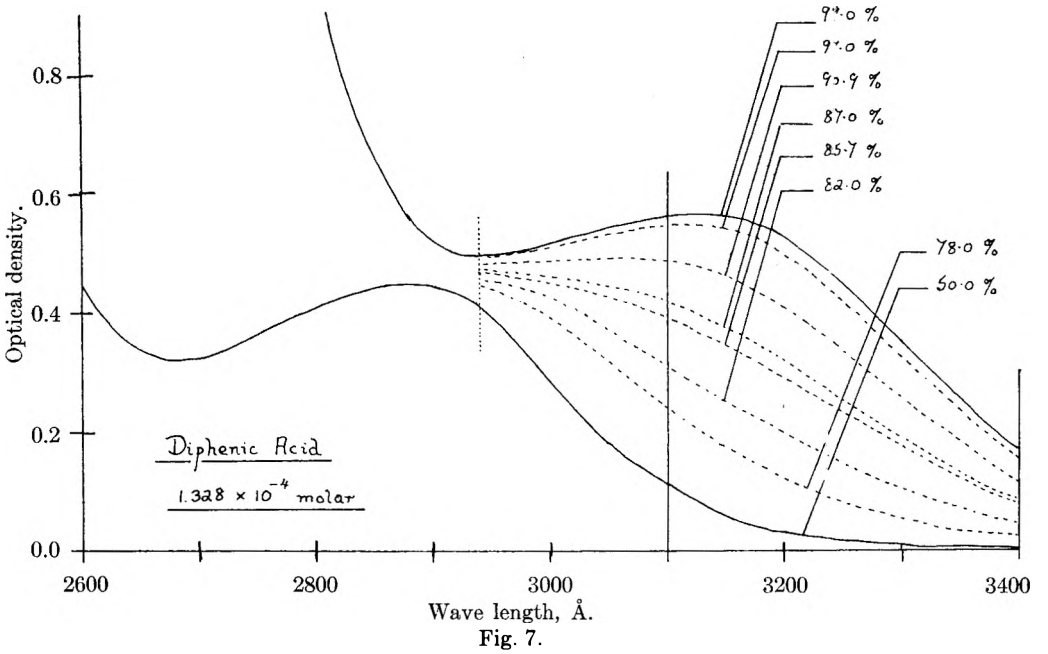

Fig. 7.

solvent composition is exemplified by Fig. 5, which relates to 2,2′-diphenic acid itself; a similar dependence is shown by other acids. Activation energies for each acidity were obtained from measurements of rate constants over a temperature range of 20 to 30°, and are good to ±0.2 kcal.

Activation entropies calculated from eq. 2, with the pre-exponential factor "A" in min.$^{-1}$, showed a dependence on solvent composition as indicated in Fig. 6, which is relevant to 2,2′-diphenic acid.

The interpretation of such relationships is difficult; but it is suggested (Discussion) that the sharp decrease in ΔS^* occurring in the neighborhood of 99.5 to 100% w./w. H_2SO_4 is due to the elimination of a water molecule from the protonated carboxyl group, with the formation of an acylium ion.

$$\Delta S^* = 4.575 \log A - 66.9 \qquad (2)$$

The Degree of Protonation of 2,2′-Diphenic Acid.—A solution of 2,2′-diphenic acid in 50% w./w. aqueous sulfuric acid has an ultraviolet absorption spectrum almost identical to that in water. An increase in sulfuric acid concentration causes a displacement of the absorption band to longer wave lengths, and at the same time increases its intensity; Fig. 7.

A similar behavior of solutions of weak organic bases in sulfuric acid has been reported,[6] the inference being that such displacement is due to protonation.

To determine the degree of protonation at each acidity, spectral measurements were made on a series of solutions in sulfuric acid of concentrations in the range 50–99% w./w. (Fig. 7 and 8). As the molarity of diphenic acid was the same in all the solutions, a single measurement of optical density at a predetermined wave length was sufficient to determine the degree of protonation.

The fraction of diphenic acid protonated, x, is given by

$$x = \frac{D_{obs.} - D_u}{D_p - D_u} \qquad (3)$$

where D_{obs} is the observed optical density; D_u is the optical density when the diphenic acid is unprotonated (50% w./w. H_2SO_4); and D_p is the optical density when protonation is complete (99% w./w. H_2SO_4).

If the diphenic acid acts as a simple Hammett base then a plot of log $[(D_{obs} - D_u)/(D_p - D_{obs})]$ against $-H_0$ should be linear and of unit slope.

Such a plot is shown in Fig. 9 but the slope has a value of only 0.57.

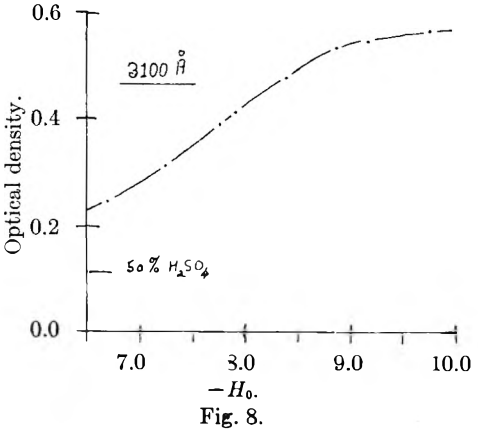

Fig. 8.

Discussion

The results presented here are best interpreted in terms of the reaction sequences[7]

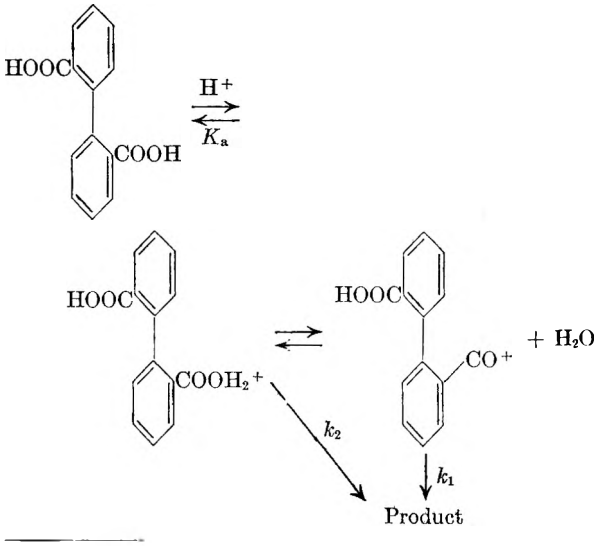

(6) L. A. Flexser, L. P. Hammett, and A. Dingwall, *J. Am. Chem. Soc.*, **57**, 2112 (1935).

(7) F. A. Long and M. A. Paul, *Chem. Revs.*, **57**, 947 (1957).

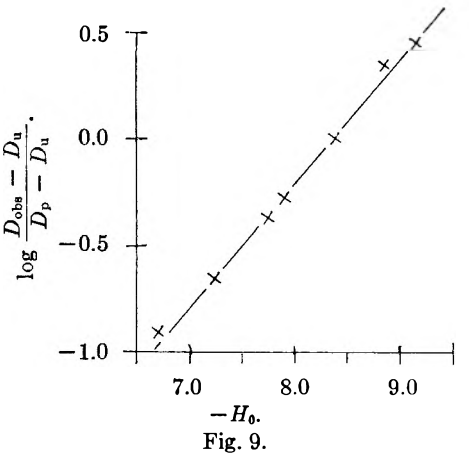

Fig. 9.

The dependence of the energy of activation on solvent composition then is accountable as follows. Consider the first sequence

$$DCOOH + H^+ \overset{K^a}{\rightleftharpoons} DCOOH_2^+ \xrightarrow{k_2} \text{Product}$$

in which H^+ denotes the acid solvent. The reaction rate hence is given by eq. 4

$$v = k_2[DCOOH_2^+] = k_2x[DCOOH]_t \qquad (4)$$

where "x" is the degree of protonation, and $[DCOOH]_t$ the total diphenic acid concentration.

The value of "x" is obtained from a consideration of the protonation equilibrium and is given by eq. 5.

$$x = \frac{K_aF(H^+)}{1 + K_aF(H^+)} \qquad (5)$$

in which $F(H^+)$ is an acidity function relevant to the system.

The observed energy of activation E_a will be given by

$$\frac{E_a}{RT^2} = -\frac{d}{dt}(\ln k_o) = -\frac{d}{dt}(\ln k_2) + \frac{d}{dt}(\ln x) \qquad (6)$$

where k_o is the experimentally observed rate constant and

$$k_o = k_2x \qquad (7)$$

In solutions where the extent of protonation is small eq. 6. may be approximated by

$$\frac{E_a}{RT^2} = -\frac{d}{dt}(\ln k_o) = -\frac{d}{dt}(\ln k_2) + \frac{d}{dt}(\ln [K_aF(H^+)] \qquad (8)$$

$$i.e., E_a = E + \Delta H_1 \qquad (9)$$

where E is the activation energy for the cyclization of the protonated diphenic acid and ΔH_1 is the heat change accompanying protonation.

In conditions of complete protonation x will be unity and eq. 6 will reduce to

$$\frac{d}{dt}(\ln k_o) = \frac{d}{dt}(\ln k_2)$$

$$i.e., E_a = E \qquad (10)$$

Thus as the degree of protonation is increased, a fall in the activation energy equal to ΔH_1 might be expected. This agrees well with experiment; for over the region 77 to 95% w./w. H_2SO_4 the degree of protonation of 2,2′-diphenic acid increases from 25 to 95%, while E_a for the reaction decreases by 5 kcal.

Exactly similar reasoning may be applied to the second equilibrium; and in an acid solution approaching anhydrous this might be expected to be displaced predominantly to the right with the resultant elimination of the heat change ΔH_2, for the loss of the elements of water, from the observed energy of activation. Again, experiment shows a fall of 7 kcal. over the narrow range 99.5 to 100%. This agrees well with the known decrease of a_{H_2O}, the activity of water, to very low values over this range.

Since the protonation of diphenic acid is so clearly related to the Hammett acidity function (Fig. 9) a correlation was sought between log k_o and H_0.[8] Surprisingly enough, in view of the extent of the protonation over the region studied, a linear relationship was found between the two (Fig. 4). Moreover the slope has the value 1.34 instead of 0.57, as might be expected from the results on the protonation of the acid.

From a consideration of the extended reaction sequence proposed above, it is possible, by making certain assumptions, to formulate a rate equation which is in reasonable agreement with the experimental results over the range of acidity in which these assumptions are valid.

viz. $DCOOH + H^+ \underset{K_a}{\rightleftharpoons} DCOOH_2^+ \underset{K_b}{\rightleftharpoons} DCO^+ + H_2O$

$\downarrow k_1$

Product

If the second equilibrium is assumed to lie predominantly to the left, then

$$[DCO^+] = K_b \frac{[DCOOH^+_2]}{a_{H_2O}} \frac{f_{(DCOOH_2^+)}}{f_{(DCO^+)}} \qquad (11)$$

where "a" and "f" denote activity and activity coefficient, respectively, and K_b is the equilibrium constant.

Therefore from eq. 4

$$[DCO^+] = \frac{K_bx[DCOOH]_tf_{(DCOOH_2^+)}}{a_{H_2O}f_{(DCO^+)}} \qquad (12)$$

The reaction rate "v" then is given in terms of both the experimentally determined rate constant k_o, and k_1, relating to the theoretical rate equation in

$$v = k_o[DCOOH]_t = k_1[DCO^+]$$

$$i.e., k_o = k_1K_b \frac{f_{(DCOOH_2^+)}}{f_{(DCO^+)}} \frac{x}{a_{H_2O}} \qquad (13)$$

Then, if in eq. 13 K_1, k_b and the ratio of activity coefficients are to be considered constant, a plot of log k_o against log x/a_{H_2O} should be linear, and of unit slope.

Such a plot from $x = 0.25$ to 0.95 based on the values of a_{H_2O} given by Deno and Taft[9] is shown in Fig. 10.

The slope of 1.10, taken with the positive values of activation entropy, is considered to lend strong support for the reaction sequence proposed above.

Finally there remains to consider the effect on the reaction rate of the substituents in the 5,5′-positions. Table II gives the rates of cyclization,

(8) L. P. Hammett and A. J. Deyrup, *J. Am. Chem. Soc.*, **54**, 2721 (1930).

(9) N. C. Deno and P. W. Taft, *ibid.*, **76**, 244 (1954).

relative to the parent acid, of the disubstituted acids in 99% w./w. H_2SO_4, together with the corresponding activation energies and slopes of the Hammett plots.

TABLE II

R,R'-	$K_{60.1°}$	E_a (kcal.)	$\frac{d \log K_0}{d H_0}$
Me	72.0	26.5	1.05
Et	50.5	25.5	1.00
Tert.Bu.	12.6	26.9	1.15
H	1.00	28.4	1.34
Br	0.118	28.8	1.45
Cl	0.096	29.3	1.50

In agreement with expectation, electron releasing groups facilitate, while electron-attracting groups retard, the cyclization reaction; and the relative rates of cyclization for the 5,5′-dialkyldiphenic acids are in the order: methyl, ethyl, *t*-butyl, which is the order of hyperconjugative release of electrons by the groups.[10]

Finally, it is noteworthy that 5,5′-dinitrodiphenic acid failed to cyclize.

(10) V. A. Crawford, *Quart. Revs.* (London), **3**, 229 (1949).

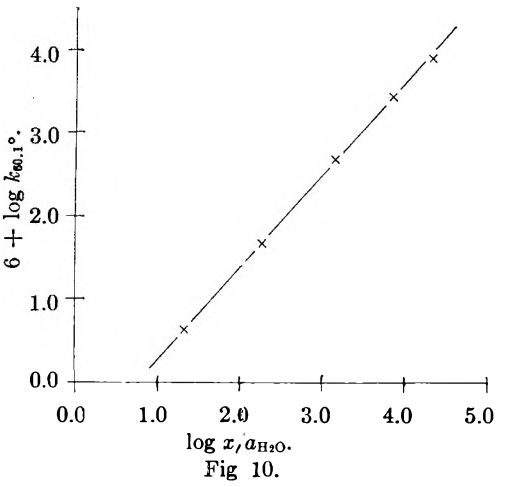

Fig 10.

Acknowledgments.—The authors wish to acknowledge the award of a Research Studentship by the Department of Scientific and Industrial Research to D.M.M., and also a grant toward the cost of materials by Imperial Chemical Industries Ltd.

AN SCF-LCAO-MO STUDY OF H_2^+ AND H_2[1a]

BY VINCENT DECARLO[1b] AND VIRGINIA GRIFFING

Department of Chemistry, Catholic University of America, Washington D. C.

Received September 27, 1961

A variational calculation of the electronic energy of H_2^+ as a function of the distance between the nuclei has been carried out using 1s, 2s, and 2p Slater-type orbitals on each atom. The exponential factor was chosen to be the same for all of the basis functions, but this factor was varied as a parameter in the variational calculations. The results obtained in this way are compared with previous calculations on H_2^+. By increasing the basis set and varying the exponential factor, the energy of H_2^+ converges toward the known exact solution. The best basis set for H_2^+ then was shown to give the best results in a self-consistent field calculation on the H_2 molecule. The energy of H_2^+ calculated from the H_2 molecule calculations using Koopman's theorem were not quite as good as the direct H_2^+ ion calculations.

Introduction

In this paper, an attempt is made to find for H_2^+ the best analytical wave-function expanded in a limited basis set of atomic orbitals (a.o.) chosen so that all a.o. appear with the same exponential factor.[2] The energy for H_2^+ then is minimized with respect to the variation of the screening parameter. These same a.o. using the best screening parameter for the H_2^+ then are used to calculate the energy of the H_2 molecule. This is found to give a value of the energy very close to the Hartree–Fock self-consistent field solution for the H_2 molecule. The basis set then is expanded and the H_2 calculation repeated to determine the sensitivity of the results to an extended basis set. Some interesting comparisons are made between the eigenvectors and eigenvalues of H_2^+ and H_2 determined in various ways.

(1) (a) The work in this paper was supported in part by the Office of Naval Research and is a dissertation submitted to the faculty of the Graduate School of Arts and Sciences of the Catholic University of America in partial fulfillment of the requirements for the degree of Doctor of Philosophy; (b) now at Melpar, Inc., Falls Church, Virginia.

(2) This method was more successful for He_2 than extended configuration interaction using excited states. See F. Webner, *J. Chem. Phys.*, **23**, 1024 (1955).

Theory.—The LCAO–MO method of approximation has been used in this study. The details of this theory are well known[3]; thus only the unique features of this study will be discussed in any detail. The problem is one of trying to find the best approximate solution to the Schroedinger equation. The energy is calculated according to eq. 1

$$E_0 = \int \Psi_0^* \hat{H} \Psi_0 d\tau \qquad (1)$$

where $\hat{H}$ is the Hamiltonian operator and Ψ_0 is a Slater determinant formed from molecular spin orbitals. The Hamiltonian can be written as

$$\hat{H} = \hat{H}_1^0 + \hat{G}_{\nu\mu}$$

where $\hat{H}_1^0$ is the one-electron operator and $\hat{G}_{\nu\mu}$ is the electron–electron interaction operator. In the conventional Roothaan[3a] procedure the molecular orbitals are chosen as a linear combination of Slater orbitals

$$\phi_i = \sum_j C_{ij} x_j(Z_a; r_{ia})$$

and a self-consistent field calculation under the variational procedure is carried out varying the co-

(3) (a) C. C. J. Roothaan, *Revs. Mod. Phys.*, **23**, 69 (1951); (b) R. F. Mulligan, *J. Chem. Phys.*, **19**, 347 (1951).

efficients. This procedure has the advantage that the variational problem remains linear giving distinct computational advantages; however, no satisfactory method of selecting the scale-parameter Z_a has been developed. It now is firmly established in the literature that Slater's rules for choosing the scale parameter give energies which are of the correct order of magnitude. This choice of the scale factor enables one to obtain 95–99% of the total energy for a molecule by SCF–LCAO–MO procedure. However, the virial theorem[4] is not always satisfied by these calculations, the wave-functions are far from approaching accuracy and thus dissociation energies are unreliable. The next step is to vary the screening constants. In principle, one would like to vary each scale factor independently. However, this procedure leads to non-linear variational equations. Hence such a computational task still is prohibitive except in a few cases even when using large digital computers. In this study two modifications have been introduced. First, the one electron problem is solved, *i.e.*, the following set of eigenvalue problems are solved

$$\int \phi_i(1)\hat{H}_1^0\phi_i(1)d\tau_1 = \epsilon_i \qquad i = 1 \text{ to } n \qquad (2)$$

where n = number of electrons, $\hat{H}_1^0$ is the one-electron operator, where σ_j are normalized symmetry orbitals formed from Slater-type atomic orbitals except that for a given ϕ_i the same exponential factor is used throughout. A variational procedure then is followed in which the scaling parameter and coefficients are varied for a minimum.

When this variational calculation is completed, the best set of symmetry orbitals σ_j and the best scaling parameter Z_a are used in the many-electron problem and a standard SCF-calculation is carried through. There is no *a priori* guarantee that this criterion for selecting the molecular orbitals is a useful one until it has been tested for many particle systems of varying complexity.

In principle, all the screening parameters could be varied independently for the one-electron problem. This would be much simpler than for the many-electron problem.

In the next two sections, this procedure is tested for the H_2^+ and H_2 problem near the equilibrium distance. In addition to testing the procedure, this particular problem gives us an opportunity to compare the results with the exact calculations on the H_2^+ and the accurate calculations for the H_2 molecule. Since we are using the exact solutions for the separated atoms and have the results for the ion and the molecule both, we can evaluate which approximations compensate most for the change from spherical symmetry to cylindrical symmetry and to what extent this approximation compensates for the electron correlation factor if at all.

The Calculations for H_2^+.—In this calculation eq. 2 is solved with

$$\hat{H}_\nu^0 = -\frac{1}{2}\nabla_\nu^2 - \frac{1}{r_{\nu a}} - \frac{1}{r_{\nu b}} \qquad (3)$$

and the following molecular orbital

$$\phi_i = C_{i1}\frac{(1s_a + 1s_b)}{N_1} + C_{i2}\frac{(2s_a' + 2s_b')}{N_2} + C_{i3}\frac{(2p\sigma_a + 2p\sigma_b)}{N_3} \qquad (4)$$

where

$$1s_a = (Z/\pi)^{1/2}\exp(-Zr_{1a})$$
$$2s_a' = 2(Z^5/3\pi)^{1/2} r \exp(-Zr_{1a}) - \sqrt{3}\, 1s_a$$
$$2p\sigma_a = (Z^5/\pi)^{1/2} r\cos\theta \exp(-Zr_{1a})$$

N_1, N_2, and N_3 with all Z's the same are the normalization factors for the corresponding normalized symmetry orbitals σ_i. That is

$$\phi_i = C_{i1}\sigma_1 + C_{i2}\sigma_2 + C_{i3}\sigma_3 \qquad (5)$$

and

$$\epsilon_i = \int \phi_i^* \hat{H}_\nu^0 \phi_i d\tau_\nu \qquad (6)$$

A variational calculation is carried through varying the coefficients for a minimum keeping the ϕ_i's normalized and orthogonal. This leads to the set of secular equations

$$\sum_j C_{ij}(H_{ij} - ES_{ij}) = 0 \text{ for } i = 1 \text{ to } 3 \qquad (7)$$

where

$$H_{ij} = \int \sigma_i(\nu)\hat{H}_\nu^0\, \sigma_j(\nu)d\tau_\nu$$

and

$$S_{ij} = \int \sigma_i(\nu)\sigma_j(\nu)d\tau_\nu$$

Since this is a set of linear dependent equations the only non-trivial solution requires that the determinant of the coefficients of the C_{ij} must be set equal to zero leading to the secular equation

$$\begin{vmatrix} H_{11} - E & H_{12} - ES_{12} & H_{13} - ES_{13} \\ H_{21} - ES_{21} & H_{22} - E & H_{23} - ES_{23} \\ H_{31} - ES_{31} & H_{32} - ES_{32} & H_{33} - E \end{vmatrix} = 0 \qquad (8)$$

This equation was solved for two special cases before eq. 8 was solved varying the scale factor. These results are included for comparison.

Case I. The second row and second column were eliminated. In this case only the $2p\sigma_g$ symmetry orbital was mixed in. This was done as a function of internuclear distance and $Z = 1$. These results are shown in Table I.

Case II. The third row and third column were set equal to zero, *i.e.*, only the $2s\sigma_g'$ orbital was mixed in. This was only done at the equilibrium distance for $Z = 1$. These results are shown in Table I.

Case III. All three symmetry orbitals were included. These were calculated as a function of distance and Z was varied for this case. These results are in Table II. Previous calculations on H_2^+ are reviewed in the Discussion. These results are summarized in Table III and compared with our best results in Table IV.

Discussion of Results

A large number of different wave functions for H_2^+ have been developed by various investigators. They range in complexity from Pauling's[5] simplest calculation to Bates and co-workers exact calculation.[6]

The results of these calculations for the equilibrium distance of the hydrogen molecule-ion and the

(4) P. O. Löwdin, *Mol. Spectroscopy*, **3**, 46 (1959).

(5) L. Pauling, *Chem. Revs.*, **5**, 173 (1928).

(6) D. R. Bates, K. Ledsham, and A. L. Stewart, *Phil. Trans. Roy. Soc. London*, **A246**, 215 (1953).

TABLE I[a]

ELECTRONIC ENERGIES (E) FOR CASES I AND II

R / basis set	1	2	3	4	6	8
$1s\sigma_g$, $2p\sigma_g$	−1.31174	−1.06589	−0.90172	−0.79392	−0.67817	−0.62739
$1s\sigma_g$, $2s\sigma_g$		−1.08917				
Bates	−1.45178	−1.10262	−0.91084	−0.79608	−0.67863	−0.62757

[a] All units are in atomic units: lengths in units of the Bohr radius a_H = 0.5293 Å.; energies in units of e^2/a_H = 27.204 e.v.

TABLE II

ELECTRONIC ENERGY OF H_2^+ USING FULL BASIS SET

Z \ R	1.4	1.5	2.0	2.5
1.0		−1.24038	−1.0982	
1.1			−1.09930	
1.2	−1.28023		−1.09959	−0.98979
1.3		−1.24573	−1.10007	− .992112
1.4			−1.10099	− .992987
1.425				− .993078
1.45		−1.24657	−1.101143	− .993108
1.475				− .993025
1.5			−1.10022	
Bates	−1.28427	−1.24898	−1.10263	− .99382

form of the best variational wave-functions obtained in each of these calculations are given in Table III.

In Table IV, those calculations that were carried out as functions of internuclear distance are compared with our calculations in the appropriate range of distance.

Hirschfelder and Kincaid[7] have found that Pauling's[5] wave-function did not satisfy the virial theorem. Finkelstein and Horowitz[8] improved the wave-function by introducing a scale factor Z which improved the agreement with the virial theorem.[9]

In a further analysis of our results the kinetic and potential energies were calculated separately for all the calculations at R = 2 a.u. in order to

TABLE III

Investigator		$-E$	R	Wave function (non-normalized)
Pauling[5]		1.0654	2.5	$\exp(-r_a) + \exp(-r_b)$
Bates, Ledsham, and Stewart[6]		1.10262	2.0	Numerical solution
Finkelstein and Horowitz[8]		1.0831	2.0	$\exp(-1.228r_a) + \exp(-1.228r_b)$
Guillemin and Zener[10]		1.1024	2.0	$\exp(-1.13r_a)\exp(-0.23r_b) + \exp(-0.23r_a)\exp(-1.13r_b)$
Dickinson[11]		1.1008	2.0	$\exp(-zr_a) + cr_a\cos\theta_a\exp(-\epsilon zr_a) + \exp(-zr_b) + cr_b\cos\theta_b \exp(-\epsilon zr_b)$ $\epsilon = 1.15$, $z = 1.247$, $c = 0.145$
James[12]		1.1024	2.0	$\exp\{-1.35(r_a + r_b)\}\{1 + 0.448(r_a - r_b)^2\}$
Gray, Pritchard, and Sumner[13,14]		1.1002	2.0	See original reference
Dalgarno and Poots[15]				$\exp\{-\alpha(r_a + r_b)\} + p\{\exp(-\beta r_a) + \exp(-\beta r_b)\}$
	(a)	1.0538	2.0	$p = \infty$, $\beta = 1$
	(b)	1.0866	2.0	$p = \alpha$, β variable (best value 1.239)
	(c)	0.9678	2.0	$p = 0$, $\alpha = 1$
	(d)	1.0798	2.0	$p = 0$, α variable (best value 0.667)
	(e)	1.0927	2.0	$\alpha = 1 = \beta$, p variable (best value 0.155)
	(f)	1.1005	2.0	α from (a), β from (b), p variable (best value 0.412)
	(g)	1.10246	2.0	α, β, and p all variable (best value $\alpha = 0.677$, $\beta = 1.354$, $p = 0.375$)
Hurley[16]		1.098	1.98	$\{\exp(-1.23r_a') + \exp(-1.23r_b')\}$
Shull and Ebbing[17]		1.094158	1.985	$\exp(-1.2455r_a') + \exp(-1.2455r_b')$
Chen[18]		1.059616	2.0	See original reference
Pritchard and Sumner[19]		1.102607	2.0	See original reference

TABLE IV

LOWEST ELECTRONIC ENERGIES AS FUNCTION OF DISTANCE

Investigator	R 1.2	1.5	1.6
Dalgarno and Poots	−1.36203		−1.21571
Shull and Ebbing		−1.074951	
Chen	−1.336039		−1.181146
De Carlo and Griffing		−1.24657	
Bates	−1.36230	−1.24898	−1.21593
Investigator	**R 2.0**	**2.4**	**2.5**
Dalgarno and Poots	−1.10245	−1.01306	
Shull and Ebbing	−1.094146		−1.085128
Chen	−1.059616	−0.962082	
DeCarlo and Griffing	−1.101143		−0.993108
Bates	−1.10262	−1.01321	−0.99382
Pritchard and Sumner	−1.102607		

(7) J. O. Hirschfelder and J. Kincaid, *Phys. Rev.*, **52**, 658 (1937).

(8) B. N. Finkelstein and G. E. Horowitz, as reported in Pauling and Wilson, "Introduction to Quantum Mechanics," McGraw-Hill Book Co., New York, N. Y., 1935, p. 331.

(9) J. C. Slater, *J. Chem. Phys.*, **1**, 317 (1933).

(10) V. Guillemin, Jr., and C. Zener, *Proc. Natl. Acad Sci.*, **15**, 214 (1929).

(11) B. N. Dickinson, *J. Chem. Phys.*, **1**, 317 (1933).

(12) H. M. James, *ibid.*, **3**, 9 (1934).

(13) H. O. Pritchard and H. A Skinner, *J. Chem. Soc.*, 945 (1951).

(14) B. F. Gray, H. O. Pritchard, and F. H. Sumner, *ibid.*, 2631 (1956).

(15) A. Dalgarno and G. Poots, *Proc. Phys. Soc.* (London), **A66**, 343 (1954).

(16) A. C. Hurley, *Proc. Roy. Soc.* (London), **A226**, 179 (1954).

(17) H. Shull and D. D. Ebbing, *J. Chem. Phys.*, **28**, 866 (1958).

(18) T. C. Chen, *ibid.*, **29**, 347 (1958).

(19) H. O. Pritchard and F. H. Sumner, *J. Phys. Chem.*, **65**, 641 (1961).

see how the variation of Z affected the restrictions set by the virial theorem.

For comparison the same criteria have been applied to these calculations reviewed above where sufficient detail enabled us to obtain the kinetic and potential energies separately. These also are presented in Table V for comparison.

In order to get some idea of the accuracy of our best wave-function ($1s\sigma_g$, $2s\sigma_g$, $2p\sigma_g$) the value of this wave-function was compared with Bates' exact wave function for selected values of the coördinates. This comparison for points along the internuclear axis is shown in Table VI and for points perpendicular to the internuclear axis is shown in Table VII. The coefficients for the calculated molecular orbitals are given in Table VIII.

In a more recent paper, Pritchard and Sumner[19] have carried out a much more extensive calculation on H_2^+ for the distance $R = 2$ a.u. They have included calculations using hydrogen-like a.o.'s as well as Slater a.o.'s including σ-type orbitals as high as $n = 4$, $l = 3$. Those values which they have calculated which are for the same set of parameters as the calculations given in this paper are in good agreement. Their results are compared with ours in Table IX. They also found that the energy was improved as one increased the screening constant from $Z = 1$ to $Z = 1.4$.

TABLE V

VIRIAL THEOREM

		$\left\|E\right\| - \left\|\frac{V}{2}\right\|$
Dalgarno and Poots		
	Calculation No. 1	−0.084
	2	.000
	3	.250
	4	− .020
	5	− .021
	6	− .026
	7	.001
DeCarlo and Griffing	$Z = 1.0$	−0.0069
	1.05	− .00288
	1.1	− .00100
	1.2	− .00072
	1.3	− .00316
Bates, *et al.*	1.45	− .00450
		− .0005

TABLE VI

CALCULATION OF ϕ ALONG THE INTERNUCLEAR AXIS

R \ Z	1.0	1.2	1.3	LCAO	Exact
0	0.288	0.296	0.308	0.233	0.315
1	.469	.483	.494	.360	.458
2	.115	.121	.118	.132	.120
3	.024	.026	.027	.049	.030
4	.004	.005	.006	.018	.007

TABLE VII

CALCULATION OF ϕ PERPENDICULAR TO THE INTERNUCLEAR AXIS

R \ Z	1.0	1.05	1.1	1.2	Exact
0.5	0.25	0.25	0.25	0.25	0.27
1.0	.17	.17	.17	.18	.18
1.5	.12	.12	.11	.11	.10
2.0	.06	.06	.06	.07	.07

TABLE VIII

COEFFICIENTS FOR ϕ

R	Z	C_1	C_2	C_3
1.5	1.0	0.94544	−0.267310	0.085795
	1.333	.94244	− .01892	.10730
2.0	1.0	.95280	− .19636	.11384
	1.05	.95093	− .15381	.12055
	1.1	.94909	− .11250	.12288
	1.2	.94049	− .03532	.12504
	1.3	.92887	.03318	.12215
	1.4	.91607	.09163	.11646

TABLE IX

THE CALCULATED MOLECULAR ENERGY FOR H_2^+ AT $R = 2$ a.u.

	6 Basis functions		Pritchard and Sumner complete set (10 basic functions)
Z	DeCarlo and Griffing	Pritchard and Sumner	
1.0	−1.09820	−1.098223	−1.102350
1.1	−1.09930	−1.099313	−1.102489
1.2	−1.09959	−1.099578	−1.102561
1.3	−1.10007	−1.100114	−1.102593
1.4	−1.10099	−1.101022	−1.102607
1.45	−1.101143		
1.5	−1.10022		

TABLE X

TOTAL MOLECULAR ENERGY (H_2) USING 1s, 2s, AND 2p AS BASIS FUNCTIONS

Z \ R	1.1	1.3	1.4	1.6
1	−1.101720	−1.126726	−1.1294279	−1.1235994
1.2	−1.1079019	−1.1302330	−1.1320771	−1.1250915
1.45	−1.1073357	−1.1284517	−1.1296498	−1.1211857

TABLE XI

MOLECULAR ENERGY CALCULATED WITH EXTENDED BASIS SET (1s, 2s, $2p\sigma$, $3d\sigma$, $4d\sigma$, $4f\sigma$)

$R = 1.4$ $Z = 1.2$

H_2	−1.132412	
H_2^+	−0.54088	(electronic energy = −1.255174)

TABLE XII

H_2^+ ELECTRONIC ENERGIES OBTAINED FROM H_2 SCF CALCULATION LIMITED BASIS SET (1s, 2s, $2p\sigma$)

Z \ R	1.1	1.3	1.4	1.6
1.0	−1.363711	−1.286224	−1.250781	−1.186013
1.2	−1.370811	−1.290414	−1.254151	−1.188555
1.45	−1.375144	−1.295521	−1.259680	−1.194793
	Bates exact value		−1.284265	−1.21593

Here it is found that using the same basis set as for H_2^+, the best H_2 molecule energy (see Table X) is obtained for $Z = 1.18$–1.2, even though the internuclear distance for the minimum is decreased to $R = 1.4$ a.u. From the united atom approach one would expect the optimum Z for H_2 might be larger, but presumably the shielding effect of the extra electron is just sufficient to counteract the decrease in distance. Further light on this subject can be obtained by considering the calculations on H_2 made by McLean, Weiss, and Yoshimine.[20] These authors used

(20) A. D. McLean, A. Weiss, and M. Yoshimine, *Rev. Mod. Phys.*, **32**, 211 (1960).

symmetry orbitals for a five configuration wavefunction and used an open shell (1s,1s′) configuration in place of the $1s\sigma_g$ symmetry orbital. They found the optimum $Z = 1.43$ for the 1s and $Z' = 0.965$ for the 1s′ giving an average of $Z = 1.1975$, in agreement with our result. However, the split Z gives a nice physical picture if it is interpreted as the increased $Z = 1.43$ for the inner electron and the decreased $Z' = 0.965$ for the effective charge of the shielded nuclei. In approximate agreement with our results for H_2, these authors find for $R = 2$ a.u. that $Z = 1.275$ and $Z' = 1.01$. Since they also varied the $2p$ screening parameter independently, one might expect this much deviation. Ransil[21] has also carried out a SCF calculation on H_2 where he obtained a Hartree–Fock solution varying the three Z's indpendently, obtaining $Z_{1s} = 1.5$, $Z_{1s}' = 1.16$, and $Z_{2p}' = 1.96$. This also confirms the fact that the inner electron shields the outer electron and the average value is close to 1.2.

The energy of the H_2 molecule was calculated using the same basis functions used in the H_2^+ calculations. The results of these calculations are given in Table X. Even though the equilibrium internuclear distance for the H_2 molecule is at 1.4 a.u., the *same* screening constant, $Z = 1.2$, which gave the best solution for the H_2^+ problem, gives the best energy for the molecule. A further calculation was made on the H_2 molecule using an extended basis set with a common screening constant of $Z = 1.2$. In this calculation, 1s, 2s, $2p\sigma$, $3d\sigma$, $4d\sigma$, and $4f\sigma$ Slater atomic orbitals were included on each atom. The results are given in Table XI. This greatly increased basis set gave only slight improvement in the energy for the H_2 molecule. This indicates that these solutions are very close to the self-consistent field solution. Some slight improvement might be obtained by independent Z variation. However, any significant improvement will require inclusion of correlation effects in some way.

Koopman's theorem has been used to calculate the energy of the H_2^+ ion from the H_2 molecule calculations given in Table X. This electronic energy for the H_2^+ ion is given in Table XII. These values are higher than the energies obtained in direct calculation on the ion as can be seen by comparing the values in Table IX. This is in agreement with the conclusions of Lorquet[22] that the direct calculations for ions give better energies than those obtained from the neutral molecule by Koopman's theorem.

Conclusions

These calculations indicate that one can obtain accurate results for the H_2^+ molecule ion by using only a few basis functions with the same screening constant. This set of basis functions gave good results for the H_2 molecule. It would be of interest to extend this calculation to the excited states of H_2^+ and to the one-electron solutions of more complicated homonuclear diatomic systems.

(21) B. J. Ransil, private communication.

(22) J. C. Lorquet, *Rev. Mod. Phys.*, **32**, 312 (1960).

ELECTRON SPIN RESONANCE INVESTIGATION ON NEUTRON IRRADIATED POLYPROPYLENE

By Ramdas P. Gupta

Institute for Elektrowerkstoffe, Freiburg. i. Br., Germany

Received September 29, 1961

Investigation on neutron irradiated isotactic polypropylene has been done by electron spin resonance experiments to study the effect of the ionizing radiation on radical formation, cross linking, and formation of the chemical bond. The samples of polypropylene were pile irradiated at the Brookhaven reactor to the neutron dosages of 5.4×10^{17}, 6.8×10^{17}, 5.7×10^{18}, and 14.0×10^{18} nvt. As the irradiation dose increases, the line becomes more sharp. There is a marked decrease in half-width with increase in irradiation dose. There has been evidence of the presence of some methyl groups in the irradiated specimen, though some of the methyl groups are destroyed by irradiation. It is more likely that color formation could be due to a conjugated double bond structure than to a long life radical. Narrowing of the line width, in this case, is not due to exchange interaction of the unpaired electrons but is due to an increase in the conjugated region of the double bond structure with the stable radical formed by neutron irradiation. The increase in the conjugated region lowers the neighbor interaction, on account of which there is a narrowing of the line width with increase in dose at high neutron dosages.

Introduction

Electron spin resonance experiments with neutron irradiated polypropylene have been conducted to study the effect of ionizing radiation on radical formation, cross linking, and formation of chemical bonds. The results and conclusions obtained by n.m.r. experiments on the same samples have been compared. Effects of radiation damage on polypropylene and some other polymers have been studied by several workers,[1-7] using the e.s.r. method but under conditions different from ours. Dynamic mechanical properties of these samples have been studied by Merril.[8] By this present experiment it has been possible to compare the results of n.m.r. experiments on the effect of radiation damage.[9] In this case samples irradiated to high neutron dosages have been studied.

(1) B. R. Loy, *J. Polymer Sci.*, **44**, 341 (1960).

(2) A. A. Miller, *J. Phys. Chem.*, **63**, 1755 (1959).

(3) Ohnishi, Ikeda, Sugimoto, and Nitta, *J. Polymer Sci.*, **47**, 503 (1960).

(4) B. R. Loy, *ibid.*, **50**, 245 (1960).

(5) Lawton, Balwit, and Powell, *ibid.*, **32**, 257 (1958).

(6) Libby, Ormerod, and Charlesby, *Polymer*, **1**, 212 (1960).

(7) Ohnishi, Ikeda, Kashiwagi and Nitta, *ibid.*, **2**, 219 (1961).

(8) Merril, results in press.

(9) R. P. Gupta, *Kolloid Z.*, **B174**, Heft 1, 74 (1961).

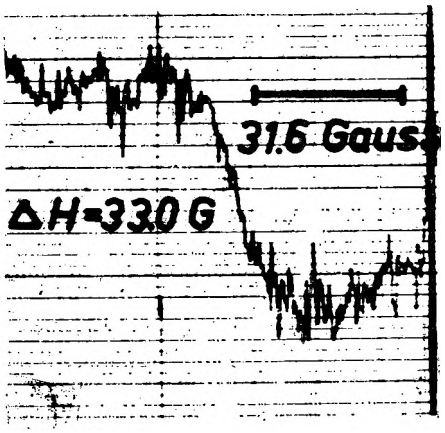

Fig. 1a.—E.p.r. line shape for polypropylene irradiated to 5.4×10^{17} nvt.

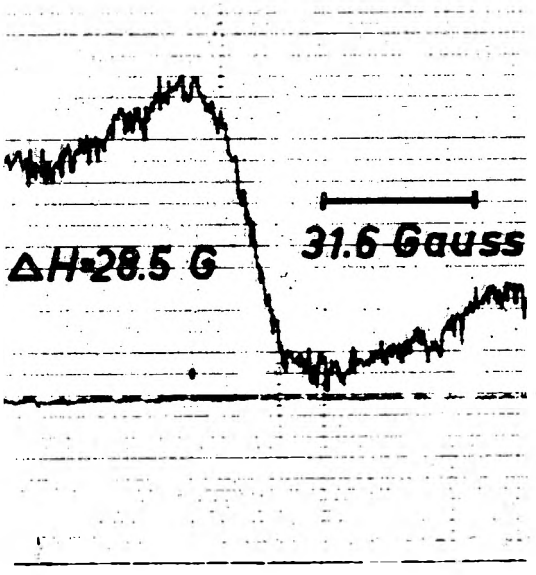

Fig. 1b.—E.p.r. line shape for polypropylene irradiated to 8.6×10^{17} nvt.

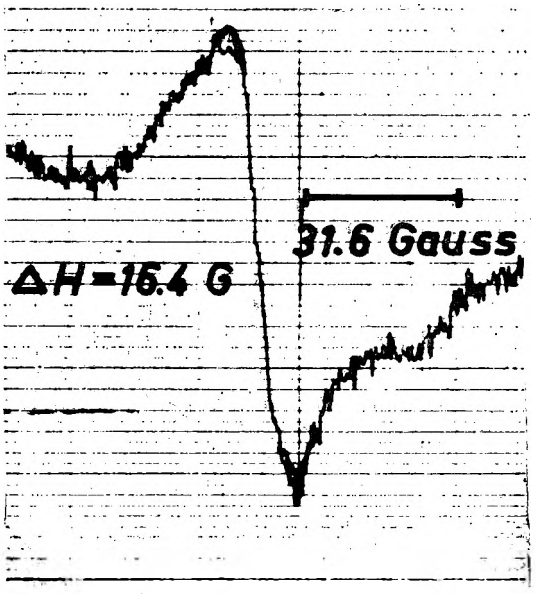

Fig. 1c.—E.p.r. line shape for polypropylene irradiated to 5.7×10^{18} nvt.

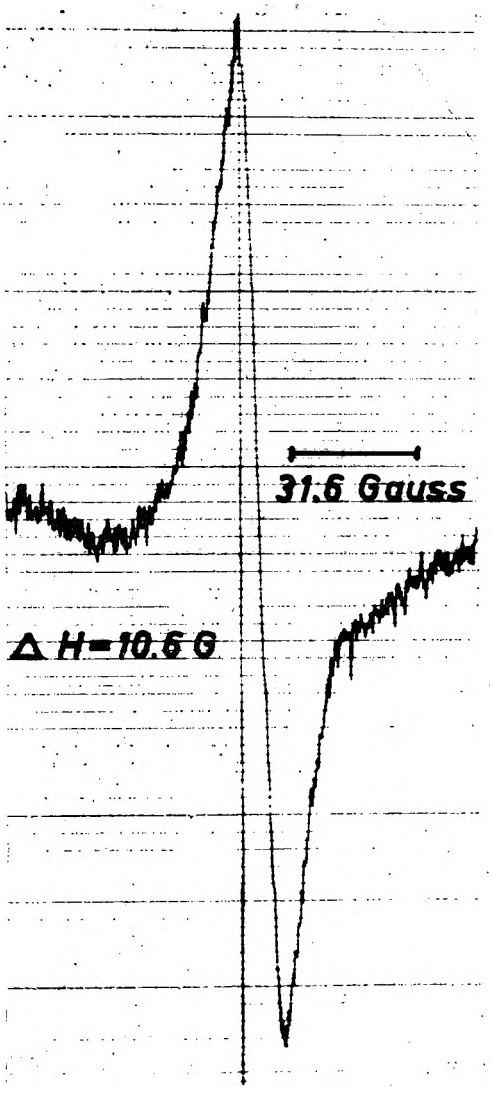

Fig. 1d.—E.p.r. line shape for polypropylene irradiated to 14×10^{18} nvt.

Experimental

Investigation on the electron spin resonance in isotactic polypropylene has been done using a Varian spectrometer, model V-4500 (X-Band, 100 kc. s. modulation) with a 6-in. electromagnet. Measurements have been made at room temperature. The samples of polypropylene were pile irradiated at the Brookhaven reactor to the neutron dosages of 5.4×10^{17}, 8.6×10^{18}, 5.7×10^{18}, and 14×10^{18} nvt. about six months before this experiment was performed. N.m.r. experiments on these samples have been conducted using a dual purpose, 40 Mc. s. Varian model spectrometer, and the results have been reported elsewhere.[9]

Results and Discussion

Figures 1a, 1b, 1c, and 1d show the e.s.r. derivative line shapes for the irradiated samples of isotactic polypropylene used in this experiment. As the irradiation dose is increased the line becomes more sharp, and there is a marked decrease in the half-width with increase in irradiation dose, as shown in Fig. 2. In the beginning, the decrease in line width is very abrupt but later at high dosages it is nearly constant. This result will be discussed later. Irradiation is more effective in the amorphous region than the crystalline region. Radical formation, cross linking, and

formation of the chemical bond is easier in the amorphous region of the polymer. This conclusion is supported by n.m.r. experiments with the same samples, the results of which have been published elsewhere.[9] If the experiments had been conducted just after the samples were irradiated, this effect would have been observed more correctly. Though these samples were irradiated about six months before the experiments, it has been possible to mark the change in signal amplitude and line width with increase in dose, because some of the formed radicals and chemical bonds have a long lifetime and are very stable. By the n.m.r. experiments on the above samples[9] it is found that the transition near liquid nitrogen temperature, which probably is due to methyl group rotation, is not affected by irradiation. This shows that the protons of some of the methyl groups certainly are not affected and some of the methyl groups remain unchanged by the process of neutron irradiation.

Specimens of polypropylene irradiated by weak X-rays (50 kv.) up to 10^5 roentgen and by strong X-rays (150 kv.) up to 3×10^4 roentgen have been studied in this Laboratory by n.m.r. and e.p.r. methods, and it has been found that weak X-rays are not energetic enough for the formation of a sufficient number of radicals and cross links. On the other hand strong X-rays are able to form a sufficient number of free radicals and cross links. The e.p.r. line shape of the polypropylene specimen irradiated to 2×10^4 roentgen by a 150 kv. source of strong X-rays has been shown in Fig. 3. The line shape in this case is not symmetric. This is due to variation in the g-value. If the paramagnetic center does not coincide with the crystal axis, it gives rise to anisotropy in the g-factor. Such asymmetric line shapes also have been observed by other workers.[10-13] If this asymmetry is due to resonance of bound oxygen present in the specimen irradiated by strong X-rays, one could assume that there is no bound oxygen present in the case of the neutron irradiated specimen.

Color formation might be due to long and short life radicals or chemical bonds. As shown by Loy,[4] color is due to a conjugated double bond structure. Miller has shown that the presence of free radicals is necessary for color development. Spectrometric analysis shows that optical density of the red colored portion of the spectrum varies inversely as the concentration of long lived radicals. Ohnishi, *et al.*, have pointed out that irradiation produces double bonds and as the irradiation dose increases the conjugated region of the double bond extends, and when the polymer is heated the short length bond decays faster than the long conjugated bond.

In the case of neutron irradiated samples a single line spectrum has been observed, as shown in Fig. 1. It is because the fine structure, which is observed at lower dosages, disappears due to broadening at very high irradiation dose that one observes a single

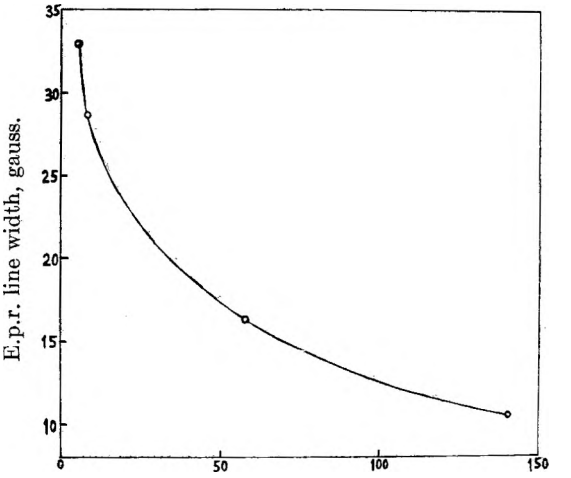

Fig. 2.—E.p.r. line width *vs.* neutron dose for irradiated polypropylene.

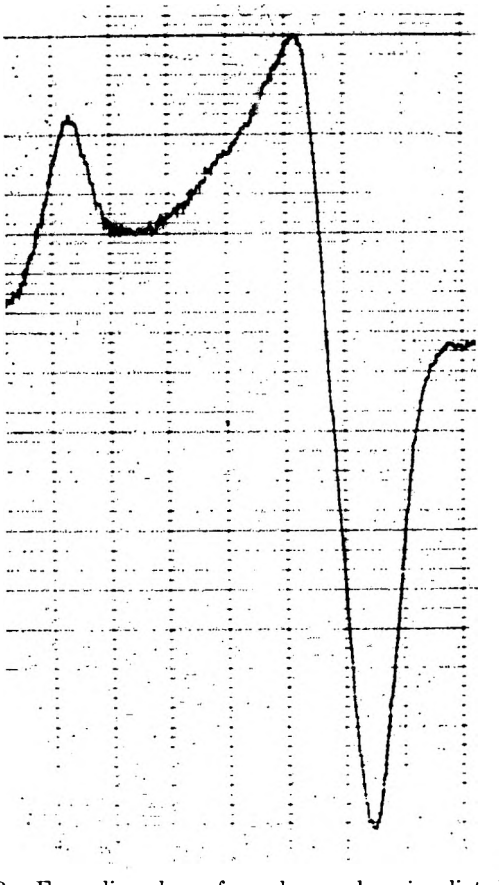

Fig. 3.—E.p.r. line shape for polypropylene irradiated to 2×10^4 r.

line spectrum. When the specimen is irradiated to neutron dosages there is formation of short and long life radicals and chemical bonds, as in the case of γ-irradiation. At low dosages mainly the short life radicals are produced, whereas at high dosages there is formation of long life radicals and chemical bonds. At low dosages the chemical bonds are unsaturated and short length and at high dosages they have a long-conjugated region. If color is due to the presence of free radicals then it may be the long lived radicals that are responsible for color formation, which is not in ac-

(10) Gordy, Miyagawa, Watabe, and Wilbur, *Proc. Natl. Acad. Sci. U. S.*, **44**, 613 (1958).
(11) B. Bleaney, *Proc. Phys. Soc.*, **A63**, 407 (1950).
(12) R. H. Sands, *Phys. Rev.*, **99**, 1222 (1955).
(13) Searl, Smith, and Wyard, *Proc. Phys. Soc.*, **74**, 491 (1959).

cordance with the results of spectrometric analysis as mentioned previously. The color we observe in this case may be due to chemical bonds.

The process of ionization by neutrons is somewhat different than by electrons or γ-rays. Neutrons interact with atoms and produce γ-rays and electrons, which in turn produce free radicals. The net process is similar in both cases of irradiation, still a marked difference in the line shape can be noticed. The radicals formed in the two cases seem to be different, in one case the paramagnetic center is axially symmetric and in the other case it is asymmetric.

Usually there is a decrease in line width in the beginning of the irradiation dose due to collision narrowing, and later at high dosages there is an increase in e.p.r. line width with increasing dose. It does not seem to be true in the case of very high neutron dosages, as used in this experiment; rather a decrease in line width with increase in dose has been observed, as shown in Fig. 2.

When the polymer is irradiated, in the initial stages there is fine structure in the e.p.r. spectrum, as observed and shown by others,[1-7] with increase in dose the fine structure reduces and finally at high dosages the spectrum becomes a single wide line due to the most stable radical formed,[7] or due to the formation of chemical bonds. As mentioned above, there is an increase in the conjugated region of the double bond with increase in dose. When the sample is exposed to the atmosphere for a long time, as in this case, there is decay in radicals and short life chemical bonds; and also by interaction with atmospheric oxygen there is formation of carbonyl and peroxyl radicals. Probably, the narrowing observed in this case is not due to exchange interaction of the unpaired electrons. The increase in the conjugated region of the double bond with increase in dose may give rise to narrowing of the line width. It could be assumed that increase in the conjugated region would lower the neighbor interaction, on account of which there is narrowing of the line width with increase in dose.

Acknowledgment.—The author wishes to thank Prof. Dr. R. Mecke under whom this work was carried out, and to Miss A. Zweng for helpful discussions.

THE THERMAL PRESSURE COEFFICIENT AND THE ENTROPY OF MELTING AT CONSTANT VOLUME OF POLYETHYLENE OXIDE

BY G. N. MALCOLM AND G. L. D. RITCHIE

University of Otago, Dunedin, New Zealand

Received October 2, 1961

Measurements have been made of the thermal pressure coefficients of three different molecular weight samples of polyethylene oxide at temperatures above the melting points. The results have been used to calculate the entropy of melting at constant volume of the highest molecular weight polymer sample using known values of the volume change on melting and the entropy of melting at constant pressure. The entropy of melting at constant volume is in good agreement with the value predicted by a calculation of the change of rotational entropy on melting.

Although the entropies of melting of several crystalline polymers have been determined at constant pressure, there is as yet little information about the corresponding entropies of melting at constant volume.[1] Such information is of particular value in the examination of the relationship between the melting behavior of a polymer and its molecular structure.[2] We report here the result of a determination of the entropy of melting at constant volume of polyethylene oxide.

The entropy of melting at constant volume is related to that at constant pressure by the equation

$$(\Delta S_m)_V = (\Delta S_m)_P - \left(\frac{\partial S}{\partial V}\right)_T \Delta V_m$$

$$= (\Delta S_m)_P - \left(\frac{\partial P}{\partial T}\right)_V \Delta V_m \qquad (1)$$

ΔV_m is the volume change on melting and $(\partial P/\partial T)_V$ is the thermal pressure coefficient of the polymer at its melting point. Both $(\Delta S_m)_P$ and ΔV_m already have been determined for polyethylene oxide.[3,4] (ΔV_m was calculated by means of the Clapeyron equation from values of $(\Delta S_m)_P$ and the pressure coefficient of the melting point.) The measurement of the thermal pressure coefficient over a range of temperatures for several different molecular weight samples of polyethylene oxide is reported in this paper. The symbol γ_V is used to denote the thermal pressure coefficient.

Experimental

Apparatus.—The measurements were made with the same kind of constant volume thermometer apparatus as was used by Hildebrand, *et al.*[5] The application of this method to the study of polymers has been described recently.[6] The polymer was degassed under vacuum and poured into a cylindrical Pyrex glass vessel with a capillary neck. At the point where the vessel was constricted to form the neck the walls of the main part of the vessel were extended by a cylindrical tube surrounding the capillary tube. The outer tube was closed by a cup-shaped Teflon plug, and the end of the capillary tube dipped into a pool of mercury contained in the Teflon plug. A small hole in the outer glass tube above the Teflon plug permitted equalization of pressure between the interior and exterior of the vessel. A

(1) L. Mandelkern, *Rubber Chem. and Technol.*, **32**, 1392 (1959).

(2) H. W. Starkweather, Jr., and R. H. Boyd, *J. Phys. Chem.*, **64**, 410 (1960).

(3) L. Mandelkern, *J. Appl. Phys.*, **26**, 443 (1955).

(4) L. R. Fortune and G. N. Malcolm, *J. Phys. Chem.*, **64**, 934 (1960).

(5) W. Weatwater, H. W. Frantz, and J. H. Hildebrand, *Phys. Rev.*, **31**, 135 (1928).

(6) G. Allen, G. Gee, D. Mangaraj, D. Sims, and G. J. Wilson, *Polymer*, **1**, 467 (1960).

tungsten wire sealed into the closed end of the main vessel projected partway down the capillary.

The glass vessel was suspended inside a steel pressure bomb which was fitted with a cone-in-cone type pressure seal similar to that described by Edeskuty and Chrisman.[7] A thin brass rod passed through a hollow steel bolt and through the mica insulating seal into the bomb. The tungsten wire protruding from the glass vessel was screwed to the end of the brass rod which served both to support the glass vessel inside the pressure bomb and also to provide the necessary insulated electrical lead into the vessel. A thin platinum wire attached to the inside surface of the pressure bomb dipped into the mercury pool surrounding the capillary neck of the glass vessel. In this way an electrical connection was provided from the insulated brass rod through the tungsten wire to the mercury pool and thence to the wall of the pressure vessel. The circuit was completed by a battery and a pilot light in series. By means of this circuit it was possible to detect when the polymer–mercury interface in the capillary was just at the tip of the tungsten wire.

The steel pressure bomb was placed inside a large well-lagged aluminum heating block. The temperature of the block was controlled by both permanent and intermittent heaters and could be maintained at any temperature from room temperature up to 200° within ±0.2°. The fluctuation of temperature inside the pressure vessel would be much less than the temperature variation in the aluminum block itself.

The pressure bomb was connected through a pressure gage to a compressor which consisted of a cylindrical steel chamber into which a thin rod was inserted through a packing gland. After assembly the apparatus was evacuated and filled with distilled water. The pressure was adjusted to any required value by screwing the rod into the compressor.

The measurements were made with the polymer samples in the liquid phase. To commence a run the apparatus was heated gently at atmospheric pressure to expel a little of the liquid from the capillary neck of the glass vessel. On cooling, mercury was pushed up the capillary and with the application of a little pressure, contact was made between the mercury and the tungsten wire. After equilibrium had been established at this temperature and pressure, the temperature was raised slightly and the new pressure required to maintain the electrical contact was determined. A period of at least 1 hr. was allowed for thermal equilibrium to be reached at each temperature. Measurements were made over a pressure range of about 400 atm. After a set of pressure–temperature values had been obtained for a given amount of polymer the temperature of the apparatus was raised at atmospheric pressure to expel a little more polymer from the glass vessel. On cooling the electrical contact was re-established and a new set of pressure–temperature readings was obtained.

The plot of temperature against pressure for each amount of polymer was linear within experimental error over the whole pressure range of 400 atm. Consequently the slope of the line could be determined easily and the line could easily be extrapolated over a short pressure interval of about 10 atm. down to a pressure of 1 atm. In this way the slope of the line at the temperature corresponding to 1 atm. pressure could be determined. The slope of the line did not give the true thermal pressure coefficient of the sample at 1 atm. pressure, but rather a quantity which may be called γ_{obs}. This quantity was corrected for the thermal expansion and the isothermal compressibility of the glass cell by the relation

$$\gamma_v = \gamma_{obs.}\left[1 + \frac{\alpha_g}{\alpha_p} - \frac{\beta_g}{\beta_p}\right]$$

α_p and α_g are the coefficients of thermal expansion and β_p and β_g are the coefficients of isothermal compressibility of the polymer and the glass, respectively. For Pyrex glass α_g was taken as 9.9×10^{-6} deg.$^{-1}$ and β_g as 3.00×10^{-6} atm.$^{-1}$. A value of $\alpha_p = 7.1 \times 10^{-4}$ deg.$^{-1}$ was calculated from the specific volume–temperature plot obtained by Mandelkern.[3] A value of β_p was obtained from the relation $\beta_p = \alpha_p/\gamma_v$ by successive approximations, using a value $\alpha_p/\gamma_{obs.}$ as a first approximation. The magnitude of the correction term was only from 4 to 6% of γ_{obs}.

(7) F. J. Edeskuty and R. H. Chrisman, *Rev. Sci. Instr.*, **29**, 178 (1958).

Materials.—The samples of polyethylene oxide had number average molecular weights 300, 1500, and 5000. They were carefully dried and degassed under high vacuum.

Results

The values of γ_{obs} and γ_v at 1 atm. pressure for the three different molecular weight samples of polyethylene oxide are shown in Table I. All the results refer to polymer samples in the liquid phase, although the values marked with an asterisk refer to samples in a supercooled liquid state. Nevertheless these latter values were not obtained by direct measurements on the polymer below its melting point. Rather they were obtained by making pressure–temperature measurements on a certain amount of polymer at several temperatures above the melting point. The linear plot of pressure against temperature which was obtained

TABLE I

THERMAL PRESSURE COEFFICIENTS OF POLYETHYLENE OXIDE AT 1 ATM. PRESSURE

T, °C.	$\gamma_{obs.}$	γ_v, atm. deg.$^{-1}$
Polyethylene oxide, 300		
37.5	17.5	16.4
48.0	16.6	15.6
60.5	15.8	14.9
74.0	15.1	14.3
92.0	14.0	13.3
Polyethylene oxide, 1500		
33.5	16.2	15.3*
42.0	15.8	14.9*
61.0	14.9	14.1
68.0	14.4	13.7
Polyethylene oxide, 5000		
50.0	14.8	14.0*
58.0	14.3	13.6*
73.0	13.6	13.0
80.0	13.2	12.6
94.5	12.5	12.0
103.0	11.9	11.4

then was extrapolated down to the point corresponding to one atmosphere pressure. The temperature at this point gave the temperature at which the thermal pressure coefficient (γ_{obs}) was equal to the slope of the line when the pressure was 1 atm. It is estimated that the experimental error in the thermal pressure coefficients is ±3%.

Discussion

Molecular Weight Dependence of γ_v.—It has been observed that for several series of homologous oligomers the values of γ_v increase slightly with molecular weight to a limiting value about 5–15% above the low molecular weight value.[6] But in the case of the polyethylene oxide samples studied here the values of γ_v decrease to a limiting value with increase in molecular weight. This trend is supported by two other isolated measurements for polyethylene oxides which have been reported.[6,8] There is little change in γ_v after the molecular weight reaches 3000. It is possible that the decrease in γ_v is related to the reduced effect of the terminal hydroxyl groups as the chain length in-

(8) G. Allen, University of Manchester, England, private communication.

creases. This suggestion is supported by the fact that at 20° γ_v for polyethylene oxide dimethyl ether 400 in which the hydroxyl groups are entirely absent is only 15.8 atm. deg.$^{-1}$ whereas that for polyethylene oxide 400 is 17.5 atm. deg.$^{-1}$. Furthermore the limiting value to which γ_v for polyethylene oxide decreases at any temperature is about the same as the limiting value to which it has been estimated that γ_v for polyethylene oxide dimethyl ether increases.[6]

The Entropy of Melting at Constant Volume.—By interpolation from Table I the value of γ_v for high molecular weight polyethylene oxide at its normal melting point (66°)[3] is 13.3 atm. deg.$^{-1}$. Substitution of this value in eq. 1 together with the values $(\Delta S_m)_P$ = 5.85 cal. deg.$^{-1}$ mole^{-1} and ΔV_m = 5.1 cc. mole^{-1} gives $(\Delta S_m)_V$ = 4.22 cal. deg.$^{-1}$ per mole of repeating units. This is equivalent to $(\Delta S_m)_V$ = 1.41 cal. deg.$^{-1}$ per mole of chain atoms.

Starkweather and Boyd[2] have described a method of calculating the entropy of melting of linear polymers from a lattice model. They write the entropy of melting at constant volume per mole of chain atoms as

$$(\Delta S_m)_V = \Delta S_R + \Delta S_D = (\Delta S_g - 0.86R) + \Delta S_D \quad (2)$$

The rotational isomerism contribution ΔS_R is written as the sum of the gain in entropy due to rotational isomerism without regard to the lattice interferences (ΔS_g) and the decrease per bond due to packing on the lattice (0.86 R). ΔS_D is a term added to allow for the over restrictiveness of a lattice treatment and is called the long range disorder contribution. A reasonable value of ΔS_D would be of the order of R cal. deg.$^{-1}$ per mole of chain atoms.

The authors have applied their theory to polyethylene and polymethylene oxide. In both these polymers the chain bonds are all alike, either C–C or C–O. But in polyethylene oxide there are two C–O bonds and one C–C bond in each repeating unit. If the difference in potential energy between *gauche* and *trans* forms for the C–C bond is the same in polyethylene oxide as in polyethylene then at the melting temperature of polyethylene oxide (339°K.) the theory gives ΔS_g = 1.57 cal. deg.$^{-1}$ per mole of C–C bonds. Similarly if the difference between *gauche* and *trans* forms for the C–O bond is the same in polyethylene oxide as in polymethylene oxide then at the melting temperature of polyethylene oxide ΔS_g = 0.89 cal. deg.$^{-1}$ per mole of C–O bonds. Hence for the repeating unit in polyethylene oxide ΔS_g = 1.57 + (2 × 0.89) = 3.35 cal. deg.$^{-1}$ per mole of repeating units. This is equivalent to ΔS_g = 1.12 cal. deg.$^{-1}$ per mole of chain atoms. When this value is used for ΔS_g the value of ΔS_D calculated by difference from eq. 2 is 2.0 cal. deg.$^{-1}$ per mole of chain atoms. The theory applied in this way thus gives a reasonable account of the entropy of melting of polyethylene oxide.

According to this analysis the gain in entropy per chain atom due to rotational isomerism on melting is lower for polyethylene oxide than for either polymethylene oxide or polyethylene. The low value for polyethylene oxide is in agreement with the observation of Davison[9] from infrared studies that the configuration of the O·$(CH_2)_2$·O group in polyethylene oxide is substantially the same in the molten and crystalline states, so that only a limited amount of rotation must occur on melting.

(9) W. H. T. Davison, *J. Chem. Soc.*, 3270 (1955).

THE REACTION OF ACTIVE NITROGEN WITH SIMPLE HYDROCARBONS*

BY E. R. ZABOLOTNY AND H. GESSER

Parker Chemistry Laboratory, University of Manitoba, Winnipeg, Canada

Received October 3, 1961

The reaction of methane with active nitrogen produced by passing both nitrogen and nitrogen–argon mixtures through a condensed discharge was studied in an unheated reaction vessel. The reactions of ethane and acetylene with active nitrogen from the nitrogen–argon system also were investigated. Hydrogen cyanide and ammonia were found as products. It is concluded that excited argon atoms increased the chemical reactivity of active nitrogen by augmenting the percentage of excited species in active nitrogen.

Introduction

The reactions of active nitrogen with a number of hydrocarbons have been studied by many investigators, in particular Winkler[1] and co-workers. The studies to date have for the most part utilized active nitrogen from a discharge through nitrogen. Hydrogen cyanide generally is reported to be the only major nitrogen containing compound in these reactions. Dewhurst,[2] however, found that significant quantities of ammonia also were present. The results of the active phosphorus–hydrocarbon reactions[3] investigated in this Laboratory also led to the expectation that ammonia is an intermediate product which might be found in large quantities if the reactions were carried out at low nitrogen concentrations.

Experimental

The apparatus was essentially that described by Winkler and co-workers,[4] the difference being that the discharge tube and the reaction system, a spherical 500-cc. bulb, were not poisoned. In most of the experiments argon, at a flow rate of 3.0 × 10^{-3} mole/min., was used as a carrier gas to

(*) The research for this paper was supported by the Defence Research Board of Canada, under grant number 95-30-28, Project D76-95-30-28.

(1) H. G. Evans, G. R. Freeman, and C. A. Winkler, *Can. J. Chem.*, **34**, 1271 (1956).

(2) H. A. Dewhurst, *J. Phys. Chem.*, **63**, 1976 (1959).

(3) E. R. Zabolotny and H. Gesser, *J. Am. Chem. Soc.*, **81**, 6091 (1959).

(4) D. A. Armstrong and C. A. Winkler, *J. Phys. Chem.*, **60**, 1100 (1956).

sweep different concentrations of nitrogen through the discharge.

All reactants were fractionated by bulb-to-bulb distillation. The condensable products and reactant were separated by a LeRoy still; the temperature was varied so that the substance being distilled had a vapor pressure of about 20 μ. The amounts of reactant and products were measured in a combined Toepler pump and gas buret. Ammonia, identified by its infrared spectrum, was found to be associated with hydrogen cyanide as ammonium cyanide at low temperatures and was distilled at $-85°$. At room temperature the ammonium cyanide was an equimolar mixture of ammonia and hydrogen cyanide.

Results

Methane, ethane, and acetylene all were reacted with active nitrogen in an argon atmosphere. In each case hydrogen cyanide and ammonia were found as the major gaseous products with little or no polymer formation. Trace amounts of ethane were found when methane was used as the reactant and correspondingly small amounts of butane and cyanogen were found when ethane was reacted.

On the basis of the hydrogen cyanide formed, about 5% of the methane reacted at 27° when nitrogen was used without a carrier gas. The molecular nitrogen flow rate was 1.6×10^{-3} mole/min., corresponding to a reaction zone pressure of 1.30 mm. When argon was used as a carrier for nitrogen flowing at a rate of 33×10^{-6} mole/min. ($Ar/N_2 > 100$), to obtain a reaction zone pressure of 2.23 mm., the rate of formation of ammonia was increased fivefold and the yield of hydrogen cyanide was approximately doubled in comparison with experiments using pure nitrogen. The rate of production of hydrogen cyanide increased rapidly with increase in methane flow, but the ammonia remained relatively constant. The increase in the rates of formation of products in the argon–nitrogen system might be attributed to the fact that argon decreases the rate of recombination of nitrogen atoms thus effectively increasing the nitrogen atom concentration. However, the nitrogen atom flow rate in the nitrogen system ($> 100 \times 10^{-6}$ mole/min.) as determined by the maximum yield of hydrogen cyanide from ethylene was greater than twice the molecular nitrogen flow rate in the nitrogen–argon system. Since blank experiments using only argon in the discharge indicated no hydrocarbon decomposition, the increase in the rates of formation of products in the argon–nitrogen system, as compared to the pure nitrogen system, must be due to collisions between excited argon atoms and nitrogen atoms and molecules. The results are shown in Fig. 1. Similar results, shown in Fig. 2, were obtained when the methane flow was kept constant at about 20×10^{-6} mole/min. and the molecular nitrogen flow in the argon stream was varied. The pressure in the reaction system was 1.45 mm. The increase in hydrogen cyanide production with increase in molecular nitrogen concentration can be interpreted as proportional to the increase in the excited species concentration.

One reason that the rate of production of ammonia was constant may be the fact that, at least to a smaller extent, ammonia itself is used up as a reactant.[5] Thus the rate of production of ammonia observed experimentally may be called an "equilibrium rate." At flow rates of molecular nitrogen of about one μmole/min., about 40% of the nitrogen reacted to form ammonia and hydrogen cyanide. When active nitrogen from the argon–nitrogen discharge was passed over ammonia, ethane, and ethylene at $-196°$ in the "product trap," no decomposition was observed.

In order to find the optimum conditions for the production of ammonia both nitrogen and methane flow rates (33×10^{-6} and 16×10^{-6} mole/min.,

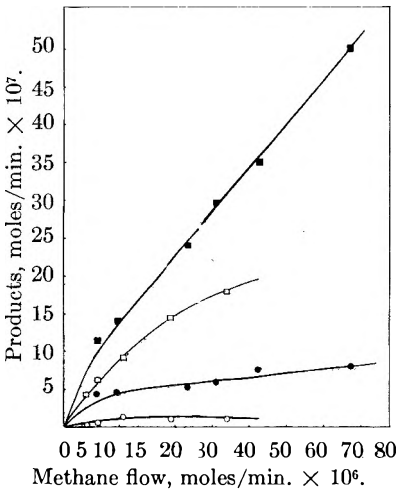

Fig. 1.—Relation between hydrogen cyanide and ammonia production with methane flow rate: ■, HCN (argon-nitrogen mixture); □, HCN (pure nitrogen system); ●, NH_3 (argon–nitrogen mixture); ○, NH_3 (pure nitrogen system).

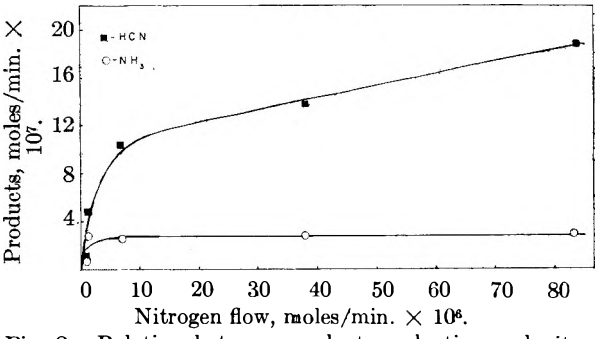

Fig. 2.—Relation between product production and nitrogen flow rate in the reaction of methane with active nitrogen.

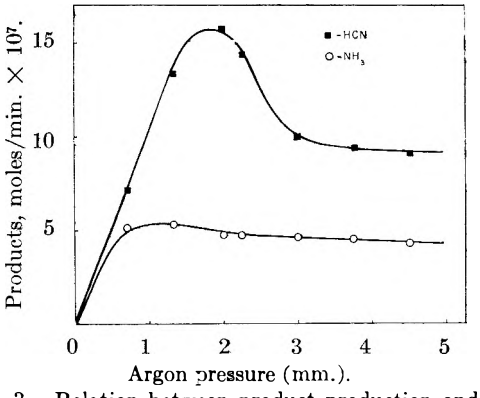

Fig. 3.—Relation between product production and reaction zone pressure for the reaction of active nitrogen with methane.

(5) G. R. Freeman and C. A. Winkler, *J. Phys. Chem.*, **59**, 371 (1955).

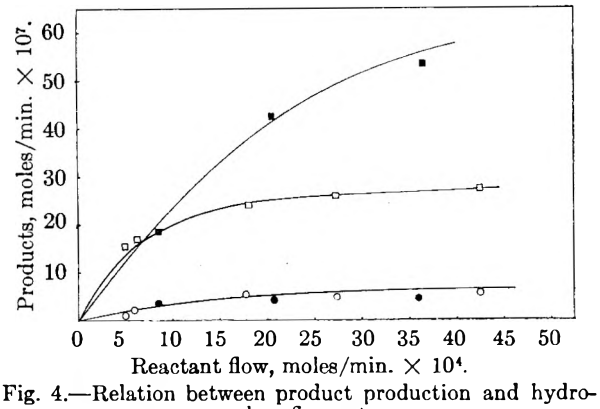

Fig. 4.—Relation between product production and hydrocarbon flow rate.

Reactant	HCN	NH_3
C_2H_2	□	○
C_2H_4	■	●

respectively) were kept constant and the reaction pressure was varied by adjusting the flow of argon. The results are illustrated in Fig. 3. The yield of ammonia decreased much less rapidly with increase in pressure than did the yield of hydrogen cyanide. The maximum rate of hydrogen cyanide production may be taken to correspond to the maximum excited species concentration. The destruction of ammonia produced in the reaction of course also would be a maximum at this point.

The yields of ammonia and hydrogen cyanide for the active nitrogen reaction with ethane and acetylene are given in Fig. 4. The reaction zone pressure was 2.23 mm. and the molecular nitrogen flow rate was 33×10^{-6} mole/min. Lower hydrogen cyanide yields in the case of acetylene indicates that there was more polymer formation than in the methane and ethane reactions. In the ethane reaction about 70% of the ethane destroyed was recovered as hydrogen cyanide but only 50% of the acetylene destroyed was recovered as hydrogen cyanide.

Discussion

Since ammonia is formed as a product from the active nitrogen reaction with acetylene it would seem likely that one of the primary processes is a hydrogen atom abstraction to form an NH radical. The reaction $CH_4 + N \rightarrow CH_3 + NH$ (1) has a minimum activation energy of 14 kcal. for ground state nitrogen atoms. It therefore becomes necessary to assume that either excited nitrogen atoms or molecules are responsible for the initial reactions. Excited atoms, which are known to exist in active nitrogen in very small concentrations,[6,7] may react with the hydrocarbon as[8]

$$CH_4 + N(^2D) \longrightarrow CH_3 + NH + 40 \text{ kcal.} \quad (2)$$
$$CH_3 + CH_3 \longrightarrow C_2H_6 \quad (3)$$

$$CH_3 + N(^4S) \longrightarrow [CH_3N] \longrightarrow HCN + H_2 \quad (4)$$
$$CH_3 + N(^4S) \longrightarrow [CH_3N] \longrightarrow HCN + 2H \quad (4a)$$
$$NH + NH \longrightarrow N_2 + H_2 + 175 \text{ kcal.} \quad (5)$$
$$NH + H_2 + M \longrightarrow NH_3 + 90 \text{ kcal.} \quad (6)$$

The heat of reaction for reaction 2 is based on the formation of a ground state NH radical. With increase in concentration of NH radicals reaction 5 would be favored over reaction 6. According to the above mechanism, the hydrogen concentration would be at least as great as the yield of hydrogen cyanide, which is always greater than the yield of ammonia.

Reaction 6, unfortunately, does not conserve spin and must be considered to be very slow. The formation of ammonia then would have to occur by reactions such as

$$NH + H + M \longrightarrow NH_2 + M \quad (7)$$
$$NH_2 + H + M \longrightarrow NH_3 + M \quad (8)$$

The initial reaction

$$CH_4 + N \longrightarrow [CH_4N] \longrightarrow HCN + H_2 + H \quad (9)$$

postulated by Winkler[9,10] undoubtedly also occurs. In a nitrogen discharge system, reaction 7 would be the predominant first step. In the nitrogen–argon discharge system, however, reactions 2 and 7 would become competitive. Reaction 2 would be favored with decrease in molecular nitrogen flow rate.

The mechanism for the ethane reaction would involve similar steps

$$C_2H_6 + N(^2D) \longrightarrow C_2H_5 + NH + 45 \text{ kcal.} \quad (10)$$
$$C_2H_5 + N \longrightarrow [C_2H_5N] \longrightarrow CH_3 + HCN + H \quad (11)$$
$$C_2H_6 + N \longrightarrow [C_2H_6N] \longrightarrow CH_3 + HCN + H_2 \quad (12)$$

Reaction steps, corresponding to eq. 4 and 9, in the acetylene–active nitrogen reaction, unfortunately cannot be written. This of course would mean that the hydrogen produced in reaction 5 is the only hydrogen available for reaction 6. The small differences in the rates of formation of ammonia would seem to indicate that ammonia production depends to a greater extent on reaction 5 than on reactions of the type corresponding to eq. 4.

It can be argued that the formation of an NH complex is not necessary even with acetylene. A complex of the type $[C_2H_2N]$ might, on interaction with itself, yield ammonia in a one-step reaction without intervention of NH. The nitrogen atom is far removed from the hydrogen atoms and the reaction

$$2[C_2H_2N] \longrightarrow NH_3 + C_4H \quad (13)$$

seems very unlikely if the radical models are considered. However, reactions between C_2H_2N radicals could produce NH or NH_2 radicals. If one could prove that reactions of this type did occur to a significant extent it might not be necessary to assume hydrogen atom abstraction. Reactions of the type

$$2[CH_3N] \longrightarrow NH_3 + [C_2H_3N] \quad (14)$$

may occur in the methane–active nitrogen reaction but certainly to only a small extent since the lifetime of the $[CH_3N]$ radical would be very short.

(6) H. P. Broida and O. S. Lutes, *J. Chem. Phys.*, **24**, 484 (1956).
(7) H. I. Schiff, *Ann. N. Y. Acad. Sci.*, **67**, 518 (1957).
(8) Heats of reaction are based on:
$D(N\text{–}H) = 87$ kcal. G. Pannetier and A. G. Gaydon, *J. chim. phys.*, **48**, 221 (1951).
$D(CH_3\text{–}H) = 101$ kcal. T. L. Cottrell, "The Strength of Chemical Bonds," Sec. Ed., Butterworths, Washington, D. C., 1958.
$D(N_2) = 225$ kcal. J. M. Hendrie, *J. Chem. Phys.*, **22**, 1503 (1954).
$N(^2D) = 55$ kcal. "Atomic Energy Levels," National Bureau of Standards, Circular 467.
(9) H. Blades and C. A. Winkler, *Can. J. Chem.*, **29**, 1022 (1951).
(10) P. Gartaganis and C. A. Winkler, *ibid.*, **34**, 1457 (1956).

PHOTOVOLTAIC EFFECT OF SILVER BROMIDE

BY W. COOPER

Communication No. 2216 from the Kodak Research Laboratories, Eastman Kodak Company, Rochester, N. Y.

Received October 7, 1961

The open-circuit photovoltaic effect of silver bromide sheet crystals–electrolyte systems has been investigated. Initial negative potentials that characterize the effect for most cases were found to be a function of electrolyte concentration and composition, crystal thickness, wave length, and incident intensity. The incorporation of impurities in the silver bromide crystals caused large changes in the observed photopotentials. The addition of Pb^{++} or Cd^{++} ions resulted in decreased potentials. In the presence of sulfide as an added impurity, a large diminution in the photopotential occurred. Thallous and cuprous ions in silver bromide behaved as temporary hole-acceptors. Silver sulfide molecules, adsorbed as a monolayer on pure and mixed crystals, caused significant decreases in the photopotential.

Introduction

Although photovoltaic effects in silver bromide for a large number of different types of electrodes have been studied, the results of such investigations generally have been incompatible. Copeland and co-workers[1] have given an account of the literature of this older work. The electrodes used were invariably of the silver–silver halide type, in which a thin layer of silver halide is coated upon a metallic silver electrode. Vanselow, Sheppard, and collaborators[2–4] have studied extensively photovoltaic effects for this type of cell and have reported both positive and negative changes, generally the latter for the first moment of irradiation followed by a change to the former with continued exposure.

Kolthoff and Sanders[5] have reported that the photovoltaic effect at a fused-disk, membrane-type silver bromide electrode is always negative in sign. In view of the fact that prior work dealt with photovoltaic changes not solely at a silver bromide surface, but at a silver–silver bromide interface and with polycrystalline material, it was of interest to study the effect in silver bromide of known purity and in the form of sheet crystals made from the melt by the methods described by Mitchell and his co-workers.[6,7]

It would be anticipated that the absorption of light by the intrinsic absorption process of silver bromide results in the creation of a hole-electron pair. The photoelectrons, owing to a larger mobility, diffuse into the bulk of the crystal, some reaching the silver bromide–metal junction. Others are trapped within the crystal but probably induce changes at the junction where contact barrier effects might be operative. The range and concentration of these carriers contribute directly to the output voltage of the cell.

Holes produced by the process diffuse primarily to the surface for non-penetrating irradiation, and are accepted to a limited degree by the electrolyte whose efficiency is related to constitution and concentration. Alteration of crystal structure that manifests changes in recombination, trapping, etc., would be expected to affect the photopotential.

Such studies of photovoltaic effects in single crystals of silver bromide should provide not only additional fundamental information concerning semiconductor surfaces, but also information of photographic interest, since Mitchell and co-workers[6–10] and West and Saunders[11] have shown the utility of such crystals for performing experiments on fundamental problems of photographic sensitivity.

Experimental Procedure

Except for slight modifications, the photovoltaic cell was similar to that used by Vanselow and Sheppard.[2] Sheet crystals of silver bromide were sealed to openings located at the rear wall of a U-tube, directly opposite quartz windows. External connections to the sheet crystals were made with silver paste[12] and a pressure contact of platinum or silver sheet. In some experiments NESA,[13] thin evaporated layers of stannic oxide or glass, was used instead of silver paste for electrical contact. A British Thomson-Houston ME/D 250-watt high-intensity mercury source was employed and the radiation passed through a Bausch and Lomb 500-m. focal length grating monochromator. The entire area of the exposed crystal (1.13 $cm.^2$) was covered by the light. Measurement of the photopotential was accomplished with a Tektronic 536 oscilloscope, equipped with a high-gain differential preamplifier, Tektronix 53/54 D. The input impedance of the device was 2 megohms compared to dark resistances of the order of 10^5 ohms for most of the crystal–electrolyte systems studied. Two methods were used to measure the light intensity. In one method, a Cambridge circular thermopile was calibrated with a Bureau of Standards radiation standard and this was used to measure the intensity of the source. The other involved the procedure of Hatchard and Parker.[14] This technique involves the photoreduction of potassium ferrioxalate as the basis of a sensitive chemical actinometer. The two independent methods agreed within 10%. Neutral density filters were used to measure the intensity-dependence of the photo-e.m.f.

A Keithley Model 200B electrometer, equipped with a decade shunt which enabled the input impedance of the instrument to be varied by factors of ten up to 10^{14} ohms, was used to determine the effect of the dark resistance of the cell on the photopotential. It was found that for most of the crystals studied the photovoltaic effect was relatively independent of the input impedance in the range of 10^6 to 10^{14} ohms, and as a consequence the measurements with the oscilloscope at an impedance of 2 megohms were valid.

Prior to each measurement of the photo-e.m.f., the dark

(1) A. W. Copeland, O. D. Black, and A. B. Garrett, *Chem. Revs.*, **32**, 177 (1943).

(2) W. Vanselow and S. E. Sheppard, *J. Phys. Chem.*, **33**, 331 (1929).

(3) S. E. Sheppard, W. Vanselow, and V. C. Hall, *ibid.*, **33**, 1403 (1929).

(4) S. E. Sheppard, W. Vanselow, and G. P. Happ, *ibid.*, **44**, 411 (1940).

(5) H. L. Sanders and I. M. Kolthoff, *ibid.*, **44**, 936 (1940).

(6) J. M. Hedges and J. W. Mitchell, *Phil. Mag.*, [7] **44**, 357 (1953).

(7) P. V. McD. Clark and J. W. Mitchell, *J. Phot. Sci.*, [2] **4**, 1 (1956).

(8) J. W. Mitchell, *ibid.*, [2] **1**, 110 (1953).

(9) T. Evans, J. M. Hedges, and J. W. Mitchell, *ibid.*, [2] **3**, 73 (1955).

(10) J. W. Mitchell, *ibid.*, [2] **5**, 49 (1957).

(11) W. West and V. I. Saunders, *J. Phys. Chem.*, **63**, 45 (1959).

(12) Silver Conducting Paint, SC 12, Micro-Circuits Company, New Buffalo, Michigan.

(13) Pittsburgh Plate Glass Company, Pittsburgh, Pa.

(14) C. G. Hatchard and C. A. Parker, *Proc. Roy. Soc.* (London), **A235**, 518 (1956).

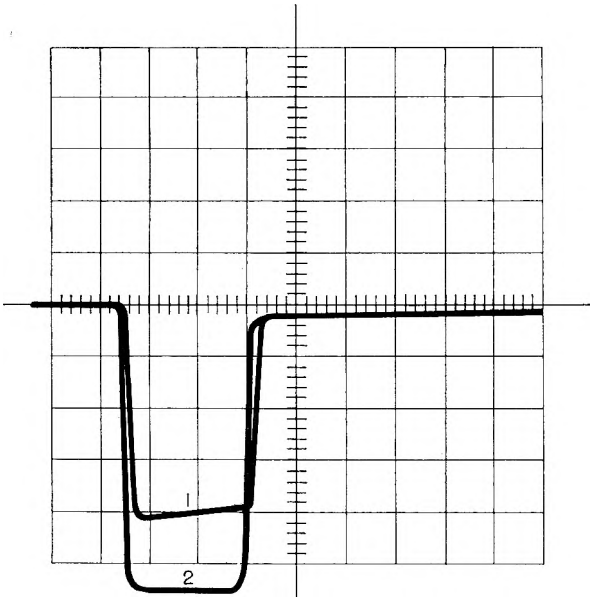

Fig. 1.—Photovoltaic effect as a function of halogen-acceptor: AgBr, (50 μ); exp., 10 msec. at 365 mμ; electrolyte (1) 10^{-5} M KBr; (2) 10^{-5} M KBr + 10^{-1} M acetone semicarbazone: one large division vertical equals 0.020 v.; one large division horizontal equals 5 msec.

resistance of the system was recorded. For crystals 10–180 μ thick, the values of the dark resistance were randomly distributed, ranging in value from 5–60 $\times$ 10^4 ohms. In this specified range of crystal thickness, the dark resistance of the photocell was of negligible importance in determining the photopotential.

For thicker crystals, *i.e.*, those greater than 200 μ, the dark resistance of the circuit was significantly higher and undoubtedly placed some limitation on the photopotential. However, beyond 200 μ, the photopotential reached an almost constant value which seemed independent of crystal thickness and the dark resistance of the cell. Corrections made by changing the input impedance of the electrometer to yield values independent of dark resistance in this range of crystal thickness do not yield potentials of the same order of magnitude as those of the thinner crystals.

A graded-bleach-etch technique developed by West and Saunders[11] was used to study the relation between the photovoltaic effect and the distribution of latent-image centers. Sulfur sensitization of pure and mixed silver bromide crystals was accomplished by treatment with 10^{-6} M sodium thiosulfate at room temperature. The adsorption of thiosulfate results in the formation of silver sulfide and it is assumed that the sulfide is in the form of an adsorbed monolayer.

Experimental Results

I. Reproducibility and Electrolyte Constitution and Concentration.—One basic difficulty encountered in previous studies of photovoltaic effects in silver halides has been the preparation of reproducible electrodes. As a stringent test of reproducibility in this investigation, experiments were performed at short exposures (10 msec.) and with 365 mμ radiation. The conducting electrolyte was potassium bromide. Reasonable reproducibility (20% generally) was obtained for the crystals under the conditions specified. Crystals obtained from the same large sheet gave results well within the limits of reproducibility indicated; usually values agreed within 10%. The phenomenon is characterized by a potential which is negative in sign.

In the range of electrolyte concentration of 10^{-3}–10^{-1} molar potassium bromide, little change was noticed in the photopotential, and saturating the electrolyte with silver bromide had no effect on the potentials. A comparison of photopotential and equilibrium solubility of silver bromide in bromide ion at various concentrations showed no correlation between solubility[15] and photopotential. At concentrations smaller than 10^{-3} M KBr decreases in photopotentials were noticeable and are attributed to the large increases in dark resistances of the solutions.

The addition of 10^{-1} M concentrations of halogen-acceptors, acetone semicarbazone, and phenol, and smaller concentrations of sodium nitrite[2] likewise could increase significantly the magnitude of the negative potentials in single sheet crystals. Acetone semicarbazone appeared most effective, although its addition increased the dark resistance of the cell. The effect of acetone semicarbazone appeared to be a function of both wave length and bromide-ion concentration, being more effective for non-penetrating radiation and low bromide-ion concentrations. Such an observation appears as a logical consequence of a greater concentration of holes appearing at the interface for non-penetrating wave lengths, and the acceptor at low bromide-ion concentrations, adsorbed at or near the surface due to less competition with bromide ion for available adsorption sites. Figure 1 shows the response of a sheet crystal first in 10^{-5} M bromide, and then the increased negative effect observed with the same crystal in 10^{-5} M bromide + 10^{-1} M acetone semicarbazone.

Cadmium bromide also was used as an electrolyte. This compound in aqueous solution is known to contain a larger number of undissociated molecules.[16] In all cases studied, cadmium bromide reduced the magnitude of the photopotentials by approximately 20% as compared to potentials obtained in the presence of potassium bromide of the same molar concentration.

Mercuric bromide, which has a dissociation constant of 4.8 $\times$ 10^{-16} at 25°,[17] also was used as an electrolyte at concentrations of 0.001 and 0.0001 M. The nature of the photopotential was markedly changed in the presence of this very weakly dissociated electrolyte; in fact, the photopotentials were found to be positive, as shown in Table I. The data also include experiments performed with cadmium bromide as electrolyte.

When saturated bromine in water was added in the dark to one electrode, a direct-positive potential, which equilibrated within the order of seconds, was obtained, corroborating the earlier work.[2] Subsequent illumination of the electrode caused a further increase in the positive potential. The potential returned to the equilibrium value after the light was removed.

Changing the nature and valency of the electrolyte cation from K^+ ion to In^{+++} ion had essentially no effect on the magnitude of the potentials. The photovoltage, at a given concentration of

(15) M. A. Hill, C. W. Zuehlke, and A. E. Ballard, *Phot. Sci. and Tech.*, [II] **3**, 101 (1956).

(16) H. L. Riley and V. Gallafent, *J. Chem. Soc.*, 514 (1932).

(17) O. Bethge, I. Jonevall-Westöö, and L. G. Sillen, *Acta Chem. Scand.*, **2**, 828 (1948).

TABLE I
DEPENDENCE OF THE PHOTOVOLTAIC EFFECT IN SILVER BROMIDE CRYSTALS ON WEAKLY DISSOCIATED ELECTROLYTES
Exposure, 10 msec.; wave length, 365 mμ

Description	Electrolyte	Molar concn.	Photoeffect (v.)
AgBr (82 μ)	$HgBr_2$	0.0001	+0.015
	KBr	.0001	− .024
	$HgBr_2$	.001	+ .027
	KBr	.001	− .031
AgBr (74 μ)	KBr	.001	− .051
	$CdBr_2$	.001	− .037
	$HgBr_2$	.001	+ .016

electrolyte, seems independent of the cation charge and valency as long as the ion does not function as a halogen-acceptor.

Thallous ions in solution appeared to have some ability to accept escaped holes in the form of photobromine, since successive 10-msec. exposures of the crystal in the presence of a potassium bromide solution resulted in decreases in the photopotential, whereas no decrease was found in the presence of the thallous bromide. Undoubtedly the reaction between photobromine and thallous ion at the electrolyte–AgBr interface prevented the introduction of holes into the crystal by the well known Wagner mechanism.[18]

II. Photovoltaic Effect and Crystal Thickness.—For a range of crystal thickness from 10–870 μ, the photovoltaic effect was characterized by small potentials for thin crystals and for crystals thicker than 200 μ and by maximum potentials for crystals of 20–65 μ average thickness. Figure 2 shows a plot of electrode potential *vs.* crystal thickness.

As the thickness of the crystal increases, the ratio of the number of holes to the number of electrons reaching the metal contact decreases, resulting in an increase in the photovoltage to a value of approximately 0.11 volt. A maximum in the photopotential in the range of 20–65 μ may be a reflection of the diffusion length of the electrons. For crystals thicker than 65 μ, the probability of an electron diffusing to the metal contact is drastically reduced.

The limiting value obtained from approximately 200–870 μ may represent merely a potential as a result of the separation of the photoproduced carriers due to the higher mobility of the electrons and electrolyte acceptance of holes.

III. Photovoltage *vs.* Wave Length and Intensity.—It was observed that the onset of the photovoltaic effect appeared to coincide with the absorption edge of pure silver bromide, *i.e.*, the absorption due to the excitation of an electron from the valence to the conduction band.

Figure 3 depicts a typical determination of the wave length dependency of a thick crystal for exposures of a constant number of photons. Also included is the absorption spectrum of pure silver bromide.[19] As one would suspect, a close analogy exists between optical absorption and the photovoltaic effect, since the latter becomes measurable only when absorption becomes significant.

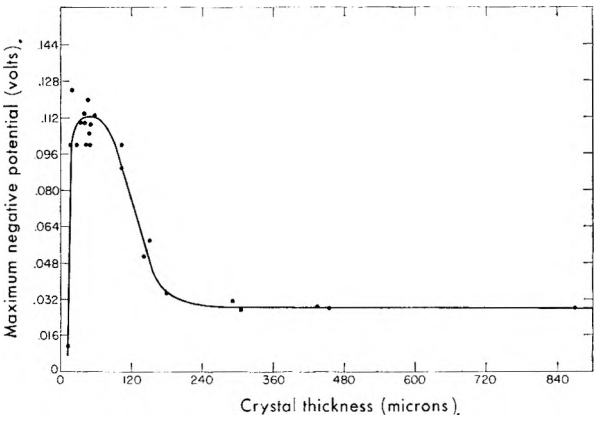

Fig. 2.—Photovoltaic effect as a function of crystal thickness: crystals, AgBr; electrolyte, 0.001 *M* KBr; exposure, 10 msec. at 365 mμ and incident intensity of 5.3×10^{14} quanta/sec./cm.^{2}.

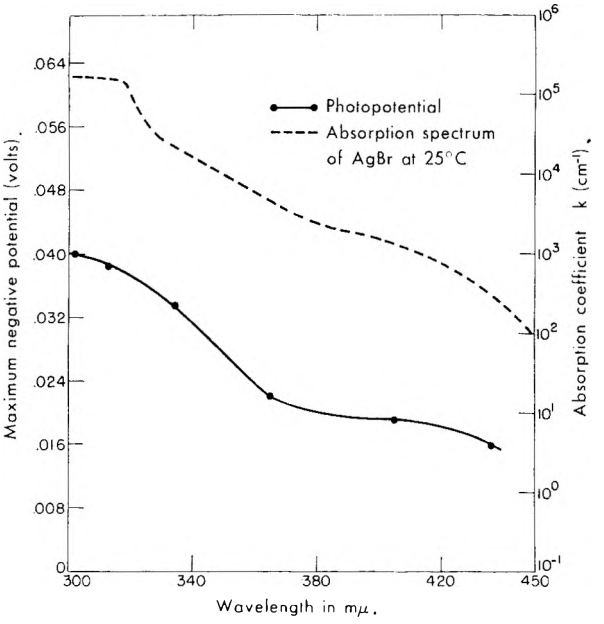

Fig. 3.—Wave length-dependence of photovoltaic effect: crystal, AgBr (306 μ); electrolyte: 0.001 *M* KBr; 10-msec. exposure; intensity, 2.6×10^{14} quanta/sec./cm.^{2}. ●—●, photopotential; – – – –, absorption spectrum of AgBr at 25°.[18]

The photo-e.m.f. also was studied as a function of light intensity both at high-intensity and at low-intensity radiation levels. At low-intensity levels the voltage varied linearly with relative intensity and at high intensity a logarithmic dependence was found. This is in agreement with the theory of the photovoltaic effect.[20] Slopes proportional to the values of kT/e, compiled from six different experiments, show that the photo-e.m.f. is related to the diffusion of photoproduced carriers. Neglecting the ratio of electron to hole mobility at low intensity, the photovoltaic effect of pure silver bromide might be expressed as $V \cong kT/e\ f(I)$ and at high intensity as $V \cong kT/e\ f(\log I)$; $f(I)$ and $f(\log I)$ represent complex functions of the intensity.

(18) C. Wagner, *Z. physik. Chem.*, **B32**, 449 (1936).
(19) F. Moser and F. Urbach, *Phys. Rev.*, [2] **112**, 1519 (1956).
(20) J. Tauc, *Rev. Mod. Phys.*, **29**, 308 (1957).

IV. The Nature of the Contacts.—When the cell was illuminated at the silver bromide–electrolyte interface, the usual negative response was obtained, but exposure of the crystal through the transparent tin oxide conducting glass yielded positive potentials, although the crystal contained a sufficient concentration of hole-acceptor, Cu^+ ions, to trap effectively the number of holes produced by the exposures.[11] The response from this type of exposure was a mirror-image of that obtained from exposure of the silver bromide–electrolyte interface. Such data strongly suggest that the exposed surface takes on a relatively positive charge with respect to the unexcited regions of the crystal which become negative owing to bulk diffusion of the more mobile photoelectrons.

To understand the photovoltaic effect process better, a knowledge of the charge-transfer mechanisms at the silver bromide–electrolyte and silver bromide–metal interfaces was necessary. Since at room temperature ionic conductivity in silver bromide due to motion of interstitial silver ions is relatively large, voltage pulses of 1.0-μsec. duration at 100 kc. and ranging in magnitude from -5 to $+5$ volts were applied to a silver bromide crystal of 88 μ average thickness, as a means of minimizing electrolysis of the crystal. In this way measurements of the current for externally applied voltages were conducted first in the dark and then in the presence of high-intensity ultraviolet radiation.

The current, recorded with an oscilloscope, varied linearly with the applied voltage both in the absence and in the presence of light. Similar results were obtained using a Tektronix 575 Transistor-Curve Tracer. It was assumed that, for the small current densities used, the potential drop across the silver reference electrode was negligible compared to that at the electrolyte–AgBr interface. The results tend to show that current flow is as readily accomplished from the crystal to the silver contact as it is across the silver bromide–electrolyte interface; *i.e.*, there are no rectifying junctions in the system. However, if rectification does occur at the junctions, it is small in comparison to the 54,0000-ohm dark resistance of the cell.

V. Photovoltaic Effect and Latent-Image Distribution.—For determining the relationship between latent-image distribution and the photopotential, two crystals of approximately the same average thickness, 41 and 38 μ, respectively, were used. The crystals were prepared so that they differed significantly in their latent-image distributions, as shown by exposing in air, to 365-mμ irradiation, samples taken from the two crystals, and subsequently etching into the interior of the crystal and then developing the samples with a non-solvent developer.[11] The experiments revealed a shallow distribution of image to the depth of about 16 μ in the sheet crystal 41 μ thick, while the latent image was found distributed throughout the depth of the other sample. With the absorption of a number of quanta of the same order of magnitude and at the same wave length, the crystals gave nearly identical values of photo-e.m.f. It appears that the photographic record, as shown by latent image, is not a true indication of the diffusion length of the photoelectrons, assuming that depth diffusion of photoelectrons is of primary importance in the photovoltaic effect. Apparently in one case deep trapping occurred only to the extent of 16 μ, and further diffusion at reduced electron concentration resulted only in the formation of latent sub-image specks.

VI. The Effect of Incorporated Impurities on the Photopotential.—A modification of the structure of silver bromide with respect to the nature and concentration of crystal defects, including ionic defects, by the incorporation of impurity ions was found to have an appreciable effect on the observed photopotentials. The fusion of copper ion into silver halides probably results in substitutional occupation of silver-ion lattice sites by Cu^+ ions.[11,21] Exposure of a crystal containing 0.1 mole % Cu^+ ion to 365-mμ radiation of incident intensity 5.3×10^{14} quanta cm.$^{-2}$ sec.$^{-1}$ in the absence and then in the presence of halogen-acceptor showed negligible differences in photopotential. Decreasing the Cu^+ ion concentration to 0.001 mole % resulted in increases of potential in the case of penetrating light. The incorporated Cu^+ ion appeared to function as a hole trap.

The depth of the hole trap was found to be relatively shallow, since after crystals containing 0.1 and 0.0001 mole % Cu^+ were exposed for 50 msec. to penetrating light and allowed to stand overnight, they reverted to the original state with respect to the initial photoresponse at 365 mμ. In contrast, pure silver bromide was more or less permanently desensitized. The data are consistent with observations on the thermal fading of the photolytic image in similar crystals as reported by West and Saunders.[11]

Thallous ions incorporated at a concentration of 0.03 mole % gave results similar to those found for incorporated Cu^+ ions. The impurity, believed to be substitutionally incorporated,[22] also served as a fairly deep, but only temporary, trap for positive holes, as had been suggested by Mueller.[23]

Divalent cadmium or lead ions substitutionally incorporated in the silver bromide lattice introduce an equivalent concentration of silver-ion vacancies.[24] Such defects which are centers of negative charge were found to affect greatly the photovoltage of silver bromide. Incorporated Pb^{++} ions at a concentration of 0.1 mole % decreased the photovoltaic effect to less than 50% of that obtained with the pure material. The cationic vacancies appear to serve as recombination centers for positive holes and electrons. Substantiation of hole-trapping and eventual recombination was provided by the observation of only negligible increases in photopotential in the presence of halogen-acceptors. In the range of concentration from 0.1–0.0001 mole % Cd^{++} ion,

(21) (a) N. R. Nail, F. Moser, P. E. Goddard, and F. Urbach, *Phys. Rev.*, [2] **98**, 1557 (1955); (b) F. Moser, N. R. Nail, and F. Urbach, *J. Phys. and Chem. Solids*, **3**, 153 (1957).

(22) Y. Wakabayashi, *Phot. Sci. and Eng.*, **4**, 1 (1960).

(23) T. W. H. Mueller, "Science and Applications of Photography: Proceedings of the R.P.S. Centenary Conference," London, September, 1953, p. 13.

(24) (a) E. Koch and C. Wagner, *Z. physik. Chem.*, **B38**, 295 (1937); (b) J. Teltow, *Ann. Physik*, [6] **5**, 62 (1949).

the magnitude of the photovoltaic effect increased as the divalent-ion concentration decreased.

The incorporation of sulfide in the silver bromide lattice results in increased electrolytic conduction,[25] in agreement with the principle that the substitutional sulfide ions are balanced by interstitial silver ions.

Studies at 365 mμ on crystals containing from 0.0001–0.01 mole % sulfide tended to substantiate strong electron-trapping by the impurity, the photopotential decreasing as the sulfide concentration was increased. This suggested a very short diffusion length for the photoelectrons; in some instances it was necessary to give a series of exposures before a photopotential was produced, indicating that deep electron traps had to be saturated before depth diffusion of electrons or charge separation of holes and electrons occurred. Furthermore, unlike pure silver bromide crystals, which exhibited decreases in the photopotential with successive exposures, these sulfide-incorporated crystals showed increased potentials with increased exposure. The results show that the electron-trapping depth of $S^=$ ions appears much deeper than that of latent-image particles. Addition of a halogen-acceptor, 10^{-1} *M* acetone semicarbazone, to the electrolyte caused slight increases in the photoeffect. Luckey[26] has studied the evolution of halogen on specimens of silver bromide containing 0.004% silver sulfide and reported that since the quantum yield of bromine evolution was not affected by the internal sulfide, it appears unlikely that the primary influence of the sulfide is to trap holes. Instead it would seem to be quite definite that the silver sulfide must be effective in providing electron traps. The relevant data describing the effect of ionic impurities on the photopotential are given in Table II.

TABLE II

EFFECT OF IONIC IMPURITIES ON THE PHOTOVOLTAIC EFFECT OF SHEET CRYSTALS

Exposure time, 10 msec.; electrolyte, 10^{-3} *M* KBr; wave length, 365 mμ; intensity, 5.3 × 10^{14} quanta/sec./cm.²

Description	Av. thickness, μ	Initial max. negative potential, v.
AgBr	36	0.110
AgBr + 0.1 mole % Pb^{++}	31	.042
AgBr + 0.01 mole % $S^=$	33	.0014
AgBr + 0.01 mole % $S^=$	38	.0000
AgBr	60	.113
AgBr + 0.03 mole % Tl^+	56	.100
AgBr + 0.0001 mole % Cu^+	54	.093
AgBr + 0.1 mole % Cu^+	59	.122
AgBr	73	.130
AgBr + 0.1 mole % Pb^{++}	74	.046
AgBr + 0.001 mole % Cd^{++}	92	.079
AgBr (annealed)	90	.100
AgBr + 0.0001 mole % Cu^+	91	.090
AgBr + 0.1 mole % Cu^+	90	.088

In all cases, sulfur-sensitizing the exposed surface resulted in a desensitization of the photovoltaic effect of a variety of crystals to the extent of 10–70% for penetrating and non-penetrating exposures. These observations may be especially relevant to elucidating the role of adsorbed silver sulfide in the photographic process. Mitchell[27] believes that adsorbed molecules of silver sulfide during the early stages of the formation of surface latent image provide traps for positive holes, and thereby supply silver ions important for latent-image formation.

In a study of interlayer effects in sheet crystals, West and Saunders[28] have reported that a layer of silver sulfide traps both electrons and positive holes. The implication of the result that halogen-acceptor could increase the magnitude of the photopotential of sulfur-sensitized crystals is that adsorbed silver sulfide molecules appear limited in their ability to trap positive holes at the surface, and if other halogen-acceptors are present during exposure, they will preferentially accept photobromine. These data are presented in Table III. Sutherns and Loening[29] have reported a similar conclusion on the role of adsorbed silver sulfide molecules in the photographic process.

Discussion

To prevent recombination of the holes and electrons produced on exposure of silver bromide, deep traps must be provided. Mitchell[30] believes that traps for positive holes are provided initially by bromide ions which form Br_2^- ions on trapping positive holes on surface kink sites and on jogs along edge dislocation lines. Herz and Helling,[31] in studies involving the adsorption isotherm of bromide ions on silver bromide, have found that the saturation level for adsorbed bromide ion is reached at a concentration of 10^{-4} *M* bromide. Thus, further increases in bromide-ion concentration should have little or no effect on the magnitude of the potentials which are highly dependent on hole removal. Such a postulation is consistent with the observations of this study.

The electrons produced on absorption either recombine, are permanently trapped, or diffuse through the depth of the crystal. A similar interpretation of the source of negative potentials was given by Sheppard and co-workers.[4]

The field set up by the diffusion of the more mobile electrons to the unilluminated surface and by electrolyte acceptance of holes is opposed mainly by interstitial silver-ion flow, so that at the steady state there is no net current flow through the sample. The photodiffusion voltage is measured between the illuminated surface and the dark barrier, provided the thickness of the crystal lies within the range of the diffusion length of the photoelectrons. Recently Williams,[32] in a similar study of the photovoltaic effect of binary compounds by an electrometer, has classified silver bromide as a p-

(25) I. Ebert and J. Teltow, *Ann. Physik.*, [6] **15**, 268 (1955).

(26) In F. Seitz, "Photographic Sensitivity," Vol. I, Hakone Symposium, S. Fujisawa, editor, Maruzen Co. Ltd., Tokyo, 1956, p. 5.

(27) J. W. Mitchell, "Wissenschaftliche Photographie," Köln, 1956, O. Helwich, editor, Helwich-Verlag, Darmstadt, 1958, p. 29.

(28) W. West and V. I. Saunders, *Phot. Sci. and Eng.*, **3**, 258 (1959).

(29) E. A. Sutherns and E. E. Loening, *J. Phot. Sci.*, [2] **4**, 154 (1956).

(30) J. W. Mitchell, "Photographic Sensitivity," Vol. II, Maruzen Co. Ltd., Tokyo, 1958, p. 47.

(31) A. Herz and J. O. Helling, *J. Colloid Sci.*, **16**, 199 (1961).

(32) R. Williams, *J. Chem. Phys.*, **32**, 1505 (1960).

Table III

Dependence of the Photovoltaic Effect of Pure and Doped Silver Bromide Crystals on Sulfur Sensitization and the Role of Halogen-Acceptors

Exposure time, 10 msec.

Description	λ, mμ	Electrolyte	Potential (v.) prior to S^- sens.	Potential (v.) after S^- sens.
AgBr + 0.1 mole % Pb^{++} (31 μ)	365	10^{-3} *M* KBr + 10^{-1} *M*	−0.040	−0.027
		Acetone semicarbazone (A.S.C.)	...	− .030
AgBr (42 μ)	365	10^{-3} *M* KBr	− .050	− .040
		10^{-3} *M* KBr + 10^{-1} *M* A.S.C.	...	− .047
AgBr (44 μ)	365	10^{-3} *M* KBr	− .066	− .038
AgBr + 0.1 mole % Cu^+ (59 μ)	365	10^{-3} *M* KBr	− .101	− .095
		10^{-3} *M* KBr + 10^{-1} *M* phenol	...	− .099
AgBr (84 μ)	436	10^{-3} *M* KBr	− .042	− .014
AgBr (435 μ)	436	10^{-3} *M* KBr	− .020	− .015

type semiconductor, and has predicted positive potentials for the halide. Such a prediction was based on the thermodynamically favored process of preferential solution of the bromide ion, leaving excess positive charge. No evidence for the dissolution of bromide lattice ion as an important step in determining the polarity and magnitude of the photo-e.m.f. has been found in this study. Matejec,[33] for a similar system, reported initial positive potentials that become negative with continued exposure. Differences in sensitivity of measuring devices might account for the conflicting data on the sign of the photopotential. In this study a comparison of the electrometer and the high-gain, differential preamplifier used with the oscilloscope showed that in many cases the response time of the electrometer was not adequate to register the initial negative potentials for exposures as long as 5 sec.

The non-ionic reaction between acetone semicarbazone and the photobromine which increases the magnitude of the negative potentials does not support the proposition that the bromide ion formed from the hydrolysis of bromine is the source of the negative potentials, as originally suggested by Kolthoff and Sanders.[5]

The inability of thallous ions to accept photobromine as efficiently as acetone semicarbazone or phenol was unexpected. There is some indication that Tl^+ ion changes the surface charge of silver bromide.[34] The ease of formation of thallic bromide by the reaction of Tl^+ ions with the photoproduced bromine should readily increase the magnitude of the photopotentials, but undoubtedly much of the thallic halide formed rapidly reverted to the initial state. Oxidation potential data indicate the thallous state to be more stable in aqueous systems than the thallic state.

The change of sign of the photovoltaic effect and the sensitivity to changes in carrier concentration as brought about by adsorption of molecular bromine is believed due primarily to the introduction of holes into the crystal. Luckey and West[35] have shown that the dark conductivity of silver bromide increases in the presence of halogen vapor as a result of the introduction of positive holes which can diffuse at least 500 μ at room temperature. It is reasonable to believe that the reaction of holes with the silver of the electrical contact plays an important role in the mechanism of the positive potentials observed.

Equivalent energy exposures of the crystals at different wave lengths confirm the role of the actinic layer in determining the photo-e.m.f.; the thinner the absorption layer the greater will be the ability of holes to escape at the silver bromide–electrolyte interface and therefore give rise to relatively large photopotentials. At the longer wave lengths, which penetrate deeply within the crystal, the removal of holes is rendered difficult because of the long diffusion distance to the surface, and as a result the photo-e.m.f. is decreased. The interpretation is supported by the extensive study of the vacuum photolysis of silver halides by Luckey,[36,37] where increased quantum yields of bromine production with decreased wave lengths were found.

Acknowledgments.—This work was greatly assisted by the advice of W. Vanselow. Thanks are extended to W. West and V. I. Saunders for many of the crystals used in the study and for information concerning their properties. The author also is grateful for the aid and advice given by members of the Physics Division of these Laboratories.

(33) R. Matejec, *Z. Elektrochem.*, **62**, 400 (1958).

(34) T. H. James and W. Vanselow, *J. Phys. Chem.*, **62**, 1189 (1958).

(35) G. W. Luckey and W. West, *J. Chem. Phys.*, **24**, 879 (1956).

(36) G. W. Luckey, *J. Phys. Chem.*, **57**, 791 (1953).

(37) G. W. Luckey, *J. Chem. Phys.*, **23**, 882 (1955).

RADIATION INDUCED EXCHANGE OF PHOSPHORUS IN THE PCl_3–$POCl_3$ SYSTEM[1,2]

By LeRoy F. Grantham and Herbert C. Moser

Department of Chemistry, Kansas State University, Manhattan, Kansas

Received October 14, 1961

Phosphorus-32 was used as a tracer to measure the rate of radiation induced exchange of phosphorus in PCl_3–$POCl_3$ binary solutions. Ultraviolet and γ-radiation induced sufficient exchange to permit a study of the kinetics of the system, but exchange was not induced by visible light. The amount of phosphorus exchanged was found to obey the equation $M = k'bD + k''abD$, where a and b are concentrations of PCl_3 and $POCl_3$, respectively, and D is the gamma or ultraviolet dosage. Values for $k\gamma'$ and $k\gamma''$ were found to be $(3.19 \pm 0.16) \times 10^{-10}$ rad^{-1} and $(4.24 \pm 0.31) \times 10^{-11}$ g. mmole^{-1} rad^{-1}. For γ-rays the ratio k'/k'' was 15 times larger than it was for ultraviolet radiation.

Introduction

Exchange of phosphorus between its compounds does not occur generally, *e.g.*, the P_4–PCl_3 system[3,4] or the PCl_3–$PSCl_3$ system,[3] although a slow exchange was found in the P–PCl_5 system dissolved in CS_2.[5] The exchange of chlorine in phosphorus chlorides is rapid.[6–8] This accounts for the phosphorus exchange found in the PCl_3–PCl_5 system.[6] A γ-ray induced exchange in the P_4-(white)–PCl_3 system was found,[4] and a similarly induced exchange of phosphorus between $POCl_3$ and PCl_3 was postulated to occur during reactor irradiation of $POCl_3$.[9]

Study of the γ-ray induced phosphorus exchange in the PCl_3–$POCl_3$ system was undertaken to help interpret the results of neutron irradiations of these compounds.

Experimental

Reagents.—Reagent grade PCl_3 and $POCl_3$ were purified by double distillation through an 8-in. glass helix packed column. Only the center fraction from each distillation was kept. These purified reagents were stored in glass-stoppered flasks and were redistilled if they were not used within a month after purification. The high boiling carrier in the separation procedure was *n*-decane The first 100 ml. of decane was purified[9] but in subsequent experiments the commercial grade reagent was used. Purified grade xylene was used as a diluent in counting sample preparation.

Phosphorus-32 labeled PCl_3 and $POCl_3$ were prepared by irradiating fused silica ampoules containing these materials in the Oak Ridge Graphite Reactor. The labeled stock solutions were purified by distillation through a column having twelve theoretical plates.[4,9] The results were independent of the compound initially labeled.

Procedure.—Large volumes (100 ml.) of mixtures containing the correct concentrations of PCl_3 and $POCl_3$ were prepared by pipetting (in air) the carriers and labeled material into glass-stoppered flasks. After the solutions were thoroughly mixed, 5-ml. aliquots were vacuum distilled into previously outgassed, fused silica ampoules. The ampoules were sealed under vacuum (<50 μ) at liquid nitrogen temperatures. Early experiments indicated that trace amounts of water enhanced the rate of exchange, therefore during final encapsulation precaution was taken to ensure that the samples were free of water and hydrolysis products.

The γ-irradiations were performed in the high level γ-facility at Argonne National Laboratory which used spent reactor fuel elements as the gamma source. Intensities in the range of 0.9×10^4 to 3.7×10^4 rads min.$^{-1}$ (in water) were used.[10] The aqueous ferrous sulfate dosimetry measurements of dosage made by Argonne National Laboratory were corrected for density differences in the absorbing media to obtain the γ-ray dosages received by the samples.

A Sylvania G15T8 Germicidal-A 15-watt mercury vapor lamp was used for the ultraviolet light source. The fused silica ampoules were held adjacent to the external surface of the lamp. The ambient temperature of the samples during irradiation was 50°. Approximately 20% of the light emitted by this lamp had a wave length of 2537 Å. (4.9 e.v.).

The mixtures were separated by distillation through a glass helix packed column (twelve theoretical plates). At least three PCl_3 and three $POCl_3$ distillate fractions were collected and radioassayed. If the results did not agree within 2% the fractions were recounted along with other fractions of the same component. A graph illustrating the separating efficiency of this column was given in a previous publication.[4]

Radioassays were made with a Tracerlab TGC5 Geiger dipping tube in conjunction with a Berkeley Decimal Scaler, Model 2000. Appropriate aliquots of radioactive materials were used to give approximately 5000 counts per minute after dilution to 15 ml. with xylene.

Results

Rate of exchange (R) was determined from the quantitative exchange law

$$R = -ab \ln (1 - F)/(a + b)t \qquad (1)$$

where a and b are the concentrations of PCl_3 plus $P^{32}Cl_3$ and $POCl_3$ plus $P^{32}OCl_3$, respectively, F is the fraction of exchange, and t is time. Fraction of exchange was calculated from

$$F = (\bar{F} - F_0)/(1 - F_0) \qquad (2)$$

where $\bar{F}$ is the apparent fraction exchange and F_0 is the fraction exchange due to incomplete separation. Values of F_0 varied from 0.006 to 0.024 depending on the labeled stock solution used. Concentrations (a and b) are expressed in millimoles per gram of solution in keeping with the radiation unit, rad (100 ergs absorbed per gram of solution).

Visible Light.—Forty-four samples of various PCl_3–$POCl_3$ concentrations were analyzed after they had been subjected to visible light (maximum energy, 3.1 e.v.). Negligible exchange (<2%) was found, even after exposing with a high intensity source for 23 days at a temperature of 250°. Exchange in samples subjected to similar condi-

(1) (a) Work supported by the Atomic Energy Commission under Contract AT 11-1-584; (b) Presented in part at the 138th National Meeting, American Chemical Society, New York, 1960.

(2) From the Ph.D. Thesis of L. F. Grantham.

(3) P. K. Conn and R. E. Hein, *J. Am. Chem. Soc.*, **79**, 60 (1957).

(4) D. W. Setser, H. C. Moser, and R. E. Hein, *ibid.*, **81**, 4162 (1959).

(5) R. Muxart, O. Chalvet, and P. Daudel, *J. chim. phys.*, **46**, 373 (1949).

(6) W. E. Becker and R. E. Johnson, *J. Am. Chem. Soc.*, **79**, 5157 (1957).

(7) J. Lewis and D. Sowerby, *J. Chem. Soc.*, 336 (1957).

(8) B. Masters, D. Asher, T. Norris, and N. Potter, *J. Am. Chem. Soc.*, **78**, 4252 (1956).

(9) T. J. Clark and H. C. Moser, *J. Inorg. & Nuclear Chem.*, **17**, 210 (1961).

(10) H. G. Swope, "Dosimetry in the Argonne High-Level Gamma Irradiation Facility," ANL-5819 (1958).

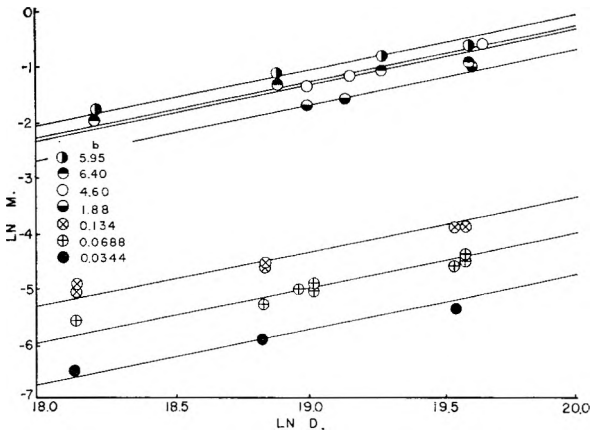

Fig. 1.—Dependence of exchange on γ-ray dosage: 25°, M in millimoles per gram, D in rad.

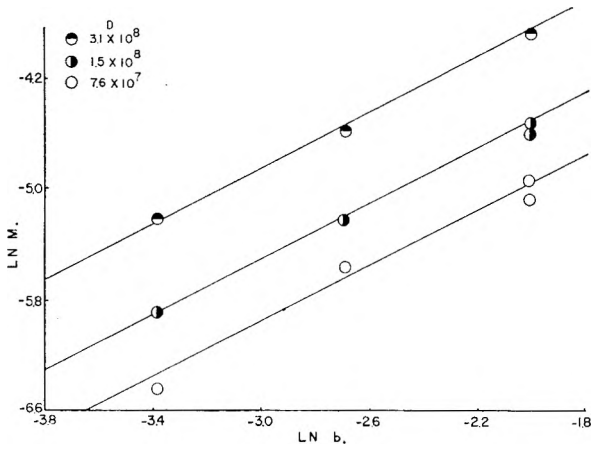

Fig. 2.—Dependence of exchange on $POCl_3$ concentration: 25°, M and b in millimoles per gram.

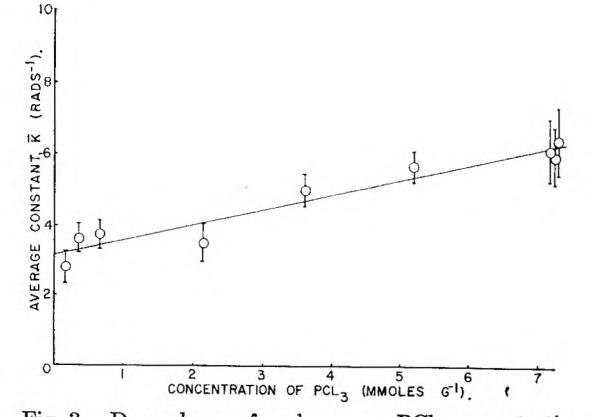

Fig. 3.—Dependence of exchange on PCl_3 concentration: 25°, a in millimoles per gram, K calculated from the equation $M = KbD$.

tions but containing trace amounts of water was 70% complete in less than 12 days.

γ-Irradiations.—Samples of PCl_3–$POCl_3$ mixtures received γ-ray dosages of 7.5×10^7 to 3.4×10^8 rads. After irradiation the solutions were clear but the quartz ampoules were violet colored; the pressure inside the capsules was considerably less than 1 atm. Results of these irradiations are given in Fig. 1 and 2. Exchange induced by γ-radiation is expressed as the total millimoles exchanged (M) to conform with the total gamma dosage (D) received by the sample; thus, a time expression that may be confusing is eliminated. The millimoles of exchange induced by γ-rays was calculated from the expression

$$M = -ab \ln (1 - F)/(a + b) \qquad (3)$$

If it is assumed that the amount of exchange can be represented by the equation

$$M = Ka^n b^\alpha D^\beta \qquad (4)$$

then the kinetic order of the variables can be established. A graph of ln M *vs.* ln D at constant concentration is given in Fig. 1. Within experimental error the slopes (β) of these lines are unity; thus, the exchange that occurred was first order in γ-ray dosage. Similarly the exchange was found to be first order in $POCl_3$ ($\alpha = 1$, Fig. 2). The slope of a similar graph of ln M *vs.* ln a is 0.14. Values of the proportionality constant, calculated from eq. 4 using experimentally determined values of the exponents, have a 15-fold variation, but K calculated from the same equation assuming n equals zero has only a twofold variation. Thus it would appear that eq. 4 is in error and is not a true representation of the exchange.

The variation of the average values of K with a is demonstrated in Fig. 3. This plot indicates that K has two components, one of which is a linear function of a. Therefore, the exchange (M) is best represented by the equation

$$M = k'bD + k''abD \qquad (5)$$

The values of k' and k'' were found to be $(3.19 \pm 0.16) \times 10^{-10}$ rad^{-1} and $(4.24 \pm 0.31) \times 10^{-11}$ g. mmole^{-1} rad.$^{-1}$, respectively, by the method of least squares. Equation 5 indicates that the exchange proceeds by two paths simultaneously. The calculated and experimental values of the exchange agreed within 10%. The amount of exchange was found to be first order in dosage over the γ-intensity range used.

The G-value for exchange (atoms of phosphorus exchanged per 100 e.v. of energy absorbed) was not constant but varied from 0.017 to 2.1 throughout the concentration range. This relatively low yield would suggest that the exchange mechanism is not a chain reaction. The radiation yield for each exchange path was calculated from eq. 6 and 7.

$$G' = \frac{M}{D} \times \frac{k'b}{k'b + k''ab} (9.63 \times 10^8) \qquad (6)$$

$$G'' = \frac{M}{D} \times \frac{k''ab}{k'b + k''ab} (9.63 \times 10^8) \qquad (7)$$

Plots of these G-values against mole fraction $POCl_3$ are given in Fig. 4 and 5. The maximum yield (Fig. 4) for the second-order mechanism (G'') occurs at equal concentrations of $POCl_3$ and PCl_3; this is typical of second-order reactions. The plot of G' (Fig. 5) is linear, as expected; however, a maximum occurs at approximately 0.96 mole fraction $POCl_3$. This behavior would be expected of a pseudo first-order reaction, *i.e.*, an exchange in which a fast reaction becomes rate controlling due to its concentration dependence. These results are consistent with the possible exchange mechanisms postulated.

Ultraviolet Irradiations.—Phosphorus exchange induced by ultraviolet light proceeded at a meas-

urable rate. The results of five experiments are given in Table I. The concentrations of $PCl_3(a)$ and $POCl_3(b)$ are expressed in units previously defined; irradiation time is given in days.

TABLE I
ULTRAVIOLET INDUCED EXCHANGE OF PHOSPHORUS IN PCl_3–$POCl_3$ SYSTEMS

a (mmole g.$^{-1}$)	b (mmole g.$^{-1}$)	Time exposed (days)	Fraction exchange (F)	Rate of exchange[a] Found	Calcd.[b]
3.54	3.32	9.8	0.030	0.0028	0.0027
3.54	3.32	37.6	.071	.0028	.0027
1.40	5.27	37.6	.076	.0019	.0020
0.346	6.21	37.6	.131	.0011	.0011
0.346	6.21	37.6	.126	.0011	.0011

[a] Expressed in mmole g.$^{-1}$ day^{-1}. [b] Calculated from eq. 8.

The exchange observed in samples subjected to ultraviolet light obeyed the equation

$$R = k'_{uv}b + k''_{uv}ab \qquad (8)$$

where R is the rate of exchange, a and b as defined previously, $k'_{uv} = (1.06 \pm 0.01) \times 10^{-4}$ day^{-1}, and $k_{uv}'' = (2.02 \pm 0.02) \times 10^{-4}$ g. mmole^{-1} day^{-1}. The values of the proportionality constants were calculated using the method of least squares. The experimental and calculated values of the rate of exchange agree within 3%.

Discussion

γ-Irradiations.—Exchange in this system probably proceeds through the transfer of oxygen between $POCl_3$ and PCl_3 instead of phosphorus. Radiation induced dissociation of the P–O bond (5.4 e.v.) followed by recombination of the oxygen atom with another PCl_3 molecule would provide one mechanism of exchange.

$$POCl_3 \rightsquigarrow PCl_3 + O$$
$$O + PCl_3 \longrightarrow POCl_3$$

G' (eq. 6) was observed to have a maximum value at a high $POCl_3$ concentration and a corresponding low PCl_3 concentration. This is reasonable if exchange proceeds by a dissociation mechanism. If a PCl_3 molecule formed by dissociation of $POCl_3$ combines with the oxygen atom before it can react with another PCl_3, exchange would not occur. Recombinations of this type should become prominent at low PCl_3 concentration. An estimate of the size of the oxygen atom cage can be obtained from location of the maximum in Fig. 5. Recombination becomes important when the number of PCl_3 molecules is less than one in twenty-five.

The dipole moments of PCl_3 and $POCl_3$ are 0.78 and 2.40 D.,[11] respectively; therefore, weakly coupled dipoles probably exist in solution. Experimental results indicated that there was a negligible volume change (<0.2%) upon mixing PCl_3 and $POCl_3$, and that a small negative enthalpy change (<20 cal. per mole of solution) accompanied the mixing of equal volumes of the two components. Therefore, a portion of the PCl_3 and $POCl_3$ molecules would be expected to couple through dipole

$$PCl_3 + POCl_3 = \overset{\alpha-}{Cl_3}\ \overset{\alpha+}{P};\overset{\alpha-}{O}\ \overset{\alpha+}{PCl_3}$$

(11) J. R. Van Wazer, "Phosphorus and Its Compounds," Vol. I, Interscience Publishing Co., Inc., New York, N. Y., 1958, pp. 53–55.

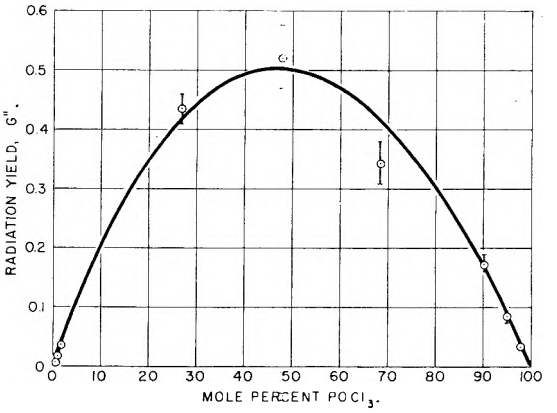

Fig. 4.—Radiation yield, G'', of second-order exchange reaction.

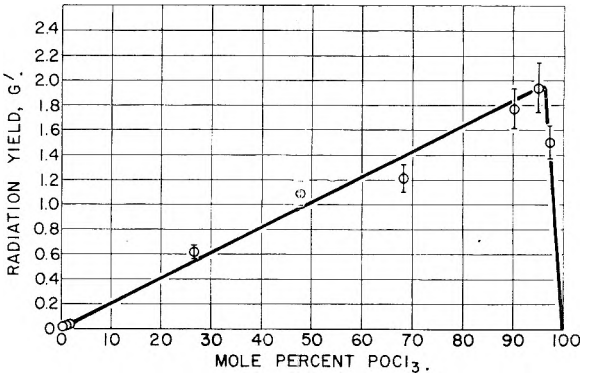

Fig. 5.—Radiation yield, G', of first-order exchange reaction.

interaction. Secondary effects from the γ-radiation may induce an oxygen transfer between the components of these weakly coupled dipoles. Such

$$\overset{\alpha-}{Cl_3}\ \overset{\alpha+}{P};\overset{\alpha-}{O}\ \overset{\alpha+}{PCl_3} \rightsquigarrow POCl_3 + PCl_3$$

an oxygen transfer would be indistinguishable from phosphorus exchange in this system and would be first order in a and b. This mechanism may account for that portion of the exchange (eq. 5) which is PCl_3 dependent ($k''abD$).

Another possible mechanism that could account for the observed PCl_3 dependent exchange would be the transfer of oxygen between excited PCl_3* or $POCl_3$* by collision with the other component

$$POCl_3 \rightsquigarrow POCl_3^*$$
$$POCl_3^* + PCl_3 \longrightarrow PCl_3 + POCl_3$$

in solution. Assuming that a steady state exists, that the sum of the concentrations of PCl_3 and $POCl_3$ is constant (<10% variation over the entire concentration range), and that the excited molecule can be deactivated by collision or by radiation, the proper kinetic expression also can be derived for this mechanism of exchange. A similar expression can be derived for the exchange that may occur upon collision of an excited PCl_3 molecule and a $POCl_3$ molecule in solution.

Ultraviolet Irradiation—The similarity in the forms of eq. 5 and 8 suggest that the mechanism of exchange was the same regardless of whether the exchange was induced by ultraviolet or γ-radiation. The ratio k'/k'' was fifteen times larger for γ-rays than for ultraviolet light. The quantum

yield varied with concentration, but a yield on the order of 10^{-3} atoms exchanged per quanta of ultraviolet light absorbed was found.

Acknowledgments.—The authors wish to express their appreciation to Miss H. Gladys Swope, Argonne National Laboratory, for her valuable assistance in obtaining the γ-irradiations. They are grateful for a fellowship sponsored by the Dowell Division of the Dow Chemical Company for L.F.G.

OXIDE-COATED ELECTRODES. I. ALUMINUM IN ACID SOLUTIONS

BY ROBERT C. PLUMB

Worcester Polytechnic Institute, Worcester, Massachusetts

Received October 20, 1961

An investigation of the electrode potentials of aluminum as a function of the oxide thickness and the nature of the electrolyte is reported. The study was made using a specially designed apparatus for producing variably oxidized surfaces and precluding the effects of oxidation in solution by observing the potentials as transients. Knowing the nature of the effect of the oxide film permits one to obtain the potentials of oxide-free surfaces. Using an appropriate model for the electrode reaction one obtains values for the free energy of formation of aluminum ions and the solubility of undissociated aluminic acid which are in substantial agreement with and probably somewhat better than previously accepted values.

Introduction

Oxidation–reduction potentials and the free energy changes which they represent may be derived from direct measurement of galvanic cells, from equilibrium data, and from thermal data. In order for the measured potential of a galvanic cell to be thermodynamic it is necessary that the electrode reactions be reversible and rapid and that the reduction and oxidation reactions be isolated from each other. The majority of metals do not readily form cells which satisfy the criterion of reversibility, and thermodynamically significant galvanic potential measurements may be made on only a relatively small number of metals. Thus the free energy changes for the reactions of many metals are based largely upon thermal and equilibrium data.

Two physical processes occurring at the metal–solution interface which will prevent thermodynamic potentials from being realized in galvanic cell measurements are the presence of oxide films which prevent free passage of metal ions between metal and solution and the simultaneous occurrence of more than one chemical reaction producing "mixed potentials" which are not readily interpreted in terms of fundamental thermodynamic quantities. It may be expected that the effects of oxide films will be most pronounced with metals forming barrier types of oxides of which aluminum and tantalum are the most noteworthy. Many other metals such as iron, titanium, and nickel form oxides which have barrier properties and with these metals, too, the oxide may affect the galvanic potential measurement. An extreme example of the mixed potential phenomena is the "corrosion potential" resulting from anodic and cathodic reactions taking place simultaneously at a metal–electrolyte interface. This complication will be discussed at greater length in a later section of this paper.

The effects of oxide films upon metal electrodes have been encountered by many investigators. Many of the experimental procedures designed to produce reversible metal electrodes such as etching, cleaning with emery paper, generating high surface areas, and amalgamating the metal, serve to obviate the effects of oxide films.[1] In this paper an essentially new method for approaching the problem of oxide films will be described. This experimental procedure permits one to measure and correct for the effects of surface oxide films upon galvanic cell measurements and enables one to obtain thermodynamic potentials of metals which form barrier type oxides. Most of the work which will be described here has been performed on aluminum. The technique seems to be applicable to many other metals.

Description of Experiments

The objective of the experiments has been to measure the electrode potential of a metal under a known and reproducible condition of oxidation. This has been accomplished by generating initially oxide-free metal surfaces, letting them oxidize for varying periods of time under reproducible conditions, and then measuring the potential of a cell formed at the moment when the metal is brought into contact with an electrolyte and a reference electrode but before the specimen oxidizes further in the solution. The experimental procedures for doing this have evolved through two distinct stages. Early crude experiments gave some extremely promising results which made the construction of more elaborate equipment desirable. A brief review of the early experiments will be given because the results were surprisingly good when compared to the more refined experiments.

An area of about 2 cm.^{2} of initially oxide-free metal surface was generated by scraping with a ceramic (to prevent contamination with a foreign metal) cutting tool, a calomel reference electrode was placed over the initially oxide-free area, and, after a predetermined time, electrolyte was introduced and the flowing front of electrolyte made contact with the reference electrode and the scraped region. The transients in potential were displayed on an oscilloscope and recorded photographically. Two very significant types of observations came from these early experiments. First it was found that the potentials varied directly as the logarithm of the time of oxidation. Second it was found that the potentials obtained by extrapolation to zero time of oxidation varied in a very systematic way with the *p*H of the electrolyte and the concentration of metal ion in the electrolyte and were directly related to the existing thermo-

(1) NOTE ADDED IN PROOF.—While this paper was in press some interesting experiments on generating oxide-free aluminum surfaces beneath the surfaces of an electrolyte have been described by Hagyard[5] and co-workers [T. Hagyard and J. R. Williams, *Trans. Faraday Soc.*, **57**, 2288 (1961); T. Hagyard and M. J. Prior, *ibid.*, **57**, 2295 (1961)].

dynamic data. With this apparatus the shortest oxidation times which could be observed were of the order of 2 or 3 sec. The experimental uncertainty in the potentials observed was of the order of 10 mv. and the uncertainty in time of oxidation was of the order of 0.5 sec. The uncertainty in the potentials obtained by extrapolation to zero time was about 20 mv. Aside from the inherent uncertainties in oxidation time and potential there were several other features of the early experiments which were objectionable and in which improvement was sought in the design of the more refined apparatus. One of those was the difficulty of generating a sizeable oxide-free region by scraping.

The transient potential apparatus which was developed is shown schematically in Fig. 1. Metal electrodes are prepared by evaporation *in vacuo*, the evaporation is interrupted and the metal electrode is dropped into a cell and the transients in potential as an electrolyte flows between the metal and the reference electrode are observed.

The metal is evaporated (from a tungsten filament held by water cooled electrodes) through an opening into a second compartment of the vacuum chamber containing a glass microscope slide substrate which previously has been cleaned by ion bombardment. The metal films produced are about 4000 Å. thick and non-porous.[2] The evaporation rate is high enough to preclude contamination of the film with oxide formed from residual gas in the system. After a suitable amount of charge has evaporated, the evaporation is interrupted by turning the main switch on the sequence timer. This starts a series of operations each having a preset time delay. The flap valve separating the two chambers closes first and at the same time the filament power is cut off. This is necessary to prevent the tungsten from burning when the vacuum is broken in the sample compartment. Then the fast operating slide valve to the atmosphere is opened and the sample is released so that it can drop into the cell. The oscilloscope trigger signal is set to start a sweep at the same time that the vacuum is broken so that it gives a direct measure of the time of oxidation. The electrode drops into the cell and is stopped by a platinum wire spring which also serves to make electrical contact with it. The tip of the calomel reference electrode is about 0.5 mm. away from the metal surface. After a variable time the electrolyte in the cell is displaced upwards making electrical contact between the electrode and the reference electrode. The transients in potential are displayed on the oscilloscope and recorded photographically. The time delay before each of the operations in the sequence may be programmed to within 10 msec. and the time required for each of the operations seems to be reproducible to within 10 msec. The times of atmospheric oxidation before contact is made by the electrolyte are known within at least 20 msec.

The vacuum system contains a variety of seals. The two poorest seals are rubber O rings on the flap valve and on the slide valve. They limit the ultimate vacuum for the pumping system used to 3×10^{-7} mm. Evaporations are performed at pressures of 6×10^{-6} mm. routinely with a pump-down time of 2 to 3 hr.

The transients are displayed on the oscilloscope screen at a sensitivity of 50 mv./cm. using a variable bucking potential to balance out most of the d.c. signal. The oscilloscope is calibrated against a laboratory potentiometer. Sweep rates of 0.5 sec./cm. have been most commonly used. The observed potentials are reproducible within 5 mv.

The Transients in Potential.—Two distinctly different types of oscilloscope traces generally are obtained with the above apparatus. A third type of trace may be obtained by adjustment of the initial state of electrification of the electrolyte but will not be included in this discussion. The type of trace observed depends upon whether or not the electrolyte has solvent action on the oxide film. Figure 2 shows the type of trace observed in weakly acidic and neutral solutions. The beginning of each of the traces represents the time at which contact is made between the metal sample and the reference electrode by means of the electrolyte. The oxidation time prior to contact with the electrolyte is shown on each trace. The potential at the moment of contact is not reproducible and depends upon the accidental state of electrification of the parts of the cell.

(2) R. C. Plumb and J. W. Swaine, accepted by *J. Appl. Phys.*

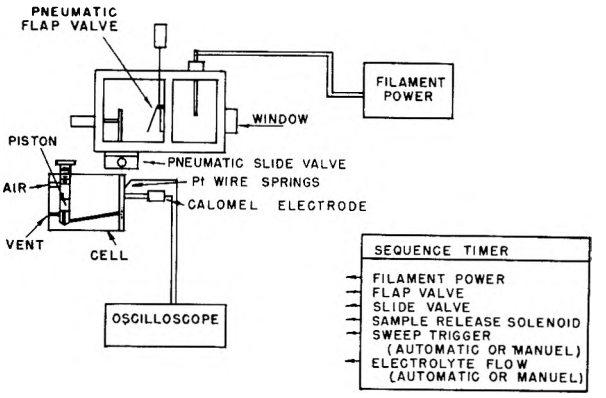

Fig. 1.—Apparatus used for study of effects of oxide films upon electrode potentials. In a short time period an evaporation of metal may be interrupted, the vacuum broken, and the metals' electrode potential measured by means of a group of pneumatically operated valves and devices the operation of which is controlled by an electronic sequence timer.

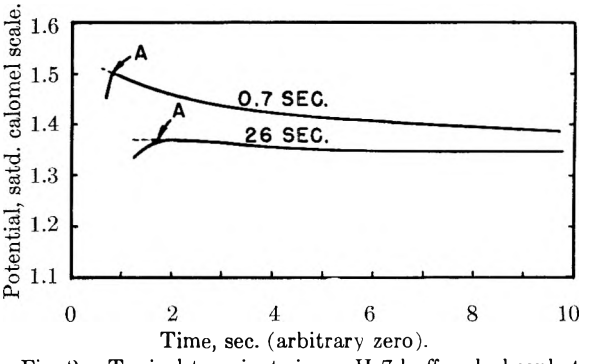

Fig. 2.—Typical transients in a *p*H 7 buffered phosphate electrolyte showing effects of the two different periods of air oxidation before contact with the electrolyte.

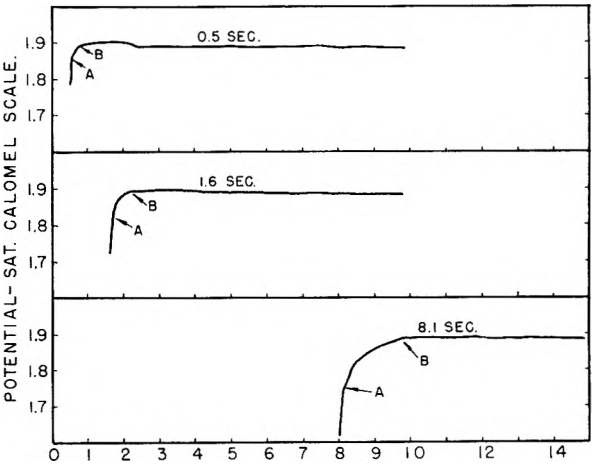

Fig. 3.—Typical transients in a *p*H 12 electrolyte showing effects of different periods of air oxidation before contact with the electrolyte.

The transient in potential up to the point labelled A is the phase charging transient associated with establishing the electric double layer. The time required for this transient depends upon the oxide film thickness and has been observed to vary from a few milliseconds through ten or more seconds. This phase charging transient is being studied further and will be discussed elsewhere. The rather slow decrease in potential after the maximum is associated with oxidation in the solution. The rate of this decrease

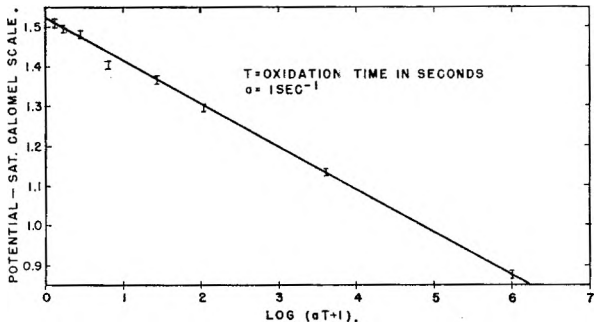

Fig. 4.—The potential as a function of time of oxidation in air for a *p*H 7.0 phosphate buffered electrolyte. Potentials obtained by extrapolation to eliminate the phase charging transient.

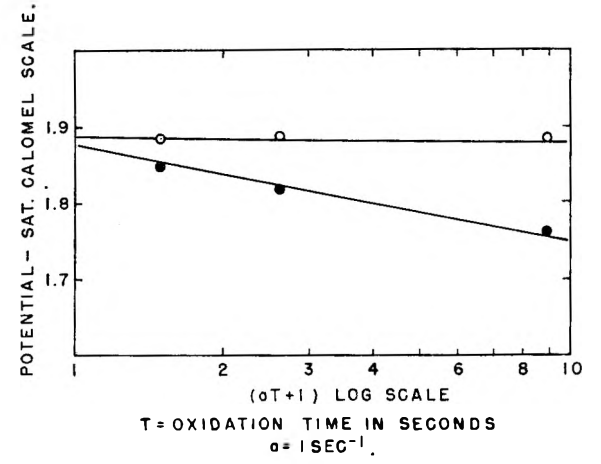

Fig. 5.—Potential as function of time of oxidation for aluminum measured with a *p*H 12 electrolyte showing the potential after the oxide dissolution transient, O, and the potential after the phase charging transient, ●.

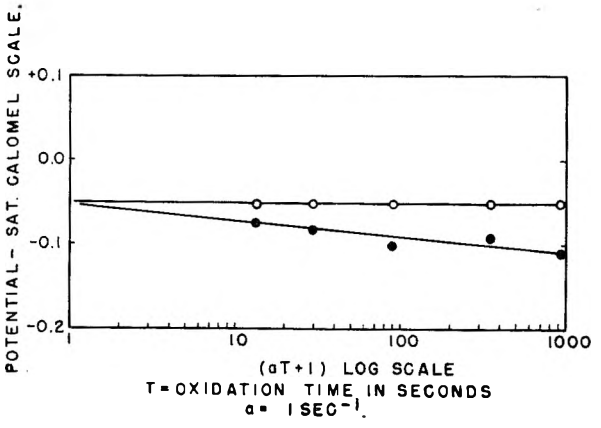

Fig. 6.—Potential as a function of time of oxidation for copper measured with a solution of copper sulfate showing the potential after the oxide becomes hydrated, O, and the potential at the time of contact, ●.

of potential is dependent upon the amount of air oxidation which preceded contact with the electrolyte. The potential characteristic of the metal with its air-formed oxide film may be obtained by extrapolation through the phase charging transient to the time of electrolyte contact as shown by the dashed lines. The potentials thus obtained are reproducible for the metal and electrolyte for a given period of air oxidation. It is these potentials with which we will be primarily concerned in the discussion to follow.

The type of trace observed with an alkaline electrolyte is shown in Fig. 3. The point A is the end of the phase charging transient. The transient from A to B is associated with oxide dissolution. The horizontal and vertical duration of this second transient depends upon the length of air oxidation prior to introducing the electrolyte. The potential at point B after the oxide dissolution transient is independent of the amount of air oxidation.

The potential transients associated with oxide growth in the electrolyte and with oxide dissolution by the electrolyte were observed in similar form with both the original crude apparatus and the present refined equipment. The phase charging transients were not observed with clarity in the original scraping experiments but were revealed in the recent experiments using evaporated films.

Variation of Potential with Oxidation Time.—The potential obtained by extrapolating through the phase charging transient to the moment of electrical contact varies in a systematic and reproducible way with the time of oxidation. It may be expressed by the equation

$$V = V_0 - K \log (at + 1)$$

A linear relationship is obtained for $a = 1.0 \pm 0.2$ sec.$^{-1}$. In neutral solutions K has the value 0.11 volt/decade. The value of K depends somewhat upon the atmosphere in which the air oxidation is carried out. If the sample is flooded with tank hydrogen the value of K is reduced to about $^1/_3$ of the value observed with a normal atmosphere. Using the ambient atmosphere and scraped specimens in the original apparatus K was found to be 0.10 volt/decade which is in excellent agreement with the value 0.11 observed on the evaporated films in an entirely different apparatus. In acid solutions at a *p*H 3 or less, K was found to be 0.18 volt/decade. The decrease in potential with time and the value of the potential for a given oxidation time does not depend upon the nature of the electrolyte except for the dependence upon *p*H. Essentially the same dependence of potential on time was observed with electrolytes at a *p*H of 7 in which the principal anions were PO_4^{---}, Cl^-, or SO_4^{--}.

We are not prepared as yet to discuss the dependence of potential upon oxide film thickness in detail. We present these empirical observations as well established facts. Measurements of oxide growth kinetics and Volta potentials of growing oxide films are underway in these Laboratories and we will discuss this question quantitatively in the near future.

Figure 4 shows the observed potential *vs.* time for times ranging from 0.3 through more than 10^6 sec.

The Potential at Zero Oxide Thickness.—From $V = V_0 - K \log (at + 1)$ one obtains V_0 as the potential at zero time of oxidation or the potential of an oxide-free surface. (The value of V_0 obtained by extrapolation to $t = 0$ is not dependent upon the value of "a" chosen.) There are two pieces of experimental evidence which indiate that it is correct to interpret the value V_0 as the potential of an oxide-free surface. In Fig. 5 the potential after the phase charging transient is plotted together with the potential after the oxide dissolution transient for a series of measurements made in an alkaline electrolyte which dissolves the oxide film. The potentials after the oxide dissolution transient are all the same and independent of the length of time in which the specimen oxidized. The potentials

after the phase charging transients vary in the usual way with the time of oxidation. The potential obtained by extrapolating these potentials to zero time of oxidation is the same as that obtained after the oxide dissolution transient. Similar observations were made on copper as shown in Fig. 6. The oxide film formed on copper shows the same ability to polarize the copper electrode as is observed on aluminum. However, the oxide film on copper is readily hydrated and its ability to polarize the electrode is destroyed rapidly by contact with the solution. The potentials at the moment of contact may be extrapolated to zero time of oxidation and the potential obtained is the same as that observed after the oxide film becomes hydrated.

Further evidence that it is correct to interpret V_0 as the potential of an oxide-free surface will be seen in the next section when it will be shown that the potentials thus obtained are reasonably related to thermodynamic potentials.

The Potentials of the Aluminum Electrode.—The potentials obtained by extrapolation to zero oxide film thickness for aluminum in acidic and neutral solution are shown in Fig. 7. The points are experimental and the curves are calculated. The potentials are related quite precisely to accepted thermodynamic potentials if one assumes the following model for the reaction at the interface. The model is, to the author's knowledge, a new one for describing reactions of this type of electrode but is physically reasonable. The proof of its correctness lies in its successful prediction of the observed potentials from thermal measurements.

The small size of the aluminum ion together with its large charge make it an unreasonable species to be present, even in hydrated form, in an aqueous solution. For this reason we will postulate that an aluminum ion popping into the solution from the metal surface and suddenly being surrounded by an atmosphere of water molecules will react with the water molecules to displace protons and acquire an hydroxyl ion atmosphere. Thus we have

$$Al_{Me}^{+++} + 3H_2O \longrightarrow Al^{+++}\cdot 3OH^- + 3H^+$$

Latimer measured the free energy change for formation of aluminum ions in solution as -116.9 kcal./mole,[3] and later revised this value to -115.0 kcal./mole.[4] Being consistent with the model for the aluminum ion just postulated we will assume that the ions Latimer worked with were like the ions in our model and that Latimer measured the free energy of the aluminum ion with an anion atmosphere.

In acid solutions the hydroxyl anion atmosphere will be neutralized and one will obtain aluminum ions surrounded by an atmosphere of the prevalent anions.

The free energy for the reaction

$$3H_2O \longrightarrow 3OH^- + 3H^+$$

is $+57.3$ kcal./mole so that one obtains for the postulated electrode reaction $\Delta F = -57.1$ kcal./mole. This is obtained using -114.4 kcal./mole rather than Latimer's value of -115.0 kcal./mole, a value more consistent with the results of this investigation. We obtain for the electrode potential on the saturated calomel scale

$$E = 1.070 - \frac{0.0592}{3} \log [Al^{+++}\cdot 3X^-] + 0.0592\ pH$$

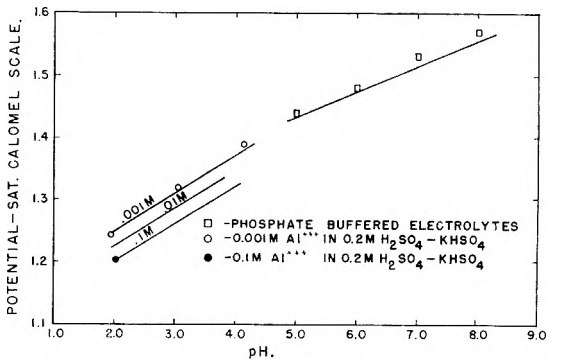

Fig. 7.—Potentials of oxide-free aluminum surfaces in acidic and neutral solutions: points, experimental; lines, calculated.

The solid lines drawn in acid solutions on Fig. 7 represent this equation. The agreement with the experimental points is extremely good. It will be especially noted that the dependence of potential on pH is correct.

The equilibria involving the aluminum ion in neutral and alkaline solutions are complex. We will assume, as a first approximation, the reactions

$$Al(OH)_3 \xrightarrow{K_s} Al^{+++}\cdot 3OH^- \xrightarrow{K_2} H^+ + H_2AlO_3^-$$

Undoubtedly further ionization of aluminic acid takes place. K_s is the solubility constant for the undissociated neutral entity, K_2 is the ionization constant, and $K_{sp} = K_sK_2$ is the solubility product in alkaline solutions. The electrode reaction then may be described as

$$Al^{+++} + 3H_2O \xrightarrow{(1)} Al^{+++}\cdot 3OH^- + 3H^+ \xrightarrow{(2)} H^+ + H_2AlO_3^- + 3H^+$$

The free energy change for this reaction is given by

$$\Delta F = \Delta F^0_{(1)} + \Delta F^0_{(2)} + RT \ln K_{sp} + 2\ RT \ln [H^+]$$

where specific allowance is made for the fact that neutralization reaction involving the proton from the aluminic acid does not affect the electrode process. This is to be expected because a charge separation must take place in order for a chemical reaction to develop an electric potential. Putting in the equilibrium constant for the ionization of aluminic acid explicitly one obtains

$$\Delta F = \Delta F^0_{(1)} + RT \ln K_s + 2\ RT \ln [H^+]$$

and using our measured value of $\Delta F^0_{(1)}$ one may write

$$E = 1.070 - 0.0197 \log K_s + 0.0394\ pH$$

where E is expressed on the saturated calomel scale. From the observed potential at pH 5 one obtains

$$K_s = 10^{-8.6}$$

This value for the solubility of the undissociated aluminic acid is reasonable compared to what is

(3) W. M. Latimer and B. S. Greensfelder, *J. Am. Chem. Soc.*, **50**, 2202 (1928).

(4) W. M. Latimer, "Oxidation Potentials," Prentice-Hall Book Co., New York, N. Y., 1952, 2nd ed., p. 281.

judged the most reliable solubility data, that of Szabo,[5] from which one may calculate the total solubility of the various species present at the isoelectric point as $10^{-7.2}$. The solid line drawn in Fig. 7 from a *p*H of 5 up represents the above equation. The agreement is good but an error of up to 15 mv. is observed at high *p*H values. This probably results from neglecting the second ionization constant of aluminic acid. Further work in neutral and alkaline solutions is underway and will be described in a later publication.

The Possibility of Interpretation in Terms of Mixed Potentials.—It has been seen that the potentials of oxide-free aluminum surfaces are explicable in terms of the electrochemical process

$$Al_{Me}^{+++} \longrightarrow Al_{sol}^{+++}$$

followed immediately by

$$Al_{sol}^{+++} + 3H_2O \longrightarrow Al^{+++}{\cdot}3OH^- + 3H^+$$

One might suspect that mixed potentials are involved in which the anodic reaction is transfer of an ion from the metal to the solution and the cathodic reaction is evolution of hydrogen. The free energy change for a model involving mixed potentials might be the same as that for the model in which aluminum causes the deprotonation of water molecules.

One may inquire how large an electrical potential will appear for the mixed potential model. Several cases can be distinguished

1. Anode and cathode at the same point on the surface with neither reaction polarized—the aluminum ions and the electrons will tend to leave the surface at different rates depending upon their vibrational frequencies and activation energies. Some potential difference between solution and metal will be established but the potential will not be related to the net free energy change for the combined reactions. To the extent that the different rates of escape are neglected there will be no potential developed. It is believed that this model would be most correct for the uniform evaporated oxide-free surfaces.

2. Anode and cathode at the same point on the surface with one reaction or the other polarized—the potential then will be that potential produced by the anodic or cathodic current passing through the resistance. The potential will not be directly related to the free energy of the combined anodic and cathodic reactions but will depend upon the polarization.

3. Anode and cathode at different points on the surface—if the anodes and cathodes were sufficiently far apart to be called separate then the experiment would consist of measuring one of the local half cells. The measured potentials are not consistent with either the cathodic or anodic reactions separately.

One piece of experimental evidence that the observed zero oxide potentials are not "mixed potentials" is the fact that the potentials observed with scraped samples and with evaporated samples agree within the scatter of the data over the whole range of oxidation times and electrolytes studied. If both anodic and cathodic reactions were involved then the homogeneous surface obtained by scraping would be expected to give different results than the more homogeneous surface obtained by evaporation.

Acknowledgments.—Appreciation is expressed to Mr. C. A. Kiesling for his great aid in the design and construction of the apparatus; to Mr. H. Rook for his assistance in obtaining the experimental data; and to the Aluminum Company of America for permission to quote from the results of exploratory experiments carried out while the author was employed at the Alcoa Research Laboratories. This research was supported by Atomic Energy Commission Basic Research Contract AT(30–1) 2479.

(5) Z. G. Szabo, *Z. Anal. Chem.*, **146**, 401 (1955).

THE MECHANISM OF POTASSIUM PROMOTION OF CHROMIA–ALUMINA DEHYDROGENATION CATALYSTS

BY JOANNE M. BRIDGES, G. T. RYMER, AND D. S. MACIVER

Gulf Research & Development Co., Pittsburgh, Pa.

Received October 25, 1961

A study has been made of the mechanism of the alkali promotion of chromia–alumina dehydrogenation catalysts by investigating the reaction of cyclohexane over a variety of promoted and unpromoted chromia catalysts. At the same time the magnetic and adsorptive properties of these materials have been determined and correlated with catalyst activity and selectivity. From the results obtained it was shown that there are, in general, two types of active sites on chromia–alumina, a dehydrogenation type associated with the chromia portion of the surface and an acid type associated with the alumina surface. The acid sites catalyze the formation of methylcyclopentane, which acts as a poison for the chromia dehydrogenation sites. The addition of potassium as a promoter "neutralizes" these acid sites, thereby preventing the formation of methylcyclopentane and hence increasing the dehydrogenation activity. Potassium in excess of that required for this "neutralization" is associated with the chromia portion of the surface in such a way that it blocks some of the dehydrogenation sites and thus lowers the dehydrogenation activity. The interaction of the potassium with the chromia apparently results in the formation of a potassium–chromium complex with the chromium in a +6 oxidation state, which under reaction conditions reduces to a +3 state.

Introduction

Chromia–alumina has been widely used as a catalyst for a variety of reactions, notably the dehydrocyclization and dehydrogenation of alkanes and naphthenes,[1] and it has been well established[1,2] that both catalyst activity and selectivity often are improved by adding a salt of an alkali metal such as potassium nitrate to the catalyst. Several workers have studied the influence of potassium on the chemical and physical characteristics of chromia–alumina and have attempted to relate their findings to variations in catalytic properties. Voltz and Weller[3] reported that potassium tended to partially stabilize the catalyst against reduction and to decrease the surface acidity; these latter results were later confirmed by Voltz, Hirschler, and Smith.[4] It also was found[3] that potassium decreased the activity for ethylene hydrogenation, cyclohexane dehydrogenation, double bond isomerization, and carbon monoxide oxidation, while it increased the activity for hydrogen peroxide decomposition. More recently, the structures of chromia–alumina–potassium oxide catalysts have been studied, and the results related to activity and selectivity in decomposing isopropyl alcohol.[5] To date, however, information is lacking on the precise mechanism by which alkali functions as a promoting agent, especially with respect to hydrocarbon reactions. For this reason, an investigation has been carried out in this Laboratory on the physical properties of alkali promoted chromia–alumina catalysts and the role of these properties in determining the manner in which various hydrocarbons react over the catalysts. The present paper reports the effect of potassium on the dehydrogenation of cyclohexane.

Experimental

Materials.—Hydrogen, helium, and prepurified nitrogen were obtained from the Air Reduction Company; oxygen and argon from the Linde Company. The hydrogen used in the kinetic studies was purified by passage, first through a "Deoxo" unit, then through magnesium perchlorate, over platinized asbestos at 300°, through magnesium perchlorate again, and finally through a −78° trap. The argon was purified by passing it over reduced copper at 400° and then through magnesium perchlorate. The treatment of the gases used in the magnetic and adsorption studies has been described elsewhere.[6] Cyclohexane (Phillips Research Grade) and methylcyclopentane (Phillips Pure Grade) were used as received.

Chromia–alumina catalysts were prepared by impregnating Davison η-Al_2O_3 with reagent grade chromic acid. Emission analysis of the original alumina indicated the presence of Si, Cu, and Ca to the extent of about 0.03% each, all other contaminants being present in amounts less than 0.01%. Ferromagnetic impurities were virtually absent as determined by magnetic susceptibility. The alumina, ground to 50–140 mesh, was contacted with chromic acid solutions of various concentrations for 24 hr. The liquid phase then was removed by filtration, and the solid was dried at 100° for 24 hr. and calcined at 500° for another 24 hr. The calcined catalysts were subjected to three cyclic treatments at 500°, first in hydrogen for 1 hr. and then in oxygen for 1 hr. A blank alumina sample was prepared in exactly the same manner except that distilled water was used in place of the chromic acid solution. Samples of chromia–alumina (10.5 wt. % Cr) obtained as indicated and a sample of the original alumina were promoted with potassium by impregnating with potassium nitrate solutions and treating in the same manner as described above for the chromia impregnation. Again, a blank chromia–alumina was made by substituting water for the potassium nitrate solution. Pure chromia was obtained by a method described earlier,[6] and a portion was promoted with potassium in the same fashion as the chromia–alumina samples.

Apparatus.—The kinetic measurements were made at atmospheric pressure using an all-glass gas flow system. The flow rates of the carrier gases, argon and hydrogen, were regulated to within 1% in the fashion described by Bailey.[7] These gases were saturated with cyclohexane at 15° and passed through the catalyst reactor. Periodic mass spectrometric analysis indicated that the partial pressure of cyclohexane in the reactant mixture was 57 ± 1 mm. throughout the course of the work. For certain experiments it was necessary to add an arbitrary amount of methylcyclopentane to the reactant stream. This was accomplished by passing the stream through a U-tube containing a small amount of liquid methylcyclopentane at room temperature. The amount of methylcyclopentane so introduced was not sufficient to appreciably change the partial pressure of cyclohexane in the reactant stream. When not in use the U-tube was isolated from the rest of the system. The reactor consisted of a 70 cm. long glass tube having a diameter of 12 mm. The catalyst bed, which was 10 cm. long, was located in the center of this tube, the remainder of the tube being packed with Pyrex wool. The entire reactor was enclosed in

(1) F. G. Ciapetta, R. M. Dobres, and R. W. Baker, "Catalysis," Vol. VI, ed. by P. H. Emmett, Reinhold Publ. Corp., New York, N. Y., 1958, Chapter 6.

(2) R. C. Archibald and B. S. Greensfelder, *Ind. Eng. Chem.*, **37**, 356 (1945).

(3) S. E. Voltz and S. W. Weller, *J. Phys. Chem.*, **59**, 569 (1955).

(4) S. E. Voltz, A. E. Hirschler, and A. Smith, *ibid.*, **64**, 1594 (1960).

(5) A. H. Rubinstein, N. A. Pribytkova, V. A. Afanasyev, and A. A. Slinkin, "The Second International Congress on Catalysis," Paris, France, July 4–9, 1960, Paper No. 100.

(6) D. S. MacIver and H. H. Tobin, *J. Phys. Chem.*, **64**, 451 (1960).

(7) S. W. Bailey, *J. Sci. Instr.*, **31**, 93 (1954).

a tube furnace whose temperature was regulated by an automatic temperature controller. The temperature gradient across the bed was 0.5°, and the maximum temperature fluctuation during the course of a run was ±0.5°. Product analyses were made chromatographically. The product gases passed directly from the reactor to a manually operated Aerograph 6-way sampling valve which was used in conjunction with a Fisher-Gulf Partitioner chromatographic unit. The chromatographic column was 12 feet long and contained 10% 8-N-8 Flexol supported on an inert carrier.

Magnetic susceptibility measurements were made over the temperature range from −78 to 200° using a Faraday type susceptibility balance previously described.[8] The −78° temperature was attained by a Dry Ice–acetone bath. Temperatures above room temperature were maintained to within ±0.1°, as measured with a calibrated copper–constantan thermocouple, by use of a platinum heating coil actuated by an automatic temperature control device.

Adsorption studies were carried out gravimetrically using a quartz spiral balance described in an earlier publication.[9] Liquid nitrogen and Dry Ice–acetone were used to maintain temperatures of −195 and −78°, while elevated temperatures were obtained with a small, automatically controlled, ceramic furnace. Temperature measurements were made using nitrogen or carbon dioxide vapor pressure thermometers and with calibrated thermocouples.

Procedure.—In making the kinetic measurements 4.6 g. of catalyst (except in the case of unsupported chromia where 1.3-g. samples diluted to a 5 cc. volume with either 50–140 mesh Pyrex chips or alumina were used) were reduced *in situ* with hydrogen at 500° and a gaseous hourly space velocity of 5000 for 16 hr. The catalyst then was cooled to the initial reaction temperature of 416° in the hydrogen stream, and the reactant charge was passed over the catalyst. In the majority of the experiments this charge consisted of argon, hydrogen, and cyclohexane in a molar ratio of 6:6:1, although a few runs were made using an argon–cyclohexane charge in which the molar ratio of argon to cyclohexane was 12:1. In both cases the argon was used as a "tracer" to permit conversions to be calculated from the chromatograms according to the method described by Hall, MacIver, and Weber.[10] Conversions were measured at 416° as a function of feed rate in the order 40, 30, 20, 15, 80, and 40 cc. (STP)/min., the identical rates at the beginning and end serving as a check of catalyst stability. The catalyst was allowed to equilibrate at least 30 min. at each feed rate before analyzing the product gas. At the end of this run the temperature was lowered to 400°, and the catalyst was allowed to remain overnight at this temperature in the presence of the reactant stream. The following day, rate studies were made as a function of space velocity at 400, 380, and 355°. The 416° run then was repeated in order to determine whether any catalyst aging had occurred.

Susceptibility measurements were made on chromia–alumina samples in both the oxidized and reduced state. Ten-mg. samples, contained in a spherical quartz bucket, were treated, *in situ*, with a stream of oxygen or hydrogen at 500° for 6 hr. and then evacuated for 16 hr. at this same temperature. During the course of the susceptibility measurements, the samples were maintained in a helium atmosphere. At each temperature susceptibilities were determined at five field strengths ranging from 4200 to 7760 oersteds. The apparent paramagnetic susceptibilities at a particular temperature, after correction for the diamagnetic contributions of the quartz sample container and the alumina support, were plotted as a function of the reciprocal field. The field plots at the various temperatures for any one sample were parallel with small positive slopes. True paramagnetic susceptibilities were obtained from these plots by extrapolation to infinite field.

Surface areas of the catalysts were determined with nitrogen at −195° by the BET method using a value of 16.2 Å.^{2} for the cross sectional area of the adsorbed nitrogen molecule. Oxygen chemisorption on chromia–alumina at −195° was measured following the general procedure of Bridges, MacIver, and Tobin.[11]

(8) J. R. Tomlinson, R. O. Keeling, Jr., G. T. Rymer, and Joanne M. Bridges, "The Second International Congress on Catalysis," Paris, France, July 4–9, 1960, Paper No. 90.

(9) D. S. MacIver and H. H. Tobin, *J. Phys. Chem.*, **65**, 1665 (1961).

(10) W. Keith Hall, D. S. MacIver, and H. P. Weber, *Ind. Eng. Chem.*, **52**, 421 (1960).

Results

The surface areas of the catalysts used in this work are presented in Table I along with oxygen chemisorption values for several of the chromia–alumina samples. The oxygen adsorption at −195° is defined in the manner described by Bridges, MacIver, and Tobin,[11] namely, as the amount of oxygen retained after the reduced catalyst has been exposed to oxygen at −195° and then evacuated for 1 hr. at −78°. In order to put these data on a comparable basis for the various catalysts the oxygen chemisorption values in column 6 of Table I have been divided by the BET nitrogen monolayer values; these ratios are given in column 7.

TABLE I

CATALYST SURFACE PROPERTIES[a]

Sample	Wt. % Cr	Wt. % K	Surface area, m.^{2}/g.	V_m (N_2), cc. (STP)/g.	V (O_2), cc. (STP)/g.	V (O_2)/V_m (N_2)
Al_2O_3	...	0	141	32.2	..	..
Al_2O_3	...	2.30	139	31.7	..	..
Cr_2O_3	...	0	17	3.8	1.8	0.47
Cr_2O_3	...	5.26	6.4	1.5	..	..
Cr_2O_3/Al_2O_3	2.11	0	126	28.6	..	..
Cr_2O_3/Al_2O_3	4.35	0	128	29.2	..	..
Cr_2O_3/Al_2O_3	6.10	0	132	30.1	..	..
Cr_2O_3/Al_2O_3	10.60	0	125	28.5	2.7	0.10
Cr_2O_3/Al_2O_3	11.05	0.20	123	28.1	2.8	.10
Cr_2O_3/Al_2O_3	10.47	.36	122	27.8	2.5	.09
Cr_2O_3/Al_2O_3	10.57	.86	113	25.8	2.0	.08
Cr_2O_3/Al_2O_3	10.04	1.25	111	25.3	2.1	.08
Cr_2O_3/Al_2O_3	10.34	2.25	92	20.9	1.5	.07

[a] $V_m(N_2)$ is nitrogen monolayer value (BET) at −195°. $V(O_2)$ is volume of oxygen chemisorbed at −195°.

The magnetic susceptibilities of the potassium promoted chromia–alumina samples were found to obey the Curie–Weiss law, and, hence, from plots of the susceptibility *vs.* reciprocal temperature one could obtain the effective magnetic moments, μ_{eff}, and the Weiss constants, Δ. These quantities are presented in Table II for the various catalysts studied. The precision of measurement was ±0.02 Bohr magneton for the moments and ±5°K. for the Weiss constants. Also included in Table II are the ratios $(\mu_{eff}/\mu_{Cr^{+3}})^2$ where $\mu_{Cr^{+3}}$ is the theoretical spin-only moment of Cr^{+3} (*i.e.*, $\mu_{Cr^{+3}} = 3.87$). This ratio also is equal to the fraction of chromium in the +3 state assuming that this is the

TABLE II

MAGNETIC PROPERTIES OF CHROMIA–ALUMINA CATALYSTS AS A FUNCTION OF PRETREATMENT

Wt. % Cr	Wt. % K	μ_{eff}, Bohr magnetons: Oxidized	μ_{eff}, Bohr magnetons: Reduced	Δ, °K.: Oxidized	Δ, °K.: Reduced	$(\mu_{eff}/\mu_{Cr^{+3}})^2$: Oxidized	$(\mu_{eff}/\mu_{Cr^{+3}})^2$: Reduced
10.60	0	3.23	3.41	220	200	0.696	0.776
11.05	0.20	3.23	3.39	220	210	.696	.767
10.47	.36	3.04	3.52	160	210	.617	.827
10.57	.86	2.98	3.48	160	210	.593	.808
10.04	1.25	2.92	3.39	180	220	.569	.767
10.34	2.25	2.69	3.43	170	240	.483	.785

(11) Joanne M. Bridges, D. S. MacIver, and H. H. Tobin, "The Second International Congress on Catalysis," Paris, France, July 4–9, 1960, Paper No. 110.

only paramagnetic species present and that each Cr^{+3} ion realizes its full theoretical moment of 3.87.

Preliminary studies in which an argon–cyclohexane charge was passed over an unpromoted chromia–alumina catalyst (10 wt. % Cr) showed that the products of the reaction were cyclohexene, benzene, and a small amount of methylcyclopentane. Traces of 3-methylcyclopentene, which would have appeared as part of the cyclohexane peak on the chromatogram, could have been present, although more detailed chromatographic and infrared analyses indicated that it was not a significant product. The 1-methyl and 2-methyl isomers were not found. Unfortunately, the catalyst aged so rapidly during the course of the run that reliable kinetic measurements could not be made, and it was necessary to add hydrogen to the charge in order to obtain stable catalyst activities. Under these conditions the activity was essentially constant over a 48-hr. period and, consequently, all subsequent experiments were carried out using the argon–hydrogen–cyclohexane charge. In addition to stabilizing the catalyst the hydrogen also changed the product distribution by increasing the amount of methylcyclopentane formed. Again, while small quantities of the methylcyclopentenes may have been present, they were formed only in trace amounts at best. In view of the observed product distribution, the rates which were measured for the present study were the rate of cyclohexane reaction (r_{CH}) and the rates of methylcyclopentane (r_{MCP}), benzene (r_B), and cyclohexene (r_{CHe}) production. In general, the conversion of cyclohexane varied from 0.5 to 96.0% depending upon temperature, space velocity, and catalyst; the amounts of benzene, cyclohexene, and methylcyclopentane in the product stream ranged from 0.4 to 96.0, 0.1 to 0.6, and 0.5 to 4.0%, respectively.

To determine the rate of cyclohexane reaction both an integral and differential method of treating the data were tried. For the case of a flow reactor the rate of cyclohexane reaction may be expressed by the steady state mass balance equation

$$r_{CH}dA = Fdf_{CH} \qquad (1)$$

where

r_{CH} = rate of cyclohexane reaction (moles/min.-m.^{2})
F = feed rate (moles cyclohexane/min.)
A = surface area (m.^{2})
f_{CH} = fraction of cyclohexane reacted

Therefore, if the conversion, f_{CH}, is plotted against the quantity, A/F, then the differential reaction rate, r_{CH}, at any particular conversion is given by the slope of the curve at that conversion. In the present work rates were obtained by measuring the slopes of such curves with a tangentimeter. As discussed elsewhere,[12,13] it often is useful to determine differential reaction rates at very low conversions (*i.e.*, infinite space velocity) where the effect of reaction products upon the kinetics is minimal. Obviously, the rate at infinite space velocity, r_{CH}^0, may be obtained directly by measuring the initial slope of the conversion *vs.* A/F curve. Such a procedure, however, places considerable weight on the extrapolated portion of the curve and for this reason an alternative method was used to obtain r_{CH}^0. Weller[14] has indicated that for many heterogeneous reactions the rate may be expressed as a simple power dependency of rate on concentration. In the present case of cyclohexane conversion, therefore, the rate was assumed to be given by

$$r_{CH} = kp_{CH}^n \qquad (2)$$

where

k = constant
p_{CH} = partial pressure of cyclohexane
n = reaction order

and plots were made of log r_{CH} *vs.* log p_{CH}. Examples of such plots are shown in Fig. 1. In all cases these plots were linear, and values of n could be obtained from the slopes; these values were than substituted in eq. 2 and by setting $p_{CH} = p_{CH}^0$, the initial partial pressure of cyclohexane, values of r_{CH}^0 were calculated. If eq. 2 is valid over the entire range of conversions studied and assuming for the moment that $n = 1$, then combining eq. 1 and 2 gives, upon integration at constant total pressure

$$kp_{CH}^0(A/F) = -[(1 + \delta y)\ln(1 - f_{CH}) + \delta y f_{CH}] \qquad (3)$$

where

δ = increase in the no. of moles of the reacting system/mole of reactant converted (*i. e.*, $\delta = 3$ for the dehydrogenation of cyclohexane to benzene)
y = mole fraction of cyclohexane in the entering feed

The fit of the data obtained in this work to eq. 3 is illustrated in Fig. 2 for several chromia–alumina catalysts. The slopes of these lines give $kp_{CH}^0 = R_{CH}$, the integral reaction rates.

In Table III, the values of n, r_{CH}^0, and R_{CH} at 416° are given for the various chromia–alumina catalysts tested. From this it may be seen that n is very close to unity for all the catalysts, indicating that the rate of cyclohexane reaction is approximately first order, and that, within experimental error, $R_{CH} = r_{CH}$. These facts justified the use of the integral method represented by eq. 3 and, be-

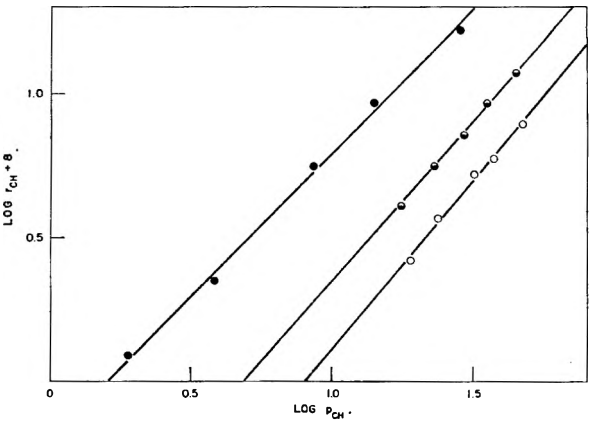

Fig. 1.—Log of the rate of cyclohexane reaction at 416° obtained from conversion-reciprocal space velocity plots *vs.* log of the partial pressure of cyclohexane: ●, 10.47 wt. % Cr, 0.36 wt. % K; ◒, 10.34 wt. % Cr, 2.25 wt. % K; ○, 6.10 wt. % Cr, 0.0 wt. % K.

(12) C. D. Prater and R. M. Lago, *Advances in Catalysis*, **8**, 293 (1956).
(13) P. B. Weisz and C. D. Prater, *ibid.*, **6**, 143 (1954).
(14) S. Weller, *A.I.Ch.E. Journal*, **2**, 59 (1956).

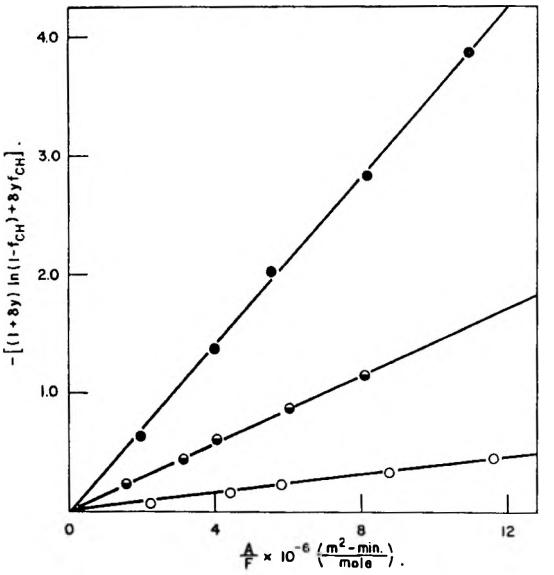

Fig. 2.—First-order rate plots for the reaction of cyclohexane at 416°: ●, 10.47 wt. % Cr, 0.36 wt. % K; ◒, 10.34 wt. % Cr, 2.25 wt. % K; ○, 6.10 wt. % Cr, 0 wt. % K.

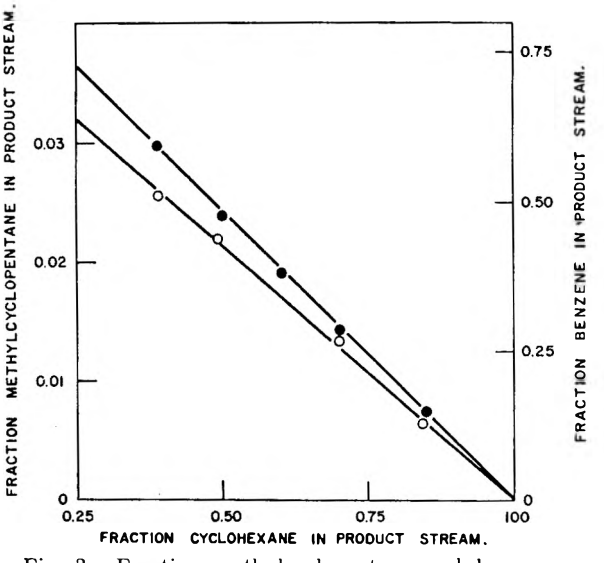

Fig. 3.—Fraction methylcyclopentane and benzene *vs.* fraction cyclohexane in the product stream in the case of 6.10 wt. % Cr_2O_3–Al_2O_3 at 416: ○, fraction methylcyclopentane; ●, fraction benzene.

cause of its convenience, this method was used, generally, to obtain the rate of cyclohexane reaction (r_{CH}^0).

For the case of the rate of formation of a product an equation analogous to eq. 1 may be written as

$$r_p dA = F\, df_p \qquad (4)$$

where

r_p = rate of formation of product p (moles p/min.-m.²)
f_p = fraction of reactant converted to p

Equations 1 and 4 may be combined to give

$$\frac{r_p}{r_{CH}} = \frac{df_p}{df_{CH}} \qquad (5)$$

and, therefore, if f_p is plotted against f_{CH}, the slope of the curve at a particular conversion level is equal to the ratio of the two rates at this conversion. Typical examples of such plots are shown in Fig. 3 for benzene and methylcyclopentane. The linearity of these curves indicates that the rate of formation of both products was first order with respect to cyclohexane, and, hence, it was possible to obtain the initial rates r_B^0 and r_{MCP}^0 by taking the product of the slopes and r_{CH}. In Table IV are summarized values of r_B and r_{MCP}^0 at 416° for all the chromia–alumina catalysts studied.

TABLE III

RATE OF CYCLOHEXANE REACTION OVER CHROMIA–ALUMINA AT 416°

Wt. % Cr	Wt. % K	Reaction order, n	r_{CH} × 10⁸, moles/ min.-m.²	R_{CH} × 10⁸, moles/ min.-m.²	E_{CH},[a] kcal./ mole
2.11	0	1.11	1.18	1.17	31
4.35	0	0.95	3.56	3.64	30
6.10	0	1.15	7.56	7.60	30
10.60	0	1.05	12.6	12.9	31
11.05	0.20	1.00	11.6	11.9	30
10.47	.36	1.00	31.5	32.0	31
10.57	.86	0.99	32.0	32.7	30
10.04	1.25	1.14	22.3	23.2	30
10.34	2.25	1.12	14.6	14.3	31

[a] E_{CH} = activation energy for cyclohexane reaction.

TABLE IV

RATES OF BENZENE AND METHYLCYCLOPENTANE FORMATION OVER CHROMIA–ALUMINA AT 416°

Wt. % Cr	Wt. % K	r_B^0 × 10⁸, moles/ min.-m.²	E_B,[a] kcal./ mole	r_{MCP}^0 × 10⁸, moles/ min.-m.²	E_{MCP}[b] kcal./ mole
2.11	0	0.86	35	0.31	23
4.35	0	3.11	35	.38	24
6.10	0	7.20	31	.27	20
10.60	0	12.9	31	.26	27
11.05	0.20	11.9	30	Small	..
10.47	.36	32.0	30	0	..
10.57	.86	32.7	30	0	..
10.04	1.25	23.2	30	0	..
10.34	2.25	14.3	30	0	..

[a] E_B = activation energy for benzene formation. [b] E_{MCP} = activation energy for methylcyclopentane formation.

Under the reaction conditions employed in the present work only trace quantities of cyclohexene were produced. At cyclohexane conversions of less than 60% only 0.5 ± 0.1% of the cyclohexane was converted to cyclohexene and, as near as could be determined at those low levels, this conversion was independent of cyclohexane concentration. In other words, the cyclohexene was present in steady state concentrations (*i.e.*, $r_{CHe} = 0$). Above 60% cyclohexane conversion, the amount of cyclohexene in the product dropped off; the analytical data, however, were insufficient to permit expression in the form of a rate equation. In all cases the amount of cyclohexene found in the product stream was considerably less than the equilibrium value.

Activation energies for the various reactions were computed in the usual fashion from the Arrhenius equation using the differential rates at infinite space velocities. The Arrhenius plots are illustrated for several catalysts in Fig. 4 and the

energy values obtained are presented in Tables III and IV for all the chromia–alumina catalysts investigated. It should be mentioned that, under the experimental conditions employed, diffusion effects did not have any appreciable influence upon the observed rate constants. Using the procedure described by Wheeler,[15] an effectiveness factor of >0.99 was calculated for each of the several catalysts employed, indicating that the entire internal surface area of each catalyst was effective in the reaction.

In order to obtain information on the respective roles of alumina and chromia in the reaction mechanism the dehydrogenation of cyclohexane was studied over pure chromia, pure alumina, and mechanical mixtures thereof. The results at 416° are summarized in Table V. Only in the case of pure chromia was an activation energy for the cyclohexane reaction measured, and a value was found of 40 ± 3 kcal./mole. It is interesting to compare the activity of pure chromia with the chromia mixed with alumina. In the former case about 30% of the cyclohexane was converted to benzene at 416° and a feed rate of 40 cc. (STP)/min.; this catalyst activity level was constant throughout the length of the run (3 hr.). In the case of the mechanical mixture a complete mass balance was not possible because of extensive cracking. Under the same conditions as above, however, 6% of the cyclohexane was converted to benzene and methylcyclopentane at the beginning of the experiment; after 3 hr. on-stream, the conversion had dropped to 3%. When the alumina, prior to mixing, was treated with potassium, the mixed catalyst behaved essentially the same as pure chromia. The pure alumina did not catalyze the conversion to either cyclohexene or benzene; instead, a large amount of cracking took place.

TABLE V

REACTION RATES AT 416° OVER MIXED CATALYSTS

Catalyst	r_{CH}^0 × 10⁶, moles/min.-m.²	r_B^0 × 10⁶, moles/min.-m.²	r_{MCP}^0 moles/min.-m.²
Al_2O_3	[a]	0	0
Cr_2O_3	1.88	1.88	0
Cr_2O_3 (5.2 wt. % K)	0.06	0.03	0
$Cr_2O_3 + Al_2O_3$	[a]	[b]	[b]
$Cr_2O_3 + Al_2O_3$ (2.3 wt. % K)	1.18	1.18	0

[a] Extensive cracking of cyclohexane. Conversion data too erratic to permit calculation of specific rate. [b] Product was obtained but the conversion data was too erratic to permit calculation of specific rate.

A final experiment consisted of saturating the argon–hydrogen–cyclohexane charge with methylcyclopentane at 25° and passing it over a potassium promoted chromia–alumina catalyst (10.5 wt. % Cr and 0.86 wt. % K). Before addition of the methylcyclopentane 76% of the cyclohexane was dehydrogenated to benzene at 421° and a feed rate of 40 cc. (STP)/min.; in the presence of methylcyclopentane only 50% of the cyclohexane was converted. The poisoning was irreversible.

(15) A. Wheeler, "Catalysis," Vol. II, ed. by P. H. Emmett, Reinhold Publ. Corp., New York, N. Y., 1955, Chapter 2.

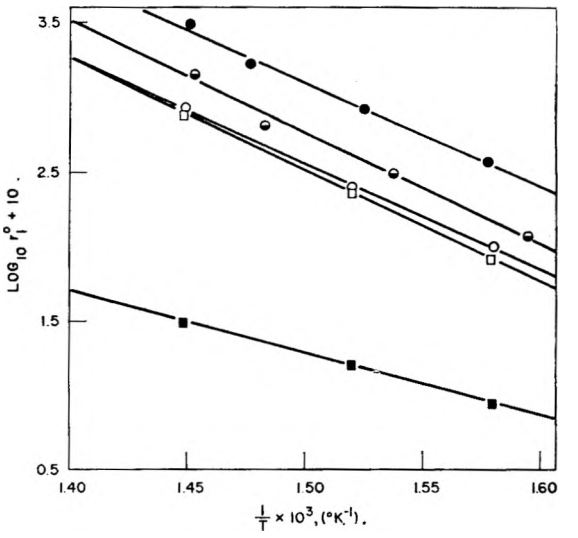

Fig. 4.—Arrhenius plots: ●, cyclohexane reaction and benzene production over 10.47 wt. % Cr, 0.36 wt. % K; ◒, cyclohexane reaction and benzene production over 10.34 wt. % Cr, 2.25 wt. % K; ○, cyclohexane reaction over 6.10 wt. % Cr; □, benzene production over 6.10 wt. % Cr; ■, methylcyclopentane production over 6.10 wt. % Cr.

Discussion

In general, chromia–alumina may be considered as a dual functional catalyst,[1] having an acid function which catalyzes reactions such as isomerization and a hydrogenation–dehydrogenation function. It has been proposed[1] that cyclohexane reacts over a catalyst of this type according to the scheme

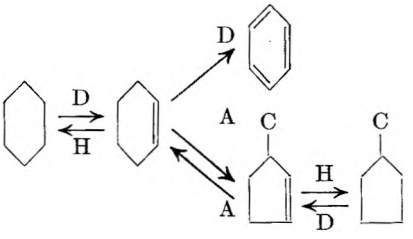

where H–D represents reaction over hydrogenation–dehydrogenation sites and A, reaction over acid sites. The data obtained during the present work is consistent with this mechanism in that, using an unpromoted chromia–alumina, the cyclohexane reacted to give benzene, cyclohexene, and methylcyclopentane. Because of this distribution of products it was possible to consider the promoting action of potassium in terms of both activity and selectivity.

The variation of activity with potassium content may be seen from Fig. 5, where the rate of cyclohexane reaction at 416° has been plotted as a function of the amount of potassium in the catalyst. It will be noted that the first increment of potassium added to the catalyst did not change the activity; beyond this point, however, the activity increased abruptly and then declined as additional potassium was added. As may be seen from Table IV, a change in the selectivity of the reaction accompanied this sudden rise in activity, in that, at this point, the methylcyclopentane disappeared from the product stream. That these two phe-

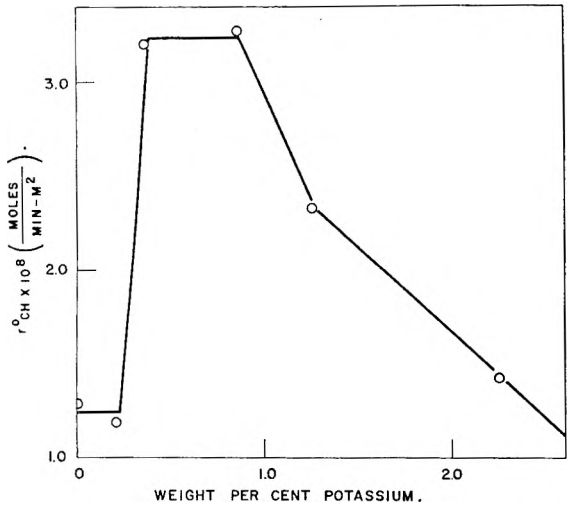

Fig. 5.—Rate of cyclohexane reaction at 416° *vs.* weight % potassium for those catalysts containing approximately 10.5 weight % chromium.

nomena were related was apparent from the experiment in which methylcyclopentane was deliberately added to the charge over a promoted chromia–alumina catalyst; the resulting irreversible decrease in catalyst activity strongly suggested that the methylcyclopentane was acting as a poison or a precursor to a poison and that the promoting role of the potassium was one of suppressing the formation of methylcyclopentane. According to the reaction scheme given above this latter compound is formed by the isomerization of cyclohexene over acid sites, and it is significant that potassium has been found to decrease the surface acidity of chromia–alumina catalysts.[3,4]

Further evidence bearing on this point is provided by the data in Table V on the activity of mechanical mixtures of chromia and alumina. It is to be noted that no methylcyclopentane was formed over pure chromia and that the catalyst was quite stable. A mixture of alumina and chromia, on the other hand, produced methylcyclopentane, and, in this case, the catalyst aged quite rapidly. As indicated earlier, a mixture of potassium-treated alumina and pure chromia behaved essentially the same as chromia alone. Thus it would appear that, under the conditions employed, chromia did not cause the C_6- to C_5-ring isomerization and that the acid sites of an alumina surface were required for the reaction. The potassium apparently serves to poison these sites, thereby destroying the acid function associated with the alumina and hence preventing the formation of the methylcyclopentane which deactivates the chromia dehydrogenation sites. The acid nature of alumina and the effect of alkali thereon has been demonstrated recently by the studies of Pines and Haag[16] and their findings are generally consistent with those reported above. It is interesting to observe that, in the present work, the C_6- to C_5-ring isomerization did not take place over pure alumina. This demonstrates the necessity of the cyclic olefin intermediate, this latter being present only when the dehydrogenation component was included in the catalyst bed.

(16) H. Pines and W. O. Haag, *J. Am. Chem. Soc.*, **82**, 2471 (1960).

It is believed that the results just discussed for the mixed catalysts are relevant also to the impregnated chromia–alumina catalysts. Earlier work[11] has indicated that a chromia–alumina catalyst prepared in the manner indicated has only about 20% of its surface covered with chromia, the chromia probably being present as crystallites on the alumina.[17] Thus, one can consider that in such a catalyst a sizable portion of the surface is similar in chemical properties to a pure alumina surface. In other words, a chromia–alumina surface may, for certain purposes, be regarded simply as a mixture of chromia and alumina surfaces. On this basis, treating the chromia–alumina catalyst with potassium poisons the acid sites associated with the alumina portion of the surface, thereby preventing the formation of methylcyclopentane and, hence, promotes the dehydrogenation activity.

The views expressed above concerning the role of methylcyclopentane in the poisoning of the chromia dehydrogenation sites are quite similar to the conclusions reached by Myers, Lang, and Weisz[18] who found that, using a platinum re-forming catalyst, cyclopentane reacted to give a poisonous intermediate, possibly cyclopentadiene, which acted as a catalyst deactivator. They postulated that this intermediate was adsorbed on the catalyst surface, where it underwent a polymerization to form "coke." The poisonous nature of C_5-ring compounds probably is related to the tendency of such compounds to polymerize when in contact with an acid catalyst[19] and to their ability to form complexes with transition metals and transition metal ions.[20] As in the case of platinum re-forming catalysts, the presence of hydrogen in the charge to the chromia–alumina catalysts reduced the aging rate, presumably by hydrogenating the catalyst poisons.

As shown in Fig. 5 the cyclohexane reaction rate passed through a maximum as potassium was added to the catalyst, and it remains to explain the deactivating influence of excess potassium. The most obvious explanation is that this potassium decreases the number of dehydrogenation sites by causing a decrease in the chromia surface area (*i.e.*, sintering), by chemically combining with the dehydrogenation sites, or by simply physically blocking or covering a portion of the chromia surface. The magnetic data in Table II indicate that the first increment of potassium added did not have any great influence on the magnetic properties of the catalyst, probably because, at this point, the potassium was associated primarily with the alumina portion of the surface. Additional potassium, however, was directly associated with the chromia, as is indicated by the decrease of μ_{eff} in the oxidized state. It is apparent that when the catalyst is oxidized the potassium is involved with

(17) R. P. Eischens and P. W. Selwood, *ibid.*, **69**, 1590 (1947).

(18) C. G. Myers, W. H. Lang, and P. B. Weisz, *Ind. Eng. Chem.*, **53**, 299 (1961).

(19) C. Kemball and J. J. Rooney, *Proc. Roy. Soc.* (London), **257A**, 132 (1960).

(20) L. E. Orgel, "An Introduction to Transition-Metal Chemistry: Ligand-Field Theory," Methuen and Co. Ltd., London, 1960, Chapter 10.

the chromia in such a way as to stabilize the Cr^{+6} electron configuration; this is consistent with the observation of Voltz and Weller[3] that potassium increases the surface oxidation state of a chromia–alumina catalyst, possibly *via* the formation of potassium chromate or dichromate. The potassium–chromium complex, however, does not appear to be stable against reduction since, as shown in Table II, treatment with hydrogen restored the effective moments of the promoted samples to that of the unpromoted catalyst. Since activities were determined with the catalysts in the reduced state it would not appear that the decrease in activity came about simply because of a change in average oxidation state of the chromia. However, despite the fact that the potassium–chromium complex is reduced, the potassium presumably remains at least physically associated with the chromia in some way since reoxidation of a promoted catalyst gave the same effective moment as was observed prior to the reduction. This potassium may exist in some form such as K_2O on the surface of the reduced chromia and in this way block some of the dehydrogenation sites. In line with this it will be observed from the data of Table V that treating pure chromia with potassium decreased the reaction rate per unit area, suggesting that the same effect is possible when the chromia is supported on an alumina surface. Another possible explanation for the deactivation is that the potassium causes a sintering or clumping of the chromia crystallites on the alumina. It is interesting to note that pure chromia decreased in area when treated with potassium (Table I) and that the Weiss constants of the reduced potassium promoted chromia–alumina catalysts increased slightly with potassium (Table II), as would be expected if the chromia was becoming less well dispersed over the alumina surface. In any case, it appeared that the deactivation could best be explained on the basis of a decrease in available chromia area either by blocking or sintering. Earlier work by Bridges, MacIver, and Tobin[11] has shown that the amount of oxygen chemisorbed by a reduced chromia–alumina catalyst at $-195°$ is an approximate measure of the extent of chromia surface, that is, the portion of the total surface which is contributed by the chromia component. Similar oxygen chemisorption measurements made on the present series of promoted chromia–alumina catalysts are reported in Table I, where it may be seen from the data in column 7 that as the potassium concentration increases, the amount of oxygen chemisorbed per unit catalyst area decreases. This would seem to suggest that the potassium causes a decrease in the available chromia area which, as discussed above, is sufficient to explain the decline in dehydrogenation activity of the catalysts at high potassium concentrations.

It is of interest to note that the activation energy for the cyclohexane reaction was independent of both the chromium concentration and the level of potassium promotion (Table III), suggesting that there is no change in the energetics of the reactant–catalyst interaction as these two factors are varied and that the promotion does not take place *via* some "electronic" factor entering into the activation energy. Using pure chromia, however, the activation energy was significantly greater (10 kcal./mole) than that over the supported chromia catalysts, which may be indicative of a basic chemical or physical difference between supported and unsupported chromia. A change in the lattice constants of the chromia when it is placed on a support, for example, possibly would be significant since the dehydrogenation reaction is thought to involve a dual site mechanism,[21] which could be energetically dependent upon the distance between active sites on the catalyst surface.[22,23]

(21) E. F. G. Herington and E. K. Rideal, *Proc. Roy. Soc.* (London) **190A**, 289 (1947).

(22) A. Sherman and H. Eyring, *J. Am. Chem. Soc.*, **54**, 2661 (1932).

(23) A. M. Rubinshtein, S. G. Kulikov, and N. A. Pribytkova, *Doklady Akad. Nauk S.S.S.R.*, **85**, 121 (1952).

THE PRESSURE OF Ga_2O OVER GALLIUM–Ga_2O_3 MIXTURES

BY C. J. FROSCH AND C. D. THURMOND

Bell Telephone Laboratories, Inc., Murray Hill, New Jersey

Received October 28, 1961

The pressure of Ga_2O over a mixture of Ga(l) and Ga_2O_3(s) has been measured over the temperature range of 800 to 1000° by the transport method. A heat of formation at 298°K. for Ga_2O(g) of -20.7 kcal. has been obtained.

We have measured the pressure of Ga_2O over mixtures of Ga and Ga_2O_3 in the temperature range 800 to 1000° by the transport method. The loss in weight of the mixture was measured as a function of time, temperature, and flow rate. A pestled mixture of 5 moles of Ga to 1 mole of Ga_2O_3 was placed in a fused silica boat which was heated in a fused silica tube under a helium gas stream. When this mixture was heated for a sufficient length of time it reached constant weight and all of the oxide had disappeared. The weight of Ga left was that calculated for the evaporation of Ga_2O. Brukl[1] has shown that the solid phase condensed from the vapor phase obtained by heating Ga–Ga_2O_3 mixtures has the composition Ga_2O. Mass spectrometric evidence for the vapor species Ga_2O has been obtained by Antkin and Dibeler[2] and others.[3]

The experimental results are shown in Fig. 1 where the logarithm of the ratio W/V has been

(1) D. A. Brukl. *Z. anorg. allgem. Chem.*, **203**, 23 (1932)

(2) S. Antkin and V. H. Dibeler, *J. Chem. Phys.*, **21**, 1890 (1953).

(3) W. S. Chupka, J. Berkowitz, C. F. Giese, and M. G. Inghram, *J. Phys. Chem.*, **62**, 611 (1958).

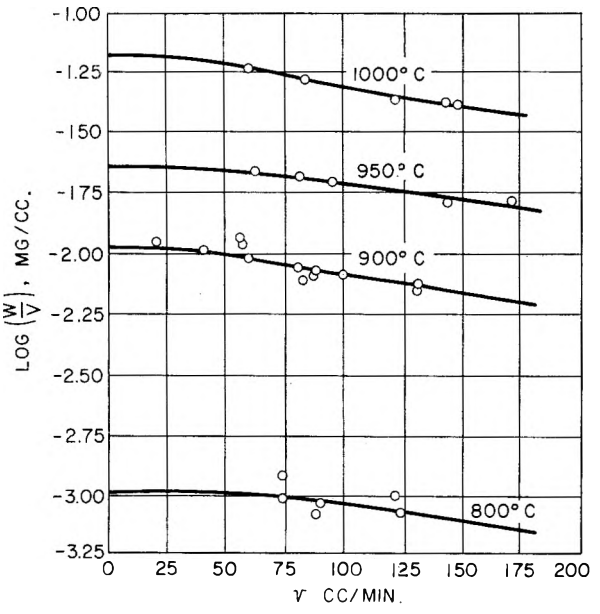

Figure 1.

plotted as a function of the flow rate v and at various temperatures to which the samples were heated: W is the weight loss of the sample when a volume V of helium is passed over it. The curves drawn through the points have been obtained from the two-constant equation

$$\left(\frac{W}{V}\right)\Big/\left(\frac{W}{V}\right)^{0} = (1 - e^{-\alpha/v}) \qquad (1)$$

A plot was made of log $(1 - e^{-\alpha/v})$ *vs.* v for various values of α. These curves were superimposed on the experimental results plotted as log W/V *vs.* v and a curve found which fit the measurements. This curve was used to extrapolate to zero flow rate to obtain $(W/V)^0$. The pressure of Ga_2O was obtained from the ideal gas law equation

$$P^{0}_{Ga_2O} = \frac{RT}{M_{Ga_2O}}\left(\frac{W}{V}\right)^{0} \qquad (2)$$

Equation 1 has not been used previously. We obtained this equation from a model which assumed that there was a uniform diffusion layer over the surface of the sample and that a steady-state condition was reached between each incremental area of the sample surface perpendicular to the gas flow stream and the element of gas volume above this area. The constant α then equals $AD/2\delta$ where A is the sample area, D the diffusion constant of Ga_2O, and δ the diffusion layer thickness. Reasonable values of α were obtained. At flow rates less than 25 cc./min., it was found that the diffusion of Ga_2O to the cooler portions of the tube became the more important transport mechanism. At flow rates smaller than this, the weight loss per unit volume of gas began to rise rapidly. This process has been discussed by Merten.[4] We propose that eq. 1 be used to extrapolate undersaturated pressures at finite flow rates to zero flow rate in order to obtain a good estimation of the equilibrium pressure under conditions where diffusional losses can be shown to occur at lower and small flow rates.

The pressures of Ga_2O obtained at the four temperatures are given in Table I. Included in the

TABLE I

T°,K.	P_{Ga_2O}, atm.	ΔH^{0}_{298}
1073	1.56×10^{-4}	65.7
1173	1.49×10^{-3}	66.3
1223	3.48×10^{-3}	66.7
1273	9.90×10^{-3}	66.6

$(\Delta H^{c}_{298}) = 66.3$ kcal./mole

$(\Delta H^{c}_{Ga_2O})_{298} = -20.7$ kcal./mole

table are the calculated values of ΔH^{0}_{298} for the reaction

$$\frac{4}{3}\,Ga(l) + \frac{1}{3}\,Ga_2O_3(s) = Ga_2O(g) \qquad (3)$$

In evaluating ΔH^{0}_{298}, the free energy function for $Ga_2O(g)$ recommended by Cochran and Foster[5] was used. They assumed that $(S^{0}_{298})_{Ga_2O(g)}$ was 69.54 e.u. from a comparison with other triatomic gaseous molecules of comparable molecular weights and that the heat capacity of $Ga_2O(g)$ was the same as for CTeS(g).[6,7] The free energy function used for Ga(l) came from Stull and Sinke.[8] The free energy function for $Ga_2O_3(s)$ is given by Cochran and Foster,[5] who used $\Delta H_T{}^{f}$ and $\Delta F_T{}^{f}$ values by Coughlin,[9] and the free energy functions for the elements given by Stull and Sinke.[8]

The value of 66.3 kcal. for the heat content change of reaction 3 at 298°K., and the heat of formation of $Ga_2O_3(s)$ at 298°K. of -261 kcal.,[10] give a heat of formation of $Ga_2O(g)$ at 298°K. of -20.7 kcal. This is in good agreement with a value of -20.4 kcal. obtained by Cochran and Foster[5] from a study of the reaction of $SiO_2(s)$ with Ga(l), and a value of -19.7 kcal. obtained by them from the reaction of MgO(s) with Ga(l). We estimate the uncertainty in ΔH^{f}_{298} or $Ga_2O(g)$ to be ± 2.5 kcal., this uncertainty arising from a 2 e.u. uncertainty in the estimated value of S^{0}_{298} for $Ga_2O(g)$.

(4) U. Merten, *J. Phys. Chem.*, **63**, 443 (1959).

(5) C. N. Cochran and C. M. Foster, *J. Electrochem. Soc.*, **109**, 144 (1962).

(6) Se_2C is probably a closer analogy to Ga_2O than CTeS. However, the heat capacity differs from that of CTeS by such a small amount that a maximum of less than 0.2 e.u. occurs in the free energy function over the temperature range of interest. This is negligible compared to an estimated error of ± 2 e.u. arising from uncertainties in S^{0}_{298}.

(7) K. K. Kelley, Bulletin 584, U. S. Bureau of Mines, 1960.

(8) D. R. Stull and G. C. Sinke, "Thermodynamic Properties of the Elements," Amer. Chem. Soc., Washington, D. C., 1956.

(9) J. P. Coughlin, U. S. Bureau of Mines, Bulletin 542, 1954.

(10) Private communication from K. K. Kelley. The value -261 ± 0.3 kcal. has been measured recently by Mrs. Alla D. Mah. The prior literature value was -258 ± 3 kcal.[9]

AN INFRARED INVESTIGATION OF XANTHATE ADSORPTION BY LEAD SULFIDE

BY ROBERT G. GREENLER

Research Division, Allis-Chalmers Mfg. Co., Milwaukee 1, Wisconsin

Received November 1, 1961

Infrared spectroscopy is used to investigate the nature of compounds formed on the surface of PbS exposed to air, the effect on these surface compounds produced by the subsequent adsorption from potassium ethyl xanthate solution, and the nature of the resulting xanthate surface layer. PbS samples which have been exposed to air show infrared evidence of $PbCO_3$, $PbSO_4$, $PbSO_3$, and other lead–sulfur–oxygen compounds of unknown composition. Carbonate ions and, in some cases, sulfur–oxygen ions are displaced by treatment with an aqueous solution of potassium ethyl xanthate but not by similar treatment with water alone. PbS samples which are heated in air to produce more oxidation of the sulfide ions adsorb more xanthate from solution than do less-oxidized samples. A surface xanthate compound is formed on the PbS which has the infrared spectrum of lead ethyl xanthate. Part of the surface xanthate is readily removed by washing in acetone. The amount of xanthate which remains on the surface after repeated washing in acetone corresponds approximately to a monolayer of xanthate ions on the PbS surface. A structure is suggested for the xanthate surface compound which is formed.

Introduction

The specific nature of the adsorption of xanthates on sulfides has been debated at some length in the literature dealing with the flotation of sulfide ores using xanthate collectors. Reviews[1-3] of the experimental data and its significance in view of various theories of flotation still leave the mechanism of adsorption undecided. There are many difficulties in trying to determine the nature of surface layers by analyzing the material after it has been removed from the surface. The technique of studying surface layers by their infrared spectra[4] permits an examination of the surface compounds or adsorbed layers without their removal and so has an obvious advantage for this problem.

Since much of the earlier work has been done on the flotation of galena by potassium ethyl xanthate (KEX), the PbS–KEX system has been chosen for this investigation. It is known that the xanthate ion is attached to the sulfide surface; however, after reviewing the evidence for the existence of lead xanthate at the surface, Gaudin[5] concludes: "These observations do not necessarily indicate that lead xanthate exists as a distinct phase at a xanthated galena surface but they show that the components of lead xanthate are available there." It generally is accepted[5,6] that a xanthate ion cannot directly replace a sulfide ion in lead sulfide, but probably exchanges with a sulfate ion (or some other oxidized sulfur ion), carbonate ion, or hydroxide ion formed on the surface by exposure to the atmosphere. Hagihara,[7] examining the cleavage surface of galena crystal by electron diffraction, identified $PbSO_4$ and Pb_2SO_5. He identified a crystalline carbonate only after long (40-day) exposure to water. In no case did he observe any of the lower sulfoxides, PbS_mO_n, with n/m less than 4. He also reports[8] that the PbS_mO_n surface compounds are removed by washing in distilled water leaving an unoxidized surface.

The work reported here investigates the existence of surface compounds on PbS exposed to air, the effects on these compounds of treatment with KEX solution, and the nature of the surface xanthate which is formed.

Experimental Details

Preparation of PbS.—The fact that PbS absorbs in the infrared limits the amount of this material which can be used in a transmission sample. As the particle size of the PbS is reduced, the greater surface-to-volume ratio of the particles permits a greater ratio of surface compound absorption to PbS absorption. In addition, the energy lost due to scattering becomes less as the particle dimensions become small compared to the infrared wave lengths employed. Fine PbS was precipitated in hot basic solution by homogeneous precipitation with thioacetamide and lead acetate. The precipitate was filtered, washed in distilled water, and dried in a vacuum desiccator.

Surface Area Determination.—The surface areas of the PbS samples were determined by a continuous-flow nitrogen adsorption method[9] in a modified apparatus which will be described elsewhere.[10]

Xanthate Preparation and Treatment.—Potassium ethyl xanthate from American Cyanamide Company was purified by washing with ether, dissolving in acetone, and extraction with ether. The xanthate was used within three weeks after purification. For xanthate treatment, 500 mg. of PbS was placed in 50 ml. of distilled water containing 250 mg. of KEX, and stirred for 1 hr. The PbS was filtered out and enough material for a sample was air-dried on filter paper.

Infrared Spectra.—Samples were made into KBr pellets by grinding 5 mg. of PbS with 700 mg. of KBr in a hand mortar, then pressing the powder in an evacuated die. Spectra were scanned on a Perkin–Elmer Model 21 spectrometer as soon as the various treatments were completed.

Results and Discussion

Spectrum of Adsorbed Xanthate.—Figure 1 shows the spectra of KEX, $Pb(EX)_2$, and PbS which has been treated with a KEX solution. Recent investigators[11,12] disagree on the assignments of the xanthate bands in the 1000 to 1200 $cm.^{-1}$ region, although they agree that the bands represent C=S and C–O–C stretching modes.

(1) A. M. Gaudin, "Flotation," McGraw-Hill Book Co., Inc., New York, N. Y., 1957, Chapt. 9.

(2) K. L. Sutherland and I. W. Wark, "Principles of Flotation," Australasian Institute of Mining and Metallurgy, Inc., Melbourne, 1955, pp. 102–112.

(3) P. L. deBruyn, "The Chemical Theory of Flotation, Mineral Engineering Techniques," American Institute of Chemical Engineers, New York, N. Y., 1954, pp. 12–14.

(4) R. P. Eischens and W. A. Pliskin, "Advances in Catalysis," Vol. 10, Academic Press, Inc., New York, N. Y., 1958, pp. 1–56.

(5) A. M. Gaudin, ref. 1, p. 236.

(6) K. L. Sutherland and I. W. Wark, ref. 2, p. 110.

(7) H. Hagihara, *J. Phys. Chem.*, **56**, 610 (1952).

(8) H. Hagihara, *ibid.*, **56**, 616 (1952).

(9) F. M. Nelsen and F. T. Eggertsen, *Anal. Chem.*, **30**, 1387 (1950).

(10) R. J. Jasinski and J. R. Huff, to be published.

(11) L. H. Little, G. W. Poling, and J. Leja, *Can. J. Chem.*, **39**, 745 (1961); **39**, 1783 (1961).

(12) M. L. Shankaranarayana and C. C. Patel, *ibid.*, **39**, 1633 (1961).

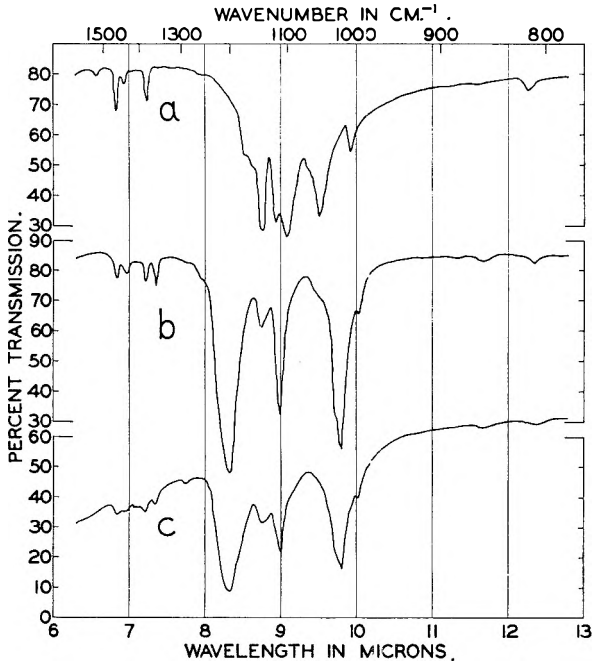

Fig. 1.—Spectra of (a) KEX, (b) $Pb(EX)_2$, and (c) PbS which has been treated in KEX solution.

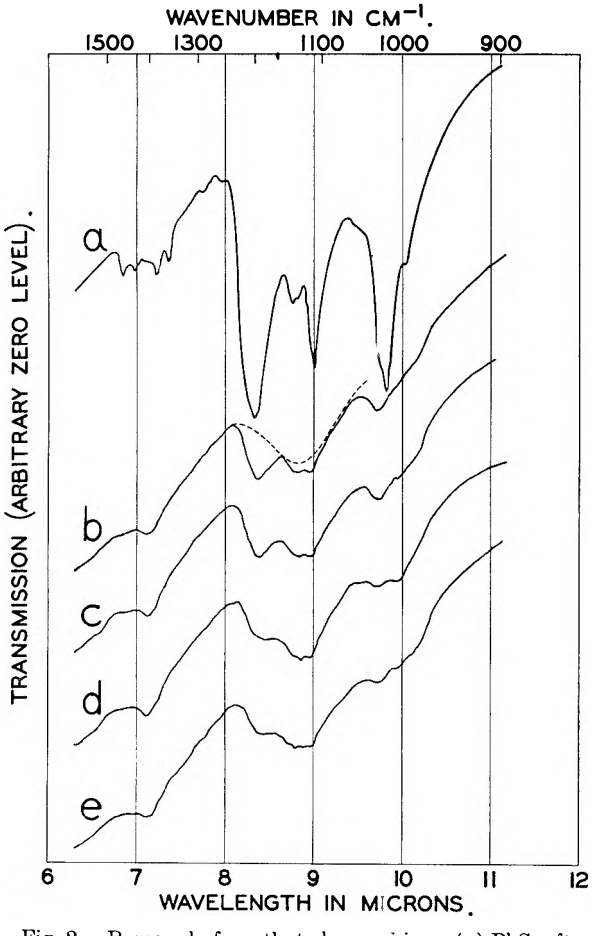

Fig. 2.—Removal of xanthate by washing: (a) PbS, after treatment with KEX solution; (b) after one wash in acetone; (c) after two washes; (d) after four washes; (e) after six washes. Spectrum (b) shows (dashed) the remaining absorption band after the xanthate spectrum is subtracted.

Without an exact assignment it is quite clear, however, that the surface coating on the PbS particles has a spectrum which agrees in detail with that of $Pb(EX)_2$ and is significantly different from KEX.

Dissolution of Surface Xanthate Compounds.—$Pb(EX)_2$ is quite soluble in acetone. Figure 2 shows the spectra of PbS samples which were treated with an excess of KEX and then treated to different numbers of acetone washes. An acetone wash consists of stirring the material for 12 min. in 100 ml. of acetone. This washing procedure is sufficient to dissolve a weight of $Pb(EX)_2$ equal to the total sample weight (PbS + surface xanthate) in 5 min. Such an amount exceeds by a factor of 10 the maximum amount of surface xanthate present in any sample. Superimposed on the xanthate spectrum in Fig. 2 are some broader absorption bands which will be discussed later. It is seen that the xanthate concentration decreases rapidly with the first wash but that an easily detectable amount remains even after six washes. Figure 3 shows, on the left ordinate scale, the amount of surface xanthate (calculated as moles of $Pb(EX)_2$ per 6-mg. sample of PbS) remaining after various numbers of acetone washes. The amount is determined by comparison with reference spectra of $Pb(EX)_2$ of known concentration. The ordinate scale at the right expresses this concentration in terms of the number of xanthate ions present for each lead atom in the surface of the PbS. This conversion is made, assuming that the density of lead atoms in the surface is the same as that in the (100) face of a PbS crystal, and using the measured value of 2.8 $m.^2$ per g. for the surface area of this batch of PbS. From the results of his electron diffraction experiments, Hagihara[8,13] concludes that the arrangement of xanthate ions on the surface of a PbS crystal is the same as the arrangement of the lead (or sulfur) atoms. If this result is accepted, it follows that a monolayer of surface xanthate consists of one xanthate ion per surface lead atom, and the ordinate scale on the right of Fig. 3 also may represent the number of layers of xanthate ion on the surface of the PbS. It is seen that, initially, an amount of xanthate corresponding to several layers is present. With the first acetone wash almost 90% of this xanthate is removed; after several washes the amount remaining corresponds to roughly a monolayer of xanthate ions. It is significant that both the easily removed xanthate and the more tightly bound xanthate have the spectrum of $Pb(EX)_2$. The data of Fig. 3 would suggest that more than just the surface monolayer of the PbS have taken part in the reaction with the xanthate solution; xanthate ions have replaced anions in several layers at the PbS surface. The identity of these displaced anions is discussed in the following section.

It is suggested that the easily removed xanthate is $Pb(EX)_2$ but that the remaining monolayer is

(13) H. Hagihara, H. Uchikoshi, and S. Yamashita, "Proceedings of the Second International Congress of Surface Activity," Vol. 3, Butterworths Publications, London, 1957, p. 343.

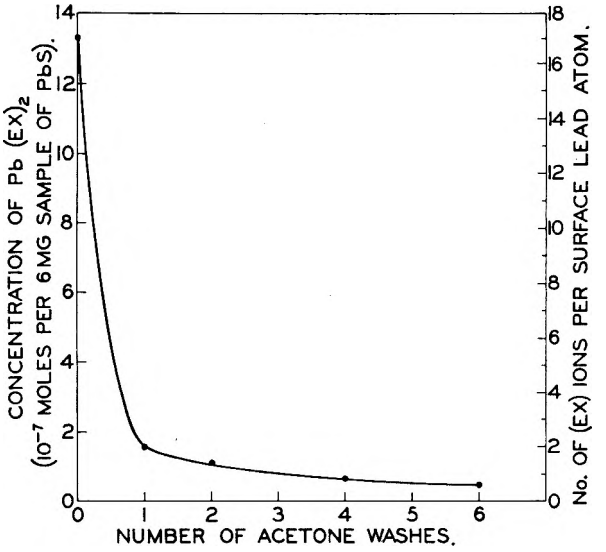

Fig. 3.—Concentration of surface xanthate remaining on PbS after being washed with acetone.

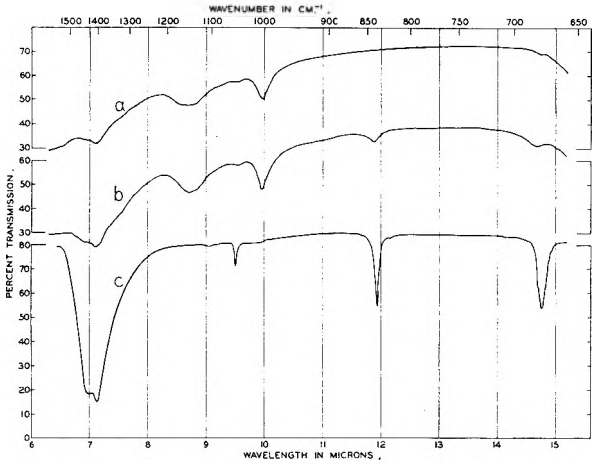

Fig. 4.—Spectra of surface compounds formed on PbS after different aging treatments: (a) stored in vacuum desiccator for 90 hr. after preparation and (b) stored in CO_2 for 90 hr. after preparation. (c) reference spectrum of $PbCO_3$.

bound to the surface as

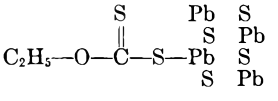

Except for some low frequency, skeletal vibrations, the infrared spectrum of such a surface compound might be expected to closely resemble that of $Pb(EX)_2$ which has the structure

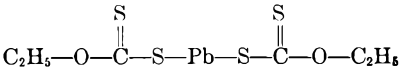

In both cases the structure involves xanthate ions attached to lead atoms which are in turn attached to sulfur atoms, the sulfur atoms belonging to the PbS lattice in one case and to a xanthate ion in the other case.

The proposed surface xanthate structure would satisfy the two experimental observations that the compound has a xanthate ion attached to a lead ion (from the spectrum of the surface compound) and also that it is tenaciously bound to the PbS surface.

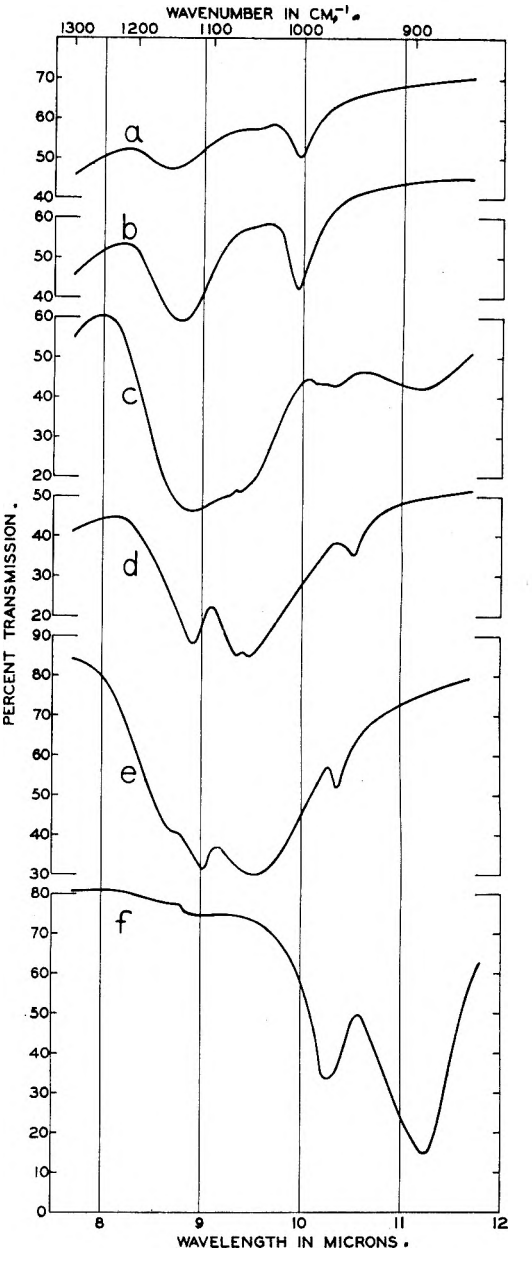

Fig. 5.—Spectra of surface compounds formed on PbS after various aging treatments: (a) stored in vacuum desiccator for 90 hr. after preparation; (b) stored in O_2 atmosphere for 90 hr.; (c) held at 150° in air for 6 hr.; (d) held at 150° in O_2 atmosphere for 6 hr. Reference spectra of (e) $PbSO_4$ and (f) $PbSO_3$.

Surface Compounds on PbS.—Several absorption bands appear in the spectrum of this small-particle-size PbS which vary with sample treatment and can be ascribed to surface compounds. Figure 4 shows the spectrum, A, of PbS which was stored in a vacuum desiccator for 90 hr. after preparation. Spectrum B shows the effect of storing some of the freshly-prepared PbS in an atmosphere of CO_2 for 90 hr. With this treatment certain of the bands are intensified; in fact, each band which appears in the reference spectrum, C, of $PbCO_3$ appears stronger after CO treatment, while the others remain relatively unchanged. It is concluded that

the 1400 cm.$^{-1}$ band is a $PbCO_3$ band along with the weaker bands at 1050, 840, and 680 cm.$^{-1}$.

Portions of the spectra of four samples of PbS are shown in Fig. 5 along with reference spectra of $PbSO_4$ and $PbSO_3$. Spectra A and B are from the same batch of PbS, part of which was stored for 90 hr. in a vacuum desiccator while the other was sealed in a tube of O_2 for 90 hr. C and D were from samples which were, respectively, heated in air to 150° for 6 hr. and sealed in a tube of O_2, heated to 150° for 6 hr.

The intensities of the bands in B were increased over those of A by aging in O_2. These same bands remained relatively unchanged from those shown in A in the spectrum (not shown) of a sample aged in N_2. Aging at 150° in O_2 gives a spectrum, D, which looks very much like $PbSO_4$. In addition to absorption bands in the $PbSO_4$ region, the sample aged at 150° in air, C, shows absorption bands characteristic of $PbSO_3$. It is concluded that all of these bands arise from sulfur ions in various states of oxidation. It is difficult to determine the exact structure associated with each of these bands since one would expect that sulfur–oxygen compounds may form on the surface of a PbS lattice structure which are not stable compounds in a free state.

The carbonate bands can be produced by several treatments; *e.g.*, extended washing in distilled water (where they probably form from dissolved CO_2), heating in air, or exposure to CO_2. Unlike the sulfur–oxygen bands, the carbonate bands show very little difference in position when produced under different conditions. This may reflect the fact that the sulfur atom is part of the PbS lattice and may exist at the surface in a variety of states (at corners, edges, plane surfaces, and surface steps of the crystal lattice) while the carbon atom is not a part of the lattice. The differences in the environment of the Pb atoms at different locations on the PbS surface will show only a small effect on the bands in the spectral region examined here. The Pb–C vibration would be expected to occur at lower frequencies; the vibrations in the region shown here predominantly involve the carbonate ion.

Interaction between Xanthate and Other Surface Compounds.—After the PbS sample has been treated with KEX, absorption bands of the surface xanthate are superimposed on the large sulfur–oxygen band at 1130 cm.$^{-1}$, and on the carbonate band at 1400 cm.$^{-1}$. It would be of interest to measure the concentration of CO_3 and S_mO_n ions on the surface of PbS both in the presence and in the absence of the surface xanthate. The most intense band in the xanthate spectrum at 1200 cm.$^{-1}$ is located where there is little absorption by the other surface compounds. The intensity of this band may be used to determine the concentration of xanthate present by reference to spectra of known xanthate concentrations. Once the xanthate concentration is known, its spectrum may be subtracted from the sample spectrum leaving the absorption bands of the other surface compounds to be measured. See, for example, Fig. 2B. In some cases there is a small amount of S_mO_n absorption at the 1200 cm.$^{-1}$ xanthate band. Once the general shape of the S_mO_n band is known, a correction can be made to the determination of the concentration of surface xanthate. The resulting correction to the calculated peak absorption of the S_mO_n or CO_3 compounds usually is quite small.

A sample of PbS which had been stored in a vacuum desiccator for five days after preparation was treated with a KEX solution and then given an acetone wash. Another portion of the same material, used as a control, was treated similarly with water and given an acetone wash. After each step, the spectrum of a sample was obtained and the absorption of the surface compounds was calculated. The same procedure was repeated with a portion of the sample which was aged at 150° for 6 hr. in air. Using reference spectra, the absorption can be converted to concentration; however, no reference spectra are available for some of the sulfur–oxygen compounds observed on the surface. To get an approximate idea of the concentration of these substances involved, the absorption at 1130 cm.$^{-1}$ was converted to a concentration by assuming: (a) the sulfur–oxygen compound has the same peak absorption as $PbSO_4$ and (b) the peak absorption is the same as that of $PbSO_3$. The concentration then was expressed as the number of adsorbed ions per surface lead atom using the measured values of surface area. Table I shows these concentrations after the various treatments. The surface areas measured for the PbS samples of Table I are 7.7 m.^{2} per g. for the first sample and 4.3 m.^{2} per g. for the sample heated in air for 6 hr.

Several things can be seen from the data in Table I. CO_3 ions are removed by xanthate treatment and are added by water treatment for the PbS samples with either aging treatment. S_mO_n ions remain relatively unaffected in the first (lightly oxidized) sample but are removed from the second (heavily oxidized) sample by xanthate treatment. For either sample, the S_mO_n concentrations in the control samples remain about constant with water and acetone washes. The amount of surface xanthate produced by KEX treatment is greater in the case of the heavily oxidized sample. In each case, the amount of xanthate remaining after the acetone wash is calculated to be about a monolayer, although quite different amounts are present before the acetone wash. It is of interest to note that in this experiment a significant amount of CO_3 and S_mO_n ions is left even after the treatment with KEX.

The data in Table I would seem to be consistent with the view that xanthate ions do displace CO_3 ions and, in some cases, S_mO_n ions from the surface layers of PbS. From this data, no ion exchange balance is evident. Although both samples show the same low CO_3 ion concentration after xanthate treatment, it may be that, during treatment in the KEX solution, more carbonate is produced on the surface by reaction with CO_2 dissolved in the water (as in the case of the control samples) and then removed by exchange with xanthate ions. No attempt was made in these experiments to

TABLE I

CONCENTRATION OF SURFACE COMPOUNDS AFTER VARIOUS TREATMENTS (NUMBER OF ADSORBED IONS PER SURFACE LEAD ATOM)

	Sample				Control		
	CO_3	SmO_n calcd. as either SO_4 or SO_3		EX	CO_3	SmO_n calcd. as either SO_4 or SO_3	
Before treatment	0.9	0.7	0.4		0.9	0.7	0.4
After KEX treatment (water treatment for control)	.2	.9	.5	4.8	1.5	.9	.6
After acetone wash	.2	.7	.4	1.2	1.7	.9	.6
PbS sample heated in air to 150° for 6 hr.							
Before treatment	1.9	12.0	7.6		1.9	12.0	7.6
After KEX treatment (water treatment for control)	0.4	4.4	2.6	33.4	3.6	13.3	8.4
After acetone wash	.5	2.1	1.4	1.3	3.1	11.2	7.1

measure surface OH ion exchange. Such measurements might be possible but would call for special precautions in drying PbS samples and in excluding atmospheric moisture picked up by the KBr while the sample pellets are made. Both of these factors would have to be examined to determine an ion balance.

Acknowledgments.—The author wishes to thank Mr. Robert J. Wagner, Mr. Edwin S. Rousseau, and Mr. Donald F. Lowe for helpful discussions and aid in the preparation of samples, and Dr. James R. Huff and Dr. Raymond J. Jasinski for making the surface area measurements.

THE SLIDING OF LIQUID DROPS ON SOLID SURFACES

BY DOUGLAS A. OLSEN, POWELL A. JOYNER, AND MARVIN D. OLSON

Minneapolis-Honeywell Research Center, Hopkins, Minnesota

Received November 6, 1961

The equations for predicting the tilt angle at which a liquid drop begins to slide on an inclined solid surface have been developed. The validity of these equations has been verified experimentally.

Introduction

The sliding motion of liquid drops on inclined surfaces originally was studied by Frenkel.[1] In this study Frenkel reported an equation which would predict the angle, α, at which a liquid drop would begin to slide down an inclined surface. The equation is

$$mg \sin \alpha = w(\gamma_{LV} + \gamma_{SV} - \gamma_{SL}) \qquad (1)$$

where

m = mass of the liquid drop
g = gravitational acceleration
α = tilt angle
w = maximum width of the contact area between the drop and the surface
γ_{LV} = liquid–vapor interfacial tension
γ_{SV} = solid–vapor interfacial tension
γ_{SL} = solid–liquid interfacial tension

The expression $(\gamma_{LV} + \gamma_{SV} - \gamma_{SL})$ in the right-hand side of eq. 1 is recognizable immediately as the reversible work of adhesion.

In a later study Aron and Frenkel[2] determined from eq. 1 values for the reversible work of adhesion of liquid drops on several different surfaces. They also showed that in order for a liquid drop to slide down an inclined surface the following inequality must be true (since sin α cannot be greater than unity)

$$m > \frac{wE_a}{g} \qquad (2)$$

where E_a = reversible work of adhesion.

(1) Ya. I. Frenkel, *Zhur. Eksptl. i Teoret. Fiz.*, **18**, 659 (1948).
(2) Ya. B. Aron and Ya. I. Frenkel, *ibid.*, **19**, 807 (1949).

In the entire study, however, no definitive experimental verification of eq. 1 was given.

In the present study it has been shown that the previous conclusions can be expanded upon so as to permit estimation of tilt angles from readily measurable quantities. The equations which are developed also are experimentally verified.

Theory

If it is assumed that the entire initial resistance to sliding of the liquid drop is at the rear of the drop, then eq. 1 can be derived. Consider a liquid drop on an inclined plane surface (Fig. 1). Assume the drop will begin to move at an angle, α, where the accelerating force exceeds the retarding force at the rear of the drop. From Fig. 1 the work, dW, at the rear of the drop due to the retarding force, f_R, acting through a distance, ds, is given by

$$dW = f_R\, ds \qquad (3)$$

At the trailing edge of the liquid drop a new liquid surface and a new solid surface are formed and the interfacial surface is destroyed (or more rigorously there is exposure of liquid–vapor and solid–vapor interfaces and destruction of a solid–liquid interface). Consequently the work done at the rear of the drop as an area dA of the solid surface becomes exposed can be given by

$$dW = (\gamma_{LV} + \gamma_{SV} - \gamma_{SL})dA \qquad (4)$$

Since $dA = w\, ds$ where w is the width of the drop and since eq. 3 and 4 may be equated, the retarding force is given by

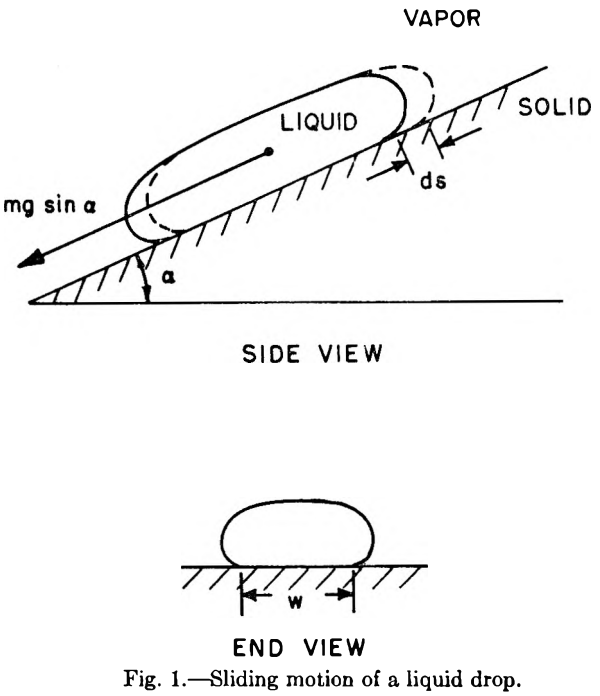

Fig. 1.—Sliding motion of a liquid drop.

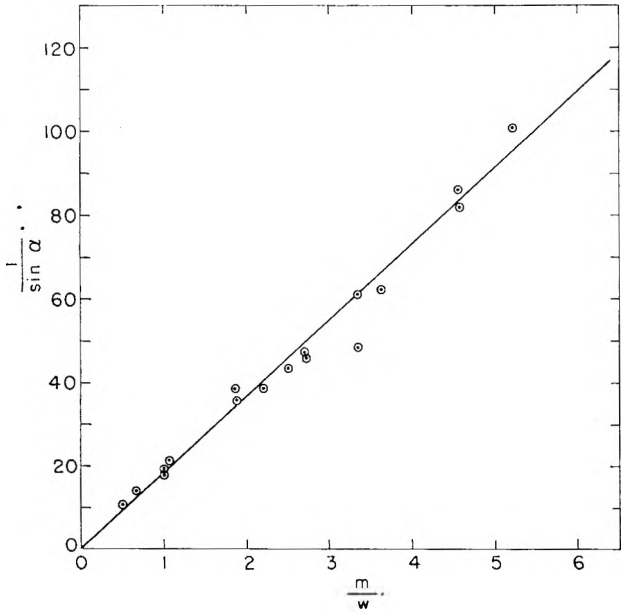

Fig. 2.—Graph of m/w vs. $1/\sin \alpha$ for water drops sliding on polytetrafluoroethylene.

$$f_R = \frac{(\gamma_{LV} + \gamma_{SV} - \gamma_{SL})w\ ds}{ds} = (\gamma_{LV} + \gamma_{SV} - \gamma_{SL})w \quad (5)$$

Equation 5 for the retarding force also can be equated with the accelerating force $mg \sin \alpha$ to give

$$mg \sin \alpha = w(\gamma_{LV} + \gamma_{SV} - \gamma_{SL}) \quad (6)$$

which can be solved to give α, the angle at which the drop begins to slide on the inclined surface.

Data are not generally available for solid–vapor, γ_{SV}, and solid–liquid, γ_{SL}, interfaces; however, they are related by the theoretical relation[3]

$$\gamma_{SV} = \gamma_{SL} + \gamma_{LV} \cos \theta \quad (7)$$

where θ = equilibrium contact angle. If eq. 7 be substituted in eq. 6 then

$$mg \sin \alpha = w\gamma_{LV}(1 + \cos \theta) \quad (8)$$

The often used expression $\gamma_{LV}(1 + \cos \theta)$ which appears in eq. 8 is rigorously true only if one can neglect the adsorption of the liquid vapor upon the solid surface.[4] However, this should be a good approximation for the case of water in contact with low energy solid surfaces such as polytetrafluoroethylene (Teflon)and polyethylene.

Thus, it has been demonstrated that the tilt angle, α, at which the drop begins to slide can be calculated if values are available either for $(\gamma_{LV} + \gamma_{SV} - \gamma_{SL})$ or for $\gamma_{LV}(1 + \cos \theta)$, which are expressions for the reversible work of adhesion, E_a. However, the latter expression is only applicable within the limitations discussed in the previous paragraph. Equation 8 is of considerable importance in that it allows measurements of the equilibrium contact angle, θ, to be made on a flat surface and then to be applied to the prediction of the tilt angle, α.

Equations 6 and 8 can be stated more generally by

$$mg \sin \alpha = wE_a \quad (9)$$

Thus, the work of adhesion also is related to the tilt angle.

The general validity of eq. 6 and 8 can be tested by the behavior of a series of liquid drops of different size sliding on a given surface. This is discussed further in the following sections.

As noted earlier the preceding equations predict the tilt angle at which the drop begins to slide. Several authors[5,6] have investigated sliding drops and have derived appropriate equations for drops already in motion at any given tilt angle. Other authors[7] have described the minimum tilt angle in terms of parameters which are not easily measured. However, there is no provision in any of these equations for predicting the minimum tilt angle from simple measurements.

Experimental Procedure

Three cases were chosen for investigation, water on polytetrafluoroethylene (Teflon), glycerol on polytetrafluoroethylene, and water on polyethylene.

Materials.—The polymers used were thin translucent sheets about 0.025 in. thick. The sheets were mounted in shallow troughs with lined paper beneath them to facilitate measurement of drop dimensions. The polymer sheets were rinsed in a chromic acid cleaning solution followed by an aqueous cleaning solution of "Alconox" detergent. The sheets then were rinsed in distilled water. Several sheets were cleaned only in "Alconox" solutions; no apparent differences in tilt angles were observed.

The liquids used were water and reagent grade glycerol. The surface tensions of each were determined using the sessile drop method[8] on Teflon. Our experimental values all were within 1% of the accepted value of 72.75 dynes/cm. for water and within 2.5% of the accepted value of 63.4 dynes/cm. for glycerol.

Procedure.—The inclinometer for measuring tilt angles was constructed of the following components: light source,

(3) T. Young, *Trans. Roy. Soc.* (London), **95**, 65 (1805).

(4) D. H. Bangham and R. I. Razouk, *Trans. Faraday Soc.*, **33**, 1463 (1937).

(5) G. Macdougall and C. Ockrent, *Proc. Royal Soc.* (London), **180A**, 151 (1942).

(6) K. Kawasaki, *J. Colloid Sci.*, **15**, 402 (1960).

(7) E. Baer and T. F. McLaughlin, *J. Appl. Polymer Sci.*, **5**, 240 (1961).

(8) A. M. Worthington, *Phil. Mag.*, **20**, 51 (1885).

lens (focal length 1 m.), ½ in. diameter mirror with cross hairs, graduated scale with increments of 3 min. which could be estimated to 1 min., and tilting plate. Located axially with the plate, the mirror reflects its cross hairs onto a scale to give direct readings of the tilt angle. The trough lined with the polymer sheet was placed on the tilting plate. A known volume of the appropriate liquid was added to the trough and the plate then was tilted through the necessary angle to obtain sliding of the drop at constant velocity. The tilt angle was observed with an accuracy of ±1 min.

All data were observed in a room thermostated at 70°F. The relative humidity range was 38 ± 2%.

Results and Discussion

Representative data for each system are given in Fig. 2, 3, and 4. In each case several sets of measurements were made to determine that the data were reproducible. The values for the observed tilt angle, α_{obs}, were determined directly from the inclinometer discussed in the previous section.

Equation 8 predicts that a graph of m/w plotted *vs.* $1/\sin\alpha$ for a series of drops of different size on a given surface should give a straight line through the origin with a slope of

$$\frac{\gamma_{LV}(1 + \cos\theta)}{g} \qquad (10)$$

From Fig. 2, 3, and 4 it is seen that a straight line does result which indicates a verification of the theory discussed above.

As further verification of the theory the contact angles have been calculated from eq. 10 and are shown in Table I along with the observed contact angles. There is excellent agreement for water and glycerol on polytetrafluoroethylene. Somewhat poorer agreement is obtained for water on polyethylene; however, this could be expected since eq. 8 neglects the adsorption of the liquid vapor upon the solid surface and its consequent effect upon the angle.[9] In this instance better agreement is obtained by considering eq. 6. Normally eq. 6 gives intractable results, since values usually are not available for the surface tension of the solids, γ_{SV}, and the interfacial tension, γ_{SL}. However, the difference between these quantities can be determined. From eq. 6 and the graphs of m/w *vs.* $1/\sin\alpha$ the resulting straight line has a slope of

$$\frac{\gamma_{LV} + \gamma_{SV} - \gamma_{SL}}{g}$$

which can be solved to give $(\gamma_{SV} - \gamma_{SL})$.

For polyethylene and water, $(\gamma_{SV} - \gamma_{SL})$ was found to be −29.9 dynes/cm.

In a few limited cases, direct estimations of these quantities are now possible. Fox and Zisman[10] have developed the concept of the critical surface tension, γ_C, of a solid which is the best estimate available at the present time for the surface tension of a solid, γ_{SV}. They found a value of 30 dynes/cm. for polyethylene. This value, along with an interfacial tension of 55.6 dynes/cm.[11] between high molecular weight hydrocarbons and water, permits an estimation of $(\gamma_{SV} - \gamma_{SL})$ for the polyethylene–water system. A value of −25.6 dynes/cm. was obtained, which is in good agreement with the value of −29.9 dynes/cm. obtained graphically.

TABLE I
CALCULATED AND OBSERVED CONTACT ANGLES

Liquid/solid	θ_{calcd}	θ_{obsd}
Water on polytetrafluoroethylene	105°	103 ± 2°
Glycerin on polytetrafluoroethylene	98°	100 ± 2°
Water on polyethylene	114°	96 ± 2°

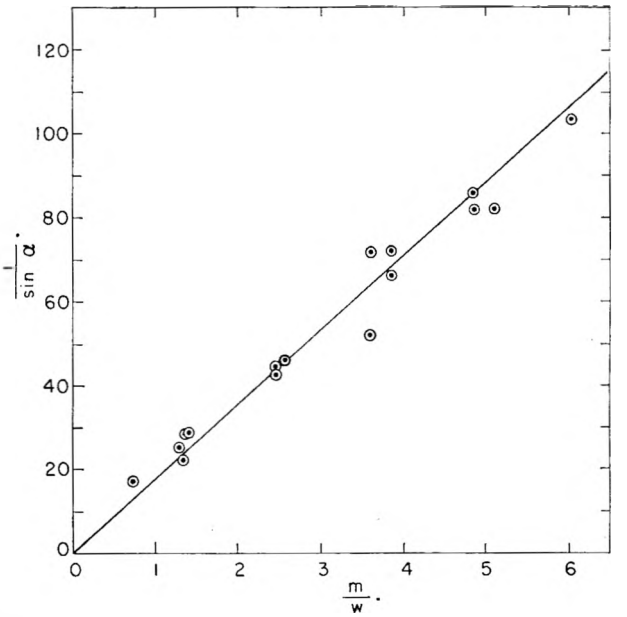

Fig. 3.—Graph of m/w *vs.* $1/\sin\alpha$ for glycerol drops sliding on polytetrafluoroethylene.

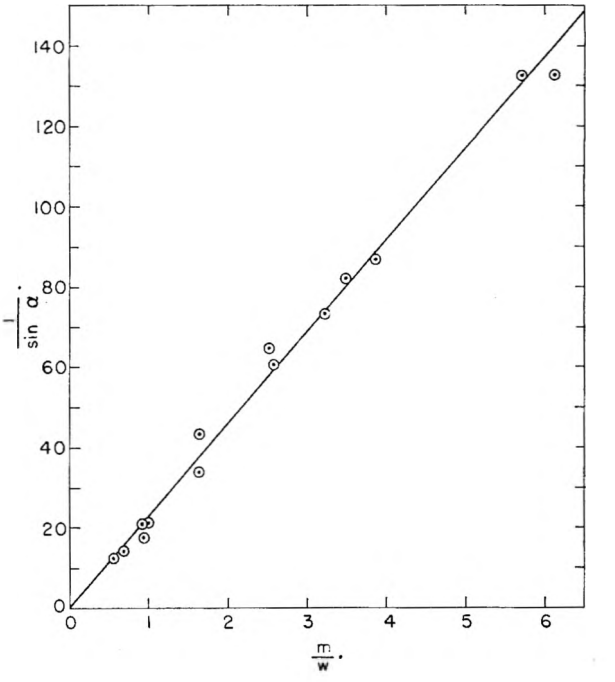

Fig. 4.—Graph of m/w *vs.* $1/\sin\alpha$ for water drops sliding on polyethylene.

(9) An alternate explanation may be found in the fact that, as shown by A. J. G. Allan (*J. Polymer Sci.*, **38**, 297 (1959)), surface oxidation increases the wettability of polyethylene. Increased wettability will reduce the observed contact angle. Since the polyethylene used in this study was rinsed in chromic acid cleaning solution, surface oxidation probably occurred which could account for the low contact angle.

(10) H. W. Fox and W. A. Zisman, *J. Colloid Sci.*, **7**, 428 (1952).

(11) D. J. Donahue and F. E. Bartell, *J. Phys. Chem.*, **56**, 480 (1952).

In conclusion it has been shown that the equations developed in the previous sections predict linear plots of m/w *vs.* $1/\sin\alpha$. This has been shown to be experimentally true. As a further verification of theory the observed and calculated values of the contact angles were shown to be in generally good agreement. The calculated and estimated values of $(\gamma_{SV} - \gamma_{SL})$ were shown to be in good agreement for the polyethylene–water system. Thus, the predicted results are consistent with those observed.

Acknowledgment.—The authors wish to thank Professor George Gubareff for his aid in translating references 1 and 2.

ARSENIC(III)–ARSENIC(V) EXCHANGE REACTION IN HCl SOLUTIONS[1]

BY LEWIS L. ANDERSON[2] AND MILTON KAHN

Department of Chemistry, The University of New Mexico, Albuquerque, N. M.

Received November 10, 1961

A measurable exchange has been observed between As(III) and As(V) in 10.8 to 12.6 *f* HCl at 29.7°, and in 10.9 *f* HCl at 48.6 and 67.3°. Complex exchange curves were observed at each temperature. The complexity is attributed to the slow interconversion, *via* hydrolytic reactions, among two or more forms of As(V) which exchange at different rates with As(III). Spectrophotometric studies revealed that As(V) species in 10.9 *f* HCl were not in chemical equilibrium even after 19.3 days of aging at room temperature. There is spectrophotometric evidence for the existence of polymeric forms of As(V) in 10.9 *f* HCl.

Introduction

This paper deals with the As(III)–As(V) exchange in HCl solutions. In the course of a study of the "hot atom" chemistry of arsenic, Maly and Simanova[3] observed exchange on heating a mixture of As(III) and As(V) in concentrated HCl. We have observed an easily measurable exchange at 29.7, 48.6, and 67.3° in 10.9 *f* HCl. This exchange, however, is generally complex; that is, the exchange curves are not straight lines. This system is complicated further by the slow attainment of chemical equilibria at room temperature among species of As(V) over several weeks as evidenced by the dependence of exchange curves on the age of the As(V) solutions. Spectrophotometric studies corroborated this aging phenomenon and revealed an extreme dependence of the equilibria among As(V) species on the HCl concentration. Although the data presented here do not permit the postulation of a mechanism for exchange, we are able to report a number of interesting observations which point up the complexity of this system.

Experimental

Tracer.—The 17.5-day As^{74} tracer was obtained from Abbott Laboratories, Oak Ridge, in the form of high specific activity sodium arsenate solution. This solution was made 11 to 12 *f* in HCl and distilled in a stream of Cl_2 to one-fourth its original volume (~20 ml.). Excess Cl_2 was removed from the cooled residue by either a stream of nitrogen or the addition of excess powdered $FeCl_2 \cdot 4H_2O$. The residue then was saturated with HCl at 0° and rapidly distilled for 2 min.; the distillate was received in 5 ml. of 12 *f* HCl at 0° and served as the stock solution of high specific activity As(III).

The As(III) tracer solutions used in runs 1–8 were prepared by inoculation of inactive As(III) solutions and used directly; for subsequent runs, the inoculated As(III) was oxidized, reduced, and distilled as described above.

The As(V) tracer solutions were prepared by exchange in 10.9 *f* HCl between inactive As(V) and high-specific-activity As(III) at 95° for 4 hr. in a sealed Pyrex tube.

To test for radiochemical purity, a sample of purified high-specific-activity As(III) was sealed in a test-tube and counted from time to time, over at least 5 half-lives of As^{74}, on a scintillation counter. The decay curves contained 17.5- and 71-day components which correspond to 17.5-day As^{74} and 76-day As^{73}. Also, the specific activity of an aliquot of an inoculated As(III) solution was within 2% of that of an aliquot subjected to oxidation, reduction, and distillation.

Reagents and Analyses.—The HCl solutions were prepared by dilution of Analytical grade 37% HCl with doubly-distilled water.

The As(III) stock solutions were prepared by dissolving C.P. As_2O_3 in HCl. The solutions were analyzed for As(III) by titrating aliquots with standard $KBrO_3$ solution to the methyl orange end-point in 2.4 *f* HCl.[4]

Stock solutions of As(V) were prepared by dissolving C.P. As_2O_5 in HCl. The As(V) concentration was determined by thiosulfate titration of the iodine liberated from KI by aliquots of the solution.[5]

All stock solutions except those used in runs 1–4 were stored at room temperature under the normal fluorescent light of the laboratory; the solutions used in runs 1–4 were stored in the dark.

Chloride analyses were performed by a modified Volhard method.[6]

The acid concentration of a stock solution was calculated from the concentrations of As(III) or As(V) and total chloride assuming that As(III) and As(V) exist in these solutions as $AsCl_3$ and $AsCl_6^-$, respectively. It is noteworthy, however, that whereas >98% of As(III) should exist in 10.9 *f* HCl as $AsCl_3$,[7] there is no evidence for the existence of $AsCl_6^-$.[8] Because the extent of hydrolysis of As(V) in HCl solutions is unknown, the actual HCl concentration of an As(V) stock solution probably was somewhat greater (<2%) than that calculated as described above.

Magnesia mixture was prepared as described by Hillebrand and Lundell.[9]

Nitrogen was scrubbed with water. All other gases were used directly from the tank.

Counting Procedures.—All activities were determined by gamma counting of liquid samples contained in selected

(1) This communication is based on work done under the auspices of the Los Alamos Scientific Laboratory and the Atomic Energy Commission (Contract No. AT (11-1)-733) and submitted in partial fulfillment of the requirements for the degree of Doctor of Philosophy in the Graduate School of the University of New Mexico, June, 1961, by Lewis L. Anderson.

(2) Eastman Kodak Fellow, 1959–1960.

(3) J. Maly and R. Simanova, *Chem. Listy*, **49**, 814 (1955).

(4) I. M. Kolthoff and E. B. Sandell, "Textbook of Quantitative Inorganic Analysis," 3rd ed., The Macmillan Co., New York, N. Y. 1959, p. 606.

(5) D. Ya. Evdokimov, *Med. Prom. S.S.S.R.*, **13**, No. 1, 46 (1959).

(6) I. M. Kolthoff and E. B. Sandell, ref. 4, p. 546.

(7) G. M. Arcand, *J. Am. Chem. Soc.*, **79**, 1865 (1957).

(8) "Gmelins Handbuch Der Anorganischen Chemie," 8th ed., No. 17, Verlag Chemie, GMBH, Weinheim Bergstrasse, 1952, pp. 391, 392.

(9) W. F. Hillebrand and G. E. F. Lundell, "Applied Inorganic Analysis," John Wiley and Sons, Inc., New York, N. Y., 1929, p. 211.

Pyrex test-tubes filled to a standard height and placed in a well-type scintillation detector. All solutions counted to furnish exchange data were of the same density. Except for very low-counting samples, all were counted long enough so that the standard deviation was less than 1%. In order to avoid corrections for decay, all samples for a given exchange run were counted within a few hours. The day-to-day variation in the operational characteristics of the counter was checked by counting a Cs^{137} standard.

Exchange Procedure.—For the runs at 29.7° exchange mixtures were prepared and sampled under a red safe-light. Appropriate portions of stock solutions of HCl, As(V), and As(III) were brought to temperature over at least 2 hr. in a water-bath regulated to ±0.05° and then mixed with the aid of a Teflon-coated magnetic stirring bar in blackened 50-ml. round-bottom flasks. Reaction time was reckoned from the instant the As(III) and As(V) solutions were mixed.

Exchange mixtures for the runs at 48.6 and 67.3° were prepared under ordinary fluorescent light from appropriate portions of stock solutions of HCl, As(V), and As(III) tracer at room temperature; aliquots of a mixture immediately were sealed in *ca.* 1.6-ml. Pyrex tubes which then were wrapped in aluminum foil to exclude light. A minimal air space was left in each tube in order to accommodate expansion of the solution at the reaction temperature. All tubes containing a given exchange mixture were immersed simultaneously in a constant-temperature water-bath; reaction time was reckoned from the time of immersion. The reaction mixtures attained thermal equilibrium within 1 min. as evidenced by thermocouple measurements.

Separation Procedure.—The two oxidation states were separated by precipitation of $MgNH_4AsO_4$ at 0°.[10] In runs 1–4, the volume of the sample withdrawn from the exchange mixture was 10 ml.; in all other experiments the sample volume was 1 ml. The separation procedure described below was applied to 1-ml. samples; except for the volume of reagents, however, the separation procedure was the same for runs 1–4.

For the runs at 48.6 and 67.3° the ampoules were cooled 2 min. in an ice-bath prior to the withdrawal of a 1-ml. sample. Samples from the 29.7°-runs were delivered immediately into 1 ml. of ice-cold concentrated HCl which was approximately 0.05 *f* in As(III) and 0.05 *f* in As(V). This solution was diluted with 2 ml. of ice-cold water and nearly neutralized with 1.5 ml. of ice-cold concentrated NH_4OH. Ten ml. of magnesia mixture then was added; the solution was neutralized with concentrated NH_4OH, treated with an additional 1 ml. of concentrated NH_4OH, and allowed to stand in an ice-bath for 10 to 20 min. The precipitate was filtered through Whatman #50 paper, washed with 2 *f* NH_4OH, and dissolved in hot 4 *f* HCl. The solution was transferred to a counting tube and diluted to a standard height with 4 *f* HCl. The recovery of As(V) as determined from iodometric analyses of As(V) generally ranged from 92 to 100%. In most experiments there was essentially no zero-time exchange, indicating the absence of separation-induced exchange.

In order to check the activity balance, the arsenic in the filtrate from the $MgNH_4AsO_4$ precipitation was precipitated with H_2S, dissolved in NH_4OH, and diluted to a standard height in a counting tube. In general, at least 97% of the activity was recovered.

Spectrophotometry.—All spectra were taken on a Cary Model-PM-14 recording spectrophotometer. Measurements were made in the ultraviolet region (2000 to 3000 Å.) at room temperature. Solutions were contained in 1-cm. glass-stoppered fused silica cells. The reference cell contained HCl of the same concentration as the solution in the sample cell; prior to each measurement, the reference cell was filled with fresh HCl.

Exchange Results

A complex exchange curve typical of this system is shown in Fig. 1. The straight lines represent the short-lived and long-lived components. The results of typical experiments carried out at 29.7° and of all the experiments performed at 48.6 and 67.3° are summarized in Table I. Runs 1–4 suggest that equilibrium among species in at least one

(10) J. Wilson and R. G. Dickinson, *J. Am. Chem. Soc.*, **59**, 1358 (1937).

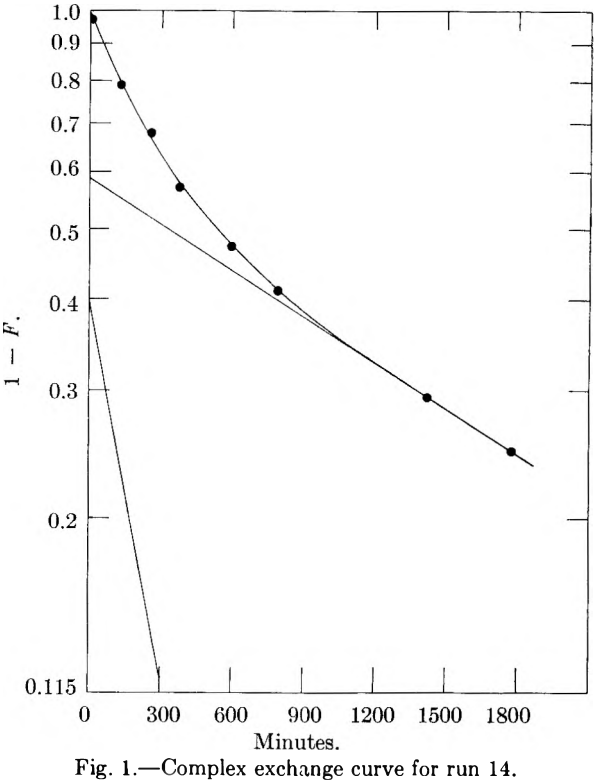

Fig. 1.—Complex exchange curve for run 14.

of the oxidation states of arsenic was not attained even after 7 days of aging at room temperature in 11.2 *f* HCl. From a comparison of runs 5 and 6 with runs 7 and 8, respectively, it was concluded that only As(V) solutions aged.

The reproducibility of experiments at 29.7° is indicated by a comparison of runs 5 and 6 with runs 7 and 8, respectively. Because the degree of hydrolysis of As(V) in these solutions is unknown, it was difficult to prepare stock solutions of As(III) and As(V) of identical HCl concentration on the basis of total chloride and arsenic determination. Therefore, inasmuch as the slow hydrolytic reactions which occur among As(V) species are extremely sensitive to the HCl concentration (see spectrophotometric results) it is doubtful that the reaction mixtures were at chemical equilibrium immediately after preparation and especially during the course of the reaction (at 29.7°) when a small amount of HCl (<1%) was lost through volatilization. The difficulty in preparing reaction mixtures which are at chemical equilibrium is emphasized by the disparity between the results of runs 12 and 21. The essential difference between these runs lies in the preparation of the As(V) stock solution. Thus, the As(V) solution which had been 10.9 *f* in HCl when used in run 12 was found to be 10.7 *f* in HCl the day before run 21 was carried out. Accordingly, at that time the HCl concentration was increased to 10.9 *f* by addition of hydrogen chloride. In this connection it is of interest to compare run 25 with run 29 (also, compare run 31 with run 35); these runs were carried out in sealed tubes to avoid volatilization of HCl. Run 25 was identical with run 29 except that for run 29 both stock solutions had been aged an additional 13 days at 48.6°, cooled, and then used to prepare the reac-

TABLE I

SUMMARY OF EXCHANGE DATA

Run no.	As(III)[a,b] × 10², f	As(V)[b] × 10², f	HCl, f	Temp., °C.	1st Component[c] $t_{1/2}$, min.	2nd Component[d] $t_{1/2}$, min.	Intercept of second component
1	0.490 (1)	1.16 (1)	11.2	29.7	109	17,650	0.44
2	.490 (7)	1.16 (7)	11.2	29.7	140	600	.35
3	.490 (22)	1.16 (22)	11.2	29.7	140	490	.21
4	.490 (42)	1.16 (42)	11.2	29.7	141	491	.21
5	.691 (4)	3.24 (185)	10.9	29.7	198	960	.71
6	.276 (11)	1.61 (192)	10.9	29.7	231	930	.67
7	.691 (19)	3.24 (200)	10.9	29.7	193	1,100	.74
8	.276 (25)	1.61 (206)	10.9	29.7	222	926	.65
9	4.74 (1)	4.18 (56)	10.9	29.7	131	358	.69
10	1.42 (1)	4.18 (56)	10.9	29.7	152	495	.65
11	0.474 (1)	4.18 (56)	10.9	29.7	210	2,863	.42
12	.420 (1)	0.837 (62)	10.9	29.7	418	3,568	.52
13	.420 (1)	8.37 (62)	10.9	29.7	115	558	.57
14	.420 (1)	2.51 (62)	10.9	29.7	176	1,426	.59
15	1.26 (1)	2.51 (62)	10.9	29.7	260	1,860	.40
16[e]	0.231 (1)	0.446 (319)	6.91	29.7	..	...	..
17[e]	.231 (1)	.448 (319)	8.88	29.7	..	...	..
18	.235 (1)	.450 (319)	9.98	29.7	56,640	...	..
19	.233 (1)	.453 (319)	10.8	29.7	450	47,600	0.93
20	.230 (1)	.453 (319)	12.6	29.7	372	22,350	.49
21[f]	.416 (1)	.829 (133)	10.9	29.7	~80	320,000	.94
22[f,g]	.416 (1)	.829 (133)	10.9	29.7	..	320,000	.94
23[f,h]	.416 (1)	.829 (133)	10.9	29.7	..	320,000	.94
24[f]	.132 (2)	0.777 (179)	10.9	48.6	142	2,900	.73
25[f]	.132 (2)	1.55 (179)	10.9	48.6	88	1,160	.81
26[f]	.132 (2)	3.88 (179)	10.9	48.6	320	...	..
27[f]	.264 (2)	1.55 (179)	10.9	48.6	307	1,450	.67
28[f]	.660 (2)	1.55 (179)	10.9	48.6	..	2,220	.96
29[f,i]	.132 (15)	1.55 (192)	10.9	48.6	240	1,265	.74
30[f]	.132 (1)	0.777 (178)	10.9	67.3	69	...	..
31[f]	.132 (1)	1.55 (178)	10.9	67.3	45	...	..
32[f]	.132 (1)	3.88 (178)	10.9	67.3	23	...	..
33[f]	.264 (1)	1.55 (178)	10.9	67.3	~40	~130	~0.47
34[f]	.660 (1)	1.55 (178)	10.9	67.3	~43	~196	~ .70
35[f,i]	.132 (15)	1.55 (192)	10.9	67.3	81	...	..

[a] As(III) was traced in all instances. [b] Number in parentheses indicates age of stock solutions, in days. [c] Short-lived component of complex exchange curve. [d] Long-lived component of complex exchange curve. [e] No measurable exchange was observed in 5 days. [f] For runs 21–35 the As(V) stock solutions had the following history: After 133 days the HCl concentration, which was originally 10.9 *f*, had decreased to 10.7 *f*. At this time the HCl concentration was increased to 10.9 *f* by addition of hydrogen chloride. [g] Exchange reaction conducted under fluorescent light. [h] Exchange mixture was in contact with 0.21 g. of Pyrex glass wool. [i] The As(III) and As(V) stock solutions were aged an additional 13 days at reaction temperature.

tion mixture. The results suggest that the reaction mixtures for runs 25 and 31 were not at chemical equilibrium when brought to reaction temperature. The preparation of reaction mixtures may be complicated further by the existence of polymeric forms of As(V) which dissociate on dilution (see spectrophotometric results). In spite of these difficulties, there was very little scattering of points about any one exchange curve where As(III) tracer was used. Attempts, however, to reproduce several runs using As(V) tracer resulted in such a wide scattering of points in the exchange plots that it was difficult to place a curve among them.

No measurable exchange (see runs 16 and 17) was observed at 29.7° in 6.91 *f* HCl and 8.88 *f* HCl in 5 days. It is noteworthy that other investigators have not observed As(III)–As(V) exchange in alkaline or slightly acidic solutions.[10-12] With increasing HCl concentration the first component of the complex exchange curves becomes more prominent and the half-time decreases (see runs 18, 19, and 20).

From the results of runs 21, 22, and 23, it is concluded that effects due to ordinary fluorescent light and surface area are not appreciable.

Attempts to analyze the data of runs 9–15 according to the procedure applied by Bonner and Goishi[13] to the Sb(III)–Sb(V) exchange in HCl solutions were unsuccessful, as evidenced by the large variation in the calculated values (0.08–0.66) of the fraction of As(V) present in a less-hydrolyzed form. These calculations were based on the assumption that As(III) exchanges with two nonequivalent forms of As(V) which, in turn, are in slow hydrolytic equilibrium; the rate of exchange between As(III) and the more-hydrolyzed form of As(V) was assumed to be zero.

(11) R. Daudel, P. Daudel, and M. Martin, *Compt. rend.*, **219**, 129 (1944).

(12) H. Muller and E. Broda, *Monatsh.*, **82**, 48 (1951).

(13) N. A. Bonner and W. Goishi, *J. Am. Chem. Soc.*, **83**, 85 (1961).

Spectrophotometric Results

This spectrophotometric study shows that there is slow interconversion at room temperature among As(V) species in HCl solutions *via* hydrolytic reactions; there is no evidence for such slow reactions in HCl solutions of As(III).

As(III) in 10.9 *f* HCl.—A shoulder and an absorption band were observed at 2130 and 2550 Å., respectively. The absorbancy at 2130 Å. followed Beer's law over a concentration range from 4.90×10^{-5} to 1.96×10^{-4} *f* As(III) and remained constant over 9 months; the apparent extinction coefficient at this wave length is $12{,}000 \pm 600$ f^{-1} cm.$^{-1}$. The absorbancy at 2550 Å. also remained constant over 9 months but did not follow Beer's law; the absorbancy of a 0.00393 *f* As(III) solution is ~4.5.

As(V) in 10.9 *f* HCl.—Weak absorption bands were observed at 2300 and 2700 Å. The absorbancy at 2700 Å. followed Beer's law over the concentration range from 0.0090 to 0.126 *f* As(V) and remained constant over 9 months; the maximum value of the apparent extinction coefficient at this wave length is ~16 f^{-1} cm.$^{-1}$.

The 2300 Å. band was found to be dependent on the age of the solution. For example, the absorbancy at 2300 Å. of a freshly prepared 0.00410 *f* As(V) solution was 5% of that (0.543) of a 9-months-old solution and gradually increased to 42% in 19.3 days. It is noteworthy that the absorbancy of freshly prepared As(V) solutions increased more rapidly at the shorter wave lengths. The aging process is accelerated by an increase in temperature. Heating a freshly prepared solution of 0.00410 *f* As(V) 1 hr. at 95° increased the absorbancy to within ~54% of a 9-month-old solution. Ordinary illumination does not affect the aging process to any appreciable extent. A 0.00410 *f* As(V) solution, stored in the dark for 19.3 days immediately after preparation, yielded an absorption spectrum identical with that of an aliquot which was exposed for the same time to ordinary fluorescent light.

The 2300 Å. band of 9-month-old As(V) solutions was found to be extremely sensitive to small changes in the HCl concentration. For example, when the HCl concentration of an aged 0.00373 *f* As(V) solution was increased ~1% by the addition of hydrogen chloride, the absorbancy at 2300 Å. increased ~12% in 40 min. and then decreased slowly; after 5 hr. the absorbancy was ~8% higher than that of the original untreated solution. Decreasing the HCl concentration of this solution ~1% with an air stream caused a 33% drop in absorbancy in less than 3 min., an additional 8% drop over 50 min., and a subsequent 8% growth over 5 hr. These results and the aging of freshly prepared As(V) solutions suggest the existence of several As(V) species which are slowly interconverted *via* hydrolytic reactions.

The 2300 Å. band of 9-months-old As(V) solution did not follow Beer's law over a concentration range from 7.45×10^{-4} to 1.86×10^{-2} *f* As(V). Plots of the logarithm of the absorbancy for various wave lengths *vs.* log [As(V)] yield straight lines with different slopes. Thus, at 2200, 2300, 2400, and 2500 Å., the slopes are 1.73, 2.66, 2.63, and 2.17, respectively. The deviation of these slopes from unity indicates the existence of polymeric forms of As(V). In this connection it is noteworthy that there is no evidence for polymers in alkaline solutions of As(V),[14,15] and copolymers of arsenate and phosphate have been reported[16,17] to dissociate in water.

Discussion

The most significant observations and conclusions drawn from this investigation are (1) an easily measurable complex exchange has been observed in 10.8 to 12.6 *f* HCl at 29.7°. No exchange was observed in 5 days at 29.7° in 6.91 and 8.88 *f* HCl. (2) The complexity of the exchange is the result of the existence of at least two As(V) species which are slowly interconverted through hydrolytic reactions. There is no evidence for slow interconversion among As(III) species. (3) As(V) species do not attain chemical equilibrium in 10.9 *f* HCl even after 19.3 days of aging at room temperature. (4) Polymeric forms of As(V) exist in 10.9 *f* HCl.

It is of interest to compare the As(III)–As(V) exchange in HCl solutions with the Sb(III)–Sb(V) exchange, which exhibits complex exchange curves because of slow hydrolytic reactions among Sb(V) species. The Sb(III)–Sb(V) exchange[18] is complex only in the 6.5 to 8.0 *f* HCl region and was easily measurable in HCl concentrations as low as 6.84 *f*. Chemical equilibrium among Sb(V) species in HCl solutions is reached in less than 1 day at room temperature.

Acknowledgments.—We wish to express our appreciation to Dr. J. D. Knight of the Los Alamos Scientific Laboratory for fruitful discussions throughout the course of this work. We also wish to thank the Sandia Corporation Department 5150 for the privilege of using the Cary recording spectrophotometer.

(14) H. Brintzinger and C. Ratanarat, *Z. anorg. u. allgem. Chem.*, **222**, 317 (1935).
(15) H. Brintzinger and C. Ratanarat, *ibid.*, **230**, 28 (1936).
(16) E. Thilo and I. Plaetschke, *ibid.*, **260**, 297 (1949).
(17) E. Thilo and K. Dostal, *ibid.*, **298**, 100 (1958).
(18) C. H. Cheek, N. A. Bonner, and A. C. Wahl, *J. Am. Chem. Soc.*, **83**, 80 (1961).

POISONING EFFECT OF TELLURIDE IONS ON HYDROGEN EVOLUTION AND CATHODIC FORMATION OF HYDROGEN DITELLURIDE

BY S. A. AWAD

Chemistry Department, University College for Girls, Ain Shams Univ., Heliopolis, Cairo, Egypt

Received November 18, 1961

The overpotential phenomena at tellurium cathodes in 0.003–0.02 *N* HCl solutions containing excess lanthanum ions were studied at 30°. The results indicate that the rate-determining step in the formation of hydrogen telluride, H_2Te, at the cathode is the electrochemical dissociation of tellurium molecules, Te_2. Telluride ions were found to behave as a catalytic poison for hydrogen evolution. It is suggested that tellurium forms another hydride, namely, hydrogen ditelluride, H_2Te_2. The standard potentials for Te_2/H_2Te and Te_2/H_2Te_2 equal −0.50 and −0.365 v., respectively.

Introduction

It has been reported that hydrogen telluride is prepared by the electrolysis of acid solutions with tellurium cathodes.[1] However, the overpotential obtained for 0.005–5 *N* HCl solutions suggests that the reaction taking place at tellurium cathodes involves the evolution of hydrogen since the cathode potential, within the current density range studied, always was less negative than the reversible potential for H_2Te formation.[2] To investigate the conditions and the mechanism of formation of this compound, we tried to obtain potentials suitable for its formation by applying the limiting current principle. Therefore, the overpotential at tellurium cathodes in very dilute HCl solutions containing excess neutral salts was studied in the present work.

Experimental

The electrolytic cell, which is similar to that used by Ammar and Awad,[2] was made of an arsenic-free glass known as "Hysil." It consists of three compartments: the anode compartment, the cathode compartment, and a compartment used for electrolytic purification of the solution. A sintered glass disk was inserted between the latter and the cathode compartment in order to minimize the diffusion of gaseous anodic products toward the cathode. Water sealed taps and ground glass joints were used to minimize the diffusion of atmospheric oxygen into the cell.

The electrodes were made of spectroscopically pure tellurium rods (7 mm. diameter), supplied by Johnson and Matthey. A thin tungsten wire was wrapped around one end of the rod. This end was inserted into a clean glass tubing and the glass sealed over the tungsten wire. The glass tubing then was sealed to the piston of a hypodermic syringe, whose barrel was fixed to the top of the cathode compartment of the cell. Each electrode was used to trace one Tafel line only.

The hydrogen was purified by passing it over copper heated to 450° to remove any oxygen. It then was passed over a mixture of MnO_2 and CuO (technically known as "Hopcalite") to oxidize the CO to CO_2, which was removed by soda lime. The purification apparatus, which was made of Hysil glass, was connected to the cylinder by a Polythene tube. A movable glass bridge was used to connect the purification apparatus with the cell.

Analar grade reagents and conductivity water were used. Hydrochloric acid solutions were made up from the constant boiling acid which was prepared by a three-stage distillation of a mixture of HCl and water in an all-glass (Hysil) apparatus. The solutions of lanthanum chloride and potassium chloride contained 100 g. of salt/l. HCl solution.

Before each run, the cell was cleaned with a mixture of nitric and sulfuric acids, followed by thorough washing with water. The cell then was completely filled with water and this water was completely displaced by pure hydrogen. The HCl or NaOH solution then was introduced into the cell and pre-electrolyzed at $10^{-3}-10^{-2}$ amp./cm.^{2} for 20 hr. with a platinum pre-electrolysis electrode. These conditions gave reproducible results within 10 mv. After this preliminary treatment, part of the pure solution was introduced under hydrogen into the cathode compartment. The test tellurium cathode then was adjusted to touch the Luggin capillary in order to avoid the interference of resistance overpotential. The direct method of measurement and the rapid technique were used.[3] The current density was calculated from the apparent surface areas. The current was measured with a multi-range micro-milliammeter and the potential by a valve potentiometer.

A saturated calomel electrode with a saturated KCl bridge was used as a reference electrode. The potential of the hydrogen electrode in the same solution and at the same temperature as the test cathode was measured against the calomel electrode with a salt bridge. The temperature was maintained at 30° with an air thermostat controlled to ±0.5°.

Results

In this investigation the overpotential at tellurium cathodes was measured at 30° in 0.003–0.02 *N* HCl solutions containing excess lanthanum chloride. Potassium chloride which was used in some cases gave almost exactly the same results. The Tafel line was traced from 10^{-6} to 10^{-2} amp./cm.^{2} and then traced again in the reverse direction. Each result included in this investigation is the mean of six individual values (with six different electrodes in six runs), which agree within 10 mv.

Figures 1, 2, and 3 show the results obtained in 0.003, 0.005, and 0.02 *N* HCl. It is clear from these figures that the overpotential values exhibit a Tafel relation only within a certain current density range (curve I). At a certain current density depending on the acid concentration, a sudden numerical increase in the overpotential is observed, after which the overpotential values fit another straight line (curve II). When the Tafel line was traced in the reverse direction, it was found to follow a totally different path. Thus, after the sudden numerical decrease in overpotential, a straight line (curve III) situated above curve I is obtained. In the case of 0.003 *N* HCl, the sudden numerical decrease is not observed; the descending straight line (curve II) flattens out to become parallel to the log c.d. axis. At comparatively low current densities a region of constant potential for curves I and III is observed in all solutions. The results in 0.01 *N* HCl exhibit the same general characteristics as those obtained in 0.005 and 0.02 *N* solutions; the position of the sudden numerical

(1) J. W. Mellor, "A Comprehensive Treatise on Inorganic and Theoretical Chemistry," Longmans, Green and Co., London, Vol. 11, 1947, p. 37.

(2) I. A. Ammar and S. A. Awad, *J. Electrochem. Soc.*, **103**, 182 (1956).

(3) A. Azzam, J. O'M. Bockris, B. Conway, and H. Rosenberg, *Trans. Faraday Soc.*, **46**, 918 (1950).

decrease in overpotential in this solution is included in Fig. 2.

Tables I, II, and III contain the mean values of the slopes b_1 (in the low current density range) and b_2 (in the high current density range) for curves I, II, and III, respectively. The values at which the potential does not change with the current density (stationary potential), referred to the reversible hydrogen electrode, also are included.

TABLE I

Concn. *N* HCl	*p*H	b_1	b_2	Stationary potential in mv. (*vs.* R.H.E.)
0.003	2.70	42	..	−290
.005	2.40	40	96	−275
.01	2.05	40	110	−295
.02	1.85	42	92	−290

TABLE II

Concn. *N* HCl	b_1	b_2	Stationary potential in mv. (*vs.* R.H.E.)
0.003	40	..	−500
.005	..	95	
.01	..	110	
.02	..	92	

TABLE III

Concn. *N* HCl	b_1	b_2	Stationary potential in mv. (*vs.* R.H.E.)
0.003	..	..	
.005	40	..	−348
.01	40	110	−380
.02	38	90	−367
		Mean value	−365

The current–potential relation at 10° in 1 *N* NaOH also was measured. The results are shown in Fig. 4, in which the potential values, E_H, are referred to the normal hydrogen electrode. The curve shows successive breaks at half-wave potentials of −0.74, −0.93, and −1.1 v.; the potential becomes constant at about −2.2 v.

Discussion

1. Curve I and Limiting Current Density.—The overpotential results in 0.003–0.02 *N* HCl solutions containing excess neutral salt are quite similar to those obtained in pure dilute HCl solutions,[2] which indicates that the hydrogen evolution reaction on tellurium cathodes is governed by a simple electrochemical mechanism. This mechanism requires two Tafel slopes of 0.04 and 0.12 v. at 30°, in good agreement with the values given in Table I.

With increase of cathodic polarization, a limiting current density, whose value increases with the acid concentration, is reached at which the activity of H^+ ions at the electrode surface decreases appreciably. Accordingly, the overpotential exhibits a rapid numerical increase until a value between −0.520 and −0.585 v. is attained. Above this value, the Tafel line is linear (curve II), indicating that another cathode reaction, probably the formation of H_2Te, takes place.

When the Tafel line was traced downward, limiting current densities were observed in all solutions except 0.003 *N* HCl; but these values are smaller than the corresponding values for Tafel lines in the opposite direction. This can be explained on the basis of a relative decrease in the H^+ ion activity in the region around the cathode since these ions continue to be consumed during the formation of H_2Te. Accordingly, one expects that with an increase of the acid concentration, the difference between the two limiting values will decrease since the removal of a small amount of H^+ ions will be less effective. Actually in 0.02 *N* HCl the two limiting current densities are nearly the same. In 0.003 *N* HCl no limiting current is observed, but the overpotential varies asymptot-

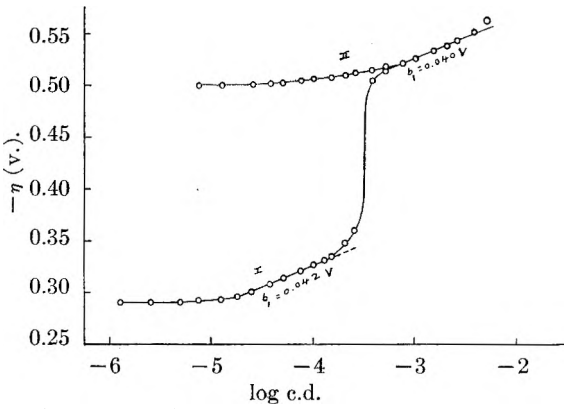

Fig. 1.—Tafel lines for Te cathodes in 0.003 *N* HCl.

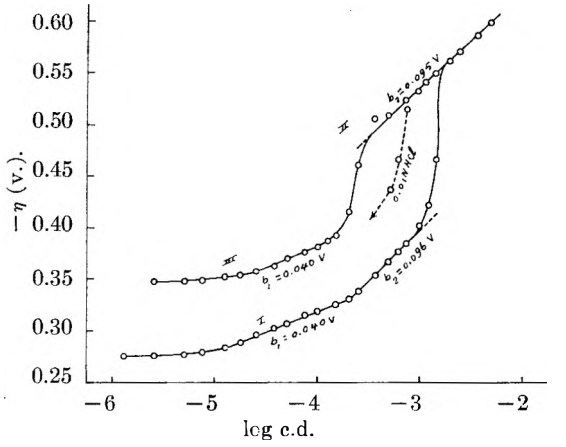

Fig. 2.—Tafel lines for Te cathodes in 0.005 *N* HCl.

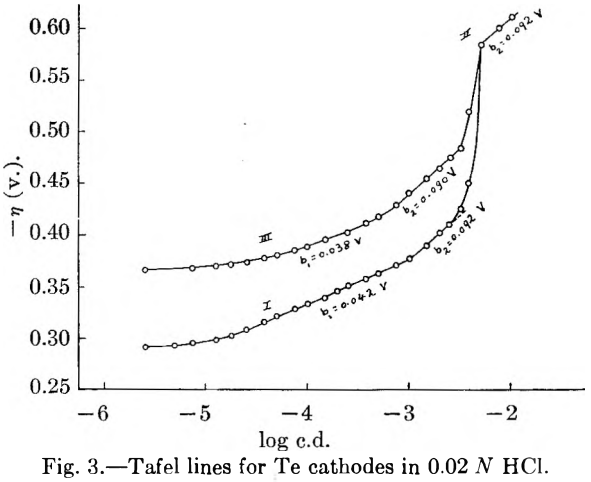

Fig. 3.—Tafel lines for Te cathodes in 0.02 *N* HCl.

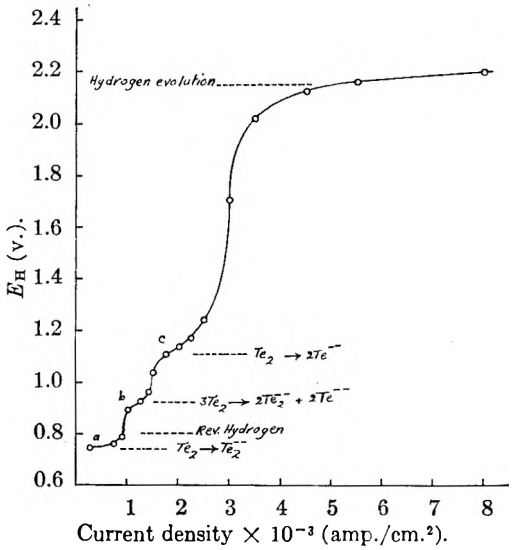

Fig. 4.—Current–potential curve for Te in 1N NaOH at 10°.

ically with log c.d. until a constant value of −0.50 v. is obtained.

2. **Curve II.**—When the potential becomes sufficiently cathodic at the limiting current, tellurium reacts eventually giving hydrogen telluride.[1] The mechanism suggested for the formation of this compound is represented by the following equations in which: (a) owing to the marked decrease in H^+ ions at the electrode surface, K^+ or La^{+++} ions are involved in "depolarization reactions" giving intermediate tellurides; and (b) tellurium is represented as Te_2 since evidence for its diatomic nature in cathodic dissolution has been obtained.[4] Thus

$$Te_2 + K^+ + e \longrightarrow KTe_2 \quad (1)$$

$$KTe_2 \longrightarrow Te_2 + K^+ + e \quad (2)$$

$$KTe_2 + K^+ + e \longrightarrow 2KTe \quad (3)$$

$$KTe + e \longrightarrow Te^{--} + K^+ \quad (4)$$

Telluride ions diffuse away from the electrode and combine with H^+ ions migrating toward the cathode

$$Te^{--} + 2H^+ \longrightarrow H_2Te \quad (5)$$

It is assumed that the electrochemical dissociation of the tellurium molecule, represented by eq. 3, is the rate-determining reaction. The velocities of reactions 1, 2, and 3 are given by[5]

$$V_1 = k_1(a_{K^+})_{d.l.}(1 - x)\exp\left(-\frac{\Delta\phi F}{2RT}\right) = a_1(1 - x) \quad (6)$$

$$V_2 = k_2 x\, 10^{-9}\exp\left(\frac{\Delta\phi F}{2RT}\right) = a_2 x \quad (7)$$

$$V_3 = k_3 x\, 10^{-9}(a_{K^+})_{d.l.}\exp\left(-\frac{\Delta\phi F}{2RT}\right) = a_3 x \quad (8)$$

where k_1, k_2, and k_3 are the rate constants for reactions 1, 2, and 3, respectively; a_1, a_2, and a_3 are the electrochemical constants; $(a_{K^+})_{d.l.}$ is the activity of K^+ ions in the double layer; and x is the fraction of the surface covered with KTe_2. If we assume that (4) is a very rapid reaction, KTe can remain on the surface for only a very short time. $\Delta\phi$ is the potential difference between the electrode and the Helmholtz double layer.

The rate of formation of hydrogen telluride is governed by the rate of reaction 3 under the condition[5]

$$a_1 + a_2 > 10a_3 \quad (9)$$

At the steady-state corresponding to a constant surface coverage, current, and potential

$$V_1 - V_2 - V_3 = 0 \quad (10)$$

From eq. 6, 7, 8, 9, and 10, the surface coverage becomes

$$x = \frac{a_1}{a_1 + a_2} \quad (11)$$

When a_1 is much smaller than a_2

$$x = \frac{a_1}{a_2} = \frac{k_1}{k_2 \times 10^{-9}}(a_{K^+})_{d.l.}\exp\left(-\frac{\Delta\phi F}{RT}\right) \quad (12a)$$

On the other hand when a_1 is much larger than a_2

$$x = 1 \quad (12b)$$

When x is given by (12a), the net cathodic current becomes

$$i = 2FV_3 = \frac{2Fk_1k_3}{k_2}(a_{K^+})^2_{d.l.}\exp\left(-\frac{3\Delta\phi F}{2RT}\right) \quad (13)$$

and accordingly, the Tafel line slope is equal to 0.04 v. at 30°. With increasing cathode polarization, x increases and approaches unity (eq. 12b). The net cathodic current, therefore, becomes

$$i = 2FV_3 = 2Fk_3 \times 10^{-9}(a_{K^+})_{d.l.}\exp\left(-\frac{\Delta\phi F}{2RT}\right) \quad (14)$$

indicating a slope of 0.12 v. at 30°.

It is clear from Table II that the Tafel slopes obtained experimentally are in good agreement with the theoretically deduced values. The finding that only the higher slope was observed in the 0.005–0.02 N solutions (*cf.*, Fig. 2 and 3) is due to the fact that the limiting current density corresponds to high cathodic polarization. In 0.003 N solution, the limiting current density is reached at low cathodic polarization, and, therefore, the lower slope is observed. In order to observe the higher slope in this solution, currents higher than those applied are required.

According to the mechanism suggested above, the number of electrons, λ, required to complete one act of the rate-determining step must be 2. From Fig. 1, the exchange current, i_0, for curve II amounts to 2×10^{-4} amp./cm.^{2}. The plot of current density against η at very low cathode polarization gives a value of −68 (v./amp./cm.^{2}) for $(\partial\eta/\partial i)_{\eta\to 0}$. Using the relation

$$\lambda = \frac{RT}{i_0F}\left(\frac{\partial i}{\partial\eta}\right)_{\eta\to 0} \quad (15)$$

we obtain λ = 1.93, which is in good agreement with the expected value.

3. **Curve III.**—After the rapid numerical decrease in overpotential, the values of η fall along curve III which lies above curve I. However, until the limiting current density is applied, curves I and III, coincide; this indicates that the new pathway is intimately associated with the presence of Te^{--} ions in solution.

We can account for the effect of telluride ions by

(4) S. A. Awad, *J. Electrochem. Soc.*, in press.

(5) J. O'M. Bockris and E. C. Potter, *ibid.*, **99**, 169 (1952).

assuming that they are specifically adsorbed on the cathode. When a large fraction of the surface is covered with these ions, the bare areas will be subjected to current densities higher than those calculated; and so the overpotential values are numerically larger. However, if the adsorbed telluride ions had no effect other than decreasing the surface area, curve III would continue as a straight line to current densities lower than those for curve I in order to become parallel to the log c.d. axis at the same overpotential. However, curve III deviates from linearity at higher current densities and, thus, becomes parallel to the log c.d. axis at overpotentials more negative than curve I by about 80 mv. It is, therefore, evident that this new path does not represent hydrogen evolution.

It has been shown by Bockris and Conway[6] that arsenic compounds, carbon monoxide, and potassium cyanide poison the cathode surface even when present in small quantities. It is probable that Te^{--} ion has a similar effect; and so evolution of hydrogen is inhibited. Direct experimental evidence for the poisoning effect of Te^{--} ion was obtained by measuring the potential at which hydrogen is evolved at tellurium cathodes from a 1 *N* NaOH solution. The measurement was carried out at a relatively low temperature (10°) in order to decrease the rate of diffusion of the telluride ions formed at the cathode. The accumulation of these ions at the cathode surface with increasing current permits the onset of a limiting current density, and leads, therefore, to the evolution of hydrogen. Figure 4 shows that hydrogen evolves at about −2.2 v., while the reversible value is −0.8 v. This high overpotential can be reasonably attributed to Te^{--} ion.

These considerations suggest that instead of the evolution of hydrogen, "hydrogen ditelluride" is formed at the cathode. The probable mechanism can be represented by the equations

$$Te_2 + H^+ + e \longrightarrow HTe_2 \qquad (16)$$

$$HTe_2 + H^+ + e \longrightarrow H_2Te_2 \qquad (17)$$

If reaction 17 is rate determining, slopes of 0.04 and 0.12 v. for the low and high current density ranges can be theoretically deduced. The values in Table III confirm this assumption. It may be asked why Te^{--} ion does not inhibit the formation of H_2Te_2 since H^+ ions also are directly involved. This may be due to the heterogeneity of the surface, the effect of which is more complex in the case of electrochemical reactions than in catalysis. However, with increasing Te^{--} ion activity (due to decreasing acid concentration) a state is reached in which H_2Te_2 formation also is inhibited (*cf.* Fig. 1).

It is obvious from Table III that the reversible potential of H_2Te_2 formation is −0.365 v., with respect to the reversible hydrogen electrode. One would, therefore, expect that, during hydrogen evolution when the overpotential becomes more negative than −0.365 v., hydrogen ditelluride would be formed (although at a lower rate) as an alternative reaction. This conclusion provides an explanation for the observation that "this electrode disintegrates into black colloidal tellurium in solutions containing traces of oxygen".[2] This observation was peculiar since it formerly was thought that H_2Te was the only hydride of tellurium, and its formation requires a highly negative potential.

4. **Determination of Standard Potential Values.** —No experimental values have been reported for the standard potential of the reaction

$$\tfrac{1}{2}Te_2 + 2H^+ + 2e \longrightarrow H_2Te \qquad (18)$$

The present investigation permits the direct determination of this potential. According to reaction 18, the potential of the Te_2/H_2Te electrode varies with *p*H in a manner similar to the hydrogen electrode. Thus, under conditions of thermodynamic reversibility, the potential difference between these two electrodes in a given solution is equal to the standard potential of the Te_2/H_2Te couple. According to the constant potential value in curve II (*cf.* Table II and Fig. 1) the standard potential of this couple is equal to −0.50 v. The standard free energy of formation of H_2Te is, thus, equal to 23.06 kcal. at 30°, which is about 10 kcal. less than 33.1 kcal., the value reported for 25°. Latimer[7] has suggested that a value of 33.1 may be too large.

Similar arguments could be applied to the case of hydrogen ditelluride. The values given in Table III indicate that the standard potential of the reaction

$$Te_2 + 2H^+ + 2e \longrightarrow H_2Te_2 \qquad (19)$$

is − 0.365 v. The standard free energy of formation of this hydride is, therefore, 16.83 kcal.

The shape of the current–potential relation shown in Fig. 4 indicates that tellurium undergoes three cathode reactions before hydrogen evolution begins. In agreement with earlier results obtained in 5–0.05 *N* NaOH,[8] wave (a) at − 0.74 v. represents the formation of Te_2^{--} according to

$$Te_2 + 2e \longrightarrow Te_2^{--} \qquad (20)$$

From polarographic studies together with controlled potential coulometric analysis, Lingane and Niedrach[9] found that Te^{--} ion gives a well developed anodic wave which involves two electrons. This fact indicates that Te^{--} ion goes directly to the elemental state without the intermediate formation of Te_2^{--}. We can, therefore, conclude that neither wave (b) nor wave (c) represents a further reduction of Te_2^{--} into Te^{--}; but in both reactions elemental tellurium still is involved. Since a highly negative potential facilitates the electrochemical dissociation of tellurium molecules, wave (c) at − 1.1 v. may well be related to the reaction

$$Te_2 + 4e \longrightarrow 2Te^{--} \qquad (21)$$

The existence of wave (b) at an intermediate potential of − 0.93 v. may indicate a partial dissociation of tellurium molecules, leading to simultaneous formation of Te_2^{--} and Te^{--} ions according to

$$3Te_2 + 8e \longrightarrow 2Te_2^{--} + 2Te^{--} \qquad (22)$$

(6) J. O'M. Bockris and B. Conway, *Trans. Faraday Soc.*, **45**, 989 (1949).

(7) W. M. Latimer, "Oxidation Potentials," Second Edition, Prentice–Hall, New York, N. Y., 1952, p. 85.

(8) S. A. Awad, *J. Electrochem. Soc.*, **108**, 468 (1961).

(9) J. J. Lingane and L. W. Niedrach, *J. Am. Chem. Soc.*, **70**, 4115 (1948).

If − 0.74 and − 1.1 v. are taken as approximate values for the standard potentials of reactions 20 and 21, the standard free energies of formation of Te_2^{--} and Te^{--} are 34.13 and 50.7 kcal., respectively. From these values, the standard potential of reaction 22 was estimated to be − 0.92 v., which is quite close to the value observed experimentally.

VISCOSITY OF AQUEOUS SOLUTIONS. III. TETRAMETHYLAMMONIUM BROMIDE AND THE ROLE OF THE TETRAALKYLAMMONIUM IONS

BY E. R. NIGHTINGALE, JR.[1]

Esso Research & Engineering Co., Linden, N. J., and University of Nebraska, Lincoln 8, Neb.

Received November 13, 1961

The viscosities of aqueous tetramethylammonium bromide solutions have been measured at 20, 25, and 30° in the concentration range 0.0005 to 1 *m*. The viscosity data have been interpreted in terms of the Jones–Dole equation for strong electrolytes. Using this relation, the viscosity *B*-coefficients for the salt and for the tetramethylammonium ion at 25° are calculated to be +0.1014 and 0.1434 l./mole, respectively. Unlike that for the larger tetraalkylammonium ions, the *B*-coefficient for $(CH_3)_4NBr$ increases with temperature yielding a negative activation energy for viscous flow. This behavior is interpreted and corroborates a previous conclusion that the $(CH_3)_4N^+$ ion is weakly hydrated at the ionic surface, much in the same manner as are the Ba^{+2}, IO_3^-, and SO_4^{-2} ions. The energies and entropies of activation for viscous flow for the R_4N^+ ions are demonstrated to be congruous with those for the common inorganic ions if corrected (a) to the molal scale to compensate for the varying amounts of solvent in a molar solution and (b) for the excess activation free energy which results from the large molar volume of the R_4N^+ ions.

Recent discussions from these Laboratories[2,3] have emphasized that transport processes can provide significant information concerning the nature of ion–solvent interactions and the effective size of the hydrated entities. The infrared spectra of aqueous solutions[4] and the influence of ionic charge on the viscosity[5] indicate, however, that the ionic interactions with water are highly specific and greatly dependent upon the charge, size, and shape of the ions. One class of ions whose role has not been adequately characterized is that of the tetraalkylammonium ions. Recently, Frank[6,7] has suggested that the tetraalkylammonium ions increase the "ice-like" structure in water *away* from the ionic surface because the non-polar alkyl group participates only very weakly in the "flickering ice-like clusters." This concept accounts not only for properties such as viscosity in which the tetraalkylammonium ions behave as if appreciably hydrated, but also for the excessive molal heat capacity and increased dielectric relaxation time of their solutions. However, the behavior of the smaller ions in this series, particularly the tetramethylammonium ion, has remained less certain. In the previous discussion on the effective size of hydrated ions,[2] the tetramethylammonium ion was assumed to be hydrated at the surface much like the sodium or iodate ion. Because accurate viscosity data are not available in the literature, the viscosity of tetramethylammonium bromide has been re-examined. The viscosity coefficients for the $(CH_3)_4N^+$ ion have been calculated and compared with those for the other tetraalkylammonium ions.

(1) Esso Research & Engineering Co., Linden, N. J.
(2) E. R. Nightingale, Jr., *J. Phys. Chem.*, **63**, 1381 (1959).
(3) E. R. Nightingale, Jr., and R. F. Benck, *ibid.*, **63**, 1777 (1959).
(4) E. R. Nightingale, Jr., and H. S. Frank, unpublished work.
(5) E. R. Nightingale, Jr., and J. F. Kuecker, to be published.
(6) H. S. Frank, *Proc. Roy. Soc.* (London), **A247**, 481 (1958).
(7) H. S. Frank and W. Y. Wen, *Discussions Faraday Soc.*, **24**, 133 (1957).

Experimental

Eastman Kodak white label tetramethylammonium bromide was purified by twice recrystallizing the salt from conductivity water and drying at 110° for 4 hr. The salt solutions were prepared on the molal basis with conductivity water. The densities of the solutions were measured at 20, 25, and 30 ± 0.05° with 25-ml. specific gravity bottles and are precise within ±0.0001 g./ml. As described previously,[3] the viscosities were measured within ±0.02° of the specified temperatures using an Ostwald viscometer which was calibrated with water by means of eq. 1

$$\eta/\rho = Kt - L/t \qquad (1)$$

where η is the absolute viscosity, ρ is the density, and t is the flow time. The characteristic viscometer constants K and L were 0.00005251 and 0.00011, respectively. The absolute viscosity of water at 20, 25, and 30° is 0.01002, 0.008903, and 0.007976 poise, respectively.[8] The densities are 0.99823, 0.99707, and 0.99568 g./ml., respectively.[9]

Results

The viscosities of the salt solutions were computed by means of eq. 1. The absolute viscosities at 20, 25, and 30° for ten tetramethylammonium bromide solutions in the concentration range 0.0005 to 1.0 molal are presented in Table I. The data

TABLE I

ABSOLUTE VISCOSITIES OF AQUEOUS TETRAMETHYLAMMONIUM BROMIDE SOLUTIONS AT 20, 25, AND 30°

m, moles/1000 g.	Absolute viscosity, poise 20°	25°	30°
0.0005137	0.010021	0.008905	0.007978
.0009992	$.010023$	.008906	.007979
.002997	$.010027$	.008909	.007982
.009939	$.010032$	.008918	.007992
.01685	$.010038$	.008926	.008001
.03384	$.010053$	.008944	.008022
.06015	$.010073$	.008971	.008054
.1013	$.010102$	.009012	.008103
.4065		.009289	
1.043		.009847	

(8) J. R. Coe and T. B. Godfrey, *J. Appl. Phys.*, **15**, 625 (1944).
(9) L. W. Tilton and J. K. Taylor, *J. Research Natl. Bur. Standards*, **18**, 205 (1937).

have been analyzed using the Jones–Dole equation.[10]

$$\eta/\eta_0 = 1 + A\sqrt{C} + BC \qquad (2)$$

where η/η_0 is the viscosity of the salt solution relative to that of the solvent water, C is the molar concentration, and A and B are constants characteristic of the electrolyte. The A-coefficient represents the contribution from interionic electrostatic forces.[11] The B-coefficient is a measure of the effective hydrodynamic volume of the solvated ions and is proportional to the entropy of hydration of a gaseous ion.[2] This coefficient denotes the order or disorder introduced by the ions into the solvent structure, and is a specific and approximately additive property of the ions of a strong electrolyte at a given temperature,[12] although no satisfactory theoretical treatment has yet been given. Plotting $(\eta/\eta_0 - 1)/\sqrt{C}$ *vs.* $\sqrt{C}$, the A-coefficient is the ordinate intercept, and the B-coefficient is given by the slope of the resulting straight line. The experimental values for the A-coefficient for tetramethylammonium bromide solutions at 20, 25, and 30° are 0.0062, 0.0066, and 0.0064, respectively. The experimental value at 25° compares fairly well with the theoretical value of 0.00623 calculated according to theory of Falkenhagen and Vernon.[11] The B-coefficients are observed to be +0.0627, 0.1014, and 0.137 at 20, 25, and 30°. Taking the value of the B-coefficient for the bromide ion to be −0.049,[13] −0.042,[14] and −0.0355,[13] respectively, we calculate the magnitude of the B-coefficient for the tetramethylammonium ion as +0.112, 0.1434, and 0.172 at these three temperatures.

Discussion

Previously, it has been demonstrated that the theory of absolute reaction rates as applied by Eyring, *et al.*, to viscosity[15] may be adapted to aqueous salt solutions to calculate ionic activation energies and entropies for viscous flow.[3] Table II records the energies and entropies of activation for viscous flow for the tetraalkylammonium ions calculated from this work and data available in the literature.[16] The positive activation energies for the tetraalkylammonium ions other than $(CH_3)_4N^+$ are consistent with the interpretation of Frank[6,7] that large R_4N^+ ions increase the viscosity of water by increasing the ice-like structure *apo-surface*.[17] As the temperature is increased, the already ordered structure of the solution is diminished more than is that of the pure solvent, and the relative viscosity and hence the B-coefficient decreases.

TABLE II

FREE ENERGY, ENERGY, AND ENTROPY OF ACTIVATION FOR VISCOUS FLOW AT 25° (C = 1 MOLE/L.)

Salt	$B\eta$	ΔF^*, kcal.	ΔE^*, kcal.	ΔS^*, e.u.
(H_2O)		(2.19)	(4.01)	(6.1)
NaBr	+0.0443[a]	2.21	3.79	5.3
$(CH_3)_4NBr$	.1014[b]	2.30	2.82	1.7
$(C_2H_5)_4NBr$	.343[c]	2.44	3.93	5.0
$(C_3H_7)_4NCl$	1.085[d]	2.75	4.41	5.6
$(C_4H_9)_4NBr$	1.354[e]	2.88	5.00	7.1
Ion	$(B\eta)_i$	ΔE_i^*, cal.		ΔS_i^*, e.u.
Br^-	−0.042	−240		−0.85
$(CH_3)_4N^+$	+0.1434	−950		−3.55
$(C_2H_5)_4N^+$	0.385	+160		−0.4
$(C_3H_7)_4N^+$	1.092	+620		+0.25
$(C_4H_9)_4N^+$	1.396	+1230		+1.85

[a] Ref. 14; dB/dT estimated from Cl^- and I^-. [b] This work. [c] V. D. Laurence and J. H. Wolfenden, *J. Chem. Soc.*, 1144 (1934). [d] "International Critical Tables," Vol. V, McGraw-Hill Book Co., New York, N. Y., p. 13. [e] P. Goldberg and R. M. Fuoss, *Proc. Natl. Acad. Sci. U.S.*, **38**, 758 (1952); dB/dT from W. Y. Wen, Ph.D. Thesis, University of Pittsburgh, 1957.

The negative activation energy for $(CH_3)_4N^+$ is congruous with our previous conclusion that this ion, unlike the other tetraalkylammonium ions, is weakly *peri-surface* hydrated.[2,17] The ion–dipole interaction energy for a univalent ion the size of $(CH_3)_4N^+$ is approximately $10kT$ and is sufficiently large compared with that for hydrogen bond formation to orient some of the water dipoles at the ionic surface more strongly than in bulk water itself. The effective hydrated radius of $(CH_3)_4N^+$ closely approximates that of the iodate ion (3.67 *vs.* 3.74 Å.) although the latter is somewhat more extensively hydrated by virtue of charge delocalization in the iodine–oxygen bond.[3,18] It is clear that there cannot be appreciable apo-surface hydration as with the larger R_4N^+ ions since this type of structure making always is accompanied by a negative temperature dependence for the B-coefficient. It may be emphasized that the conclusion that $(CH_3)_4N^+$ is weakly peri-surface hydrated is not inconsistent with the data of Haggis, Hasted, and Buchanan[19] on the change of the dielectric relaxation wave length in aqueous solutions. These workers have demonstrated that "hydrogen bond-forming" molecules and ions increase the dielectric relaxation time in water, but it is not possible to differentiate between apo-surface and peri-surface hydration by these measurements. For instance, both structure-making salts such as LiCl and structure-breaking salts like RbCl decrease the relaxation time while the structure-ordering ions F^-, $(CH_3)_4N^+$, and $(C_2H_5)_4N^+$ all increase the relaxation time. It appears that the major difference between the structure-breaking I^- ion and the structure-making $(CH_3)_4N^+$ ion is one of size: the normal water structure about an iodide ion collapses because the first-layer water about the ion behaves as a disturbing center and

(10) G. Jones and M. Dole, *J. Am. Chem. Soc.*, **51**, 2950 (1929).

(11) H. Falkenhagen and E. L. Vernon, *Physik. Z.*, **33**, 140 (1932).

(12) W. M. Cox and J. H. Wolfenden, *Proc. Roy. Soc.* (London), **A145**, 475 (1934).

(13) Estimated from known temperature dependence of Cl^- and I^-.

(14) M. Kaminsky, *Discussions Faraday Soc.*, **24**, 171 (1957).

(15) S. Glasstone, K. J. Laidler, and H. Eyring, "The Theory of Rate Processes," McGraw-Hill Book Co., New York, N. Y., 1941.

(16) A plot of $B\eta$ *vs.* r_H^3 (see ref. 2) suggests that $B\eta$ for $(C_3H_7)_4NCl$ is too large by *ca.* 0.18 unit. The literature value for dB/dT is approximately correct, however, and thus yields consistent values for ΔE_i^* and ΔS_i^*.

(17) Literally—*away* from the surface of the ion. Ions for which the force field is sufficient to order water molecules *at* the ionic surface maybe said to be hydrated *peri-surface*—meaning at and round-about the ionic surface. The latter class includes, however, both structure makers such as Li^+ and F^- and structure breakers such as Rb^+ and Cl^-.

(18) E. R. Nightingale, Jr., *J. Phys. Chem.*, **64**, 162 (1960).

(19) G. H. Haggis, J. B. Hasted, and T. J. Buchanan, *J. Chem. Phys.*, **20**, 1452 (1952).

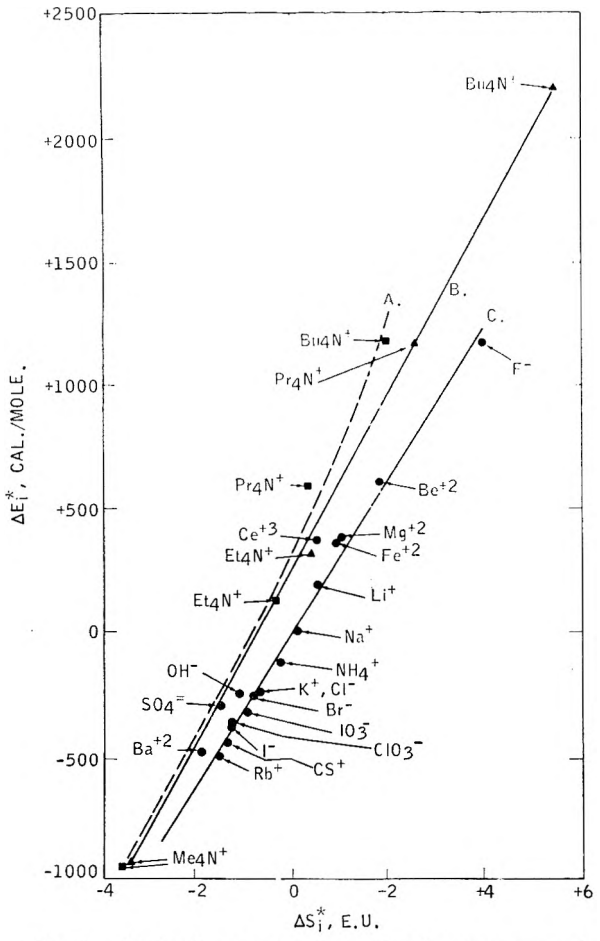

Fig. 1.—Activation energy *vs.* activation entropy: A, R_4N^+ ions on molar scale; B, R_4N^+ ions corrected to molal scale; C, common ions on molar scale.

interferes with the ice-like water structure,[6] whereas the weakly oriented water about the larger $(CH_3)_4N^+$ ion participates more readily in the fluctuations of the water structure.

In the previous discussion on activation energies and entropies for viscous flow[3] it was shown that the apparently anomalous relation of positive *B*-coefficients accompanying negative activation energies occurs for ions such as Ba^{+2}, IO_3^-, $SO_4^=$, and now $(CH_3)_4N^+$, which are minimally peri-surface hydrated. Furthermore this relation is temperature-dependent, for if a higher reference temperature, say 40°, is chosen in place of 25°, "normal" ions such as K^+ and Cl^- likewise appear anomalous. This behavior is characteristic of ions for which extensive hydration beyond the primary solvent sheath is not significant and for which the temperature independent ion–dipole solvation forces predominate. Thus the viscosity temperature coefficient of aqueous solutions containing $(CH_3)_4N^+$ is like that described previously: as the temperature increases, the normal ordering of the water structure is destroyed, and the water molecules become more susceptible to peri-surface ordering in the relatively weak field of the ion.

It is instructive to compare the activation energies and entropies for viscous flow of the tetraalkylammonium ions with those calculated in the previous paper.[3] In Fig. 1, these data are compared for a wide variety of ions. Curves A and C appear to infer that the energy–entropy relation for the R_4N^+ ions does not in general conform to that for the more common ions. However, it must be recognized that these calculations all have been based on the molar concentration scale. For common ions, this scale is satisfactory since the density of most common inorganic salt solutions is such that one liter of a molar solution contains very close to 54 moles of water. For $(CH_3)_4NBr$, $(C_2H_5)_4NBr$, $(C_3H_7)_4NCl$, and $(C_4H_9)_4NBr$, however, one liter of a molar solution contains only 49, 46, 43, and 39 moles of water, respectively. Thus for these latter species, the viscosity and the apparent *B*-coefficient of a molar solution are appreciably greater than for a molal solution. The appropriate corrections in ΔE^* and ΔS^* may be made as follows. Assuming[20] that

$$\left(\frac{dB}{dT}\right)_c = \left(\frac{dB}{dT}\right)_m \qquad (3)$$

it may be shown[3] that

$$\Delta E_m^* = \Delta E_c^* \left(\frac{1 + B_c}{1 + B_c f}\right) \qquad (4)$$

where the fraction f is given by

$$f = n_c/n_m \leqq 1$$

where n_c and n_m are the number of moles of water in a molar and molal solution, respectively.

Table III lists the corrected values for ΔE^* and ΔS^* for both the salts and the cations calculated using eq. 4. In correcting these values, ΔF^* was assumed to remain constant since the change in the logarithm of the particle volume is negligibly small.[3] Curve B in Fig. 1 demonstrates that when corrected to the molal scale,[21] the behavior of the activation energies and entropies for the tetraalkylammonium ion closely parallels that of the common ions. The apparent deviation between curves B and C in Fig. 1 stems directly from the large activation free energy of the tetraalkylammonium ions (Table II), which in turn results from their abnormally large molar volume (ref. 3, eq. 6). If allowance is made for this difference in ΔF^*,

TABLE III

CORRECTED ACTIVATION ENERGIES AND ENTROPIES FOR VISCOUS FLOW AT 25° (CONCN. = 1 MOLE/1000 G.)

Salt	$(B\eta)_+$	ΔE^*, kcal.	ΔE_+^*, cal.	ΔS^*, e.u.	ΔS_+^*, e.u.
$(CH_3)_4NBr$	0.131	2.85	−920	+1.85	−3.40
$(C_2H_5)_4NBr$	.327	4.11	+350	5.61	+0.35
$(C_3H_7)_4NCl$	.882	5.00	+1230	7.54	+2.25
$(C_4H_9)_4NBr$	.987[a]	6.05	+2280	10.6	+5.35

[a] For internal consistency, this value has been used instead of that measured by Wen (Table II, ref. *e*), although Wen's value for dB/dT has been used to calculate ΔE^* and ΔE_+^*. Using Wen's value for B_η, ΔE^* is decreased about 10%.

(20) The error introduced by this assumption is proportional to $(\partial m/\partial C)_C - 1$ and is negligibly small.

(21) The Jones–Dole equation originally was used with both the molal and molar concentration scales (ref. 10) but virtually all recent viscosity data have been interpreted on the basis of the molar scale (ref. 14). Curve C in Fig. 1 is based on the molar scale (*ca.* 54 moles of water per liter of solution).

it may be seen that the activation energies and entropies of the tetraalkylammonium ions are in fact consistent with those of the common ions.

Acknowledgment.—The assistance of Mr. R. F. Benck in determining the viscosities of some of the solutions is gratefully acknowledged.

HIGH SPEED STIRRING TECHNIQUES IN SOLUBILITY STUDIES: A CRITICAL APPRAISAL AND APPLICATION TO HIPPURIC ACID ESTERS[1]

By R. J. Larese, D. A. Robinson, W. F. Brassine, and W. J. Canady[2]

West Virginia University Medical Center, Department of Biochemistry, Morgantown, West Virginia

Received November 16, 1961

Since a possible relationship between the variation of rate of hydrolysis with ionic strength and the variation of solubility with ionic strength has been suggested, it was considered desirable to determine the effects of ionic strength upon the solubility of a series of hippuric acid esters. Some difficulties involving hydrolysis before reaching equilibrium were encountered. A method is outlined using very rapid stirring at approximately 30,000 r.p.m. Equilibrium was reached within less than one hour. In order to test the high-speed technique, the temperature dependence of the solubility of free hippuric acid was determined, and the thermodynamical values obtained were compared to the results of an earlier work which made use of conventional agitation. The agreement was found to be entirely satisfactory.

Introduction

It has been suggested by Miles, Robinson, and Canady[3] that the variation with ionic strength of certain kinetic constants associated with some enzyme catalyzed reactions may be related to the variation of the solubility of the substrate with ionic strength. Since it has been shown that a homologous series of hippuric acid esters, up to and including butyl hippurate, are hydrolyzed in the presence of α-chymotrypsin,[4] it was deemed advisable to study the effect of ionic strength on the solubility of those substrates.

One problem which might be anticipated in regard to such a study of these esters in aqueous solvents would be the possibility of hydrolysis while equilibrium was being reached. This problem was indeed encountered, the apparent solubility slowly increasing with time. Even after 4–6 days of equilibration with the mild agitation used in a previous study of the solubility of free hippuric acid,[5] the readings still were rising. This continuous rise was accompanied by a corresponding drop in *p*H. The decision was reached that a much more rapid method was required in order to study the solubilities of such esters.

It was judged that the most likely way to keep the ester in contact with water for the minimum length of time was to employ extremely high-speed agitation in order to reach equilibrium very rapidly. After examination of available equipment, it was decided that the Virtis Model 23 homogenizer supplied the necessary features. Four blades are used, and according to the manufacturer, the speed attained with solutions of the visocosities encountered in this study is approximately 30,000 r.p.m.

No material change in reading could be detected with any of the substances investigated here after treatment for 30 min., and it was assumed that equilibrium had been reached in this time. It still remained necessary to demonstrate the validity of the high-speed technique before it could be applied with any certitude to the study of the hippuric acid esters. A suitable test was considered to be a study of the temperature dependence of the solubility of hippuric acid itself, which already has been investigated using conventional stirring techniques.[5] Agreement of the thermodynamical quantities for the solutions of hippuric acid obtained by both methods could be taken to constitute a good test of the method employed. For this reason, the work presented consists of the study of the temperature dependence of hippuric acid in water, and the effect of potassium chloride on the solubility of methyl, ethyl, propyl, isopropyl, and butyl hippurates at 25°.

Experimental

Materials.—The materials for the temperature dependence studies on hippuric acid were the same as those previously described.[5] The esters were prepared by the method of Nelson, Miles, and Canady.[4] The potassium chloride was Fisher's "Certified A.C.S.," and was used without further treatment.

Equipment.—Constant temperature was maintained by means of a Sargent thermistor controlled water-bath, which is capable of maintaining the temperature within ±0.01°. The temperature was measured with two EXAX solid-point thermometers having temperature ranges of 0 to 30 and 20 to 50° in increments of 0.1°. These thermometers were calibrated against a Leeds and Northrup platinum resistance thermometer over the entire experimental range. The platinum resistance thermometer had been calibrated previously by the U. S. Bureau of Standards. A Beckman DUV spectrophotometer was used for the photometric determinations. As mentioned earlier, the Virtis Model 23 homogenizer was used to provide agitation.

Procedure.—The homogenizer was placed near the water-bath and the head of the instrument swung around to extend out over the bath. The flask supplied with the homogenizer was supported in the bath by means of a tripod, and the clamp supplied with the instrument tightened down to make it secure. Thus the temperature within the homogenizer flask was maintained by the water-bath.

Agitation for protracted periods of time was found to appreciably warm the solution in the homogenizer flask, hence intermittent agitation was used.

Three-tenths of a gram of hippuric acid or ester of hippuric

(1) Supported by Grant No. NSF-G-7587 from the National Science Foundation and by Grant No. RG-8122 from the National Institutes of Health.

(2) Reprint requests to this author.

(3) J. L. Miles, D. A. Robinson, and W. J. Canady, *Federation Proc.*, **20**, 231 (1961).

(4) G. H. Nelson, J. L. Miles, and W. J. Canady, *Arch. Biochem. Biophys.*, in press.

(5) R. J. Larese and W. J. Canady, *J. Phys. Chem.*, **65**, 1240 (1961).

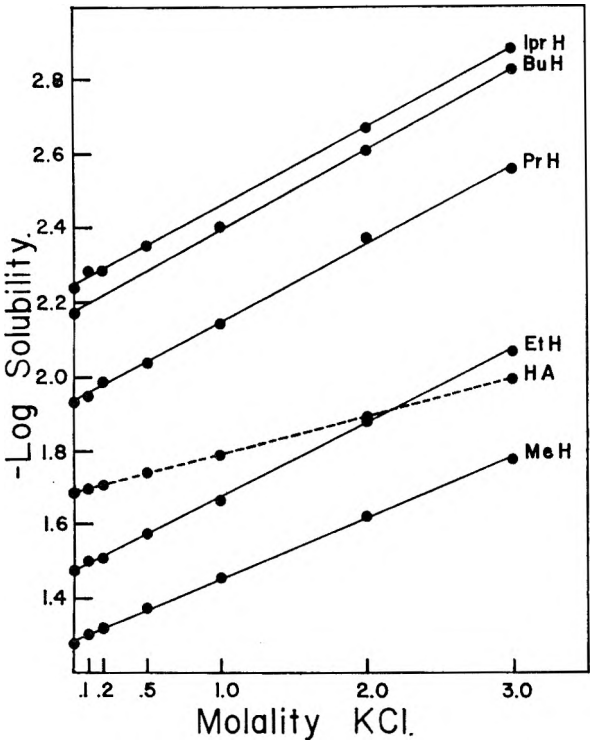

Fig. 1.—Logarithm of the solubilities of hippuric acid esters plotted against ionic strength. The dotted line represents free hippuric acid.

acid was added to 35 ml. of solvent in the homogenizer flask. The contents then were agitated at full speed for approximately 20 sec. This process was repeated every 5 min. for 1 hr. In this way no detectable rise in temperature occurred within the flask. At the end of the hour, the solution was transferred by suction through a sintered glass disk to a 10-ml. volumetric flask which was suspended in the bath. After a 10-min. equilibration the volume of the contents of the flask was exactly adjusted. The solution then was diluted in such a way as to produce a solution of approximately $3 \times 10^{-5} M$. The unknown then was read against a standard solution of that concentration in the Beckman DUV spectrophotometer at 230 mμ. All of the substances investigated in this work were found to follow Beer's law.

The only deviation from the above procedure was in the case of butyl hippurate. Since butyl hippurate is an oil rather than a solid as are the other esters, it was necessary to place a piece of fine filter paper, previously dampened with solvent, over the sintered disk for transfer to the volumetric flask. Aside from this one detail, the treatment was the same as for the other esters.

The values to be quoted are those obtained after 1 hr., while it was stated previously that equilibrium was apparently reached, in all cases, within 30 min. It is considered that this allows a comfortable margin of safety.

The solubility of hippuric acid in water was studied at seven temperatures ranging from 15 to 45°. The solubilities of the hippuric acid esters were studied in solvents of seven ionic strengths at 25°. One exception is again butyl hippurate which, because of limited quantities being available, was studied at only four ionic strengths.

Results

The logarithms of the solubilities of hippuric acid in water at various temperatures are to be seen in Table I. These values were obtained by plotting the experimental results against the reciprocal of the absolute temperature on large scale graph paper. The values were read from this smoothed curve. The experimental measurements were found to be repeatable within a mean deviation of 1.5%.

TABLE I

LOGARITHMS OF THE SOLUBILITIES OF HIPPURIC ACID IN WATER AT VARIOUS TEMPERATURES

Solubilities are expressed in terms of molarity

t, °C.	$-\log s$, moles/l.	t, °C.	$-\log s$, moles/l.
15	1.8425	35	1.5342
20	1.7725	40	1.4520
25	1.6960	45	1.3625
30	1.6178		

The values listed in Table I were fitted to an equation of the form

$$\ln s = \frac{\Delta H_0}{RT} + \frac{\Delta C_p}{R} \ln T + C \qquad (1)$$

where

$$\Delta H = \Delta H_0 + \Delta C_p T$$

The assumption is made that the conventional activity coefficient is independent of concentration.

Some thermodynamical quantities of interest are ΔF^0, written as equal to $-RT \ln s$, ΔH, ΔS^0, and ΔC_p. There are two values quoted for each of the above terms, the first being that obtained in this work while the second value, in parentheses, is the value obtained using conventional agitation.[5] The standard free energy change, $\Delta F^0 = 2293$ (2293) cal., $\Delta H = 6342$ (6264) cal., $\Delta S^0 = 13.6$ (13.3) e.u., and $\Delta C_p = 90.6$ (103.7) cal./°. It may be seen that agreement between the two methods is very good. At first glance it might seem that closer agreement between the ΔC_p values could have been expected. Since fitting the data to such an equation involves the use of a second derivative, very small variations in the experimental values can cause a considerable apparent variation of ΔC_p. In light of this fact, the agreement must be considered to be excellent. A possible explanation might be that slight hydrolysis of the peptide bond took place, especially at the higher temperatures, with the old method which involved equilibration for more than 2 days. Hydrolysis of this peptide bond would tend to cause higher readings than the current ones at the higher temperatures, and hence more curvature in a plot of $\ln s$ against $1/T$, giving rise, of course, to a higher apparent value for ΔC_p. The authors are convinced that the results obtained with high-speed stirring actually are more reliable than those obtained by means of the old technique.

The constants in eq. 1 are

$$\frac{\Delta H_0}{R} = -10{,}402, \frac{\Delta C_p}{R} = 45.59802, \text{ and } C = 298.59768$$

Table II shows the variation of the logarithms of the solubilities of the hippuric acid esters with ionic strength at 25°. The experimental values of $\log s$ when plotted against ionic strength were found to be linear. The equation for each straight line was obtained by the method of least squares; the values listed in Table II were obtained in this way. That good linearity was indeed obtained in each case may be ascertained by inspection of Fig. 1.

Discussion

It may be deduced from Table II that the salting out effect on the esters exerted by potassium

TABLE II

EFFECT OF POTASSIUM CHLORIDE CONCENTRATION ON THE SOLUBILITY OF HIPPURIC ACID AND HIPPURIC ACID ESTERS AT 25°

Solubility is expressed in terms of molarity

Ester of hippuric acid	Molality of KCl						
	0.0	0.1	0.2	0.5	1.0	2.0	3.0
	− log solubility						
Free acid	1.6828	1.6931	1.7034	1.7344	1.7859	1.8891	1.9922
Methyl	1.2865	1.3030	1.3195	1.3690	1.4516	1.6166	1.7817
Ethyl	1.4742	1.4941	1.5141	1.5738	1.6734	1.8726	2.0718
Propyl	1.9352	1.9563	1.9774	2.0407	2.1463	2.3574	2.5685
Isopropyl	2.2485	2.2696	2.2907	2.3539	2.4593	2.6701	2.8808
Butyl	2.1777	2.1994	2.2211	2.2863	2.3949	2.6121	2.8293

chloride increases with the increasing chain length as might be expected from electrostatic theories such as that of Butler.[6] Insufficient data on the physical characteristics of the esters are available at this time for attempting to interpret the results in terms of the more sophisticated treatment of Bockris, Bowler-Reed, and Kitchener.[7]

The good agreement of the temperature dependence studies with previous studies using conventional agitation techniques is encouraging. It must be pointed out, however, that the procedure outlined above does not lend itself to studies approaching equilibrium from oversaturation. It would seem that this is a small disadvantage when one considers that such a method is a very practical way to study the solubility of relatively unstable solids. The solution suggested for this problem is simple and inexpensive.

Acknowledgments.—The authors are indebted to the National Science Foundation and to the National Institutes of Health for their support. The authors also wish to thank Mr. M. C. Parkinson of the Virtis Company for his helpful advice and suggestions.

(6) J. A. V. Butler, *J. Phys. Chem.*, **33**, 1015 (1929).

(7) J. O. M. Bockris, J. Bowler-Reed, and J. A. Kitchener, *Trans. Faraday Soc.*, **47**, 184 (1951).

MUTUAL DIFFUSION IN NON-IDEAL LIQUID MIXTURES. III. METHYL ETHYL KETONE–CARBON TETRACHLORIDE AND ACETIC ACID–CARBON TETRACHLORIDE

BY D. K. ANDERSON AND A. L. BABB

Department of Chemical Engineering, University of Washington, Seattle, Washington

Received November 17, 1961

Mutual diffusivities and viscosities have been measured for the methyl ethyl ketone–carbon tetrachloride and acetic acid–carbon tetrachloride systems at 25.0°. The experimental data are discussed in terms of an equation similar in form to that of Hartley and Crank. The present equation was derived by assigning intrinsic diffusivities to the dimer of the associating component as well as to the monomeric species of both components.

Introduction

In a previous paper[1] the authors presented diffusion data for the diethyl ether–chloroform system in which the non-ideal behavior was explained by assuming that a one:one complex forms between components. In this paper, diffusivities and viscosities are reported for the systems methyl ethyl ketone–carbon tetrachloride and acetic acid–carbon tetrachloride at 25.0°.

Experimental

Diffusivities were measured with the use of a Mach–Zehnder diffusiometer described fully elsewhere[2] and viscosities were determined using an Ostwald viscometer. Temperatures were controlled at 25.0 ± 0.05°. The reagent-grade solvents were obtained from Mallinckrodt Chemical Works and were used without further purification.

The experimental diffusivities were obtained by measuring the interdiffusion of two solutions of very nearly equal concentrations. The measured value was taken to be that of a solution with a concentration equal to the average of the two solutions. The results are given in Tables I and II and in Fig. 1 and 2. Experimental viscosities are listed in Tables III and IV.

Discussion

Comparison of Results with Hartley and Crank Equation.—Hartley and Crank[3] have shown that for non-ideal systems the concentration dependence of mutual diffusivities could be described by an equation of the form

$$D_{AB} = \mathfrak{D}_A(V_B C_B) + \mathfrak{D}_B(V_A C_A) \qquad (1)$$

where D_{AB} is the mutual diffusivity, $\mathfrak{D}$ is the so-called intrinsic diffusivity, V is the molar volume, C is the molar concentration, and the subscripts A and B refer to components A and B in binary solution. They also have shown that if the driving force for diffusion is the gradient of the chemical potential, the intrinsic diffusivity is given by

$$\mathfrak{D}_i = \frac{RT}{N_T f_i} \frac{\mathrm{d} \ln a_i}{\mathrm{d} \ln c_i} \qquad (2)$$

(1) D. K. Anderson and A. L. Babb, *J. Phys. Chem.*, **65**, 1281 (1961).

(2) C. S. Caldwell, J. R. Hall, and A. L. Babb, *Rev. Sci. Instr.*, **28**, 816 (1957).

(3) G. S. Hartley and K. Crank, *Trans. Faraday Soc.*, **45**, 801 (1949).

Table I

Summary of Experimental Diffusivities for Methyl Ethyl Ketone–Carbon Tetrachloride

Mole fraction ketone, solution A	0	0.0363	0.1954	0.397	0.499	0.745	0.9894
Mole fraction ketone, solution B	0.0186	.0545	.2030	.405	.509	.752	1.000
Av. mole fraction	.0093	.0454	.1992	.401	.504	.749	0.9947
$D_{AB} \times 10^5$, cm.²/sec.	1.552	1.453	1.436	1.680	1.878	2.363	3.007

Table II

Summary of Experimental Diffusivities for Acetic Acid–Carbon Tetrachloride

Mole fraction acetic acid, solution A	0	0	0	0.00475	0.1820	0.4004	0.6008	0.8011	0.9896
Mole fraction acetic acid, solution B	0.00427	0.00453	0.00981	.01759	.1920	.4106	.6108	.8105	1.000
Av. mole fraction	.00219	.00227	.00491	.0112	.1870	.4055	.6058	.8058	0.9948
$D_{AB} \times 10^5$, cm.²/sec.	1.416	1.414	1.365	1.356	1.208	.916	.820	.881	1.277

Table III

Viscosities of Methyl Ethyl Ketone–Carbon Tetrachloride

Mole fraction ketone	0	0.1954	0.405	0.397	0.499	0.509	0.745	0 752	1.000
Viscosity at 25° (cp.)	0.887	0.736	0.620	0.623	0.576	0.576	0.483	0.472	0.393

Table IV

Viscosities of Acetic Acid–Carbon Tetrachloride

Mole fraction % acetic acid	0.00	21.4	41.8	60.8	80.5	100.0
Viscosity at 25° (cp.)	0.887	0.820	0.804	0.816	0.920	1.126

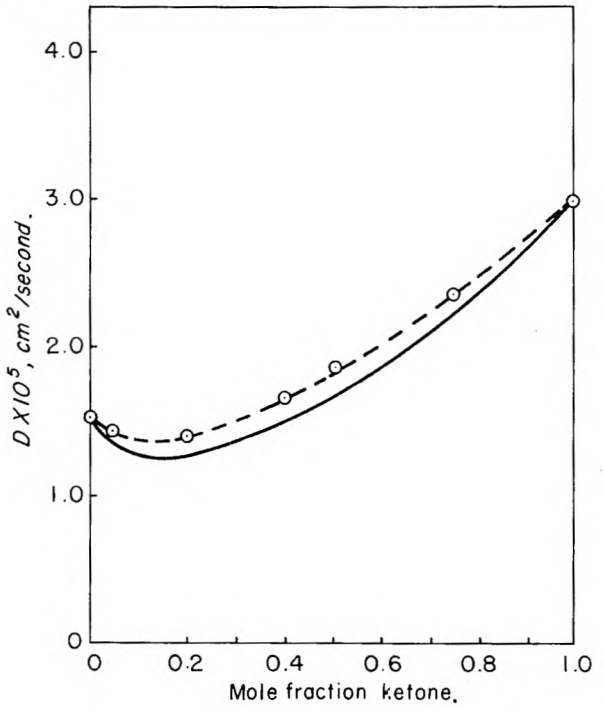

Fig. 1.—Diffusion coefficients for the system methyl ethyl ketone–carbon tetrachloride: ⊙, experimental; ———, calculated, eq. 3; – – – –, calculated, eq. 4.

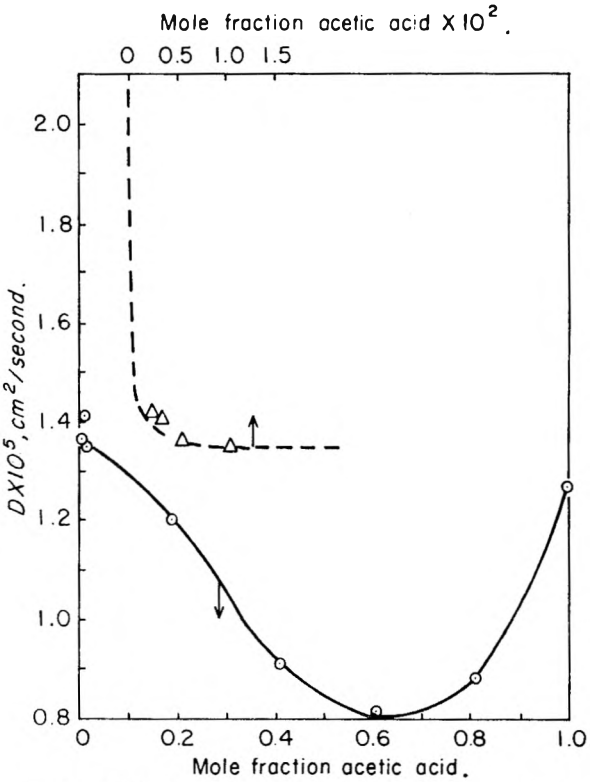

Fig. 2.—Diffusion coefficients for the system acetic acid–carbon tetrachloride: △, ⊙, experimental; – – – –, calculated, eq. 4.

where a_i is the activity of the component, η is the solution viscosity, and f_i is a friction coefficient dependent only on molecular size. These intrinsic diffusion coefficients are defined with respect to a reference frame through which no volume flow by bulk motion occurs. If eq. 1 and 2 are combined, the well-known Hartley and Crank equation is obtained.

$$D_{AB} = \frac{RT}{N\eta}\left[\frac{X_A}{f_B} + \frac{X_B}{f_A}\right]\frac{d \ln a}{d \ln X} \qquad (3)$$

Equation 3 was tested on the ketone–carbon tetrachloride system by calculating the values of f_A and f_B from the intercepts of the experimental diffusivity–mole fraction (X) curve. These values along with activities calculated from data available in the literature[4] were used to compute the diffusivity–mole fraction curve shown in Fig. 1. The lack of agreement with the experimental data probably lies in the assumption inherent in eq. 3 that the diffusing species are simple molecules; whereas, in fact, association occurs so that the diffusing species may be dimers, trimers, etc., as well as simple monomers.

Modified Form of the Hartley and Crank Equation.—In the previous paper, it was shown that diffusivity data for the system diethyl ether–

(4) R. T. Fowler and G. S. Norris, *J. Appl. Chem.*, **5**, 266 (1955).

chloroform could not be explained by the Hartley and Crank equation unless it was modified by assigning intrinsic diffusivities to the three species present in solution, *i.e.*, the two monomers and the ether–chloroform complex. For the system methyl ethyl ketone–carbon tetrachloride, hydrogen bonding can occur between ketone molecules. These interactions cause positive deviations from Raoult's law as opposed to the ether–chloroform system where the cross interaction causes negative deviations.

For the present investigation, it is assumed that the ketone exists in solution as monomers and dimers only and that the concentrations of these species can be related by an equilibrium constant

$$K = \frac{X_{II}}{X_I^2}$$

where X_{II} and X_I are the true mole fractions of the dimer and monomer, respectively. The methods outlined by Hildebrand and Scott[5] were used along with activity data[4] to estimate an equilibrium constant of 5.6 for the methyl ethyl ketone in carbon tetrachloride.

Intrinsic diffusivities were assigned to the dimer as well as to both monomers in solution and a modified form of the Hartley and Crank equation was derived[6]

$$D_{AB} = \frac{RT}{N\eta}\left[\left(\frac{X_I^0}{f_I X_A} + \frac{4X_{II}^0}{f_{II}X_A}\right)X_B + \frac{1}{f_2}X_A\right]\frac{d\ln a}{d\ln X} \quad (4)$$

$$X_I^0 = \frac{C_I}{C_A + C_B} = \frac{X_I}{1 + X_{II}}$$

$$X_{II}^0 = \frac{C_{II}}{C_A + C_B} = \frac{X_{II}}{1 + X_{II}}$$

Equation 4 reduces to eq. 3 for the case when no association occurs (*i.e.*, $X_I^0 = X_A$ and $X_{II}^0 = 0$). Values of X_I^0 and X_{II}^0 can be calculated from the equilibrium constant.

(5) J. H. Hildebrand and R. L. Scott, "The Solubility of Nonelectrolytes," 3rd. ed., Reinhold Publ. Corp., New York, N. Y., 1950.

(6) D. K. Anderson, Ph.D. Thesis, University of Washington, 1960, *Dissertation Abstr.*, **XXI**, No. 6, 1388 (1960).

Application of the Modified Equation.—It is not possible at present to assign a definite value to f_{II} since not enough is known about the diffusion mechanism. However, a qualitative check of the validity of eq. 4 may be obtained by determining a single value of f_{II} empirically from the data of Fig. 1 and then using eq. 4 to see how well the entire diffusivity–mole fraction curve is predicted.

The parameters f_1 and f_2 as calculated from the intercepts of the experimental curve were 29.0 and 34.7 Å., respectively. These correspond to Stokes–Einstein radii of 1.54 and 1.84 Å., respectively. Using the empirical value of 2.44 Å. for the Stokes–Einstein radius of the dimer, the curve shown in Fig. 1, which fits the experimental data very closely, was calculated.

The system acetic acid–carbon tetrachloride also provides an interesting test of eq. 4. Although it is not possible to estimate the degree of association of the acetic acid in concentrated solutions, it dimerizes very strongly in dilute solution. Davies, *et al.*, have found[7] the dimerization constant to be 2.07×10^{-3} g.-mole/l. at 25°,[8] so that over 96% of the acid is associated to dimers at a mole fraction of acetic acid of 0.04. Calculations based on eq. 4 indicated that a very sharp increase in the diffusivity should be observed at low concentrations of acetic acid. Data taken at concentrations as low as possible are shown in Fig. 2. It is seen that the diffusivity does increase sharply near the carbon tetrachloride intercept as predicted. This fact is not predictable from eq. 3. It would be of interest to have values at even lower concentrations.

Additional experimental data are being obtained for systems with known degrees of association and will be reported in future communications.

Acknowledgment.—This work was supported by the U. S. Army Research Office (Durham).

(7) M. Davies, P. Jones, D. Patnail, and E. A. Moelwyn-Hughes, *J. Chem. Soc.*, 1249 (1951).

(8) Their equilibrium constant was defined as C_I^2/C_{II}.

NUCLEAR MAGNETIC RESONANCE STUDIES OF THE P^{31} NUCLEUS IN PHOSPHORUS COMPOUNDS

By Leo C. D. Groenweghe, Ludwig Maier, and Kurt Moedritzer

Monsanto Chemical Company, Research Department, Inorganic Chemicals Division, St. Louis, Missouri

Received November 22, 1961

A study of two hundred new P^{31} nuclear magnetic resonance chemical shifts shows that the P^{31} relative shift contributions of common organic ligands directly bonded to a quadruply connected phosphorus atom lie in the order $C_6H_5 \geq CH_2Cl > CH_3 > C_2H_5$. Since these contributions are relatively unaffected by other groupings connected to the phosphorus, their value can be used in the estimation of chemical shifts—a fact of considerable interest in the structural analysis by n.m.r. of mixtures of organic phosphorus compounds. Consecutive substitution of one organic ligand for another on triply connected phosphorus leads to approximately equal stepwise changes in the P^{31} chemical shift. However, the effect of other ligands bonded to the phosphorus is so large that characteristic shift contributions cannot be assigned readily.

Since the discovery of the chemical shift in the nuclear magnetic resonance (n.m.r.) of the P^{31} nucleus by Knight[1] some ten years ago, about 400 n.m.r. spectra of individual phosphorus compounds have been reported in the literature. Various authors[2–7] have published impressive lists of P^{31} chemical shifts and have shown that P^{31} n.m.r. spectros-

(1) W. D. Knight, *Phys. Rev.*, **76**, 1259 (1949).

(2) H. S. Gutowsky, D. W. McCall, and C. P. Slichter, *J. Chem. Phys.*, **21**, 279 (1953).

(3) H. S. Gutowsky and D. W. McCall, *ibid.*, **22**, 162 (1954).

(4) N. Muller, P. C. Lauterbur, and J. Goldenson, *J. Am. Chem. Soc.*, **78**, 3557 (1956).

copy is an extremely valuable tool for structure proofs and for qualitative as well as quantitative analysis of mixtures of phosphorus compounds.[8]

This paper is based on previously unreported chemical shifts on 200 phosphorus compounds, published elsewhere by these authors.[9] With these data, empirical shift correlations have been carried out to a precision not obtained in previous publications. Such shift correlations are of great importance in the practical application of n.m.r. to the analysis of mixtures of phosphorus compounds.

Experimental

All n.m.r. measurements were made with a Varian Model V-4300B high-resolution spectrometer with a radio-frequency of 16.2 Mc. and a magnetic field of approximately 9395 gauss, using a Varian magnet, Model V-4012-HR. Chemical shifts are reported in p.p.m. of the applied field using 85% H_3PO_4 as a standard (zero shift). Upfield shifts are denoted by a plus sign and downfield shifts by a minus sign. The chemical shifts were determined by the concentric-tube technique, whereby a narrow tube containing the reference compound is inserted in the sample giving an accuracy depending on the broadness of the peak of *ca.* ±0.5 p.p.m. for well-resolved resonances. The few data obtained by the tube-interchange technique are accurate within *ca.* ±1.5 p.p.m. Most of the samples were contained in 15 mm. o.d. Pyrex tubes. When only a small quantity (as little as 100 mg.) of sample was available, either a 5 mm. o.d. tube was used with the proper probe insert or the tube in the sample holder was adjusted to a depth at which maximum response from the coil was obtained.

Most of the n.m.r. shifts have been obtained with pure samples. However, some of the compounds or phosphorus structure-building units have not been separated. In almost every case, compounds which were not isolated were contained in the reaction products of random reorganization reactions[8,10,11] carried out in sealed Pyrex tubes.

Results and Discussion

The chemical shift of phosphonic acids is dependent on the *p*H; therefore, the shifts of 16 sodium phosphonates have not been included in the published list. It was found that, in contrast with the case of phosphoric acid,[12] the chemical shift for phosphonates becomes more positive with increasing *p*H. The chemical shifts of the monosodium and disodium phosphonates were, respectively, from 2 to 4 and from 3 to 8 p.p.m. more positive than the shifts of the corresponding acids.

Contribution of Atoms and Ligands Connected to the Phosphorus.—In the past, one could calculate with a certain broad approximation the chemical shift of a phosphorus compound from additive "shift constants" attributed to the individual ligands attached to the phosphorus atom. The shift of quadruply-connected compounds could be estimated roughly through the knowledge of the shift of similar compounds; whereas, for triply-connected compounds, only a sometimes useful estimation could be obtained. Complications which one could encounter in estimating chemical shifts are illustrated in the following example.

The chemical shifts of $POCl_3$ and $POBr_3$ are −2.2 and +103.4 p.p.m., respectively. This would mean that on the average this shift becomes 35.2 p.p.m. more positive each time a bromine is substituted for a chlorine. This corresponds within ±3.4 p.p.m. to the experimental findings ($POCl_2Br$ = +29.6 p.p.m. and $POClBr_2$ = +64.8 p.p.m.[8]). However, the chemical shifts of $PSCl_3$, $PSCl_2Br$, $PSClBr_2$, and $PSBr_3$ are −28.8, +14.5, +61.4, and +111.8 p.p.m., respectively,[8] averaging an increase of 46.9 p.p.m. for each bromine substituted. Although here too, an agreement with the experiment of within ±3.6 p.p.m. was observed, the findings in the first series of compounds do not seem to be related to those of the second series. Furthermore, the correlation becomes worse when one compares the effect of substituting sulfur for oxygen in $POCl_3$ and $POBr_3$. A change in chemical shift of −26.6 and +8.4 p.p.m., respectively, then is obtained.

Obviously, changes in chemical shift as a result of substitution may be very much dependent on other atoms connected to the phosphorus. Consequently, the prediction of the chemical shift of a compound in which all but one ligand is different from a compound with known chemical shift is only possible when such dependency does not occur to an appreciable extent, unless one would be able to include the proper corrections for this effect. At the present time, however, such corrections do not seem possible.

Quadruply-Connected Phosphorus Compounds.—The change in chemical shift due to substituting one organic ligand for another is shown in Table I. Cases studied comprise substitution of either a methyl, chloromethyl, ethyl, or phenyl group directly connected to the phosphorus by another group of this series. The table gives average values for changes due to the substitution of one specific ligand for another one as computed for at least three structures which are identical except for different organic ligand(s) (R) and/or a bromine atom instead of a chlorine directly attached to the phosphorus. In such related structures, identical substitution results in a change in chemical shift which is the same within relatively close limits as shown by the reported standard deviations. Furthermore, from the data in this table, it is apparent that such substitutions also result in the same change in chemical shift, although with somewhat broader limits, if one disregards the nature of the other ligands. As a matter of fact, it appears possible to assign a fixed relative contribution for each of these ligands, such as +7 p.p.m. for methyl, +12 p.p.m. for chloromethyl, and +15 p.p.m. for phenyl, if one assigns a contribution of 0 p.p.m. for ethyl. It is highly probable that similar relationships can be written for other organic ligands when a sufficient amount of data becomes available.

Table II shows the change in chemical shift as a result of substitutions other than one organic ligand

(5) J. R. Van Wazer, C. F. Callis, J. N. Shoolery, and R. C. Jones, *J. Am. Chem. Soc.*, **78**, 5715 (1956).

(6) H. Finegold, *Ann. N. Y. Acad. Sci.*, **70**, 875 (1958).

(7) W. A. Henderson, Jr., and S. A. Buckler, *J. Am. Chem. Soc.*, **82**, 5794 (1960).

(8) L. C. D. Groenweghe and J. H. Payne, *ibid.*, **81**, 6357 (1959).

(9) K. Moedritzer, L. Maier, and L. C. D. Groenweghe, *J. Chem. Eng. Data*, **7**, 307 (1962).

(10) E. Fluck, J. R. Van Wazer, and L. C. D. Groenweghe, *J. Am. Chem. Soc.*, **81**, 6363 (1959); L. C. D. Groenweghe, J. H. Payne, and J. R. Van Wazer, *ibid.*, **82**, 5305 (1960).

(11) L. C. D. Groenweghe and J. H. Payne, *ibid.*, **83**, 1811 (1961).

(12) R. A. Y. Jones and A. R. Katritzky, *J. Inorg. & Nuclear Chem.*, **15**, 193 (1960).

TABLE I

EFFECT ON N.M.R. CHEMICAL SHIFT BY SUBSTITUTION OF ONE ORGANIC LIGAND BY ANOTHER IN QUADRUPLY-CONNECTED PHOSPHORUS COMPOUNDS

(R = any alkyl or aryl group, X = either Cl or Br)

Original structure	Substituted structure	Av. change in shift, p.p.m.	Stand. dev., p.p.m.	No. of substitutions considered
C_6H_5 replaced by another organic ligand				
C_6H_5RPSCl	C_2H_5RPSCl	−16.1	2.1	4
C_6H_5RPOCl	C_2H_5ROPCl	−16.7	0.9	3
C_6H_5RPSCl	$CH_2ClRPSCl$	− 1.1	3.3	3
C_6H_5RPOCl	$CH_2ClRPOCl$	− 3.7	1.7	3
CH_3 replaced by another organic ligand				
CH_3RPOCl	C_2H_5ROPCl	− 7.0	1.8	3
CH_3R_2PS	$C_2H_5R_2PS$	+ 1.5	1.3	3
CH_3RPSX	C_2H_5RPSX	−12.8	4.5	6
CH_3RPOCl	$CH_2ClRPOCl$	+ 7.2	0.8	3
CH_3RPSX	$CH_2ClRPSX$	+ 2.9	1.0	3
CH_3RPOCl	C_6H_5RPOCl	+10.8	1.3	3
CH_3RPSX	C_6H_5RPSX	+ 5.2	2.5	4

for another one. Once again, it appears that the same substitution results in the same change in chemical shift within relatively close approximation when carried out in structures which are identical except for different other organic ligands.

TABLE II

EFFECT ON N.M.R. CHEMICAL SHIFT BY SUBSTITUTION OF ONE INORGANIC LIGAND BY ANOTHER, ORGANIC OR INORGANIC, IN QUADRUPLY-CONNECTED PHOSPHORUS COMPOUNDS

(R and R′ = any alkyl ar aryl group)

Original structure	Substituted structure	Av. change in shift, p.p.m.	Stand. dev., p.p.m.	No. of pairs of structures considered
O Replaced by S				
$(RO)_3PO$	$(RO)_2PS$	−70.1	1.0	3
$RP(O)Cl_2$	$RP(S)Cl_2$	−37.5	2.8	4
RR′P(O)Cl in CCl_4	RR′P(S)Cl	−31.0	3.9	8
R_3PO in $CHCl_3$	R_3PS in $CHCl_3$	− 8.9	5.9	3
Miscellaneous substitutions				
$RP(O)Cl_2$	$RP(O)(OH)_2$	+19.1	4.9	4
$RP(O)(OH)_2$	$RP(O)(OC_2H_5)_2$	+ 0.8	1.4	4
$RP(O)Cl_2$	$RP(O)(OC_2H_5)_2$	+18.9	2.7	6
RR′P(O)Cl	RR′P(O)OH	+12.6	5.1	5
RR′P(S)Cl	RR′P(S)Br	+18.2	4.6	4
$R_2P(O)Cl$	$R_2P(O)CH_2Cl$	+12.3	6.6	4
$R_2P(O)Cl$	$R_2P(O)$-O-$P(O)R_2$	+11.5	1.6	5
$R_2P(O)CH_2Cl$	$R_2P(O)$-O-$P(O)R_2$	− 4.2	5.8	3
$R_2P(O)OH$	$R_2P(O)$-O-$P(O)R_2$	− 1.3	6.1	5
$R_2P(O)Cl$	$R_2P(O)OH$	+12.6	4.4	6
$RP(O)(OH)_2$	$(RPO_2)_n$	+17.0	1.3	3
$RP(O)Cl_2$	$(RPO_2)_n$	+30.4	5.7	3
$RP(O)(OC_2H_5)_2$	$(RPO_2)_n$	+17.3	0.8	3

It should be noted that these relationships also have been tested on similar substitutions for which only two examples are available, and that disagreement with the above conclusions could not be found.

Consequently, it appears possible to predict the chemical shift of a quadruply-connected phosphorus compound generally within 5 p.p.m., using the known chemical shift of a compound having the same structure except for one ligand on the phosphorus. Such predictions are valuable in the structural analysis of mixtures of organic phosphorus compounds by n.m.r. technique.

Triply-Connected Phosphorus Compounds.—The changes in chemical shift due to consecutive substitution of one organic ligand for another one are shown in Table III. It is apparent from this table

TABLE III

EFFECT ON N.M.R. CHEMICAL SHIFT OF SUBSEQUENT EXCHANGES OF HALOGENS OR R-GROUPS IN TRIPLY-CONNECTED PHOSPHORUS COMPOUNDS

Original compound	Substituted compound	Change in chemical shift for— 1st substitution	2nd substitution	3rd substitution
$(CH_3)_3P$	$(C_2H_5)_3P$	−13.5	−14.5	−13.6
$(C_2H_5)_3P$	$(C_6H_5)_3P$	− 5.3	− 1.6	− 6.5
$(CH_3)_3P$	$(C_6H_5)_3P$	−15.0	−19.0	−21.0
$(CH_3)_2PH$	$(C_2H_5)_2PH$	−22.5	−21.5	
$(CH_3)_2PH$	$(C_4H_9)_2PH$	−19.8	−10.3	
$(CH_3)_2PH$	$(C_6H_5)_2PH$	−27.2	−31.2	
$(CH_3)_2PCl$	$(C_2H_5)_2PCl$	−13.8	−13.2	
$(CH_3)_2PCl$	$(C_6H_5)_2PCl$	+ 8.6	+ 1.9	
$(C_2H_5)_2PCl$	$(C_6H_5)_2PCl$	+22.0	+15.5	
$(CH_3)_2PBr$	$(C_2H_5)_2PBr$	−10.6	−17.7	
$(CH_3)_2PBr$	$(C_6H_5)_2PBr$	+10.7	+ 6.2	

that all the changes studied fall within 5 p.p.m. of the average change obtained by dividing the change in chemical shift due to substitution of all the ligands by the number of ligand sites involved. Predictions of chemical shifts made on the basis of these findings can be expected to be relatively accurate, especially when one considers the wide range of chemical shifts covered by the triply-connected phosphorus compounds (−230 p.p.m. to +240 p.p.m.).

In certain cases, relationships as in quadruply-connected phosphorus compounds also can be found. For instance, substitution of a bromine for a chlorine in compounds of the type RR′PCl results in an average change of +6 ± 2.7 p.p.m. as calculated for five examples. Substitution of two bromines for two chlorines in structures of the type $RPCl_2$ increases the chemical shift by 6.6 ± 3.9 p.p.m. (three examples).[4] However, one cannot generalize these findings, since substitution of a phenyl group for a methyl group in $(CH_3)_2PH$ and in $(CH_3)_2PCl$ causes a change in chemical shift of −27.2 and +8.6 p.p.m., respectively. For the same substitution in $CH_3(C_6H_5)PH$ and $CH_3(C_6H_5)PBr$, a respective change of −31.2 and +6.2 p.p.m. is obtained.

An interesting phenomenon can be seen in the family of the aminophosphines. If one replaces all the dimethylamino groups by diethylamino groups, the chemical shift increases between 4 and 8 p.p.m., regardless of the number of amino groups connected to the phosphorus atom.

It also is of interest to note the surprising fact that the ethyl group takes a separate place in the aliphatic series of ligands. It can be seen from the data[9] that certain ethyl-substituted triply-connected phosphorus compounds have a much more

negative chemical shift than either the methyl or the higher alkyl-substituted compounds (*e.g.*, $(C_2H_5)_2PH$, $CH_3(C_2H_5)PH$, and $(C_2H_5)_3P$ [6]). Even in the quadruply-connected compounds, the ethyl group takes a separate place in the aliphatic series of ligands, but then only in a few cases does this ligand exhibit a more negative contribution than either methyl or higher alkyl (*e.g.*, $(C_2H_5)_2PSBr$ and $CH_3(C_2H_5)PSBr$.

Spin–Spin Coupling.—Table IV shows some average coupling constants resulting from interaction of hydrogen and fluorine in various structures.

TABLE IV

RANGE OF SPLIT MAGNITUDE AS A RESULT OF SPIN–SPIN INTERACTION WITH HYDROGEN AND FLUORINE IN VARIOUS STRUCTURES

X = halogen, Y = either halogen or hydrogen, Z = any ligand, n = integer from 1 to 3.

Structure of interacting ligand(s)	Av. coupling constant, c.p.s.	Stand. dev., c.p.s.	No. of compounds checked
$(ZCH_2\text{–}S)_nPX_{3-n}$	11	3	7
$YCH_2\text{–}PX_2$	19	5	3
$XCH_2\text{–}P(O)Z_2$	13	3	6
$H\text{–}PR_2$	198	14	8
F–P(O)RX	1110	89	3

Once again, averages of less than three examples have not been reported.

It is interesting to note that the hydrogen directly attached to the phosphorus in phosphines gives an average coupling constant of 197 c.p.s. (standard deviation = 14 c.p.s.), whereas this value becomes 606 c.p.s. (standard deviation = 85 c.p.s.) for the same hydrogen in quadruply-connected compounds.[6] Coupling constants for hydrogen connected to phosphorus over more than one bond do not seem to exceed 25 c.p.s. and depend on the number of bonds which separate the two atoms, the kind of atoms through which they are linked, and the other atoms connected to the phosphorus. Splits resulting from hydrogen connected to the phosphorus through two intermediate carbon atoms (–C–C–P) have not been observed at 9395 gauss fields, which means that the corresponding constants are less than *ca.* 5 c.p.s. However, coupling over a carbon and a sulfur, a carbon and an oxygen, or a carbon and a nitrogen seems to give constants of about 10–15 c.p.s. in both triply- and quadruply-connected compounds.

Acknowledgment.—The authors wish to thank Dr. J. R. Van Wazer for helpful discussions and John Yoder for taking some n.m.r. spectra, as well as John Chupp and Steven Fitch for some samples.

THE MECHANISM OF FORMATION OF LIVING α-METHYLSTYRENE DIMER AND TETRAMER

BY C. L. LEE, J. SMID, AND M. SZWARC

Department of Chemistry, State University College of Forestry at Syracuse University, Syracuse 10, New York

Received November 24, 1961

The mechanism of formation of living α-methylstyrene dimer and tetramer was investigated. These oligomers result from an electron transfer reaction: alkali metal + $\alpha MS \rightarrow \alpha MS^-$, $alkali^+$. It was shown that the monomeric radical-ions (αMS^-) do not dimerize into dimeric dianons ($^-\alpha MS\text{–}\alpha MS^-$); their reaction with the monomer yielding dimeric radical-ions ($^-\alpha MS\cdot\alpha MS\cdot$) is preferred. In the absence of a large alkali metal surface, the dimeric radical-ions dimerize into tetrameric dianions, but in systems having a large metal surface, *e.g.*, in the presence of sodium emulsion, the dimeric radical-ion acquires an electron and is transferred into dimeric dianion. The structure of the dimer and the tetramer was discussed. The kinetics of dissociation of the living tetramer into living dimer was investigated.

It was recognized by Dainton and Ivin[1] that the conversion of monomer to *high* molecular weight polymer is restricted by certain thermodynamic conditions. Their treatment of polymerization processes leads to the concept of ceiling temperature which is determined by the heat and entropy of polymerization. This temperature becomes particularly low when a strained polymer is formed, the polymerization of α-methylstyrene being an example. Indeed, at 0° the conversion of this monomer to a high molecular weight polymer is possible only if its concentration exceeds 0.7 *M*, and a still higher concentration is needed for the polymerization to proceed at room temperature.[2,3]

The thermodynamic restrictions outlined by Dainton and Ivin do not apply to processes yielding *low* molecular weight polymers,[1] and it is indeed possible to form a low molecular weight poly-α-methylstyrene under conditions which forbid the formation of a high molecular weight material. It is the purpose of this paper to discuss such reactions, to investigate their mechanisms, and to establish the structure of the resulting oligomers.

Dimerization of α-Methylstyrene.—A slow addition of α-methylstyrene to a vigorously stirred emulsion of sodium in tetrahydrofuran produces dimeric dianions which yield 2,5-diphenyl-2,5-dimethyladipic acid on carboxylation.[4] The dimerization is quantitative, and the addition of aromatic hydrocarbons such as naphthalene seems to catalyze the process.

It was recognized by Paul, Lipkin, and Weissman[5] that the reaction of alkali metals with aro-

(1) F. S. Dainton and K. J. Ivin, *Nature*, **162**, 705 (1948); *Quart. Revs.* (London), **12**, 61 (1958).

(2) H. W. McCormick, *J. Polymer Sci.*, **25**, 488 (1957).

(3) D. J. Worsfold and S. Bywater, *ibid.*, **26**, 299 (1957).

(4) C. F. Frank, *et al.*, *J. Org. Chem.*, **26**, 307 (1961).

(5) D. E. Paul, D. Lipkin, and S. I. Weissman, *J. Am. Chem. Soc.*, **78**, 116 (1956).

matic hydrocarbons, or with monomers such as styrene or α-methylstyrene, proceeds by an electron transfer process and yields negative radical-ions. The primary radical-ions derived from monomers undergo further reactions yielding either dimeric dianions or dimeric radical-ions.[6] Using α-methylstyrene as an example, these processes may be described by the equations

$$\text{electron donor (}e.g.\text{, alkali metal)} + \alpha\text{-Me-styrene} \longrightarrow \alpha\text{-Me-styrene}^- \quad (1)$$

$$2\ \alpha\text{-Me-styrene}^- \longrightarrow (\alpha\text{-Me-styrene})^{=}_2 \quad (2)$$

or

$$\alpha\text{-Me-styrene}^- + \alpha\text{-Me-styrene} \longrightarrow {}^-\alpha\text{-Me-styrene-}\alpha\text{-Me-styrene}\cdot \quad (3)$$

$${}^-\alpha\text{-Me-styrene-}\alpha\text{-Me-styrene}\cdot + \text{electron donor} \longrightarrow (\alpha\text{-Me-styrene})^{=}_2 \quad (4)$$

This means that the dianion may be formed either by direct dimerization of the monomeric radical-ions (reaction 2), or through a sequence of reactions yielding first the dimeric radical-ions (reaction 3), and then, as result of further electron transfer, the dimeric dianions (reaction 4). The electron donated in reaction 4 may come from the original donor, from the monomeric radical-ion, or from the dimeric radical-ion (in the latter case the electron transfer represents a disproportionation of the dimeric radical-ions).

The electron transfer from an alkali metal to a monomer or to a dimeric radical-ion seems to be enhanced by the presence of aromatic hydrocarbons. Apparently the flat molecules of these hydrocarbons react with the metal surface faster than the monomer does, and thus the indirect electron transfer proceeds more rapidly than the direct one. This is an interesting point which may be of some significance in surface chemistry.

$$\text{alkali surface} + \text{aromatic hydrocarbon} \longrightarrow \text{aromatic hydrocarbon}^-$$

$$\text{aromatic hydrocarbon}^- + \text{monomer} \longrightarrow \text{aromatic hydrocarbon} + \text{monomer}^-$$

The dimers formed from the monomeric radical-ions of styrene or its derivatives possess phenyl groups on their terminal carbon atoms. Such dimers, whether dianions or dimeric radical-ions, are more stable and more readily formed than any other conceivable dimer.[6,7] The dimers of styrene or α-methylstyrene yield on carboxylation the respective 2,5-substituted adipic acids,[4] and the dimer of 1,1-diphenylethylene gives 2,2,5,5-tetraphenyladipic acid.[8]

All the facts given above fail to distinguish between the two alternative ways of formation of the dimeric dianions: namely, the reaction proceeding through direct dimerization of the respective monomeric radical-ions and the one involving the dimeric radical-ions as an intermediate. To shed more light on this problem it was decided to investigate processes yielding low molecular weight poly-α-methylstyrenes of degree of polymerization greater than 2.

Tetramerization of α-Methylstyrene.—A 0.4–0.5 *M* solution of α-methylstyrene in tetrahydrofuran reacts at room temperature with sodium, deposited as a mirror, and yields dianions of α-methylstyrene tetramer in about 6 hr. Titration of the resulting solution, freed from excess of sodium, showed that the molar ratio of Na:α-methylstyrene was 1:2. The living ends may be destroyed by adding water and the polymer precipitated. Two samples prepared in this way by Dr. Ladacki were investigated. The molecular weights determined by ebullioscopic technique were found to be 484 and 433, respectively, whereas the theoretical value is 474. On carboxylation a tetrameric dicarboxylic acid was formed and its molecular weight determined ebullioscopically and by titration. The results agreed again with the calculated one (ebullioscopic 582, electrometric titration 570, theoretical 562).[9]

Studies of equilibria between the monomer and the tetramer[10] demonstrated that the tetramer may add the monomer and grow to higher *n*-mers, but it cannot degrade to a lower molecular weight polymer and the monomer. These observations prove that the tetramer is not a mixture of oligomers having an average degree of polymerization of 4, but it is essentially a single species. Consideration of the relevant reactions leads to the conclusion[7] that such a tetramer results from the dimerization of the dimeric radical-ions formed by the reaction of the monomeric radical-ions with the monomer (reaction 3). Therefore, this structure is proposed for the oligomer

$$-C(Ph)(CH_3)\cdot CH_2\cdot CH_2\cdot C(Ph)(CH_3)\cdot C(Ph)(CH_3)\cdot CH_2\cdot CH_2\cdot C^-(Ph)(CH_3)$$

Further observations verified this conclusion. The addition of two equivalents of α-methylstyrene to the dimeric dianions of this monomer produces also tetrameric dianions. The equilibrium concentration of the monomer in contact with a 0.06 *M* solution of these tetramers is about 0.01 *M* at 0°,[11] whereas its concentration in a similar solution of the directly formed tetramer is less than 0.001 *M*. Hence, the tetrameric dianions formed directly from α-methylstyrene and metallic sodium must differ from those formed from the dimeric dianions. The mode of preparation of the latter implies that their structure is

$$-C(Ph)(CH_3)\cdot CH_2\cdot C(Ph)(CH_3)\cdot CH_2\cdot CH_2\cdot C(Ph)(CH_3)\cdot CH_2\cdot C^-(Ph)(CH_3)$$

or

$$C^-(Ph)(CH_3)\cdot CH_2\cdot C(Ph)(CH_3)\cdot CH_2\cdot C(Ph)(CH_3)\cdot CH_2\cdot CH_2\cdot C^-(Ph)(CH_3)$$

These tetramers possess the head-to-tail linked monomeric units, and therefore they are expected to decompose into trimers and the monomer. Hence, in agreement with our observations, the respective equilibrium concentration of the monomer should not be negligible in such systems. The stability of the directly formed tetramer indi-

(6) M. Szwarc, *Nature*, **178**, 1168 (1956).

(7) M. Szwarc, *Makromol. Chem.*, **35**, 132 (1960).

(8) These facts are challenged by Wenger, *J. Am. Chem. Soc.*, **82**, 4281 (1960)) who states that the head-to-tail dimer should be more readily formed although it is *less* stable. No evidence is given to support this claim.

(9) We are indebted to Dr. L. H. Tung of the Midland Division of Dow Chemical Co. for carrying out the ebullioscopic molecular weight determinations.

(10) A. Vrancken, J. Smid, and M. Szwarc, *J. Am. Chem. Soc.*, **83**, 2772 (1961); also *Trans. Faraday Soc.*, in press.

(11) A. Vrancken, unpublished results from this Laboratory.

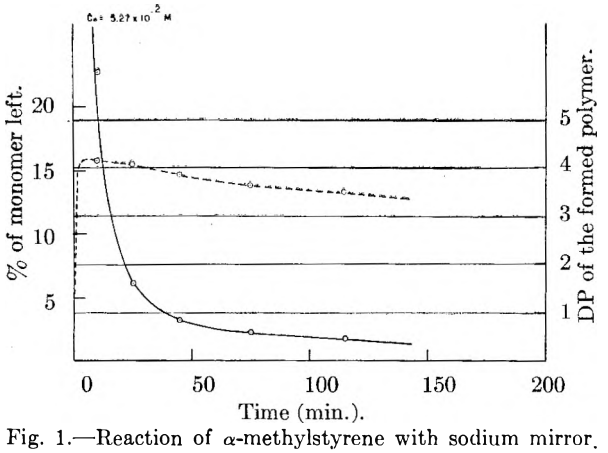

Fig. 1.—Reaction of α-methylstyrene with sodium mirror.

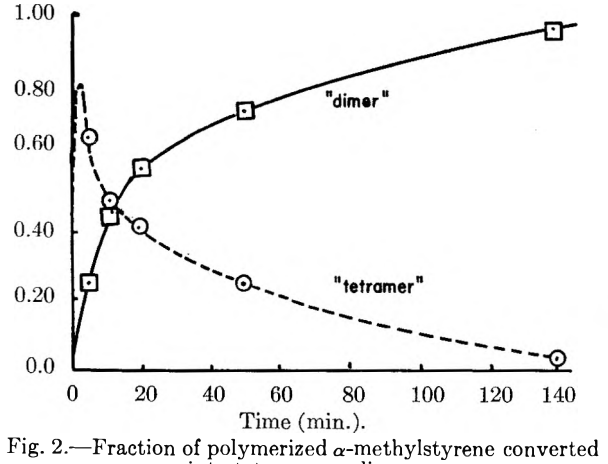

Fig. 2.—Fraction of polymerized α-methylstyrene converted into tetramer or dimer.

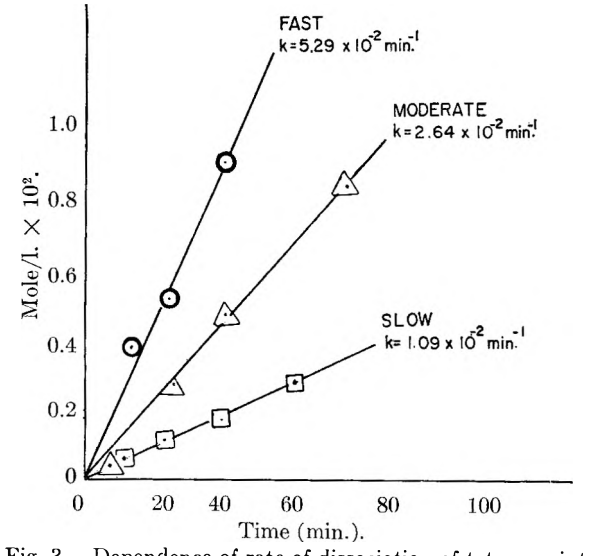

Fig. 3.—Dependence of rate of dissociation of tetramer into dimer on speed of stirring at 25°.

cates the absence of the head-to-tail links in its molecule. Thus, the structure proposed in the preceding paragraph is the only one consistent with this requirement.

The tetrameric dianion formed from α-methylstyrene and sodium is a convenient and efficient initiator for the polymerization of styrene or α-methylstyrene.[7,11] Actually, recent work, carried out in this Laboratory,[12] has demonstrated that the rate constant for styrene addition to this dianion is larger than the propagation rate constant of anionic homopolymerization of styrene.

Reaction of α-Methylstryene with Sodium and with Sodium–Potassium Alloy.—Formation of living α-methylstyrene tetramers indicates that the reaction of the monomeric radical-ions with the monomer is faster than their dimerization. Further evidence supporting this view comes from studies of the kinetics of the monomer–alkali metal interaction. Solutions of α-methylstyrene (0.05 M) were treated with sodium deposited as mirror, and with liquid sodium–potassium alloy. The rate of the process depends on the rate of stirring, which therefore was kept reasonably uniform in each experiment. Aliquots were withdrawn and analyzed and thus the momentary concentrations of living ends and of the residual monomer were determined.

The results obtained in the reaction with the sodium mirror are shown in Fig. 1. The continuous line gives the % of the residual monomer as a function of time. One notices the rapid consumption of the monomer—in 0.5 hr. 95% had reacted and in about an hour only 2% was left. The dotted line gives the momentary average degree of polymerization ($\overline{DP}$)

$$\overline{DP} = 2\ [\text{concn. of polymerized monomer}]/[\text{concn. living ends}]$$

and shows that the initial product is essentially a tetramer which slowly degrades in the later stages of the reaction.

The reaction with sodium–potassium alloy was much faster. The results of the analysis are given in Fig. 2 as fractions of the polymerized monomer which is present as a tetramer and a dimer, respectively, assuming that these were the only two polymers formed in the reaction. Inspection of Fig. 2 again shows that the tetramer seems to be the first product of the reaction, although under these conditions its degradation to the dimer is much faster.

These results confirm our suggestion that the reaction

$$\text{alkali metal} + \alpha\text{MS} \longrightarrow \alpha\text{MS}^-, \text{A}^+$$

is followed by the rapid reaction of the radical-ions with the monomer giving dimeric radical-ions (reaction 3) which subsequently dimer-

$$2\ ^-\alpha\text{MS}\cdot\alpha\text{MS}\cdot \longrightarrow\ ^-\alpha\text{MS}\cdot\alpha\text{MS}\cdot\alpha\text{MS}\cdot\alpha\text{MS}^- \quad (5)$$

ize producing the head-to-head tail-to-tail tetramer. The results also indicate that the dimerization of the dimeric radical-ions is preferred to their disproportionation

$$2\ ^-\alpha\text{MS}\cdot\text{MS}\cdot \longrightarrow\ ^-\alpha\text{MS}\cdot\alpha\text{MS}^- + 2\alpha\text{MS} \quad (6)$$

It is implied in this mechanism that the dimerization of the monomeric radical-ions (reaction 2) is much slower than their addition to the monomer (reaction 3). This is plausible since the concentration of the latter is much higher than that of the former, and the respective rate constants probably are not too different. Actually, the recently com-

(12) C. L. Lee, J. Smid, and M. Szwarc, *J. Am. Chem. Soc.*, **83**, 2961 1961).

pleted studies of the 1,1-diphenylethylene system showed that the rate constant for the dimerization of $(Ph)_2C{=}CH_2^-$ is $\sim 10^{-1}$ l./mole sec. whereas that for the reaction $(Ph)_2C{=}CH_2^- + CH_2{=}C(Ph)_2 \rightarrow$ dimeric radical-ion is about 10^{-2} l./mole sec. In view of the large difference in the concentration of $(Ph)_2C{=}CH_2$ and its radical-ions the latter reaction is much faster than the former. The rate constant for the dimerization of the monomeric radical-ions is much smaller than that observed for the recombination of conventional radicals. The recombination of the dimeric radical-ions is expected to proceed faster, although it still may be somewhat slower than that of conventional radicals.

In the previously discussed reactions electrons were not easily available since the surface of the metal was relatively small. If sodium emulsion is used, the surface is much larger and electrons are more readily provided. Under such conditions the reaction of dimeric radical-ions with sodium (reaction 4) may compete efficiently with their dimerization, and then α-methylstyrene may be directly converted into dimeric dianions. The presence of catalytically acting aromatic hydrocarbons makes this process even more favorable.

Conversion of the "Living" Tetramer of α-Methylstyrene into the Dimer.—Although the interaction between a sodium mirror and α-methylstyrene in tetrahydrofuran solution initially yields the tetramer, prolonged contact with the metal leads to a much slower reaction which results in the formation of additional "living" ends and a decrease in the degree of polymerization. This slow depolymerization is enhanced if sodium is replaced by potassium or sodium–potassium alloy. Its progress may be followed conveniently either by titrating with methyl iodide aliquots of the solution filtered from the remaining alkali metal, or by measuring the increase in the optical density of the solution at 340 mμ (the absorption peak of the living poly-α-methylstyrene).

The kinetics of depolymerization of the living α-methylstyrene tetramer by sodium–potassium alloy is shown in Fig. 3. It can be seen that the rate of reaction depends on the rate of stirring, indicating that the process is heterogeneous and takes place on the surface of the metal. Since the living dimer is the final product of the reaction one has to conclude that the equilibrium in the system

living tetramer + solid alkali metal $\longrightarrow$ 2 living dimers

is displaced to the right.

Although the living tetramer is degraded to the dimer on the surface of an alkali metal, such a reaction is not observed with "killed" tetramer. Apparently the presence of negative charges on both ends of the tetramer facilitates the dissociation process. Dissociation of a C–C bond by an alkali metal is a known reaction observed in some hydrocarbons, such as $(C_6H_5)_2CH{\cdot}CH(C_6H_5)_2$.[13]

The financial support of this study by The National Science Foundation (Grant G-14393) and the Quartermaster Corps (Grant No. DA-19-129-QM-1297) is gratefully acknowledged.

(13) G. E. Coates, "Organo-Metallic Compounds," Methuen, London, 1956, p. 16.

A RAMAN-SPECTRAL STUDY OF SOME GALLIUM(III) CHLORIDE SYSTEMS[1]

By Kenneth Schug and Leonard I. Katzin[2]

Chemistry Division, Argonne National Laboratory, Argonne, Illinois

Received November 24, 1961

Raman spectral observations and related chemical studies have been employed to investigate the nature of the species present in diisopropyl ether–aqueous extraction systems of gallium(III) chloride and in certain other gallium chloride solutions. Evidence is presented that tetrahedral $GaCl_3OH_2$ is an important species in the ethereal phase when the molar ratio of chloride to gallium is low and/or in the absence of a cation capable of accompanying the species $GaCl_4^-$ in the ether phase.

Introduction

The extraction of gallium(III) chloride from aqueous solutions into diisopropyl ether has been the subject of several investigations which provide evidence for the nature of the species present in the ethereal phase. Analytical results[3] and spectral studies[4] in these systems as well as those in the apparently analogous iron(III) chloride systems[4-8] can be interpreted in terms of the extraction of a tetrahedral MCl_4^- ion, accompanied by a hydrated proton. Extensive association of the ionic species presumably occurs in the low-dielectric ethereal phase.[9]

In this paper we report some Raman-spectral and chemical observations on extraction systems at high gallium(III) concentrations, and on certain other gallium(III) chloride solutions in ether.

Experimental

Materials.—Aqueous gallium(III) chloride stock solutions of about 4 *M* concentration were prepared by the

(1) Based on work performed under the auspices of the U. S. Atomic Energy Commission.

(2) To whom inquiries should be addressed.

(3) N. Nachtrieb and R. E. Fryxell, *J. Am. Chem. Soc.*, **71**, 4035 (1949).

(4) L. A. Woodward and M. J. Taylor, *J. Chem. Soc.*, 4473 (1960).

(5) N. Nachtrieb and R. E. Fryxell, *J. Am. Chem. Soc.*, **70**, 3552 (1948).

(6) R. J. Myers, D. E. Netzler, and E. H. Swift, *ibid.*, **72**, 3767 (1950).

(7) H. L. Friedman, *ibid.*, **74**, 5 (1952).

(8) A. H. Laurene, D. E. Campbell, S. E. Wiberley, and H. M. Clark, *J. Phys. Chem.*, **60**, 901 (1956).

(9) N. Nachtrieb and R. E. Fryxell, *J. Am. Chem. Soc.*, **74**, 897 (1952).

(slow) reaction of a slight excess of 99.99% pure Ga metal with concentrated HCl. The solutions were removed from contact with the excess metal some time before use, to assure complete oxidation of the gallium to the +3 state.

Pure $GaCl_3$(c) was prepared by the reaction of gallium metal with gaseous HCl, at 375–400°, on the vacuum line. It was further handled by vacuum line techniques to prepare anhydrous gallium(III) chloride solutions in several solvents.

Aqueous gallium perchlorate solutions were prepared by the reaction of gallium metal with hot 72 weight % perchloric acid.

Fisher certified diisopropyl ether was used, usually without further purification.

All other chemicals used were of reagent quality.

Analytical Methods.—Gallium was determined gravimetrically as the 8-hydroxyquinolate, by the oxidative method described by Kolthoff and Sandell,[10] or by the EDTA method of Flaschka.[11] Chloride was determined by the Volhard method. Lithium was determined by flame photometry, with the kind coöperation of Ralph Bane. Water was determined directly by the Karl Fischer method, using a dead-stop end-point method.

The ethereal phase analyses were performed on solutions made by adding an aliquot of the ether phase to some water in a volumetric flask, allowing the ether to evaporate, and then making to volume.

Measurements.—Spectra were obtained on a Model 81 Cary Raman spectrophotometer, with 7-mm. sample cells (solution volume, *ca.* 4 ml.). Single slit conditions were used, with the slit set 10 cm. long and 10 $cm.^{-1}$ wide. Most spectra were taken by slow scanning from the low-frequency limit to about 600 $cm.^{-1}$, since preliminary runs indicated no significant solute peaks appear above 600 $cm.^{-1}$. The solution spectra were measured at 34 ± 1°, the normal operating temperature of the spectrophotometer's cell compartment. No special precautions appeared to be necessary in the preparation of the samples. For the Raman study of solid Ga_2Cl_6 a special cell designed to increase the amount of Raman light collected was employed.

Polarization studies were carried out by enclosing the sample tube in the cylindrical Polaroid shields provided with the spectrophotometer for this purpose.

Results

Aqueous Solutions.—The Raman spectra of a large number of aqueous Ga(III) solutions have been obtained over the frequency region 60–650 $cm.^{-1}$. The Cl/Ga ratio has been varied from zero to about 10 by the appropriate mixing of aqueous stock solutions of $GaCl_3$, $Ga(ClO_4)_3$, HCl, and LiCl. The only Raman lines observed have had their peaks at 117, 152, 346, and 380 $cm.^{-1}$. These correspond closely in position and character with those reported by Woodward and Nord[12] for $GaCl_4^-$ ion in aqueous $GaCl_3$–HCl solutions. There appears to be a systematic variation in the ratio of the area of these peaks to the concentration of total gallium ("specific area") as LiCl progressively replaces HCl as the source of excess chloride.

Extractions.—The analytical results from typical extraction systems are given in Table I. The extraction of aqueous gallium chloride solutions, containing an excess of HCl, by diisopropyl ether gave results in substantial agreement with previous work[3,4]: nearly complete extraction of gallium, a solute composition in the ethereal phase agreeing with the formulation $HGaCl_4 \cdot (3.5\text{–}5\ H_2O)$, and a Raman spectrum very similar to that found in aqueous HCl–$GaCl_3$ solutions. The gallium concentration achieved in the ethereal phase ranged from 0.36 to 1.49 moles per l. in the acid extractions. In extractions with less than one mole of HCl per mole of $GaCl_3$ the extraction of Ga was incomplete and, at high total gallium, the Cl/Ga ratio was less than 4.

It is well known that in certain composition regions, the ether phase separates into two phases, the "light" and the "heavy" phases. The low gallium concentration in the light ether phase (*ca.* 0.1 *M*) made it difficult to obtain a satisfactory Raman spectrum for that phase, due to the interference of weak solvent peaks, and due to high "noise" levels. However, each ether phase has its strongest peak at 346 $cm.^{-1}$, and certain other peaks occur in agreement with the $GaCl_4^-$ frequencies cited above.

TABLE I

ANALYTICAL DATA FOR THE EQUILIBRIUM ETHEREAL PHASES IN SOME TYPICAL EXTRACTIONS[a]

Electrolyte added to initial aq. soln.	Total Ga, *M*	Total Cl, *M*	H_2O, *M*	Li, *M*	Cl/Ga	H_2O/Ga
None	1.21[b]	4.15	..	..	3.4	
	0.89[b]	2.83	..	..	3.2	
	1.04[b]	3.75	3.64	..	3.7	3.6
HCl	0.68	2.65	3.4	..	3.9	5.0
	.98	3.93	4.1	..	4.0	4.2
	1.49	5.64	5.4	..	3.8	3.6
	0.71[b]	2.75	3.36	..	4.0	4.7
	1.68[b,c]	5.81	..	..	3.5	..
LiCl	0.97	3.48	..	0.35	3.6	..
	.97	3.61	..	.45	3.7	
	.96	3.81	4.70	.67	4.0	3.0
	1.55	5.89	2.9		3.8	3.0
HCl + LiCl[d]	0.98	4.1	5.1	.04	4.2	5.0
$CaCl_2$	1.85[b]	6.13	3.9	..	3.3	2.1

[a] Usually 3 ml. of aqueous solution was shaken with 5 ml. of ether; the volume of the ether phase always increased. [b] Gallium extraction was incomplete in these cases. [c] Initial aqueous solution had a $HCl/GaCl_3$ ratio of ~0.5. [d] Approximately equimolar LiCl and HCl used.

In contrast to the extractions from solutions with excess acid present, the extractions from solutions corresponding to $GaCl_3$ in pure water showed the following characteristics: gallium extraction was incomplete; Cl/Ga and H_2O/Ga ratios in the extract were lower: and several new peaks appeared in the Raman spectrum of the ethereal phase. In Fig. 1 are shown typical Raman spectra for ether phases equilibrated with a solution of $GaCl_3$ with excess acid, and equilibrated with a solution of $GaCl_3$ in water, respectively. Both are of about the same total gallium concentration. The most striking differentiating features in the second spectrum are the appearance of a strong, sharp, highly polarized peak with its maximum at 363 $cm.^{-1}$, and a broad depolarized peak at 405 $cm.^{-1}$. Lesser, but significant, differences also are seen in the 100–200 $cm.^{-1}$ range. A plausible, though not unique, resolution of the altered low frequency region may be made by introducing peaks at 130 and 142 $cm.^{-1}$. Spectral interpretation in the low-frequency region is complicated both by extensive overlapping of genuine Raman peaks, and by the presence of a spurious double peak in the 150–

(10) I. M. Kolthoff and E. B. Sandell, "Textbook of Quantitative Inorganic Analysis," The Macmillan Co., New York, N. Y., 1952, p. 607.

(11) H. Flaschka and H. Abdine, *Chem. Analyst*, 44, 96 (1954).

(12) L. A. Woodward and A. A. Nord, *J. Chem. Soc.*, 3721 (1956).

170 cm.$^{-1}$ region. The latter is an instrumental artefact of undetermined origin.

Measurements of the peak areas show that the sum of the areas under the 346 and 363 cm.$^{-1}$ peaks bears nearly the same ratio to the total gallium concentration in the ether phase as does the 346 cm.$^{-1}$ peak alone in the acid extracts. A similar relationship, constant total peak area in relation to gallium concentration, seems to hold for the low-frequency cluster, although the imprecision in measurement is greater.

Effects of Neutral Chlorides.—Some extractions were performed in which chloride salts were added to the aqueous phase containing $GaCl_3$ without excess HCl. Halides used were LiCl, NH_4Cl, and $CaCl_2$.

A moderate excess of LiCl resulted in complete extraction of gallium. The ether phases had Cl/Ga and H_2O/Ga ratios less than 4, contained appreciable concentrations of Li^+, and gave Raman spectra which were intermediate between those for extractions from solutions with excess HCl and those from solutions of $GaCl_3$ alone. With increasing LiCl concentrations, the Cl/Ga ratio in the ether approached 4, the Li^+ concentration increased, and the H^+ concentration showed little change. The spectrum approached that of the extracts from excess-HCl solutions. The 363 cm.$^{-1}$ peak was evident only as a shallower-than-usual minimum between the 346 and 380 cm.$^{-1}$ peaks of $GaCl_4^-$. One starting aqueous phase contained approximately equimolar LiCl and HCl (Cl/Ga = 10). The ethereal extract contained very little lithium, its Cl/Ga ratio was about 4, and its Raman spectrum was almost identical to that of the extract from solutions containing HCl without LiCl.

NH_4Cl in the initial aqueous $GaCl_3$ solutions results in a slight increase in the fraction of gallium extracted, an increase in the Cl/Ga ratio in the ether phase, and an increase in the 346 cm.$^{-1}$ peak at the expense of the 363 cm.$^{-1}$ peak. $CaCl_2$ in the initial aqueous $GaCl_3$ solution gave a slight increase in the ethereal 346 cm.$^{-1}$ peak area relative to the 363 cm.$^{-1}$ peak.

Upon addition of NH_3 or NaOH to the initial aqueous solutions, less gallium was extracted than in their absence, but the extract Cl/Ga ratio was not greatly affected, and the Raman spectrum showed no qualitative changes. If $HClO_4$ were added to the initial aqueous solution, the extent of gallium extraction, and the extract Cl/Ga ratio both increased, and the 346 cm.$^{-1}$ peak area increased sharply at the expense of the 363 cm.$^{-1}$ peak and area. The fraction of gallium extracted approached 75% at high $HClO_4$.

Other Solutions.—To aid in the identification of the species responsible for the peaks not ascribable to $GaCl_4^-$ (the 405, 363, 142, and 130 cm.$^{-1}$ peaks) pure crystalline $GaCl_3$ was dissolved in diisopropyl ether. When the ether was distilled onto the solid gallium trichloride at Dry Ice temperature there was no apparent reaction. On slowly increasing the temperature to about 0° the crystalline $GaCl_3$ was converted into a much more voluminous flocculent white solid. Simultaneously

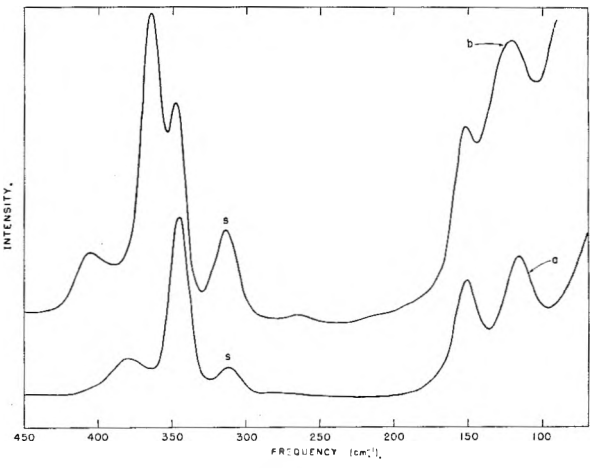

Fig. 1.—Raman spectra of sopropyl ether phase in extraction of (a) aqueous $GaCl_3$ with excess HCl; (b) aqueous $GaCl_3$. The total gallium concentration in the ether is about 1 *M* in each case. Solvent peaks are denoted by s. The spectra were obtained at different gain settings, as is indicated by the relative sizes of the solvent peaks.

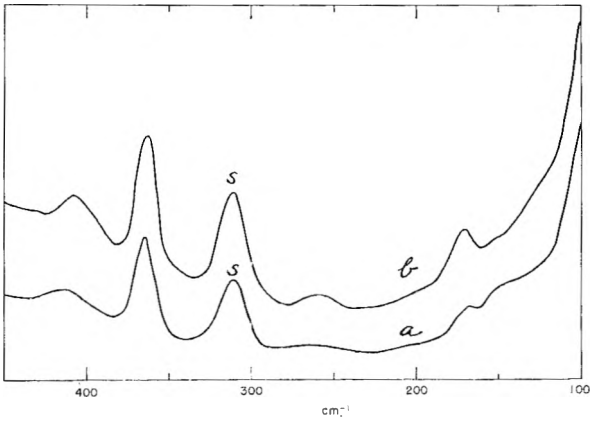

Fig. 2.—Raman spectra of $GaCl_3$: (a) in anhydrous diisopropyl ether, and (b) the same after addition of about one equivalent of water. Peaks due to the solvent are designated by s.

a small amount of yellow to orange material formed. The flocculent white solid could be reversibly dissolved and reprecipitated by alternate warming and cooling of the solution between room temperature and ice temperature. No further increase in the intensity of the color occurred on long standing of the ether solution at room temperature.

In the best (least colored) solution of $GaCl_3$ in diisopropyl ether a strong, highly polarized peak was observed at 367 cm.$^{-1}$, and a weaker unpolarized one at about 420 cm.$^{-1}$. The low frequency region again is complicated by the spurious peak in the 150–170 cm.$^{-1}$ region, but shows evidence for several weak peaks. On the addition of about one mole of water per mole of gallium, a precipitate formed and redissolved. The strongest (polarized) peak was now found at 363 cm.$^{-1}$ and a medium-sized one at about 410 cm.$^{-1}$. In addition, changes occurred in the low frequency region, with the appearance of a peak near 130 cm.$^{-1}$. Further addition of water had essentially no affect on the spectrum. Addition of a small amount of aqueous HCl produced a 346 cm.$^{-1}$ peak, with a decrease

in the 363 cm.$^{-1}$ peak. The spectra of these synthetic $GaCl_3$–ether solutions before and after addition of water are shown in Fig. 2.

A solution of $GaCl_3$ in diethyl ether showed a peak at 365 cm.$^{-1}$ as the only certain feature of the spectrum; the solution possessed considerable color. A solution of $GaCl_3$ in benzene (also colored) showed peaks at about 410 and 360 cm.$^{-1}$, the former seeming to be more intense, in contrast to the relative intensities of similarly positioned peaks in the diisopropyl ether solutions.

Solid Gallium Chloride.—To check on the possibility that dimeric Ga_2Cl_6 might be present in some of the solutions discussed above, the Raman spectrum of solid $GaCl_3$, which is composed of such dimers, was recorded. Reliable spectra were obtained in the region 200–600 cm.$^{-1}$; in order of decreasing intensity Raman peaks were observed as follows: 407 > 458, 330–345 (double peak?) > 250 > 550 (?) cm.$^{-1}$. These may be compared with results previously reported[13] for the solid— 466 > 277, 324, 384, 410, 545 cm.$^{-1}$ and for the liquid— 410 >> 345, 286 > 316, 458 > 479, 542 > 261. It is believed that the present results on the solid are more reliable than those previously[13] reported.

Discussion

The composition of the ether extracts showing the 405, 363, and (probable) 142 and 130 cm.$^{-1}$ peaks in addition to those of $GaCl_4^-$ suggests that the species responsible contains three chlorides per gallium. With coördination 3 unlikely, the possible presence of dimeric Ga_2Cl_6 must be considered, though it would not be expected to occur in the presence of water. The absence of a peak near 458 or 330 cm.$^{-1}$, the positions of strong peaks in solid $GaCl_3$, and the absence of a strong 363 cm.$^{-1}$ peak in the spectrum reported[13] for the liquid melt provide spectral evidence for the nonidentity with dimer. The 405 cm.$^{-1}$ peak of the ether extracts thus is not the 407 cm.$^{-1}$ peak of the dimeric solid, though of course similar vibrational modes may be involved. The new peaks in the ether, because of their relationships to those for $GaCl_4^-$, therefore may be ascribed to a second tetrahedral species, $GaCl_3X$. Here X is probably water, though it might be ether. The shifts on adding water to the dry ether solution of $GaCl_3$ are relevant to this judgment. Indirect support to the $GaCl_3X$ interpretation may be found in the Raman spectra of melts of the $GaCl_3$–$POCl_3$ adduct.[14] Though additional frequencies are present because of the $POCl_3$ vibrations, peaks at 363 and 406 cm.$^{-1}$ are found, in the same relative intensity as for our spectra. The strong 346 cm.$^{-1}$ vibration is not seen. It is known[15] that these adducts are bonded through the oxygen and not through the chloride of the $POCl_3$. The relations of the spectra for $GaCl_4^-$ and $GaCl_3X$ are consistent with the sort of differences which are found[16] in the Raman spectra of $SiBr_4$ and $SiBr_3Cl$.

The physical and spectral observations on the synthetic $GaCl_3$–isopropyl ether solutions can reasonably be interpreted as follows: (1) solid $GaCl_3$ reacts exothermically to form tetrahedral $GaCl_3 \cdot O(C_3H_7)_2$ (methyl[17] and ethyl[18] ether analogs are known); (2) local heating accompanying the above reaction leads to side reactions producing some colored product; (3) the ether addition product is dissolved and precipitated on warming and cooling the solution; (4) on the addition of water the ether is replaced by water to give $GaCl_3 \cdot OH_2$. The strong 410 cm.$^{-1}$ peak with the $GaCl_3$ solution in benzene suggests a dimeric form related to that in the fused pure salt may exist in this solvent, which is a poor electron donor.

In extraction, $GaCl_4^-$ formed in excess chloride may be accompanied into the ether phase by either H^+ or Li^+. Ammonium or calcium ions cannot be extracted in these systems, so that when their chlorides are present gallium will extract as $GaCl_4^-$ only to the extent that H^+ is available, either as excess HCl or as a product of hydrolysis of the octahedral gallium(III) or the second cation. With neither H^+ nor Li^+ available, extraction of $GaCl_3 \cdot H_2O$ occurs, though with a much lower extraction efficiency. The presence of added alkali further decreases extraction, by decreasing the amount of acid obtainable by the hydrolytic equilibria. Addition of an acid such as $HClO_4$ makes possible extraction of up to 75% of the original gallium as $HGaCl_4$, leaving in the aqueous phase chloride-deficient, octahedral hydrated gallium species.

(13) H. Gerding, H. G. Hoving, and P. A. Renes, *Rec. trav. chim.*, **72**, 78 (1953).

(14) H. Gerding, J. A. Koningstein, and E. R. van der Worm, *Spectrochim. Acta*, **16**, 881 (1960).

(15) I. Lindqvist and C. Branden, *Acta Cryst.*, **12**, 642 (1959); M. Baaz, V. Gutmann, and L. Hubner, *Monatsh.*, **91**, 537 (1960).

(16) M. L. Delwaulle, *Bull. soc. chim. France*, 1294 (1955).

(17) R. E. Van Dyke and H. E. Crawford, *J. Am. Chem. Soc.*, **72**, 2829 (1950).

(18) N. N. Greenwood, *J. Inorg. & Nuclear Chem.*, **8**, 234 (1958).

TOLUENE: THERMODYNAMIC PROPERTIES, MOLECULAR VIBRATIONS, AND INTERNAL ROTATION

BY D. W. SCOTT, G. B. GUTHRIE, J. F. MESSERLY, S. S. TODD, W. T. BERG, I. A. HOSSENLOPP, AND J. P. MCCULLOUGH

Contribution No. 111 from the Thermodynamics Laboratory of the Bartlesville Petroleum Research Center, Bureau of Mines, U. S. Department of the Interior, Bartlesville, Okla.

Received December 7, 1961

Low temperature calorimetry and vapor flow calorimetry were repeated for toluene with current accurate methods to provide the following information: values of heat capacity for the solid (11°K. to the triple point), the liquid (triple point to 371°K.), and the vapor (371 to 500°K.); the triple point temperature; the heat of fusion; thermodynamic functions for the solid and liquid (0 to 360°K.); heat of vaporization (341 to 410°K.); and parameters of the equation of state. The results were used to confirm a vibrational assignment and to show that the internal rotation is essentially free, as expected from the sixfold symmetry. Thermodynamic functions for toluene in the ideal gas state (0 to 1500°K.) were calculated by methods of statistical mechanics.

Thermodynamic data for toluene have depended on calorimetric results obtained some years ago by methods less accurate than currently employed.[1,2] In fact, the best third law entropy value until now has been Kelley's 1929 value,[3] which was determined in one of the earliest heat capacity studies of an organic compound made down to liquid hydrogen temperatures.

Because of toluene's role as the simplest member of the alkyl benzene family of petroleum hydrocarbons, accurate knowledge of its thermodynamic properties is particularly desirable for both practical and theoretical applications. Therefore, calorimetric measurements with toluene were repeated by the Bureau of Mines with the much more accurate techniques that have been developed since the earlier studies were done. The experimental values of entropy and vapor heat capacity obtained are summarized in Table I. These results were used to investigate the molecular vibration and internal rotation and to calculate thermodynamic functions by methods of statistical mechanics, as discussed in the following two sections. Presentation of the detailed experimental results is deferred to the final section.

TABLE I

OBSERVED AND CALCULATED THERMODYNAMIC PROPERTIES OF TOLUENE

	Entropy, $S°$, cal. deg.$^{-1}$ mole^{-1}			Heat capacity, $Cp°$, cal. deg.$^{-1}$ mole^{-1}	
T, °K.	Obsd.	Calcd.	T, °K.	Obsd.	Calcd.
298.15	76.77	76.64	371.20	31.09	31.09
341.27	80.39	80.24	396.20	33.19	33.18
361.06	82.04	81.90	427.20	35.65	35.66
383.77	83.92	83.80	462.20	38.32	38.31
410.11	86.08	86.00	500.20	40.98	41.00

Molecular Vibration and Internal Rotation.—Use of the observed values of thermodynamic properties in Table I to investigate molecular vibration and internal rotation required accounting for all degrees of freedom of the molecule. The 45 degrees of freedom may be classified as 3 translations, 3 over-all rotations, 1 internal rotation, and 38 vibrations. The translations and over-all rotations were treated by the standard formulas of statistical mechanics. Because the molecular structure of toluene has not been determined, the bond distances and angles were assumed to be the same as in structurally related molecules. The structure of the phenyl group was taken to be the same as in benzene[4] and that of the CH_3–C grouping the same as in acetaldehyde.[5] For the assumed structure, the product of the principal moments of inertia is 2.402×10^{-113} g.^{3} cm.^{6}, and the reduced moment of inertia for internal rotation is 5.008×10^{-40} g. cm.^{2}. The symmetry number for over-all and internal rotation is 6.

The vibrational assignment found to be consistent with the calorimetric data is given in Table II. The assignment as a monosubstituted benzene, exclusive of C–H stretching frequencies, is that of Randle and Whiffen[6] as corrected by Whiffen.[7] The two methyl rocking modes are assigned the same frequency, as suggested by Randle and Whiffen.[8] The thermodynamically unimportant C–H stretching and unsymmetrical CH_3 bending frequencies have the usual uncertainties that result from incomplete resolution and interference of Fermi resonance.

TABLE II

VIBRATIONAL ASSIGNMENT FOR TOLUENE IN CM.$^{-1}$

Species	A_1	B_1	A_2	B_2
	519	342	405	205
	785	623	842	462
	1003	1081	966	694
	1031	1155		728
	1177	1278		893
Monosubstituted	1209	1329		981
benzene	1501	1460		
	1611	1585		
	3058	3040		
	3076	3090		
	3110			
CH_3 rocking		1041		1041
CH_3 bending	1385	1436		1456
C–H stretching	2922	2954		2930

(1) K. S. Pitzer and D. W. Scott, *J. Am. Chem. Soc.*, **65**, 803 (1943) and earlier work cited therein.

(2) W. J. Taylor, D. D. Wagman, M. G. Williams, K. S. Pitzer, and F. D. Rossini, *J. Research Natl. Bur. Standards*, **37**, 95 (1946).

(3) K. K. Kelley, *J. Am. Chem. Soc.*, **51**, 2738 (1929).

(4) B. P. Stoicheff, *Can. J. Phys.*, **32**, 339 (1954).

(5) R. W. Kilb, C. C. Lin, and E. B. Wilson, Jr., *J. Chem. Phys.*, **26**, 1695 (1957).

(6) R. R. Randle and D. H. Whiffen, "Molecular Spectroscopy," G. Sell, ed., Institute of Petroleum, London, 1955, pp. 111–125.

(7) D. H. Whiffen, *J. Chem. Soc.*, 1350 (1956).

(8) R. R. Randle and D. H. Whiffen, *ibid.*, 3497 (1955).

The actual values of frequencies above 400 cm.$^{-1}$ in Table II are for the most part those reported by Wilmshurst and Bernstein.[9] Vapor state values were used whenever possible. Frequencies of two very weak Raman bands not observed by Wilmshurst and Bernstein (405 and 1278 cm.$^{-1}$) were taken from the compilation of Kohlrausch.[10]

The values of the two lowest frequencies (205 and 342 cm.$^{-1}$) are from vapor state infrared spectra obtained at the authors' request by Drs. F. A. Miller and W. G. Fateley of the Mellon Institute. These two frequencies are significantly lower than the values in the liquid state (216 and 346 cm.$^{-1}$). In the temperature range of the calorimetric entropy determinations, the entropy contribution of these two frequencies, calculated rigorously from the vapor state values, is about 0.12 cal. deg.$^{-1}$ mole^{-1} greater than the approximate contribution calculated from the liquid state values. This difference approaches the experimental uncertainty of the calorimetric entropy values. A similar shift is observed for 2-butyne (dimethylacetylene),[11] and unpublished work of the Bartlesville laboratory shows that use of the vapor state frequency of 194 cm.$^{-1}$ instead of the liquid state frequency of 213 cm.$^{-1}$ in calculating thermodynamic functions removes the 0.4 cal. deg.$^{-1}$ mole^{-1} entropy discrepancy reported for this compound over 20 years ago.[12] Shifts of low frequencies between liquid and vapor states by thermodynamically significant amounts may be more common than previously suspected. At least, the examples of toluene and 2-butyne suggest caution in using liquid state values of low frequencies for calculations of vapor state thermodynamic properties.

Internal rotation in toluene has sixfold symmetry. From empirical evidence, the barrier would be expected to be very low.[13] Pitzer and Scott[1] showed that the upper limit to the barrier height is about 1000 cal. mole^{-1}. With the more accurate calorimetric data of this research, the barrier is found to be so low that it is thermodynamically negligible. In fact, even when internal rotation is assumed free, the calculated entropy is still less than observed, although the difference is well within the combined uncertainty of the calculated and observed values.

Thermodynamic Functions.—The molecular parameters described in the foregoing section were used to compute the values of thermodynamic functions listed in Table III. Empirical anharmonicity contributions,[14] with ν = 950 cm.$^{-1}$ and Z = 0.76 cal. deg.$^{-1}$ mole^{-1}, were included to give better agreement with the experimental values of heat capacity.[15] The contributions of anharmonicity are only 0.003 and 0.02 cal. deg.$^{-1}$ mole^{-1} in $S°$ and $C_p°$ at 298.15°K. but increase to 0.95 and 1.58 cal. deg.$^{-1}$ mole^{-1} at 1500°K. Calculated values of $S°$ and $C_p°$ are compared with the observed values in Table I. The agreement well within experimental uncertainty shows that the vibrational assignment of Table II is consistent with the calorimetric data and that internal rotation is essentially free.

TABLE III

THE MOLAL THERMODYNAMIC FUNCTIONS OF TOLUENE IN THE IDEAL GAS STATE[a]

T, °K.	$(F° - H°_0)/T$, cal. deg.$^{-1}$	$(H° - H°_0)/T$, cal. deg.$^{-1}$	$H° - H°_0$, kcal.	$S°$, cal. deg.$^{-1}$	$C_p°$, cal. deg.$^{-1}$
0	0	0	0	0	0
273.15	− 60.96	13.61	3.717	74.57	22.60
298.15	− 62.19	14.45	4.309	76.64	24.77
300	− 62.28	14.52	4.355	76.80	24.94
400	− 66.96	18.20	7.281	85.16	33.48
500	− 71.43	22.03	11.02	93.46	40.98
600	− 75.78	25.72	15.44	101.50	47.20
700	− 80.00	29.17	20.42	109.17	52.33
800	− 84.11	32.34	25.87	116.45	56.61
900	− 88.09	35.24	31.72	123.33	60.23
1000	− 91.94	37.90	37.90	129.84	63.32
1100	− 95.67	40.33	44.37	136.00	65.96
1200	− 99.27	42.57	51.08	141.84	68.25
1300	−102.76	44.62	58.01	147.39	70.22
1400	−106.14	46.51	65.12	152.65	71.95
1500	−109.41	48.26	72.39	157.67	73.46

[a] To retain internal consistency, some of the values are given to one more decimal place than is justified by the absolute accuracy.

Experimental

The basic experimental techniques are described in published accounts of apparatus and methods for low temperature calorimetry[16] and vapor flow calorimetry.[17] The reported values are based on a molecular weight of 92.134 g. mole^{-1} (1951 International Atomic Weights[18]), the 1951 values of fundamental physical constants,[19] and the relations: 0° = 273.15°K.[20] and 1 cal. = 4.184 joules (exactly). Measurements of temperature were made with platinum resistance thermometers calibrated in terms of the International Temperature Scale[21] between 90 and 500°K. and the provisional scale[22] of the National Bureau of Standards between 11 and 90°K. All electrical and mass measurements were referred to standard devices calibrated at the National Bureau of Standards.

The Material.—The sample of toluene used for low temperature calorimetry was an API Research hydrocarbon

(9) J. K. Wilmshurst and H. J. Bernstein, *Can. J. Chem.*, **35**, 911 (1957).

(10) K. W. F. Kohlrausch, "Ramanspektren," Edwards Brothers Inc., Ann Arbor, Michigan, 1945, p. 380.

(11) R. C. Lord, "Investigation of Far Infrared Spectra," WADC TR 59-498, Feb., 1960.

(12) D. M. Yost, D. W. Osborne, and C. S. Garner, *J. Am. Chem. Soc.*, **63**, 3492 (1941).

(13) E. B. Wilson, Jr., "Advances in Chemical Physics," Vol. 2 I. Prigogine, ed., Interscience Publishers, Inc., New York, N. Y., 1959 pp. 367–393.

(14) J. P. McCullough, H. L. Finke, W. N. Hubbard, W. D. Good, R. E. Pennington, J. F. Messerly, and G. Waddington, *J. Am. Chem. Soc.*, **76**, 2661 (1954).

(15) The contributions of vibration and anharmonicity were computed by the Bureau of Mines Electronic Computer Service, Pittsburgh, Pa.

(16) H. M. Huffman, *Chem. Revs.*, **40**, 1 (1947); H. M. Huffman, S. S. Todd, and G. D. Oliver, *J. Am. Chem. Soc.*, **71**, 584 (1949); D. W. Scott, D. R. Douslin, M. E. Gross, G. D. Oliver, and H. M. Huffman, *ibid.*, **74**, 883 (1952).

(17) G. Waddington, S. S. Todd, and H. M. Huffman, *ibid.*, **69**, 22 (1947); J. P. McCullough, D. W. Scott, R. E. Pennington, I. A. Hossenlopp, and G. Waddington, *ibid.*, **76**, 4791 (1954).

(18) E. Wichers, *ibid.*, **74**, 2447 (1952).

(19) F. D. Rossini, F. T. Gucker, Jr., H. L. Johnston, L. Pauling and G. W. Vinal, *ibid.*, **74**, 2699 (1952).

(20) Some of the results originally were computed with constants and temperatures in terms of the relation 0° = 273.16°K. Only results affected significantly by the new definition of the absolute temperature scale [H. F. Stimson, *Am. J. Phys.*, **23**, 614 (1955)] were recalculated. Therefore, numerical inconsistencies, much smaller than the accuracy uncertainty, may be noted in some of the reported data.

(21) H. F. Stimson, *J. Research Natl. Bur. Standards*, **42**, 209 (1949).

(22) H. J. Hoge and F. G. Brickwedde, *ibid.*, **22**, 351 (1939).

made available by the American Petroleum Institute through the API Research Project 44 at the Carnegie Institute of Technology.[23] The purity, determined by calorimetric studies of melting point as a function of fraction melted, was 99.999 mole %. The sample used for vapor flow calorimetry, loaned by Phillips Petroleum Co. through the courtesy of A. O. Frenzel, had a purity of 99.96 mole %.

Heat Capacity in the Solid and Liquid States.—The observed values of heat capacity, C_s, are listed in Table IV.

TABLE IV

MOLAL HEAT CAPACITY OF TOLUENE IN CAL. DEG.$^{-1}$

T, °K.[a]	C_s[b]	T, °K.[a]	C_s[b]	T, °K.[a]	C_s[b]
Crystals		54.48	10.894	171.84	20.811[d]
11.53	0.863	56.44	11.172	Liquid	
12.46	1.082	59.35	11.558	160.09	32.326[c]
12.63	1.118	64.95	12.231	183.21	32.422
13.52	1.357	71.03	12.824	189.34	32.521
13.99	1.462	77.18	13.360	191.95	32.573
14.86	1.691	83.09	13.858	200.41	32.755
15.61	1.885	86.63	14.122	209.15	33.007
16.54	2.148	88.80	14.289	209.73	33.010
17.37	2.374	92.21	14.499	218.68	33.313
18.37	2.669	94.83	14.670	228.55	33.687
19.34	2.948	98.11	14.881	238.74	34.125
20.27	3.227	104.34	15.297	249.22	34.636
21.56	3.603	110.35	15.713	259.56	35.181
22.48	3.881	116.56	16.153	269.73	35.765
24.01	4.330	122.97	16.624	279.75	36.375
24.89	4.571	129.18	17.085	289.61	37.016
26.56	5.056	135.21	17.540	299.32	37.672
27.53	5.335	138.68	17.789	300.79	37.752
29.42	5.837	141.09	17.993	310.65	38.449
30.66	6.177	144.49	18.255	320.73	39.171
33.90	7.017	150.16	18.734	330.66	39.907
37.68	7.900	156.24	19.265	340.80	40.638
42.26	8.863	159.34	19.515	351.17	41.374
46.77	9.699	162.70	19.854	361.35	42.175
51.30	10.436	165.68	20.156	371.02	42.868

[a] T is the mean temperature of each heat-capacity measurement. [b] C_s is the heat capacity of the condensed phase at saturation pressure. [c] Undercooled liquid. [d] Results for the solid are not corrected for the effect of premelting due to the presence of impurities.

Above 30°K., the accuracy uncertainty is estimated to be no greater than 0.2%. The heat capacity values for the liquid may be represented within 0.1% between the triple point and 371°K. by the empirical equation

$$C_s(\text{liq}) = 46.884 - 0.19340\,T + 7.5592 \times 10^{-4}\,T^2 - 7.1067 \times 10^{-7}\,T^3 \text{ cal. deg.}^{-1} \text{ mole}^{-1} \quad (1)$$

Heat and Temperature of Fusion.—Three determinations of the heat of fusion, ΔHm, gave the average value 1586 ± 1 cal. mole^{-1}; the maximum deviation from the mean was taken as the uncertainty. The results of a study of the melting temperature, T_F, as a function of the fraction of total sample melted, F, are listed in Table V. Also listed in Table V are the values obtained for the triple point temperature, T_{tp}, the mole fraction of impurity in the sample, N_2*, and the cryoscopic constants[24] A = $\Delta Hm/RT_{tp}^2$ and B = $1/T_{tp} - \Delta Cm/2\,\Delta Hm$, calculated from the observed values of T_{tp}, ΔHm, and ΔCm (10.96 cal. deg.$^{-1}$ mole^{-1}).

TABLE V

TOLUENE: MELTING POINT SUMMARY

T_{tp} = 178.15 ± 0.05°K.; N_2* = AF/($T_{tp} - T_F$) = 0.00001[3] ± 0.00001; A = 0.02515 deg.$^{-1}$; B = 0.00216 deg.$^{-1}$

Melted, %	1/F	T_F, °K.	$T_{calcd.}$, °K.
11.04	9.058	178.1462	178.1462
25.90	3.861	.1487	.1486
50.67	1.973	.1493	.1495
70.49	1.419	.1497	.1498
90.33	1.107	.1499	.1499
100.00	1.000		.1499
Pure	0		178.1504

(23) The sample was purified by API Research Project 6 at the Carnegie Institute of Technology from material supplied by the Humble Oil and Refining Co.

TABLE VI

THE MOLAL THERMODYNAMIC PROPERTIES OF TOLUENE IN THE SOLID AND LIQUID STATES[a]

T, °K.	$-(F_s - (H_s - H°_0)/T$, cal. deg.$^{-1}$	$(H_s - H°_0)/T$, cal. deg.$^{-1}$	$H_s - H°_0$, cal.	S_s, cal. deg.$^{-1}$	C_s, cal. deg.$^{-1}$
Crystals					
10	0.049	0.147	1.47	0.196	0.581
12	.083	.248	2.97	.331	.971
14	.131	.386	5.40	.517	1.463
16	.193	.553	8.85	.746	1.989
18	.268	.744	13.39	1.012	2.557
20	.357	.955	19.10	1.312	3.145
25	.631	1.540	38.49	2.171	4.603
30	.967	2.168	65.03	3.135	5.997
35	1.349	2.808	98.29	4.157	7.281
40	1.765	3.439	137.54	5.204	8.401
45	2.205	4.046	182.05	6.251	9.383
50	2.662	4.623	231.14	7.285	10.234
60	3.601	5.678	340.7	9.279	11.639
70	4.547	6.613	462.9	11.160	12.730
80	5.485	7.433	594.6	12.918	13.603
90	6.404	8.161	734.5	14.565	14.353
100	7.298	8.813	881.3	16.111	15.005
110	8.166	9.407	1034.8	17.573	15.688
120	9.009	9.960	1195.2	18.969	16.404
130	9.826	10.485	1363.0	20.311	17.146
140	10.622	10.987	1538.2	21.609	17.908
150	11.397	11.475	1721.2	22.872	18.717
160	12.153	11.954	1912.7	24.107	19.591
170	12.892	12.433	2113.6	25.325	20.600
178.15	13.484	12.825	2284.8	26.309	21.407
Liquid					
178.15	13.484	21.728	3870.8	35.212	32.37
180	13.707	21.839	3931	35.55	32.39
190	14.906	22.395	4255	37.30	32.53
200	16.065	22.910	4582	38.98	32.75
210	17.198	23.381	4910	40.58	33.02
220	18.296	23.827	5242	42.12	33.36
230	19.362	24.252	5578	43.61	33.75
240	20.405	24.654	5917	45.06	34.18
250	21.416	25.048	6262	46.46	34.68
260	22.408	25.427	6611	47.84	35.21
270	23.374	25.800	6966	49.17	35.78
273.15	23.674	25.916	7079	49.59	35.97
280	24.318	26.168	7327	50.49	36.39
290	25.243	26.531	7694	51.77	37.04
298.15	25.983	26.825	7998	52.81	37.58
300	26.148	26.893	8068	53.04	37.70
310	27.037	27.252	8448	54.29	38.40
320	27.906	27.613	8836	55.52	39.12
330	28.764	27.970	9230	56.73	39.86
340	29.603	28.332	9633	57.94	40.58
350	30.43	28.691	10042	59.12	41.29
360	31.24	29.053	10459	60.29	42.07

[a] The values tabulated are the free energy function, enthalpy function, enthalpy, entropy, and heat capacity of the condensed phases at saturation pressure.

(24) A. R. Glasgow, A. J. Streiff, and F. D. Rossini, *J. Research Natl. Bur. Standards*, **35**, 355 (1945).

Thermodynamic Properties in the Solid and Liquid States.—Values of thermodynamic functions for the condensed phases were computed from the calorimetric data for selected temperatures betwen 10 and 360°K. The results are in Table VI. The values at 10°K. were computed from a Debye function for 5 degrees of freedom with $\theta = 109.5°$; these parameters were evaluated from the heat capacity data between 11 and 22°K. Corrections for the effect of premelting have been applied to the smoothed data in Table VI.

Heat of Vaporization, Vapor Heat Capacity, and Effects of Gas Imperfection.—Experimental values of the heat of vaporization and vapor heat capacity are given in Tables VII and VIII. The estimated accuracy uncertainty of the values of ΔHv and $C_p°$ are 0.1 and 0.2%, respectively. These heat-of-vaporization values and that of Osborne and Ginnings[25] at 298.15°K. may be represented within ±3 cal. mole^{-1} by the empirical equation

$$\Delta Hv = 11637 - 4.823T - 1.260 \times 10^{-2}T^{-2} \text{ cal. mole}^{-1} \quad (298\text{–}410°\text{K.}) \quad (2)$$

The effects of gas imperfection were correlated by the procedure described in an earlier paper.[26] The Antoine vapor pressure equation given in the API Research Project 44 tables[27] was used. The empirical equation for B, the second virial coefficient in the equation of state, $PV = RT(1 + B/V)$, is

$$B = -321 - 41.48 \exp(1200/T) \text{ cc. mole}^{-1} \quad (340\text{–}500°\text{K.}) \quad (3)$$

Observed values of B and $-T(d^2B/dT^2) = \lim_{P\to 0}(\partial C_p/\partial P)_T$ and the ones calculated from eq. 3 are compared in Tables VII and VIII.

TABLE VII

THE MOLAL HEAT OF VAPORIZATION AND SECOND VIRIAL COEFFICIENT OF TOLUENE

T, °K.	P, atm.	ΔHv, cal.	B, cc. Obsd.	B, cc. Calcd.[a]
341.27	0.250	8521 ± 4[b]	−1718	−1717
361.06	.500	8254 ± 3	−1497	−1472
383.77	1.000	7933 ± 3	−1280	−1267
410.11	2.000	7538 ± 2	−1057	−1095

[a] Calculated from eq. 3. [b] Maximum deviation from the mean of three or more determinations.

Entropy in the Ideal Gas State.—The entropy in the ideal gas state at 1 atm. pressure was calculated as shown in Table IX. At 298.15°K., the value of heat of vaporization reported by Osborne and Ginnings[25] was used.

Comparison with Previous Work.—The earlier results of Kelley[3] differ from the present results by +0.3% to −1.9% for the heat capacity of the crystals outside of the premelting region, −0.2% to −1.9% for the heat capacity of the liquid, and negligibly for the heat of fusion. Kelley's value of entropy, S_s, at 298.15°K., 52.4 ± 0.3 cal. deg.$^{-1}$ mole^{-1} differs from the present value, 52.81 ± 0.10 cal. deg.$^{-1}$ mole^{-1}, by about the sum of the claimed uncertainties.

The vapor heat capacity values of Montgomery and De Vries[28] and Bennewitz and Rossner[29] differ from those of this study by 2–3%. The values of Pitzer and Scott[1] agree with the present data within 1%.

The values of the second virial coefficient measured by Cox and Andon[30] agree reasonably well with those in Table VII. However, the deviations are larger than the estimated combined accuracy uncertainties. Their derived value of heat of vaporization at 383.77°K., 7954 ± 5 cal. mole^{-1}, also deviates from the measured value in Table VII more than would be expected. The measured value of heat of vaporization of Osborne and Ginnings[25] at 298.15°K. is, however, consistent with the present results. In fact, a quadratic equation based only on the values in Table VII gives an extrapolated value at 298.15°K. within 0.25% of the Osborne and Ginnings datum.

TABLE VIII

THE MOLAL VAPOR HEAT CAPACITY OF TOLUENE IN CAL. DEG.$^{-1}$

T, °K.	371.20	396.20	427.20	462.20	500.20
C_p (2.000 atm.)			36.901	39.122	41.547
C_p (1.000 atm.)		34.045	36.207	38.678	41.230
C_p (0.500 atm.)	31.709	33.608			
C_p (0.375 atm.)	31.560				
C_p (0.250 atm.)	31.394	33.390	35.785	38.404	41.041
$C_p°$	31.09	33.19	35.65	38.32	40.98
$-T(d^2B/dT^2)$, obsd.[a]	1.18	0.79	0.52	0.34	0.24
$-T(d^2B/dT^2)$, calcd.[b]	1.16	0.80	0.53	0.35	0.23

[a] Units: cal. deg.$^{-1}$ mole^{-1} atm.$^{-1}$ [b] Calculated from eq. 3.

TABLE IX

THE MOLAL ENTROPY OF TOLUENE IN THE IDEAL GAS STATE IN CAL. DEG.$^{-1}$

T, °K.	298.15	341.27	361.06	383.77	410.11
S_s (liq)[a]	52.81	58.09	60.43	63.05	66.02
$\Delta Hv/T$	30.46	24.97	22.86	20.67	18.38
$S^* - S$[b]	0.03	0.09	0.13	0.20	0.30
$R \ln P$[c]	−6.53	−2.76	−1.38	0.00	1.38
$S°$ (obsd.) ± 0.15[d]	76.77	80.39	82.04	83.92	86.08

[a] By interpolation in Table VI or extrapolation by use of eq. 1. [b] The entropy in the ideal gas state less that in the real gas state, calculated from eq. 3. [c] Entropy of compression, calculated from Antoine eq. of ref. 27. [d] Estimated accuracy uncertainty.

(25) N. S. Osborne and D. C. Ginnings, *J. Research Natl. Bur Standards*, **39**, 453 (1947).

(26) J. P. McCullough, H. L. Finke, J. F. Messerly, R. E. Pennington, I. A. Hossenlopp, and G. Waddington, *J. Am. Chem. Soc.*, **77**, 6119 (1955).

(27) F. D. Rossini, K. S. Pitzer, R. L. Arnett, R. M. Braun, and G. C. Pimentel, "Selected Values of Physical and Thermodynamic Properties of Hydrocarbons and Related Compounds," Carnegie Press, Pittsburgh, Pa., 1953.

(28) J. B. Montgomery and T. De Vries, *J. Am. Chem. Soc.*, **64**, 2375 (1942).

(29) K. Bennewitz and W. Rossner, *Z. physik. Chem.*, **B39**, 126 (1938).

(30) J. D. Cox and R. J. L. Andon, *Trans. Faraday Soc.*, **54**, 1622 (1958).

ACID–BASE EQUILIBRIA BETWEEN BROM PHENOL BLUE AND SELECTED N-HETEROCYCLICS IN NON-AQUEOUS SOLVENTS

BY OREST POPOVYCH

Analytical Research Division, Esso Research and Engineering Company, Linden, New Jersey

Received December 9, 1961

The equilibria between an indicator acid and an amine in hydrocarbon and hydroxylic media have been described by a series of equations and constants and a method outlined for their experimental evaluation by a combination of visible spectrophotometry and electrolytic conductance. The ion-pair formation constant $K_B = (BH^+A^-)/(HA)(B)$ was adopted as a measure of basicity of an amine B relative to a reference acid HA. Basic reactivity of six N-heterocyclics—pyridine, 2-, 3-, 4-picoline, 2,4-lutidine, and isoquinoline—toward brom phenol blue, expressed as K_B, was determined as a function of solvent by visible spectrophotometry. The solvents ranged from hydrocarbons to isopropyl alcohol–toluene mixtures containing up to 50% alcohol. In the latter, ionic dissociation constants of the indicator–amine and the indicator–solvent ion-pairs were evaluated by electrolytic conductance. It was found that while the relative strengths of the bases remained independent of the solvent, the absolute values of the K_B's were a sensitive function of the medium. The acid–base reactions were most favored by polar and hydroxylic media, with the major increase in reactivity observed upon addition of isopropyl alcohol to toluene. It was concluded that preferential solvation of the neutralization products was the major factor in determining the medium effects; bulk properties of the solvent were of secondary importance. A good correlation was obtained between the indicator and the potentiometric determinations of basicity.

I. Introduction

The general objective of the work reported here was to investigate the effect of solvents on the acidity and basicity of solutes. Due to the well known limitations of potentiometry in correlating acid–base reactivities measured in different solvents, particularly in aprotic media, we resorted to indicators for purposes of defining and measuring acid–base equilibria in widely differing solvent systems. Furthermore, by employing one indicator for all the media we were able to study solvent effects on the same acid–base pair in each case.

The advantages of using indicators were reviewed by Davis and co-workers[1] in connection with their own extensive contributions in this field.[1-8] Other workers[9-11] reported determinations of basicity in non-aqueous solvents with the aid of indicators. Specifically, the present study was designed to investigate the basic reactivity of six structurally similar N-heterocyclics—pyridine, 2-, 3-, 4-picoline,[12] 2,4-lutidine,[13] and isoquinoline—toward a single reference acid—brom phenol blue—in hydrocarbons and in mixtures of isopropyl alcohol and toluene. Visible spectrophotometry of the acid–base reaction mixtures comprised the core of our study, since it could be applied to all the media. It was supplemented by electrolytic conductance in the most polar solvent.

In contrast to most of the earlier indicator work, the present study was not limited to "inert" solvents, but included partially hydroxylic media in which protolysis and ionic dissociation became appreciable. As a result, a generalized method of describing acid–base equilibria had to be applied.

II. Experimental

Materials.—All commercial solvents used were of spectrophotometric grade (Matheson Company). In addition, the isopropyl alcohol was freshly distilled over (Linde 5A) Molecular Sieves. A colorless solution of brom phenol blue in a hydrocarbon was taken as the criterion of the latter's purity for our purpose (*i.e.*, as the absence of hydroxylic and other basic impurities). Brom phenol blue (Eastman Kodak white label) was recrystallized from benzene to yield nearly colorless crystals. The amines used as the starting materials in this work were of the best grades commercially available. Pyridine (spectrograde) and the picolines (white label) were from the Eastman Kodak Company, isoquinoline and 2,4-lutidine, from the Matheson Company. All were dried with Linde 5A Molecular Sieves and fractionated. Isoquinoline was distilled at reduced pressure, the remaining amines, at atmospheric. Only the middle constant-boiling fraction was collected and used.

Measurements—Spectrophotometric.—Visible absorption spectra were recorded on a Cary spectrophotometer Model 11 MS, using 1-cm. silica cells. The measurements were made in a spectroscopy laboratory with controlled temperature (25.0°) and humidity.

Indicator solutions of fixed initial concentration (2.00–8.00 $\times$ 10^{-5} M) were reacted with increasing concentrations of a base (10^{-5} M and up), until the absorbance of a reaction mixture reached its maximum value, which remained constant on addition of a moderate excess of base ($\sim 10^{-2}$ M).[14] This maximum absorbance (at λ_{max} 410–425 mμ) was assumed to correspond to a complete conversion of brom phenol blue to its basic form and was used to calculate its molar absorptivity. Within experimental error, a_{max} was found to be 2.40 $\times$ 10^4 for all the systems investigated. The same value also was obtained for solutions of the sodium salt of brom phenol blue. Thus, it appeared to be the property of the univalent anion of brom phenol blue, fairly independent of the associated cation.

Using the above a_{max}, the equilibrium concentration of the basic form in each reaction mixture was calculated from its absorbance by applying Beer's law. The equilibrium concentration of the (unreacted) indicator in acid form was obtained by difference from its known initial concentration. Because the initial base concentration also was known, the concentrations of the remaining components also could be calculated by a method dependent on the complexity of the system. These calculations will be discussed in detail later in the text.

(1) M. M. Davis and P. J. Schuhmann, *J. Research Natl. Bur. Standards*, **39**, 221 (1947).

(2) M. M. Davis, P. J. Schuhmann, and M. E. Lovelace, *ibid.*, **41**, 27 (1948).

(3) M. M. Davis and E. A. McDonald, *ibid.*, **42**, 595 (1949).

(4) M. M. Davis and H. B. Hetzer, *ibid.*, **46**, 496 (1951).

(5) M. M. Davis and H. B. Hetzer, *ibid.*, **48**, 381 (1952).

(6) M. M. Davis and H. B. Hetzer, *J. Am. Chem. Soc.*, **76**, 4247 (1954).

(7) M. M. Davis and H. B. Hetzer, *J. Research Natl. Bur. Standards*, **60**, 569 (1958).

(8) M. M. Davis and J. Paabo, *J. Am. Chem. Soc.*, **82**, 5081 (1960).

(9) R. P. Bell and J. W. Bayles, *J. Chem. Soc.*, 1518 (1952).

(10) J. W. Bayles and A. Chetwyn, *ibid.*, 2328 (1958).

(11) R. G. Pearson and D. C. Vogelsong, *J. Am. Chem. Soc.*, **80**, 1038 (1958).

(12) Methylpyridine.

(13) Dimethylpyridine.

(14) It is known that a large excess of base may lead to a secondary neutralization step with the formation of blue or purple reaction products. However, at the concentration levels employed here, this secondary reaction was never encountered.

Measurements—Conductometric.—The apparatus employed for measurements of electrolytic conductance and of dielectric constants in the present study was described in detail elsewhere.[15] Its main components were a specially-built Leeds and Northrup capacitance–conductance bridge, an oscillator to energize the bridge at 19.5 kc., and a radio receiver as the tuned amplifier–detector. A telephone was used to determine the bridge balance. The conductance cell was a Balsbaugh Laboratories 100T3 electrical cell, which consisted of two assemblies of concentric nickel cylinders as the electrodes. This cell had a nominal constant of 0.001. The exact value, determined from capacitance measurements with air and benzene as the dielectrics, was found to be 0.0008496. Its performance checked well against that of a platinum cell with a constant of 0.0100, as determined from the conductance of aqueous KCl.

Although the above apparatus was suitable for conductance work of highest precision and accuracy, the system under study was handicapped by large solvent corrections and by extensive molecular dissociation of the ion-pairs (salts) into their component acid and bases. The accepted way of studying such systems[16,17] is to determine the conductance of a salt in the presence of a large enough excess of its constituent acid or base to repress the molecular dissociation. Therefore, stock solutions of the salts were prepared *in situ* by reacting 8.00×10^{-5} *M* indicator with 2.00×10^{-2} *M* base. The electrolyte concentrations were checked by visible spectrophotometry.

As a result of high and uncertain solvent corrections and of the reduced accuracy of determining the electrolyte concentration, all our solutions were prepared volumetrically. The conductances were read to the nearest 0.1 μmho, so that the sensitivity of our measurements was a specific conductance of 8×10^{-11} mho-cm. All measurements were made at 25.00 ± 0.02°, and sorption effects due to the large electrode area were minimized by using at least three fillings and equilibrations for each solution. The results are reported to three significant figures. Concentration ranges over which the conductances were measured were 8×10^{-5}–4×10^{-6} *M* for each salt and 10^{-3}–10^{-5} *M* for the indicator. Although the linearity of the log λ *vs.* log *C* and of the $1/\lambda$ *vs.* *C*λ plots seemed to indicate that corrections for interionic attractions and activity coefficients could be largely neglected, definitive results were obtained by the Fuoss–Shedlovsky calculation.[18]

III. Results and Discussion

The Generalized System.—When an acid HA reacts with a weak uncharged base B in a medium of low dielectric constant, the main equilibrium to be considered is the formation of a 1:1 salt, or an ion-pair

$$B + HA = BH^+A^- \qquad K_B = \frac{(B^+HA^-)}{(B)(HA)} \qquad (1)$$

Visible[1–11] and infrared[19,20] spectrophotometry, as well as conductance[21] and dipole-moment[22] data, show that in dilute hydrocarbon solutions, the above equilibrium suffices to describe the system completely, at least as a very good approximation. As a result, the ion-pair formation constant (eq. 1) has been adopted as a quantitative expression for the reactivity of a base toward a reference acid (or *vice versa*) in all of the recent indicator work not only in "inert" solvents, but even in glacial acetic acid.[23,24]

(15) P. E. Rouse, Jr., F. D. Bailey, and J. A. Minkin, *Proc. API, Sect.* (III), **30**, 54 (1950).

(16) M. A. Elliott and R. M. Fuoss, *J. Am. Chem. Soc.*, **61**, 294 (1939).

(17) C. R. Witschonke and C. A. Kraus, *ibid.*, **69**, 2472 (1947).

(18) R. M. Fuoss and T. Shedlovsky, *ibid.*, **71**, 1496 (1949).

(19) G. M. Barrow and E. A. Yerger, *ibid.*, **76**, 5211 (1954).

(20) E. A. Yerger and G. M. Barrow, *ibid.*, **77**, 4474, 6206 (1955).

(21) C. A. Kraus, *J. Phys. Chem.*, **60**, 129 (1956).

(22) A. A. Maryott, *J. Research Natl. Bur. Standards*, **41**, 7 (1948).

(23) I. M. Kolthoff and S. Bruckenstein, *J. Am. Chem. Soc.*, **78**, 1 (1956).

(24) S. Bruckenstein and I. M. Kolthoff, *ibid.*, **78**, 10 (1956).

Ion-pairs can further associate into higher aggregates

$$n BH^+A^- = (BH^+A^-)_n \qquad (2)$$

and dissociate into ions

$$BH^+A^- = BH^+ + A^- \qquad K_s = \frac{(BH^+)(A^-)}{(BH^+A^-)} \qquad (3)$$

Complications due to the association reaction can be minimized by the use of very dilute solutions, while their presence can be recognized readily from spectrophotometric and conductometric data. The ionic dissociation is known to be negligible in hydrocarbons, but becomes increasingly important as the dielectric constant of the medium is raised.

Further complications arise from the formation and the dissociation of solvent–indicator ion-pairs when the solvent possesses pronounced basic properties, as do the common hydroxylic solvents

$$ROH + HA = RO^+H_2A^- \qquad K_p = \frac{(RO^+H_2A^-)}{(ROH)(HA)} \qquad (4)$$

hydroxylic solvent; solvent–indicator ion-pair

$$RO^+H_2A^- = RO^+H_2 + A^- \qquad K_A = \frac{(RO^+H_2)(A^-)}{(RO^+H_2A^-)} \qquad (5)$$

protonated solvent

Equilibria 4 and 5 can be combined to yield the familiar acid ionization constant of the indicator HA in the basic hydroxylic solvent ROH

$$HA + ROH = RO^+H_2 + A^-$$

$$K_i = \frac{(RO^+H_2)(A^-)}{(HA)} = K_p \times K_A \qquad (6)$$

Thus, for a complete description of an acid–base reaction mixture in the generalized case, including the evaluation of the ion-pair formation constant K_B, we have to know the equilibrium concentrations of seven species (B, HA, BH^+A^-, BH^+, A^-, $ROH_2^+A^-$, ROH_2^+). This excludes higher aggregates (eq. 2), assumed to be negligible in dilute solutions. In order to obtain an expression for (BH^+A^-) in terms of experimentally determinable quantities, we start with the total indicator present in its basic form, (A_T)

$$(A_T) = (B^+HA^-) + (ROH_2^+A^-) + (A^-) \qquad (7)$$

where to preserve electroneutrality

$$(A^-) = (BH^+) + (ROH_2^+) \qquad (8)$$

We then define a new quantity, S_T

$$(S_T) = (A_T) - (ROH_2^+A^-) = (BH^+A^-) + (BH^+) + (ROH_2^+) \qquad (9)$$

Finally, eq. 3 and 6 first are rewritten as

$$K_s = \frac{(BH^+)(BH^+ + ROH_2^+)}{(BH^+A^-)} \qquad (10)$$

and

$$K_i = \frac{(ROH_2^+)(BH^+ + ROH_2^+)}{(HA)} \qquad (11)$$

respectively, and then combined with (9) to give

$$(BH^+A^-)^2 - (2S_T + K_s)(BH^+A^-) - K_i(HA) + S_T^2 = 0 \qquad (12)$$

It is generally accepted that electronic spectra are incapable of showing any appreciable difference between free ions, ion-pairs, or any other aggregates containing the same absorbing species.[23,24] All

TABLE I

BASICITY (ION-PAIR FORMATION) CONSTANTS OF THE AMINES[a]

	$K_B \times 10^{-3}$					
	Pyridine	Isoquinoline	2-Picoline	3-Picoline	4-Picoline	2,4-Lutidine
Chlorobenzene	2.50 ± 0.10	...	...	14.6 ± 0.2	28.6 ± 0.9	438 ± 34
Benzene	1.88 ± 0.10	4.75 ± 0.17	19.8 ± 0.8	9.51 ± 0.16	18.0 ± 1.2	179 ± 13
Toluene	1.40 ± 0.13	3.64 ± 0.11	12.9 ± 0.6	6.67 ± 0.06	11.8 ± 0.4	113 ± 11
Vol. % Isopropyl alcohol in toluene						
10	2.54 ± 0.23	6.67 ± 0.33	15.8 ± 0.7	9.40 ± 0.7	23.0 ± 0.9	96.2 ± 7
20	3.12 ± 0.36	6.62 ± 0.33	19.0 ± 1.2	11.2 ± 0.3	24.2 ± 0.6	116 ± 4
40	3.21 ± 0.00	6.89 ± 0.11	20.6 ± 0.6	10.8 ± 0.5	23.7 ± 0.9	110 ± 3
50	3.49 ± 0.21	7.24 ± 0.18	19.1 ± 0.6	10.6 ± 0.9	21.3 ± 1.1	119 ± 12

[a] In general, each constant is an average of about ten determinations at different concentrations of indicator and base. Standard deviation of individual measurements is indicated.

three species in eq. 7 contain a common component responsible for visible absorption—the univalent anion of the indicator acid. Thus, to a very good approximation, all basic forms will absorb in the same spectral region and their combined concentration will be measured by the visible absorbance of an equilibrium mixture. The ionic dissociation constant of the amine–indicator ion-pair, K_s, (eq. 3) can be obtained, in principle, from the observed electrolytic conductance of solutions containing the ion-pair as the only electrolyte. The constants K_p and K_i, which govern solvent–indicator interactions, can be evaluated by combining spectrophotometric and conductometric data obtained on solutions of the pure indicator in the media and the concentration ranges of interest. Finally, total absorbance in conjunction with K_p will evaluate S_T (eq. 9), required to complete the list of known variables in eq. 12. Thus, an experimental solution to the generalized system can be obtained by a combination of visible spectrophotometry and electrolytic conductance.

Hydrocarbon Systems.—In an equilibrium mixture of brom phenol blue and an N-heterocyclic base in a hydrocarbon solvent, the only species absorbing in the visible is the amine–indicator ion-pair BH^+A^-, which is the only basic form of the indicator present in any appreciable concentration. The unreacted acid and base are colorless. Thus, visible absorbance determines (BH^+A^-) directly, and K_B is calculated simply by eq. 1. Considering that the ion-pair concentration in this work was of the order of 10^{-5} M, the above K_B's should be good approximations of thermodynamic equilibrium constants.

The only complication could arise from a further association of the ion-pairs, in a manner represented by eq. 2. However, if the association were appreciable, the equilibrium constants calculated by eq. 1 would increase rapidly with increasing concentration of added base.[25] No such systematic variation was observed for our systems (standard deviations are indicated in Table I) and this was accepted as satisfactory proof for the validity of the ion-pair assumption over the concentration range investigated. Incidentally, for the 50–50 isopropyl alcohol–toluene mixture, this was corroborated further by our conductance data, where plots of log λ *vs.* log C were straight lines with slopes of $-1/2$.

The basicity constants K_B of the selected N-heterocyclics in terms of their reactivity with brom phenol blue are listed in Table I. We find that the order of basic strength remains quantitatively the same from one solvent to another. In hydrocarbons, the order of increasing basicity is always: pyridine, isoquinoline, 3-picoline, 4-picoline, 2-picoline, and 2,4-lutidine. A good linear relationship is obtained between a series of corresponding basicity constants measured in any two hydrocarbons (Fig. 1).

Hydrocarbon–Hydroxylic Systems.—Our studies of basicity were extended to mixture of isopropyl alcohol and toluene. All the amines were studied in 10, 20, 40, and 50% isopropyl alcohol in toluene (by volume).[26] Selected measurements also were made in the 1–10% range. Strictly speaking, the generalized solution in eq. 12 should be used to evaluate K_B's in all the mixtures of isopropyl alcohol and toluene. However, the dielectric constants of most isopropyl alcohol–toluene mixtures employed by us are so low (Table II) that the extent of ionic dissociation in their solutions is outside the realm of reliable measurements. Thus, our conductometric determinations of the ionic dissociation constants (Table III) were confined to the most polar solvent mixture (D = 8). It is only for the 50–50 isopropyl alcohol–toluene mixture that we obtained all the constants necessary to use eq. 12.

TABLE II

DIELECTRIC CONSTANTS OF ISOPROPYL ALCOHOL–TOLUENE MIXTURES (at 25°)

% Isopropyl alcohol in toluene, by volume	D	% Isopropyl alcohol in toluene, by volume	D
0	2.374	6	2.620
1	2.416	8	2.718
2	2.462	10	2.817
3	2.501	20	3.492
4	2.541	40	6.098
5	2.581	50	7.903

(25) A. Weissberger and K. Fasold, *Z. physik. Chem.*, [A] **157**, 65 1931)

(26) At 25°, 10% isopropyl alcohol by volume is 1.31 M.

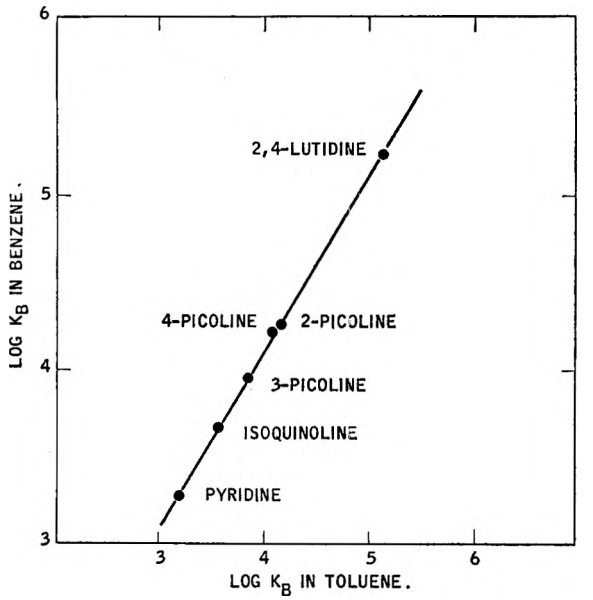

Fig. 1.—Relationship between basicity constants of amines in toluene and in benzene.

TABLE III

LIMITING EQUIVALENT CONDUCTANCES AND IONIC DISSOCIATION CONSTANTS OF THE ION-PAIRS

Ion-pair of brom phenol blue and	Λ_0	$K_s \times 10^7$
Pyridine	26.0	4.47
Isoquinoline	23.4	6.13
3-Picoline	26.7	3.72
2-Picoline	20.3	8.50
4-Picoline	23.0	6.43
2,4-Lutidine	29.4	3.72
Isopropyl alcohol	23.8	$K_i = 1.68 \times 10^{-7}$ (eq. 6)
		$K_p = 0.0318$ (eq. 4)

Fortunately, our inability to measure accurately the extent of ionic dissociation in the remaining alcohol–toluene mixtures also meant that there the dissociation could be largely neglected. For example, the dissociation constants of the ion-pairs encountered in these systems were estimated to be of the order of 10^{-7}, 10^{-13}, and 10^{-17} in the 40, 20, and 10% isopropyl alcohol–toluene mixtures, respectively.

What could not be neglected was the protolysis reaction between the indicator and the hydroxylic solvent (eq. 4) and its contribution to visible absorbance. In order to evaluate the concentration of an amine salt in an equilibrium mixture, the fraction of absorbance due to the indicator–solvent ion-pairs must be subtracted from the total observed absorbance. In the absence of conductance data, this was done by determining spectrophotometrically the concentration of the basic form of the indicator as a function of the equilibrium concentration of unreacted indicator. An empirical correction was obtained in each medium over a short concentration range of interest, which corresponded approximately to a subtraction of $(ROH_2^+A^-)$ (plus a negligible amount of (A^-)) from the total basic form measured by spectrophotometry. The remaining basic form corresponded then to (BH^+A^-). In effect, such simplified treatment combines $(ROH_2^+A^-)$ with (ROH_2^+) on the one hand, and (BH^+A^-) with (BH^+), on the other hand, along with the assumption that there are no common-ion effects, because there are no free ions. We found that even for the 50% isopropyl alcohol–toluene mixture, the agreement between results obtained by the exact and the empirical calculation was remarkably good (Table IV). Below is a sample calculation by both methods.

Example: I. Exact Method (Using Eq. 12). Data.—6.00×10^{-5} *M* 4-picoline reacted with 4.00×10^{-5} *M* indicator in the 50–50 isopropyl alcohol–toluene mixture: A_{max} at equilibrium = 0.500; $K_s = 6.43 \times 10^{-7}$; $K_p = 0.0318$; $K_i = 1.68 \times 10^{-7}$.

Calculation: $(A_T) = 0.500/2.40 \times 10^4 = 2.08 \times 10^{-5}\ M$

$(HA) = 4.00 \times 10^{-5} - (A_T) = 1.92 \times 10^{-5}\ M$

$(ROH_2^+A^-) = K_p \times (HA) = 0.0318 \times 1.92 \times 10^{-5} = 6.1 \times 10^{-7}\ M$

$(S_T) = (A_T) - (ROH_2^+A^-) = 2.08 \times 10^{-5} - 6.1 \times 10^{-7} = 2.02 \times 10^{-5}\ M$

$(BH^+A^-)^2 - (2S_T + K_s)(BH^+A^-) - K_i(HA) + S_T^2 = 0$ (eq. 12)

Solving (12): $(BH^+A^-) = 1.65 \times 10^{-5}\ M$

$(A^-) = S_T - (BH^+A^-) = (2.02 - 1.65) \times 10^{-5} = 0.37 + 10^{-5}\ M$

$$(ROH_2^+) = \frac{K_i(HA)}{(A^-)} = \frac{(1.68 \times 10^{-7})(1.92 \times 10^{-5})}{(0.37 \times 10^{-5})} = 8.7 \times 10^{-7}\ M$$

$(BH^+) = (A^-) - (ROH_2^+) = (0.37 - 0.09) \times 10^{-5} = 0.28 \times 10^{-5}\ M$

$(B) = (B)\text{ added} - (BH^+A^-) - (BH^+) = (6.00 - 1.65 - 0.28) \times 10^{-5} = 4.07 \times 10^{-5}\ M$

$$K_B = \frac{(BH^+A^-)}{(B)(HA)} = \frac{1.65 \times 10^{-5}}{(4.07 \times 10^{-5})(1.92 \times 10^{-5})} = 21.1 \times 10^3$$

II. Empirical Method. Data.—The same as in I, except that K_s and K_i are unknown (assumed to be zero) and instead of K_p, an empirical correction for $(ROH_2^+A^-)$ is used. On the basis of a short study on pure indicator solutions, a solution of 1.92×10^{-5} *M* indicator should contribute (by interpolation) about 0.22×10^{-5} *M* basic form.

Calculation.—Let total basic form of the indicator, A_T, be composed of the basic form due to reaction with solvent, A_1, and, with the amine, A_2.

$(A_T) = (A_1) + A_2)$

$(A_2) = (A_T) - (A_1) = (2.08 - 0.22) \times 10^{-5} = 1.86 \times 10^{-5}\ M$

(A_1 should correspond roughly to $(ROH_2^+A^- + ROH_2^+)$, A_2, to $(BH^+A^- + BH^+)$).

(BH^+) is assumed to be negligible, compared to (BH^+A^-).

$$K_B = \frac{(BH^+A^-)}{(B)(HA)} \frac{1.86 \times 10^{-5}}{4.14 \times 10^{-5} \times 1.92 \times 10^{-5}} = 23.4 \times 10^3$$

Except for the 50% isopropyl alcohol in toluene, where eq. 12 was used, equilibrium constants for

TABLE IV

BASICITY CONSTANTS CALCULATED BY THE EXACT AND THE EMPIRICAL METHOD

(50% isopropyl alcohol in toluene)

Base	$K_B \times 10^{-3}$ Eq. 12	$K_B \times 10^{-3}$ Empirical
Pyridine	3.49	3.81
Isoquinoline	7.24	8.28
3-Picoline	10.6	11.6
2-Picoline	19.1	21.7
4-Picoline	21.3	23.7
2,4-Lutidine	119	122

the reaction of brom phenol blue with N-heterocyclics (K_B, eq. 1) in isopropyl alcohol–toluene mixtures were calculated directly by eq. 1, preceded by an empirical subtraction for the contribution of the alcohol to total absorbance. As in pure hydrocarbons, we find the order of basic strengths to be quantitatively the same in each mixture of isopropyl alcohol and toluene. Furthermore, except for a reversal in the case of 2- and 4-picoline, which are very close in basicity, the order is the same as in hydrocarbons (Fig. 2).

However, the absolute values of the basicity constants are a sensitive function of the medium. In hydrocarbons, they increase in the order toluene, benzene, chlorobenzene. The major increase in acid–base reactivity is observed upon addition of the alcohol to toluene, which reaches an approximate plateau between 10 and 50% alcohol. In order to shed more light on the effect of alcohol on the position of the acid–base equilibria, the basicity constants of 4-picoline were measured over its 1–10% range in toluene. Addition of alcohol to toluene caused a rapid initial rise in reactivity, which reached a plateau at about 5% of added alcohol (Fig. 3). Further addition had a comparatively slight effect.

An unusual effect was produced by adding 0.5% water to the 50–50 isopropyl alcohol–toluene mixture at the expense of the alcohol. This increased the ion-pair formation constants and the ionic dissociation constants by factors of about 1.5 and 2, respectively (Table V). Obviously, this effect of water goes far beyond that which could be expected from the slight increase in the dielectric constant alone.

TABLE V

THE EFFECT OF 0.5% WATER

50–50 isopropyl alcohol–toluene

Base	Anhydrous $K_B \times 10^3$	Anhydrous $K_s \times 10^7$	With 0.5% water $K_B \times 10^3$	With 0.5% water $K_s \times 10^7$
Pyridine	3.49	4.47	4.68	8.97
Isoquinoline	7.24	6.13	11.0	11.4
3-Picoline	10.6	3.72	16.4	8.12
2-Picoline	19.1	8.50	28.0	11.2
4-Picoline	21.3	6.43	32.0	8.27
2,4-Lutidine	119	3.72	187	6.04

From the above evidence it is clear that bulk properties of mixed solvents, such as their basicities and dielectric constants, cannot be the governing factors in determining the observed variation of solute basicities with the medium. However, these phenomena can be explained if in mixtures with toluene, isopropyl alcohol is assumed to be segregated by the polar neutralization products and solvating them in preference to the uncharged reactants. Once enough alcohol is added to a hydrocarbon to overcome the latter's competition for solvation sites, its effect on the acid–base reactivity of solutes attains a saturation value. Stabilization of ion-pairs and ions by solvation seems to be the major factor leading to increased basicities in solutions containing hydroxylic components. Addition of a small quantity of water to the 50–50 alcohol–toluene mixture leads to great increases in acid–base reactivity, probably by a similar mechanism. Apparently, water tends to replace isopropyl alcohol in the solvation sphere, and itself exerts an even more stabilizing effect on the polar products. Similarly in hydrocarbons, the relative enhancement of basicities in chlorobenzene is due to its greater dipolar character with resulting stabiliza-

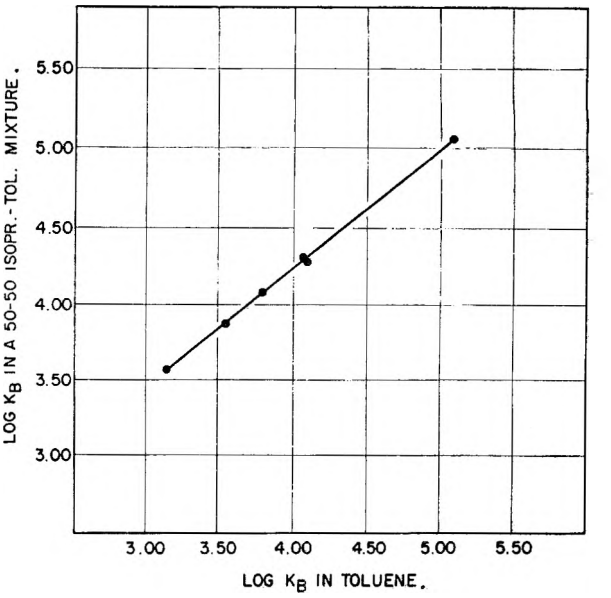

Fig. 2.—Relationship between basicity constants of amines in toluene and in 50–50 mixture of isopropyl alcohol and toluene.

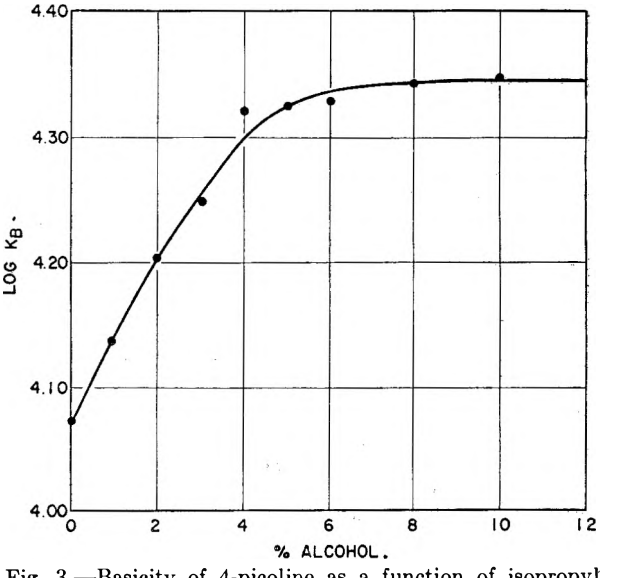

Fig. 3.—Basicity of 4-picoline as a function of isopropyl alcohol concentration in toluene.

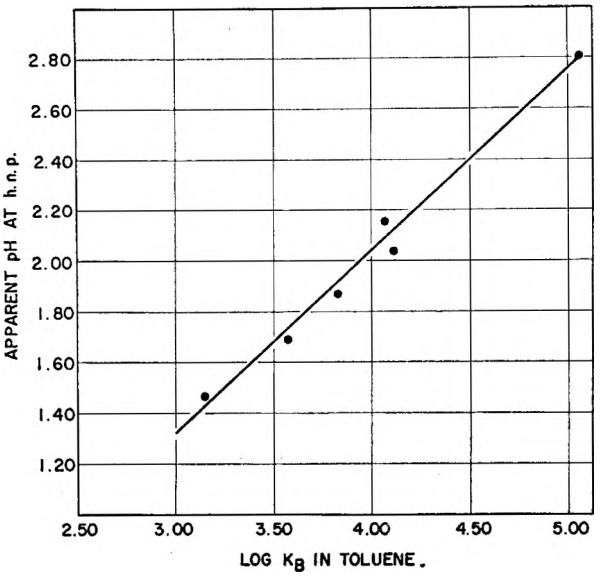

Fig. 4.—Half-neutralization points in methyl isobutyl ketone *vs.* indicator measures of basicity in toluene. 10^{-2} *M* amines titrated with 0.1 *N* $HClO_4$ in dioxane. Electrodes: glass–calomel with methanolic KCl. Beckman expanded scale *p*H meter, Model 76.

tion of polar products. Slight differences such as observed between benzene and toluene are not easily explained.

Shifting of the acid–base equilibrium in eq. 1 due to preferential solvation was elucidated further by dissolving known quantities of the indicator–amine salts in the various solvents and measuring their absorbance. Only a fraction of the calculated absorbance was observed in pure solvents, which showed that in solution the ion-pairs tend to dissociate into their molecular constituents to an extent inversely related to the solvation ability of the medium for polar solutes. The full absorbance always could be restored by the addition of excess base.

It should be emphasized that the above medium effects are evaluated in terms of basicity defined as the extent of ion-pair formation, while the role of the medium in promoting ionic dissociation is excluded. In media where ionic dissociation is appreciable, a slightly better measure of effective basicity than K_B may be the expression: $K_B' = [(BH^+A^-) + (BH^+)]/(B)(HA)$, though it corresponds to no true equilibrium. Such "over-all basicity constants" have been calculated for the most polar medium, where both (BH^+) and (BH^+A^-) were known (Table VI).

TABLE VI

OVER-ALL BASICITY CONSTANTS OF THE AMINES

(50% isopropyl alcohol in toluene)

Base	$K_B' = \frac{[(BH^+A^-) + (BH^+)]}{(B)(HA)}$
Pyridine	3.93
Isoquinoline	8.61
3-Picoline	12.0
2-Picoline	23.0
4-Picoline	25.1
2,4-Lutidine	132

Comparison with Potentiometry.—An accepted measure of relative acidic or basic strength in nonaqueous solvents is the half-neutralization point (h.n.p.) in a potentiometric acid–base titration. In order to compare our indicator measures of basicity with their potentiometric counterparts, the selected N-heterocyclics were titrated potentiometrically in methyl isobutyl ketone with perchloric acid. Figure 4 shows that their h.n.p.'s are quantitatively related to the basicity constants determined in terms of reactivity toward brom phenol blue. A similar relationship holds for potentiometric titrations in other media and for the literature values of their basic ionization constants in water. Such good correlations between indicator and potentiometric measurements of basicity are not the general rule. Usually, they are distorted due to complications from hydrogen bonding and other specific solvent–solute interactions. However, in this case both methods seem to measure the same single property of the amines—their tendency to accept protons from a reference acid. Thus, for the series of structurally similar bases studied here, the order of strengths is quantitatively the same not only in different solvents, but for different methods of determination as well.

Acknowledgments.—The author wishes to thank Professors R. M. Fuoss and S. Bruckenstein for stimulating discussions of this work. Also, the capable assistance of Mr. H. F. Rundlett in many of the experiments is acknowledged.

FORMATION OF HYDROGEN ATOMS IN IRRADIATED CATALYSTS

BY P. H. EMMETT, R. LIVINGSTON, H. ZELDES, AND R. J. KOKES

Department of Chemistry, Johns Hopkins University, Baltimore, Md., and the Oak Ridge National Laboratory, Oak Ridge, Tenn.

Received December 11, 1961

Irradiation of silica gel, alumina, and silica–alumina catalysts at −195° with a Co^{60} γ-ray source produces hydrogen atoms detectable by the use of an electron spin resonance spectrometer on the cold (−195°) sample. About 1×10^{17} hydrogen atoms per gram were produced in silica gel and in alumina; about 12×10^{17} per gram of sample were produced in the silica–alumina catalyst and also in a sample of catalyst that had been base exchanged with Ba^{++} ions. A silica–alumina catalyst originally equilibrated with 70% relative humidity at 25° showed hydrogen atom yields increasing with an increase of temperature of sample evacuation up to about 250° and then decreasing as the temperature of evacuation was increased to 500°.

The mechanism of cracking of hydrocarbons by silica–alumina catalysts is believed to occur by carbonium ion formation[1] promoted by the acid nature of these catalysts.[2] The formation of carbonium ions by olefins adsorbed on clay catalysts has been demonstrated by spectral studies[3]; more recent studies[4] of the spectra of adsorbed molecules indicate that both olefins and paraffins form carbonium ions on the surface of silica–alumina catalysts. Although carbonium ion formation on cracking catalysts is well supported by experimental evidence, the mechanism of its formation and the role of the catalyst is not completely clear. Positive ion formation by adsorption of olefins can occur by reaction with a proton from a Brönsted acid; it also can occur by the addition of a Lewis acid to the double bond.[4] Thus, a question of considerable importance is whether the catalytic action depends on Lewis acid sites or Brönsted acid sites. The spectra of chemisorbed ammonia[5] gives an indication that the sites are primarily Lewis acids[6]; studies of the exchange of hydrocarbons[1] with deuterated catalysts seem to indicate that the active centers are Brönsted acids, *i.e.*, hydrated Lewis acids.

Recent studies[7] of the electron spin resonance of frozen acids suggested a new way of studying the acidity of cracking catalysts. When frozen acids of the third period elements (*e.g.*, $HClO_4$, H_2SO_4, and H_3PO_4) are irradiated at −195° with a Co^{60} γ-ray source, hydrogen atoms are formed. The number of trapped hydrogen atoms formed varies from acid to acid, but in general, the number is greater the stronger the acid. In view of these observations on other acids it seemed worthwhile to explore the question as to whether the hydrogen atoms in the water content of the silica–alumina catalysts might tend to give higher yields of hydrogen atoms on irradiation at −195° than the water content of either silica gel or alumina.

Experimental

Pretreatment.—The samples used in this study were Fisher activated alumina, Davison silica gel, and Davison (high density) silica–alumina catalyst (~500 $m.^2/g.$). The barium exchanged catalysts were prepared by the technique described by Haldeman and Emmett.[8] Prior to pretreatment all samples were stored for several days in a desiccator containing a solution of potassium iodide at such a concentration that the relative humidity was 70%. For irradiation studies samples of these solids in a thin-walled tube were pretreated as indicated in a conventional vacuum system.

Radiation and Electron Spin Resonance Measurements.—The samples were irradiated at the temperature of liquid nitrogen at a dose rate of about 2×10^{17} e.v. $g.^{-1}$ $min.^{-1}$ in a Co^{60} γ-ray source. The irradiated samples were kept cold until after the atomic hydrogen assays were completed. The assays were accomplished with an electron spin resonance spectrometer which displayed the absorption spectrum on an oscilloscope. The number of hydrogen atoms was deduced by comparing the strength of an atomic hydrogen absorption line with that of a known sample of the stable free radical α,α-diphenyl-β-picrylhydrazyl. The line strengths were estimated visually by comparing signal to noise at the same microwave power level for all samples.

Results

The results of thirty-four experiments on silica–alumina cracking catalysts, on base exchanged silica–alumina catalysts, and on silica gel and alumina gel are shown in Table I and Fig. 1. The number of hydrogen atoms per gram of sample varies from 1.0 and 1.6×10^{17}, respectively, for alumina and for silica to as high as 14×10^{17} for silica–alumina catalysts. For purposes of comparison we may note that prolonged irradiation of 12.9% H_2SO_4 yields a steady state corresponding to 3×10^{18} hydrogen atoms for the glassy solid; for 12.5% $HClO_4$ the corresponding figure is 3×10^{19} hydrogen atoms per gram of solid.

Several experiments were carried out to ascertain the effect of base exchange on the hydrogen atom production from silica–alumina catalysts. In only one of the eighteen experiments listed in Table I (D8-122 hr.) was the difference in corresponding samples of base exchanged and non-exchanged catalyst greater than the assumed experimental error; hence, base exchange has little effect on the potential hydrogen atom production of these catalysts.

Figure 1 shows a plot of the number of hydrogen atoms produced by irradiation as a function of the temperature of evacuation. (Points at 25° corre-

(1) H. H. Voge, "Catalysis," P. H. Emmett, ed., Vol. VI, Reinhold Publ. Corp., New York, N. Y., 1958, p. 407.

(2) L. B. Ryland, M. W. Tamele, and J. N. Wilson, "Catalysis," P. H. Emmett, Ed., Vol. VII, Reinhold Publ. Corp., New York, N. Y., 1960, p. 1.

(3) A. G. Evans, *Discussions Faraday Soc.*, **8**, 302 (1950).

(4) H. P. Leftin, *J. Phys. Chem.*, **64**, 1714 (1960).

(5) J. E. Mapes and R. P. Eischens, *ibid.*, **58**, 1059 (1954); R. P. Eischens, *Z. Elektrochem.*, **60**, 782 (1956).

(6) N.m.r. spectra of the hydrogen content of silica–alumina catalysts suggest the surface-O–H group is more like an alcohol group than an acid group [D. E. O'Reilly, "Advances in Catalysis," Vol. XII, Academic Press, New York, N. Y., 1960, p. 71]. The spectra observed, however, may be due primarily to Si–O–H groups and, in such a case, the results do not rule out protons that may be found in Al–O–H groups, the assumed sites of acid activity.[2]

(7) R. Livingston, H. Zeldes, and E. H. Taylor, *Discussions Faraday Soc.*, **14**, 166 (1955); R. Livingston and A. J. Weinberger, *J. Chem. Phys.*, **33**, 499 (1960).

(8) R. G. Haldeman and P. H. Emmett, *J. Am. Chem. Soc.*, **78**, 2917, 2922 (1956).

TABLE I

TRAPPED HYDROGEN ATOMS IN VARIOUS SOLIDS[a]

Run	Sample	Treatment: Evac. time, hr.	Treatment: Evac. temp.	Atomic hydrogen/g. cat. × 10^{-17}: Irradiation 18 hr.	50 hr.	66 hr.	122 hr.
D1	Blank	16	250°	0	0	..	~0
D2	Catalyst	16	250°	4	6	..	9
D3	Ba^{++} exchanged catalyst	16	250°	4	5	..	10
D8	Twice Ba^{++} exchanged catalyst	16	250°	4	7	..	14
D6	Blank	16	500°	0	0	..	~1.0
D4	Catalyst	16	500°	~2	2	..	5.6
D5	Ba^{++} exchange catalyst	16	500°	~2	3.0	..	4.0
D7	Twice Ba^{++} exchanged	16	500°	~0	2.0	..	4.0
A1	Alumina	16	250°	..	..	1.0	...
A2	Silica gel	11	250°	..	..	1.6	...

[a] The relative accuracy ($< \pm 1.0$) is far better than the absolute accuracy. The A and D series were performed at different times.

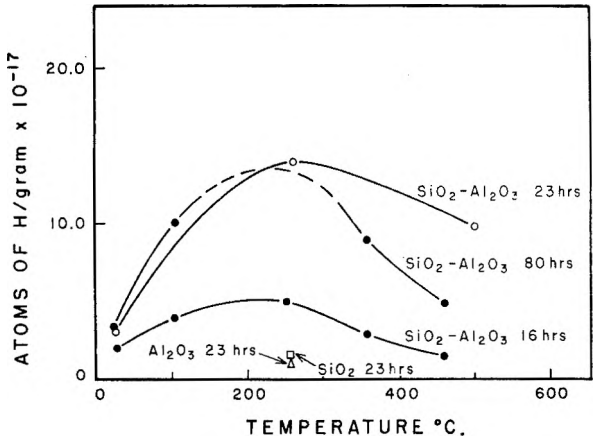

Fig. 1.—Atomic hydrogen signal as a function of the temperature of Al_2O_3, SiO_2, and SiO_2–Al_2O_3 for different times of radiation. The filled and open circles refer to runs carried out at widely different times.

spond to the catalyst equilibrated at 70% relative humidity.) Since there is a correspondence between evacuation temperature and water content,[8] this is effectively a plot of the number of hydrogen atoms *vs.* the amount of water removed from the catalyst. (For comparison we also have included points for silica gel and alumina.) The plot shows a definite maximum at about 250° regardless of the length of the irradiation. These data, together with those in Table I, suggest that for prolonged irradiation the number of hydrogen atoms produced in the catalyst evacuated at 250° is $12 \pm 2 \times 10^{17}$/g.; for the catalyst evacuated at 500° the corresponding value is $7 \pm 2 \times 10^{17}$/g.

Discussion

Before any discussion of the above results, it must be re-emphasized that the number of hydrogen atoms produced on irradiation is a function not only of the strength of the protonic acid present but of the stability of the hydrogen atom trapping sites. For example it has been shown[9] that even ice will form hydrogen atoms when subjected to irradiation if the temperature of the sample is kept at about 4°K. At higher temperatures (such as the −195° used in our experiments) the hydrogen atoms disappear so rapidly that in irradiated ice they have not been detected. In the light of the dependence of hydrogen atom concentration on the effectiveness both of the production and of the recombination factors, the following conclusions seem warranted from the present work:

1. The number of hydrogen atoms observed on the silica–alumina cracking catalysts appears to be higher by a factor of about ten than those produced on silica gel or on alumina. This can be contrasted with the observations by nuclear magnetic resonance[6] which suggest that the type of OH groups on silica–alumina catalysts and on silica gel are similar.

2. The number of hydrogen atoms produced in the silica–alumina catalysts is small, amounting to about 0.2% of the hydrogen equivalent to the water content of the catalyst. Stated in another way the hydrogen atom concentration is equivalent to about 0.01 atom per 1000 Å.^{2} of surface. This compares and contrasts with a figure of 1 active site per 1000 Å.^{2} as judged by poisoning experiments with quinoline and about 14 sites per 1000 Å.^{2} as judged by the amount of Ba^{++} or K^+ incorporated into the silica–alumina catalysts by base exchange procedures.[10]

3. The results obtained here are consistent with but are by no means conclusive in proving the existence of some Brönsted acid sites on the silica–alumina catalysts. Furthermore, they do not preclude the existence of Lewis acid sites on the catalyst. The failure of base exchange with barium to sharply lower the hydrogen atom formation would indicate that any Brönsted acids responsible for the hydrogen atom formation would be from the range of acid strengths that have been shown by Benesi[11] still to exist on a base exchanged catalyst and that may well be responsible for the cracking of cumene as observed by Danforth[12] on base exchanged catalysts.

4. The change in the hydrogen atom content with the residual water content suggested by the curves in Fig. 1 parallel similar observations on the influence of water on isobutane adsorption,[13] on the isomerization of hydrocarbons, and on the cracking of hydrocarbons on silica–alumina catalysts.[14] The

(9) L. H. Piette, R. C. Rempel, H. E. Weaver, and J. M. Flournoy, *J. Chem. Phys.*, **30**, 1623 (1959).

(10) *Cf.* ref. 2, p. 43 and p. 79.

(11) H. A. Benesi, *J. Am. Chem. Soc.*, **78**, 5490 (1956); *J. Phys. Chem.*, **61**, 970 (1957).

(12) J. D. Danforth, *ibid.*, **58**, 1030 (1954).

(13) D. S. MacIver, P. H. Emmett, and H. S. Frank, *ibid.*, **62**, 935 (1958).

existence of a maximum in the curves of Fig. 1 with respect to water content is also in keeping with similar maxima observed in the curves representing the rate of exchange of hydrogen atoms of isobutane with deuterated cracking catalysts.[2] This again is consistent with the hydrogen atom production being associated with a Brönsted acid but unfortunately it does not prove the existence of such acids on the catalyst surface.

Taken as a whole, the present radiation experiments suggest that part of the water content of the silica–alumina catalysts is present in some special form capable (like other inorganic acids) of yielding hydrogen atoms on irradiation with γ-rays at $-195°$. Whether these atoms may be said to come from Brönsted acid sites on the catalyst or to result from special trapping effects of Lewis acid sites cannot be stated with certainty at the present time. This hydrogen atom producing capability then is to be added to a long list of distinctive acid-type properties possessed to a markedly greater extent by silica–alumina cracking catalysts than by silica gel or by alumina.

(14) S. G. Hindin, A. G. Oblad, and G. A. Mills, *J. Am. Chem. Soc.*, **77**, 535, 538 (1955).

PROPERTIES OF ELECTROLYTES IN HYDROGEN PEROXIDE–WATER SOLUTIONS. I. SOLVATION OF ALKALI NITRATES[1]

BY MARTIN E. EVERHARD,[2] PAUL M. GROSS, JR.,[3] AND JAMES W. TURNER[2]

Cobb Chemical Laboratory of the University of Virginia, Charlottesville, Va., and the Department of Chemistry of Wake Forest College, Winston-Salem, N. C.

Received December 18, 1961

The partial pressures of hydrogen peroxide and water in the systems alkali nitrate–H_2O_2–H_2O over the full range of hydrogen peroxide–water compositions at 50° have been determined. The results are discussed in terms of the preferential solvation of the smaller ions by water and the larger ions by hydrogen peroxide in agreement with the previously reported solubility of these salts in this solvent.

Introduction

Aqueous solutions of hydrogen peroxide exhibit significantly different solvent effects on the solutions of cations of differing size based on a series of solubility measurements of the alkali metal salts over the full range of hydrogen peroxide–water concentrations at 0, 15, and 25°.[4,5] Considering only the data obtained for nitrates, it was found that the solubilities of $LiNO_3$ and $NaNO_3$ decreased on the addition of hydrogen peroxide to water. On the other hand, the solubilities of KNO_3, $RbNO_3$, and $CsNO_3$ were considerably greater in hydrogen peroxide-rich solutions than in water. Furthermore, $LiNO_3$ forms hydrates while KNO_3 and $RbNO_3$ form hydroperoxidates. It was concluded that the smaller Li^+ and Na^+ ions were more easily solvated by water molecules than by hydrogen peroxide in the mixed solvent and that the larger K^+, Rb^+, and Cs^+ ions were preferentially solvated by the hydrogen peroxide.

A more quantitative approach to this preferential solvation might be obtained by determining the partial pressures of H_2O_2 and H_2O at a fixed mole fraction of salt over the full hydrogen peroxide–water concentration range. To accomplish this it is necessary to have available accurate vapor pressures and vapor compositions of this mixed solvent over the full range of hydrogen peroxide–water concentrations. Accurate vapor pressure determinations were made earlier by Scatchard and co-workers[6] and reliable vapor compositions and pressures were measured by Floyd[7] in essentially the same equipment described below. The most convenient temperature at which to make the vapor pressure determinations proved to be 50° since at lower temperatures excessive equilibration time was required and at higher temperatures decomposition of the H_2O_2 occurred.

Experimental

The equilibrium still consists of a boiler with a resistance wire heater and a thermocouple well. The hot vapors are heated to avoid condensation and fractionation and then are condensed, dripping into a trap where they can be removed for analysis. An overflow from the trap returns excess condensate to the boiler. The volume of solution contained in the boiler is about 17 ml. while that in the vapor trap is about 1 ml. The apparatus for the measurement and regulation of pressure is similar to that used by Scatchard[8] and values can be determined to better than 1%.

The temperature was measured by a four junction thermal of copper–constantan to better than 0.05°. The temperature of the boiling solution was regulated by adjustment of the total pressure by a needle valve. A 30-l. ballast vessel was contained in the system to avoid erratic pressure changes.

The hydrogen peroxide used was 95% by weight[9] except for the most concentrated solutions, which were prepared by distillation following a procedure described by Gross and Taylor.[10] The hydrogen peroxide was analyzed by the method of Huckaba and Keyes.[11] The solids were analyzed by dry weight determination.

For one of the systems discussed here, the thermody-

(1) This work was supported in part by the Office of Ordnance, U. S. Army.

(2) Philip Francis du Pont Fellows. Based in part on the Ph.D. Theses of M. E. E. and J. W. T. at the University of Virginia.

(3) To whom inquiries should be addressed at Wake Forest College.

(4) J. D. Floyd and P. M. Gross, Jr., *J. Am. Chem. Soc.*, **77**, 1435 (1955).

(5) M. E. Everhard and P. M. Gross, Jr., *J. Phys. Chem.*, **66**, 548 (1962).

(6) G. Scatchard, G. M. Kavanaugh, and L. B. Ticknor, *J. Am. Chem. Soc.*, **74**, 3715 (1952).

(7) J. D. Floyd, Ph.D. Thesis, Univ. of Virginia, 1955.

(8) G. Scatchard, C. L. Raymond, and H. H. Gilmann, *J. Am. Chem. Soc.*, **60**, 1275 (1938).

(9) Donated by the Becco Division, F. M. C. Corp.

(10) P. M. Gross, Jr., and R. C. Taylor, *J. Am. Chem. Soc.*, **72**, 2075 (1950).

(11) C. E. Huckaba and F. G. Keyes, *ibid.*, **70**, 2578 (1948).

namic consistency of the data was considered using the method of Boissonnas,[12] which requires the assumptions that the vapors are ideal and that the volume of the liquid is negligible compared to the volume of the vapor. Also Raoult's law is assumed to hold at the origin of the partial pressure curves. The low pressures at which these experiments were conducted makes these assumptions tenable. The average deviation of the partial pressure of water in the $RbNO_3$ system calculated in this way from the experimental value was 0.52 mm., indicating good internal consistency of the data. The maximum deviation was 1.54 mm.

Results

The experimental data are presented in Tables I through IV. The $RbNO_3$ concentration was lower than the other salts due to the excessive decomposition found at higher concentrations.

TABLE I

VAPOR PRESSURE AND COMPOSITION OF THE $LiNO_3$–H_2O_2–H_2O SYSTEM AT 50°, MOLE FRACTION $LiNO_3$ = 0.0632 ± 0.001

Total pressure (mm.)	Mole fraction H_2O_2 In solvent	Mole fraction H_2O_2 In vapor
74.3	0.0424	0.0004
67.7	.1167	.0004
58.6	.2124	Very small
40.5	.3628	.0221
32.8	.4469	.0489
25.6	.5376	.113
21.6	.6185	.154
16.1	.7101	.314
12.4	.8160	.583
10.0	.9042	.824
9.1	.9452	.893

TABLE II

VAPOR PRESSURE AND COMPOSITION OF THE $NaNO_3$–H_2O_2–H_2O SYSTEM AT 50°, MOLE FRACTION $NaNO_3$ = 0.0647 ± 0.001

Total pressure (mm.)	Mole fraction H_2O_2 In solvent	Mole fraction H_2O_2 In vapor
82.0	0.0127	Very small
81.5	.0228	0.0002
79.8	.0451	.0002
73.0	.1239	.0005
61.2	.2391	.0036
47.8	.3717	.0085
37.2	.4734	.0305
35.0	.5017	.0330
29.1	.5785	.0502
18.4	.7391	.1884
13.6	.8285	.4430
11.0	.8854	.6957
10.5	.9250	.7381
9.5	.9638	.8952
9.0	.9949	.9702

From these data the partial pressures of water and hydrogen peroxide were calculated using the equation $P_x = (P_t)(N_x')$, where P_x is the partial pressure of constituent x, P_t is the total pressure, and N_x' is the mole fraction of this constituent in the vapor phase.

The deviation of the partial pressure curves from that of ideal vapors is an indication of the solvation occurring in solution. According to Hildebrand,[13]

(12) C. B. Boissonnas, *Helv. Chim. Acta*, **22**, 541 (1939).

TABLE III

VAPOR PRESSURE AND COMPOSITION OF THE KNO_3–H_2O_2–H_2O SYSTEM AT 50°, MOLE FRACTION KNO_3 = 0.0646 ± 0.001

Total pressure (mm.)	Mole fraction H_2O_2 In solvent	Mole fraction H_2O_2 In vapor
84.1	0.0217	Very small
79.1	.1022	Very small
75.3	.1527	Very small
58.5	.3313	0.0011
35.3	.5617	.0395
34.7	.5670	.0365
34.5	.5712	.0276
25.7	.6789	.0843
16.1	.8243	.236
15.2	.8417	.344
11.8	.9016	.530
11.7	.9246	.452
10.0	.9579	.832
9.5	.9669	.916

TABLE IV

VAPOR PRESSURE AND COMPOSITION OF THE $RbNO_3$–H_2O_2–H_2O SYSTEM AT 50°, MOLE FRACTION $RbNO_3$ = 0.0397 ± 0.001

Total pressure (mm.)	Mole fraction H_2O_2 In solvent	Mole fraction H_2O_2 In vapor
87.1	0.0000	0.0000
76.8	.1293	.0022
51.6	.3763	.0108
30.6	.5926	.1219
24.7	.6480	.1509
15.6	.8303	.3611
10.8	.9179	.7235
10.2	.9282	.8000
9.84	.9421	.8601

negative deviations from Raoult's law and increased solubilities tend to occur when the components of a solution have an attraction for one another which leads to the formation of solvates. In order to help separate the solvent–solvent interactions from the solute–solvent interactions, the difference between the total pressure of the salt solutions from that of the pure solvent was calculated. The results are shown in Table V. Since the vapor pressure of water is about ten times greater than that of hydrogen peroxide at the temperature studied, the effects noted are largely those exhibited by water. These data will be used in the following discussion.

In the case of the $LiNO_3$ system, the partial pressure or the escaping tendency of water is decreased over the full range of concentration while that of the hydrogen peroxide is decreased only up to about 0.9 mole fraction hydrogen peroxide. The negative deviations from ideality are due in part to the interaction of the hydrogen peroxide and the water. This causes the change in the total pressure to be always negative, see Table V. A consistent picture of the solution structure would be one in which the solute–solvent solvation is largely with water molecules and only involves solute–hydrogen peroxide bonding to a small extent, possibly in the second solvation layer. The slight increase in the

(13) J. H. Hildebrand, "Solubility," Reinhold Publ. Corp., New York, N. Y., 1936, p. 113.

TABLE V

THE DIFFERENCE IN THE TOTAL PRESSURE IN THE PURE MIXED SOLVENT FROM THAT IN THE ELECTROLYTE SOLUTION

Mole fraction H_2O_2	ΔP $LiNO_3$ system, mm.	ΔP $NaNO_3$ system, mm.	ΔP KNO_3 system, mm.	ΔP $RbNO_3$ system, mm.
0.0	−13.2	−9.8	−7.5	−5.6
.1	−12.4	−6.8	−2.8	−2.7
.2	−12.2	−5.0	−0.2	−0.2
.3	−11.9	−4.4	0.2	0.7
.4	−11.0	−3.7	0.4	1.3
.5	−9.6	−3.0	0.6	1.3
.6	−7.6	−2.0	1.0	1.1
.7	−5.3	−1.4	1.2	0.7
.8	−3.5	−1.3	0.6	0.4
.9	−1.4	−0.9	0.3	−0.6
1.0	−1.1	−1.0	−1.2	−1.4

escaping tendency of the hydrogen peroxide, at about 0.9 mole fraction hydrogen peroxide, indicates that very little solute–hydrogen peroxide interaction occurs. That is, as the water content becomes small, very little water is "left-over" from the solute–water interaction to bond with hydrogen peroxide. Consequently, the hydrogen peroxide is freer than if the solute were not present and shows an increase in its partial pressure.

The partial pressures in the $NaNO_3$ system show a slightly smaller negative deviation than in the $LiNO_3$ system. The negative deviations of the total pressure also are somewhat less, indicating less extensive solvation than in the $LiNO_3$ system. It is expected that the solvation in the $NaNO_3$ system is quite similar to the $LiNO_3$ system but, due to the smaller charge density of the Na^+ ion as compared to the Li^+ ion, the solvation is somewhat weaker.

When the KNO_3 system is considered, some striking changes are evident. The solute has such a strong affinity for hydrogen peroxide that in solutions containing high concentrations of water the hydrogen peroxide is bonded to the solute so that the expected hydrogen peroxide water clusters are broken down. The result is an increase in the escaping tendency of the water molecules, as shown by the positive values of the total pressure change in Table V. As more hydrogen peroxide is introduced into the system, the hydrogen peroxide–water bonding increases and results in a decreased escaping tendency for the water. The solvation sheath is smaller than in the cases discussed above due to the decrease in charge density, however, for K^+ ions the hydrogen peroxide would be expected to be present in the primary solvation layer.

The $RbNO_3$ system shows the same trends as noted for the KNO_3 system discussed above. The escaping tendency for water is somewhat higher than for the ideal case at lower concentrations of hydrogen peroxide. As more hydrogen peroxide is added to the system, the escaping tendency decreases, as in the KNO_3 system. The change in the total pressure, Table V, is even more positive than in the KNO_3 system. This indicates even stronger solute–hydrogen peroxide bonding in the $RbNO_3$ system even though the solute concentration was lower. This lower concentration was necessary due to the decomposition at higher concentrations. The stronger solvation by hydrogen peroxide in the $RbNO_3$ system as compared to that in the KNO_3 system also is evident from the formation of a hydroperoxidate at lower H_2O_2 concentration in the former system.[4,5] In the $RbNO_3$ system the solute–water coördination would be expected to be slight as it is when water is the only solvent. The solvation that does occur would be expected to be mostly by hydrogen peroxide.

Vapor pressure measurements for the $CsNO_3$ system were attempted but excessive decomposition, even at low solute concentrations, prevented the completion of these experiments. From the solubility data[5] it appears that the $CsNO_3$ is solvated preferentially by hydrogen peroxide. This solvation would not be expected to be as strong as in the case for the smaller ions since a hydroperoxidate was not found.

These results support those found earlier from solubility considerations.[4,5] In these previous studies, it was reported that the smaller cations were solvated better by water and formed solid hydrates while the larger ions were solvated better by hydrogen peroxide and formed solid hydroperoxidates. Similarly the increase in solubility of the larger ions as the solvent became richer in hydrogen peroxide was taken as evidence that these ions were better solvated by hydrogen peroxide than by water. The converse was found to be true for the smaller ions, that is the poorer solvation of these ions by hydrogen peroxide resulted in a decreased solubility as the solvent became richer in hydrogen peroxide. It seems likely that the hydrogen peroxide molecule is capable of replacing two water molecules in the coördination of the cation since hydrogen peroxide has two oxygens compared to one for water. However, since the exact number of molecules in the solvation cluster cannot be determined by the experiments reported here, it cannot be concluded that each hydrogen peroxide in the cluster replaces two water molecules.

The ability of the hydrogen peroxide molecule to solvate large ions can be attributed to the increased distance separating the non-bonding orbitals on adjacent oxygens in conjunction with the large dipole moment of the molecule. The increased distance presumably allows the dipole to orient itself into a more favorable energy position than the water molecule.

In order to compare the diameters of the cations with the distance separating the non-bonding oxygen orbitals of hydrogen peroxide, an approximate distance of separation was calculated. The angle between the non-bonding oxygen orbital and the O–O axis was calculated by Schatz.[14] By using the length of the OH bond minus the radius of the hydrogen atom, a reasonable, minimum length for the non-bonding orbital can be found. From this information the length of the skew line between the non-bonding orbitals on adjacent O atoms was calculated to be 2.1 Å. This would be a minimum distance since the non-bonding orbitals actually would extend out an infinite distance from the oxygens. This calculated distance is smaller than the diameter of the potassium ion, 2.66 Å., and con-

(14) P. N. Schatz, personal communication, Univ. of Virginia, Charlottesville, Va.

siderably smaller than the diameter of the rubidium ion, 2.96 Å., but larger than the 1.90 Å. of the Na^+ ion. It thus seems that ions smaller than potassium are too small to coördinate effectively with the hydrogen peroxide molecule; however, the larger charge densities of the smaller ions lead to very effective coördination with the smaller water molecule.

THE EFFECT OF IRRADIATION UPON THE KINETICS OF AN ENDOTHERMIC SOLID REACTION. THE DEHYDRATION OF MANGANOUS OXALATE DIHYDRATE[1]

BY TED B. FLANAGAN[2] AND CHANG HWAN KIM[3]

Brookhaven National Laboratory, Upton, L. I., New York

Received December 20, 1961

The kinetics of dehydration of virgin and reactor-irradiated manganous oxalate dihydrate have been examined with the aid of a quartz helix balance. The maximum rate of dehydration was noted to increase by a factor of approximately 3 times (70°) while the activation energy was reduced from 22.3 ± 0.7 to 17.3 ± 0.7 kcal./mole after a total neutron dose of 6.05×10^{18} n. cm.$^{-2}$.

Introduction

The dehydration of manganous oxalate dihydrate has been studied by Topley and Smith[4] and Volmer and Seydel.[5] Indeed manganous oxalate dihydrate is of some historic interest because the "Topley–Smith effect," *i.e.*, an unusual dependence of the rate of dehydration upon the surrounding water vapor pressure, first was observed with this compound (*e.g.*, see ref. 6). Topley and Smith found an activation energy of 24.3 kcal./mole for the dehydration; their rate constants were determined somewhat arbitrarily, as the rate of loss of water vapor per decigram of manganous oxalate dihydrate at 20% dehydration.

While there have been many recent studies of the effects of irradiation, *e.g.*, γ-ray and neutron, upon exothermic solid decompositions, (see especially ref. 7 to 11), there has been a lack of such studies for endothermic reactions.[12,13] Manganous oxalate dihydrate was chosen since the dehydration of virgin material had been investigated previously and because the subsequent thermal decomposition of the anhydride also could be investigated.[14]

Experimental

Materials.—Manganous oxalate dihydrate was prepared by the addition of potassium permanganate to a stirred oxalic acid solution at 80°[15] and also by addition of manganous carbonate to a hot, stirred oxalic acid solution. Microscopic examination revealed that the dihydrate resulting from both preparations was predominately in the form of rhombohedral plates; in addition, however, some long, prismatic crystals were noted. Several preparations using the manganous carbonate and oxalic acid procedure failed to eliminate the long prisms completely.[15] Finally a preparation with a great majority of crystals in the rhombohedral platelet form was employed for the dehydration studies. It was observed, however, that there was negligible difference between the dehydration–time curves of material from the two preparative procedures. The particle size was less than 5 μ. Elemental analysis gave: C = 13.42% and H = 2.21% compared to the theoretical values of C = 13.41% and H = 2.25% for the dihydrate.

Apparatus.—The dehydration was studied with the aid of a quartz helix balance (sensitivity 1 cm./1 mg., Microchemical Specialties, Berkeley, California). One to 2-mg. samples were employed. In the study of endothermic solid state reactions self-cooling often is present[16] and consequently the temperature of the sample may be lower than that measured in the furnace. Self-cooling corrections can be made if the sample's area is known accurately, *i.e.*, if large single crystals are employed.[16] To eliminate self-cooling when employing fine particles, hydrogen gas may be added to the reaction vessel to aid in heat transfer to the sample during dehydration. Topley and Smith[4] used this procedure. Helium gas was employed in the present investigation and it was observed that the rate was sensitive to small variations in the helium pressure. The effect of the helium pressure on the rate of dehydration at both 85 and 95° was investigated. In both cases a maximum in the rate of dehydration occurred at approximately 0.15 mm. of helium; hence, this pressure was employed for determination of the activation energy. A self-cooling curve also was determined for an irradiated sample (6.05×10^{18} n. cm.$^{-2}$); it was found that self-cooling was also of importance in this case, but the rate was not so sensitive to the helium pressure (70°) as was the rate of virgin samples. A pressure of 0.15 mm. of helium also was chosen for the determination of the activation energy of the irradiated sample.

Irradiation Procedure.—Small samples, 10 to 40 mg., were placed in quartz containers (5 cc.) and evacuated to approximately 10^{-6} mm. before sealing off *in vacuo*. The samples then were irradiated in a water-cooled "hole" of the Brookhaven graphite research reactor. In the absence of any appreciable radiation heating due to the presence of a large sample or sample container, the measured temperature of the "hole" is 40 to 50°. The sample vessels were equipped with a break-off seal and could be opened into the high vacuum system to determine the gas evolved after irradiation. One sample was irradiated in air. This

(1) Work performed under the auspices of the U. S. Atomic Energy Commission.

(2) To whom inquiries should be sent regarding this work; present address: Chemistry Department, University of Vermont, Burlington, Vermont.

(3) Participant summer student program, Brookhaven National Laboratory.

(4) B. Topley and M. L. Smith, *J. Chem. Soc.*, 321 (1935).

(5) M. Volmer and G. Seydel, *Z. physik. Chem.*, **A179**, 153 (1937).

(6) W. E. Garner, in "Chemistry of the Solid State," ed. Garner, Butterworths, London, 1955, Chap. 8.

(7) E. G. Prout, *J. Inorg. & Nuclear Chem.*, **7**, 368 (1958).

(8) E. G. Prout and M. J. Sole, *ibid.*, **9**, 232 (1959).

(9) P. J. Herley and E. G. Prout, *ibid.*, **16**, 16 (1960).

(10) E. G. Prout, *Nature*, **183**, 884 (1959).

(11) P. J. Herley and E. G. Prout, *J. Chem. Soc.*, 3300 (1959).

(12) T. B. Flanagan, *Trans. Faraday Soc.*, **55**, 114 (1959).

(13) P. J. Herley and E. G. Prout, *J. Am. Chem. Soc.*, **82**, 1540 (1960).

(14) T. B. Flanagan, to be published.

(15) R. W. Coltman, *Ind. Eng. Chem.*, **16**, 606 (1924).

(16) M. L. Smith and B. Topley, *Proc. Roy. Soc.* (London) **A134**, 224 (1931).

sample was wrapped with aluminum foil and placed in a small aluminum container. Several of the samples were weighed before and after irradiation.

The total neutron flux in the reactor "hole" employed was $\sim 1.0 \times 10^{13}$ n. cm.$^{-2}$ sec.$^{-1}$. The fast neutron flux (>0.4 Mev.) was 4.6×10^{11} n. cm.$^{-2}$ sec.$^{-1}$ and the approximate γ-flux was 2.7×10^{6} r./hr.

Results

Dehydration of Virgin Samples.—A typical dehydration run is shown in Fig. 1 (70°, 0.15 mm. of helium). The shape of the dehydration curve is typical of dehydration reactions which have not been artificially nucleated.[6] The time sequence of phases in the per cent. dehydration–time curve is as follows: phase (a) an induction period, phase (b) a slow reaction period, phase (c) a constant reaction rate, and finally phase (d) a deceleratory phase (Fig. 1).

In a typical run, such as shown in Fig. 1, only 90 to 95% of the two molecules of water were lost from the oxalate at temperatures from 55 to 95°. After heating in an air furnace at 110° for 30 hr., 97% of the water was lost. Heating *in vacuo* at 150° removes approximately 100% of the water. Apparently the last 5% of the water of hydration is comparatively difficult to remove; this behavior was noted to an even greater degree in irradiated samples (see below).

Garner and others[6] have studied many dehydration reactions and have established that the majority of these reactions proceed in the following way: nuclei formation on the surface (this usually is preceded by an induction period), coalescence of these nuclei to establish an interface, and growth of the interface into the volume of the crystal. The events observed in the α–time curve (Fig. 1), α = percentage dehydration, can be tentatively interpreted in terms of the mechanism outlined above: phase (a) represents prenucleation phenomena, phase (b) nuclei formation and coalescence, phase (c) penetration into the interior by a constant area interface, which was established during phase (b), and phase (d) represents deceleration of the reaction, probably in part due to complete reaction of the smaller crystals.

Microscopic observations confirmed this general picture of the dehydration process. With the aid of time-lapse photography, the dehydration process could be followed directly on a vacuum heating stage. These studies revealed that nuclei formed on the surface of the rhombohedral plates; the nuclei appeared to form preferentially at ridges and imperfections on the surface and not necessarily at the edges or corners. The nuclei then grew and coalesced. The plates became relatively opaque after dehydration as compared to the virgin samples. No change in the external shape of the crystals occurred following dehydration.

It was noted from Fig. 1 that a linear rate extends from 10 to 40% dehydration; these percentages are independent of temperature. The distribution of sizes among the crystals precluded a detailed "curve fitting" to the entire dehydration curve. Rate constants were calculated from the slope of the linear portion of the dehydration curve. Rate constants calculated in this manner correspond to penetration into the crystals by an interface of constant area judging from both microscopic observations and by

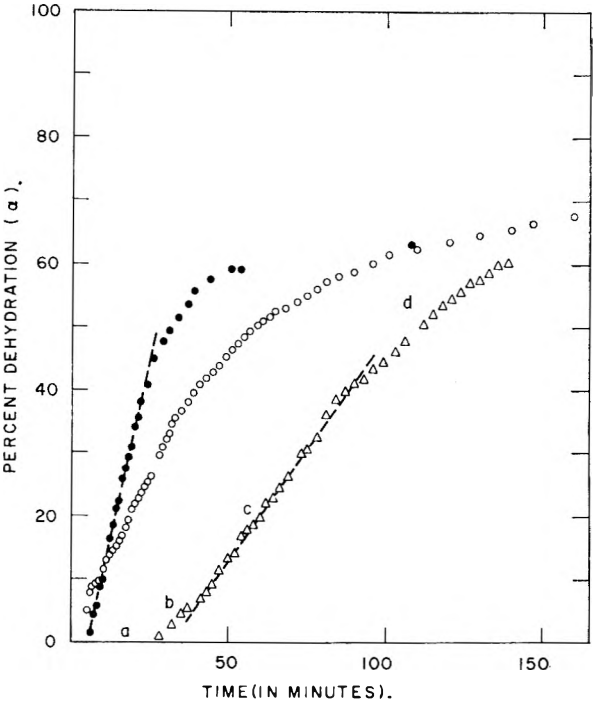

Fig. 1.—The dehydration of manganous oxalate dihydrate (70°, 0.15 mm. helium): Δ, virgin sample; ●, reactor-irradiated sample (6.0×10^{18} n. cm.$^{-2}$); ○, sample dehydrated and rehydrated prior to the dehydration shown in this figure.

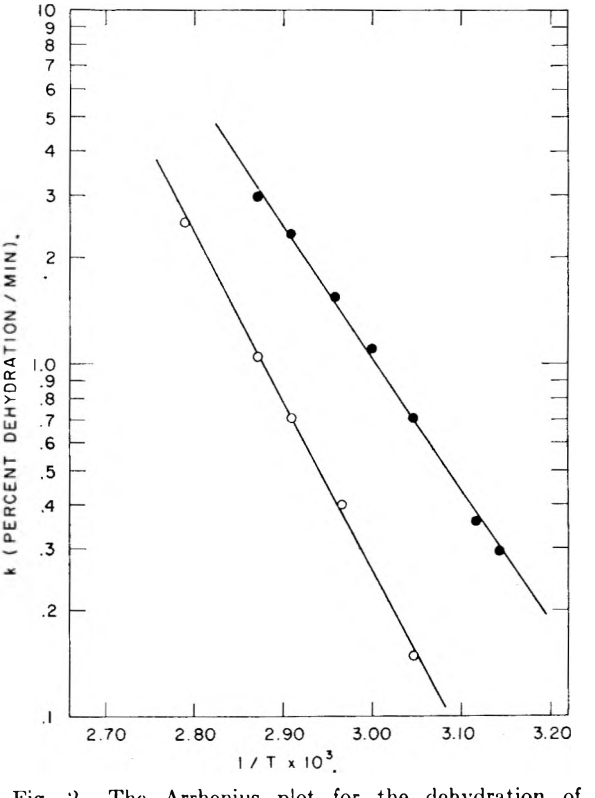

Fig. 2.—The Arrhenius plot for the dehydration of manganous oxalate dihydrate (0.15 mm. helium): ○, virgin sample; ●, reactor-irradiated sample (6.0×10^{18} n. cm.$^{-2}$).

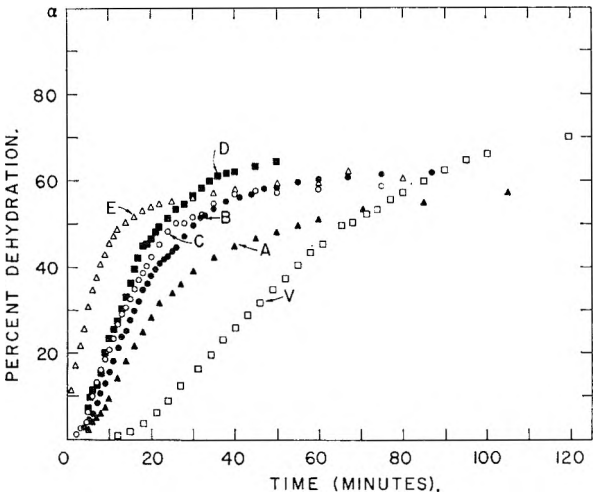

Fig. 3.—The effect of reactor-irradiation upon the dehydration of manganous oxalate dihydrate (75°, 0.15 mm. helium): V, virgin sample; A, 2.2×10^{18} n. cm.$^{-2}$; B, 4.6×10^{18} n. cm.$^{-2}$; C, 5.2×10^{18} n. cm.$^{-2}$; D, 6.0×10^{18} n. cm.$^{-2}$ (irradiated in air); E, 9.8×10^{18} n. cm.$^{-2}$.

analogy with other dehydration reactions. Figure 2 shows the Arrhenius plot of these rate constants; the activation energy is 22.3 ± 0.7 kcal./mole. Self-cooling *in vacuo* was negligible below 55°. The linearity of the Arrhenius plot (Fig. 2) attests to the successful elimination of self-cooling. The induction time also follows the Arrhenius relation with an activation energy of 24.1 ± 1.2 kcal./mole. The value of 22.3 kcal./mole is somewhat smaller than the value of 24.3 kcal./mole found by Topley and Smith.[4]

Dehydration of Reactor-Irradiated Samples.—Figure 1 shows the comparison of the dehydration curve of a virgin and a reactor-irradiated sample (6.05×10^{18} n. cm.$^{-2}$). It is noted that irradiation greatly affects the kinetics of dehydration; for example, in Fig. 1 the induction time has been decreased from 28 to 6 min. The subsequent linear rate of dehydration in the irradiated sample extends from $\alpha = 0$ to $\alpha = 40\%$ dehydration. The magnitude of the linear rate constant for dehydration of the irradiated sample is 3.2 times as great as that of the unirradiated sample (70°). It should be noted that although the rates have been enhanced the general shape of the dehydration curve has not been markedly altered after irradiation (Fig. 1).

Microscopic examination of the irradiated samples during their dehydration revealed no pronounced differences from the behavior of unirradiated samples, *e.g.*, there was no cracking or crumbling of the irradiated samples.

Figure 3 shows the effect of total neutron irradiation dose upon the percentage dehydration–time curves (75°, 0.15 mm. of helium). All but one of the samples were irradiated *in vacuo*[17]; the exception, sample D, was irradiated in the atmosphere of the reactor. (The samples henceforth will be referred to as they are labeled in Fig. 3.) It is noted from Fig. 3 that the dehydration behavior of the sample irradiated in the atmosphere of the reactor does not differ markedly from a sample irradiated *in vacuo* at a slightly smaller total neutron dose (sample C).

A plot of the rate of dehydration *vs.* total neutron dose is quite linear over the range studied, *i.e.*, to 9.8×10^{18} n. cm.$^{-2}$ (75°, 0.15 mm. He). The sample irradiated in air falls on the straight line.

An additional difference between the dehydration behavior of irradiated and virgin samples is that the amount of water lost after several hours of dehydration at 75° decreases somewhat after irradiation. For example, sample D looses approximately 75% of its water after 48 hr. of heating *in vacuo* at 75°. Upon heating to 150° the remainder of the water is lost rapidly. It is expected that samples A through D still retain 100% of their water after irradiation since there was no indication of any water vapor upon opening these samples into the vacuum system. Sample E, however, did evolve some water vapor upon opening the container. Prolonged heating of sample E *in vacuo* at 135° showed that only 94% of the two moles of water were retained after irradiation.

If decomposition occurs at 135° or lower temperatures, the dehydration data will of course be erroneous. This seems unlikely since observable decomposition of unirradiated samples does not occur readily until the temperature is raised to approximately 300° and irradiation does not increase the rate of decomposition.[14] That decomposition is not a factor was shown more conclusively by the following experiment: Sample E was dehydrated in a closed vacuum system while the water vapor was condensed into a liquid nitrogen trap. After several hours heating at 135°, pressure readings still indicated a good vacuum. Since CO is one of the decomposition products,[14] any decomposition would be indicated by an increase of pressure. Additional evidence against decomposition occurring was the visual absence of decomposition, *i.e.*, the sample still was whitish in appearance while the decomposition residue was dark.[14]

Evidence that Samples Were Not Dehydrated during Irradiation.—In order for the kinetic data of the irradiated samples to be meaningful the samples must not have been dehydrated during irradiation, either thermally or as a direct result of irradiation, and then rehydrated after removal from the reactor. The following evidence will be cited to strongly suggest that the samples were not dehydrated during irradiation. (1) While dehydration of irradiated samples was appreciable at 40 to 50° *in vacuo* (Fig. 2), dehydration of an irradiated sample (D) did not occur in the laboratory atmosphere after 120 hr. at 60°. On the basis of this evidence, sample D would not have been dehydrated during its irradiation in air (40–50°) and since its kinetic behavior resembles samples irradiated with a comparable dose *in vacuo* (Fig. 3), it is probable that these latter samples were not dehydrated during irradiation. (2) The rate of rehydration of the anhydride to the dihydrate was extremely slow under conditions

(17) The samples were sealed into quartz containers at 10^{-6} mm. pressure but radiation-induced decomposition of oxalate ions caused the pressure to increase during irradiation, *e.g.*, the pressure over sample C was ~5 mm. (CO_2 and CO) after irradiation.

more favorable for rehydration than the irradiated samples were subjected to. (3) The absence of either water vapor or significant weight loss was noted after opening samples A to D. (4) The magnitude of the rate of dehydration of a rehydrated sample (unirradiated) was closer to that of the virgin than that of an irradiated sample (Fig. 1). (5) Microscopic examination revealed that rehydrated samples appeared more opaque than either irradiated or virgin samples.

There is, however, an incongruity in the evidence; namely, the dehydration of an irradiated sample is appreciable at 45° *in vacuo* (Fig. 2), but dehydration of the samples sealed into quartz ampoules *in vacuo* apparently did not occur after many hours of irradiation. The most likely explanation of this is that the samples which were sealed into quartz ampoules were not in fact irradiated *in vacuo* because of the occurrence of radiation-induced decomposition of oxalate ions. While the percentage decomposition was small, the small size of the sample containers allowed appreciable pressures of gas to accumulate (mainly CO), *e.g.*, for sample C approximately 5 mm. of gas was present in the ampoule after irradiation. It is suggested that the presence of this gas successfully inhibited the dehydration reaction.

Dehydration of γ-Irradiated Sample.—A sample was irradiated as the dihydrate *in vacuo* at room temperature for a total dose of 1.6×10^8 r. (CO^{60}). The dehydration characteristics of this sample were studied. It was found that the subsequent dehydration curve was unaffected by this dose of γ-rays.

Activation Energies for Dehydration of Irradiated Samples.—The Arrhenius plot of the activation energy for dehydration of a reactor-irradiated sample (6.05×10^{18} n. cm.$^{-2}$, irradiated in air) is shown in Fig. 2 in comparison with a virgin sample. The activation energy has been reduced by irradiation from 22.3 ± 0.7 to 17.3 ± 0.7 kcal./mole. This means that there must be a compensating reduction in the pre-exponential factor for dehydration of irradiated samples because the decrease in the activation energy is too large to account for the observed increase in rate. The activation energy for the induction period is also 17 kcal./mole (this should be regarded as an approximate value); it is, however, significantly lower than the value of 24 kcal./mole found for virgin samples.

Discussion

As has been pointed out above, the shape of the per cent. dehydration–time curve for the dehydration of virgin manganous oxalate dihydrate (*e.g.*, Fig. 1) is to be expected for a contracting envelope mechanism when the particles have not been artificially nucleated.[6] The linear rate extends over a significant fraction of the dehydration curve because nucleation and growth are confined to the two large surfaces of the rhombohedral plates. The activation energy calculated from the induction time is larger than that obtained from the linear rate constants. This suggests that the activation energy for nucleation is greater than that for nuclei growth (interfacial penetration); this is reasonable.[6]

The following discussion pertains to the irradiated sample most completely investigated, that is, sample D (total neutron dose of 6.05×10^{18} n. cm.$^{-2}$) (see Fig. 1 and 3). In virgin samples the early non-linear region, phase (b), usually extends from 0 to 10% dehydration; in the irradiated sample shown in Fig. 1 the linear region commences from almost the start of the dehydration. This implies that nucleation and the establishment of the constant area interface must occur simultaneously. Reactor irradiation introduces many potential nucleation sites which will be homogeneously distributed throughout the crystals. The damaged regions on the surface of the plates rapidly nucleate and coalesce upon heating. The resulting interface penetrates into crystals as for unirradiated samples, but the rate of penetration into the irradiated matrix will be enhanced due to the presence of internal radiation damage. The final deviations from linearity occur near 40% dehydration; this is comparable to the point of deviation in unirradiated samples and is consistent with the fact that essentially the same mechanism of dehydration occurs in irradiated and virgin samples.

Damaged regions in the lattice may arise from decomposition of oxalate ions by ionizing radiation or by atomic displacements resulting from either fast neutron knock-on collisions or recoil of manganese atoms from the Mn^{55} (n,γ) Mn^{56} reaction. Walker[18] has estimated that slow neutron capture by manganese will cause approximately $^1/_2$ of the total atomic displacements in pure manganese. It is believed that ionizing radiation, which decomposes isolated oxalate ions, does not contribute significantly to the increase in the rate of dehydration, because isolated defects would not affect the progression of the interface as markedly as regions of damage extending over several hundred molecules (resulting from displacement or thermal spikes). In support of this a γ-ray dose close to that obtained during the reactor irradiation of sample A (Fig. 3) did not affect the subsequent dehydration. The majority of the damage will arise from fast neutron knock-on collisions onto C, H, O, and Mn. There also will be a significant contribution by the recoil damage caused by Mn^{56}.

The effects of nuclear irradiation upon the subsequent exothermic decomposition of solids have been studied by a number of workers.[7-11,19-22] In most cases sample irradiation increases the rate of decomposition and decreases the induction period (if an induction period is present before irradiation). In exothermic decomposition reactions radiation may alter the mechanism of decomposition.[22] The possibility of a change in the mechanism of an endothermic dehydration reac-

(18) R. M. Walker, *J. Nuclear Materials*, **2**, 147 (1960).

(19) T. B. Flanagan, *Nature*, **181**, 42 (1958); *J. Phys. Chem.*, **66**, 416 (1962).

(20) J. Jach, "Proc. Int. Symp. on Reactivity Solids," Amsterdam, 1960.

(21) J. M. Groocock, *Proc. Roy. Soc.* (London), **246A**, 225 (1958).

(22) R. M. Haynes and D. A. Young, *Discussions Faraday Soc.*, **31**, 229 (1961).

tion after irradiation is less likely, since the simple contracting envelope mechanism invariably observed for dehydration reactions[6] is not likely to be significantly altered by radiation unless macrodisruption of the crystals occurs. Hence the evaluation of radiation damage as reflected by the subsequent decomposition kinetics would be expected to be more unequivocal in endothermic systems.

Both dehydration reactions studied to date,[12] (this investigation) have required comparatively large doses of reactor-irradiation[10] for their subsequent dehydration–time curves to be affected. In addition Herley and Prout[13] found that the decomposition of silver oxide was unaffected after an exposure of 1.8×10^{17} n. cm.$^{-2}$ (fast). Judging from these results endothermic solid state decomposition reactions are less affected by irradiation than are exothermic reactions.

Acknowledgments.—Dr. G. J. Dienes is thanked for his encouragement and advice. The coöperation of the Picatinny Arsenal Explosives Research group at Brookhaven National Laboratory is gratefully acknowledged.

CONDUCTANCE OF THE ALKALI HALIDES. III. THE ISOTOPIC LITHIUM CHLORIDES[1]

BY ROBERT W. KUNZE AND RAYMOND M. FUOSS

Contribution No. 1687 from the Sterling Chemistry Laboratory of Yale University, New Haven, Connecticut

Received December 26, 1961

The conductances of the chlorides of Li^6 and Li^7 in water at 25° have been measured over the concentration range 0.002–0.01 *N*. The limiting conductances are $\Lambda_0(Li^6Cl) = 115.23$ and $\Lambda_0(Li^7Cl) = 115.10$. The difference of 0.13 (6 times experimental error) corresponds to a 0.35% greater mobility for the ion of Li^6.

Natural lithium consists predominantly (92.02%) of the heavier isotope; present availability of each isotope in a state of high purity suggested a comparison of their conductances in order to verify the expected existence of a small difference in mobility. It has been shown that a small isotope effect exists for lithium nitrate dissolved in sodium–potassium nitrate eutectic,[2,3] although considerably smaller than the difference in masses (0.089 *vs.* 1/7). Arnikar recently[4] reported a relative mobility difference $\Delta v/v = 0.0036$, based on measurements of migration of lithium chloride in agar gel. The purpose of this paper is to present the results of a series of measurements of the conductance of the chlorides of Li^6 and Li^7 in water at 25°. We find $\Delta\lambda_0/\lambda_0(Li^+) = 0.0035$, in complete agreement with Arnikar's result.

Experimental

Materials.—The lithium chloride was used as received from the Isotopes Division of the Oak Ridge National Laboratory. The isotopic compositions reported for the samples were Li^6Cl (95.62% Li^6) and Li^7Cl (99.9926% Li^7). According to spectrographic analysis, other cations were present at most in only trace amounts, less than 0.01%, except the Li^6Cl, for which 0.1% calcium was reported. Assuming the calcium present as chloride, the error due to replacing LiCl by an equal weight of $CaCl_2$ is nearly compensated by the higher *equivalent* conductance of Ca^{++}. Distilled water with a specific conductance of about 10^{-6} was used; the conductance was measured in the cell before adding the first portion of lithium chloride. Our lowest solution conductances were of the order of 200×10^{-6}; since the solvent conductance was known to 1–2%, the maximum uncertainty from this source was about 0.01% in solute conductance.

Methods.—Lithium chloride was dissolved in water to give approximately 0.1 *N* solution; a portion of about 15–20 g. of this solution was weighed from a weight buret into the water in the conductance cell to give a starting solution of about 0.01 *N* in the cell. Further points were obtained by adding successive portions of water to the cell. All concentrations thus were determined by weight (and corrected to vacuum); they were computed to volume concentrations c (eq./l.) by the equation[5] $c/m = 0.99707 - 0.0182m$.

The concentrations of the master solutions were determined by differential potentiometric titration[6] of 40–50-g. samples against 0.1 *N* silver nitrate solution. The titration was carried almost to the end-point using silver nitrate solution from a weight buret; then the final part of the titration was made using 0.004 *N* silver nitrate solution from a volumetric buret. All titrations were made near 0° in order to sharpen the end-point (about 10 mv. break). The silver nitrate solutions were standardized by using them to titrate portions of our purified potassium chloride[7]; about 400-mg. portions of the latter were weighed on the microbalance. In all, three master solutions (a, b, c) of Li^6Cl and two (d, e) of Li^7Cl were prepared; the corresponding conductance data are indicated by the superscripts on the run numbers in Tables I and II. All standardizations (both of lithium chloride solutions and of the silver nitrate solutions prepared individually for each master solution) are based on (at least) triplicate analyses; the standard deviation over the 12 silver nitrate–potassium chloride titrations was 0.014%, and over the 21 lithium chloride–silver nitrate titrations was 0.007%. As a check on the method, a master solution of sodium chloride, purified for conductance, was prepared and analyzed; it then was used in a conductance run by the dilution technique used for lithium chloride; the points so obtained ($c = 0.0049266$, $\Lambda = 120.650$; $c = 0.0030570$, $\Lambda = 121.796$) agree within 0.01 Λ-unit with the average of literature values.[8–10]

The conductance cell used for all the measurements had a constant of 1.01090 ± 0.00024, based on 21 determinations

(1) Results presented in this paper will be included in a thesis to be presented by Robert W. Kunze to the Graduate School of Yale University in partial fulfillment of the requirements for the degree of Doctor of Philosophy.

(2) M. Chemla, *Compt. rend.*, **242**, 1450 (1956).

(3) H. J. Arnikar and M. Chemla, *J. Appl. Rad. Isotopes*, **2**, 261 (1957).

(4) H. J. Arnikar, *J. Inorg. & Nuclear Chem.*, **10**, 248 (1959).

(5) H. S. Harned and B. B. Owen, "The Physical Chemistry of Electrolytic Solutions," Reinhold Publ. Corp., New York, N. Y., third edition, 1958, p. 715.

(6) N. F. Hall, M. A. Jensen, and S. A. Baeckström, *J. Am. Chem. Soc.*, **50**, 2217 (1928).

(7) J. E. Lind, Jr., and R. M. Fuoss, *J. Phys. Chem.*, **65**, 999 (1961).

(8) T. Shedlovsky, *J. Am. Chem. Soc.*, **54**, 1411 (1932).

(9) G. C. Benson and A. R. Gordon, *J. Chem. Phys.*, **13**, 473 (1945).

(10) F. W. Tober, dissertation, Yale University, 1948.

TABLE I

CONDUCTANCE OF Li^6Cl IN WATER AT 25°

$10^3 c$	Λ	$10^3 c$	Λ
Run 1[a]		Run 5[a]	
11.4805	106.925	10.4000	107.283
9.1590	107.674	7.6579	108.292
6.0224	108.952	6.0048	108.995
4.1672	109.910	4.1252	109.934
2.1418	111.318	2.0690	111.953
Run 2[a]		Run 6[c]	
10.1908	107.342	8.5435	107.941
7.7767	108.224	5.8938	109.052
5.9861	108.978	4.5282	109.733
3.9496	110.043	3.3413	110.456
1.9825	111.489	1.7111	111.748
Run 3[b]		Run 7[b]	
9.2556	107.705	10.1917	107.408
6.8936	108.617	8.1427	108.128
5.4257	109.294	6.1836	108.936
3.7652	110.215	4.0315	109.992
1.8925	111.621	2.4741	111.082
Run 4[b]		Run 8[b]	
10.8679	107.166	11.8675	106.863
8.3417	108.041	8.4730	108.002
5.8886	109.085	6.7584	108.691
3.9796	110.105	4.6002	109.736
2.0095	111.548	2.4071	111.149

TABLE II

CONDUCTANCE OF Li^7Cl IN WATER AT 25°

$10^3 c$	Λ	$10^3 c$	Λ
Run 9[d]		Run 11[e]	
14.4471	105.986	9.5224	107.475
11.4300	106.862	6.9810	108.449
7.5240	108.223	5.4692	109.131
4.7675	109.492	3.9030	109.970
2.8695	110.660	1.9460	111.386
Run 10[d]		Run 12[e]	
7.5585	108.201	10.3636	107.202
5.9672	108.885	7.9567	108.064
4.3293	109.703	5.8444	108.947
3.1055	110.458	4.6051	109.573
1.5523	111.748	2.3501	111.066

made at frequent intervals during the work on lithium chloride; the method used was that proposed by Lind, Zwolenik, and Fuoss.[11] Cell design, electrical equipment, and thermostat have been described previously.[7]

The conductances of solutions of the chlorides of the two isotopes of lithium are summarized in Tables I and II.

Discussion

The data of Tables I and II were analyzed on the IBM 650 computer, using Kay's[12] program for the equation[13]

$$\Lambda = \Lambda_0 - Sc^{1/2} + Ec \log c + Jc \qquad (1)$$

which describes the conductance at low concentrations for unassociated I–I electrolytes. The values of the limiting conductances Λ_0 and linear coefficients J are summarized in Table III, together with the contact distances $\mathring{a}$ calculated from J and the standard deviation σ of the difference between the observed values of conductance in a given run and the values calculated for that run using eq. 1 and the corresponding constants from the table.

TABLE III

CONSTANTS DERIVED FROM DATA

Run	Λ_0	J	$\mathring{a}$	σ
Lithium(6) Chloride				
1	115.205	176.5	3.36	0.005
2	115.226	176.0	3.36	.011
3	115.284	173.8	3.31	.004
4	115.323	169.7	3.24	.006
5	115.237	177.7	3.39	.006
6	115.213	179.6	3.42	.024
7	115.210	184.1	3.51	.022
8	115.266	177.2	3.38	.014
Lithium(7) Chloride				
9	115.132	174.4	3.32	0.016
10	115.060	185.4	3.54	.007
11	115.093	181.1	3.46	.009
12	115.112	179.0	3.42	.008

TABLE IV

COMPARISON OF ISOTOPES

Data	Λ_0	J
Li^6Cl	115.234 ± 0.024	178
Li^7Cl	115.099 ± .023	180
LiCl[a]	115.098 ± .010	176
LiCl[b]	115.02 ± .05	190
LiCl[c]	115.044 ± .009	181
LiCl[d]	115.080 ± .013	178

[a] T. Shedlovsky, *J. Am. Chem. Soc.*, **54**, 1411 (1932). [b] K. A. Krieger and M. Kilpatrick, *ibid.*, **59**, 1878 (1937). [c] F. W. Tober, Dissertation, Yale University, 1948. [d] R. E. Jervis, D. R. Muir, J. P. Butler, and A. R. Gordon, *J. Am. Chem. Soc.*, **75**, 2855 (1953).

The average values (run 4 not included in average) for the limiting conductances are compared in Table IV with values obtained from data in the range $0.002 \leq c < 0.011$ in the literature. These were based on measurements made on solutions of lithium chloride of normal isotopic composition (92.02% Li^7). The excellent agreement between our value for the heavy isotope and those reported for natural lithium confirms the validity of our standards and methods. The data thus clearly establish the existence of a small but real difference between the mobilities of the ions of Li^6 and Li^7; the former has a limiting conductance 0.135 unit larger (0.35%) than the latter. This difference is in exact agreement within experimental error of the difference ($\Delta v/v = 0.0036$) found by Arnikar[4] by transport experiments with lithium chlorides in agar gels. The relative difference in mobilities of the two isotopic ions is, of course, much smaller than the difference in the masses of the lattice ions. As expected, the contact distances are identical (Li^6, 3.39 ± 0.04; Li^7, 3.44 ± 0.07 Å.) for the two isotopic ions in aqueous solution.

(11) J. E. Lind, Jr., J. J. Zwolenik, and R. M. Fuoss, *J. Am. Chem. Soc.*, **81**, 1557 (1959).

(12) R. L. Kay, *ibid.*, **82**, 2099 (1960).

(13) R. M. Fuoss, *ibid.*, **81**, 2659 (1959).

EFFECTS OF AMIDES ON PHOTOCHEMICAL PROCESSES AT ZINC OXIDE SURFACES[1]

BY M. CLARE MARKHAM, JOSEPH C. KURIACOSE, JOANN DEMARCO, AND CAROL GIAQUINTO

Department of Chemistry, Saint Joseph College, West Hartford, Conn.

Received January 12, 1962

Amide residues exert a stabilizing influence on hydrogen peroxide at irradiated surfaces of zinc oxide in aqueous suspension, whether the peroxide has been formed in the system by the photocatalyzed oxidation of the amide itself, or whether hydrogen peroxide has been added to the system before irradiation. In the former case the rate of oxygen uptake and the final steady-state concentration of hydrogen peroxide are related to the number of oxidizable C–H bonds in the amide. In the latter case the level of hydrogen peroxide that can be maintained is governed by both the initial concentration of added peroxide and the nature of the amide. Formamide gives rise to a surface-inactivating residue immediately on irradiation in contact with zinc oxide, and therefore stabilizes high concentrations of added peroxide, but produces very little peroxide itself. Acetanilide both produces and maintains high concentrations of hydrogen peroxide. Other amides studied include N-methylformamide, N,N-dimethylformamide, and urea. Effects of several nitrogen-containing compounds are compared with those of the amides.

Introduction

When an aqueous suspension of zinc oxide is irradiated with light in the near ultraviolet a small amount of hydrogen peroxide is formed. The presence of organic material in the system greatly increases the yield of hydrogen peroxide. Previous studies[2] using phenol as the organic additive showed an optimum rate of peroxide formation at a phenol concentration of 1×10^{-3} *M*. With this initial concentration of phenol, hydrogen peroxide builds up to a maximum concentration of 4×10^{-3} *M* in about two hours, and then gradually decreases until it reaches the steady-state concentration that would be formed at an irradiated zinc oxide surface in pure water. The first detectable oxidation products of the phenol are catechol and hydroquinone. After a few hours there is no further indication of an aromatic ring in the system, and evolution of carbon dioxide suggests exhaustive oxidation of the phenol.

During a series of experiments designed to compare reactions of various aromatic compounds in irradiated suspensions of zinc oxide, it was observed that hydrogen peroxide formed in the presence of acetanilide remained stable indefinitely for prolonged periods of irradiation following the attaining of the maximum concentration. This phenomenon is illustrated in Fig. 1.

Meanwhile, studies of the photosensitized polymerization of methyl methacrylate in aqueous suspensions of zinc oxide[3] had indicated that oxygen is essential to the initiation process, contrary to the earlier suggestion that polymerization in the absence of oxygen proved that oxygen might not be necessary for photochemical reaction at zinc oxide surfaces.[4] Several simple amides such as formamide, N-methyl-, and N,N-dimethylformamide are good solvents for oxygen. Their dielectric constants are, respectively, 109, 190, and 37. While formamide is a good solvent for the photosensitized polymerization, neither N-methylformamide nor N,N-dimethylformamide are.

The object of the present research was to study in detail the behavior of amides in these systems, in order to understand better the chemical effects produced by light at the surface of zinc oxide. Data are presented on the formation of hydrogen peroxide in the presence of various amides. In some cases it has been possible to identify intermediates. Measurements of oxygen uptake have been made in both aqueous and non-aqueous systems.

Experimental

The apparatus and method of procedure for the investigation of peroxide formation were the same as described.[4] The Hanovia H-4 high pressure quartz mercury arc lamp was used throughout with a Pyrex jacket to retain all radiation below 320 mμ. Rapid entrainment of air supplied oxygen to the system and kept the zinc oxide in suspension. The air was washed through distilled water before entrainment. For each study 0.1 g. of zinc oxide and 25–30 ml. of solution were used. Samples of 1 or 2 ml. were withdrawn periodically and analyzed for peroxide by addition of iodide to the acidified solution and titration with standard thiosulfate. All chemicals used were Analytical Reagent grade.

Ultraviolet analyses were performed with a Beckman DK-2 ratio recording spectrophotometer. Infrared analyses were made on a Perkin–Elmer Infracord. Samples of the irradiated solution, from which zinc oxide had been removed by centrifugation, were prepared for infrared analysis by evaporation to dryness, dissolving the residue in chloroform, addition of potassium bromide, and vacuum evaporation of the chloroform.

Measurements of oxygen uptake were made in Warburg respirometer flasks using the Hanovia H-4 mercury lamp in its Pyrex shield mounted horizontally above a pair of flasks to give sets of duplicate measurements. The temperature was maintained at 25° in these experiments as well as in the tests for peroxide formation. The flasks contained 0.2 g. of zinc oxide and 3 ml. of liquid reactant. A few measurements were carried out with potassium hydroxide solution in the center well to check on carbon dioxide evolution.

Concentrations of oxidation products of acetanilide were estimated by making the centrifugate from the irradiated suspension alkaline with 1 *M* sodium hydroxide and extracting the unreacted acetanilide into chloroform. The sodium hydroxide layer, containing the hydroxyacetanilides, then was neutralized with 1 *M* hydrochloric acid and analyzed on the spectrophotometer. Standards were prepared according to the same procedure. The chloroform layer was evaporated to dryness under vacuum and the residue of acetanilide redissolved in water for spectrophotometric measurements.

Hydroxylamine hydrochloride and hydrazine sulfate were neutralized with sodium hydroxide before adding zinc oxide and irradiating. The effects of the salts produced by the neutralization were tested in separate measurements of decomposition of hydrogen peroxide and were found to be negligible. For example, curve 6 of Fig. 7 shows that

(1) This work was carried out under Contract AF 19 (604)-7224, with the Geophysics Research Directorate of the Air Force Cambrdige Research Laboratories, Air Force Research Division.

(2) M. C. Markham, M. C. Hannan, and S. W. Evans, *J. Am. Chem. Soc.*, **76**, 820 (1954).

(3) J. C. Kuriacose and M. C. Markham, *J. Phys. Chem.*, **65**, 2232 (1961).

(4) M. C. Markham and K. J. Laidler, *ibid.*, **57**, 363 (1953).

the decomposition of hydrogen peroxide is the same in the presence and absence of added sodium chloride. Highest purity grades of redistilled aniline, methylamine hydrochloride, ammonia, and propionitrile were used, all at concentration 10^{-3} *M*, without further treatment. KCN was neutralized with HCl to obtain a solution of cyanide at *p*H 7.

Results

Suspensions of Zinc Oxide Containing Acetanilide.—Under the conditions used, the initial rate of formation of hydrogen peroxide in suspensions of zinc oxide containing acetanilide appears to be limited chiefly by the available light intensity at the catalyst surface. Moving the reaction vessel farther from the lamp reduces the reaction rate, but by a factor less than that predicted by the inverse square law. On the other hand, substituting oxygen for air does not increase the rate. The initial rates of formation of peroxide in solutions of acetanilide 0.001 *M* or higher apparently are independent of concentration. With the limiting concentration of 0.02 *M*, due to the solubility of acetanilide in water, there is a definite inhibition. Kinetic studies show that the reaction is zero order with respect to acetanilide between 0.001 and 0.010 *M*. The steady-state level reached by the hydrogen peroxide, however, is dependent on the initial acetanilide concentration, but in no simple numerical ratio, as shown in Fig. 1. The products of the reaction maintain a high concentration of peroxide in the system for long periods of irradiation. In some cases the time of irradiation has been extended to 40 hr. with no appreciable decrease in the peroxide concentration. The effect of temperature on these systems is slight. Activation energies of a few kilocalories can be measured in the initial stages.

Ultraviolet spectra reveal that the chief oxidation product of acetanilide is the *o*-hydroxyacetanilide. The formation of the hydroxy derivatives and the disappearance of acetanilide were studied in the initial reaction stages for several different initial concentrations of acetanilide. Results of the 0.001 *M* initial concentration of acetanilide are typical, and are shown in the following table.

TABLE I

FORMATION OF PRODUCTS AND DECOMPOSITION OF ACETANILIDE IN AQUEOUS SUSPENSIONS OF ZINC OXIDE AT 365 mμ AND 0.001 *M* INITIAL CONCENTRATION OF ACETANILIDE

Time (min.)	Concn. acetanilide, *M* (× 10^4)	Concn. *p*- and/or[a] *m*-hydroxyacetanilide, *M* (× 10^4)	Concn. *o*-hydroxyacetanilide, *M* (× 10^4)	Concn. hydrogen peroxide, *M* (× 10^4)
0	10.0	0.00	0.00	0.00
5	7.2	.47	0.86	1.90
10	5.3	.48	2.31	4.25
15	3.6	.44	3.24	6.05
20	2.2	.30	4.05	9.75

[a] *p*- and *m*-hydroxyacetanilides are not distinguished here. In any case there is not much of either. By analogy with the oxidation products of phenol in these systems, we expect more of the *para* derivative and very little *meta*.

The fact that the *ortho* derivative builds up to a much higher concentration than the *para* and/or *meta* might be taken as an indication that the latter are preferentially adsorbed at the zinc oxide surface and therefore react at a faster rate. In the dark it has not been possible to detect any appreciable adsorption of either the parent acetanilide or

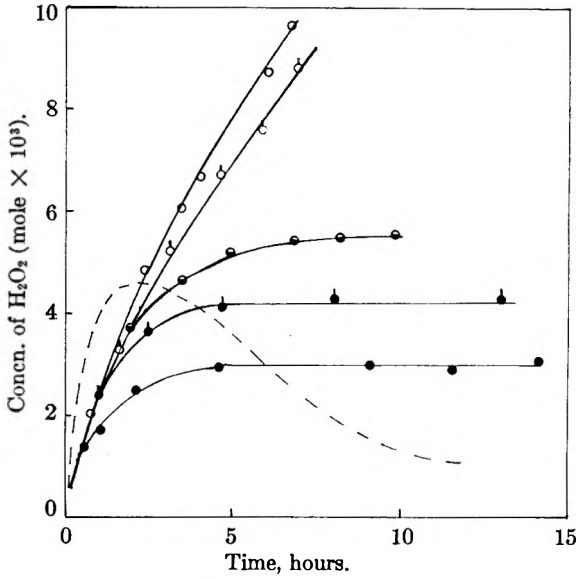

Fig. 1.—Effect of concentration of acetanilide on the formation of hydrogen peroxide: ———, phenol (0.001 *M*); ●, 0.0005 *M*; ●, 0.001 *M*; ◒, 0.002 *M*; ○, 0.005 *M*; ○, 0.01 *M*.

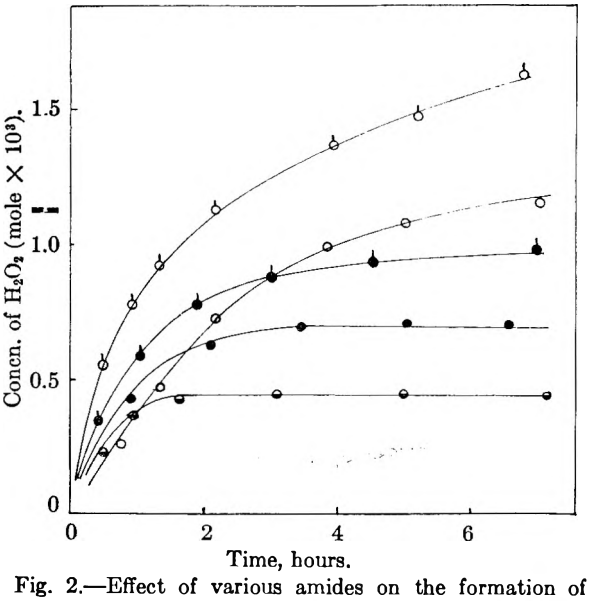

Fig. 2.—Effect of various amides on the formation of hydrogen peroxide: ◒, formamide; ●, acetamide; ●, N-methylformamide; ○, water; ○, N,N-dimethylformamide.

the hydroxy-derivatives on the surface of zinc oxide suspended in water. It cannot be ruled out, however, that there might be some difference on irradiation. Nor does the *p*-hydroxyacetanilide appear to form peroxide faster at an irradiated zinc oxide surface. Independent studies of the rate of formation of hydrogen peroxide in irradiated suspensions containing 0.001 *M* *o*-hydroxyacetanilide or *p*-hydroxyacetanilide show that, when irradiated in equal initial concentrations, these compounds produce hydrogen peroxide at equal rates, and both produce it twice as fast as acetanilide solutions of equal concentration. It seems possible nevertheless that when hydroxy compounds are present simultaneously in smaller amounts there may be competition for the surface. It is noteworthy that

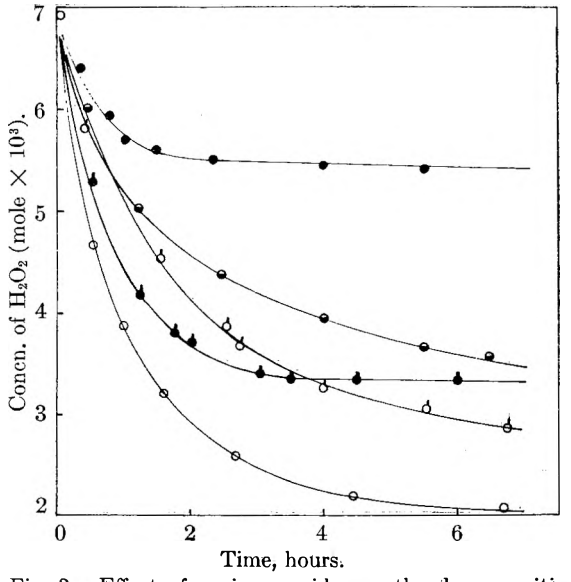

Fig. 3.—Effect of various amides on the decomposition of hydrogen peroxide: ●, formamide; ◒, acetamide; ◭, N-methylformamide; ○, water; ◌, N,N-dimethylformamide.

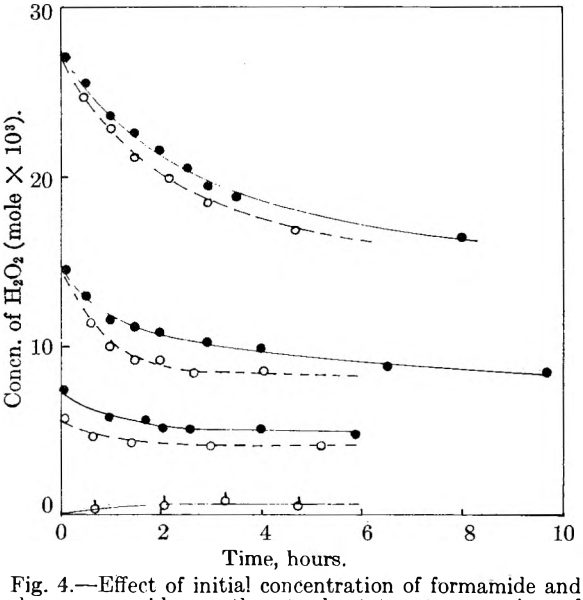

Fig. 4.—Effect of initial concentration of formamide and hydrogen peroxide on the steady-state concentration of hydrogen peroxide: ○, 0.001 *M* formamide; ●, 0.002 *M* formamide.

during the initial stages of oxidation in these irradiated suspensions of zinc oxide, 0.001 *M* *p*-hydroxyacetanilide forms a pink oxidation product, suggesting formation of an *o*-quinoid structure, whereas *o*-hydroxyacetanilide under the same conditions forms a yellow product, indicative of a *p*-quinoid structure. Since the *p*-quinone would be more stable than the *ortho*-, it is possible that the apparent persistence of the *o*-hydroxyacetanilide features in the spectra are due in part to the *p*-quinoid oxidation product. The corresponding *o*-quinone oxidation product of the *p*-hydroxyacetanilide would be expected to undergo rapid autooxidation. In fact the measured ratios of oxygen consumed to peroxide formed in these systems always are somewhat greater than 1:1.

Infrared studies of the products of irradiation of suspensions of zinc oxide containing acetanilide confirm those in the ultraviolet in indicating the presence of both *o*- and *p*-hydroxyacetanilides in the early stages of the reaction. After a few hours, when no more indication of an aromatic ring can be found in the ultraviolet spectra, infrared spectra also show the disappearance of aromatic ring vibrations. In fact, the only persistent features in the infrared spectrum after several hours or irradiation are small vibrations in regions characteristic of simple aliphatic amides. The only other final products seem to be hydrogen peroxide and carbon dioxide. One might expect the amide residue to be either acetamide or formamide. The differences in the infrared spectra for small amounts of these amides are not sufficiently unambiguous to permit a decision regarding the nature of the residue on this basis alone. It therefore was decided to carry out a comparative study of several amides in their abilities to take up oxygen and produce hydrogen peroxide, or maintain hydrogen peroxide added initially in irradiated aqueous suspensions of zinc oxide.

Comparative Study of Effects of Simple Aliphatic Amides at Irradiated Zinc Oxide Surfaces.—Besides acetamide and formamide other simple amides tested were: N-methylformamide, N,N-dimethylformamide, and urea. Figure 2 shows the rates of formation of hydrogen peroxide by several amides, as compared with water. It is evident that these substances produce peroxide much more slowly than acetanilide. Also there is evidence of some relation between the number of oxidizable methyl groups and the amount of hydrogen peroxide formed.

Figure 3 shows the effect of the same amides, also at 0.001 *M* concentration, in governing the extent of decomposition of hydrogen peroxide initially present at a concentration slightly higher than that which was formed by 0.001 *M* acetanilide. The amides appear almost in inverse order from that in Fig. 2, but peroxide decomposes fastest of all in pure water. Urea was found to have no effect on either the formation or maintenance of hydrogen peroxide in these systems, and so is not included in the figures. It appears that the other amides all are capable of producing some product that inhibits the extent of decomposition of hydrogen peroxide at irradiated zinc oxide surfaces. The inverse order of the amides in Fig. 2 and 3 may be due to the fact that the methyl groups on the nitrogen are capable of delaying the formation of this final product more than the methyl attached to the carbon as in acetamide.

In Figure 4 there are further studies with formamide, showing that doubling the concentration of formamide has very little effect on the final steady-state concentration of a given initial concentration of hydrogen peroxide. Doubling the hydrogen peroxide concentration, however, raises the steady level of hydrogen peroxide appreciably in the presence of a given amount of formamide.

Figure 5 shows the effects of 0.001 *M* formamide and 0.001 *M* acetanilide solutions with respect both to formation and decomposition of hydrogen

peroxide. Acetanilide not only preserves hydrogen peroxide added initially, but increases the concentration. Apparently the rate of decomposition of hydrogen peroxide at the surface is balanced and more than compensated by its rate of formation in the presence of acetanilide.

Oxygen absorption measurements were made with zinc oxide suspended in pure formamide, N-methylformamide, and N,N-dimethylformamide, as well as decimolar solutions of two of these. The results are presented in Fig. 6. The rate at which oxygen is taken up is highest for dimethylformamide and decreases through N-methylformamide and formamide. In water solution, too, dimethylformamide shows a higher rate of oxygen uptake than formamide, but the differences are much smaller. These results show the same trend as the rates of peroxide formation in Fig. 3. The presence of a larger number of C–H bonds increases the rate of oxygen uptake as well as the rate of peroxide formation.

In water solution dimethylformamide gives a rate of oxygen uptake lower than that with pure amide, while in the case of formamide the rate apparently is higher in aqueous solution. With potassium hydroxide in the center well of the Warburg flasks to absorb carbon dioxide, it becomes apparent that the rate of oxygen uptake by pure formamide really is higher, and that carbon dioxide is evolved right in the initial stages. Dimethylformamide shows no appreciable carbon dioxide formation in the first hour of irradiation. Formamide, having only one oxidizable C–H bond, gives rise to the final decomposition products immediately on irradiation, and these evidently inhibit peroxide formation and oxygen uptake. Water takes up oxygen less readily than the amides, hence aqueous solutions of the amides show a decrease in rate of oxygen uptake.

Comparative Study of Effects of Nitrogen-Containing Compounds other than Amides.—In order to obtain further information as to the probable nature of the amide residue, several nitrogen-containing compounds, at concentrations 10^{-3} M, were tested for their effects on inhibiting the decomposition of hydrogen peroxide in irradiated zinc oxide suspensions. The results are shown in Fig. 7. Curve 1 shows the effect of potassium cyanide, pH 9.8. Cyanide ion completely prevents the decomposition of hydrogen peroxide. Since zinc hydroxide fails to decompose hydrogen peroxide on irradiation, and the suspension at pH 9.8 contains appreciable hydroxide ion, it is not certain whether this effect is due to cyanide alone. Curve 2 shows the effect of adjusting the pH of the cyanide suspension to 7.1. There is a slight initial decomposition, but the cyanide ion certainly shows a strong inhibition of the decomposition of hydrogen peroxide. Curve 3, showing the effect of formamide, is included for comparison.

The effects of aniline and ammonia are indicated in curve 4, and that of hydrazine in curve 5. These compounds permit appreciable decomposition of hydrogen peroxide to take place before a stable concentration is attained. By comparison with water (or salts), shown in curve 6, the preceding compounds all show some inhibition. The pH of the methylamine hydrochloride was 6.0.

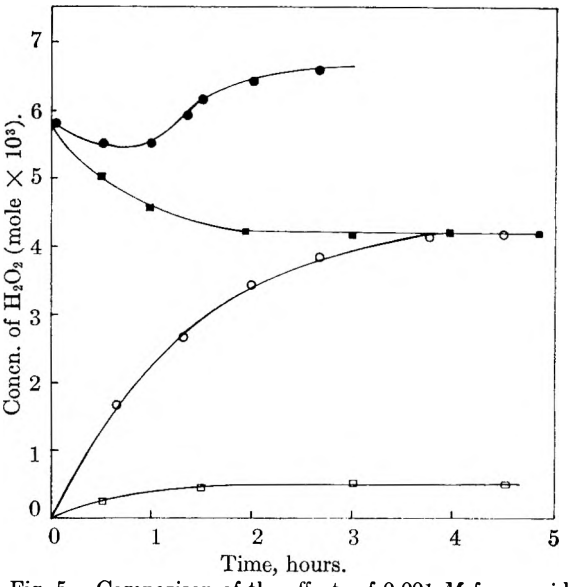

Fig. 5.—Comparison of the effects of 0.001 M formamide and acetanilide on the formation and decomposition of hydrogen peroxide: ○, ●, acetanilide; ■, □, formamide.

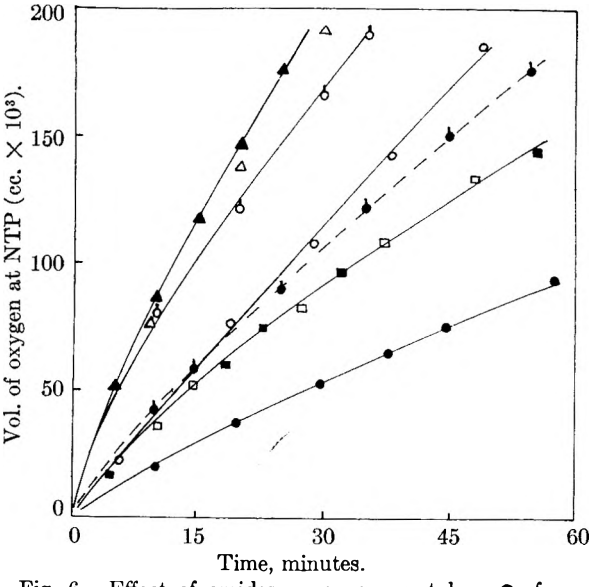

Fig. 6.—Effect of amides on oxygen uptake: ●, formamide; ○, formamide + KOH; ■, 0.1 M formamide; □, 0.1 M formamide + KOH; △, N,N-dimethylformamide; ▲, N,N-dimethylformamide + KOH; ◐, 0.1 M N,N-dimethylformamide; ◑, N-methylformamide.

Surprisingly hydroxylamine and propionitrile, curve 7, are accelerators of the decomposition of hydrogen peroxide. It seems likely that these compounds give rise to free radicals which enhance the decomposition of the peroxide. In stabilizing the hydrogen peroxide in irradiated suspensions of zinc oxide the role of the organic additive appears to be the contribution of electrons to the catalyst. According to this picture it is unlikely that propionitrile can give rise to a cyanide ion, and therefore it does not show the same inhibition as potassium or hydrogen cyanides. Similarly hydroxylamine would not be expected to produce hydroxide ions in these systems.

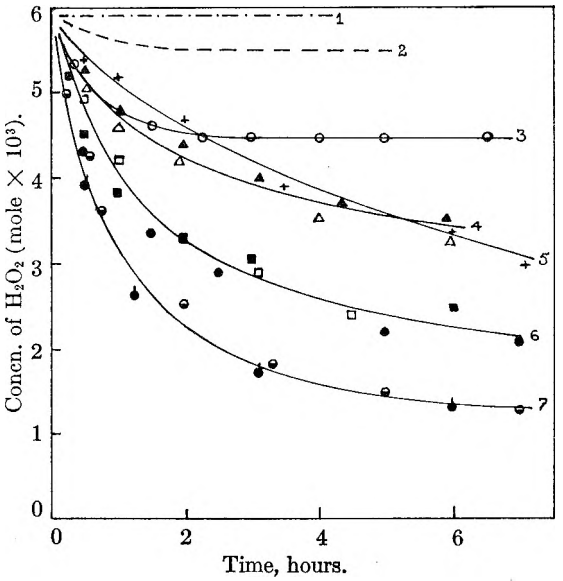

Fig. 7.—Comparison of the effect of various nitrogen-containing compounds on the decomposition of hydrogen peroxide: curve 1, potassium cyanide; 2, hydrogen cyanide; 3, ○ formamide; 4, ▲ ammonia, △, aniline; 5, + hydrazine; 6, ● no additive, □ methylamine hydrochloride, ■ sodium chloride; and 7, ◒ hydroxylamine, ◐ propionitrile.

Conclusions

Results show that the persistence of hydrogen peroxide in irradiated suspensions containing acetanilide is due to an amide residue which apparently is strongly adsorbed on the surface, and able to exclude both oxygen and hydrogen peroxide. This residue does not reach an effective concentration on the surface until after the oxidation of the ring has permitted the accumulation of a relatively high concentration of hydrogen peroxide.

Formamide on reaction at an irradiated zinc oxide surface is converted directly to the final products and at least one of these must be remaining on the surface and acting as an inhibitor for further reaction. Since the other amides have to go through several intermediate steps before they give rise to products similar to those formed from formamide, the inhibiting action prevails only at a later time. Meanwhile considerable quantities of oxygen are taken up and the rate of this uptake must be related to the number of oxidizable linkages available in the molecule. The same explanation accounts for the effect of the amides in producing hydrogen peroxide in these systems. Urea, either because it is not adsorbed or not oxidized, has no effect. Since the inhibited surface no longer can participate in the oxygen–hydrogen peroxide exchange, the remaining hydrogen peroxide is stable indefinitely on continued irradiation.

The inhibiting residue must be the nitrogen-containing part of the amide group, perhaps forming a complex with the zinc at the catalyst surface, since large amounts of carbon dioxide are produced during the initial stages of the surface inactivation by formamide. Hydrogen peroxide added initially decomposes at the surface until the inhibiting product accumulates in sufficient quantity by the oxidation of the amide. This conclusion is justified by Fig. 4, which shows that for a given initial concentration of formamide any desired steady-state concentration of hydrogen peroxide can be maintained provided the initial concentration is sufficiently high. During the initial period the decomposition of hydrogen peroxide follows an apparent second-order rate law. On the surface of zinc oxide a given amount of formamide always requires a definite amount of time for the formation of the nitrogen-containing residue, which inhibits the formation and decomposition of hydrogen peroxide. The higher the initial concentration of peroxide, the greater will be the per cent. decomposition during this time. The amide residue from 0.001 *M* formamide evidently is sufficient to produce a nearly covered surface, because doubling the concentration of formamide has practically no effect on the final level of peroxide. There is evidently an equilibrium with the aqueous phase because the zinc oxide can be filtered or centrifuged and used again for a period in a fresh solution.

The inhibiting residue evidently is not an ordinary zinc–ammonia complex, since ammonia is not able to inhibit directly. However, the fact that ammonia and hydrazine eventually do prove to be inhibitors of the decomposition of hydrogen peroxide proves that a simple nitrogen-containing residue can account for the effects of the amides. Aniline and ammonia, in spite of a large difference in basicity (K_b, ammonia, 1.8×10^{-5}; K_b, aniline, 3.8×10^{-10}), require about the same amount of time to give rise to inhibiting fragments which tentatively might be considered to contain electron-deficient nitrogen. Apparently hydroxylamine produces both radicals which can accelerate peroxide decomposition and also a surface-adsorbed fragment which leads to the maintenance of a steady-state concentration even lower than that in pure water. Certainly the inhibiting residue from the amides would not be expected to be a cyanide ion, since this ion cannot even be formed from propionitrile in this system.

The probability that the inhibiting fragment formed at the irradiated zinc oxide surface can be an electron-deficient nitrogen group is of interest to the various theoretical explanations of photochemical processes at zinc oxide surfaces. If in accordance with the interpretations of several investigators of surface reactions at irradiated zinc oxide,[5-8] the effect of light is to reduce an adsorbed oxygen molecule which subsequently reacts to form hydrogen peroxide in aqueous suspensions, the zinc oxide will be left in an electron-deficient state. The now positively charged zinc oxide is neutralized by regaining an electron from an oxidizable substrate. This process may lead to an electron deficient nitrogen-containing fragment which becomes strongly adsorbed on zinc oxide.

(5) I. Veselovskii and D. M. Shub, *Zhur. Fiz. Khim.*, **26**, 509 (1952).

(6) T. R. Rubin, J. G. Calvert, G. T. Rankin, and W. M. MacNevin, *J. Am. Chem. Soc.*, **75**, 2850 (1953).

(7) J. G. Calvert, K. Theurer, G. T. Rankin, and W. M. MacNevin, *ibid.*, **76**, 2575 (1954).

(8) V. A. Garten and K. Eppinger, *Solar Energy*, **5**, 77 (1961).

ELECTRON SPIN RESONANCE OF SOME NITROGEN-CONTAINING AROMATIC FREE RADICALS[1,2]

BY L. DALLAS TUCK AND DAVID W. SCHIESER

Department of Pharmaceutical Chemistry, School of Pharmacy, University of California, San Francisco Medical Center, San Francisco, California

Received January 20, 1962

The results of electron spin resonance studies at room temperature on free radicals formed from phenazine, phenoxazine, and phenothiazine, together with two derivatives of the latter, thionine and methylene blue, are reported in sulfuric acid or in acidified ethanol. The *g*-values for the spectra were determined, and the hyperfine splitting measured. The hyperfine structure observed was interpreted as that due to splitting by the nitrogen-14 nuclei on the center ring and protons attached directly thereto.

We report here the results of electron spin resonance studies on the positive ion free radicals formed in acid solution from several nitrogen-containing aromatic compounds, *viz.*, phenazine, phenoxazine, phenothiazine, thionine, and methylene blue. They are similar in structure to the free-radical ions formed from such hydrocarbons as anthracene and naphthalene, but they are considerably more stable, owing to the greater possibilities of resonance due to the presence of nitrogen in the center ring. Each of the free radicals studied is a semiquinone, intermediate in oxidation state between a reduced (leuco) form and an oxidized (dye) form.

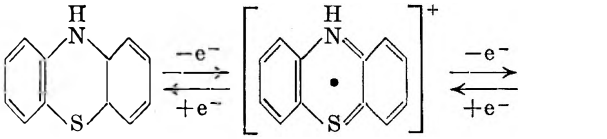

Phenothiazine Semiquinone ion

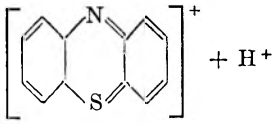

Phenazothionium ion

To emphasize the involvement of all three rings in the aromatic resonance, it appears to be realistic to draw the bonding of the radical as though it is the oxidized form to which a single electron is added. Considerations below show that in the conditions of our experiments all ring nitrogens of the free radicals are protonated. The parent forms other than phenothiazine, shown above, are

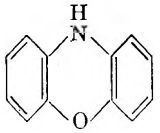

Phenoxazine

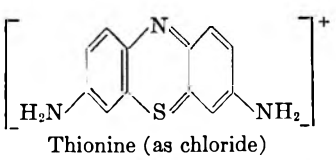

Thionine (as chloride)

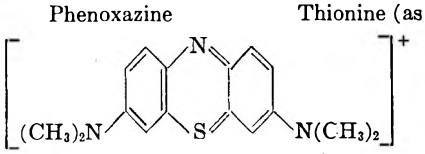

Methylene blue (as chloride)

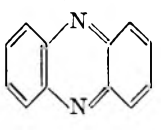

Phenazine

The stability and conditions for stability of these semiquinone free radicals were predicted by L. Michaelis,[3] and existence of stable examples of this series has been proved by e.s.r. studies.[4-6] Hyperfine studies of phenazine in essential agreement with ours have been reported by Matsunaga and McDowell.[7]

Instrumental

The spectrometer was an X-band reflective type using 1000-cycle field modulation and a lock-in detector with first-derivative presentation. The spectrometer is similar to that of Abraham, Ovenall, and Whiffen.[8] Power incident on the sample usually was of the order of 20 mwatts, depending upon instrumental settings, and was generated by a Varian V-58 Klystron operating at 9300 Mc. A Varian power supply and six-in. electromagnet spaced at 1.75-in. gap were employed for the steady field. For presentation of the spectra, the steady field was swept over an appropriate range of field strength by injection of a linearly varying voltage into the magnet power supply from a motor-driven helipot in a potentiometer circuit. The resonant cavity operated in the TE_{103} mode, and the solutions were inserted therein in Pyrex tubing of about 1.5 to 2.0 mm. internal diameter. All measurements were made at room temperature, and no measurement or control of temperature was attempted.

Magnetic Field Strength Measurements.—Values of magnetic field strength for line splittings and *g*-values were determined by calibration of the helipot dial against the proton magnetic resonance line in water. Frequency measurements of the proton resonance signal were determined by comparison with harmonics of a General Radio frequency calibrator, Type 1213-C. Diphenylpicrylhydrazyl was used as a standard fixed point for *g*-value measurements.

Experimental

Preparation of Solutions.—Solutions for which the most satisfactory spectra were obtained were prepared by dissolving approximately 10–50 mg. of the solid parent compound in 10 ml. of concentrated sulfuric acid, to which then was added, depending upon the oxidation state of the parent compound, 0.1 ml. of 0.5 *M* stannous chloride or 0.1 ml. of 30% hydrogen peroxide. Variations in technique are indicated below. In some instances the sulfuric acid effected oxidation without addition of hydrogen peroxide.

1. Phenazine radical ion: To prevent precipitation of solid phenazyl radical salt, it was found desirable to dilute the sulfuric acid solution by addition of 3 ml. of ethanol or water. An identical spectrum was obtained from a solution in 95% ethanol to which were added 0.2 ml. of concentrated hydrochloric acid and 0.1 ml. of 0.5 *M* stannous chloride.

(1) Presented before the 138th National Meeting of the American Chemical Society, New York City, N. Y., September, 1960.

(2) Based on a thesis presented by David W. Schieser in partial fulfillment of the requirements for the Ph.D. degree, University of California, January, 1960.

(3) L. Michaelis, *Chem. Revs.*, **16**, 243 (1935).

(4) A. N. Holden, W. A. Yager, and F. R. Merritt, *J. Chem. Phys.*, **19**, 1319 (1951).

(5) Y. Fellion and J. Uebersfeld, *Arch. sci.* (Geneva), **10**, Spec. no., 95 (1957).

(6) P. Camagni and G. Lanzi, *Intern. Conf. Mesons and Recently Discovered Particles 43° Congr. Nazl. Fis., Padua-Venice, 1957, Comun.*, Vol. XII, pp. 4–5.

(7) Y. Matsunaga and C. A. McDowell, *Proc. Chem. Soc.*, 175 (1960).

(8) R. J. Abraham, D. W. Ovenall, and D. H. Whiffen, *Trans. Faraday Soc.*, **54**, 1128 (1958).

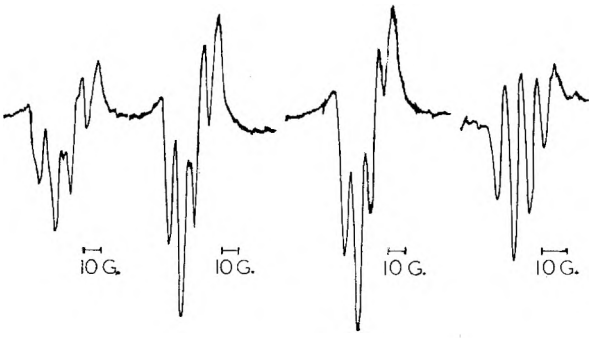

Fig. 1.—E.s.r. spectra of positive ion free radicals formed from phenoxazine, phenothiazine, thionine, and methylene blue in sulfuric acid.

Thiourea (saturated aqueous solution) was a satisfactory substitute for stannous chloride as a reducing agent.

2. Phenoxazine radical ion: Hydrogen peroxide produced an e.s.r. spectrum immediately. However, on standing for a few days the sulfuric acid solution yielded an identical spectrum without addition of the oxidant. A series of dilutions in concentrated sulfuric acid produced spectra which were identical except for intensity.

3. Phenothiazine radical ion: No oxidizing agent other than the sulfuric acid was needed. An identical spectrum was obtained from an ethanolic solution acidified by hydrochloric acid to which a drop of hydrogen peroxide was added. A series of dilutions in concentrated sulfuric acid produced identical spectra except for intensity.

4. Thionine radical ion: Reduction by stannous chloride was required to produce the free radical ion. A series of dilutions up to eightfold from the original with concentrated sulfuric acid produced the same spectrum.

5. Methylene blue radical ion: Reduction was required for the production of the semiquinone radical. In addition, a strong spectrum of different structure is obtained from an ethanolic solution containing potassium hydroxide and without oxidizing or reducing agent.

Solid Radical Salts.—Several of the substances showed a tendency to precipitate the solid radical salt if the solution was made sufficiently concentrated. This usually resulted in a spectrum in which a single sharp line is superimposed on the more complex spectrum of the solute species.

In the case of phenazine, the solid, presumably the semiquinone radical chloride, was separated from the supernatant, washed, and dried. Its g-value was determined to be 2.0033 in agreement with Holden, Yager, and Merritt,[4] who observed a "weak line" with g-value of 2.0031. Its line width, measured as the separation of points of maximum slope, was found to be 3.3 gauss. The line width increases slowly with time without apparent change in the over-all intensity, no doubt owing to physical adsorption of oxygen.[9-11] The rate of increase in width is greater in a powdered sample than in the crystals obtained from the preparation.

The hyperfine coupling constants and line widths were computed by comparison of the experimental curves with theoretical gaussian curves drawn with appropriate line intensities (1:2:2:1 for phenothiazine-type radicals) and having various ratios of splitting to component line width. A choice of the best model was made on the basis of relative heights of peaks. A plot of the positions of the maximum and minimum points on the experimental curve (in gauss) against the corresponding points on the theoretical curve (in standard deviation units) yielded the line width as twice the slope of the resulting straight line. The coupling constant then was calculated from the splitting-to-width ratio.

Results and Discussion

The phenazine radical ion produces a relatively symmetrical seven-line spectrum in agreement with the results of Matsunaga and McDowell.[7] The experimental spectrum shows almost quantitative agreement with a theoretical curve constructed with uniform line spacing of 6.60 gauss, line widths of 5.74 gauss, and relative line intensities of 1:4:8:10:8:4:1. The latter intensities are consistent with a hyperfine splitting by the two equivalent nitrogen-14 nuclei and an identical or nearly identical splitting by the two protons attached to the nitrogen in the strongly acidic solution.

Phenoxazine, phenothiazine, and thionine, as shown in Fig. 1, produce radical ions having uniformly spaced four-line spectra of appreciably asymmetry. Comparisons with calculated spectra having line intensities in the ratio 1:2:2:1 show reasonable agreement, and yield the coupling constants and line widths shown in Table I. Measured g-values also are shown in the table.

TABLE I

CHARACTERISTICS OF THE E.S.R. SPECTRA

Parent compound	g-Value	Number of lines	Coupling constant, gauss	Line width, gauss
Phenazine	2.0026	7	6.60	5.74
Phenoxazine	2.0049	4	9.83	8.19
Phenothiazine	2.0050	4	7.10	5.69
Thionine	2.0045	4	7.05	6.13
Methylene blue	2.0043	4	6.89	4.92
Methylene blue in base	2.004	3	7.8	8

The interpretation of the hyperfine splitting from the number of lines and their intensities is similar to that for phenazine, namely, a basic three-line splitting by the single nitrogen-14 nucleus of the center ring and a nearly identical splitting due to the attached acidic proton. The sulfur-32 and oxygen-16 nuclei produce no splitting as they have no magnetic moment.

The large difference between the N^{14} coupling constant in the oxygen-containing molecule as compared with the sulfur-containing one should be noted. We are tempted to ascribe this effect to the relative negativities of the two elements, but recognize that other factors may contribute. This difference in terms of the spin density on the nitrogen would be a sensitive point for confirmation in a molecular orbital model of these molecules.

Compared to phenothiazine, the very slightly smaller coupling constant in thionine suggests that the amine group possibly enhances the resonance contribution of the side rings, as might be expected. The effect does not seem to be so important, however, as suggested by the work of Michaelis, Schubert, and Granick.[12] The substitution of methyl groups on the amines to give methylene blue results in a further enhancement of the same type.

The asymmetry of these spectra is the same type and produced under the same conditions as that described by Blois, Brown, and Maling,[13] and may be ascribed to a phase shift by the solvent, sulfuric acid, which produces a spectrum having partial dispersive character. It is possible that in addition there is some asymmetry caused by the presence of an "impurity" free radical, as there is evidence that

(9) N. S. Garif'yanov and B. M. Kozyrev, *Doklady Akad. Nauk SSSR*, **118**, 738 (1958).

(10) J. J. Lothe and G. Eia, *Acta Chem. Scand.*, **12**, 1535 (1958).

(11) J. E. Bennett and E. J. H. Morgan, *Nature*, **182**, 199 (1958).

(12) L. Michaelis, M. P. Schubert, and S. Granick, *J. Am. Chem. Soc.*, **62**, 204 (1940).

(13) M. S. Blois, Jr., H. W. Brown, and J. E. Maling, "Free Radicals in Biol. Systems," Proc. Symposium, Stanford, Calif., 1960, p. 117.

the oxidation of these compounds does not occur without complications.[14]

Agreement of each of the spectra is found with a model in which the coupling constant of the nitrogen is equal to that of a single proton, presumed to be the N proton. To the precision of the present measurements, it is not possible to ascribe individual values to the nitrogen and the proton. This result differs from the results of Billon, Cauquis, Cambrisson, and Li,[15] who interpreted their four-line spectrum of phenothiazine free radical ion, formed by electrochemical oxidation in acetonitrile solution, as derivable from a nitrogen coupling constant of 7.5 gauss and a proton coupling constant of 4.5 gauss. Their larger value for the nitrogen splitting and smaller value for the proton may be due to partial acidic dissociation of the radical ion in the absence of excess acid. Models based on their constants gave spectra which were not in agreement with our experimental spectra. The N^{14} splitting constant could be determined separately and to a better precision by obtaining the e.s.r. spectra in D_2SO_4, in which circumstance deuterium rather than the proton would be attached to the nitrogen.

No hyperfine splitting by the side-ring protons was found in these studies. Preliminary results on phenazine have been reported by Schieser and Zvirblis[16] showing that modification of the solvent yields resolvable splitting by these protons. The envelope of their spectrum corresponds to ours, showing that our line width is the result principally of unresolved hyperfine splitting.

(14) J. C. Craig, M. E. Tate, F. W. Donovan, and W. P. Rogers, *J. Med. Pharm. Chem.*, **2**, 669 (1960).

(15) J. P. Billon, G. Cauquis, J. Cambrisson, and A. M. Li, *Bull. soc. chim. France*, 2062 (1960).

(16) D. W. Schieser and P. Zvirblis, *J. Chem. Phys.*, **35**, April (1962).

NOTES

THE HYDROLYTIC DEGRADATION OF SODIUM TRIPHOSPHATE

By A. G. Buyers[1]

Colgate-Palmolive Company

Received August 4, 1961

A brief investigation of the hydrolytic degradation of aqueous sodium triphosphate, concentration 14 w/o, in the temperature range 108–121° has been carried out. A second-order kinetic interpretation has disclosed that these data are in reasonable agreement with previous studies carried out in aqueous solution, and using solid sodium triphosphate hexahydrate.[2,3]

Experimental

Accurately weighed amounts of recrystallized sodium triphosphate hexahydrate, about 2.74 g., were dissolved in 15 ml. of distilled water for hydrolysis studies. Immediately after preparation, 5 ml. of a given solution contained in a platinum crucible were sealed within a 22-ml., 98% nickel, flame ignition, Parr peroxide sulfur bomb. The bombs were completely immersed beneath the surface of an oil-bath maintained at the desired temperature. After 30 min., the bombs were removed, chilled, and the contents were subjected to analysis for ortho-, pyro-, and triphosphates.[4,5]

Discussion of Hydrolytic Data

The currently accepted first-order mechanism for the hydrolytic degradation of sodium triphosphate is written

$$HP_3O_{10}^{-4} + H_2O \rightleftharpoons HP_2O_7^{-3} + HPO_4^{-2} + H^+ \quad (1)$$

However, this equation is not always in accord with quantitative chemical analysis for reaction products, which frequently reveals pyro- to ortho-phosphate mole ratios exceeding one. Quimby has suggested that the solid state degradation of the sodium triphosphate hexahydrate may be represented by the second-order reaction

$$2Na_5P_3O_{10} + H_2O \rightleftharpoons Na_4P_2O_7 + 2Na_3HP_2O_7 \quad (2)$$

The equation is written for this same process, for sodium triphosphate dissolved in water

$$2HP_3O_{10}^{-4} + H_2O \rightleftharpoons 3HP_2O_7^{-3} + H^+ \quad (3)$$

and either reaction would be followed by

$$H_2O + HP_2O_7^{-3} \rightleftharpoons 2HPO_4^{-2} + H^+ \quad (4)$$

Accordingly, summarized in Table I are approximate rate data in the temperature range 25–150° for the hydrolysis of sodium triphosphate in aqueous solution and for the hydrolytic degradation of solid sodium triphosphate hexahydrate. In all cases pyro/orthophosphate mole ratios are greater than one. It is easily seen that reactions 2, 3, and 4 will disclose pyro/ortho-phosphate mole ratios which exceed one when analyses are carried out upon a degraded triphosphate system.

In some instances, tabulated values for the decimal fraction $Na_5P_3O_{10}$ remaining at 30 min. were the product of extrapolation. The time, 30 min., was chosen as an interval which permitted measurements as the initial step in the degradation process took place. Data so obtained were used to yield eq. 5 from the plot of this Arrhenius relation, Fig. 1, and the second-order interpretation represented by eq. 2 or 3. The rate equation is

$$\log k = 13.9 - \frac{6061}{T} \quad (5)$$

where k is the second-order rate constant, (based upon the disappearance of triphosphate) and the energy of activation is calculated to be 28 ± 5 kcal./mole.

Let us assume that the activation step in the

(1) Hughes Research Laboratories, Malibu Canyon Road, Malibu, California.

(2) R. N. Bell, *Ind. Eng. Chem.*, **39**, 136 (1947).

(3) (a) O. T. Quimby, *J. Phys. Chem.*, **58**, 603 (1954); (b) A. C. Zettlemoyer, C. H. Schneider, H. V. Anderson, and R. J. Fuchs, *ibid.*, **61**, 991 (1957).

(4) R. N. Bell, *Ind. Eng. Chem.*, **19**, 87 (1947).

(5) A. G. Buyers, *Anal. Chim. Acta*, **19**, Nr. 2, 118 (1958).

TABLE I

HYDROLYTIC DEGRADATION DATA—$Na_5P_3O_{10}$

Ref.	Chemical state	Temp., °K.	10^3/Temp.	Decimal fraction $Na_5P_3O_{10}$ remaining at 30 min.	Estimated av. mole ratio P_2O_7/PO_4 for the temp. indicated	Rate constant $\times 10^2$ (2nd order) dec. fract.$^{-1}$, min.$^{-1}$
R. N. Bell	Aqueous soln. (1 w/o)	373	2.68	0.96	1.13	0.13
	(10 w/o)	373	2.68	.89	1.12	.40
	(1 w/o)	343	2.92	.99	1.70	.03
O. T. Quimby	Aqueous soln. (1 w/o)	298	3.36	.96[a]	..	.00002[a]
	(10 w/o)	355	2.82	.99	..	.03
A. G. Buyers	Aqueous soln. (14 w/o)	394	2.54	.37	1.78	5.66
		385	2.60	.74	1.30	1.17
		381	2.62	.77	1.24	1.00
O. T. Quimby	Solid $Na_5P_3O_{10}6H_2O$	423	2.36	.18	1.34	15.18
		393	2.54	.58	1.63	2.4
		378	2.65	.88	1.63	.47
		368	2.72	.96	1.35	.13
A. C. Zettlemoyer, *et al.*[b]	Solid $Na_5P_3O_{10}6H_2O$	393	2.54	.70		1.43
		388	2.58	.85		.60
					1.1	
		383	2.61	.88		.47
					→ to	
		373	2.68	.90		.37
					1.73	
		368	2.72	.93		.27
		358	2.79	.97		.10

[a] Calculated from 146-day analysis. [b] Data for 378° were not tabulated as these values were not consistent with the remaining data by these authors.

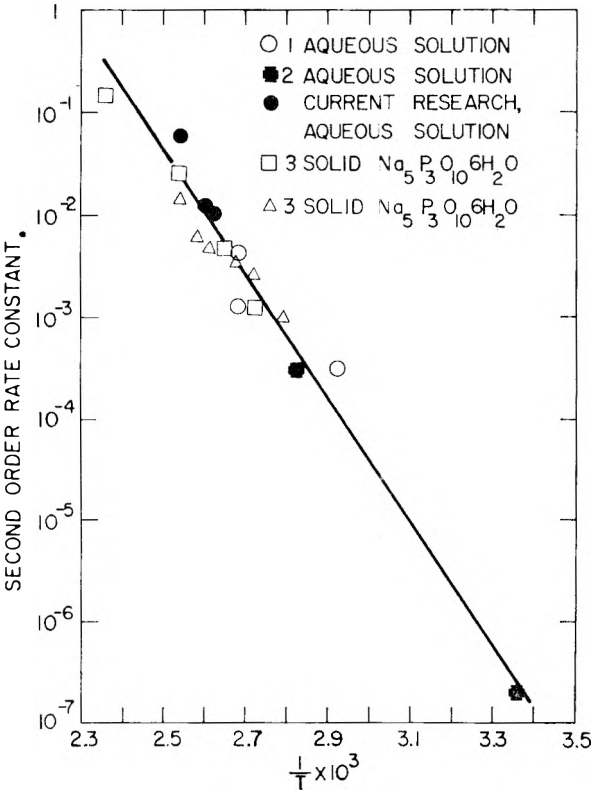

Fig. 1.—Arrhenius relation for second-order reaction based upon the disappearance of sodium triphosphate hexahydrate.

hydrolytic process is the breaking of the P–OP bond, a fact not established, but plausible. It then is interesting to note that apparently the energies of activation are not different for first or second-order interpretations. First-order mechanisms, eq. 1 or 4, require that initially one P–OP bond be broken by hydrolysis. The second-order expressions, eq. 2 or 3, suggest that two P–OP bonds are broken and one P–OP bond is formed, representing a net energy change for breaking one bond, *i.e.*, 20–25 kcal./mole.[6]

Admittedly, the mechanism for the hydrolytic degradation of sodium triphosphate to orthophosphate has not been established by this note. However, it is believed that the examined hydrolysis data and their interpretation render dubious the simple hydrolytic mechanism depicted by eq. 1. Furthermore, evaluation of available research has indicated that the initial step in this hydrolysis can be described in terms of a second-order reaction.

(6) J. R. Van Wazer, *Encyclopedia Chem. Technol.*, **10**, 403 (1953).

THE ACTIVITY COEFFICIENTS OF AMMONIUM PERCHLORATE IN WATER AT 25°

BY O. E. ESVAL AND S. Y. TYREE, JR.

Department of Chemistry, University of North Carolina, Chapel Hill, North Carolina

Received October 12, 1961

The extensive measurements of activity coefficients for 1–1 electrolytes indicate that the activity

coefficients of ammonium perchlorate should be similar to those of ammonium nitrate.[1] Harned and Owen[2] have made a rough classification of the thermodynamic properties of 1–1 electrolytes based on their ion size and structure. Basically it can be assumed that any deviation from the Debye–Hückel equation can be attributed to the hydration energy of the cation or anion. This is directly related to the charge, size, and symmetry of the ion. In addition it can be shown that an ion with a low hydration energy will tend to have a low value for a given activity coefficient as compared to an ion which is more highly hydrated. Therefore, the perchlorate ion should have a slightly lower hydration energy than the nitrate ion, since the perchlorate ion is more symmetrical and larger while having the same charge. Thus it may be concluded that the activity coefficients of ammonium perchlorate should be slightly lower than those of ammonium nitrate.

The osmotic coefficients of ammonium perchlorate were obtained by the isopiestic method of Sinclair and Robinson,[3,4] from which the activity coefficients of ammonium perchlorate were calculated over a range of 0.1 to 2.1 m.

Experimental

Materials.—Two preparations of ammonium perchlorate were used, one prepared by the method of Hartley[5] and one obtained from J. T. Baker and Company. Both preparations were recrystallized three times with demineralized water (specific conductance 10^{-7} cm.$^{-1}$ ohms^{-1}) or until a negative chloride test was obtained as indicated by silver nitrate. The salt was dried in a vacuum desiccator over P_2O_5 instead of an oven at 110° in order to prevent possible slow decomposition of the perchlorate into the chloride over long periods of time. Both preparations were analyzed for chloride by reduction of the perchlorate to chloride by the Parr bomb and gravimetric determination of the resulting chloride. Three samples were run in this manner and all agreed to within a few tenths of 1%.

Anal. Calcd. for NH_4ClO_4: Cl, 30.17. Found: Cl, 30.37.

Reagent grade KCl was used without any further purification. The salt was dried in an oven at 110°.

The apparatus for the isopiestic equilibrations and the experimental technique involved have been previously described.[6]

Results and Discussion

The isopiestic solutions of potassium chloride and ammonium perchlorate are listed in Table I. Deviations greater than 3 parts per thousand between the ammonium perchlorate solutions or the potassium chloride solutions were not used. This happened in only two instances out of 21 experimental points; in both cases, it appears that splattering of the solution from the cups had occurred.

The osmotic coefficients and the mean molal activity coefficients of ammonium perchlorate are listed in Table II. The osmotic coefficients were

Table I

Isopiestic Solutions of Ammonium Perchlorate and Potassium Chloride at 25°

$m_{NH_4ClO_4}$	m_{KCl}	$m_{NH_4ClO_4}$	m_{KCl}
0.104	0.101	1.495	1.106
.205	.197	1.544	1.346
.283	.270	1.602	1.394
.450	.420	1.670	1.445
.603	.558	1.730	1.488
.759	.703	1.811	1.550
.918	.837	1.905	1.622
1.091	.983	2.006	1.692
1.241	1.106	2.100	1.768
1.455	1.268		

calculated from the experimental data by the relation[7]

$$\phi = m_R\phi_R/m$$

where ϕ is the osmotic coefficient of ammonium perchlorate at a concentration m, and ϕ_R is the osmotic coefficient of potassium chloride, the reference salt, at a concentration m_R. The osmotic coefficients of potassium chloride were those as listed in the new edition of Lewis and Randall.[8] These values are 0.0020 greater than the values tabulated by Robinson and Stokes.[9] The physical constants for the Debye–Hückel limiting equation also were obtained from the same source.[10]

Table II

Osmotic and Mean Molal Activity Coefficients of Ammonium Perchlorate at 25°

m	ϕ	$\gamma_\pm$	m	ϕ	$\gamma_\pm$
0.1	0.901	0.730	1.0	.811	.482
.2	.879	.662	1.2	0.801	0.460
.3	.861	.617	1.4	.791	.442
.4	.848	.583	1.6	.783	.426
.5	.838	.556	1.8	.775	.411
.6	.834	.540	2.0	.767	.398
.7	.825	.521	2.1	.756	.394
.8	.820	.507			
.9	.816	.493			

The activity coefficients were determined by[11]

$$2.303 \log \gamma_\pm = -(1 - \phi) - 2\int_0^m \frac{(1 - \phi)}{m^{1/2}}\, dm^{1/2}$$

where a plot of $(1 - \phi)/m^{1/2}$ *vs.* $m^{1/2}$ is sufficient to evaluate the integral of the above equation and consequently log $\gamma_\pm$. However, since the range of concentration of the experimental data was 0.1 to 2.0 m, an extrapolation function was needed which would extend the plot of $(1 - \phi)/m^{1/2}$ *vs.* $m^{1/2}$ to zero concentration. The extrapolation function used is the one based on the Debye–Hückel equation and described by Harned and Owen.[12] In addition, the equation used for extrapolation was found to give a very close fit over the entire range of the experimental results. By using a value of 0.606 for A_m', the deviation from the experimental

(1) R. A. Robinson and R. H. Stokes, "Electrolyte Solutions," 2nd Ed., Butterworths Scientific Publ., London, England, 1959, p. 495.

(2) H. S. Harned and B. B. Owen, "The Physical Chemistry of Electrolytic Solutions," 2nd Ed., Reinhold Publ. Corp., New York, N. Y., 1950, p. 394.

(3) D. A. Sinclair, *J. Phys. Chem.*, **37**, 495 (1933).

(4) R. A. Robinson and D. A. Sinclair, *J. Am. Chem. Soc.*, **56**, 1830 (1934).

(5) H. Hartley, *Proc. Roy. Soc.* (London), **A132**, 429 (1930).

(6) C. S. Patterson, S. Y. Tyree, and K. Knox, *J. Am. Chem. Soc.*, **77**, 2195 (1955).

(7) Reference 2, p. 288.

(8) G. N. Lewis and M. Randall, Revised by K. S. Pitzer and L. Brewer, "Thermodynamics," 2nd Ed., McGraw-Hill Book Co., New York, N. Y., 1961, p. 643.

(9) Reference 1, p. 484.

(10) Reference 8, p. 640.

(11) Reference 2, p. 292.

(12) Reference 2, pp. 289–294.

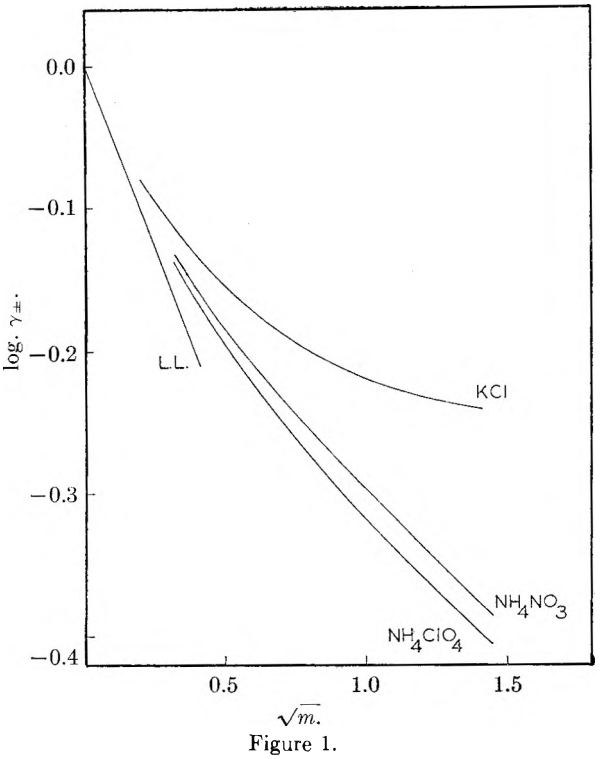

Figure 1.

log $\gamma_{\pm}$ was found to be ± 0.001 over a range of 0.1 to 1.2 m and ± 0.010 up to 2.0 m. This value of A_m' corresponds to 1.84 Å. for $\mathring{a}$, the mean distance of closest approach. Use of the further extended Debye–Hückel equation with the added term of B_m did not give a better fit after the proper adjustment of A_m' and B. As is expected for ammonium salts, the value of $\mathring{a}$ is much lower than the values for the alkali halides, which range between 3.5 and 6.2 Å. The small value of $\mathring{a}$ would seem to indicate that other important effects are present in addition to the very low hydration energies of the cation and anion.

The logs of the mean molal activity coefficients of ammonium perchlorate along with some other 1–1 electrolytes[13] are plotted in Fig. 1. It can be seen that the plot is slightly lower than that of ammonium nitrate, as was expected. The L. L. line represents the Debye–Hückel limiting slope.

(13) Reference 1, pp. 479–480.

CONDUCTIVITY OF SODIUM DODECYL SULFATE SOLUTIONS BELOW THE CRITICAL MICELLE CONCENTRATION

BY G. D. PARFITT AND A. L. SMITH[1]

Department of Chemistry, University of Nottingham, Nottingham, England

Received October 16, 1961

Colloidal electrolytes such as sodium dodecyl sulfate show a more or less abrupt discontinuity in physical properties over a relatively short concentration range termed the critical micelle concentration (c.m.c.). Above this concentration it is well established that the amphipathic ions aggregate to form micelles. Below the c.m.c. it generally has been assumed that, in the absence of hydrolysis, such electrolytes consist of simple ions though the suggestion has been made from time to time that aggregation occurs below the c.m.c.

We have made accurate measurements of the electrical conductivity of aqueous solutions of sodium dodecyl sulfate at 25° at concentrations below the c.m.c. down to 4×10^{-4} M in order to investigate the extent of aggregation of anions to form dimers or small pre-micelles which, alone, presumably would increase the conductivity, or of association to ion pairs which would decrease the conductivity. The results have been analyzed in the light of the theory of electrolytic conductance given by Fuoss and Onsager.[2]

Experimental

The sodium dodecyl sulfate was a pure sample kindly supplied by Thomas Hedley & Co., Ltd., having a purity of 99.9% as determined by partition end-point titration.[3] It was purified further by a liquid/liquid extraction technique.[4] The water used was obtained from an ion exchange column and, equilibrated with air, had a conductivity 1.1×10^{-6} ohm^{-1} cm.$^{-1}$.

Conductivities were measured on a conventional 1000 cycles/sec. bridge incorporating a Wagner earth using resistance boxes of 0.05% grade. The cell, similar in design to that of Flockhart and Graham,[5] was of 400 ml. capacity and required 50 ml. to cover the electrodes. Dilution additions were by weight and concentrations calculated from measured densities. Equilibrium was reached about 30 min. after dilution. Resistances were taken after about 1 hr. and remained constant for at least 7 days.

Results and Discussion

The results are shown in Fig. 1 by a plot of Λ *vs.* $c \times 10^3$ which is of the form expected for a 1:1 strong electrolyte. Both the internal consistency and the agreement between the three overlapping series of measurements were ~0.05%.

Fuoss and Onsager[2] give for an unassociated 1:1 electrolyte (neglecting a small viscosity term)

$$\Lambda = \Lambda_0 - Sc^{1/2} + Ec \log c + Jc \qquad (1)$$

where S is the Onsager limiting slope, E is a function of Λ_0 and the solvent properties, and J is a function of Λ_0, the solvent properties, and the ion size parameter "a." For an associated electrolyte this becomes

$$\Lambda = \Lambda_0 - Sc^{1/2}\gamma^{1/2} + Ec\gamma \log c\gamma + Jc\gamma - K_A c\gamma f^2 \Lambda \qquad (2)$$

Treating the sodium dodecyl sulfate as a simple unassociated 1:1 electrolyte Λ_0 was found from the data by a Shedlovsky extrapolation[6] so that S and E could be calculated and eq. 1 applied. A plot of $\Lambda + Sc^{1/2} - Ec \log c$ *vs.* c (Fig. 2) is straight up to concentrations very close to the c.m.c., after which an abrupt change is obvious. The slope, J, of the portion below the c.m.c. is 195, which corresponds to a value for "a" of 5.0 Å. This is rather less than the average value of 5.5 Å. found[7] for this electrolyte in dioxane–water mixtures at lower dielectric constants with appreciable values of the

(1) At the time of this work at the College of Technology, Northampton, England.

(2) (a) R. M. Fuoss and L. Onsager, *J. Phys. Chem.*, **61**, 668 (1957); (b) R. M. Fuoss and L. Onsager, *ibid.*, **62**, 1339 (1958).

(3) T. Barr, J. Oliver, and W. V. Stubbings, *J. Soc. Chem. Ind.*, **67**, 45 (1948).

(4) S. P. Harrold, *J. Colloid Sci.*, **15**, 280 (1960).

(5) B. D. Flockhart and H. Graham, *ibid.*, **4**, 367 (1949).

(6) T. Shedlovsky, *J. Am. Chem. Soc.*, **54**, 1405 (1932).

(7) G. D. Parfitt and A. L. Smith, awaiting publication.

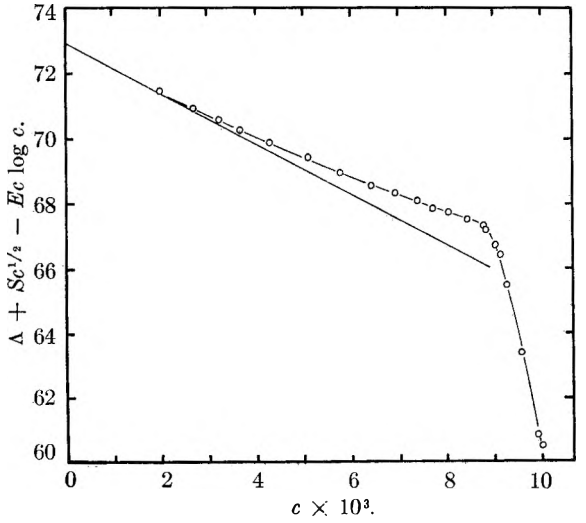

Fig. 1.—Equivalent conductivity of solutions of sodium dodecyl sulfate (c in moles $l.^{-1}$): ——, Onsager tangent.

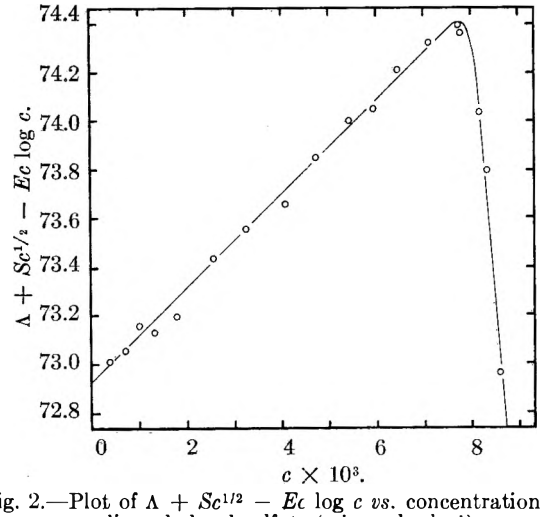

Fig. 2.—Plot of $\Lambda + Sc^{1/2} - Ec \log c$ *vs.* concentration for sodium dodecyl sulfate (c in moles $l.^{-1}$).

association constant K_A. At low values of K_A with γ, the degree of dissociation, nearly unity it would need almost impossibly precise data to separate the Jc term from the $K_A c f^2 \Lambda$ term. The difference between the two "a" values would be accounted for by a K_A of about 0.5.

Thus, in water, at concentrations below the c.m.c. sodium dodecyl sulfate has been found to behave as a simple 1:1 electrolyte. The appreciable formation of dimers or larger aggregates would cause deviations from eq. 1 which have not been observed.

In the work of Mukerjee, Mysels, and Dulin[8] on sodium dodecyl sulfate and other similar electrolytes the conductivity data are explained in terms of dimer formation below the c.m.c. to account for equivalent conductivities well above the Onsager limiting slope. Although the latter work preceded the Fuoss–Onsager theory, a footnote points out that the higher terms introduced by this theory would not account for the observed deviations. However, the analysis of these workers starts by an extrapolation of Λ *vs.* $c^{1/2}$ plots to obtain Λ_0 from which the Onsager limiting slope is drawn. Such an extrapolation naturally gives overwhelming weight to the least accurate data at greatest dilution where the solvent correction is stated to be 10–40%. In this work the maximum solvent correction is rather less than 4%.

In a recent investigation[9] of sodium dodecyl sulfate below the c.m.c. by e.m.f. measurements it was found that dimerization was at most small and the results are, in fact, in good agreement with a zero dimerization constant.

We conclude, therefore, that there seems no reason to postulate that sodium dodecyl sulfate below its critical micelle concentration is other than a 1:1 strong electrolyte.

(8) P. Mukerjee, K. J. Mysels, and C. I. Dulin, *J. Phys. Chem.*, **62**, 1390 (1958).

(9) F. van Voorst Vader, *Trans. Faraday Soc.*, **57**, 110 (1961).

THE NATURE OF THE BINDING OF COUNTERIONS ON CHARGED COLLOIDS AND MACROMOLECULES

BY PASUPATI MUKERJEE

Indian Association for the Cultivation of Science, Jadavpur, Calcutta-32, India

Received October 17, 1961

Various different kinds of investigations, such as counterion activity determination, conductivimetry, and transport studies leave little doubt that for highly charged colloids such as polyelectrolytes and micelles of association colloids a large fraction of the counterions remains bound to the colloidal particles, strongly enough to form part of the kinetic entity. A question of some importance in the theoretical study of ion-binding and the energetics of these species concerns the nature of this binding, *i.e.*, is it entirely non-specific binding arising out of the strong electrical forces or are there perhaps more specific forces such as covalent forces involved? Recent studies using Raman spectra[1] and nuclear magnetic resonance[2] suggest that the binding is non-specific. The purpose of this note is to show that an equilibrium method, involving the use of partial molal volumes, $\bar{V}$, is a useful general method for studying this question. The method is applied to a micellar system and a polyelectrolyte.

The basis of the method can be derived from the properties of simple electrolytes.[3] For these, at infinite dilution, $\bar{V}$'s are strictly additive, being the sums of $\bar{V}$'s of individual ions, so that $\Delta\bar{V}$, the difference in $\bar{V}$ of two electrolytes of the same charge-type with one ion in common, is independent of the nature of the common ion. The concentration dependence of $\bar{V}$ for strong electrolytes can be expressed over a wide range as $\bar{V} = \bar{V}_0 + S\sqrt{C}$ where $\bar{V}_0$ is the value at infinite dilution and S is a constant characteristic of the electrolyte. An important property of S is that its values also are reasonably additive with respect to individual ions, particularly for 1:1 electrolytes. As a result, even at fairly high concentrations, in spite of consider-

(1) S. Lapanje and S. A. Rice, *J. Am. Chem. Soc.*, **83**, 496 (1961).

(2) L. Kotin and M. Nagasawa, *ibid.*, **83**, 1026 (1961).

(3) H. S. Harned and B. B. Owen, "The Physical Chemistry of Electrolytic Solutions," 3rd Edition, Reinhold Publ. Corp., New York, N. Y., 1958.

able changes in $\bar{V}$, $\Delta\bar{V}$ is almost independent of the common ion. Table I gives some examples for pairs of electrolytes at 1 M concentration and at infinite dilution. In many cases $\Delta\bar{V}$ (1 M) is actually close to $\Delta\bar{V}_0$, showing little concentration dependence. In some other cases (see last row of Table IB) it shows appreciable concentration dependence. An example of special interest to us is $\Delta\bar{V}$ between a strong acid and its salt. Thus $\bar{V}_{HCl} - \bar{V}_{NaCl}$ is 1.2 ml./mole at infinite dilution, 0.8 ml./mole in 0.25 M, −0.2 ml./mole in 1 M, and −2.0 ml./mole in 2 M solutions in water, and shows appreciable concentration dependence.

The situation changes sharply for weak acids. On association of a proton to a negative ion, two charges disappear and the electrostriction of the solvent is regained so that the partial volumes are considerably greater. Thus $\bar{V}_0$ of undissociated acetic acid is greater than that of sodium acetate by 12.7 ml./mole[4] and that of H_2SO_4 is greater than that of $NaHSO_4$ by 21.6 ml./mole.[3] Compared to their salts, therefore, $\bar{V}$'s for weak acids are considerably larger than those of strong acids.

For charged colloidal systems we extend our definition of $\bar{V}$ and $\Delta\bar{V}$ to partial equivalent volumes. The comparison of this $\Delta\bar{V}$ with the value expected for simple strong electrolytes forms the basis of our method. If the interactions between the charges on the colloid are only electrostatic, the $\Delta\bar{V}$'s should be substantially the same. Specific interactions, on the other hand, should affect different counterions differently and, therefore, affect the $\Delta\bar{V}$ for the colloidal systems. Covalent bonding, charge transfer, and desolvation all may be expected to influence $\Delta\bar{V}$.

It is important to note that for comparison with simple electrolytes the ambient ionic strength is not the significant one for colloidal systems. Even at high dilutions of the colloid the local concentration of counterions near the surface of a micelle, or a protein, or on a polyelectrolyte chain, is high, and not adequately determinable. The concentration, however, is not so high as to make comparisons meaningless. The micelles of association colloidal electrolytes exhibit one of the densest packings of charges on a colloid. But even so, assuming a perfectly smooth surface, the average separation between the charges is about 7 Å., corresponding to a 3 M solution in 1:1 electrolytes. Considering that the surface must be rough[5] the actual local concentration should be less. At such concentrations of simple strong electrolytes, $\bar{V}$ continues to be additive for many pairs of counterions. In those cases where $\Delta\bar{V}$ shows little concentration dependence the difficulty is minimized. On the other hand, from the concentration dependence of $\Delta\bar{V}$, in a system where specific interactions are not considered important, some idea may be obtained about the "effective" concentration of charges on the colloid.

For applying these ideas rather accurate $\bar{V}$ values are required for systems where only the counterion is varied. Suitable data are available in the case of micelles of association colloidal electrolytes for a particularly interesting pair of systems, sodium lauryl sulfonate and the corresponding acid, in which the effect of specific interactions should be large. From the slopes of the specific volume curves above the critical micelle concentration (c.m.c.), $\bar{V}$, expressed per mole of the association colloid in the micellar form, can be obtained. From the density data of Wright, *et al.*, for sodium lauryl sulfonate over 40–70°),[6] the extrapolated value of $\bar{V}$ at 25° is 241.6 ± 1.0 ml./mole. At that same temperature, $\bar{V}$ for the acid from the density data of Kirkby[7] is 239.5 ± 0.5 ml./mole. Since about 70% of the counterions are bound to the micelle surface,[5,8] this small difference and the lower value for the acid suggest strongly that the interactions are mainly electrostatic, in agreement with similar conclusions for polyelectrolytes,[1,2] and that covalent forces, or other specific influences, are not involved. Recent estimates of electrostrictions due to ions[9] would indicate an increase of about 5 ml./mole for the acid if the protons were covalently bound. The limits of error are rather large, but the probable difference in $\bar{V}$ corresponds roughly to the difference expected in 1–3 M solutions of the chlorides, which is in good agreement with the expected local concentration of the counterions at the micelle surface.

TABLE IA

VARIATION IN V WITH COUNTERIONS

	$\Delta\bar{V}_0$	$\Delta\bar{V}$ in 1 M solutions for X =			
		Cl^-	Br^-	I^-	OH^-
LiX–NaX	0.5	−0.4	−0.3	−0.5	−1.1
KX–NaX	10.2	10.4	10.5	10.6	9.8
CsX–NaX	22.7	22.8	22.9	23.0	...

TABLE IB

	$\Delta\bar{V}_0$	$\Delta\bar{V}$ in 1 M solution for M =			
		Li^+	Na^+	K^+	Cs^+
MBr–MCl	7.1	6.6	6.5	6.6	6.6
MI–MBr	11.5	11.0	11.0	11.0	11.1
MCl–MOH	23.4	20.7	20.0	20.6	..

That charge interactions at the micelle-surface are mainly electrostatic in nature has been assumed frequently.[5,10] Our approach provides strong evidence for it.

In the case of polyelectrolytes some recent data on ammonium polyvinylsulfonate in 0.5 M NH_4Cl and potassium polyvinylsulfonate in 0.1 M KCl[11] can be interpreted similarly. Assuming that the apparent specific volume, ϕ, can be taken as the partial specific volume (*i.e.*, $d\phi/dc$ is small, as in the case of proteins[12]) the $\Delta\bar{V}$ value between the ammonium and the potassium salt is 6.7 ml./equiv. This is significantly different from $\Delta\bar{V}_0$ between

(4) O. Redlich and J. Bigeleisen, *Chem. Revs.*, **30**, 171 (1942).

(5) D. Stigter and K. J. Mysels, *J. Phys. Chem.*, **59**, 45 (1955).

(6) K. A. Wright and H. V. Tartar, *J. Am. Chem. Soc.*, **61**, 544 (1939).

(7) H. E. Kirkby, as reported by M. E. L. McBain and E. Hutchinson, "Solubilization and Related Phenomena," Academic Press, New York, N.Y., 1955.

(8) I. M. Kolthoff and W. F. Johnston, *J. Am. Chem. Soc.*, **73**, 4563 (1951).

(9) P. Mukerjee, *J. Phys. Chem.*, **65**, 740, 744 (1961).

(10) J. Th. G. Overbeek and D. Stigter, *Rec. trav. chim.*, **75**, 1263 (1956).

(11) E. F. Casassa and H. Eisenberg, *J. Phys. Chem.*, **65**, 427 (1961).

(12) M. O. Dayhoff, G. E. Perlmann, and D. A. MacInnes, *J. Am. Chem. Soc.*, **74**, 2515 (1952).

NH_4^+ and K^+ (9.3 ml./mole), but it corresponds to the difference expected for NH_4Cl and KCl if the excess concentration in the bound layer on the polyelectrolyte is about 1.5 N, a reasonable value on geometrical grounds.

The study of the variation of $\bar{V}$ with the nature of the counterion, therefore, gives us a means of examining the question of the specificity of ion-binding. The method is more general than those of Raman spectroscopy or nuclear magnetic resonance. With the available techniques of density measurements $\bar{V}$ can be determined to better than 0.1%.[4] It should be possible, from the difference of the measured $\Delta\bar{V}$ and the value at infinite dilution, to get some indication of the strength of the electrostatic interactions, as in the examples cited above, in terms of an effective concentration, or some more detailed theoretical picture of ion-binding.

An extension of the method, applicable particularly to association colloidal electrolytes, is to compare the change in $\bar{V}$ from below the c.m.c. to above it for the case of different counterions. For this precise data below the c.m.c. are needed as well. From the available data, we can compare laurylsulfonic acid at 25°[7] with sodium laurylsubmate at 23°.[13] The extra oxygen in the latter is not expected to cause much difference. On the formation of micelles from the single ions, $\bar{V}$ increases by 10.0 ± 2.0 ml./mole for sodium laurylsulfate and 11.3 ± 1.0 ml./mole for laurylsulfonic acid. This again shows that the sodium and the hydrogen forms behave in about the same manner, and that the charge interactions are mainly electrostatic.

(13) L. M. Kushner, B. D. Duncan, and J. I. Hoffman, *J. Research Natl. Bur. Standards*, **49**, 85 (1952).

FLUORINE N.M.R. SPECTROSCOPY. VIII. COUPLING CONSTANTS IN NORMAL AND ISOTOPIC C_3F_8

BY GEORGE VAN DYKE TIERS

Contribution No. 215 from the Central Research Dept., Minnesota Mining and Mfg. Co., St. Paul 19, Minn.

Received September 25, 1961

Several recent papers[1-7] have given indication of the strong dependence of fluorine shielding values[1-3,5-7] and coupling constants[3-7] upon the molecular conformation or stereostructure,[1-5] and upon the nature of substituent groups.[3,6,7] However, to place such observations upon a quantitative basis, it would be necessary to secure extremely detailed information about molecular geometry in fluorocarbon derivatives. Owing to the conformational flexibility of most of these compounds[1,3,4,6,7] it is quite unlikely that precise bond angles and dihedral angles will be secured. Two courses remain: first, the investigation of rigid molecules having a more or less well defined geometry[1,2,5]; and secondly, the study of certain symmetrical molecules (or groups) for which there is an obvious simplification of the conformational problems.

In this paper the second course is adopted, the molecule studied being perfluoropropane, C_3F_8. Owing to the symmetry, the coupling constant between CF_3 groups can only be seen for the isotopic isomer $C_2F_5C^{13}F_3$, which is present in natural abundance; this powerful method, due to Sheppard,[8] is particularly valuable for fluorine compounds.[5]

Experimental

The n.m.r. equipment and techniques have been described.[5,9,10] The perfluoropropane was a purified sample available in these laboratories. It was studied as a 34% (by liquid volume) solution in CCl_3F in order to reduce the hazard due to high pressure. Fluorine shielding values,[9] ϕ^*, measured at 28.9° on this and on a 12% solution then were extrapolated to infinite dilution[9]; results, given in Table I, are the averages of six to eight separate determinations, and error values given are standard deviations in the averaged values.

TABLE I

FLUORINE N.M.R. SHIELDING VALUES FOR PERFLUOROPROPANE

Concn. of C_3F_8, %	ϕ^* (CF_3)	Std. dev.	ϕ^* (CF_2)	Std. dev.
34	+82.861	±0.006	+131.181	±0.009
12	+82.833	± .003	+131.200	± .003
0	+82.818[a]	± .005	+131.210[a]	± .006

[a] Extrapolated value; at infinite dilution in CCl_3F, $\phi^* = \phi$.

In Table II are listed the results of the coupling constant measurements, and also the associated "C^{13} isotope effect" shifts, both "direct"[11] and "distant."[10] As in all previous cases,[5,10,11] the heavier isotope produces shifts corresponding to higher shielding. In all cases it was permissible to use first-order spin–spin analysis due to the large disparity in magnitudes of the coupling constants. This was fortunate, as the spectra are very weak, the C^{13} being in natural abundance; finer details in the patterns would have been very difficult to observe reproducibly. For $J(F\text{–}C^{13})$ a 0.18 c./sec. second-order correction was applied.[5]

TABLE II

FLUORINE N.M.R. COUPLING CONSTANTS AND ISOTOPE EFFECTS FOR THE CF_3 GROUP IN PERFLUOROPROPANE

Coupling system[a]	J, c./sec.	Std. dev.[b]	$\Delta\phi$, p.p.m.[c]	Std. dev.[b]	No. of meas.
F–C^{13}	285.74[d]	±0.13	+0.135	±0.005	20
F–C–C^{13}	40.34	± .10	+0.020	±0.002	18
F–C–C–F	0.70	± .01	.....	.....	32
F–C^{13}–C–C–F	7.31	± .07	.....	.....	25

[a] Coupling is between the first- and last-mentioned nuclei in each system. [b] Std. dev. of the *average*. [c] $\Delta\phi = \phi(C^{13}$ isomer) $- \phi(C^{13}$ isomer). [d] Corrected according to ref. 5; $M_L + M_H = 285.93$ c./sec.

Discussion

It is noteworthy from Table I that there is little concentration dependence of shielding values for

(1) G. V. D. Tiers, *Proc. Chem. Soc.*, 389 (1960).
(2) G. V. D. Tiers, *J. Phys. Chem.*, in press (Part IX).
(3) J. Feeney and L. H. Sutcliffe, *Trans. Faraday Soc.*, **56**, 1559 (1960).
(4) L. M. Crapo and C. H. Sederholm, *J. Chem. Phys.*, **33**, 1583 (1960).
(5) G. V. D. Tiers, *ibid.*, in press (Part V).
(6) E. Pitcher, A. D. Buckingham, and F. G. A. Stone, *Spectrochim. Acta*, in press.
(7) G. V. D. Tiers, *J. Phys. Chem.*, **66**, 764 (1962).
(8) N. Sheppard and J. J. Turner, *Proc. Roy. Soc.* (London), **A252**, 506 (1959); *Mol. Phys.*, **3**, 158 (1960).
(9) G. Filipovich and G. V. D. Tiers, *J. Phys. Chem.*, **63**, 761 (1959).
(10) G. V. D. Tiers, *J. Phys. Soc. Japan*, **15**, 354 (1960).
(11) P. C. Lauterbur, private communication; paper in course of preparation.

C_3F_8, and indeed for nearly all purposes ϕ^* (10% to 20%) might be substituted for ϕ with negligible error, as indicated previously.[1,9] Interestingly, the weak solvent dependences for CF_3 and CF_2 groups are in opposite directions.

While shielding of the CF_3 group is slightly higher than is found in longer-chain compounds,[7] the CF_2 ϕ-value, 131.210, is very substantially increased in C_3F_8. For *n*-perfluoroalkanes the average values are 122.5 ϕ and 126.64 ϕ for mid-chain CF_2 and for CF_2 adjacent to CF_3[12]; in the present case proximity to two CF_3 groups brings about a further, almost linear, increase in shielding.

The n.m.r. isotope shifts due to attached and to "distant" C^{13} correspond reasonably well with previous values for CF_3 groups.[5,10] Coupling constants between fluorine and C^{13} also have magnitudes close to those previously reported[5,10]; a further treatment of this subject[11] will demonstrate the range of variation observed in $J(F-C^{13})$ in a variety of compounds. No information could be obtained as to the relative sign of $J(F-C^{13})$ and $J(F-C-C^{13})$.

The coupling constant between dissimilar fluorines in the perfluoroethyl group is now known to be somewhat dependent upon structure. Thus, in C_2F_5I $J(FCCF)$ is 4.6 c./sec.,[6] and in several (perfluoroethyl)-metal compounds it ranges from 1.4 to 1.8 c./sec.[6]; however, when the C_2F_5 group is attached to carbonyl, the coupling varies from 1.48[13] to 0.7 c./sec.[6] The value measured here for C_3F_8, 0.70 c./sec., corresponds well with the latter cases, provided there is no inversion in sign.

The principal outcome of the carbon-13 study is the observation of the coupling constant between the otherwise equivalent CF_3 groups in C_3F_8. Such "distant" coupling has often been measured between CF_3 and CF_2 groups so located,[6,7] and it has been suggested[6] that there is a correlation between high coupling constants, $J(CF_3-C-CF_2X)$, and low shielding values for the CF_2X group, and *vice versa*. However, in the present case (X = F) a "low" coupling constant, 7.3 c./sec., accompanies a low shielding value; the suggested correlation[6] is thus seen to be based upon too limited a choice of data.

Acknowledgment.—I thank R. B. Calkins for excellent operation of the n.m.r. spectrometer, and Jane E. H. Tiers for careful measurement of the spectra.

(12) G. V. D. Tiers, paper to be submitted shortly.
(13) C. A. Reilly, *J. Chem. Phys.*, **25**, 604 (1956).

A SIMPLE METHOD OF MEASURING LIQUID INTERFACIAL TENSIONS, ESPECIALLY AT HIGH TEMPERATURES, WITH MEASUREMENTS OF THE SURFACE TENSION OF TELLURIUM

BY CYRIL STANLEY SMITH[1] AND DONALD P. SPITZER

Institute for the Study of Metals, University of Chicago, Chicago, Illinois

Received October 25, 1961

The common methods of measuring surface tensions at elevated temperatures have been reviewed by Kozakevitch.[2] Perhaps the best method is the use of the profile of a sessile drop, as in the work of Kingery, *et al.*,[3] but this is difficult to apply to the interface between two liquids, although good results have been obtained by the use of radiography.[4] An alternate method has been devised, which involves only the measurement of the height of a column of liquid at the moment that its meniscus breaks away from a sharp-edged circular hole in a flat plate. It may be called the "Meniscus Break-through Method." In principle it is identical with the maximum bubble pressure method, but it uses the liquids under study as manometric fluids. The method can be used at room temperature, but is especially advantageous in the difficultly-accessible interiors of furnaces or cryostats, since the observation of the sudden instability of the interface is independent of the measurement of height, and can be done telescopically in a vertical direction. The method also has the advantage that the interface is easily renewed and is, therefore, fresh and relatively uncontaminated.

The orifice plate, sealed to the end of a tube of appropriate length, is either raised or lowered through the interface (depending on whether the contact angle of the lower liquid against the orifice material is less or greater than 90°) until the liquid under higher pressure breaks through. To a first approximation the interface energy

$$\gamma = \frac{rhg}{2}(\rho_2 - \rho_1) \qquad (1)$$

where ρ_1 and ρ_2 denote the densities of the upper and lower liquids, respectively; g is the gravitational constant; and h, the critical hydrostatic head, is experimentally the difference between the height, H_0, of the plate at the point where the interface first touches the orifice plate and the point, H, where it breaks through (both of which are easily identified by watching the meniscus from above with a telescope), corrected for the thickness of the disk and for the change in external liquid level caused by the displacement of the orifice tube. The correction for non-sphericity of the meniscus due to the gravitational pressure gradient in the liquids is done by the Sugden method, as in the conventional maximum bubble pressure method.

In practice it has been found convenient to mount the orifice tube on a rod attached to the carriage of a vertical cathetometer which also carries a horizontal telescope (sighted, *via* a prism, on the meniscus) and a suitable light, all moving together. The rod enters a vertical furnace containing the crucible with the experimental materials through a small hole in the lid, which also is arranged to admit thermocouples and an inert gas.

If large amounts of both liquids are available, it is simplest to allow the upper liquid to maintain its own level within and without the tube support-

(1) Massachusetts Institute of Technology, Cambridge, Massachusetts.
(2) P. Kozakevitch, "Surface Tension" in "Physicochemical Measurements at High Temperatures," Edited by J. O'M. Bockris, J. L. White, and J. D. Mackenzie, Academic Press, New York, N. Y., 1959, pp. 208–224.
(3) W. D. Kingery and M. Humenik, Jr., *J. Phys. Chem.*, **57**, 359 (1953).
(4) P. Kozakevitch, S. Chatel, G. Urbain, and M. Sage, *Rév. Métallurgie*, **52**, No. 2, 139 (1955).

ing the orifice plate, either by making a perforation at a suitable height or by using a short tube with its upper end below the upper meniscus, attached to a rod for support. The interface energy is then

$$\gamma = \frac{Xg}{2}\left[(H - H_0)\left(1 + \frac{d^2}{D^2 - d^2}\right) - t\right] \times (\rho_2 - \rho_1) \quad (2)$$

where X is r multiplied by the value of X/r, obtained by successive approximations from the table of Sugden,[5] given also by Adam,[6] and Harkins.[7] D is the inside diameter of the crucible containing the liquids and d is the outside diameter of the orifice tube.

It also is satisfactory to allow a layer of the upper liquid to be entrapped in the tube, for its volume remains unchanged from the moment that the bottom of the orifice plate touches the interface and cuts off connection with the upper layer. In this case, the density function in equation 1 becomes ρ_2 alone, and a correction is applied to the pressure term to allow for the displacement of the liquid within the thickness of the plate, *i.e.*

$$\gamma = \frac{Xg}{2}\left\{\left[(H - H_0)\left(1 + \frac{d^2}{D^2 - d^2}\right) - t\right] \times \rho_2 - t\rho_1 r^2/R^2\right\} \quad (3)$$

As in the capillary-height and maximum-bubble-pressure methods, it is necessary to use a sufficiently large vessel to ensure that the change in pressure due to the curvature of the meniscus between the container wall and the tube will be insignificant: a clearance of 1 cm. or more usually is adequate. The densities of the liquids may be determined by measuring as a function of depth the change of pressure of a neutral gas bubbling through the orifice, using, of course, an external manometer.

For visual observation the upper liquid must be reasonably transparent. The method could, however, be adapted to opaque liquids by the use of electrical probes, force-displacement measurements, or X-ray fluoroscopy to observe the critical heights.

In high temperature studies it is often difficult to find a material for making the orifice and crucible that will be inert. In some cases a solid soluble in the liquid under study but in equilibrium with it may be used. For example, sintered sodium fluoride has been used in studies of the interface between fused alkali halides and tellurium.

The method was proven by measuring the well known water–air and water–carbon tetrachloride interfaces at room temperature, and then employed for the metal–salt systems recently reported.[8] As an example we report here measurements of the surface tension of tellurium. Tellurium of moderately high purity was used (less than 0.001% each of Si, Mg, Cu, Al, Cr, and Ni; 0.002% Ag and Fe; and 0.005% Pb) in an atmosphere of purified nitrogen. The orifice plate, tube, and crucible were made of Pyrex glass. The density at 460° was found to be 5.58 g./cc. Six different experiments at 460° gave the results shown in Table I, the average being 178.4 ± 1.5 ergs/cm.^{2}. Measurements on fresh interfaces only are reported: the surface tension decreased with time, eventually by as much as 10%, probably as a result of the pick-up of impurities.

TABLE I

THE SURFACE TENSION OF TELLURIUM AT 460°

r, cm.	$(H - H_0)$, cm. obsd.	$(H - H_0)$, cm. cor.[a]	a^2	Surface tension, ergs./cm.^{2}
0.0853	0.860	0.812	0.06426	175.7
.0853	.870	.824	.06528	178.5
.0853	.877	.832	.06597	180.3
.0853	.872	.826	.06525	178.4
.0855	.846	.822	.06528	178.5
.0855	.848	.824	.06545	178.9
				178.4 ± 1.5

[a] Corrected for liquid displacement as in eq. 2.

The interface energy of the Te–CsCl interface, measured in a Pyrex apparatus at 640° was found to be 133.5 ± 1.2. The interface energy between these same liquids saturated with NaF, (measured using an orifice and crucible made of sintered NaF powder) was 97.1 ± 0.5 ergs/cm.^{2} at 600°.

A TECHNIQUE FOR THE RAPID DETERMINATION OF IONIZATION AND APPEARANCE POTENTIALS[1]

BY ROBERT W. KISER[2] AND EMILIO J. GALLEGOS

Department of Chemistry, Kansas State University, Manhattan, Kansas

Received November 30, 1961

A number of methods have been reported[3] and used for obtaining ionization and appearance potentials from ionization efficiency curves. The ionization efficiency curves (a plot of ion intensity *vs.* electron energy) are obtained from electron impact investigations using a mass spectrometer.

A method of obtaining approximate ionization and appearance potentials has been developed and employed in our Laboratory, using a Bendix time-of-flight mass spectrometer. The general features of our mass spectrometric system have been described.[4] Using this new method, which we term the "energy compensation technique," ionization and appearance potentials may be obtained usually in less than one minute. The energy compensation (e.c.) technique follows the concept of the method introduced by Lossing, *et al.*[5] The e.c. method,

(1) This work was supported in part by the U. S. Atomic Energy Commission under contract No. AT(11-1)-751 with Kansas State University.

(2) Address reprint requests to this author.

(3) See, for example, F. H. Field and J. L. Franklin, "Electron Impact Phenomenon and the Properties of Gaseous Ions," Academic Press, New York, N. Y., 1957, pp. 24–37.

(4) E. J. Gallegos and R. W. Kiser, *J. Am. Chem. Soc.*, **83**, 773 (1961).

(5) F. P. Lossing, A. W. Tickner, and W. A. Bryce, *J. Chem. Phys.*, **19**, 1254 (1951).

(5) S. Sugden, *J. Chem. Soc.*, **121**, 858 (1922).

(6) N. K. Adam, "The Physics and Chemistry of Surfaces," London, 1941, p. 372.

(7) W. D. Harkins, "Determination of Surface and Interfacial Tensions," in "Physical Methods of Organic Chemistry," edited by A. Weissberger, 3rd Ed., Interscience Publishers, New York, N. Y., 1959, Vol. I, part 1, pp. 757–814.

(8) D. P. Spitzer, *J. Phys. Chem.*, **66**, 31 (1962).

being instrumental in character, eliminates the necessity of obtaining the usual ionization efficiency curve in the determination of ionization and appearance potentials. A similar method, termed "simplified procedure," has been employed[5] to determine ionization potentials. Using the e.c. method, the ion currents of the calibrating gas and the gas under investigation are measured at 50 e.v. and recorded on separate channels of a dual channel recorder. The sensitivity of the two amplifiers (one for each ion out-put) is increased 100-fold (or, if desired, 1000-fold) and the electron energy decreased until the ion current intensity reads the same for each ion as previously at 50 e.v. The difference in the voltages is taken as the difference in the appearance potentials of the calibrating gas and the gas under study. Although this method has been used only with a time-of-flight instrument for appearance potential determinations, it also should prove suitable for use with other types of mass spectrometers. The nearly identical "simplified procedure" of Lossing, *et al.*,[5] has been used previously for ionization potential determinations.

Table I summarizes some results of ionization potentials determined for various compounds using the linear extrapolation method, the logarithmic plot method,[5] the extrapolated voltages difference method,[6] and the e.c. method. Xenon was used as the calibrating gas for the determinations shown in Table I. An ionization potential of 12.13 e.v. was taken for xenon.[7] Most of the values shown as having been determined by extrapolated voltage differences already have been reported.[8-11] From this table it is seen that the e.c. method gives results for ionization potentials which may be taken as acceptable to within about ±0.2 e.v.

TABLE I

IONIZATION POTENTIALS OBTAINED USING VARIOUS METHODS OF INTERPRETING IONIZATION EFFICIENCY CURVES COMPARED TO THOSE OBTAINED USING THE ENERGY COMPENSATION TECHNIQUE

	Ionization potential (e.v.)[a]				
Molecule	L.E.	L.P.	E.D.	E.C.	Lit.[b]
Nitrogen dioxide	11.1	11.3	11.39	11.3	
Ethylenimine	10.2	9.8	9.94	9.8	
Ethylene sulfide	9.1	8.7	8.87	8.9	
Azetidine	9.1	9.2	9.1	8.9	
Trimethylene oxide	9.9	9.9	9.85	9.7	
Trimethylene sulfide	9.2	9.1	8.9	8.9	
Pyrrolidine	9.2	9.1	9.0	8.9	
Tetrahydrofuran	9.5	9.2	9.45	9.3	
Tetrahydrothiophene	8.7	8.5	8.57	8.4	
Piperidine	8.8	9.0	8.9	8.7	
Tetrahydropyran	9.6	9.6	9.53	9.7	
Tetrahydrothiapyran	9.0	8.6	8.5	8.5	
Thiadioxane	8.6	8.3	8.50	8.5	
Dioxane (1,4-)	9.7	9.2	9.56	9.8	
Hexamethylenimine	8.9	8.6	8.76	8.5	
Tetramethylsilicon	10.0	10.1	9.80	9.8	
Tetramethyltin	8.9	8.0	8.25	8.4	
Krypton(II)				24.2	24.56
Benzene				9.7	9.25
Nitrogen				15.7	15.6
Oxygen				12.5	12.2
Ammonia				10.3	10.15–10.50
Phosphine				10.3	10.1

[a] L.E. = linear extrapolation; L.P. = logarithmic plot; E.D. = extrapolated voltage difference; E.C. = energy compensation. [b] A comparison to literature values is made only for those molecules where comparisons to L.E., L.P., and E.D. were not made. For a summary of literature values, see R. W. Kiser, "Table of Ionization potentials," TID-6142, U.S. Atomic Energy Commission, June 20, 1960.

A similar study was made of the determination of appearance potentials of fragment ions. Our studies have shown that appearance potentials of fragment ions determined by the linear extrapolation method and the logarithmic plot method for interpretation of the ionization efficiency curves are not always reliable. The method due to Warren[6] has given results which we generally find satisfactory for the determination of appearance potentials. The results we have obtained using the e.c. method indicate that appearance potentials so obtained are generally low by about 0.1–0.2 e.v. (even though the determinations were reproducible) for fragment ions whose appearance potentials are less than the ionization potential of the xenon calibrating gas. Using the e.c. method, values of appearance potentials greater than the ionization potential of the xenon calibrating gas were observed to be high by 0.2 e.v. or more, and the results became considerably less reliable with an increase of the appearance potential. Nevertheless, fairly accurate (±0.2 e.v.) appearance potentials may be obtained rapidly with the e.c. method if their values lie near to or lower than the ionization potential of the calibrating gas.

(6) J. W. Warren, *Nature*, **165**, 811 (1950).
(7) C. E. Moore, Natl. Bur. Standards Circ. 467, Vol. 3, 1958.
(8) E. J. Gallegos and R. W. Kiser, *J. Phys. Chem.*, **65**, 1177 (1961).
(9) E. J. Gallegos and R. W. Kiser, *ibid.*, **66**, 136 (1962).
(10) R. W. Kiser and I. C. Hisatsune, *ibid.*, **65**, 1444 (1961).
(11) B. G. Hobrock and R. W. Kiser, *ibid.*, **65**, 2186 (1961).

THE THERMAL EXPANSION OF POTASSIUM CHLORIDE[1]

BY THOR RUBIN, H. L. JOHNSTON, AND HOWARD W. ALTMAN

Cryogenic Laboratory of the Department of Chemistry, The Ohio State University, Columbus 10, Ohio

Received October 31, 1961

The apparatus and the experimental techniques used for the determination of the thermal expansion of potassium chloride were the same as those described for the determination of the expansion coefficient of copper.[2]

Large pieces of potassium chloride were obtained from the Harshaw Chemical Company. They were cut into three pillars, then filed to approximately the same length. These pillars separated the plates of the interferometer. By carefully filing one pillar or another, circular fringes finally were obtained with the interferometer which did not expand or contract to the eye moving transversely

(1) This work was supported in part by the Air Material Command, Wright Field.
(2) T. Rubin, H. W. Altman, and H. L. Johnston, *J. Am. Chem. Soc.*, **76**, 52 (1956).

over the whole field of the plate. Then the pillars were judged to be of the same length to within about one fifth of a wave length of the radiation used (sodium-D radiation). This parallel plates interferometer gave interference patterns which virtually were unaffected by tilting motion of the apparatus. Such motion is almost unavoidable since differential thermal expansion of the apparatus on cooling or heating always will occur.

Results

Absolute values for expansion coefficients for potassium chloride are given in Table I. r_1^2 and r_2^2 are the apparent first fringe diameters measured at temperature equilibrium. The apparent diameters of these rings were measured with a filar micrometer eye piece. The constant O' (smoothed) is a measure of the change of the square of the fringe diameter by one fringe order. They are smoothed according to the method described by Rubin, Johnston, and Altman.[3] T_{avg} °K. is the mean of the initial and final temperature of the determination, ΔT is the temperature interval of the determination, F is the number of fringes passing a fiduciary mark during a determination, l_0 is the length of the sample at room temperature, and α is the coefficient of linear expansion. The asterisks represent initial values of r^2 which are equal to the final value of the previous run. Thus, all measurements with asterisks are members of a continuous series of which there are four.

TABLE I

l_0 = 0.4955 cm.

ΔT	T_{avg}	O' smoothed	r_1^2	r_2^2	F	$\alpha \times 10^6$
12.138	144.157	14.87	28.944	16.892	6.1895	3.033
15.201	157.83	14.83	*	17.098	8.0138	3.136
14.499	172.68	14.79	*	29.757	7.8559	3.222
15.962	187.91	14.75	*	27.140	8.82258	3.287
13.749	202.70	14.73	*	23.717	7.7676	3.361
16.084	217.68	14.69	*	27.668	9.2691	3.427
16.281	233.86	14.63	*	20.839	9.5332	3.482
21.438	252.72	14.58	*	17.893	12.7975	3.550
17.428	272.15	14.55	*	26.884	10.6184	3.623
15.283	288.51	14.52	*	19.097	9.4637	3.682
7.650	83.050	14.63	29.214	27.040	2.8507	2.223
9.724	91.74	14.57	*	25.705	3.9078	2.391
10.462	101.83	14.55	*	18.276	4.4894	2.548
9.107	111.62	14.52	*	20.250	4.1359	2.702
9.627	120.99	14.50	*	28.222	4.55169	2.813
12.391	132.00	14.49	*	29.160	6.0647	2.912
6.241	16.560	14.91	14.822	15.288	0.03127	0.017
6.116	22.74	14.84	*	16.851	0.01053	0.102
6.011	28.80	14.80	*	21.160	0.2911	0.286
6.057	34.83	14.75	*	28.516	0.4987	0.490
6.921	41.32	14.72	*	27.046	0.9001	0.774
11.077	50.32	14.68	*	29.160	2.1440	1.156
10.951	61.33	14.64	*	28.196	2.9342	1.597
8.279	70.95	14.60	*	22.562	2.6138	1.881
7.728	78.95	14.56	*	19.184	2.7681	2.131
17.816	266.288	14.79	22.373	18.927	10.7667	3.594
23.144	286.77	14.71	*	23.424	14.3062	3.676

All temperature values determined below 41.32° K. are measured with only a standard thermocouple. All those above this temperature have temperatures determined from the thermocouple in conjunction with a precise resistance thermometer.

The resistance values as a function of temperature were graphed and new values at equal temperature intervals were smoothed and tabulated. The tabulated values were used to calculate the ΔT and T_{avg} values at the higher temperatures.

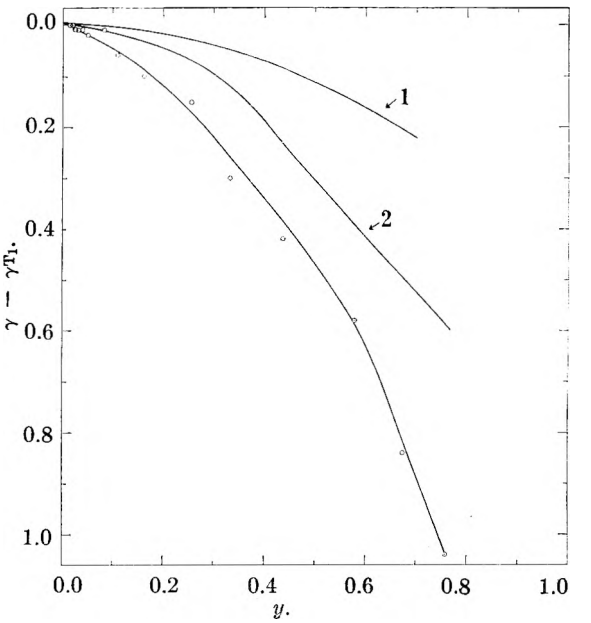

Fig. 1.—The variation of the Grüneisen parameter with temperature.

The thermocouple was calibrated in terms of the Ohio State University Cryogenic Laboratory temperature scale.[4]

Since these data are taken with rather large temperature intervals, the derivatives of length with respect to temperature were computed at the mean temperature from each series of length–temperature measurements by the method of divided differences.[5,6] First to fourth divided differences alone were needed. Division of the first derivative by l_0 yields the α of Table I.

Errors.—Absolute temperatures are accurate to about 0.03°K. Those temperature intervals measured by the thermocouple are precise to about 0.01° K., whereas those intervals which were measured by means of the resistance thermometer are precise to a few thousandths of a degree. Errors in F are of the order of 0.007 fringe. The error in F is the largest source of error and determines the error in α at all temperatures.

Srinivasan[7] and Henglein[8] have measured expansion coefficients of potassium chloride over a part of the temperatures covered by the present work. Their results are presented in Table II together with α values of the present work taken at corresponding temperatures. These were read from a large scale smooth graph. α_s and α_h refer, respectively, to the values of Srinivasan and Henglein. The agreement is only fair.

Theory.—Using a simple model which already has been described[3,10] the results of this work are best

(3) T. Rubin, H. L. Johnston, and H. W. Altman, *J. Phys. Chem.*, **65**, 65 (1961).

(4) T. Rubin, H. L. Johnston, and H. Altman, *J. Am. Chem. Soc.*, **73**, 3401 (1951).

(5) F. A. Willers, "Practical Analysis," R. T. Beyer translation, Dover Publications, 1947, p. 77.

(6) J. B. Scarborough, "Numerical Analysis," Johns Hopkins Press Baltimore, Maryland, 1930, p. 115.

(7) R. Srinivasan, *J. Indian Inst. Sci.*, **37A**, 232 (1955).

(8) Fr. D. Henglein, *Z. physik. Chem.*, **115**, 91 (1925).

TABLE II

t_{avg}, °C.	$\alpha \times 10^6$ this research	$\alpha_s \times 10$	
−164	2.671	2.20	
−141.4	2.916	2.59	
−122.5	3.076	2.93	
−109.5	3.172	3.06	
− 92.0	3.261	3.26	
− 75.6	3.336	3.35	
− 61.0	3.374	3.42	
− 30.2	3.518	3.45	
0	3.627	3.52	
+ 15.0	3.683	3.59	
		$\alpha_h \times 10^5$	ΔT
−132	2.998	2.99	(−184) − (−79)
− 39.5	3.485	3.37	(− 79) − 0
+ 25	3.721	3.67	0 − 50

described in terms of the Grüneisen parameter γ,[9] where $\gamma = 3\alpha/\beta C_V$. V is the molar volume and β is the isothermal compressibility. The rest of the symbols have their usual meaning.

Using the specific heat work of Berg and Morrison,[11] the compressibility data of Durand,[12] a value of the compressibility at the absolute zero given by Slater,[13] and the present data, the Grüneisen parameters were calculated. The results for the computation of the Grüneisen parameters are shown in Fig. 1. The ordinate $\gamma - \gamma_{275°K.}$ is self explanatory. The abscissa $y = \sigma^2/(1 + \sigma^2)$ where $\sigma = h\nu_{max}/2\pi kT$. Here ν_{max} is the maximum lattice vibration frequency. The rest of the symbols have their usual meaning. The value of the vibration frequency ν_{max} was taken as proportional to $\theta = 233°K.$, which is near the maximum value in the high-temperature region.[11] This is within certain limits an arbitrary choice which does not seem to modify the discussion of the variation of the Grüneisen function with temperature. The use of the function y has been justified previously.[3]

The scatter of the individually computed points in Fig. 1 arises mainly from errors in the compressibility values. Below 80°K. the values of the compressibilities used depend upon an extrapolation of Durand's[12] compressibility data to a value at the absolute zero given by Slater.[13] The largest reasonable error this procedure can introduce into the values of γ is about 4%.

Barron[14] has developed a theory for the variation of γ with temperature. For the model, we shall consider that the interionic potential consists of a coulomb term and a repulsion term which was assumed to be of inverse ninth power.

Using the methods outlined previously,[3] for potassium chloride we have

$$\gamma - \gamma_\infty = -0.44y^2 \qquad (1)$$

This function is included in Fig. 1 as curve 1.

The relation 1 does not agree with the experimental curve of $\gamma - \gamma_{275°\alpha}$ of potassium chloride. A comparison of eq. 1 for potassium chloride to relation 6 given by Rubin, Johnston, and Altman[3] shows that there is less curvature in the $\gamma - \gamma_\infty$ function for potassium chloride than that function for sodium chloride. On the other hand, the experimental curve of $\gamma - \gamma_\infty$ for potassium chloride has significantly greater curvature than $\gamma - \gamma_\infty$ for rock salt, curve 2. It is interesting, though, that the experimental values for potassium chloride can be superimposed upon those for rock salt using one multiplying constant. Thus the $\gamma - \gamma_\infty$ function for both salts is a corresponding state function of y. That much is, of course, expressed in relation 1 of this work and the relation for the rock salt work.

Thus, the Kellermann model for NaCl and the corresponding model for KCl do not provide the correct values of the moments $\gamma(2)$ and $\gamma(4)$ used in computing the coefficient in relation 1. There is little hope that addition of higher moments will improve the agreement between this theory and experiment.[15]

Determination of the expansion coefficients of potassium chloride was made from 17 to 275°K. Grüneisen coefficients as a function of temperature were computed using known heat capacities and compressibilities. Correlation of these Grüneisen coefficients with those expected for a sodium chloride lattice has been made.

(9) E. Grüneisen, "Handbuch der Physik," Vol. 10, Springer, Berlin, 1920.

(10) D. Bijl and H. Pullan, *Physica*, **21**, 285 (1955).

(11) W. Berg and J. A. Morrison, *Proc. Roy. Soc.* (London), **A 242**, 467 (1957).

(12) M. A. Durand, *Phys. Rev.*, **50**, 449 (1936).

(13) J. C. Slater, *ibid.*, **23**, 492 (1924).

(14) T. H. K. Barron, *Phil. Mag.*, [7], **46**, 720 (1955).

(15) T. H. K. Barron, private communication.

A MICRO-REACTOR STUDY OF SOME REACTIONS OF C_5 HYDROCARBONS OVER ALUMINA

BY J. C. ROHRER AND J. H. SINFELT

Esso Research and Engineering Co., Linden, N. J.

Received October 31, 1961

The use of a micro-reactor coupled with apparatus for gas chromatographic analysis of the reaction products, as described by Kokes, Tobin, and Emmett,[1] has become a valuable tool in the study of heterogeneous catalysis. In this technique, a small amount of reactant, say 0.05 ml., is injected into a stream of carrier gas which passes over a small charge of catalyst and directly to a chromatographic column for analysis of the reaction products. The technique is rapid, easy to use, and is particularly well suited to applications where one is primarily interested in comparing conversions or product distributions, rather than making detailed kinetic studies.

The present paper discusses the application of the micro-reactor technique to the study of some reactions of a series of C_5 hydrocarbons over alumina. Since alumina is widely used as a catalyst and as a catalyst support for hydrocarbon reactions, there is considerable incentive to learn more about the catalytic properties of alumina. The application of the micro-reactor technique to determine the nature of the products formed from a variety of different hydrocarbons over alumina has added to our knowledge in this area.

(1) R. J. Kokes, H. Tobin, Jr., and P. H. Emmett, *J. Am. Chem. Soc.*, **77**, 5860 (1955).

TABLE I

PRODUCT DISTRIBUTIONS FROM 1-PENTENE, 2-PENTENE, AND 2-METHYL-2-BUTENE[a]

Reactant→	1-Pentene		2-Pentene[b]			2-Methyl-2-butene		
Carrier gas	H_2	He	H_2	He	He	H_2	He	H
Temp., °C.	527	527	527	527	372	527	527	372
Products, wt. %								
C_5-	3.9	2.7	5.0	3.0	..	4.2	2.4	..
2-Methyl-1-butene	7.6	7.6	7.3	7.1	1.3	26.5	23.7	25.6
2-Methyl-2-butene	13.3	12.2	15.0	18.5	5.0	54.5	59.2	71.7
3-Methyl-1-butene	1.4	1.2	1.7	1.5	..	3.3	4.2	2.7
1-Pentene	40.4	41.3	7.7	9.9	10.8	2.2	1.9	..
trans-2-Pentene	21.5	21.8	29.4	25.7	39.5	6.0	5.6	..
cis-2-Pentene	11.9	13.2	33.9	34.3	43.4	3.3	3.0	..

[a] Conditions: carrier gas rate = 1200 cc. (STP) per min., pressure = 1.7 atm. [b] 85% *cis*, 15% *trans*.

Experimental

Procedure.—A small amount of liquid reactant (0.05 ml.) was injected by means of a hypodermic syringe into the carrier gas in the inlet line to the reactor. The reactor pressure was 1.7 atmospheres. The carrier gas was either hydrogen or helium, at a flow rate of 1200 cc. (STP) per min. The reactor was a 1.3-cm. i.d. stainless steel tube (total volume = 20 cc.) surrounded by an electrically heated aluminum block to maintain isothermal operation. A catalyst charge of 1 g., diluted with inert ceramic beads to fill the reactor volume, was used throughout.

The reaction products were analyzed by a chromatographic column coupled directly to the reactor outlet. The column (0.63 mm. i.d., 16 m. in length) contained hexamethylphosphoramide impregnated on firebrick, and was operated at 40°. The data obtained on any given hydrocarbon were not sufficient to obtain a carbon balance. Only the composition of the hydrocarbon fraction, and not the total concentration of hydrocarbons in the reactor effluent, was determined. The amount of carbonaceous deposit on the catalyst at the end of the study indicated that less than 1% of the total hydrocarbon charge was retained by the catalyst.

Materials.—The 1-pentene, cyclopentane, cyclopentene, and 2-methyl-2-butene used in this study were greater than 99 mole % pure. The 2-pentene was a mixture of 85% *cis*-2-pentene and 15% *trans*-2-pentene, while the piperylene (1,3-pentadiene) was a mixture of 70% *trans*-piperylene and 30% *cis*-piperylene. The hydrocarbons were all obtained from Matheson Coleman and Bell. The alumina catalyst was prepared by calcination of β-alumina trihydrate[2] in air for 4 hr. at 593°. The β-alumina trihydrate was obtained from Davison Chemical Co. X-Ray diffraction measurements confirmed that it was β-alumina trihydrate. The surface area of the alumina resulting from the calcination of the trihydrate was 210 $m.^2/g$.

Results

Product distribution data are shown in Tables I and II for each of the hydrocarbons: 2-pentene, 2-methyl-2-butene, 1-pentene, piperylene (1,3-pentadiene), cyclopentane, and cyclopentene. The data were obtained using both helium and hydrogen as carrier gas.

The data on 2-pentene, 2-methyl-2-butene, and 1-pentene in Table I show that all three olefins undergo skeletal isomerization as well as double bond migration at 527° over the alumina catalyst used in this work. In general, the effect of the carrier gas (H_2 or He) on these reactions appears to be small. However, the extent of cracking to lower carbon number compounds (C_5-) appears to be consistently higher in the presence of hydrogen. In the case of 1-pentene and 2-pentene, the relative amounts of the methylbutenes formed are at least directionally in accord with thermodynamic equilibrium data.[3] Furthermore, the relative amounts of 2-methyl-1-butene and 3-methyl-1-butene formed from 2-methyl-2-butene are in rough agreement with thermodynamic data, as are the relative amounts of *trans*- and *cis*-2-pentene formed from 2-methyl-2-butene or 1-pentene. Runs on 2-pentene and 2-methyl-2-butene also were made at a somewhat lower temperature, 372°. These runs showed double bond migration comparable to that observed at 527°, but the extent of skeletal isomerization was appreciably lower and, in the case of 2-methyl-2-butene, none of the latter was observed. This is in line with the general observation that double bond migration takes place more readily than skeletal isomerization.[4]

TABLE II

PRODUCT DISTRIBUTIONS FROM PIPERYLENE, CYCLOPENTANE, AND CYCLOPENTENE[a]

Reactant	Piperylene[b]		Cyclopentane		Cyclopentene	
Carrier gas	H_2	He	H_2	He	H_2	He
Temp., °C.	527	527	527	527	527	527
Products, wt. %						
C_5-	10.1	8.8	1.4	0.5	0.9	
2 Methyl-1-butene	1.9	0.9	0.7			
2-Methyl-2-butene	5.2	2.9	0.8			
3-Methyl-1-butene	0.4					
1-Pentene	1.9	0.8	0.2			
trans-2-Pentene	4.9	1.6	0.3			
cis-2-Pentene	2.4	0.5	0.2			
Cyclopentane			96.4	99.5	1.8	
Cyclopentene	2.1				92.6	100.0
trans-Piperylene	43.1	53.0				
cis-Piperylene	25.2	28.7				
Other pentadienes	2.8	2.8			4.7	

[a] Conditions: carrier gas rate = 1200 cc. (STP) per min., pressure = 1.7 atm. [b] 30% *cis*, 70% *trans*.

Product distribution data for piperylene, cyclopentane, and cyclopentene at 527° are shown in Table II. With respect to the effect of carrier gas, the extent of cracking to lower carbon number compounds (C_5-) again was found to be greater in the presence of hydrogen. Furthermore, there also was a noticeable effect of hydrogen on the other reactions of these compounds. Thus, hydrogen was found to promote the ring splitting of cyclopentane and cyclopentene to C_5 olefins and diolefins, respectively. Furthermore, in the presence of hydrogen increased amounts of C_5 olefins

(2) H. C. Stumpf, A. S. Russell, J. W. Newsome, and C. M. Tucker, *Ind. Eng. Chem.*, **42**, 1398 (1950).

(3) "Selected Values of Physical and Thermodynamic Properties of Hydrocarbons and Related Compounds," API Research Project 44, Carnegie Press, Inc., New York, N. Y., 1953.

(4) F. E. Condon, "Catalysis," Vol. 6, Reinhold Publishing Corp., New York, N. Y., 1958, p. 98.

were formed from piperylene, suggesting direct hydrogenation by hydrogen. In addition, some hydrogenation of cyclopentene to cyclopentane was observed in the presence of hydrogen.

In the case of piperylene, hydrogen transfer reactions also appear to occur, as evidenced by the formation of C_5 olefins from the piperylene in the complete absence of hydrogen, *i.e.*, in the presence of helium as a carrier gas. The piperylene also was found to cyclize to cyclopentene in the presence of hydrogen. Some double bond migration to other pentadienes also was observed.

Discussion

Double bond migration and skeletal isomerization of olefins over alumina have been interpreted in terms of carbonium ion mechanisms.[5] In a similar manner, the hydrogen transfer and cyclization reactions of piperylene observed in this work can be explained by carbonium ion mechanisms

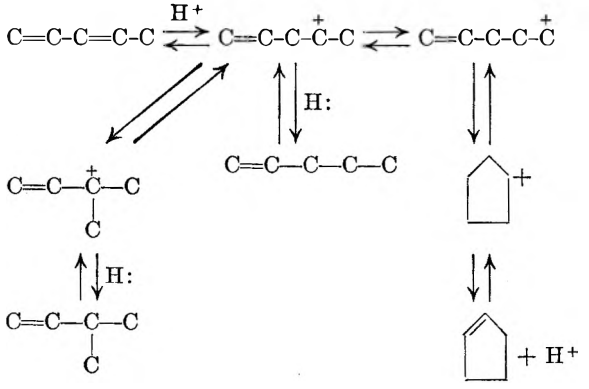

where H: represents a hydride ion donated by piperylene or another hydrocarbon molecule in the system. In the case of cyclization of piperylene, a primary carbonium ion is an intermediate. Since a primary carbonium ion is quite unstable compared to secondary and tertiary ions, the extent of cyclization is limited. One would expect hexadiene, for example, to cyclize more readily to a five-membered ring structure (methylcyclopentene) since the intermediate would be a secondary carbonium ion.

That alumina possesses hydrogenation activity is evident from the observed hydrogenation of some of the olefins in the presence of hydrogen. The hydrogenation activity of alumina has been noted before.[6,7] The effect of hydrogen on the ring splitting reaction also has been observed in a previous study on methylcyclopentane,[8] in which it was suggested that hydrogen might enhance the acidity of the alumina and hence increase the catalytic activity for these reactions. However, it is also conceivable that the role of hydrogen may be one of keeping the surface free of carbonaceous residues which lower the activity of the alumina.[8]

(5) W. O. Haag and H. Pines, *J. Am. Chem Soc.*, **82**, 2488 (1960).
(6) V. C. F. Holm and R. W. Blue, *Ind. Eng. Chem.*, **43**, 501 (1951).
(7) S. W. Weller and S. G. Hindin, *J. Phys Chem.*, **60**, 1501 (1956).
(8) J. H. Sinfelt and J. C. Rohrer, *ibid.*, **65**, 2272 (1961).

EQUILIBRIUM CONSTANT OF A HYDROGEN BONDING SYSTEM: PHENOL–PYRIDINE

By Asish Kumar Chandra and Shantimoy Banerjee

Department of Chemistry, University College of Science and Technology, Calcutta 9, India

Received November 6, 1961

Although the existence of intermolecular hydrogen bonds in solution can be recognized from the observation of anomalous absorption spectra of π-electron systems, few values have been reported for hydrogen bond energies of various proton donors interacting with proton acceptors. In a previous communication, Chandra and Basu[1] reported the free energy change of hydrogen-bonded complexes of some π-electron systems with different aliphatic alcohols. In their paper, equilibrium constants were measured from the $n\rightarrow\pi^*$ blue-shift and the optical density measurements at the peak, while Nagakura and Baba[2] measured the equilibrium constants and the hydrogen bond energies of phenol with ether and dioxane from the $\pi\rightarrow\pi^*$ red-shift of the aromatic molecule and the temperature dependence of the spectra. In all the previous cases, the physico-chemical basis underlying the method of calculating the equilibrium constants was the Benesi and Hildebrand equation or its modifications. These methods have a common failing, namely, they cannot be applied to the cases where both the donor and the acceptor have comparable absorption in the wave length region of interest. It is the purpose of the present note to develop a simple expression which will treat the spectral data specifically in the region where both of the components, donor and acceptor, and the complex have appreciable absorption and permit a direct evaluation of equilibrium constants with minimum computation.

Method of Calculation.—Let the equilibrium be represented by

$$A + B \rightleftarrows AB \qquad K = \frac{C}{([A] - C)([B] - C)} \quad (1)$$

where [A] and [B] represent the initial concentrations of the two components, and C, the equilibrium concentration of the hydrogen bonded complex. The optical density per cm. of path (O.D.) of a solution containing the molecular species (1) is given by

$$\text{O.D.} = \epsilon_c C + \epsilon_1([A] - C) + \epsilon_2([B] - C) \quad (2)$$

where ϵ_0, ϵ_1, and ϵ_2 are the molar extinction coefficients of AB, A, and B, respectively.

Suppose

$$[B] = m[A] \quad (3)$$

whence

$$\text{O.D.} = (\epsilon_c - \epsilon_1 - \epsilon_2)C + (\epsilon_1 + m\epsilon_2)[A] \quad (4)$$

Let us write

$$D = \text{O.D.} - (\epsilon_1 + m\epsilon_2)[A] = \bar{\epsilon}C \quad (5)$$

where

$$\bar{\epsilon} = (\epsilon_c - \epsilon_1 - \epsilon_2)$$

(1) A. K. Chandra and S. Basu, *Trans. Faraday Soc.*, **56**, 632 (1960).
(2) S. Nagakura and H. Baba, *J. Am. Chem. Soc.*, **74**, 1221 (1952).
(3) H. P. Stephenson, *J. Chem. Phys.*, **22**, 1077 (1954).

From eq. 1 and 3 and neglecting C^2 we get

$$m[A]^2K - (1 + m)[A]KC = C \qquad (6)$$

When eq. 5 is substituted into (6) there results

$$\frac{m[A]}{(1 + m)D} - \frac{1}{\epsilon} = \frac{1}{K\epsilon}\frac{1}{(1 + m)[A]} \qquad (7)$$

The relation 7 shows that the plot of $[B]/(1 + m)D$ against $1/(1 + m)[A]$ should be linear, if 1:1 complex formation occurs. From the intercept and slope of the line the equilibrium constant and molar extinction coefficient of the complex may be calculated. This method has been followed in the present investigation to obtain the equilibrium constant of the hydrogen bonded complex of phenol with pyridine and also to estimate the hydrogen bond energy from the temperature dependence of the equilibrium constant. Further investigations with similar systems are in progress.

Experimental

The compounds phenol and pyridine were obtained from commercial sources and were purified by recommended methods. The *n*-heptane, the non-hydrogen bonded solvent, was a Merck G. R. quality sample showing a cut-off at 220 mμ. Spectral measurements were made in a Beckman Model DU spectrophotometer using 1-cm. silica cells at three different temperatures (22, 30, and 40°).

Results and Discussion

The $\pi \rightarrow \pi^*$ band of phenol is known to undergo a red-shift whenever the phenol interacts with the solvent through the formation of a hydrogen bond. The magnitude of the shift in the band is about 30–40 Å., as a result of this effect. It is expected, therefore, that if to a *n*-heptane solution of phenol an increasing amount of pyridine was added, the $\pi \rightarrow \pi^*$ band of phenol should move regularly to the red, because it is established from other sources that phenol forms a strong hydrogen-bonded complex with pyridine in solution. But in view of the strong overlap between the $n \rightarrow \pi^*$ band of pyridine and the $\pi \rightarrow \pi^*$ band of phenol, the position of the new peak due to the complex cannot be located in the absorption spectra of a phenol–pyridine mixture. With the presumption that the position of the peak due to the complex should appear on the longer wave length side of the phenol band, O.D. measurements for the determination of the equilibrium constant were made on a mixture of phenol and pyridine at several wave lengths between 280–290 mμ. The plot of $[B]/(1 + m)D$ against $1/(1 + m)[A]$ was found to be linear at all wave lengths. [B] represents the variable concentration of pyridine and [A] the constant concentration of phenol. From the slope and intercept of these curves, the equilibrium constant for the hydrogen bonded complex was calculated using relation 7. No appreciable difference in K-values was noted for measurements at different wave lengths between 280–290 mμ. Figure 1 shows one such plot at 285 mμ and at three different temperatures. The results are summarized in Table I.

TABLE I

Concn. of phenol, mole/l.	Range of values of m	Temp., °C.	K	$-\Delta G$, kcal./mole	$-\Delta H$, kcal./mole	$-\Delta S$ e.u.
		22	88	2.642	6	11.4
7.68×10^{-4}	3–8	30	66	2.538	6	11.4
		40	49	2.436	6	11.4

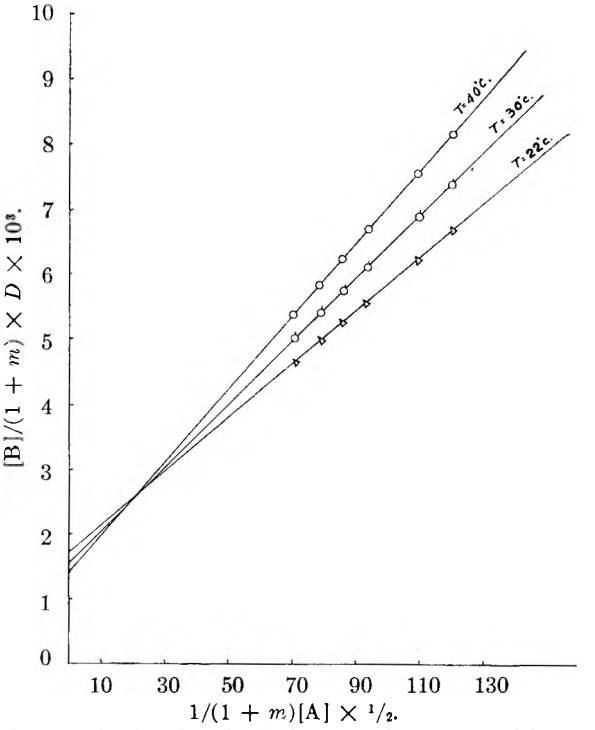

Fig. 1.—Plot for phenol–pyridine complex at three different temperatures.

It may be argued in this connection that the $n \rightarrow \pi^*$ band of pyridine which appears at 270 mμ[3] should shift to the blue when it interacts with phenol through the formation of a hydrogen bond. So from the spectral measurements at the shorter wave length side of the pyridine band the equilibrium constant for the phenol–pyridine complex may be calculated and compared with the above K-values. But the concentrations of pyridine and phenol could not be so adjusted as to make the O.D. measurements in the aforesaid region accurate to within 5%. Moreover, the calculated absorption curve of the complex (Fig. 2) shows a band at 282 mμ which has almost the same intensity as the 278 mμ band of phenol, while the blue-shift of the pyridine band is associated with some other complicating factors. The calculated absorption curve II of the complex in Fig. 2 is obtained using the optical density measurements of a particular phenol–pyridine mixture[4] in the wave length region 260–290 mμ and knowing the equilibrium constant at a definite temperature.

The enthalpy change for complex formation was calculated from the slope of the log K–$1/T$ curve and the entropy change then was calculated from the usual thermodynamic relation. Values of these quantities are recorded in Table I. It is to be noted that this value of $-\Delta H$ is distinctly higher than the 5 kcal./mole reported previously by Pimentel and McClellan[5] for the phenol–pyridine complex from infrared absorption measurements. The evidence for a higher value of $-\Delta H$ for the phenol–pyridine complex than 5 kcal./mole is obtained as follows. Using the optical

(4) The concentrations of phenol and pyridine are so adjusted as to make the O.D. measurements accurate to within 5%.

(5) G. C. Pimentel and A. L. McClellan, "The Hydrogen Bond," W. H. Freeman & Co., San Francisco, Cal., 1960.

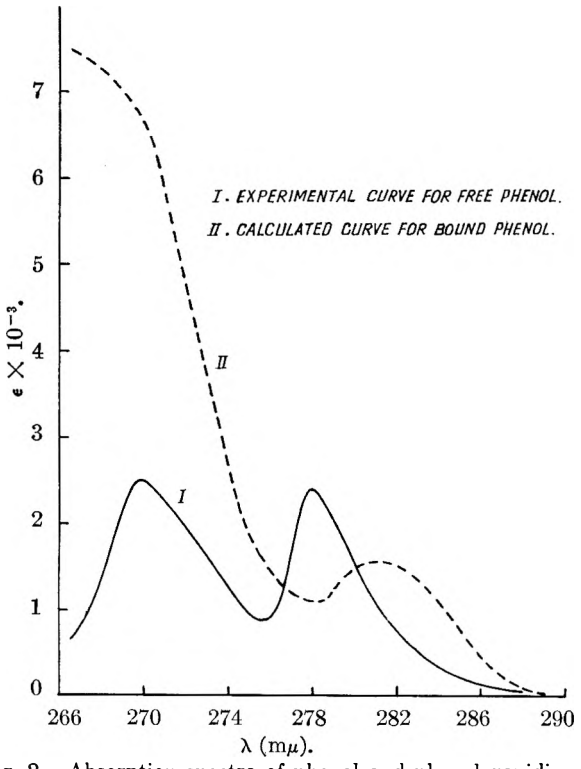

Fig. 2.—Absorption spectra of phenol and phenol–pyridine complex in *n*-heptane.

density measurements in the infrared region the integrated molar absorption coefficient B_0 for the absorption band due to the hydrogen bonded complex may be calculated. Becker[6] found a good correlation between B_0 and ΔH for a variety of hydrogen bonding systems. The reported B_0 value[7] for the phenol–pyridine complex is very high, indicating a higher $-\Delta H$ value from the ΔH–B_0 relation than 5 kcal./mole. Considering the limitation in the accuracy of the present graphical method we may conclude that the calculated shift of the phenol band on the longer wave length side in the presence of pyridine is due mainly to the hydrogen bonding effect.

Acknowledgment.—Sincere thanks are due to Professor B. N. Ghosh for providing all laboratory facilities and encouragement during the course of this work.

(6) E. D. Becker, private communication, National Institutes of Health, Bethesda 14, Maryland.

(7) N. Fuson, P. Pineau, and M. L. Josien, *J. chim. phys.*, 454 (1958).

THE CHLOROPHYLL-SENSITIZED PHOTOREDUCTION OF THIONINE BY ASCORBIC ACID

By K. G. Mathai and E. Rabinowitch

Photosynthesis Laboratory, Department of Botany, University of Illinois, Urbana, Illinois

Received November 9, 1961

Krasnovsky and Brin[1,2] reported that dyes, such as riboflavin, safranin, and Nile Blue, accelerate the regeneration of chlorophyll *a* from its pink reduced form ("eosinophyll"), which is formed by illumination of air-free solutions of chlorophyll and ascorbic acid in pyridine. Bannister[3] showed that no bleaching occurs in dry pyridine, and that 10% or more water is needed for this reaction.

In ternary systems (chlorophyll + ascorbic acid + dye) chlorophyll sensitizes the photochemical reduction of certain dyes by ascorbic acid.

The kinetics of chlorophyll-sensitized reactions of this type was studied by Livingston and Pariser.[4,5] They found that in the case of chlorophyll-sensitized photoreduction of methyl red by phenylhydrazine, the quantum yield is a function of the concentration of methyl red; over a fairly wide range, this yield is independent of light intensity and of the concentration of chlorophyll. A similar observation was made for the pheophytin-sensitized photoreduction of the dye butter yellow by ascorbic acid.

Previously, studies were made in our Laboratory of the kinetics of photoreduction of chlorophyll *a* by ascorbic acid, *cf.* Bannister[3]; and of the photoreduction of thionine by ferrous ions, *cf.* Ainsworth.[6] We were interested in the possibility of coupling these two reactions, *i.e.*, of achieving chlorophyll *a*-sensitized reduction of thionine by ascorbate, and of thionine-sensitized reduction of chlorophyll *a* by ferrous ions. Following are some observations on the first-named reaction; they are quite analogous to Livingston's observations on other chlorophyll-sensitized dye reductions.

Experimental

Thionine (biological stain of the National Aniline and Chemical Co., Inc.) was purified by repeated recrystallization; the purity of the sample was checked by spectroscopy. Chlorophyll *a* was prepared from fresh spinach by Holt's[7] method. Ascorbic acid (Mallinckrodt USP) was used without further purification. 30% aqueous pyridine was made up from Fisher's "reagent grade" pyridine and double-distilled water. Oxygen-free samples, containing appropriate amounts of chlorophyll, ascorbic acid, and thionine in 30% aqueous pyridine, were illuminated by an "actinic" beam from a 1000-watt projection lamp, operated from a 2000-watt Sola constant voltage transformer. The beam passed through a heat filter and was made parallel by a condensing lens 12 cm. in diameter. A Farrand interference filter, with maximum transmission at 670 mμ (roughly corresponding to the absorption maximum of chlorophyll in pyridine) was inserted into the beam. The photolytic cell was placed in a bath through which water from a thermostat was circulated. The "scanning" beam from a ribbon filament lamp was focused, under right angle to the actinic beam, on the center of the cell. The intensity of the scanning beam was regulated by a variable aperture and was kept low enough not to cause measurable photolysis. The intensity of the scanning beam transmitted by the reaction mixture was recorded photoelectrometrically, using a Farrand monochromator and Tektronic 520 oscilloscope. The sweep time of the latter was fast compared to the measured reaction times. The intensity of the actinic light was measured with an Eppley thermopile, calibrated as described by Bannister.[3]

By using solutions with different concentrations of chlorophyll, an empirical calibration curve, relating the transmission of actinic light to the optical density at 670 mμ, was determined with a Beckman DU spectrophotometer. Using

(1) A. A. Krasnovsky and G. P. Brin, *Compt. rend. acad. sci. U.R.S.S.*, **67**, 325 (1949).

(2) A. A. Krasnovsky and G. P. Brin, *ibid.*, **73**, 1239 (1950).

(3) T. T. Bannister, *Plant Physiol.*, **34**, 246 (1959); Thesis, Univ. of Illinois, 1958.

(4) R. Livingston and R. Pariser, *J. Am. Chem. Soc.*, **78**, 2944 (1956).

(5) R. Livingston and R. Pariser, *ibid.*, **78**, 2948 (1956).

(6) S. Ainsworth, *J. Am. Chem. Soc.*, **70**, 1510 (1948).

(7) E. E. Jacobs, A. E. Vatter, and A. S. Holt, *Arch. Biochem. Biophys.*, **58**, 228 (1954).

the known molar extinction coefficient of chlorophyll *a* in pyridine at 670 mμ (79 × 10⁴), the chlorophyll concentration could be computed from the optical density. A similar procedure was used to compute the concentration of thionine, using a calibration curve relating transmission to optical density at 600 mμ, and the molar extinction coefficient of thionine at 600 mμ given by Rabinowitch and Epstein[8] (5.7 × 10⁴). A correction was applied for the absorption of chlorophyll *a* at 600 mμ.

The photochemical reaction was initiated by opening the oscilloscope camera shutter, which was synchronized with a trigger pulse to the oscilloscope and with the opening of a shutter at the focus of the condenser. The initial quantum yields were obtained by measuring the rate of thionine bleaching during the first 5 to 10% of the reaction. The concentration of chlorophyll was checked at the beginning and at the end of each run. The results of these experiments are given in Table I.

TABLE I

SUMMARY OF RESULTS (t = 25°)

Chl = chlorophyll, A = ascorbic acid, T = thionine, I = absorbed quantum flux

Exp. no.	[Chl] × 10⁶, mole/l.	[A] × 10², mole/l.	[T] × 10⁵, mole/l., initial	[T] × 10⁵, mole/l., final	I × 10⁵, einst./sec./l.	φ × 10²	K × 10⁴
1	1.4	1.0	1.0	0.94	7.8	3	1.47
2	1.4	1.0	1.0	0.95	4.3	2.5	1.80
3	1.4	1.0	1.0	0.92	1.6	3	1.44
4	1.4	1.0	2.0	1.91	7.3	7	1.17
5	1.4	1.0	2.0	1.92	4.2	8	1.01
6	1.4	1.0	2.0	1.90	1.6	8	0.97
7	1.4	1.0	4.0	3.70	7.7	11	1.31
8	1.4	1.0	4.0	3.80	4.4	9	1.73
9	1.4	1.0	4.0	3.70	1.5	10	1.48
10	1.4	1.0	6.0	5.50	7.6	12	1.74
11	1.4	1.0	6.0	5.60	4.6	13	1.59
12	1.4	1.0	6.0	5.40	1.8	12	1.75
13	1.4	5.0	1.0	0.42	7.4	2	2.21
14	1.4	5.0	2.0	1.92	7.6	7	1.18
15	1.4	5.0	4.0	3.90	7.4	10	1.56
16	2.5	5.0	6.0	5.50	7.5	13	1.57
17	2.5	1.0	1.0	0.93	8.3	3	1.46
18	2.5	1.0	2.0	1.94	8.4	6	1.23
19	2.5	1.0	4.0	3.8	8.2	11	1.35
20	2.5	1.0	6.0	5.6	8.6	14	1.44
21	0.75	1.0	1.0	0.91	7.1	2.5	1.73
22	0.75	1.0	2.0	1.91	7.2	8	1.14
23	0.75	1.0	4.0	3.90	7.0	11	1.38
24	0.75	1.0	6.0	5.60	7.1	12	1.75
							1.47

Table I shows that the quantum yield (ϑ) is independent of the concentration of chlorophyll and of the absorbed light intensity. At high ascorbic acid concentrations, used in these experiments, ϑ is also independent of [A], and thus a function of the concentration of thionine alone. These observations are quite similar to those made by Livingston and co-workers[5] on other chlorophyll-sensitized oxidation–reduction systems, and can be interpreted by the two mechanisms suggested by Livingston

	Mechanism I	Mechanism II	
(1)	$Chl + h\nu \longrightarrow Chl^*$	$Chl + AH_2 \rightleftharpoons ChlAH_2$	(1)
(2)	$Chl^* \longrightarrow Chl + h\nu$	$Chl + h\nu \longrightarrow Chl^*$	(2)
(3)	$Chl^* \longrightarrow Chl'$	$Chl^* \longrightarrow Chl + h\nu$	(3)
(4)	$Chl' \longrightarrow Chl$	$Chl^* \longrightarrow Chl' \longrightarrow Chl$	(4), (4a′)
(5)	$Chl' + AH_2 \longrightarrow AH_2Chl'$	$ChlAH_2 + h\nu \longrightarrow AH_2Chl'$	(5)

(8) E. Rabinowitch and L. F. Epstein, *J. Am. Chem. Soc.*, **63**, 69 (1941).

$$AH_2Chl' \longrightarrow Chl + AH_2 \quad (6)$$

$$D + AH_2Chl' \longrightarrow Chl + AH + DH \quad (7)$$

$$2DH \longrightarrow DH_2 + D \quad (8)$$

$$2AH \longrightarrow AH_2 + A \quad (9)$$

Here, Chl = chlorophyll
Chl′ = chlorophyll in the triplet state
Chl* = chlorophyll in the first excited singlet state
AH_2 = reductant (ascorbic acid); D = dye (thionine)

Both mechanisms lead to eq. 1

$$\vartheta \cong \frac{1}{2}\left[\frac{[AH_2]}{K' + [AH_2]} \times \frac{[D]}{K + [D]}\right] \quad (1)$$

where ϑ is the (experimentally determined) ratio of the number of moles of dye reduced to the number of einsteins absorbed; when $[AH_2]$ is large compared to K', eq. 1 is reduced to

$$\vartheta \cong \frac{1}{2}\left[\frac{[D]}{K + [D]}\right] \quad (2)$$

In the first of the above two mechanisms, it is assumed that ascorbic acid reacts with chlorophyll, in its metastable state Chl′, forming an unstable reactive complex AH_2Chl'. In the second mechanism, the formation of a complex is postulated to occur between ascorbic acid and chlorophyll in the ground state. This complex, AH_2Chl, is activated by absorption of light, to form the reactive complex, AH_2Chl'. The latter may either decompose spontaneously or react with a dye molecule.

In both mechanisms $K = k_6/k_7$. In mechanism I, K' is determined by competition of reaction 5 with radiationless dissipation (4); while in mechanism II, K' is the dissociation constant of the complex $Chl \cdot AH_2$. The reaction is assumed to be due, in both mechanisms, to encounters between excited complexes AH_2Chl' and dye molecules. The rate equation 2 derived from these mechanisms represents satisfactorily our data obtained at the higher concentration of ascorbic acid (from 0.01 to 0.05 M) as shown by lack of regular variations in the K value in Table I. The value of K' in mechanism I, was given by Livingston and Pugh[9] as $K' = 3.2 \times 10^{-6}$ mole^{-1}; it is so small that calculating K from eq. 1 instead of eq. 2 would make no significant difference.

Discussion

The function of chlorophyll in photosynthesis may be analogous to its role in the above-discussed chlorophyll-sensitized dye reductions. The primary oxidation and reduction products must be prevented, in photosynthesis, from reacting back. Recently,[10] we have shown how the products of photochemical thionine reduction by ascorbate can be stabilized by distribution between immiscible solvents, thus storing some of the absorbed light energy. In photosynthesis, too, the energy-rich products may be stabilized by distribution between two phases–*e.g.*, a hydrophilic and a hydrophobic layer adjoining the pigment monolayer.

As suggested in schemes (I) and (II), chlorophyll acts, in sensitization, in the metastable triplet state, rather than in the unstable singlet excited state.

The existence of such a long-lived form of excited chlorophyll has been established by kinetic evidence, and by comparison of the quantum yields of fluorescence with those of certain autoöxidations sensitized by chlorophyll. "Quenching" of this state of chlorophyll by ascorbic acid was demonstrated by Livingston and Pugh[9] (quenching constant $k_q = 3.4 \times 10^5$ mole^{-1} for ascorbic acid in pyridine solution containing 2% or more water). The inverse of k_q is the constant K' used above.

(9) R. Livingston and A. C. P. Pugh, *Nature*, **186**, 969 (1960).

(10) K. G. Mathai and E. Rabinowitch, *J. Phys. Chem.*, **66**, 663 (1962).

DISPLACEMENT REACTIONS AT THE SULFUR ATOM. III. THE REACTION OF CYANIDE WITH THIOSULFATE[1]

By Robert Earl Davis

Department of Chemistry, Purdue University, Lafayette, Indiana

Received December 16, 1961

Cyanide ion has a high nucleophilic character toward displacement at saturated carbon atoms. In a previous study on the mechanism of reaction of cyanide with sulfur,[2] the term "thiophilic" was suggested to describe the displacement on sulfur atoms. Several single-sulfur transfer reactions also were discussed.

$$XS + Y \longrightarrow X + SY \qquad (1)$$

The reaction of thiosulfate ($X = SO_3^{-2}$) with cyanide ($Y = {}^-CN$) was briefly reviewed[3] and new data[2] were presented.

The rate expression

$$\text{rate} = k_2(CN^-)(S_2O_3^{-2}) \qquad (2)$$

was found[3] and confirmed.[2] Ishikawa reported a linear dependence between k_2 and the ionic strength, μ, at moderately high salt concentrations. In view of the importance of the reaction of thiosulfate and cyanide to biochemistry,[4-10] analytical chemistry,[10-12] and the theoretical chemistry of displacement reactions at the sulfur atom,[1,13-15] new data on the forward and reverse reaction are presented.

$$CN^- + SSO_3^{-2} \underset{k_{-2}}{\overset{k_2}{\rightleftharpoons}} SCN^- + SO_3^{-2} \qquad (3)$$

Experimental

All salts were Merck or Mallinckrodt analytical reagent grade. Stable salts were dried at 120° while thiosulfate solutions were standardized against potassium iodate and cyanide solutions against silver nitrate. All solutions were prepared at 25.0° using conductivity water. Experiments were performed in deoxygenated solutions under pure nitrogen. Special care was taken to avoid contamination by copper(II) and saliva, both excellent catalysts. Individual sealed tubes and closed flasks with aliquot-withdrawing ports were used. Aliquots were withdrawn and the reaction was quenched by cooling. The optical density then was measured at 270 or 260 mμ[2,16] at 25.00 ± 0.01°. Alternatively aliquots were quenched in acidified iodine solution in a good hood (*caution:* HCN) and then titrated with standard thiosulfate. Both methods gave identical results within 2%.

Results and Discussion

The rate expression (2) adequately describes the reaction when the cyanide ion concentration has been varied from 2×10^{-3} to 2.5×10^{-1} M and the thiosulfate concentration varied from 2×10^{-3} to 1.2×10^{-1} M (Table I). The value of the observed second rate constant is a function[3] of the pH. The data indicate that cyanide ion is many thousands of times more effective than hydrogen cyanide. The second-order rate constant, k_2, is a function of the ionic strength. Salts such as potassium chloride and potassium thiocyanide increase the rate. The data are in accordance with the predictions of the Brönsted–Christiansen–Scatchard

Table I

T, °C.	KCN, M	$Na_2S_2O_3$, M	Salt	μ, M	k_2, M^{-1} sec.$^{-1}$
25.00	0	0		0	1.20×10^{-5}[a]
	0.002	0.002		0.008	1.71×10^{-5}
	.005	.005		.02	2.21×10^{-5}
	.050	.050		.20	3.96×10^{-5}
	.120	.006		.14	3.90×10^{-5}
	.070	.007		.09	3.92×10^{-5}
	.251	.12		.63	4.50×10^{-5}
	.002	.002	KCl	.01	1.92×10^{-5}
	.002	.002	KCl	.02	2.18×10^{-5}
	.002	.002	KCl	.25	4.30×10^{-5}
	.002	.002	KSCN	.01	1.94×10^{-5}
	.002	.002	KSCN	.15	3.79×10^{-5}
	.002	.002	KSCN	.20	4.34×10^{-5}
69.84	0	0		0	1.23×10^{-4}[a]
	0.003	0.002		0.009	1.81×10^{-4}
	.052	.053		.20	4.01×10^{-4}
	.070	.007		.09	2.94×10^{-4}
	.250	.123		.63	6.98×10^{-4}
	.253	.125	NaCl	.88	7.68×10^{-4}
90.00	0	0		0	3.61×10^{-4}[a]
	0.002	0.002		0.008	5.12×10^{-4}
	.006	.005		.021	6.32×10^{-4}
	.140	.005		.15	8.90×10^{-4}
	.007	.026		.09	8.60×10^{-4}

[a] Extrapolated to $\mu = 0$.

(BCS) equation. A plot of log k_2 *vs.* $\mu^{1/2}$ is linear with a slope of 1.9 below $\mu^{1/2} = 0.15$. Above $\mu^{1/2} = 0.15$ the slope decreases. Ishikawa's data, obtained at $\mu^{1/2} \cong 0.70$, show a more linear dependence of log k_2 with μ. Extrapolation to infinite dilution gives $k_2 = 1.20 \pm 0.06 \times 10^{-5}$ M^{-1} sec.$^{-1}$ at 25°, $1.23 \pm 0.03 \times 10^{-4}$ at 69.84°, and $3.61 \pm 0.09 \times 10^{-4}$ at 90.00°. From these data $\Delta H^* = 12.4 \pm 0.4$ kcal./mole and $\Delta S^* = -39 \pm 3$ cal./mole deg. at 25°. The sign and magnitude of ΔS^* agrees with the positive slope of 1.9 for the reaction of two anions.[17]

A mechanism postulated by Foss[19] and consistent

(1) Part II. R. E. Davis, *J. Phys. Chem.*, **62**, 1599 (1958).

(2) P. D. Bartlett and R. E. Davis, *J. Am. Chem. Soc.*, **80**, 2513 (1958).

(3) F. Ishikawa, T. Murooka, and H. Hagisawa, *Sci. Reports Tohoku University I*, **21**, 511 (1932).

(4) Thiosulfate has been used as an antidote for cyanide poisoning.

(5) B. Mukerji, *Indian Med. Gaz.*, **72**, 353 (1937).

(6) R. G. Smith, B. Mukerji, and J. H. Seabury, *J. Pharmacol.*, **68**, 351 (1940).

(7) B. H. Sorbo, *Acta Chem. Scand.*, **7**, 32 (1953).

(8) B. H. Sorbo, *ibid.*, **7**, 1192 (1953).

(9) C. A. McChesney, *Nature*, **181**, 347 (1958).

(10) B. H. Sorbo, *Biochim. Biophys. Acta*, **23**, 412 (1957).

(11) A. Gutman, *Z. anal. Chem.*, **47**, 294 (1908).

(12) O. A. Nietzel and M. A. Desesa, *Anal. Chem.*, **27**, 1839 (1955).

(13) O. Foss, "Ionic Scission of the Sulfur–Sulfur Bond," in "Organic Sulfur Compounds," Vol. I, N. Kharasch, ed., Pergamon Press, New York, N. Y., 1961, pp. 83–96 and references cited.

(14) W. A. Pryor, "Mechanisms of Sulfur Reactions," McGraw-Hill Book Co., Inc., New York, N. Y., 1962.

(15) R. E. Davis, "A Critique of Some Reactions of Elemental Sulfur," in "Organic Sulfur Compounds," Vol. II, N. Kharasch, ed., Pergamon Press, New York, N. Y., 1962.

(16) D. P. Ames and J. E. Willard, *J. Am. Chem. Soc.*, **75**, 3267 (1953).

(17) Simple electrostatic theory[18] predicts that

$$\Delta S_{el}^* = \frac{-Z_A Z_B e^2}{Dr^*} \left(\frac{\partial \ln D}{\partial T}\right)_P$$

while the slope of the BCS equation is equal to $1.018 Z_A Z_B$ at 25°.

(18) A. A. Frost and R. G. Pearson, "Kinetics and Mechanism," 2nd ed., John Wiley and Sons, Inc., New York, N. Y., 1961, pp. 136, 150.

(19) O. Foss, *Acta Chem. Scand.*, **1**, 307 (1947).

with the data is a direct displacement of the cyanide ion on the thio sulfur. Even though this sulfur atom bears negative charge, a negatively charged thiophile can abstract it in a reaction of low activation energy. We are biased by electrostatic and symmetry considerations and suggest a linear CSS system in the activated complex.

The position of the equilibrium of reaction 3 lies far to the right. Sorbo[20] using the enzyme rhodanase could not detect more than 10^{-6} M cyanide remaining after reaction of 0.1 M cyanide with 0.1 M thiosulfate. We have heated 0.1 M thiocyanate with 0.1 M sulfite at 90° for ten weeks. No cyanide was detected using the cupric acetate benzidine reagent.[21] The limit of detection of cyanide is about 9×10^{-7} M. Thus the equilibrium constant of reaction 3 is at least 10^{+10} or greater. Assuming $K = 10^{+10}$ the upper limit of k_{-2} is of the order of 10^{-15} M^{-1} sec.$^{-1}$ at 25°. This rate constant corresponds to a first half-time of *about one billion years* at 0.01 M concentrations.

Foss[13,22] has suggested that thio-containing thiophiles can be ranked in order of their thiophilicity on the basis of their oxidation potentials for $2XS^- \rightarrow XSSX + 2e^-$. The necessary potentials are given in Table II. The values for sulfite and cyanide ion have been calculated from the free energies.[23] The usefulness of Foss's treatment can be generalized to include other ions such as cyanide. The data of Table II are of interest in several respects. (1) An ion of higher E^0 value will displace an ion of lower E^0. Thus cyanide displaces sulfite. (2) The E^0 values of sulfite and thiosulfate are nearly identical but subject to differential changes as the pH is varied. Thus thiosulfate will displace bisulfite (as in the decomposition of thiosulfate in acid[24]) and sulfite will displace thiosulfate (reaction of sulfite with sulfur).

TABLE II

OXIDATION POTENTIALS IN AQUEOUS SOLUTION

X^-	E^0	Ref.
SCN^-	−0.77	[a]
$S_2O_3^{-2}$	− .08	[b]
SO_3^{-2}	(− .03)	[c]
CN^-	+ .18	[d]

[a] Value reported by N. Bjerrum and A. Kirschner, "Die Rhodanide des Goldes und das freie Rhodan," Copenhagen, 1918. [b] Reference 23, p. 75. [c] Calculated from ΔF°'s given in ref. 23. $\Delta F^{\circ}_{S_2O_6^{-2}}$ may be too large, ref. 23, p. 77. [d] Calculated from ΔF°'s given in ref. 23, p. 129.

Acknowledgment.—This work on the theory of displacement reactions at the sulfur atom was supported by a grant from the Walter Reed Army Institute of Research.

(20) B. H. Sorbo, *Acta Chem. Scand.*, **7**, 1132 (1953).

(21) F. Feigl, "Spot Tests," Vol. I, 4th ed., Elsevier Press, Houston, Texas, 1954, pp. 258–260, 267.

(22) O. Foss, *Acta Chem. Scand.*, **1**, 307 (1947).

(23) W. M. Latimer, "The Oxidation Potentials of the Elements and their Potentials in Aqueous Solutions," 2nd ed., Prentice-Hall, Inc., New York, N. Y., 1952, pp. 72, 129.

(24) R. E. Davis, *J. Am. Chem. Soc.*, **80**, 3565 (1958).

COMMUNICATIONS TO THE EDITOR

THE IONIZATION POTENTIALS OF CYCLOPROPYL RADICAL AND CYCLOPROPYL CYANIDE[1]

Sir:

Only recently have determinations of the ionization potentials of cycloalkyl radicals been made.[2] Pottie, Harrison, and Lossing[2] made a direct determination of the ionization potential of cyclopropyl radicals formed in small yields by the thermal decomposition of cyclopropyl nitrite and found I(cyclopropyl) = 8.05 ± 0.1 e.v. From a study which is briefly described below, we have determined I(cyclopropyl) = 7.8 ± 0.4 e.v. by an indirect method.

Cyclopropyl cyanide (Aldrich Chemical Company) was admitted in the vapor phase to the ion source of the time-of-flight mass spectrometer previously described[3] and appearance potentials were determined for the various ions using both the extrapolated voltages difference method[4] and the energy compensation technique.[5] For the determination of I(cyclopropyl), we are concerned with the ions of m/e = 41 (70 e.v. relative abundance = 100%) and m/e = 26 (70 e.v. relative abundance = 14%), since their formation involves complementary reactions; *i.e.*

$$C_3H_5CN \longrightarrow C_3H_5^+ + CN + e^- \qquad (1)$$

and

$$C_3H_5CN \longrightarrow CN^+ + C_3H_5 + e^- \qquad (2)$$

We found the appearance potential of m/e = 41 to be 12.70 ± 0.15 e.v. and the appearance potential of m/e = 26 to be 19.5 ± 0.4 e.v. These deviations were derived from the reproducibility of the measurements, and do not necessarily indicate the absolute limits of error. From the above results, the heat for the reaction

$$CN^+ + C_3H_5 \longrightarrow CN + C_3H_5^+ \qquad (3)$$

is −6.8 e.v. However, the ionization potential of the CN radical has been determined to be 14.55 e.v.[6–8] Therefore, we calculate the ionization poten-

(1) This work was supported in part by the U. S. Atomic Energy Commission under Contract No. AT(11-1)-751 with Kansas State University.

(2) R. F. Pottie, A. G. Harrison, and F. P. Lossing, *J. Am. Chem. Soc.*, **83**, 3204 (1961).

(3) E. J. Gallegos and R. W. Kiser, *ibid.*, **83**, 773 (1961).

(4) J. W. Warren, *Nature*, **165**, 811 (1950).

(5) R. W. Kiser and E. J. Gallegos, *J. Phys. Chem.*, **66**, 947 (1962).

(6) V. H. Dibeler, R. M. Reese, and J. L. Franklin, *J. Am. Chem. Soc.*, **83**, 1813 (1961).

(7) D. P. Stevenson, *J. Chem. Phys.*, **18**, 1347 (1950).

(8) J. T. Herron and V. H. Dibeler, *J. Am. Chem. Soc.*, **82**, 1555 (1960).

tial of the cyclopropyl radical to be 7.8 ± 0.4 e.v., in agreement with the value reported by Pottie, *et al.*[2]

The appearance potential of m/e = 66 (70 e.v. relative abundance = 14%), the (parent–H) ion, was determined to be 13.3 ± 0.3 e.v. If the value of ~92 kcal./mole is employed for the C–H bond energy,[9] the ionization potential of the cyanocyclopropyl radical is calculated to be 9.3 e.v., in reasonable agreement with arguments and values given by Pottie and Lossing.[9] From an interpolation in Table II given by Pottie and Lossing,[9] we estimate the ionization potential of the methylcyclopropyl radical to be 7.5$_0$ e.v.

The parent molecule ion had a relative abundance of 29% at 70 e.v. The ionization potential of cyclopropyl cyanide was determined to be 11.2 ± 0.2 e.v. This result is in only fair agreement with the approximate value of 10.8 e.v. calculated by treating the cyclopropyl unit and the CN unit as groups and employing Franklin's group orbital method.[10] In so doing, we took $c^2 = -1.7$ as given by Franklin for interaction between the CN and phenyl groups, for the interaction parameter between the C_3H_5 and CN groups; I(cyclopropane) = 10.23 e.v.[11,12] and I(HCN) = 13.73 e.v.[13]

In order to determine the heats of formation of the various gaseous ions, we need to know the value of ΔH_f(cyclo-C_3H_5CN). Franklin's method[14] may be employed to give an approximate value; using the group contribution of 29.5 for CN and the C_3 ring correction (24.2), we calculate ΔH_f(cyclo-C_3H_5CN) = 43 kcal./mole. This value, together with ΔH_f(H) = 52 kcal./mole[15] and ΔH_f^+(CN) = 425 kcal./mole,[16] leads to ΔH_f^+(C_3H_5CN) = 301, ΔH_f^+(C_3H_4CN) = 298, ΔH_f(C_3H_5) = 68, and ΔH_f^+(C_3H_5) = 246 kcal./mole.

The question arises as to whether the C_3H_5 radical and ion for which energetics have been calculated are cyclic or not. Pottie, *et al.*,[2] and Stevenson[17] have noted the danger in attempting to deduce energetic properties of cycloalkyl radicals or ions from appearance potential data of cycloalkanes. However, the agreement of I-(cyclopropyl) indirectly determined by us with that determined by Pottie, *et al.*, in a direct manner indicates that the C_3H_5 and $C_3H_5^+$ of this study are both cyclic. Further, the values of ΔH_f^+(C_3H_5) = 239[2] and 246 kcal./mole are both significantly greater than the value of 220 kcal./mole reported for the allyl ion,[16,18] also suggesting that the $C_3H_5^+$ ion is cyclic. Since the appearance potential of m/e = 41 is fairly low, and in fact is quite close to the ionization potential of the xenon calibrant gas, it is considered very unlikely that our ΔH_f^+(C_3H_5) = 246 is in error by more than an electron volt. And to assign 26 kcal./mole as excitational energy to the allyl ion seems rather unreasonable.

The value of ΔH_f(C_3H_5) = 68 kcal./mole also supports our contention that C_3H_5 is the cyclopropyl rather than allyl radical, since it is expected that the heat of formation for cyclopropyl would be greater than that for allyl (ΔH_f(allyl) = 30 kcal./mole[19,20]). Our value of ΔH_f(C_3H_5) = 68 kcal./mole, although possibly somewhat high, is estimated to be correct to within about 12 kcal./mole.

We also have compared the mass spectra of allyl cyanide and cyclopropyl cyanide. The spectra are very similar, but we note than in allyl cyanide the m/e = 66 ion is only about one-half as intense as is the same ion in the cyclopropyl cyanide mass spectrum. This also suggests the retention of a cyclic structure.

We shall consider other features of the mass spectrum and energetics of cyclopropyl cyanide along with additional cyano-compounds in a future publication.

(9) R. F. Pottie and F. P. Lossing, *J. Am. Chem. Soc.* **83**, 4737 (1961).

(10) J. L. Franklin, *J. Chem. Phys.*, **22**, 1304 (1954).

(11) F. H. Field, *J. Chem. Phys.*, **20**, 1734 (1952).

(12) R. F. Pottie, A. J. Lorquet, and W. H. Hamill, *J. Am. Chem. Soc.*, **84**, 529 (1962).

(13) C. J. Varsel, F. A. Morrell, F. E. Resnik, and W. A. Powell, *Anal. Chem.*, **32**, 182 (1960).

(14) J. L. Franklin, *Ind. Eng. Chem.*, **41**, 1070 (1949).

(15) F. D. Rossini, D. D. Wagman, W. H. Evans, S. Levine, and I. Jaffe, "Selected Values of Chemical Thermodynamic Properties," National Bureau of Standards Circular 500, U. S. Government Printing Office, Washington, D. C., 1952.

(16) See F. H. Field and J. L. Franklin, "Electron Impact Phenomena and the Properties of Gaseous Ions," Academic Press, Inc., New York, N. Y., 1957.

(17) D. P. Stevenson, *J. Am. Chem. Soc.*, **80**, 1571 (1958).

(18) C. A. McDowell, F. P. Lossing, I. H. S. Henderson, and J. B. Farmer, *Can. J. Chem.*, **34**, 345 (1956).

(19) M. Szwarc, *Chem. Rev.*, **47**, 75 (1950).

(20) P. Gray and A. Williams, *ibid.*, **59**, 239 (1959).

DEPARTMENT OF CHEMISTRY
KANSAS STATE UNIVERSITY
MANHATTAN, KANSAS
ROBERT W. KISER
BRICE G. HOBROCK

RECEIVED MARCH 16, 1962

1,2-BIS-DIFLUOROAMINO-4-METHYLPENTANE: HEATS OF COMBUSTION, FORMATION, AND VAPORIZATION; AND VAPOR PRESSURE[1]

Sir:

In continuing studies of organic fluorine compounds, the Federal Bureau of Mines has determined selected thermodynamic properties of 1,2-bis-difluoroamino-4-methylpentane ($C_6H_{12}N_2F_4$)

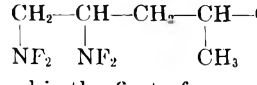

This compound is the first of a new class[2] for which accurate thermodynamic data have been determined. The heat of combustion and vapor pressure were measured, and the standard heats of formation and vaporization were calculated from the observed data.

A sample of 1,2-bis-difluoroamino-4-methylpentane was supplied through the courtesy of Dr. R. W. Walker, Rohm and Haas Co., Huntsville, Alabama. The material was purified by a preparative-scale gas–liquid chromatographic method by T. C. Davis of the Bureau's Laramie, Wyoming,

(1) This work was supported by the United States Air Force through the Air Force Office of Scientific Research under Contract No. CSO 59-9, ARPA Order No. 24-59, Task 3. Reproduction in whole or in part is permitted for any purpose of the United States Government.

(2) R. C. Petry and J. P. Freeman, *J. Am. Chem. Soc.*, **83**, 3912 (1961).

Petroleum Research Center. The sample used in the experiments was 99.8 mole % $C_6H_{12}N_2F_4$ and 0.2% $C_5H_{10}N_2F_4$; it contained $C_6H_{12}N_2F_4$ isomers other than 1,2-bis-difluoroamino-4-methylpentane, but in amounts small enough that the accuracy of the results was not affected significantly. A small correction for the $C_5H_{10}N_2F_4$ was applied in calculating the heats of combustion and formation.

Combustion calorimetry was done with apparatus and techniques previously described.[3] To avoid detonation and incomplete combustion, each sample was diluted with a paraffin oil[3] in such proportions that 58 to 75% of the energy evolved in a combustion experiment came from the diluent. The diluted sample for an experiment was contained in a bag of polyester film,[3] filled and sealed in a way that permitted accurate determination of the mass of each component. The heat of solution of the sample in paraffin oil was assumed negligible. From the results of seven satisfactory experiments, the heat of combustion of 1,2-bis-difluoroamino-4-methylpentane was found to be $\Delta Hc°_{298.15} = -1080.1_3 \pm 0.8_0$[4] kcal. mole^{-1}, for the idealized reaction 1.

$$C_6H_{12}N_2F_4(\text{soln. in oil}) + 8O_2(g) + 196H_2O(\text{liq}) = 6CO_2(g) + N_2(g) + 4[HF\cdot 50H_2O](\text{liq}) \quad (1)$$

For consistency with related published data, 1951 atomic weights and fundamental constants[5] were used with the definitions: 0°C. = 273.15°K.; 1 cal. = 4.184 joules (exactly).

The vapor pressure of the difluoroamino compound was measured with a recently developed inclined-piston gage to be described elsewhere. Successive portions of the sample were distilled from the sample container until no significant change in vapor pressure occurred. This procedure minimized errors due to the small amount of $C_5H_{10}N_2F_4$ impurity present in the original sample. The results of measurements at nine temperatures between −20.000 and +20.000° (0.236 and 4.812 mm.) are represented by the Antoine equation

$$\log p = 6.88576 - 1427.201/(209.946 + t) \quad (2)$$

where p is in mm. and t is in °C. The Clapeyron equation, eq. 2, and estimates of the second virial coefficient and liquid density were used to compute the standard heat of vaporization, $\Delta Hv°_{298.15} = 10.51 \pm 0.05$ kcal. mole^{-1}.

The results of this investigation and heat-of-formation data for carbon dioxide, water, and aqueous HF[6] were used in calculating the standard heats of formation of liquid and gaseous 1,2-bis-difluoroamino-4-methylpentane for the reaction

$$6C(c, \text{graphite}) + 6H_2(g) + N_2(g) + 2F_2(g) = C_6H_{12}N_2F_4 \text{ (l or g)} \quad (3)$$

$$\Delta Hf°_{298.15} = -60.09 \text{ kcal. mole}^{-1} \text{ (liq)}$$
$$= -49.58 \text{ kcal. mole}^{-1} \text{ (gas)}$$

Calculations of bond energies for molecules as complicated as 1,2-bis-difluoroamino-4-methylpentane are inherently uncertain. However, with a consistent set of bond energy terms, the foregoing heat-of-formation value was used to make a reasonable estimate of the N–F thermochemical bond energy, E(N–F) = 67 kcal. mole^{-1}. This value is about the same as that found for NF_3[7] (66 kcal. mole^{-1}), but it is significantly lower than the value in perfluoropiperidine,[8] 73 kcal. mole^{-1}.

Organic difluoroamino compounds are shock sensitive and possibly toxic, so care must be exercised in working with them.

(3) W. D. Good, D. W. Scott, and G. Waddington, *J. Phys. Chem.*, **60**, 1080 (1956); W. D. Good, D. R. Douslin, D. W. Scott, A. George, J. L. Lacina, J. P. Dawson, and G. Waddington, *ibid.*, **63**, 1133 (1959).

(4) The uncertainty interval is twice the final "over-all" standard deviation.

(5) E. Wichers, *J. Am. Chem. Soc.*, **74**, 2447 (1952); F. D. Rossini, F. T. Gucker, Jr., H. L. Johnston, L. Pauling, and G. W. Vinal, *ibid.*, **74**, 2699 (1952).

(6) F. D. Rossini, D. D. Wagman, W. H. Evans, S. Levine, and I. Jaffe, "Selected Values of Chemical Thermodyanic Properties," National Bureau Standards Circular 500, Washington, D. C., 1952.

(7) G. T. Armstrong, S. Marantz, and C. F. Coyle, *J. Am. Chem. Soc.*, **81**, 3798 (1959).

(8) W. D. Good, D. W. Scott, J. L. Lacina, and G. Waddington, presented at the 133rd American Chemical Soicety National Meeting, San Francisco, Calif., April 13–18, 1958; to be published.

CONTRIBUTION NO. 116 FROM THE THERMODYNAMICS LABORATORY OF THE BARTLESVILLE PETROLEUM RESEARCH CENTER, BUREAU OF MINES, U. S. DEPARTMENT OF THE INTERIOR
BARTLESVILLE, OKLAHOMA

W. D. GOOD
D. R. DOUSLIN
J. P. MCCULLOUGH

RECEIVED MARCH 3, 1962

RATE EQUATION FOR ADSORPTION OF A NEUTRAL SUBSTANCE AT A METAL-ELECTROLYTE INTERFACE[1]

Sir:

An equation was derived for the rate of adsorption of a neutral substance at a metal–electrolyte interface for processes obeying a logarithmic Temkin isotherm. The key ideas in the derivation are: (i) In the thermodynamic analysis of adsorption at a metal–electrolyte interface it is convenient to select as independent electrical variable should maintain constant the charge q on the electrode rather than the potential E (Parsons), *i.e.*, q rather than E is the "natural" variable in the treatment of adsorption. (ii) It is inferred from recent work in this Laboratory that the logarithmic Temkin isotherm is obeyed for many organic neutral substances of varied structure over a fairly wide concentration range. (Exceptions were found, however.) The validity of the logarithmic Temkin isotherm can be ascertained by noting that a plot of the surface concentration Γ (nearly equal to the surface excess for a neutral substance), at constant charge and electrolyte activity, against the logarithm of the bulk activity a is linear for the logarithmic Temkin isotherm. More simply, one can verify that a plot of E at constant q against $\ln a$ is linear[2] (Parsons). Thus, the Esin and Markov coefficient, $(\partial E/\partial \ln a)_q$, at constant charge is constant for the logarithmic Temkin isotherm. (iii) Rate equations given by Temkin for gas adsorption

(1) Work supported by the National Science Foundation.

(2) It can be shown (Mohilner and Delahay, to be published) that the logarithmic Temkin isotherm is a sufficient, but not necessary, condition for a linear plot of E against $\ln a$ at constant q. In principle an infinite number of isotherms satisfying certain conditions would yield such a linear plot but, in practice, only the logarithmic Temkin isotherm among the ten most common isotherms corresponds to a constant Esin and Markov coefficient at constant q.

on solids apply. (iv) The influence of the charge on the adsorption and desorption rates can be expressed in terms of a *charge parameter* ρ and the charge-dependent part of the standard free energy of adsorption $\delta\Delta G^q$ at charge q. This novel idea is the key to the treatment.

The net rate of adsorption is

$$v = v_0\{\exp[(-\lambda b/RT)\delta\Gamma]\exp-(\rho/RT)\delta\Delta G^q] - \exp[((1-\lambda)b/RT)\delta\Gamma]\exp[((1-\rho)/RT)\delta\Delta G^q]\} \quad (1)$$

$$v_0 = k^0 a^{1-\lambda}\exp\{[(\lambda-\rho)/RT]\Delta G^q\} \quad (2)$$

where v_0 is the *adsorption exchange rate;* k^0 the *adsorption standard rate constant;* λ the *coverage parameter* (this is not the coverage) used by Temkin in correlating rates with coverage; $\delta\Gamma$ and $\delta\Delta G^q$ represent perturbations in the values of Γ and ΔG^q; b is the parameter in the logarithmic Temkin isotherm, *i.e.*, $b\Gamma$ varies linearly with RT ln a at constant charge; R and T are as usual. At equilibrium, there is adsorption exchange between solution and metal at the rate of v_0 mole cm.$^{-2}$ sec.$^{-1}$ If ΔG^q varies, as a result of a change of the charge q by an external device, the rate of variation of Γ, $v = d\Gamma/dt$, is given by eq. 1. The equilibrium value Γ corresponding to the new value of ΔG^q is ultimately reached. The correlation between ΔG^q and q is obtained from the isotherm or, more conveniently, by integration of the Esin and Markov coefficient with respect to the charge.

It follows from eq. 2 that, at constant electrolyte composition

$$(\partial \ln v_0/\partial \ln a)_q = 1 - \lambda \quad (3)$$

$$RT(\partial \ln v_0/\partial\Delta G^q)_a = \lambda - \rho \quad (4)$$

i.e., λ and ρ can be determined experimentally.

Equation 1 recalls the Butler Erdey–Gruz–Volmer equation for electrode kinetics and it should provide a basis for adsorption kinetics, just as the latter equation allowed the development of electrode kinetics. The charge parameter ρ in eq. 1 is analogous to the transfer coefficient in the Butler Erdey–Gruz Volmer equation. Likewise, eq. 2 recalls a similar equation for the exchange current; and eq. 3 and 4 are similar to the relationship for determination of the transfer coefficient in electrode kinetics.

Correction of eq. 1 for mass transfer is immediate; and the corresponding boundary value problems have been analyzed for mass transfer controlled by semi-infinite linear diffusion and either a step variation of ΔG^q or for ΔG^q proportional to time or the square root of time (Delahay, to be published). Equation 1 and the corresponding equation with mass transfer correction can be linearized readily. Correction of v_0 for the double layer structure analogous to the Frumkin correction in electrode kinetics should be minor because the interaction of a neutral substance with the field in the *diffuse* double layer is quite small.

The theory will be published, and experimental methods for the determination of v_0 now are being developed.

COATES CHEMICAL LABORATORY
LOUISIANA STATE UNIVERSITY P. DELAHAY
BATON ROUGE 3, LA. D. M. MOHILNER

RECEIVED MARCH 5, 1962

No. 31 in the ADVANCES IN CHEMISTRY SERIES

CRITICAL SOLUTION TEMPERATURES

by **Alfred W. Francis,** consultant to Socony Mobil Oil Co., Inc.

This volume, written by an authority on hydrocarbon chemistry and liquid-liquid phase relations, lists over 6000 critical solution temperatures (the minimum temperature for mixing of two substances in all proportions *as liquids*). Also included are about 800 aniline point observations; methods for determining CST; guides to using CST data and to estimating the CST for untested systems.

Among uses of CST are: screening possible extraction solvents for selectivity; approximating liquid solubility at any temperature below the CST; characterizing hydrocarbons; analysis of mixtures, especially where water is one component, and providing an insight into molecular structure.

CONTENTS

246 pages. **Cloth bound.** **Price: $5.00**

Order from: **Special Issues Sales, American Chemical Society**
1155 Sixteenth Street, N.W., Washington 6, D. C.

NO. **26** EPR AT WORK SERIES

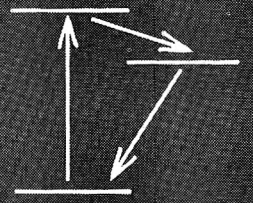

EPR OF TRIPLET STATES

(ELECTRON PARAMAGNETIC RESONANCE)

EPR study of triplet states in organic molecules is of considerable intrinsic interest and has taken on an added importance because these materials are suitable for optical masers. High sensitivity, provision for uv irradiation, and variable temperature equipment make the Varian V-4502 EPR spectrometer particularly useful in this work.

EXAMPLE

Triplet Naphthalene in Durene

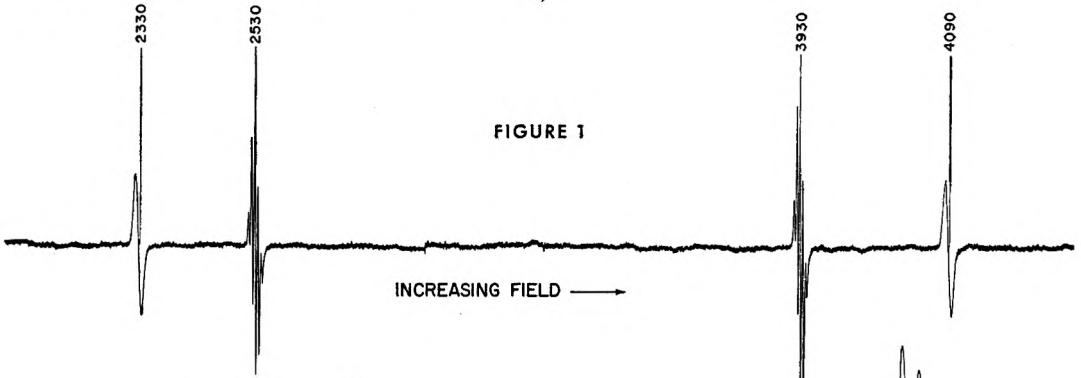

FIGURE 1

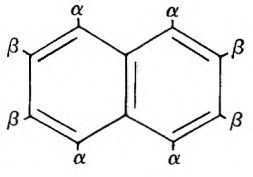

FIGURE 2

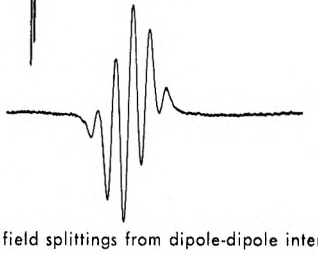

FIGURE 3

Observation by EPR of a meta-stable photo excited triplet state in an organic molecule was first reported by Hutchison and Mangum[1]. Success in their work required a dilute suspension of oriented molecules. This was achieved by growing mixed crystals of naphthalene (Fig. 2) in durene. This host substance is transparent to the uv irradiation required to excite the naphthalene triplet state.

The EPR spectrum at 77°K is illustrated in Fig. 1. The Varian F-8 NMR Fluxmeter was used to make the field measurements. There are two molecules per unit cell in durene, at approximately right angles to each other. Naphthalene substitutes isomorphically, and the high and low field lines arise from molecules which have the magnetic field perpendicular to the molecular plane. The lines with structure are associated with molecules in the other site which have the field parallel to the long axis. The difference in heights of the pair of lines from a particular orientation are caused by a difference in the transition probabilities. Zero field splittings from dipole-dipole interaction are comparable to a microwave quantum, resulting in the large anisotropy.

Hyperfine interaction with the protons on the ring positions is anisotropic. With the magnetic field parallel to the long axis of naphthalene, interaction with the 4 equivalent α protons may be resolved, and a 5-line spectrum is observed (Fig. 3). In other orientations, the resolution is poorer, and in no case is the β splitting clearly seen.

Subjects of current interest, under investigation in a number of laboratories are: optical excitation and decay processes, energy transfer mechanisms, and behavior at liquid helium temperatures. In these experiments, the details of the interaction of the naphthalene molecule with the host lattice are being probed. One may expect that the information gained in this work will have immediate practical application in optical masers.

(1) C. A. Hutchison, Jr. and B. W. Mangum, J. Chem. Phys. **29,** *952 (1958).*

For literature which fully explains the 100 kc EPR Spectrometer and its application to basic and applied research in physics, chemistry, biology and medicine, write the Instrument Division.

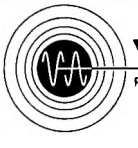

VARIAN associates

PALO ALTO 52, CALIFORNIA

595